“Biodegradable Polymer Adhesives, Hybrids and Nanomaterials”

A Thesis

Submitted to the Faculty

of

Drexel University

by

Andreas Mylonakis

in partial fulfillment of the

requirements for the degree

of

Doctor of Philosophy

September 2008

Dedications

This work is dedicated to my mom Loukia Tsoni, my brother Gewrgios Mylonakis, my grandmother Gewrgia Tsoni and my fiancé Catherine Stoupas for their encouragement, support and love. I would also like to dedicate it to Dr. Andreas Athinaios, the president of The Hellenic Foundation, that supported me not only financially but also psychologically. I know that this work makes them happy and proud.

Acknowledgements

Throughout these years in Drexel University there are many people that I have become thankful of, without whom most probably I would not be able to pursue my doctorate. First, I would like to express my gratitude to my advisor Dr. Yen Wei for his guidance, support and help. Amongst others, what I have learned from him and which will be followed throughout my scientific career was to enjoy what I am doing, be open to new ideas and remain always challenged by trying novel things. With his own unique way he kept me highly motivated, focused and inspired to reach the final goal of pursuing something that will have a small or a big impact to society. As he always keeps saying, chemistry is an art, and you need imagination to become a good artist. I express my sincere appreciation to a big mentor for my scientific career and my personal life.

Words are very little to describe my gratitude to The Hellenic Foundation, and Dr. Andreas Athinaios in particular, for supporting me with a full-time scholarship to obtain the PhD in Chemistry at Drexel University. His support, financial but more importantly psychological will be always remembered and never taken for granted. He opened new highways for my scientific career and personal life, and I am very glad to know that this thesis makes him and The Hellenic Foundation very proud. On a personal level I've learned the virtues of patience, hard work, integrity, and love, and which I will do my best to follow for the rest of my life. I will never forget that he was always there for me with a non-stop effort to reach solutions to my problems, enjoy my happy moments and support me in the bad days during my PhD years.

I would also like to thank and express my appreciation to Dr. Shuxi Li who was always the first resource of scientific guidance and information throughout this research work. I will always remember his continuous efforts to organize the laboratory, to answer questions and seek solutions to potential problems. Our great collaboration in many research projects will be always remembered. I owe my sincere appreciation to Dr. Amar Nath from University of North Carolina for his guidance and the great collaboration we had on the phthalocyanine research work. I would especially like to thank Dr. David Soll, Dr. Jack Baldwin and Dr. Cyrial Evian for their guidance, inspiration and great collaboration we had in the biodegradable adhesives I have worked on.

I want to thank my candidacy examination and/or my dissertation defense committee members, Dr. Daniel King, Dr. Lynn Penn, Dr. Robert Hutchins, Dr. Sally Solomon, Dr. Jun Xi, Dr. Shu Yang, Dr. Guoliang Yang and Dr. Jian-Min Yuan. Their time and valuable suggestions are highly appreciated.

I would like to express my appreciation to Dr. Kevin Owens for training me on several analytical instruments, all the professors in the department of Chemistry for being there for me, and Drexel University for providing me with a great working environment. I also thank Dr. Solomon Samuel who helped me with the mechanical testing of many of my research samples and the good collaboration we had. I acknowledge Dr. Nadaraj Sundar Babu for his valuable help in many of the projects. I thank Mrs. Dee Breger, Dr. Zhorro Nikolov, Dr. Edward Basgall, Dr. Boris Polyak, Dr. Anat Katsir and Mrs. Leko Lin for training me on various microscopic and spectroscopic instruments. I also want to thank Dr. Xing Geng and Dr. Giuseppe R. Palmese for assisting and facilitating the usage of the instron instrument. I would like to express my thankfullness to Mr. Edward Doherty, Mrs. Virginia Nesmith and Mrs. Edith Smith for their

assistance all these years. I would like to thank Mr. Thomas Cachaza for making many custom-made apparatus.

I want to express my appreciation to many of the graduate students past and present who have been there for me. Mrs. Widalys Gonzalez, Mrs. Laquisha Hamilton, Mr. Gordan Reeves, Mrs. Guzeliya Korneva, Mrs. Adeline Kojtari, Mrs. April Holcomb, Dr. Hung Le, Mr. Thomas Measey, Mr. Andrew Hagerman, Mr. Khalid Baig Mirza, Mrs. Stephanie Schuster, Mrs. Alma Pipic, Mr. James Rieben, Mr. Matthew Rossi, Mrs. Renata Szyszka, Mrs. Kim Kahle, Mrs. Mozhgan Bahadory, Mr. William Erb, …. the list goes on. Special thanks are due to all the past and present associates and students in Dr. Wei's lab, Dr. Zongtao Zhang, Dr. Houping Yin, Dr. Zhengfei Sun, Dr. Alpa Patel, Dr. Yi Guo, Mr. Mathew Zagorski, Mr. Indraneil Mukherjee, Mr. Somang Kim, Mr. Sudipto Das, Mr. David Berke-Schlessel, Mr. Kerry Drake, Mr. Charles Bowman, Mr. Alexksander Fisher, Dr. Siui Li. I want to also express my gratitude to Mr. Colin Murray and Mr. Tom Hughes for the valuable discussions and the financial help for the enzyme work.

I want to express my gratefulness to my mom Loukia Tsoni who has always stood by my side all these years with innumerable sacrifices and efforts to raise me and my brother with love, integrity and self-esteem. I know that this work makes her very proud. I express my gratitude to my brother and grandmother for their love and support. I also want to thank the most precious thing in my life, my fiancé Catherine Stoupas, for her unconditional love, help and support through these years.

Table of contents

Appendix D. Collaborative or On-going Work

List of Tables

List of Schemes

List of Figures

List of Symbols

A	absorbance
N_a	amount of gas adsorbed
D	average particle size
δ	chemical shift
σ	specific conductivity
θ	diffraction angle
E_{min}	maximum potential
E_{max}	minimum potential
i_c	cathodic current
i_a	anodic current
v	sweep rate
E_y	elastic modulus
T_g	glass transition temperature
C_p	heat capacity
η	viscosity
ds/dt	rate of shear
V_m	maximal velocity
K_m	Michaelis constant
D	pore size distribution
P	pressure
P/P_0	relative pressure
T	temperature
d	separation between planes
R_v	volume comductivity
λ	wavelength

List of Abbreviations

AFM	atomic force microscopy
ATQD	*N*-(4-aminophenyl)-*N'*-(4'-(3-triethoxysilyl-propyl-ureido) phenyl-1,4-quinonenediimine)
BPO	benzoyl peroxide
BET	Brunauer-Emmett-Teller
CPs	conductive polymers
CV	cyclic voltammery
DSC	differential scanning calorimetry
DHBA	3,4-dihydroxybenzoic acid
DHBA-Ch-1	modified chitosan with 3,4-dihydroxybenzoic acid (feeding mol ratio 2:1)
DHBA-Ch-2	modified chitosan with 3,4-dihydroxybenzoic acid (feeding mol ratio 4:1)
DHBA-Ch-3	modified chitosan with 3,4-dihydroxybenzoic acid (feeding mol ratio 10:1)
DOPA	L-3,4-dihydroxyphenylalanine
DMF	dimethylformamide
DMSO	dimethylsulfoxide
EDX	elemental analysis
EBAT	emeraldine form aniline trimer
ESEM	environmental scanning electron microscope
FT-IR	fourier transform infrared spectra
HIF0	0% fructose-templated hybrid material (TMOS/MTMS: 1/1)
HIF20	20% fructose-templated hybrid material (TMOS/MTMS: 1/1)
HIF50	50% fructose-templated hybrid material (TMOS/MTMS: 1/1)
HIIF0	0% fructose-templated hybrid material (TMOS/MTMS: 2/1)
HIIF20	20% fructose-templated hybrid material (TMOS/MTMS: 2/1)
HIIF50	50% fructose-templated hybrid material (TMOS/MTMS: 2/1)
HIIIF0	0% fructose-templated hybrid material (TMOS/MTMS: 3/1)

HIIIF20	20% fructose-templated hybrid material (TMOS/MTMS: 3/1)
HIIIF50	50% fructose-templated hybrid material (TMOS/MTMS: 3/1)
HIIIIF0	0% fructose-templated hybrid material (TMOS/PhTMS: 20/1)
HIIIIF20	20% fructose-templated hybrid material (TMOS/PhTMS: 20/1)
HIIIIF50	50% fructose-templated hybrid material (TMOS/PhTMS: 20/1)
HGS	HEMA-GMA-silica
GMA	glycidyl methacrylate
GPC	gel permeation chromatography
HEMA	2-hydroxyethyl methacrylate
HPLC	high performance liquid chromatography
HRP	horse radish peroxidase
ITO	indium tin oxide
IR	infrared spectroscopy
IUPAC	international union of pure and applied chemistry
NHS	N-hydroxysuccinimide
NiPAAm	N-isopropyl-acrylamide
MTMS	methyltrimethoxysilane
NMR	nuclear magnetic resonance
PhTMS	phenyltrimethoxysilane
PBS	phosphate buffered saline
PANi	polyaniline
PMMA	poly(methyl methacrylate)
PHGS	poly(2-hydroxyethyl methacrylate-glycidyl methacrylate-silica)
PHGS-2-7	poly(HEMA-GMA-silica) containing 7 wt% silica (HEMA/GMA: 2)
PHGS-2-10	poly(HEMA-GMA-silica) containing 10 wt% silica (HEMA/GMA: 2)
PHGS-2-15	poly(HEMA-GMA-silica) containing 15 wt% silica (HEMA/GMA: 2)
PHGS-2-20	poly(HEMA-GMA-silica) containing 20 wt% silica (HEMA/GMA: 2)
PHGS-2-25	poly(HEMA-GMA-silica) containing 25 wt% silica (HEMA/GMA: 2)
PHGS-2-30	poly(HEMA-GMA-silica) containing 30 wt% silica (HEMA/GMA: 2)

PPy	polypyrrole
PSD	pore size distribution
RDE	rotating disk polarography
SEM	scanning electron microscopy
TEOS	tetraethylorthosilicate
TEOS	tetraethylorthosilicate
TMOS	tetramethylorthoxysilicate
TEM	transmission electron microscopy
THBA	3,4,5-trhydroxy benzoic acid
THBA-Ch	modified chitosan with 2,5-dihydroxybenzoic acid (feeding mol ratio 2:1)
TESPIC	triethoxysilylpropyl isocyanate
TGA	thermogravimetric analysis
TSUPQD	*N*,*N*'-bis(4'-(3-triethoxysilylpropyl-ureido) phenyl)-1,4-quinonenenediimine
THF	tetrahydrofuran
TEGDMA	tri(ethylene glycol) dimethacrylate
UV-Vis	ultraviolet and visible
XRD	X-ray diffraction

Abstract

Biodegradable Polymer Adhesives,Hybrids and Nanomaterials

Andreas Mylonakis

Advisor: Dr. Yen Wei

Biodegradable polymeric products and organic-inorganic hybrid materials for a diversity of applications are the two main fields on which this research has been focused. A novel biodegradable adhesive, which mimics marine adhesive proteins, has been synthesized by the covalent incorporation of 3,4-dihydroxybenzoic acid onto the chitosan backbone. The adhesive strength of these materials varies with the molecular weight of the polysaccharide, the amount of diphenolics present and the curing time. Infrared spectroscopy (IR), nuclear magnetic resonance spectroscopy (NMR) and ultraviolet-visible spectroscopy (UV) have been used to qualitatively and quantitatively establish the amount of the diphenolic moiety present on the backbone of the biodegradable polymers. The as synthesized polymers combine both the adhesive capability of the diphenolic function and the healing effect of chitosan. The biocompatibility and biodegradability of these modified chitosans offer the promise of utility of these novel materials in dental and medical applications.

Organic-inorganic hybrid materials with low volume shrinkage and excellent mechanical properties were synthesized by the covalent incorporation of 2-hydroxyethyl methacrylate and glycidyl methacrylate on pre-hydrolyzed sol-gel silica. These hybrid materials exhibited low volume shrinkage during polymerization and were crack-free during storage for about twelve months. The mechanical properties of these materials are composition dependent. Incorporation of silica effectively increased the compressive yield stress and modulus of the obtained poly(HEMA-GMA-silica) hybrid materials.

A series of new electroactive hybrid materials have been synthesized by covalent incorporation of polyaniline into polyacrylate-silica hybrids. The formulation involves the radical co-polymerization of glycidyl methacrylate-polyaniline (GMA-PANi) and glycidyl methacrylate-2-hydroxyethyl methacrylate-silica (GMA-HEMA-silica) to yield poly(HEMA-GMA-silica)-polyaniline (PHGS-PANi) hybrids. The chromoelectrochemical study suggests that these materials can have tunable colors upon change of potential and/or pH, and thus may find applications as chemical or biological sensors and electro-optical devices. Moreover, conductivity measurements and mechanical testing of these materials show that these materials can be prepared to have both a reasonably high conductivity and excellent mechanical properties.

A novel technology for maintaining the enzymatic activity, during storage in harsh media, such as organic solvents and high pH aqueous solutions, has been explored. The non-surfactant templated sol-gel method has been utilized to incorporate horseradish peroxidase (HRP) enzyme into the pores of mesoporous organosilicas followed by the application of a second acrylic protective layer. Results indicate that such doubly encapsulated HRP showed many orders of magnitude higher residual activity after storage in harsh media, as compared to the native enzyme under the same conditions. This method is expected to be useful for stabilizing other enzymes as well, in hostile environments.

The electrochemical study of a novel electroactive aniline trimer-silane compound and other well defined aniline oligomers with end group substitution has been investigated. Results demonstrate that substitution with electron-donating or electron-withdrawing groups has a profound effect on the electrochemistry of such compounds. Additionally, the formation of interesting oxygen adducts by both wet and dry prolonged oxygenation of iron phthalocyanines (α-

and β-form) has been achieved. Finally, the fabrication of a novel fluorescent nanoelectrode with applications in neuroscience has been explored.

Chapter 1. Introduction to Polymers, Hybrid Materials and Nanomaterials

1.1 History and Motivation

Polymeric materials, hybrid materials and nanomaterials are the three important aspects that are the focus of this thesis, which includes the development of biodegradable polymers and the synthesis of a broad range of novel organic-inorganic hybrid materials and nanomaterials for a variety of applications. The majority of the hybrid materials that have been synthesized in this work belong to the class of nanocomposites and may also be thus considered as nanomaterials.

According to Charles Carraher, "Polymers are all around us and responsible for life itself, for communication (both natural and synthetic), nutrition, clothing, recording history, buildings and highways. In fact it is difficult to imagine society without synthetic polymers, and life without natural polymers".[1] The word polymer is derived from the Greek words "poly" and "meros", which mean "many" and "part' respectively. Polymeric compounds are formed by the joining of smaller, usually repeating, units linked by covalent bonds. These compounds often form large macromolecules, and the area they comprise goes from plastics, fibers and rubbers that can be seen in our everyday lives in the modern societies to proteins, carbohydrates, nucleic acids and natural fibers that are part of our bodies and biological world. Historically, polymers were known by the early humans who utilized degradation of proteins in meat by aging and cooking and learned how to process, dye and weave the natural occurring fibers of wool, silk and cotton. As with almost everything in materials science, these discoveries were first made empirically far before the science of polymers was discovered.

It was not before 1839, when Charles Goodyear started experimenting with the natural rubber, that the public was introduced to these new "man-made" materials. According to a story, Charles Goodyear, while doing experiments, accidentally dropped a lump of rubber mixed with sulfur on a hot stove. The rubber did not melt but charred instead. What he had discovered was the vulcanization of rubber, which creates a cross-linked material more durable than natural rubber, and which after many efforts of experimentation is now being used in the automobile industry.[2] Several years after Goodyear's invention, Leo Baekeland in 1907 at an American Chemical Society meeting announced the synthesis of the first synthetic polymeric material, which was later, after extensive effort for its optimization, named Bakelite.[3] Baekeland discovered this sticky, amber-colored and easily molded into different shapes, resin by subjecting mixed phenol and formaldehyde to heat and pressure. Although there is not much evidence that Baekeland recognized what polymers were, he appeared to have a sense of how to utilize them in order to get thermoplastic materials that could be converted to thermosets. Up until that time, polymer science was largely empirical, instinctive and intuitive mainly due to the lack of fundamental knowledge on the theoretical basis. Contrary to prevailing ideas at that time, Hermann Staudinger proposed, in a landmark paper published in 1920, that rubber and other polymeric substances, such as starch, cellulose and proteins, are long chains of short repeating molecular units linked by covalent bonds.[4] X-ray studies of many natural and synthetic polymers provided evidence to confirm that macromolecular compounds existed. Despite the impressive experimental evidence, Staudinger continued to encounter very strong opposition for nearly two decades from leading organic chemists. For instance, Heinrich Wieland, 1927 Nobel laureate in chemistry,[5] wrote to Staudinger, "Dear colleague, drop the idea of large molecules; organic molecules with a molecular weight higher than 5000 do not exist. Purify your products, such as

rubber, they will crystallize and prove to be low molecular compounds!" This new concept, referred to as "macromolecules" by Staudinger in 1922, and for which Staudinger was ultimately awarded the Nobel Prize in 1953,[6] covered both synthetic and natural polymers and was the key to a wide range of modern polymeric materials and innovative applications.[7] Among other great scientists of that time Wallace Hume Carothers, with his theoretical and experimental research at the DuPont Company, was the one to fully remove any doubts about whether or not macromolecules exist. Two of the 20th century's most widely used synthetic polymers, namely neoprene and nylon, originated in 1930 from his studies in his research laboratory. World War II demands and shortages were the impetus for developing substitutes and improved materials.

Since then, brought by the needs for materials with unique or better properties, the polymer science has continued to grow and has evolved into one of the fastest growing areas. The actual importance of polymers has been realized throughout the years, due to the tremendous applications in all the branches of science, including:

- Structural polymers and composites, such as fibers, textiles, proteins and carbohydrates;
- Packaging materials and coatings that combine the ease of processing with desirable mechanical properties;
- Transparent and optical materials such as windows, optical fibers, lenses, reflectors, and transparent film packages;
- Biological and medical materials including dissolvable sutures, implants, prosthetics, and drug delivery systems;
- Fluid modifiers and suspension stabilizers for applications in the food and health care industry;

- Conductive, electroactive, optoelectronic, and/or magnetic polymers with applications in electronics, optics, biotechnology and the fabrication of "smart devices".

The fields of biodegradable polymers and conductive polymers are the two subcategories of polymeric materials that have been investigated in this research and will be presented in more details in the following sections of Chapter 1.

The area of hybrid materials is another aspect that forms the foundation of this thesis. The term hybrid materials includes many different systems, spanning a wide range of various materials, such as highly ordered coordination polymers, amorphous sol-gel compounds and materials with and without interactions between the inorganic and organic components.[8] In our opinion, broad definition could be the following: a hybrid material is a material that includes two or more moieties blended, or more strictly, covalently bonded on the molecular level. They can be described as nanocomposites made of organic and inorganic components combined over length scales ranging from a few Angstroms to a few tens of nanometers. Historically, inorganic components were first added to synthetic organic polymers soon after the invention of the latter.[9] The benefit of exploring the area of hybrid materials was the lower cost and the great potential for numerous combinations of the final material's properties that could not be achieved with the conventional materials namely either pure organic or pure inorganic materials. The development of these multifunctional advanced materials has various applications in the fields of:

- Optics, electronics, ionics;
- Mechanics, membranes, coatings;
- Catalysis, sensors and biology.

In particular, hybrid materials prepared by synthetic methods, such as sol-gel chemistry, seem to present a route leading to the development of endless novel hybrid materials for a diversity of applications. The sol-gel process, which is mainly dealing with inorganic polymerization reactions, is a chemical synthesis procedure used for the preparation of inorganic materials such as glasses and ceramics. It involves an inorganic polymerization, which leads to a highly cross-linked solid through a hydrolytic polycondensation. Compared to other inorganic network forming reactions, the sol-gel method possesses mild reaction conditions and a broad solvent compatibility. These two characteristics offer the possibility to carry out the inorganic network forming process in the presence of a preformed organic polymer or to carry the organic polymerization before, during or after the sol-gel process. The properties of these organic/inorganic hybrid materials, which have been named as "ceramers" by Wilkis et al. and "ormosils" or "ormocers" by Schmidt et al.,[10] are not only determined by the properties of the inorganic or organic component, but also by the phase morphology and the interfacial region between the two moieties. In the later 1980s, our group at Drexel University developed the first hybrid material with vinyl polymers being uniformly mixed in and covalently bonded to inorganic silica at the molecular level.[11] The preparation, characterization and applications of these organic/inorganic hybrid materials have become a fast expanding area of research in the materials science, due to the novel and unique properties that these hybrids/nanocomposites can offer, compared to the traditional macroscale composites and conventional materials.

The world of nanomaterials is another big area of science on which this thesis has been focused. Nanotechnology refers to the manipulation of matter of very small scale, covering many kinds of science and also many products. According to the United States National

Nanotechnology Initiative website, “Nanotechnology is defined as the understanding and control of matter at dimensions of roughly 1 to 100 nanometers, where unique phenomena enable novel applications”.[12] The first one to mention the distinguishing concepts in nanotechnology is physicist Richard Feynman, who gave an inspiring talk called "There's Plenty of Room at the Bottom", at an American Physical Society meeting at Caltech on December 29, 1959. Feynman considered the possibility of direct manipulation of individual atoms as a more powerful form of synthetic chemistry than those used at the time. The term "nanotechnology" was actually coined by Professor Norio Taniguchi in 1974.[13] Taniguchi was the recipient of Euspen's first lifetime achievement award, which was presented in Bremen, May 1999. The citation on Professor Taniguchi's award read: "In recognition of his unique and outstanding contributions to research and development in the ultra precision materials processing technologies. Through his vision, writings and example of total dedication to this field of endeavor he has stimulated the development of what will be one of the dominant technologies in the 21st Century." In 1980s the basic idea of the “nanotechnology” definition was promoted by Dr. Eric Drexler, through speeches and various nanotechnology books written by him.[14,15] Since nanomaterials possess unique, beneficial chemical, physical, and mechanical properties, they can be used for a wide variety of applications. These applications include, but are not limited to areas such as:

- Nanocircuits and nanofabrication of electronic devices;[16,17]
- Nanoporous materials for a number of sophisticated end uses;[18]
- Self-assembled biopolymers and biomimetic structures;[19]
- Health care products;[20]
- Coatings industry;[20]

- Quantum dots,[22] metal nanoparticles[23] and catalysts.

For a better understanding of the topics discussed in the coming chapters of this dissertation, the rest of the sections in Chapter 1 will give a brief review of the types of biodegradable polymers, biodegradable adhesives, hybrid materials, hybrids prepared by the sol-gel process, conductive polymers and nanomaterials that have been studied to date.

1.2 Biodegradable Polymers

In recent years, there has been an explosion of interest in biodegradable materials for use in packaging,[24] agriculture, medicine[25] and other areas.[26] In particular for this thesis, the biodegradable polymeric materials with applications in the medical industry are of interest. There is not a completely satisfactory definition for "biodegradable" but the American Society for Testing of Materials (ASTM) defines the term as "a degradation caused by biological activity, especially by enzymatic action, leading to a significant change in the chemical structure of the material. These changes result in a loss of physical and mechanical properties, as measured by standard methods." Biodegradable polymers usually undergo degradation from the action of naturally occurring microorganisms, such as bacteria, fungi, and algae. Polymers may also be photodegradable, oxidatively degradable or hydrolytically degradable albeit for simplicity purposes all are designated as biodegradable.

Biodegradable polymers may be natural or synthetic with the latter offering more advantages, since tailoring may lead to materials with a wide range of properties.[27] Even though the biomedical applications of degradable natural polymers, such as wood, cotton, leather, etc., date back thousands of years, the application of synthetic biodegradable polymers did not start before

the 1960s.[28] The reasons for this slow evolution of biodegradable polymers can be attributed to the several unique challenges in developing resorbable medical materials, compared to developing commodity polymeric materials. In the past three decades, however, there has been a great development of a range of new generation synthetic biodegradable polymers. Apart from biodegradable, the polymers to be used in the medical field have to be biocompatible also. The response of a tissue to a material that it comes in contact with depends on many factors ranging from the chemical, physical and biological properties of the materials to the shape and structure of the material. A very important aspect that has to be taken into account when developing new biodegradable materials is the fact that the degradation products, that are produced, have to fulfill the requirement of biocompatibility as well. The general criterion for selecting a polymer for use as a biomaterial is to match the mechanical properties and the rate of degradation to the requirements of the specific application.[29] An ideal biodegradable polymer for use in the medical field:

- should not evoke an inflammatory, allergenic or toxic response;
- should have non-toxic degradation products that can be metabolized and feasibly cleared from the body;
- should have acceptable shelf life in order to be used as a consumer product;
- should have degradation times that match the healing or regeneration process of the tissue to which it is applied.

Today biodegradable polymers in the medical industry are used as drug-delivery systems,[30] implants,[31] temporary prosthetics,[32] sutures, stitches,[33] among others.

1.2.1 Classes of Biodegradable Polymers

Given the complexity and the wide range of applications that polymeric biomaterials are currently used, there is not just one polymeric system available that can be considered as an ideal biodegradable polymer. This underlines the continuous need to develop new biodegradable materials that meet the unique and specific requirements for each individual medical application. The major medical devices that biodegradable polymers find applications nowadays are shown in **Table 1-1**.

To pursue for the practical medical purposes listed in **Table 1-1**, a wide range of biodegradable materials, both synthetic and natural, have been used, and the list of the materials that are explored as potential candidates for medical devices and other applications increases every year. An effort to list the several different classes of compounds that fulfill the general requirements of biodegradability and biocompatibility and that are used nowadays in many different sections of the medical field are summarized in **Table 1-2**.[34]

1.2.2 Biodegradable Adhesives

Interest in treating wounds can be dated back to our ancestors. Primitive people closed wounds by sewing them together with muscle fibers or shreds of tendon. Early people were also looking for alternatives to thread and needle and the use of adhesive tapes and gum adhesives from plants can be dated back 4,000 years.[35] Modern people have continued to refine the suture to its current form, but the search for alternative methods and devices for wound closure continues to evolve.[36] Currently there exist a variety of different types of sutures, absorbable and non-absorbable in different sizes. Although they provide a meticulous closure and have the greatest tensile strength, compared with any other wound closure technique, they present several

disadvantages. The use of traumatic needles and the use of a foreign body to close a wound cause anxiety to patients and give them the highest infection rate as a wound closure device.[37,38] Staples can be considered as alternatives, but as in the case of sutures, they have the disadvantage of requiring the use of anesthetics and the less-than-meticulous cosmetic closure. Given the shortcomings of these wound closure devices, interest in tissue adhesives has grown in the last half century and especially in the last two decades. The utility of tissue adhesives seems to present a great potential for solving for many of the current problems in the medical industry. Tissue adhesives are nowadays used as a method to stop bleeding by sealing vascular structures, as topical wound sealants to provide an antimicrobial barrier to outside contamination, and to fixate structures where sutures and normal fixation devices, such as plates and screws, cannot be used.[39,40] Different products vary in the specific adhesion mechanism and how well they stick, adhere and/or bond. Tissue adhesives can be divided in the categories of cyanoacrylate adhesives, fibrin based adhesives and protein-based adhesives.

Synthetic cyanoacrylate adhesives are a family of liquid monomers, consisting of the alkyl esters of 2-cyanoacrylic acid. They exothermically polymerize easily at room temperature upon contact with moisture, and they form strong adhesive bonds with a variety of substrates, such as wood, metal, hard tissue (i.e. bone and enamel), and soft tissue (i.e. skin, vascular tissue). Synthetic cyanoacrylate monomers have been available since the 1950s; however their clinical use has been restricted because of the potential for thermal damage to the tissues and concerns about their cytotoxic or histotoxic effects of their degradation products. This is the reason that only a limited number of cyanoacrylate adhesive products have been so far approved for medical use for topical skin approximation by the U.S. Food and Drug Administration.[41]

Fibrin is the insoluble protein that is involved in blood clotting, which is developed in the blood from the soluble protein fibrinogen. When an injury occurs, fibrin is deposited around the wound in the form of a mesh, which dries and hardens so that bleeding stops. There is a wide range of fibrin-based adhesive products used nowadays for medical use.[42] The main advantages of all fibrin-based glues are the lack of toxicity and the complete compatibility with the human tissues. They are typically used for hemostasis and can seal tissues, while they do not have adequate tensile strength to close skin. Some limitations of these fibrin-based glues come from the fact that they are only effective in the absence of active bleeding.

Protein-based adhesives that do not belong to the above-mentioned categories are starting to gain a big interest lately. This class of adhesive materials may contain many different polymeric materials, like gelatin, albumin and several other natural and synthetic polypeptides based on proteins that are excreted from organisms.[43,44] Particularly for the latter, it has been found that proteins with a preferred amino-acid composition are responsible for the characteristic ability of several sea creatures to adhere on various surfaces underwater.[45] Accordingly, a lot of effort by many researchers has focused on developing biomimetic materials that contain these specific chemical groups or aminoacids. This methodology seems to present a key aspect towards the goal of the formulation of biocompatible, biodegradable, non-toxic and versatile glue and could provide means to adhesiveness on a diversity of surfaces.

1.3 Hybrid Materials

Although the original birth of hybrid materials is not known, it is clear that the mixing of organic and inorganic components was carried out in the ancient world. At that time, the driving force was to consistently try novel mixtures of inorganic pigments and other inorganic and

organic components to form bright paints and dyes.[46] Therefore, it can be said that hybrid materials are not an invention of the last decades but were developed a long time ago. However, recent technological breakthroughs and the desire for new functions generated an enormous demand for novel materials. Many of the well-established materials, such as metals, ceramics or plastics, cannot fulfill all technological desires for the various new applications. Scientists and engineers realized early on that mixtures of materials can show superior properties as compared to their individual components. Thus, the interest has been focused on developing materials and technologies that combine the benefits of the two different worlds, namely the inorganic and the organic.

The term hybrid materials includes many different systems spanning from a wide area of various materials, such as highly ordered coordination polymers, amorphous sol-gel compounds and materials with and without interactions between the inorganic and organic components.[47] A broad definition could be the following: a hybrid material is a material that includes two moieties blended or, more strictly, covalently bonded at the molecular level. The most obvious advantage of inorganic-organic hybrid materials is that they can favorably combine the often dissimilar properties of organic and inorganic components in one material as can be seen in **Table 1-3**. These possibilities clearly reveal the power of hybrid materials to generate complex systems from simpler building blocks.[48]

Probably the most intriguing property of hybrid materials that makes this class of materials very important for many applications is their easy processing.[49,50] Contrary to pure solid state inorganic materials that often require a high temperature treatment, hybrid materials show a more polymer-like handling because of their large organic content and the formation of crosslinked inorganic networks from small molecular precursors, just like in polymerization

reactions. These materials can acquire many shapes and forms, from films to powders and bulk materials. Material properties of hybrid materials are usually changed by modifications of the composition at the molecular scale. If, for example, more hydrophobicity of a material is desired, the amount of hydrophobic molecular components is increased. On the other hand, mechanical properties, such as toughness or scratch resistance, are tailored if hard inorganic nanoparticles are included into the polymer matrix. Because the compositional variations are carried out at the molecular scale, a gradual fine tuning of the material properties is possible.[51] Another very important subject in materials chemistry is the formation of smart materials, such as materials that react to environmental changes or switchable systems, because they open routes to novel technologies, such as electroactive materials, electrochromic materials, sensors,[52] membranes,[53,54] catalytic materials,[55] etc. The desired function of the final hybrid material can be delivered from the organic or inorganic or from both components.

1.3.1 Hybrids Prepared by the Sol-Gel Method

Sol-gel process is a method that utilizes small molecular starting materials (i.e., precursors) to produce inorganic metal oxides under relatively mild conditions. Interest in the sol-gel process can be dated back in 1800s with the investigations by Ebelman and Graham.[56,57] Owing to the sparse understanding of the physicochemical principles behind the sol-gel process though, it was not before the 1950s that this method became of significant interest to chemists.[58] Since then, there has been tremendous progress that has grown it into a separate field of science. In fact, this process shows similarities to the organic polymerization since it also starts from small molecular precursors resulting in a bulk, crosslinked solid material. Compared to other procedures, used for the preparation of inorganic materials, the sol-gel process utilizes mild

conditions, such as ambient temperatures and common solvents like alcohols. In particular, the silicon-based sol–gel process was one of the major driving forces of what has today become the broad field of inorganic–organic hybrid materials. Silicon has a special role in this process and the reason for this is its good processability and the stability of the Si-C bond during the formation of a silica network, which allows the production of organic-modified inorganic networks in one step. Sol-gel derived hybrids have the wonderful advantage of the simplicity and versatility that is associated with the sol-gel process, which allows the easy incorporation of an organic component into a ceramic network under mild conditions.[59] These organic-inorganic hybrid materials may include products from the hydrolytic condensation of tri-functional or di-functional organosilanes, where the organic group may undergo further reactions to monomeric building blocks containing two or more triethoxysilyl groups as precursors to synthesize bridged polysilsesquioxanes as illustrated in **Figure 1-1**.

1.4 Conductive Polymers (CPs)

Explosive growth of research in the field of inherently conductive polymers (CPs) was triggered when in 1974, MacDiarmid, Heeger and Shirakawa discovered that the electronic conductance of polyacetylene with π-π conjugated backbones may be increased by many orders of magnitude by "doping it" with electron acceptors (p-type dopants), such as iodine.[60,61] For this discovery of the conductive polymers, they were awarded the Nobel Prize in chemistry in 2000.[62] Conductive polymers are increasingly desired for a variety of sophisticated end-uses.[63] Very significant progress has been made in this field, as a result of the numerous potential applications of these materials in electronic, electrochromic and photoelectrochemical devices.[64-66] In 2000 the number of journal articles published related to conductive polymers reached the number of

8000. At the present time, about 40 research articles related to conductive polymers are published every week.[67] The potential applications of conductive polymers and the impact that this class of compounds has in the area of smart materials has been recognized by many investigators in numerous review articles. The chemical structure of some typical conductive polymers can be seen in **Figure 2-2**.

Most of the possible applications of conductive polymers rely on their electroactivity, their relatively easy processability, their light weight and their low price. The field of electrochromic and electroluminescent devices has been long viewed as among the most promising application areas for CPs and is basically making use of the change in color associated with a redox reaction of some of these polymers (e.g., polyaniline). In such a device, a substance is customly absorbed onto a transparent conductive substrate, such as indium-tin oxide glass, or kept in the solution form between two electrodes. In this manner, conductive polymers with good color contrast between the oxidized and the reduced form have become possible alternatives to the present technologies. Conductive polymers have found applications in another area of great interest, namely the field of sensor technology. Applications range from chemical sensors for gas detectors,[68] to pH electrodes[69] to amperometric glucose electrodes.[70] To date, conductive polymers have found applications as antistatic coatings, microelectronics, energy storage devices, photovoltaics, display windows, actuators, sensors, separation devices, electrochromic devices and anticorrosion coatings.

Among these macromolecular compounds, polyaniline has been extensively studied due to its rather easy preparation, good environmental stability and its interesting redox properties (or electroactivity).[71-73] It has the following general polymeric structure:

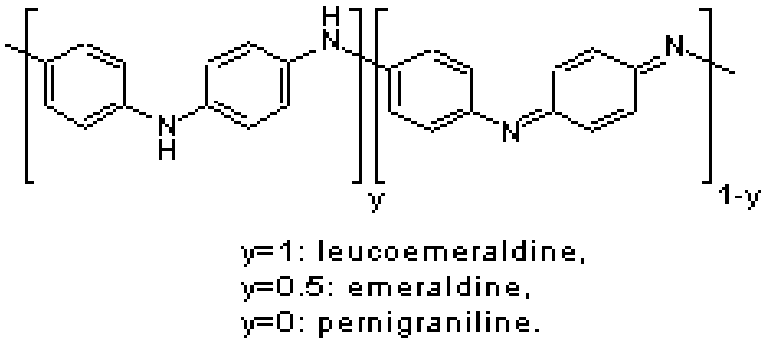

Scheme 1-1. General structure of polyaniline.

It differs from most other inherently conductive polymers, such as polypyrroles and polythiophenes, because it acquires three readily accessible oxidation states. These range from the fully reduced form of leucoemeraldine (y=1) to the half oxidized form of emeraldine (y=0.5) to the fully oxidized form of pernigraniline (y=1). Polyaniline is most commonly synthesized by either chemical or electrochemical oxidative polymerization of aniline monomers in acidic environment. However, recently several other synthesis procedures have been developed, including photochemical and enzyme-catalyzed techniques. Upon doping with an acid, polyaniline converts to its highly conductive emeraldine salt form:

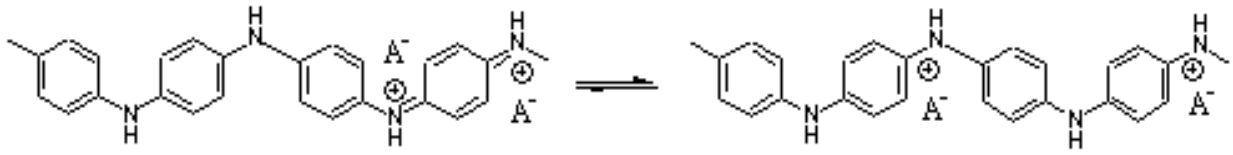

Scheme 1-2. Structure of the conductive emeraldine salt of polyaniline.

1.5 Nanomaterials

Nanoscale materials can be defined as those whose size scale lies within the nanometer range, i.e., in the range between one and about one hundred nanometers (10^{-9} meters). Within

this size scale, the properties of matter are often characteristically different from individual atoms or molecules and from bulk materials. The study has been recently recognized as a new area of science, which is generally termed as "Nanoscience". Even more popular lately has become the term "Nanotechnology", which refers to a field of applied science and technology, whose theme is the control of matter on the atomic and molecular scale, generally 100 nanometers or smaller, and the fabrication of devices or materials that lie within that size range.[74] Eric Drexler, an American scientist, who promoted the concept of nanotechnology notes in one of his books, "Coal and diamonds, sand and computer chips, cancer and healthy tissue; throughout history, variations in the arrangement of atoms have distinguished the cheap from the cherished, the diseased from the healthy. Arranged one way, atoms make up soil, air, and water arranged another, they make up ripe strawberries. Arranged one way, they make up homes and fresh air; arranged another, they make up ash and smoke".[75]

The design and development of nanoscale size materials is not considered to be another step towards miniaturization. The physical, chemical, optical, magnetic and electrical properties of these materials are size and shape dependent. The major challenge for the future in the world of "Nanotechnology" is to exploit these unique properties and develop the next generation nanodevices.[76] Funding agencies in United States, Europe, Australia, China and Japan are spending a significant part of their funds for the development of this relatively new area of study. Since the establishment of the National Nanotechnology Initiative (NNI), which is a program established in 2001 in the United States to coordinate federal nanotechnology research and development, the amount of federal spending has exceeded the amount of five billion dollars.

Likewise, the number of groups working in nanoscience or nanotechnology has increased dramatically during the past two decades.

1.6 Organization of this Dissertation

Biodegradable polymeric products, organic-inorganic hybrid materials and nanomaterials for a diversity of applications are the three main fields on which this research has been focused. In Chapter 2, the general methodologies, along with the characterization techniques, which have been used in this research, are described. Chapter 3 deals with the synthesis and characterization of novel biodegradable, biocompatible and non-toxic materials with adhesive properties on wet and/or dry surfaces. Chapter 4 presents the synthesis and the mechanical testing of novel organic-inorganic hybrid materials with low volume shrinkage and excellent mechanical properties. Chapter 5 reveals the basic concept behind the experimental approach that led to the highly transparent and monolithic hybrid materials. Chapter 6 describes the covalent incorporation of polyaniline in the hybrid materials along with the electrochromism, the conductivity, the electroactivity and the mechanical testing studies. Chapter 7 deals with the electrochemical investigation of a novel electroactive aniline trimer-silane compound and other well defined aniline oligomers with end group substitution. Chapter 8 describes the formation of interesting oxygen adducts, upon prolonged oxygenation in the dry state and in aqueous suspensions of iron phthalocyanines. Chapter 9 presents the immobilization of horseradish peroxidase and α-glucosidase in mesoporous hybrid materials, utilizing a nonsurfactant-templated sol-gel method. In the same chapter, the encapsulation and protection of HRP from harsh environments by a new double encapsulation method is also presented. Chapter 10 presents a general conclusion for all of the projects that have been investigated. Appendix A gives a

thorough description on on-going work on the fabrication of a novel fluorescent nanoelectrode for applications in neuroscience. Appendix B contains research work that has been done in the area of biodegradable adhesives with ambiguous results, along with some suggestions and ideas on future work that is going to take place in our laboratory. Appendix C is an original research proposal titled "Preservation of Historic Property Utilizing Bacteria and Biodegradable Polymeric Microspheres", which was defended successfully on December 15th, 2006, in partial fulfillment of the requirement for the Ph.D. candidacy at Drexel University. Appendix D presents preliminary results for collaborative work. Finally, Appendix E provides supporting information for the chapters presented in this PhD thesis for a better elucidation of the research projects that have been explored.

Table 1-1. Clinical applications of biodegradable polymers.[76]

Function	Purpose	Examples
Bonding	Suturing	Vascular and intestinal anastomosis
	Fixation	Fracture bone fixation
	Adhesion	Surgical adhesion
Closure	Covering	Wound cover, local hemostasis
	Occlusion	Vascular embolization
Separation	Isolation	Organ protection
	Contact inhibition	Adhesion prevention
Scaffold	Cellular proliferation	Skin reconstruction, blood vessel reconstruction
	Tissue guide	Reconstruction, nerve reunion
Capsulation	Controlled drug delivery	Sustained drug release

Table 1-2. Naturally occurring and synthetic biodegradable polymers.

Natural polymers	**Polymer examples**
Protein based polymers	Collagen, albumin, gelatin
Polysaccharides	Agarose, alginate, carrageenan, hyaluronic acid, dextran, chitosan, cyclodextrins

Synthetic polymers	**Polymer examples**
Polyesters	Poly(lactic acid), poly(glycolic acid), poly(hydroxy butyrate), poly(ε-caprolactone), poly(β-malic acid), poly(dioxanes)
Polyanhydrides	Poly(sebasic acid), poly(adipic acid), poly(terephthalic acid), and various copolymers
Polyamides	Poly(imino carbonates), polyamino acids
Phosphorous-based polymers	Polyphosphates, polyphosphonates, polyphosphazenes
Others	Poly(cyano acrylates), polyurethanes, polyortho esters, polydihydropyrans, polyacetals

Table 1-3. Comparison of general properties of typical inorganic and organic materials.[48]

Properties	**Organics (polymers)**	**Inorganics (SiO_2, transition metal oxides)**
Nature of bonds	Covalent [C-C], van der Waals, H-bonding	Ionic or iono-covalent
T_g	Low (-120 ^oC to 200 ^oC)	High (>> 200 ^oC)
Thermal stability	Low (<350 ^oC - 450 ^oC)	High (>> 100 ^oC)
Density	0.9 - 1.2	2.0 - 4.0
Refractive index	1.2 - 1.6	1.15 - 2.7
Mechanical properties	Elasticity	Hardness
	Plasticity	Strength
	Rubbery	Fragility
Hydrophobicity	Tunable	Hydrophilic
Permeability	Permeable to gases	Low permeability to gases
Electronic properties	Insulating to conductive	Insulating to semiconductors (SiO_2, TMO)
	Redox properties	Redox properties (TMO)
		Magnetic properties
Processability	High (molding, casting, film formation, control of viscosity)	Low for powders High for sol-gel coatings

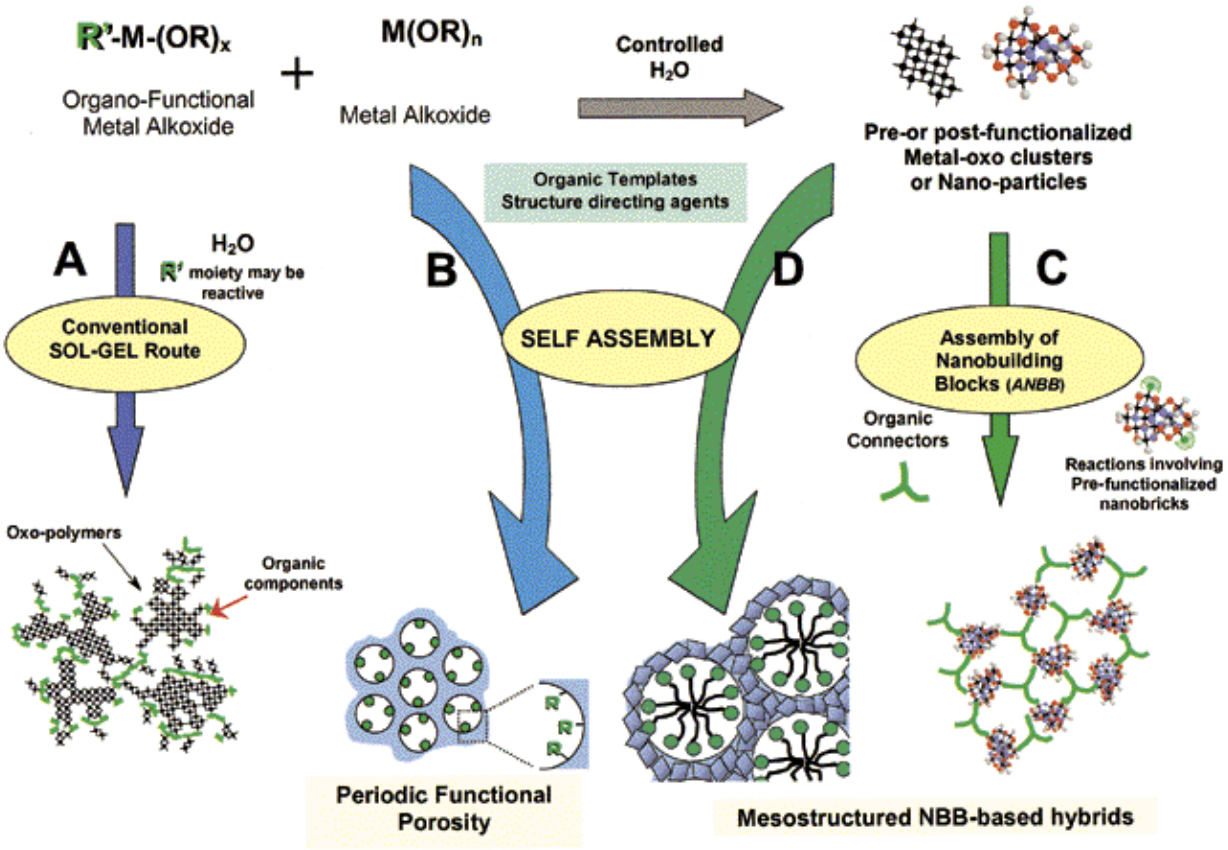

Figure 1-1. Schematic of monomeric building blocks containing two or more triethoxysilyl groups as precursors to bridged polysilsesquioxanes.[78]

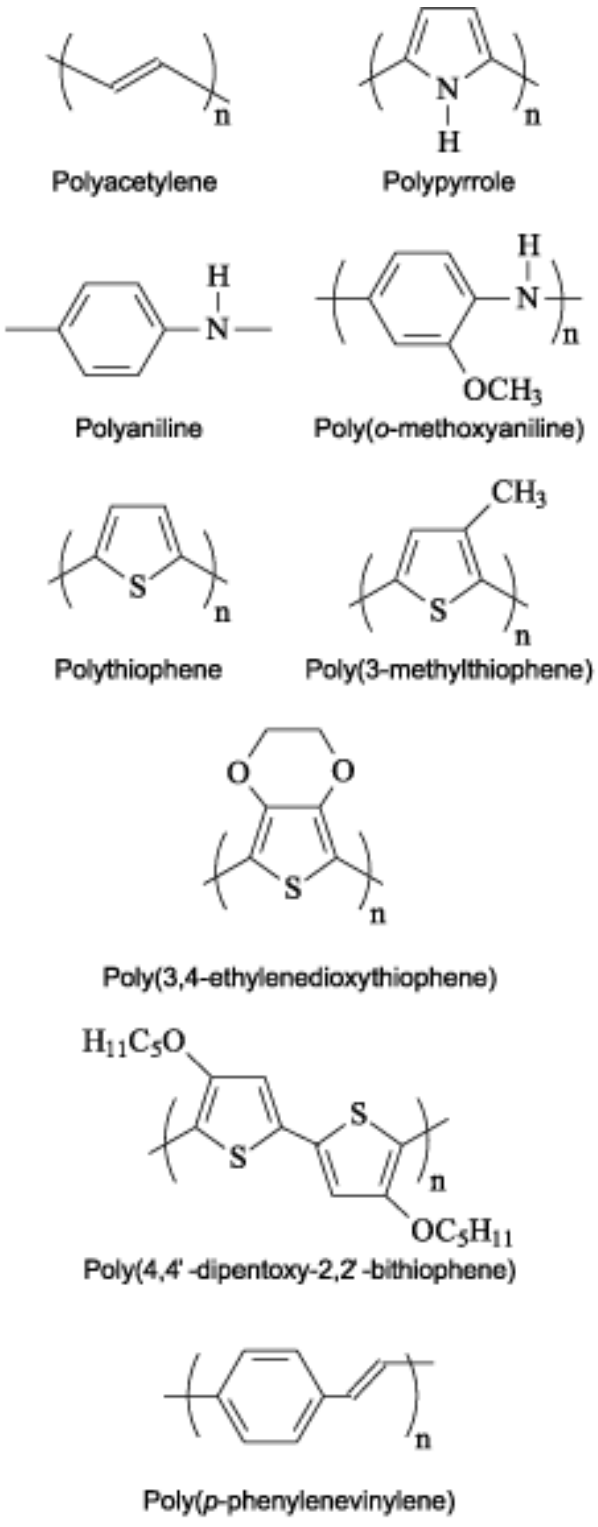

Figure 1-2. Chemical structures of some typical conductive polymers.[79]

1.7 Reference List

1. Charles, E., Carraher, Jr. Introduction to polymer chemistry. Taylor & Francis Group, Florida; 2007.

2. Department of Materials Science and Engineering, University of Illinois Urbana-Champaign. http://matse1.mse.uiuc.edu/polymers/time.html; 2007.

3. American Chemical Society. National Chemical Landmarks. http://acswebcontent.acs.org/landmarks/newproducts_t.html#bakelite; 2007.

4. Staudinger, H. "Uber polymerization", Berichte der Deutchen Chemischen Gesellscaft. (1920), 53, 1073-1085.

5. Nobel Lectures, Chemistry 1922-1941, Elsevier Publishing Company, Amsterdam; 1966.

6. Staudinger, H. Macromolecular Chemistry. Nobel Lecture; 1953.

7. American Chemical Society. National Chemical Landmarks. http://acswebcontent.acs.org/landmarks/polymer/staudinger.html; 2004.

8. Kickelbick, G. Hybrid materials-synthesis, characterization and applications. Wiley-VCH, Germany; 2007.

9. Baekeland, L. H. The synthesis, constitution, and uses of Bakelite. The Journal of Industrial and Engineering Chemistry (1909), 1, 149-169.

10. Wen, J., Wilkes, G. L. Organic/inorganic hybrid network materials by the sol-gel approach. Chemistry of Materials (1996), 8, 1667-1681.

11. Wei, Y., Bakthavatchalam, R., Whitecar, C. K. Synthesis of New Organic- Inorganic Hybrid Glasses, Chemistry of Mateials (1990), 2, 337-339.

12. National Nanotechnology Initiative. http://www.nano.gov/html/facts/whatIsNano.html; 2006.

13. Taniguchi, N. On the basic concept of nano-technology. Japan Society of Precision Engineering. International Conference Proceeding Engineering Part II; 1978.

14. Drexler, K. E. Engines of creation: the coming era of nanotechnology. Anchor Books Editions, New York; 1986.

15. Drexler, K. E. Nanosystems: molecular machinery, manufacturing, and computation. John Wiley & Sons, Inc., New York; 1992.

16. Becerril-Garcia, H. A., Harrison, R. G., Woolley, A. T. Advances in DNA templated nanofabrication of electronic devices. Abstracts of Joint Regional Meeting of the Northwest and Rocky Mountain Sections of the American Chemical Society, Logan, UT, United States, GEN-200; 2004.

17. Nagahara, L. A., Oden, P. I., Majumdar, A., Carrejo, J. P., Graham, J., Alexander, J. Nanofabrication utilizing the atomic force microscope. Proceedings of SPIE-The International Society for Optical Engineering (1992), 1639, 171-179.

18. Lu, G. Q., Zhao, X. S. Nanoporous materials science and engineering, Imperial College Press, London; 2004.

19. Xu, A. W., Ma, Y., Cölfen, H. Biomimetic mineralization. Journal of Materials Chemistry (2007), 17, 415-449.

20. Department of Health and Ageing. http://www.nicnas.gov.au/PUBLICATIONS/ Information_Sheets/General_Information_Sheets/ NIS_Nanomaterials_PDF.pdf. Australia; 2008.

21. Bohannon, J. 'Smart Coatings' research shows. The virtues of superficiality. Science (2005), 309, 376-377.

22. Patel, A. C., Wei, Y. Electrospinning of silica nanofibers containing quantum dots. Abstracts of Papers, 230th American Chemical Society National Meeting, Washington, DC, United States, INOR-158; 2005.

23. Patel, A. C., Li, S., Wei, Y., Wang, C., Zhang, W. Electrospinning of porous silica micro/nanofibers containing silver nanoparticles. Polymer Materials Science Engineering Preprints (2004), 91, 690-691.

24. Jayasekara, R., Harding, I., Bowater, I., Lonergan, G. Biodegradability of a selected range of polymers and polymer blends and standard methods for assessment of biodegradation. Journal of polymers and the environment (2005), 13, 231-251.

25. Pillai, O., Panchagnula, R. Polymers in drug delivery. Current Opinion in Chemical Biology (2001), 5, 447-451.

26. Ray, S. Biodegradable polymers for industrial applications. CRC Press, Cambridge; 2005.

27. Lu, Y., Chen, S. C. Micro and nano-fabrication of biodegradable polymers for drug delivery. Advanced Drug Delivery Reviews (2004), 56, 1621-1633.

28. Barbucci, R. Intergrated Biomaterial Science. Kluwer Academic/Plenum Publishers, New York; 2002.

29. Lakshmi, S., Cato, N., Laurencin, T. Biodegradable polymers as biomaterials. Progress in Polymer Science (2007), 32, 762-798.

30. Park, J. H., Ye, M., Park, K. Biodegradable polymers for microencapsulation of drugs. Molecules (2005), 10, 146-161.

31. Ha, C. S., Gardella, J. A. Surface chemistry of biodegradable polymers for drug delivery systems. Chemical Reviews (2005), 105, 4205-4232.

32. Middleton, J. C., Tipton, A. J. Synthetic biodegradable polymers as orthopedic devices. Biomaterials (200), 21, 2335-2346.

33. Rezwan, K., Chen, Q. Z., Blaker, J. J., Boccaccini, A. R. Biodegradable and bioactive porous polymer/inorganic composite scaffolds for bone tissue engineering. Biomaterials (2006), 27, 3413-3431.

34. Nair, L. S., Laurencin, C. T. Biodegradable polymers as biomaterials. Progress in Polymer Science (2007), 32, 762-798.

35. Majno, G. The healing hand. Man and wound in the ancient world. Cambridge (MA), Harvard University Press; 1975.

36. Forrest, R. D. Early history of wound treatment. Journal of the Royal Society of Medicine (1982), 75, 198-205.

37. Ritchie, A. J., Rocke, L. G. Staples versus sutures in the closure of scalp wounds: a prospective, double-blind, randomized trial. Injury (1989), 20, 217-218.

38. Quinn, J. V., Maw, J. L., Ramotar, K. Octyl-cyanoacrylate tissue adhesive wound repair in contaminated wound model. Surgery (1997), 122, 60-72.

39. Chao, H. H., Torchiana, D. F. Bioglue: albumin/glutaraldehyde sealant in cardiac surgery. Journal of Cardiac Surgery (2003), 18, 500-503.

40. Jackson, M., MacPhee, M., Drohan, W., Alving, B. Fibrin sealant: current and potential clinical applications. Blood Coagul Fibrinolysis (1996), 7, 737-746.

41. Quinn, J. V. Tissue adhesives in clinical medicine. BC Decker, Ontarion; 1998.

42. Sierra, D. H., Eberhardt, A. W., Lemons, J. E. Failure characteristics of multiple-component fibrin-based adhesives. Journal of Biomedical Materials Research Part A (2001), 59 (1), 1-11.

43. Bonchek, L. I. Braunwald, N. S. Experimental evaluation of a cross-linked gelatin adhesive in gastrointestinal surgery. Annals of Surgery (1967), 165, 420–424.

44. Lin, J., Iannettoni, M. D. Closure of bronchopleural fistulas using Albumin-Glutaraldehyde tissue adhesive. The Annals of Thoracic Surgery (2004), 77, 326-328.

45. Yamamoto, H., Nagai, A. Polypeptide models of the arthropodin protein of the barnacle Balanus balanoides. Marine Chemistry (1992), 37, 131-43.

46. Sanchez, C., Soler-Illia, A. A., Ribot, F., Lalot, T., Mayer, C. R., Cabuil, V. Designed hybrid organic-inorganic nanocomposites from functional nanobuilding blocks.Chemistry of Materials (2001), 13, 3061-3083.

47. Kickelbick, G. Hybrid materials-synthesis, characterization and applications. Wiley-VCH, Germany; 2007.

48. Shrap, K. G. Inorganic/ organic hybrid materials. Advanced Materials (1998), 10, 1243-1248.

49. Mammeri, F., Bourhis, E. L., Rozes, L., Sanchez, C. Mechanical properties of hybrid organic-inorganic materials. Journal of Material Chemistry (2005),15, 3787-3811.

50. Ashby, M. F., Brechet, Y. J. M. Designing hybrid materials. Acta Materiala (2003), 51, 5801-5821.

51. Li, S., Samuel, S. P., Mylonakis, A., Shah, A., Hsieh, A., Patel, A., Wei, A., Baran, G., Wei, Y. Synthesis of new organic-inorganic hybrids poly[2-hydroxethyl methacrylate (HEMA)-glycidyl methacrylate (GMA)-silica] and their mechanical properties. Journal of Materials Research (2007), 23(1), 66-71.

52. Innocenzi, P., Lebeau, B. Organic-inorganic hybrid materials for non-linear optics. Journal of Materials Chemistry (2005), 15, 3821-3831.

53. Pratheep, K. A., Pal, S. R. Novel hybrid of clay, cellulose, and thermoplastics. I. Preparation and characterization of composites of ethylene-propylene copolymer. Journal of Applied Polymer Science (2007), 104, 2672-2682.

54. Wu, C., Wu, Y., Xu, T., Fu, Y. Novel anion-exchange organic-inorganic hybrid membranes prepared through sol-gel reaction and UV/thermal curing. Journal of Applied Polymer Science (2007), 107, 1865-1871.

55. Forster, P. M., Cheetham, A. Hybrid inorganic-organic solids: an emerging class of nanoporous catalysts. Topics in Catalysis (2003), 24(1-4), 79-86.

56. Hench, L. L., West, J. K. The sol-gel process. Chemical Reviews (1990), 90, 33-72.

57. Graham, T. On the properties of silicic acid and other analogous colloidal substances. Journal of Chemical Society (1864), 17, 318-323.

58. Sayari, A., Hamoudi, S. Periodic mesoporous silica-based organic-inorganic nanocomposite materials. Chemistry of Materials (2001), 13 (10), 3151-3168.

59. Wei, Y., Jin, D., Yang, C., Kels, M., Qiu, K. Organic-inorganic hybrid materials: relations of thermal and mechanical properties with structures. Materials Science and Engineering (1998), 6, 91-98.

60. Shirakawa, H., Louis, E. J., MacDiarmid, A. G., Chiang, C. K., Heeger, A. J. Synthesis of electrically conducting organic polymers: halogen derivatives of polyacetylene, (CH)x. Journal of Chemical Society, Chemical Communications (1997) 3, 578-580.

61. Ito, T., Shirakawa, H., Ikeda, S. Simultaneous polymerization and formation of polyacetylene film on the surface of concentrated soluble Ziegler-type catalyst solution. Journal of Polymer Science (1974),12, 11-20.

62. The Nobel Foundation. Nobel Laureates. http://nobelprize.org/nobel_prizes/chemistry/laureates/2000/; 2000.

63. Doherty, W. J., Armstrong, N. R., Saavedra, S. S. Conducting polymer growth in porous sol-gel thin films: Formation of nanoelectrode arrays and mediated electron transfer to sequestered macromolecules. Chemistry of Materials (2005), 17, 3652-3660.

64. Genies, E. M., Lapkowiski, M., Santier, C., Vieil, E. Polyaniline, spectroelectrochemistry, display and battery. Synthetic Metals (1987), 18, 631-636.

65. Duek, E. A. R., De Paoli, M.A., Mastragostino, M. An electrochromic device based on polyaniline and prussian blue. Advanced Materials (1992), 4, 287-291.

66. Bauerle, P. Intrinsically conducting polymers - quo vadis?. Advanced Materials (1993), 5, 879-886.

67. Wallace, G. G., Spinks, G. M., Kane-Maquire, L. A. P., Teasdale, P. R. Conductive electroactive polymers. Intelligent Materials Systems. CRC Press, Florida; 2003.

68. Bai, H., Shi, G. Gas sensors based on conducting polymers. Sensors (2007), 7, 267-307.

69. Malkaj, P., Dalas, E., Vitoratos, E., Sakkopoulos, S. PH electrodes constructed from polyaniline/zeolite and polypyrrole/zeolite conductive blends. Journal of Applied Polymer Science (2006), 101, 1853-1856.

70. Pandey, P. C. A new conducting polymer-coated glucose sensor. Journal of Chemical Society, Faraday Transactions (1988), 1, 2259-2265.

71. Kim, E., Lee, M.H., Moon, B.S., Lee, C., Rhee, S.B. Redox cycleability of a self-doped polyaniline. Journal of the Electrochemical Society (1994), 141, L26-L28.

72. Kuzmany, H., Sariciftci, N.S. In situ spectroelectrochemical studies of polyaniline. Synthetic Metals (1987), 18, 353-358.

73. Xing, S., Zhao, C., Jing, S., Wang, Z. Preparation of polyaniline dispersions with different assembly structure. Journal of Materials Science (2006), 41, 2761-2766.

74. Siegel, R. W., Hu, E., Roco, M. C. Nanostructure science and technology. R&D status and trends in nanoparticles, nanostructured materials and nanodevices. Kluwer Academic Publishers. The Netherlands; 1999.

75. Drexler, E. Engines of Creation. Coming era of nanotechnology. Anchor Books, New York; 1986.

76. Liz-Marzan, L. M., Kamat, P. V. Nanoscale materials. Kluwer Academic Publishers, The Netherlands; 2003.

77. Reis, R. L., Cohn, D. Polymer based systems on tissue engineering, replacement and regeneration. Kluwer Academic Publishers, Portugal; 2001.

78. Sandia Corporation. http://www.sandia.gov/inorganic-organic-materials-group/bridged1.htm; 2007.

79. De Paoli, M. A., Gazotti, W. A. Electrochemistry, polymers and opto-electronic devices: A combination with a future. Journal of the Brazilian Chemical Society (2002), 13, 410-424.

Chapter 2. Introduction to the General Methodologies and Techniques Used

2.1 Introduction

In this chapter, the general methodologies that have been applied in the research projects are described. Due to the importance of analyzing and verifying the properties of the polymers, hybrid materials and nanomaterials, the major characterization techniques that have been used will be also briefly discussed in this chapter.

2.2 Biodegradable Polymers

2.2.1 Biodegradable Adhesives

The first major area of chemistry that this research has been focused on, is the biodegradable polymers. The aim of this project, which is going to be presented in full detail in Chapter 3, was to obtain a biodegradable, biocompatible and non-toxic material that would show adhesiveness on wet and/or dry surfaces. At the present time, no adhesive, that fulfills completely all of the criteria of biodegradability, non-toxicity, biocompatibility and adequate adhesiveness on tissue or bone in the presence of biological fluids, has been reported. Thus, the formulation of such an ideal adhesive is still a big challenge for the medical and dental community. Several different approaches have been tried in the present study in an attempt to solve for this problem. One approach included the incorporation of cyanoacrylates into polylactic acid and polyglycolic acid with or without covalent bonding. Another approach was to modify the end groups of polyethylene glycol with dihydroxy-benzoic acid. The grafting of diphenolic compounds on polysuccinimide has been also investigated with promising results. All of the above mentioned routes, which led to promising and/or ambiguous results, will be briefly

described in Apendix B. In this section the general methodology of a different approach, which led to some very interesting and promising results is going to be introduced.

It is well known that marine organisms, such as barnacles and mollusks adhere themselves onto wet surfaces, such as rocks, stones and others. The past twenty five years, extensive scientific research has been devoted to understand and explain the mechanism and the molecular interactions that rely behind this adhesiveness.[1-4] This led to the very interesting discovery that some proteins with specific chemical groups, which are extracted by these organisms, are responsible for this characteristic ability of these creatures to stick on various surfaces underwater.[5-7] Accordingly, a bio-mimetic system, that would contain some of these chemical groups or proteins attached on the backbone of a biodegradable, biocompatible and nontoxic polymeric backbone, could be a key aspect towards the goal of the formulation of a biocompatible, biodegradable, non-toxic and versatile glue and could provide means to adhesiveness on a diversity of wet surfaces.

The extensive research in this field has dictated that the curing of these marine adhesive proteins is happening through the polyphenolic groups that the excreted proteins contain.[8] Most studies have indicated that one of the characteristics of these proteins is the presence of L-3,4-dihydroxyphenylalanine (DOPA), which is believed to be responsible for bonding.[9] The exact mechanism behind this capability remains still under study with much controversy between scientists.[10-12] Following the polyphenolic approach, several research groups have incorporated DOPA or other compounds that contain the same functional groups onto the backbone of polymeric materials and have found that the adhesive properties of the obtained materials have improved. [13-18]

In our study the modification of chitosan via amide formation with 3,4-dihydroxybenzoic acid (DHBA) to yield a biodegradable, biocompatible and non-toxic adhesive material has been investigated. The efforts have been focused on a material that would find applications in the dental and biomedical industry and, thus, the tensile and shear adhesive strength of these materials has been tested on bone and porcine skin surfaces. This was done in order to create a controlled environment, which would simulate the surfaces on which these materials are intended to be used. Adhesiveness was achieved without added enzymes or oxidants. Infrared spectroscopy (IR), ultraviolet-visible spectroscopy (UV-vis) and nuclear magnetic resonance spectroscopy (NMR) have been used in order to qualitatively and quantitatively establish the amount of the diphenolic moiety present on the backbone of the biodegradable polymer.

2.2.2 Characterization of the Synthesized Biodegradable Polymers

2.2.2.1 Nuclear Magnetic Resonance Spectroscopy (NMR)

Nuclear magnetic resonance (NMR) spectroscopy is a form of absorption spectroscopy and a powerful tool to determine how atoms are spatially arranged in the molecules. Under proper conditions in a magnetic field, a sample can absorb electromagnetic radiation in the radio frequency (rf) region at frequencies governed by the characteristics of the sample. This absorption is a function of certain nuclei in the molecule. A plot of the frequencies of the absorption peaks versus peak intensities constitutes an NMR spectrum.[19] All nuclei intrinsically carry a charge. In some nuclei this charge spins on the nuclear axis and this circulation of nuclear charge generates a magnetic dipole along the axis:

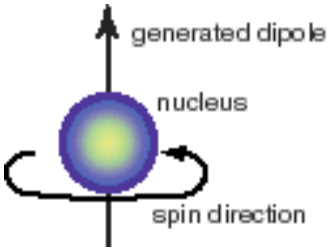

Scheme 2-1. Spinning charge on proton generates magnetic dipole.[20]

The angular momentum of the spinning charge can be described in terms of quantum spin numbers *I*; these numbers have values of 0, 1/2, 1, 3/2 and so on (*I*=0 denotes no spin). The spin number *I* can be determined from the atomic mass and the atomic number as shown in **Table 2-1**.

In quantum mechanical terms the spin number *I* determines the number of orientations a nucleus may assume in an external uniform magnetic field in accordance with the formula $2I+1$. In our case though we are only concerned about the protons whose spin number is equal to 1/2. In the following figure there are two energy levels with a slight excess of proton population in the lower energy state ($N_\alpha > N_\beta$) in accordance with the Boltzmann distribution.

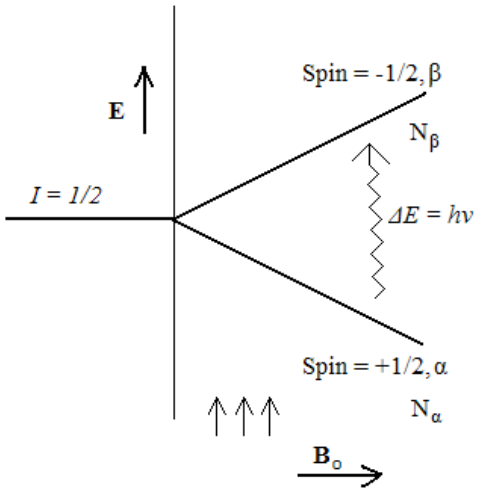

Scheme 2-2. Two proton energy levels in a magnetic field of magnitude B_o.

ΔE is given by:

$$\Delta E = \frac{h\gamma}{2\pi} B_o$$

where B_o represents the external magnetic field strength. Resonant absorption will occur when electromagnetic radiation of the correct frequency that matches this energy difference is applied. It is this resonant absorption that is detected by NMR. A proton in a molecule is "shielded" from the applied magnetic field to a very small effect by its electron cloud. In general, this electronic shielding reduces the effect of the applied magnetic field to a nucleus and as a result the energy gap is reduced, which makes the frequency required to achieve resonance to be also reduced. This shift of the NMR frequency due to the chemical environment is called chemical shift, and it explains why NMR is a direct probe of the chemical structure of a given compound.

2.2.2.2 IR Spectroscopy

Infrared (IR) spectroscopy deals with the interaction of infrared radiation with matter.[21] The IR spectrum of a compound can provide important information about its chemical nature and molecular structure. The IR spectrum of a given molecule is unique to that molecule and thus highly useful in compound identification. The infrared portion of the electromagnetic spectrum is divided into three regions: the near-, mid- and far- infrared, named after their relation to the visible spectrum. The mid-infrared, approximately 4000-400 cm^{-1} (30-1.4 μm), may be used to study the fundamental vibrations and associated rotational-vibrational structure. Infrared spectroscopy exploits the fact that molecules have specific frequencies at which they rotate or vibrate corresponding to discrete energy levels. In order for a molecule to absorb infrared

radiation though, there must be a change in the dipole moment during a vibration. With certain functional or structural groups, it has been found that their vibrational frequencies are characteristic of this group nearly independently from the rest of the molecule and are known as group frequencies. The presence thus of various group vibrations in the infrared spectrum is of great importance in identifying the absorbing compound and the chemical groups that it contains.[22]

2.2.2.3 UV-Vis Spectroscopy

Ultraviolet and visible (UV-Vis) spectroscopy is a reliable and accurate method, allowing for both qualitative and quantitative analysis of substances. Many molecules absorb a portion of ultraviolet or visible light radiation (180 to 820 nm). This absorption usually occurs over a wide range of wavelengths because molecules normally have many excited modes of vibration and rotation at room temperature. Thus, a UV-Vis spectrum of a molecule usually consists of absorption bands corresponding to structural groups.[23] According to Beer's Law, absorbance is directly proportional to the path length *l* (cm), the molar absorptivity ε and the concentration of the analyte that absorbs at this wavelength range according to the following equation:

$$A = C\,\varepsilon\,l$$

The unit of the molecule that is responsible for the absorption is called "chromophore", of which the most common are C=C (p to p* vibration) and C=O (n to p* vibration) systems. When an analyte is exposed to light having energy that matches an electronic transition within the molecule, some of this energy will be absorbed and the electron will be excited to a higher

energy orbital. A spectrometer records the wavelengths at which absorption occurs, together with the degree of absorption at each wavelength. The resulting spectrum is presented as a graph of absorbance (A) versus wavelength (nm).

2.3 Hybrid Materials

2.3.1 Introduction

Inorganic materials and organic polymers are quite different with respect to their properties. For example, inorganic materials, such as glass and ceramics are hard but not impact resistant (i.e., brittle), whereas organic polymers, such as rubber, are resilient but soft and lack scratch resistance. Organic polymers generally suffer from some of the inherent drawbacks of organic compounds, such as instability to heat and tendency of natural degradation and/or aging. As a result, the possibility of combining properties of organic and inorganic components into a unique composite material has been explored since the beginning of the industrial era. However, an explosion in interest of hybrid materials and particularly organic-inorganic hybrid materials happened with the birth of soft chemical methods that utilize mild reaction conditions, such as the "sol-gel" processes.

The sol-gel approach, which is mainly dealing with inorganic polymerization reactions, is a chemical synthesis procedure used for the preparation of inorganic materials, such as glasses and ceramics.[24] It involves an inorganic polymerization that leads to a highly cross-linked solid through a hydrolytic polycondensation. Compared to other inorganic network forming reactions, the sol-gel method possesses mild reaction conditions and a broad solvent compatibility. These two characteristics offer the possibility to carry out the inorganic network forming process in the presence of a preformed organic polymer or to carry the organic polymerization before, during or

after the sol-gel process.[25] The preparation, characterization and applications of these organic/inorganic hybrid materials have become a fast expanding area of research in the materials science, due to the new and different properties that these hybrids/nanocomposites can offer compared to the traditional macroscale composites and conventional materials.

2.3.2 Hybrid Materials by the Sol-Gel Method

Despite the many advantages that the sol-gel process offers, there are several severe, sometimes detrimental, problems associated with it. Large volume shrinkage, crack formation and brittleness of gels are amongst the most important problems, and many attempts from various groups have been focused on efforts to overcome them.[26-29] One way to solve this problem is the incorporation of organic compounds in the sol-gel matrices at the nanoscale level, which can be succeeded via various different synthetic routes.[30] These organic-inorganic hybrid materials have lately attracted great attention by many industrial and academic groups in the field of materials science, because they can provide unique combinations of properties, which cannot be achieved by conventional methods.[31] The applications of these products are innumerable, including coatings,[32] films,[33] microelectronics,[34] optoelectronics,[35] and biosensors.[36]

The properties of these materials depend, not only on the properties of the individual components, but also upon the composite's phase morphology and interfacial properties.[37,38] The resulting hybrid organic-inorganic materials can range from physical mixtures and blends (i.e. nanocomposites) of the inorganic oxide and organic molecule to covalent hybrids where covalent attachment between the two domains (e.g., organic and inorganic) exists.[39] These composites or organic-inorganic hybrid materials can be considered as nano-composites, if the size of particles is in at least one direction below 100 nm, and they remain transparent if the heterogeneity

remains below 400 nm. Sol-gel derived hybrids have the wonderful advantage of the simplicity and versatility that is associated with the sol-gel process, which allows the easy incorporation of an organic component into a ceramic network under mild conditions.[40] These organic inorganic hybrid materials may include products from the hydrolytic condensation of tri-functional or di-functional organosilanes, where the organic group may undergo further reactions, to monomeric building blocks containing two or more triethoxysilyl groups as precursors to synthesize bridged polysilsesquioxanes.[41-43]

The efforts of the present research study have been focused on the development of novel organic-inorganic hybrid materials with tunable properties for a multitude of applications. One approach has been the covalent incorporation of acrylic groups, such as 2-hydroxyethyl methacrylate (HEMA) and glycidyl methacrylate (GMA), to sol-gel intermediates and the subsequent radical polymerization of the obtained hybrid prepolymers to yield a highly crosslinked, organic-inorganic interconnected 3-dimensional network [poly(HEMA-GMA-silica)] (**Figure 2-1**). This hybrid material exhibits excellent mechanical properties while maintaining its optical transparency. Another approach that has been investigated, was the covalent incorporation of electroactive polyaniline (PANi) into the above mentioned hybrid materials to provide a conductive hybrid material [poly(HEMA-GMA-silica)-PANi] with good mechanical and electro-optical properties. Last, hybrid materials, prepared via the sol-gel route, have been used to encapsulate a variety of different enzymes for storage and protection against a diversity of harsh environments, including non-aqueous and high pH aqueous solvents. The synthesis and characterization of all of the above mentioned hybrid materials are going to be presented in the following chapters. In the following sections of this chapter, the sol-gel method

along with the major characterization techniques that have been used to analyze the as synthesized hybrid materials are going to be introduced.

2.3.3 Introduction to Sol-Gel Chemistry

The sol-gel process, as the name implies, involves the transition of a system from a liquid "sol" (mostly colloidal) to a solid "gel" phase. The process begins with the hydrolysis (**Scheme 2-3**) and polycondensation (**Scheme 2-4** and **Scheme 2-5**) of the precursors (usually inorganic salts or organic metal alkoxides) to form high molecular weight, yet soluble, polyintermediates defined as "sol". These intermediates then link together to become a three dimensional network defined as "gel".

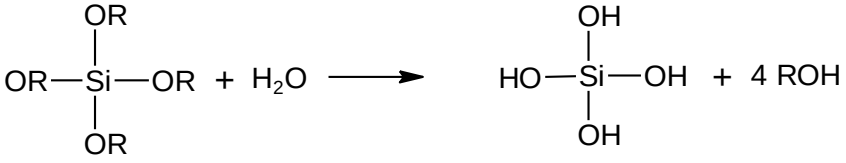

Scheme 2-3. Hydrolysis reaction of tetraalkyl orthosilicate with water in acidic or basic environment.

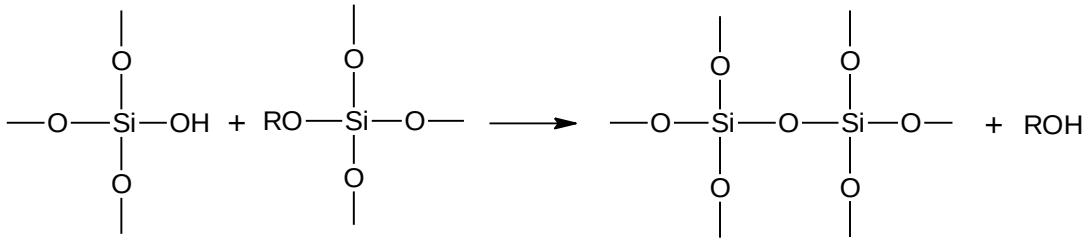

Scheme 2-4. Condensation reaction of tetraalkyl orthosilicate with hydrolyzed tetraalkylorthosilicate.

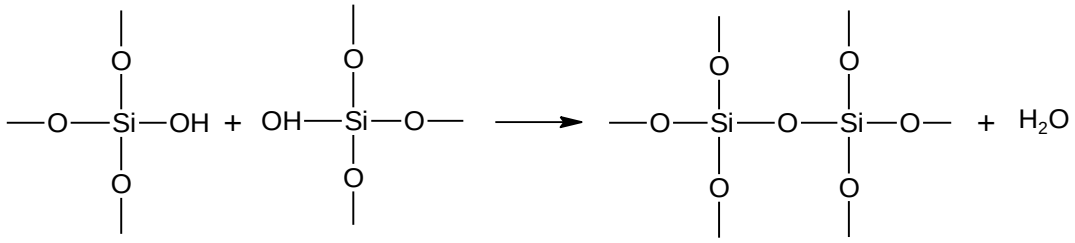

Scheme 2-5. Self condensation reaction of hydrolyzed tetraalkyl orthosilicate.

Application of this sol-gel process makes it possible to fabricate ceramic or glass materials in a wide variety of forms: ultra-fine or spherical shaped powders, thin film coatings, ceramic fibers, microporous inorganic membranes, monolithic ceramics and glasses, or extremely porous aerogel materials (**Figure 2-2**).[44]

2.3.3.1 Precursors Used

Metal salts that are readily converted to the oxide form by thermal or oxidative decomposition are good candidates for gel formation. Sodium silicates and potassium silicates are two important precursors that are used for the preparation of porous silica gels. The two steps involved in the chemical reactions are the hydrolysis of silicates (e.g., Na_2SiO_3) to $Si(OH)_4$ under acidic conditions, as depicted in **Scheme 2-6**, followed by the condensation of the hydrolyzed silicates:

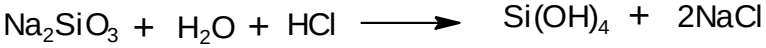

Scheme 2-6. Hydrolysis of Na_2SiO_3 under acidic environment.

Unfortunately, byproducts such as NaCl or KCl result when inorganic metal salts are used as precursors. These salts are difficult to remove and hence make the purification of the obtained materials problematic.

On the other hand, when metal alkoxides are used as precursors, they produce byproducts that are easily removed by a simple drying process, which makes them the preferred precursors for the synthesis of sol-gel materials. These compounds have the general formula $M(OR)_n$ where M is a metal ion and R is an alkyl group. Amongst silicon, zirconium, aluminum and titanium, silicon is the most widely used metal for synthesizing sol-gel materials and this is the metal that has been investigated in this research work. Typical alkoxides that have been used include tetraethyl orthosilicate (TEOS), tetramethyl orthosilicate (TMOS), methyl-trimethoxy silane (MTMS), phenyl-trimethoxy silane and others. **Scheme 2-7** shows the hydrolysis of tetraethyl orthosilicate (TEOS) with water under acidic conditions.

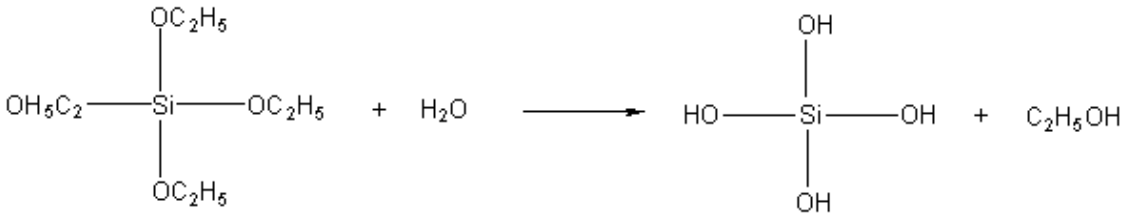

Scheme 2-7. Hydrolysis of tetraethylorthosilicate (TEOS) with water.

In the gelation step, alkoxide gel precursors in aqueous solution polymerize through alcohol or water producing condensations. These steps proceed simultaneously, and the extent to which each step goes depends on different factors that may be controlled by the reaction conditions. Amongst others, the role of the pH, the temperature and the mol ratio of water to alkoxides are extremely important in controlling the hydrolysis and polycondensation rates. In

fact, one can imagine processes all the way from condensation of colloidal particles to cluster growth and crosslinking of polymeric materials, depending on the synthesis method.[45] As Brinker and others note, gelation may be considered a rapid solidification process, which is distinctly different from precipitation.[46,47] At low pH values (e.g., < 3) relatively linear polymeric species are produced, which can then crosslink to yield a polymeric gel. On the other hand, alkoxides tend to polymerize to form colloidal silica or weakly crosslinked clusters at higher pH values. Depending on dilution and pH, these particles can then aggregate to form a colloidal gel (**Figure 2-3)**.[48]

2.3.4 Characterization Techniques of the Hybrid Materials

2.3.4.1 Mechanical Properties Measurements

In characterizing mechanical behavior of brittle materials there are a number of parameters of interest. First, the stiffness or elastic constants are important to measure. This is an indication of the resistance of the material to elastic deformation. Measuring the elastic constants in sol-gel silica and organic-inorganic hybrid materials allows for a comparison among pure sol-gel silica, pure polymers and hybrid materials prepared by various methods. For brittle materials in particular, the tensile test is difficult to carry out, and the results show a high degree of scattering. A compression test, which is more readily performed and which gives results with a lower degree of scattering, overcomes the above disadvantages. Because the stress is compressive, brittle tensile fracture is suppressed and plastic yielding may be observed in materials that under most measuring conditions are brittle.[49]

The relationship between compressive stress and strain is often used to characterize the mechanical properties of materials (**Figure 2-4**). Generally, there is a linear relationship between

stress and strain up to the yield point. Below the yield point, further increases in stress cause proportionally greater increases in strain. Within this region, the material is deforming elastically or viscoelastically and the deformation is essentially recoverable upon unloading. At some point beyond this, it yields and as the deformation proceeds further, the sample may or may not exhibit strain softening. At the yield point, the deformation ceases to be entirely elastic and the material starts to deform plastically. There is a maximum stress that a material can withstand without undergoing permanent deformation. The slope of the straight-line portion of the stress-strain curve gives a measure of the modulus of elasticity (or Young's modulus in Hooke's Law) defined as:

$$Modulus\ of\ elasticity = Stress/Strain$$

A steep slope, giving a high modulus value, indicates a rigid material, while a shallow slope, giving a low modulus value, indicates a flexible material. A hard, brittle material, such as an amorphous polymer far below its glass transition temperature (the temperature at which the transition in the amorphous regions between the glassy and the rubbery state occurs, T_g) usually has an initial slope indicative of very high modulus, moderate strength, a low elongation at break, and a low area under the stress-strain curve (**Figure 2-5**). Generally, such materials exhibit elastic deformation up to the point of fracture, which is a brittle fracture. Hard and strong polymers have high modulus of elasticity, high strength, and elongation at break of approximately 5 %. Hard, tough behaviour is shown by polymers such as cellulose acetate, cellulose nitrate and nylons. They are characterized by high yield points and high modulus, high

strengths and large elongations. On the other hand, materials that are soft and tough, show low modulus and yield values, moderate strength at break and very high elongation.

2.3.4.2 Electroanalytical Methods

The connection between chemistry and electricity goes back to Alessandro Volta's discovery in 1793 that electricity could be produced by placing two dissimilar metals on opposite sides of a moistened paper.[50] Since then, very significant progress from various contributors has been made and has led to what is defined today as electrochemistry. Nowadays, electrochemistry is a separate branch of chemistry that studies chemical reactions that take place in a solution at the interface of an electron conductor (e.g., the electrode, composed of a metal or a semiconductor) and an ionic conductor (e.g., the electrolyte), and that involve electron transfer between the electrode and the electrolyte or species in solution. Generally, voltammetry, which is a branch of electrochemistry, and which has been extensively employed in this research, is a monitoring of alterations in the concentration of a chemical species. This monitoring happens by measuring changes in current in response to an applied voltage with respect to time. According to Faraday's law, the charge is directly proportional to the amount of species that undergo a loss (oxidation) or a gain (reduction) of electrons. This is expressed by the following equation:

$$Q = \mathrm{n}\,\mathrm{F}\,\mathrm{e}$$

where Q is the total charge generated (in coulombs, C), n is the number of moles of a species undergoing oxidation or reduction, F is Faraday's constant (96,487 C/mol) and e is the number of electrons per molecule lost or gained. Since current is the change in charge as a function of time:

$$I = \frac{dQ}{dt}$$

then the current response, with respect to time (voltammogram), gives information about changes in the concentration of the species of interest.

In electrochemistry, the interface between the electrode and the electrolyte turns out to be of crucial importance, since that is where all of the interactions take place and not in the bulk of the solution. While the actual interface (electrode surface) represents only the top layer of atoms on the electrode and the layer of absorbed solvent or absorbed species, an interfacial region that is different from the bulk phases exists and extends over considerably bigger distances.[51] Various models have been proposed describing this interfacial region near the electrode surface. Helmholtz envisioned this interface as a "double layer" in which the excess charge on the metal would be neutralized by a monomolecular layer of ions of opposite charge to that on the metal phase.[52] This model though did not account for many factors, such as diffusion/mixing in solution, the possibility of absorption on to the surface and the interaction between solvent dipole moments and the electrode. A later model proposed by Stern began to address some of these limitations. A schematic representation of this model can be seen in **Figure 2-6**. In this diffusion layer the potential varies linearly with distance within the outer Helmholtz plane. Beyond the outer Helmholtz plane the variation of the potential with distance is exponential. Many modifications and improvements have been made to these early models, with the latest approaches using numerical modeling to follow the redistribution effects as the electrode potential is varied.[53] Nevertheless, interfacial interactions must be considered in the treatment of

electrochemical data, even though the exact interfacial structure near the electrode surface is not completely known.

Mass transfer is defined as the movement of a compound from one location to another in solution. In electrochemical systems, three different modes of mass transport are generally considered, namely diffusion, convection, and migration. Diffusion removes concentration gradients by the movement of material from a high concentration to a low concentration. Migration is the movement of charged species due to a potential gradient. Electroanalytical measurements are usually carried out in a solution containing a large excess of an inert electrolyte so that the current of electrons through the external circuit can be balanced by the passage of ions through the solution between the electrodes. In such a case, a minimal amount of the electroactive species will be transported by migration. Convection on the other hand, is the movement of species due to mechanical forces and usually can be eliminated on a short time scale. As a consequence, diffusion is the major mass transfer process that has to be considered in all electrochemical methods where no convection of the electrolyte solution is used.

2.3.4.2.1 Cyclic Voltammetry

Potential sweep methods, which include linear sweep voltammetry, cyclic voltammetry and pulsed voltammetric techniques, are probably the most widely used electrochemical techniques. Cyclic voltammetry is a type of a potentiodynamic electrochemical technique and the one that has been extensively utilized during this research. In a cyclic voltammetry experiment, the basic scheme involves the application of a voltage to a working electrode in solution. The current flowing at the working electrode is then plotted versus the applied voltage to give the

cyclic voltammogram. On reaching $t=t_1$ the sweep direction is inverted as shown in the following scheme and swept until E_{min}, then inverted and swept to E_{max}, etc.

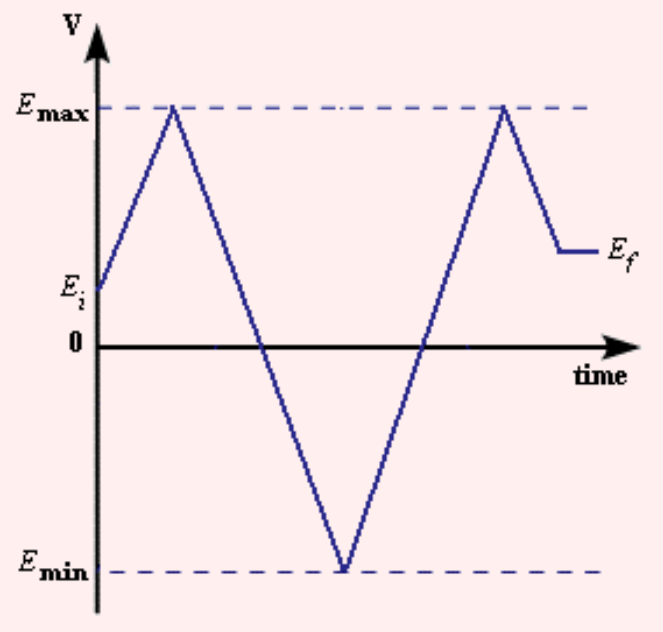

Scheme 2-8. Variation of voltage by time in a cyclic voltammetry experiment.

The important parameters in cyclic voltammetry are the initial potential E_i, the initial sweep direction, the sweep rate v (mV/sec), the maximum potential E_{max}, the minimum potential E_{min} and the final potential E_f. For the majority of experiments, the electroactive species is in the form of a solution. Electrolyte is added into the solution that is to be tested to ensure sufficient conductivity. Precise control of the external applied potential is not possible with a two-electrode system because of the potential drop across the cell due to the solution resistance and the polarization of the counter electrode. Consequently, the three-electrode system with a working, a reference and an auxiliary electrode is the most widely used (**Figure 2-7**). The potential of the working electrode is controlled relative to the reference electrode, but the current passes through

the working electrode and the auxiliary electrode. Since the passage of current through an electrode can alter its potential, a reference electrode has to comprise the following two requirements:

- a high input impedance, thereby decreasing the amount of current passing through it;
- non-polarizable electrode, so that the passage of small currents does not alter its potential.

Many different reference electrodes for both aqueous and non-aqueous solutions that meet the above requirements and which have a well-known formal potential are used in electrochemical measurements. The ones that have been utilized in this research study are the saturated calomel reference electrode (SCE), the silver/silver chloride reference electrode (Ag/AgAgCl) and the silver/silver nitrate reference electrode ($Ag/AgNO_3$). There is also a wide range of materials that can be used as working electrodes and electrolytes. Electrode materials may include noble metals (e.g., Pt, Au), active metals (e.g. Fe, Ni), carbon of various types (e.g. carbon paste, glassy carbon), semiconductors (e.g., Si, CdS), electronically conductive polymers (e.g., polyaniline, polypyrrole), inorganic conductors (e.g., indium tin oxide) and others.[47] Electrolyte phases may be basically divided in two categories, namely aqueous and non-aqueous solutions. The combination of the solvent, the electrolyte, the working electrode, the reference electrode and the auxiliary electrode determines the range of the potential that can be applied and the form of the current response that is going to be obtained.[54] An example of the basic shape of the current response for a cyclic voltammetry experiment, with a Ag/AgCl used as a reference electrode, is shown in **Figure 2-8**.

In this example, during the positive potential scan for the first half cycle, an anodic current is observed that results from the oxidation of the analyte. Now, the product generated during the forward scan is available at the surface of the electrode for the reverse scan, resulting in a cathodic current due to its reduction. Cyclic voltammetry, is nowadays commonly used, because it offers a fast and reliable method for the initial characterization of a redox-active system. In addition to providing an estimate of the redox potential, it can also present information about the rate of electron transfer between the electrode and the analyte, and the stability of the analyte in the electrolyzed oxidation states. For an electrochemical reaction to be called reversible the following should be true:

- the peak potential separation (E_{pa} - E_{pc}) is equal to 57/n mV for all scan rates, where n is the number of electron equivalents transferred during the redox process;
- the peak current ratio (i_{pa}/i_{pc}) is equal to 1 for all scan rates;
- for diffusion-controlled process, the peak current increases linearly as a function of the square root of the scan rate (v).

The situation is very different when the redox reaction is not reversible, when chemical reactions are coupled to the redox process or when adsorption of either reactants or products occurs. In fact, it is these "non-ideal" situations that are usually of greatest chemical interest and for which the diagnostic properties of cyclic voltammetry are particularly suited.[55]

2.3.4.2.2 Rotating Disk Polarography

In a rotating disk electrode (RDE) voltammetry experiment, a rotating disk electrode, which consists of a disk electrode embedded in the middle of an inert surface, rotates around its axis (**Figure 2-9**). This is the most popular hydrodynamic electrochemical method where convection is used. The act of rotation drags material to the electrode surface, where it can react and the process becomes in this case mass transport limited compared to diffusion limited, when measurements are done in stagnant solutions. The mass transport limited current arises from the fact that the system reaches a steady state, and so the current reaches a plateau once the equilibrium at the surface is driven to the products side. The variation of the mass transport limited current as a function of the rotation speed was first solved mathematically by Levich, who showed the following relationship between the current, the rotation speed and the concentration of the analyte for a reversible electron transfer reaction.[56]

$$i_l = (0.62)nFAD^{2/3}w^{1/2}v^{-1/6}C$$

where F is the Faraday constant (96485 C/mol), A is the electrode surface area (cm^2), D is the analyte's diffusion coefficient (cm^2/sec), w is the angular rotation rate of the electrode (radians/sec), v is the kinematic viscosity of the solution (cm^2/sec). The kinematic viscosity is the ratio of the solution's viscosity to its density. For pure water, v = 0.0100 cm^2/sec. An RDE experiment can provide input about the kinetics of a reaction, about whether or not a reaction is reversible, about the rate of reactivity of products, about the formal redox potentials of the redox active species and about the concentration of the analytes.

2.3.4.3 Conductimetry

The four probe method has been used for the measurement of the conductivity of the obtained materials. In this approach, a high impedance source is used to supply current through the outer two probes, and a voltammeter measures the voltage drop, across the inner two probes (**Figure 2-10**), to determine the sample resistivity. For free-standing or spin-coated polymer thin films on substrates, in situ electrical conductivity measurements, using a bandgap electrode, are greatly simplified. Their conductivity is represented by volume resistivity, R_v (also called "specific resistance"), rather than conventional resistance (e.g., R). R_v has the units of ohm centimeter. Accordingly, "conductivity" (also called "specific conductivity") (σ) is defined as the inverse of volume resistivity in siemens per centimeters. The calculation of conductivity is based on the following equation:[57]

$$\sigma = \frac{I\,l}{V\,d\,t}$$

where *I* is the current supplied between the two outer probes (mA), *V* is the voltage drop across the two inner probes (mV), *l* is the distance between two adjacent probes (cm), *d* is the width of measured film (cm) and *t* is the thickness of measured film (cm).

2.4 Nanomaterials

Another major area of science that this research has been focused on is the world of nanomaterials. According to United States National Nanotechnology Initiative website, "Nanotechnology is defined as the understanding and control of matter at dimensions of roughly 1 to 100 nanometers, where unique phenomena enable novel applications".[58] The organic-

inorganic hybrid materials that have been synthesized in this work can be considered as nano-composites, if the size of particles in at least one direction is below 100 nm.[38] As results show, and which are going to be presented in the following chapters, the domain size of in-homogeneity between the two different phases, namely organic and inorganic, remains well below 100 nm. These as-synthesized hybrid materials may thus be considered as nanomaterials.

Another project in the field of nanomaterials included the fabrication of a novel fluorescent tungsten nanoelectrode, which is expected to have a huge impact in the field on neuroscience. The fabrication includes the utilization of electron beam deposition on the apex of conventional tungsten microelectrodes followed by electropolymerization of a fluorescent insulating coating. Due to the extensive utilization of the scanning electron microscope (SEM) for this as well as for the other projects, the basic characteristics of SEM are going to be described. In addition the general principles behind X-ray diffraction spectroscopy and the gas sorption measurement (BET), which have been utilized during this research are going to be introduced in the last sections of this Chapter.

2.4.1 Characterization of Nanomaterials

2.4.1.1 Scanning Electron Microscope (SEM)

The invention of the scanning electron microscope is attributed to M. Knoll and E. Ruska in 1932. Nowadays, the scanning electron microscope (SEM) is the most versatile and widely used electron beam instrument that exists in the scientific area. It owes its popularity to the easily interpreted nature of the micrographs that it generates, to the diversity of types of information that it can produce, and to the fact that images and analytical information can be readily combined.[59,60] The basic mode of use of the SEM has always been in the imaging of surface

topography. The increasingly high level of performance of SEM, in particular, makes it an excellent complement to high resolution transmission electron microscope (TEM) imaging, as it provides the surface details lacking in the TEM, or to scanning tunneling or atomic force microscopies, where it can provide images for comparison that are readily interpretable.[61] The general arrangement of components in an SEM is shown in **Figure 2-11**. Electrons emerging from the source (electron gun) follow a vertical path and must be accelerated by some chosen voltage, which is held under high vacuum. The beam travels through electromagnetic fields and lenses, which focus the beam down toward the sample.[62] When the primary electron beam interacts with the sample, the electrons lose energy by repeated scattering and absorption within a teardrop-shaped volume of the specimen known as the interaction volume (**Figure 2-12**), which extends from less than 100 nm to around 5 μm into the surface. The size of the interaction volume depends on the electrons' landing energy, the atomic number of the specimen and the specimen's density.

Once the beam hits the sample, backscattered electrons, secondary electrons and X-rays are ejected from the sample. Detectors collect these X-rays, backscattered electrons, and secondary electrons and convert them into a signal that is sent to a screen similar to a television screen. This produces the final image. Because the SEM utilizes vacuum conditions and uses electrons to form an image, special preparations must be done to the sample. All metals are conductive and require no preparation before being used. All non-metals need to be made conductive by covering the sample with a thin layer of conductive material. This is done by using a device called “sputter coater”, which applies an ultra-thin conductive coating on the sample of interest. The highest quality images can be created from an optimized interplay of

sample preparation techniques, accelerating voltage, working distance, spot size and artifact corrections.[63]

2.4.1.2 X-ray Diffraction (XRD)

The X-ray diffraction (XRD) method is a non-destructive analytical technique used to reveal information about the crystallographic structure, the chemical composition, and the physical properties of solid materials and thin films. This technique is based on the concept of observing the scattered intensity of an x-ray beam hitting a sample, as a function of the incident beam and the scattered angle. X-rays are comparably short wavelength, high energy electromagnetic radiations. When X-rays are focused into a fine beam and hit a solid sample, they diffract through the inspected matter (**Figure 2-13**). The obtained X-ray pattern is like a fingerprint for a given compound and may even identify unknown substances by comparing diffraction data against published databases. It may even be used to characterize heterogeneous solid mixtures by determining the relative abundances of the crystalline compounds. The reflected rays have to satisfy Bragg's equation:

$$n\lambda = 2d\ sin\theta$$

Where n is an integer, λ is the wavelength of the incident beam, d is the separation between different crystallographic planes, and θ is the diffraction angle.

2.4.1.3 Gas Sorption Measurement

Porous solids can adsorb large amounts of condensed gas due to their intrinsic porosity and corresponding large surface area, and this amount of adsorbed gas can be used to deduce

information about their porous structure.[64,65] The term "adsorption", which was first introduced by Kayser in 1881, is now widely used to describe the process of condensed gases onto free surfaces.[66] Once a highly dispersed solid is exposed to a gas or a vapor of specific pressure in a closed atmosphere, the solid begins to adsorb the gas. This results in the gradual reduction of the gas pressure at that specific temperature. After some time, the gas pressure becomes constant and the amount of gas adsorbed by the sample can be calculated from the difference in gas pressure by application of gas laws. The amount of adsorbed gas per gram of solid depends on the equilibrium pressure P, the temperature T, and on the nature of the gas and of the sample. For a given gas and sample, the amount of gas adsorbed at a fixed temperature is given by the following equation:

$$X = f(P)_{T,gas,solid}$$

On the other hand, if the gas is below its critical temperature, i.e., if it is in the vapor form, the following equation is used:

$$X = f(P/P_o)_{T,gas,solid}$$

These two equations are the expressions of the adsorption isotherm, which represents the relationship between the pressure at which the gas is adsorbed and the equilibrium pressure at constant temperature. These equations are a means of determining the general pore structure of a porous material. The adsorption isotherm is usually constructed point-by-point by the aid of a volumetric dosing technique and application of the gas laws.

In 1985, IUPAC developed a standard classification that divides adsorption isotherms into six groups as illustrated in **Figure 2-14**:

- Type I isotherms are indicative of microporous solids with relatively small external surfaces. The limiting uptake is governed by accessible micropore volume instead of internal surface area.
- Type II isotherms are common for non-porous or macroporous solids. The adsorbate is compatible with surface material and forms multilayers.
- Type III isotherms rarely appear. In this case, heat of adsorption is less than heat of vaporization for the adsorbate.
- Type IV isotherms have a characteristic hysteresis loop, which is associated with capillary condensation occurring in mesoporous solids. It is always indicative of pores from 15 to 1000 Angstrom in radius.
- Type V isotherms are typical of weak adsorbent-adsorbate interactions and are somewhat similar to type III isotherms.
- Type VI isotherms are commonly indicative of multilayers on a uniform non-porous surface. After formation of the first monolayer, each following adsorbed layer is equivalent.

For Type IV isotherms, the hysteresis loops have recently been classified into four classes based on the change of geometry during the adsorption and desorption processes as shown in **Figure 2-15**.[67]

- H1 loop is usually associated with pores with regular shape and narrow size distribution.
- H2 loop is hard to interpret, as it was originally attributed to a difference in mechanism between condensation and evaporation processes occurring in pores with narrow necks

and wide bodies but now it is believed that the network effects may also play an important role.

- H3 loop is observed from aggregates of plate-like particles and it shows no adsorption limit at high P/P_0.
- H4 loop is often assigned to narrow slit-like pores.

Brunauer-Emmett-Teller (BET) gas adsorption method is nowadays the most widely used standard procedure for determining surface area of finely-divided and porous materials. The Brunauer-Emmett-Teller (BET) gas adsorption equation is given by the following equation:

$$\frac{P}{n^a \times (P - P_o)} = \frac{1}{n_m^a \times C} + \frac{(C-1) \times P}{n_m^a \times C \times P}$$

where n^a is the amount of gas adsorbed at a relative pressure P/P_0 and n_m^a is the monolayer capacity.

Table 2-1. Determination of the spin number *I*.

I	Atomic Mass	Atomic Number	Example (I)
Half integer	Odd	Odd or even	${}^{1}_{1}\mathrm{H}(\frac{1}{2})$, ${}^{17}_{8}\mathrm{O}(\frac{5}{2})$, ${}^{15}_{7}\mathrm{N}(\frac{1}{2})$
Integer	Even	Odd	${}^{2}_{1}\mathrm{H}(1)$, ${}^{14}_{7}\mathrm{N}(1)$, ${}^{10}_{5}\mathrm{B}(3)$
Zero	Even	Even	${}^{12}_{6}\mathrm{C}(0)$, ${}^{16}_{8}\mathrm{O}(0)$, ${}^{34}_{16}\mathrm{S}(0)$

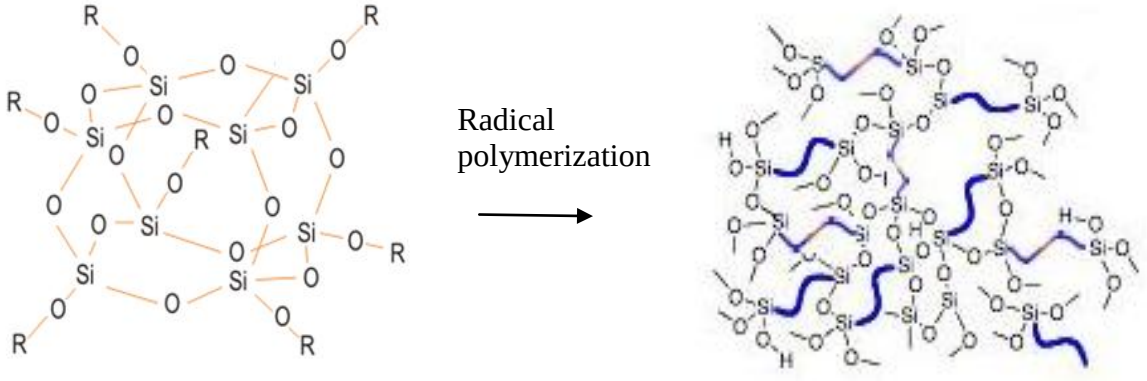

Figure 2-1. Schematic of sol-gel intermediates containing alkyl groups that have double bonds, which upon radical polymerization yield a highly crosslinked interconnected hybrid organic-inorganic 3-dimensional network.

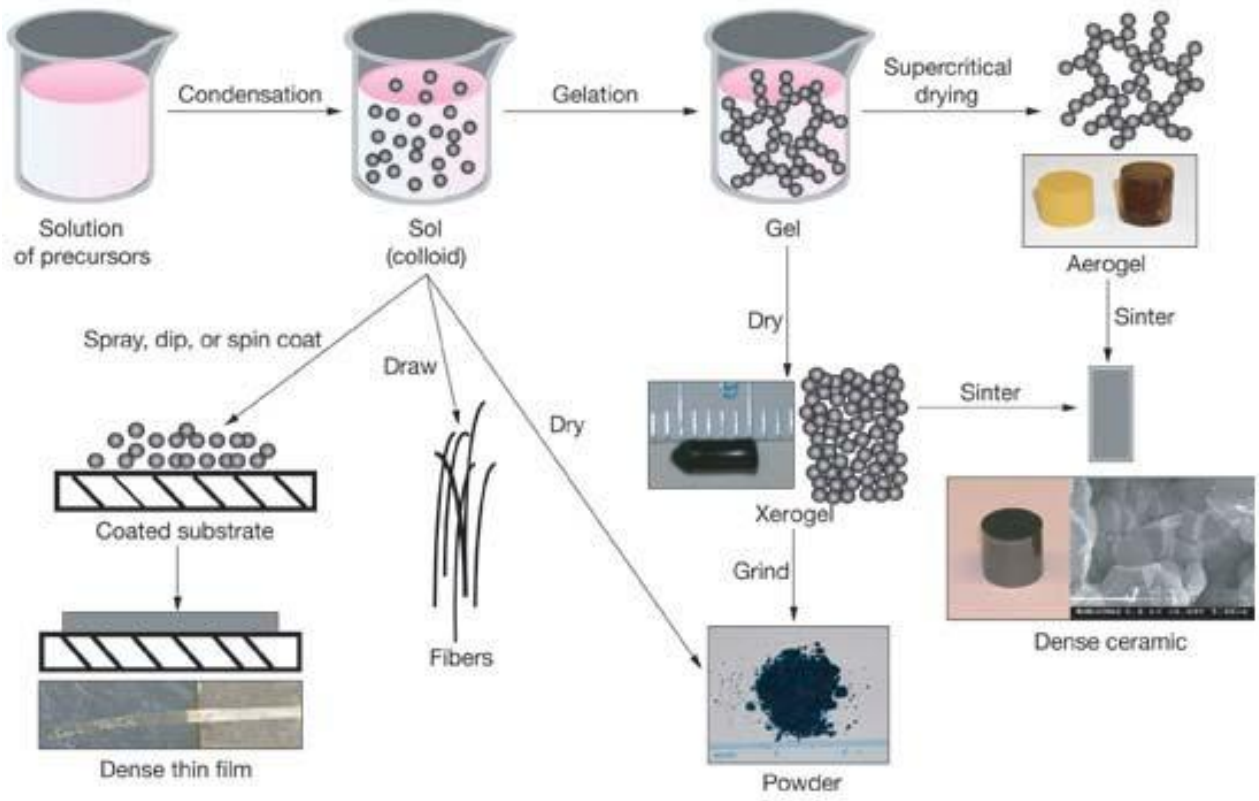

Figure 2-2. Sol-gel process and products.[68]

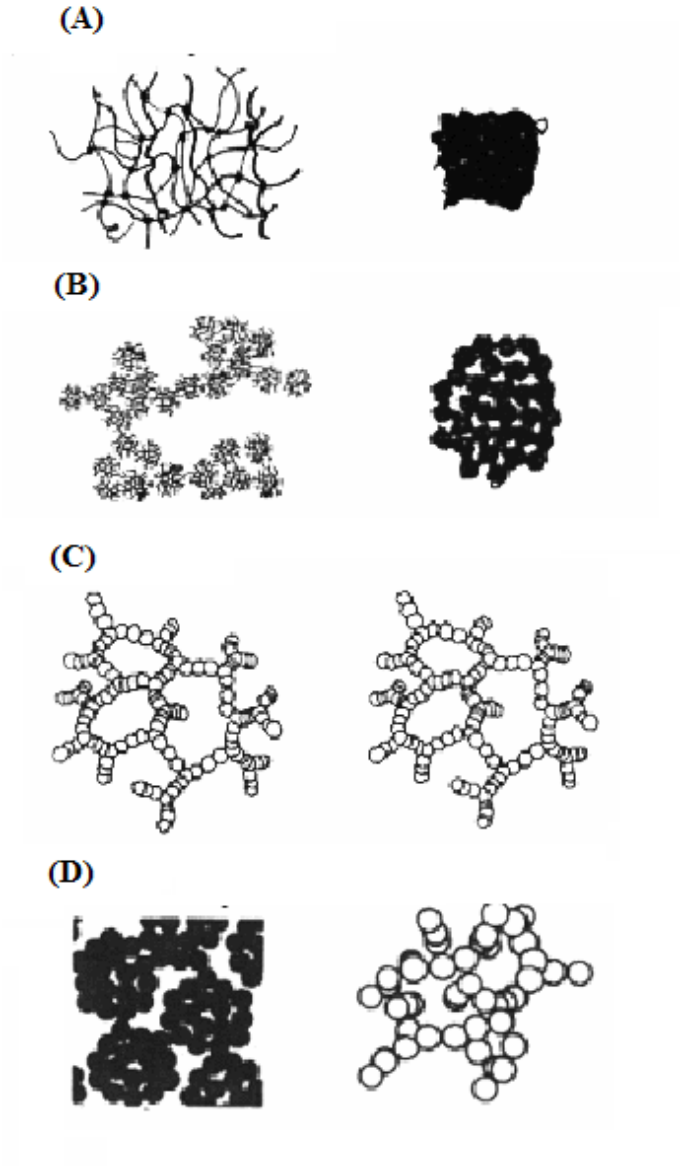

Figure 2-3. Schematic representation of gel desiccation for: (a) acid-catalyzed gels, (b) base-catalyzed gels, (c) colloidal gel aged under conditions of high silica solubility, (d) colloidal gel composed of weakly bonded particles.[25]

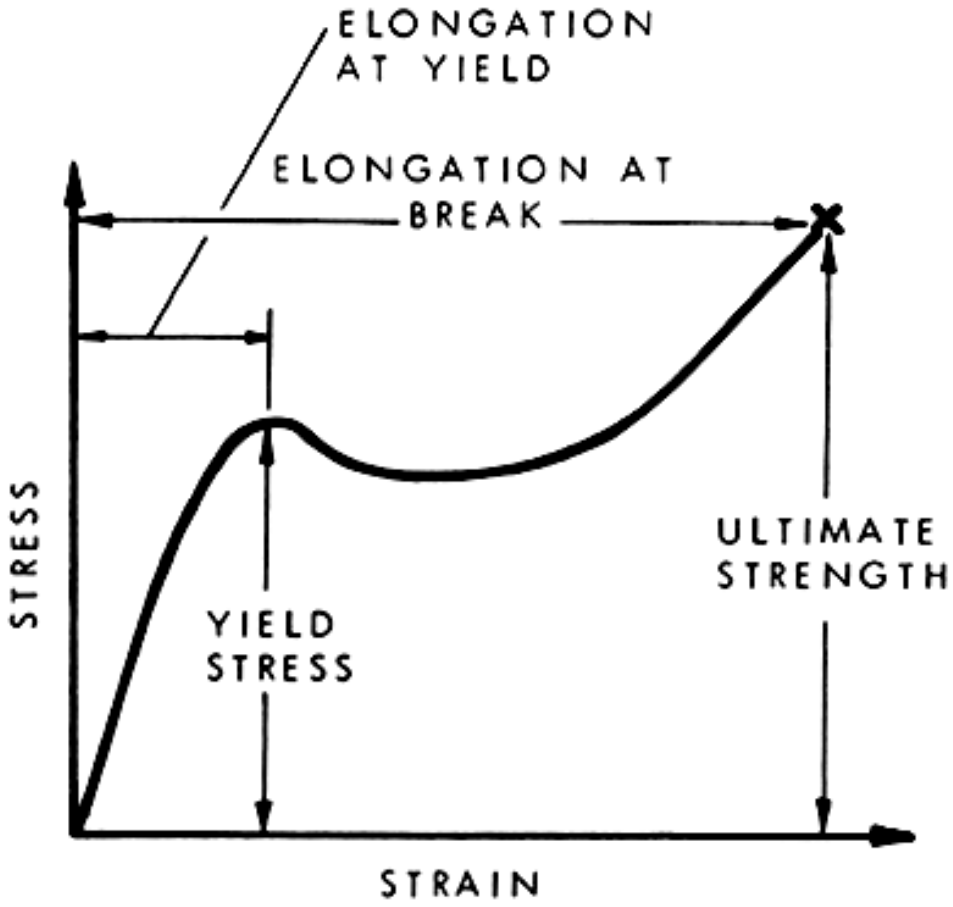

Figure 2-4. General scheme of a compressive stress-strain curve.[69]

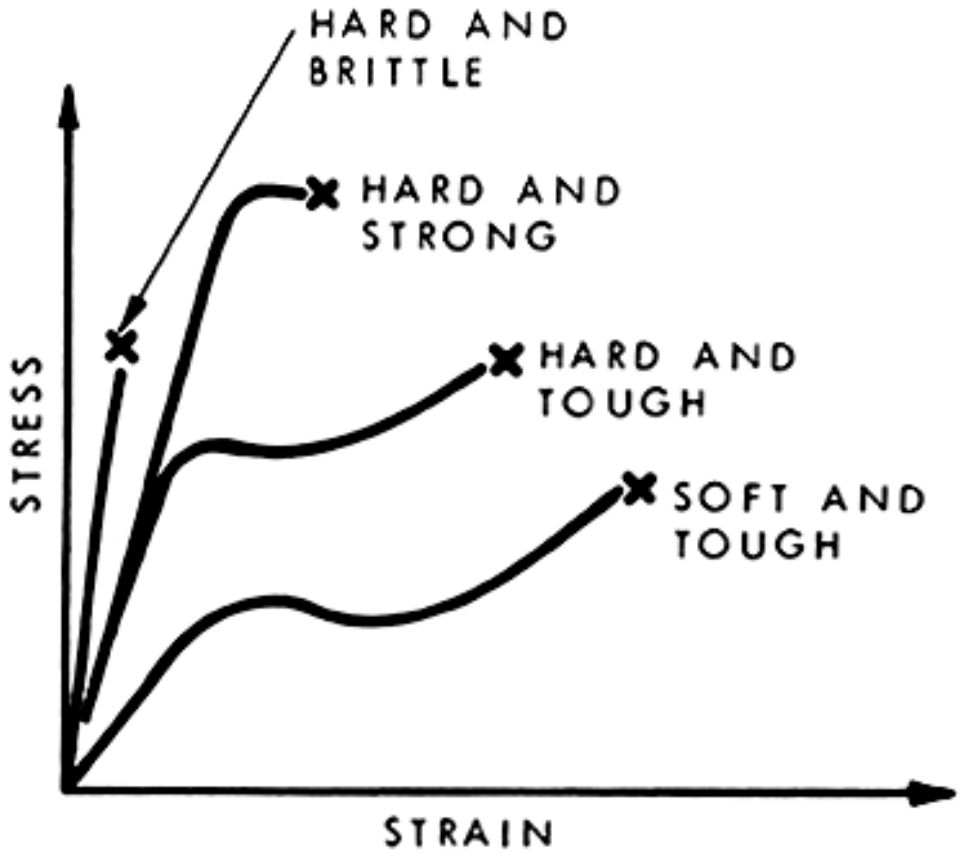

Figure 2-5. Tensile stress-strain curves for four types of polymeric materials.[69]

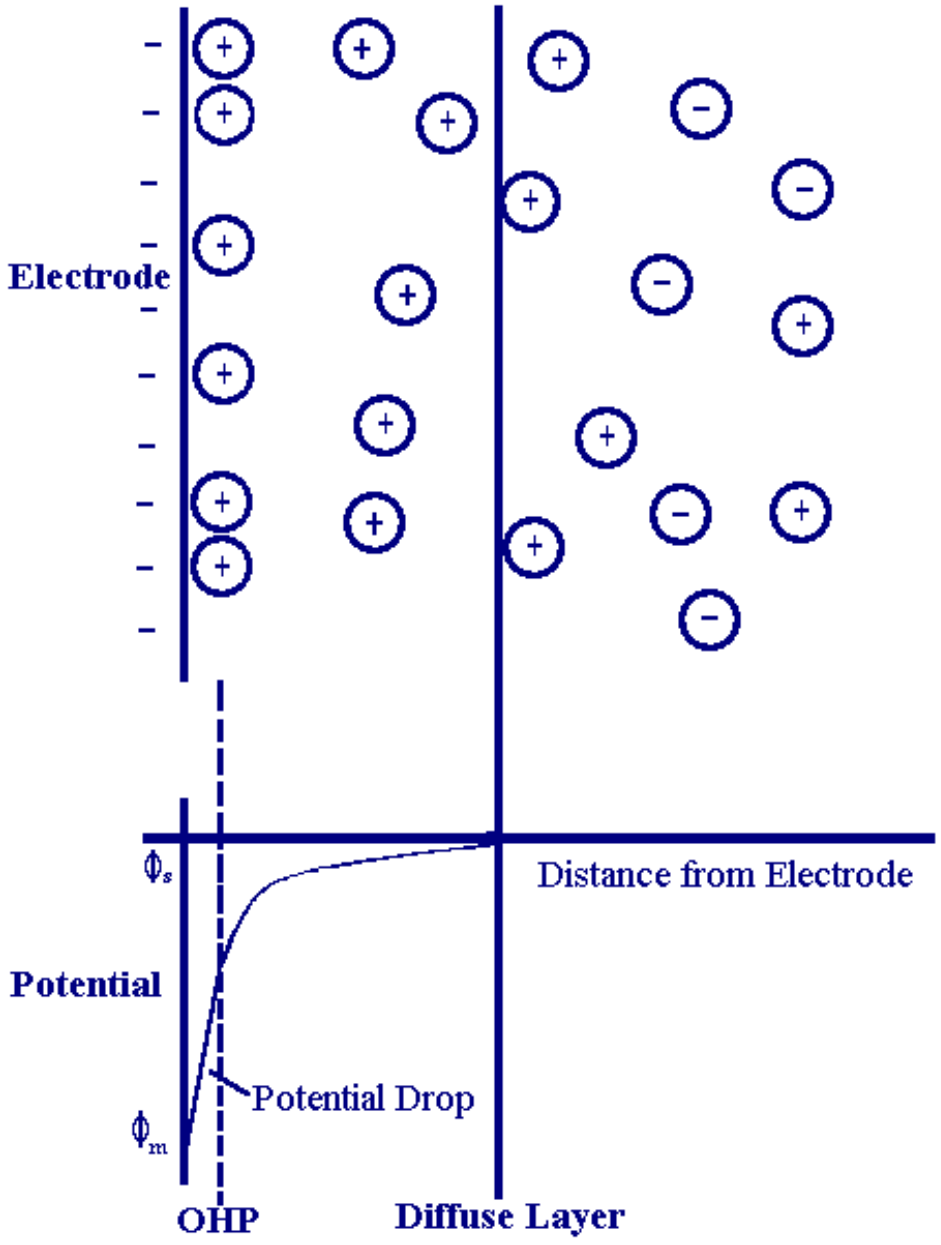

Figure 2-6. Diffusion layer at the interface of a metal in a solution. The Outer Helmholtz Plane (OHP) can be seen.[70]

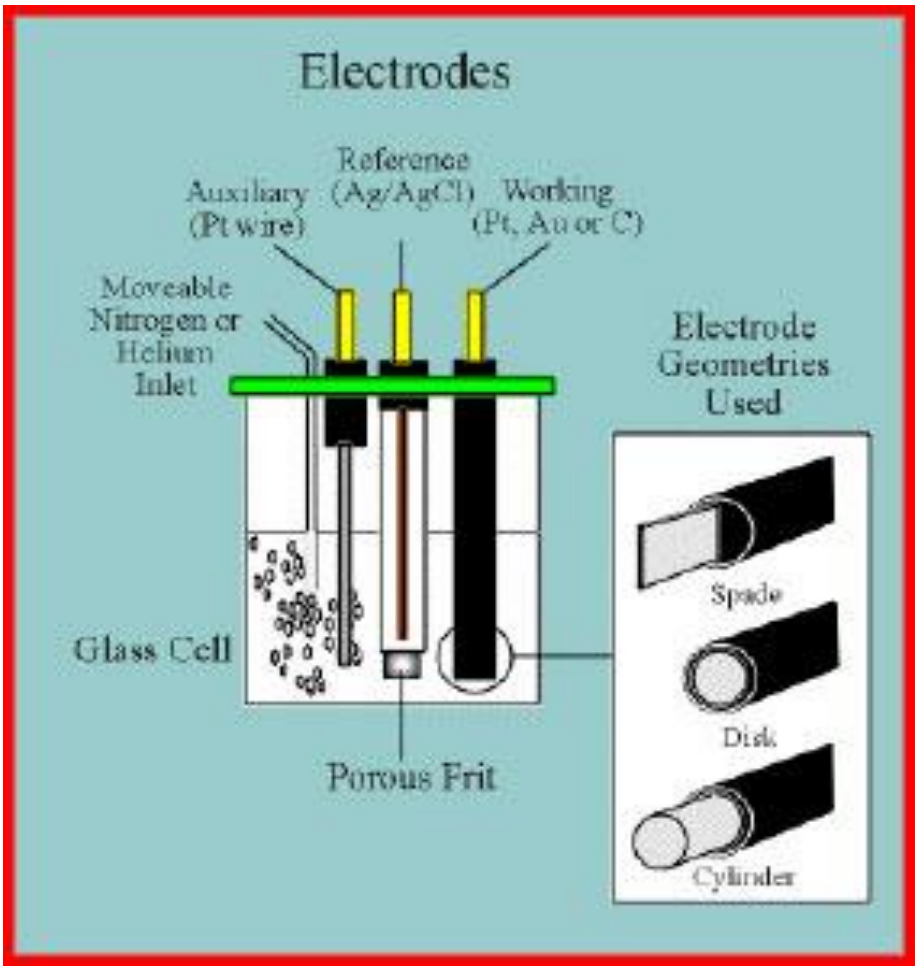

Figure 2-7. Three-electrode cyclic voltammetry system with a working, a reference and an auxiliary electrode.[71]

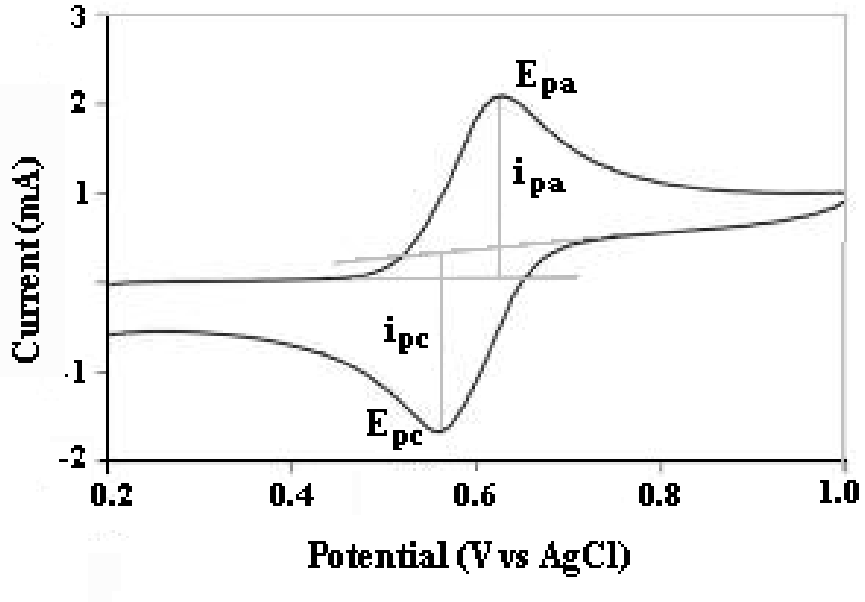

Figure 2-8. A typical cyclic voltammogram.

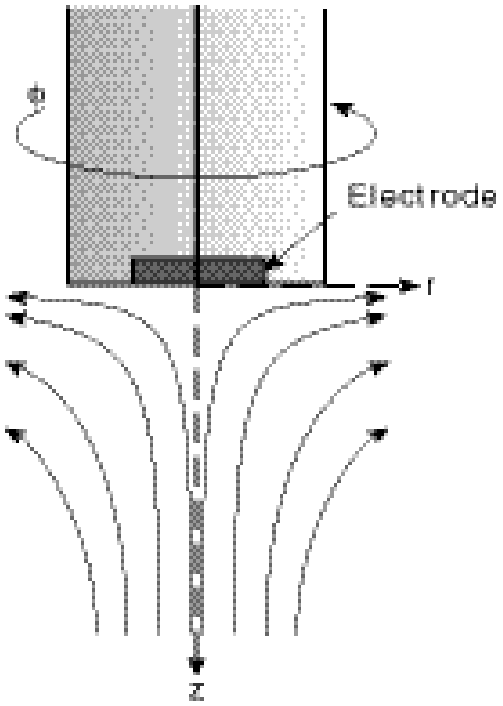

Figure 2-9. Flow profile at a rotating disc electrode.[72]

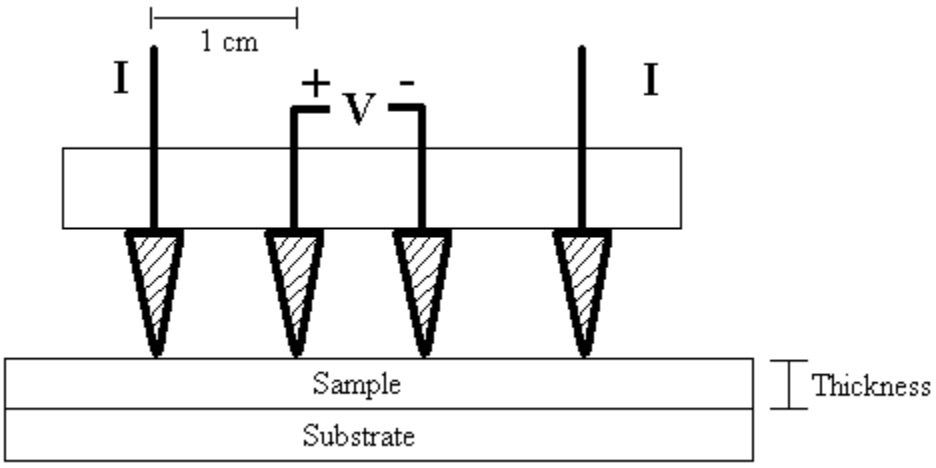

Figure 2-10. Four probe conductivity measurement method.

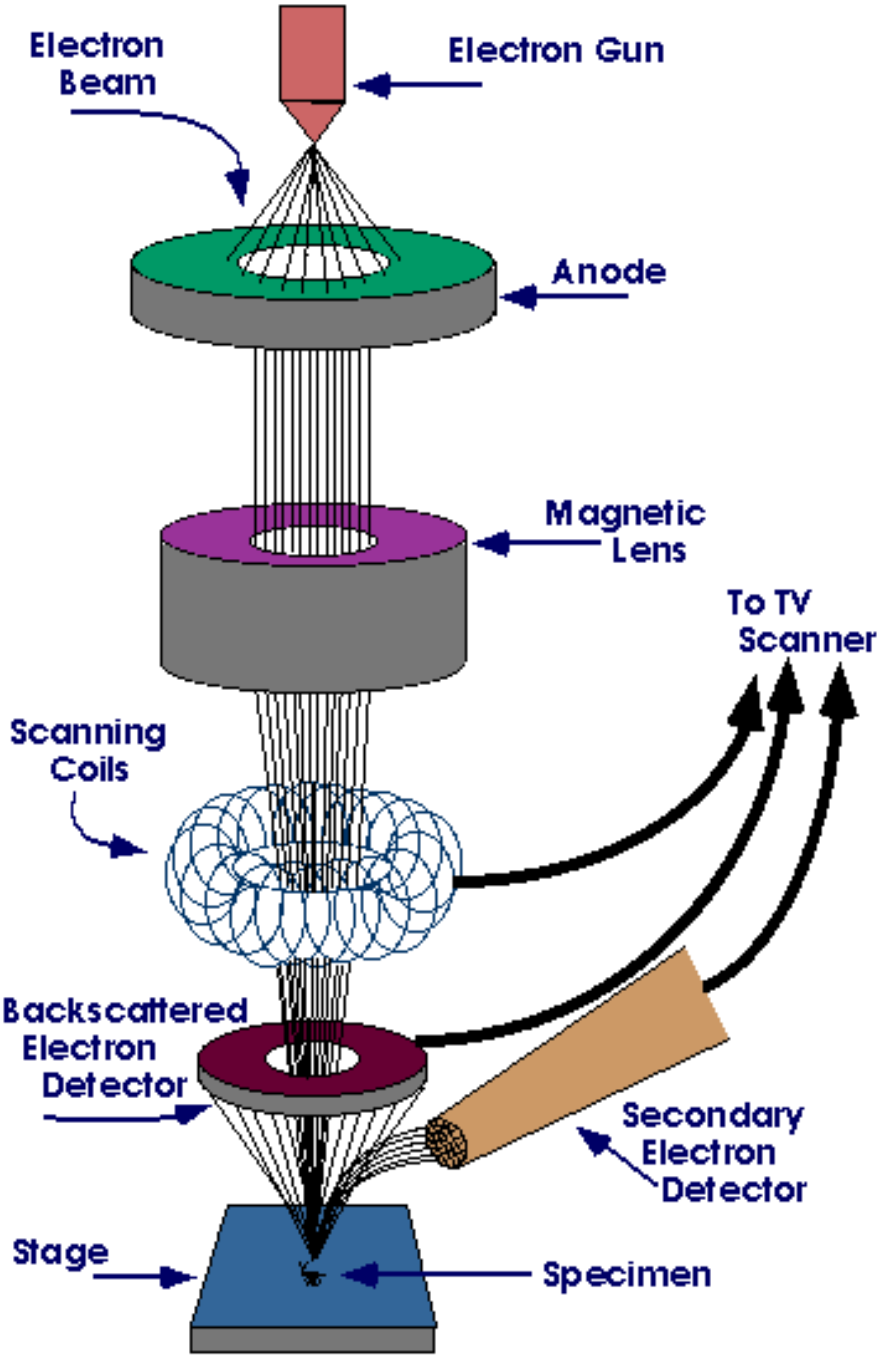

Figure 2-11. General arrangement of a scanning electron microscope.[73]

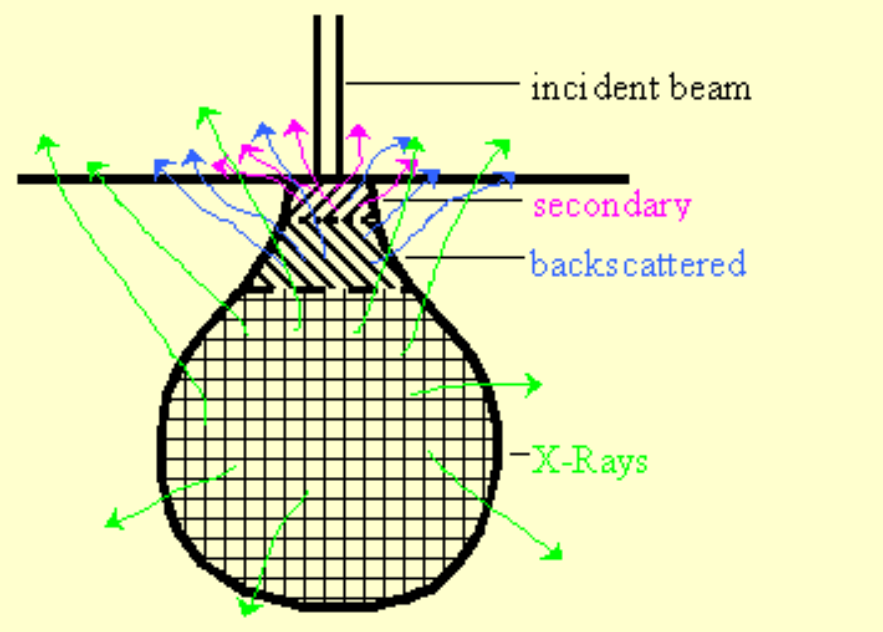

Figure 2-12. Interaction volume of the incident electron beam with the sample in a scanning electron microscope.[74]

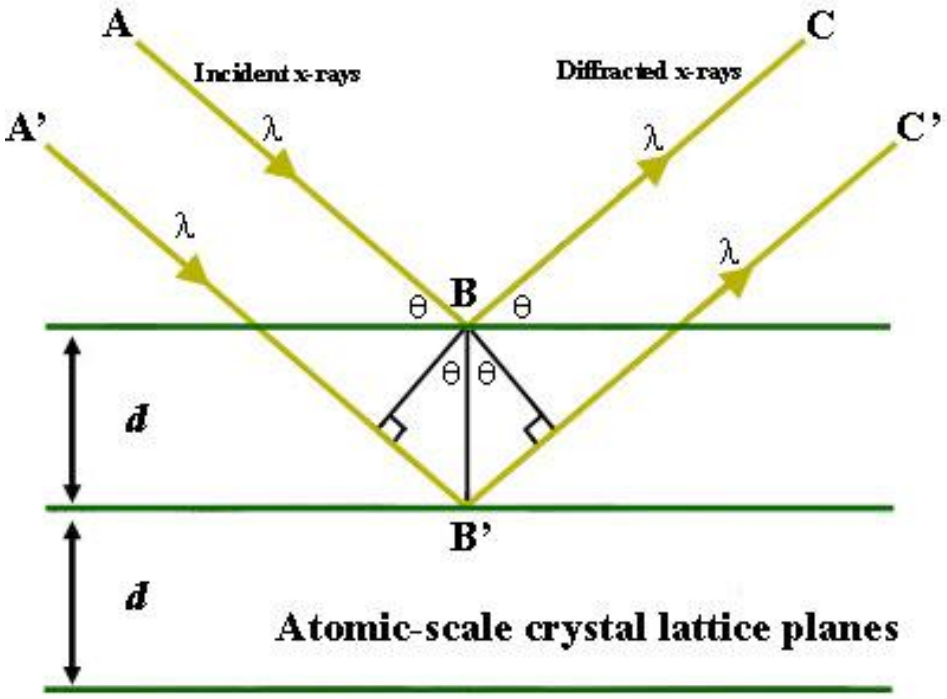

Figure 2-13. Schematic representation of diffraction of X-rays by a crystalline material.[75]

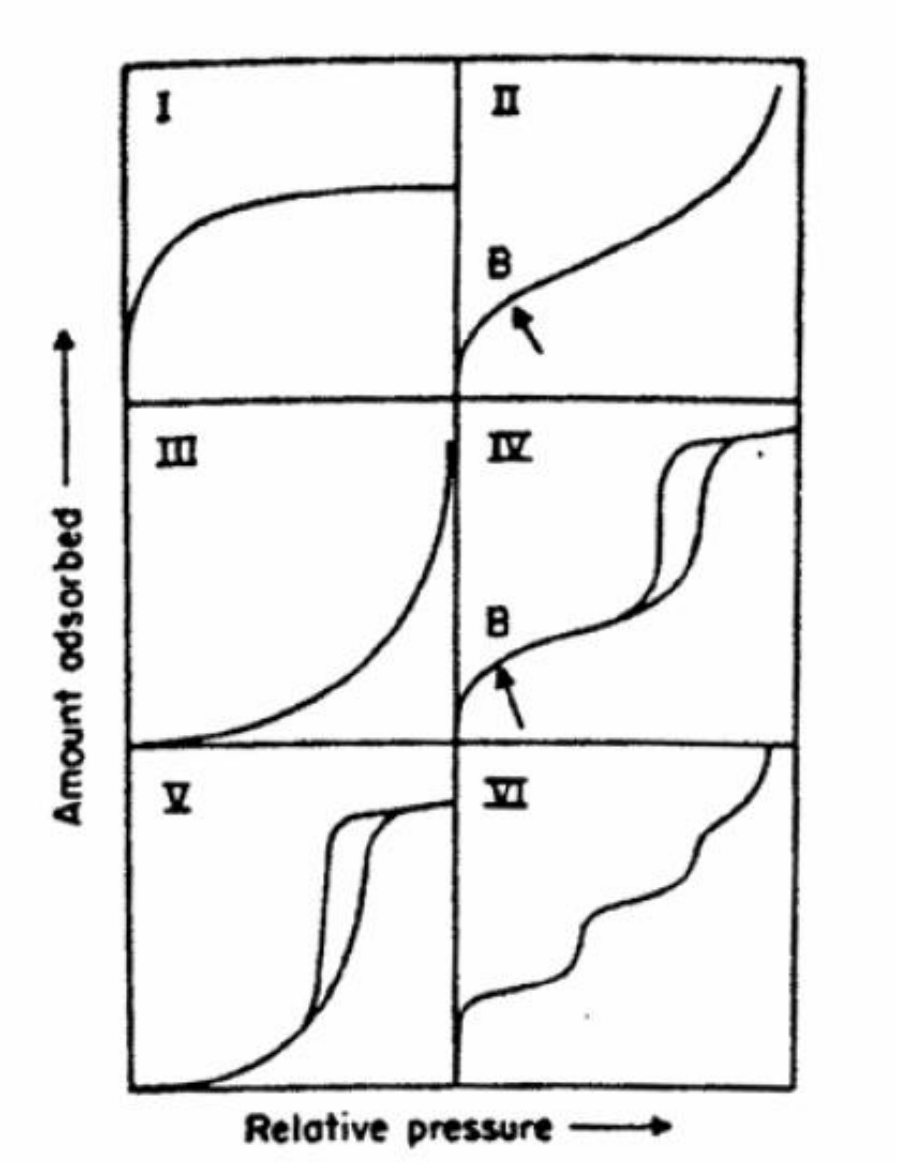

Figure 2-14. IUPAC classification of physisorption isotherms.[76]

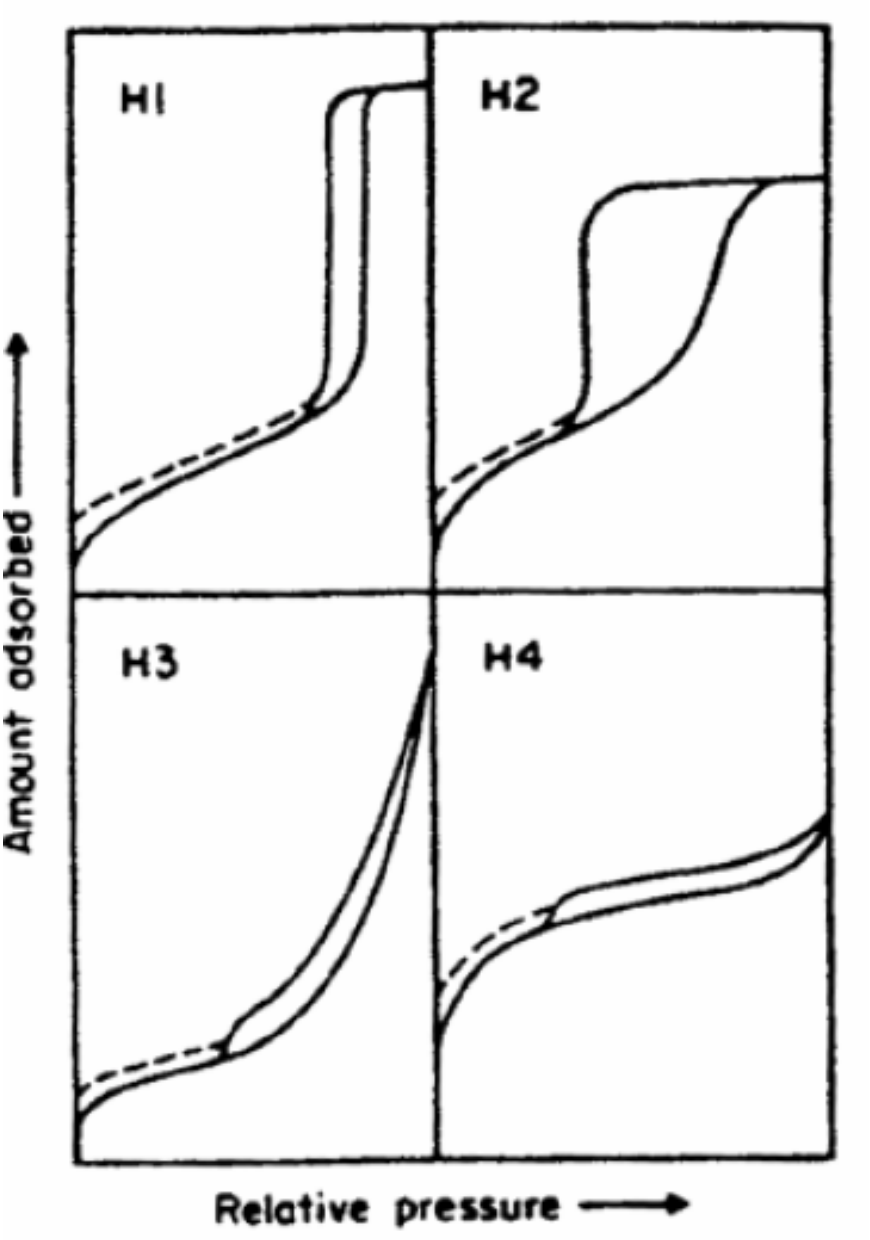

Figure 2-15. IUPAC classification of hysteresis loops.[76]

2.5 Reference List

1. Ayako, N., Kousaku, O., Ikuo, U., Hiroyuki, Y. Green mussel Perna Viridis L.: Attachment behavior and preparation of antifouling surfaces. Biomolecular Engineering (2003), 20, 381-387.

2. Camilla, F., Hans, E., Fredrik, H. The influence of cross-linking on protein-protein interactions in a marine adhesive : The case of two byssus plaque proteins from the blue mussel. Biomacromolecules (2002), 3, 732-41.

3. Baty, A. M., Leavitt, P. K., Siedlecki, C. A., Tyler, B. J., Suci, P. A., Marchant, R. E., Geesey, G. G. Adsorption of adhesive proteins from the marine mussel, Mytilus Edulis, on polymer films in the hydrated state using angle dependent X-ray photoelectron spectroscopy and atomic force microscopy. Langmuir (1997), 13, 5702-5710.

4. Ohkawa, K., Ichimiya, K., Nishida, A., Yamamoto, H. Synthesis and surface chemical properties of adhesive protein of the asian freshwater mussel, Limnoperna Fortunei. Macromolecular Bioscience (2001), 1, 376-386.

5. Yamamoto, H., Nagai, A. Polypeptide models of the arthropodin protein of the barnacle Balanus Balanoides. Marine Chemistry (1992), 37(1-2), 131-43.

6. Waite, J. H. Marine adhesive proteins: natural composite thermosets. International Journal of Biological Macromolecules (1990), 12, 139-44.

7. Yamamoto, H., Nagai, A., Okada, T., Nishida, A. Synthesis and adhesive studies of barnacle model proteins. Marine Chemistry (1989), 26, 331-8.

8. Li, K., Geng, X., Simonsen, J., Karchesy, J. Novel wood adhesives from condensed tannins and polyethilenimine. International Journal of Adhesion and Adhesives (2004), 24, 327-333.

9. Wang, J., Liu, C., Lu, X., Yin, M. Co-polypeptides of 3,4-dihydroxyphenylalanine and L-lysine to mimic marine adhesive protein. Biomaterials (2007), 28, 3456-3468.

10. Yu, M., Hwang, J., Deming, T. J. Role of L-3,4-Dihydroxyphenylalanine in mussel adhesive proteins. Journal of the American Chemical Society (1999), 121, 5825-5826.

11. Monahan, J., Wilker, J. J. Cross-linking the protein precursor of marine mussel adhesives: bulk measurements and reagents for curing. Langmuir (2004), 20, 3724-3729.

12. Monahan, J., Wilker, J. J. Specificity of metal ion cross-linking in marine mussel adhesives. Chemical Communications (2003), 14, 1672-1673.

13. Lee, B., Chao, C.Y., Nelson, N. F. Motan, E., Shull, K. R. Messersmith, P. Rapid gel formation and adhesion in photocurable and biodegradable block copolymers with high DOPA content. Macromolecules (2006), 39, 1740-1748.

14. Burke, S.A., Ritter-Jones, M., Lee, B.P., Messersmith, P.B. Thermal gelation and tissue adhesion of biomimetic hydrogels. Biomedical Materials (2007), 2(4), 203-10.

15. Lee, B.P., Huang, K., Nunalee, F.N., Shull, K.R., Messersmith, P.B. Synthesis of 3,4-dihydroxyphenylalanine (DOPA) containing monomers and their co-polymerization with PEG-diacrylate to form hydrogels. Journal of Biomaterials Science. Polymer Edition (2004),15,449-464.

16. Lee, H., Bruce P. Lee, B. P., Messersmith, P.B. A reversible wet/dry adhesive inspired by mussels and geckos. Nature (2007), 448, 338-341.

17. Lee, B. P., Dalsin, J. L., Messersmith, P. B. Synthetic polymer mimics of mussel adhesive proteins for medical applications. Bioadhesives (2006), 257-278.

18. Hu, B. H., Messersmith, P. B. Enzymatically cross-linked hydrogels and their adhesive strength to biosurfaces. Orthodontics and Craniofacial Research (2005), 8, 145–149.

19. Silverstein, R. M., Webster, F. X. Spectrometric identification of organic compounds. John Willey and Sons, Inc., USA; 1998.

20. Association of cancer online resources. http://www.acor.org/ped-onc/treatment/MRI/MRI. html; 1995.

21. Ingle J. D., Crouch, S. R. Spectrochemical analysis. Prentice Hall, New Jersey; 1988.

22. Mohrig, J. R., Hammond, C. N., Morrill, T. C., Neckers, D. C. Experimental organic chemistry-A balanced approach: Macroscale and microscale. W. H. Freeman and Company, New York; 1997.

23. Pavia, D. L., Lampman, G. M., Kriz, G. S. Introduction to spectroscopy: A guide for students of organic chemistry. Saunders College Publishing, Orlando, Florida; 1979.

24. Wen, J., Wilkes, G. L. Organic/Inorganic hybrid network materials by the sol-gel approach. Chemistry of Materials (1996), 8, 1667-1681.

25. Brinker, C. J., Scherer, G. W. Sol-Gel science: The physics and chemistry of sol-gel processing, Academic Press, San Diego; 1990.

26. Hajji, P., David, L., Gerard, J. F., Pascault, J. P., Vigier, G. Synthesis, structure, and morphology of polymer-silica hybrid nanocomposites based on hydroxyethyl methacrylate. Journal of Polymer Science: Part B: Polymer Physics (1999), 37, 3172-3187.

27. Surivet, F., Lam, T. M., Pascault, J. P., Pham, Q. T. Organic-inorganic hybrid materials. Hydrolysis and condensation mechanisms involved in alkoxysilane-terminated macromonomers. Macromolecules (1992), 25, 4309-4320.

28. Wei, Y., Bakthavatchalam, R., Whitecar, K. C. Synthesis of new organic-inorganic hybrid glasses. Chemistry of Materials (1990), 2(4), 337-9.

29. Khimich, N. N. Synthesis of silica gels and organic-inorganic hybrids on their base. Glass Physics and Chemistry (2004), 30, 430-442.

30. Innocenzi, P., Kidchob, T., Yoko, T. Hybrid organic-inorganic sol-gel materials based on epoxy-amine systems. Journal of Sol-Gel Science and Technology (2005), 35, 225-235.

31. Mukherjee, S. P. Random and block copolymerization in metal oxide gel synthesis from metalorganic compounds. Journal of Non-crystalline Solids (1985), 73, 639-641.

32. Schmidt, H. Organic modification of glass structure. Journal of Non-crystalline Solids (1989), 112, 419-423.

33. Wen, J., Wilkes, G. L. Organic-inorganic hybrid network materials by the sol-gel approach. Chemistry of Materials (1996), 8, 1667-1681.

34. Innocenzi, P., Lebeau, B. Organic-inorganic hybrid materials for non-linear optics. Journal of Materials Chemistry (2005), 15, 3821-3831.

35. Sharp, K. G. Inorganic/organic hybrid materials. Advanced Materials (1998), 10, 1243-1248.

36. Cerveau, G., Corriu, R. J. P., Framery, E. Nanostructured organic-inorganic hybrid materials: Kinetic control of the texture. Chemistry of Materials (2001), 13, 3373-3388.

37. Novak, M. Hybrid nanocomposite materials-between inorganic glasses and organic polymers. Advanced Materials (1993), 5, 422-433.

38. Kelly, A. Concise Encyclopedia of Composite Materials. Elsevier Science, New York; 1994.

39. Loy, D. A., Shea, K. J. Bridged polysilsesquioxanes. Highly porous hybrid organic-inorganic materials. Chemical Reviews (1995), 95, 1431-1442.

40. Wei, Y., Jin, D., Yang, C., Kels, M., Qiu, K. Organic-inorganic hybrid materials: relations of thermal and mechanical properties with structures. Materials Science and Engineering C (1998), 6, 91-98.

41. Wei, Y., Jin, D., Yang, C, Wei, G. A fast convenient method to prepare hybrid sol-gel materials with low volume-shrinkages. Journal of Sol-Gel Science and Technology (1996), 7, 191-201.

42. Wei, Y., Jin, D., Yang, C., Wei, G. Synthesis of organic-inorganic hybrid sol-gel materials with low volume-shrinkages. Polymeric Materials Science and Engineering (1996), 74, 244-5.

43. Guo, Y., Mylonakis, A., Zhang, Z., Lelkes, P. I., Levon, K., Li, S., Feng, Q., Wei, Y. Oligoaniline-contained electroactive silsesquioxane precursor for synthesizing novel siliceous materials. Macromolecules (2007), 40, 2721-2729.

44. Dislich, H., Hinz, P. History and principles of the sol-gel process, and some new multicomponent oxide coatings. Journal of Non-crystalline Solids (1982), 48, 11-16.

45. James, P. F. The gel to glass transition: Chemical and microstructural evolution. Journal of Non-crystalline Solids (1988), 100, 93-114.

46. Brinker, C. J., Scherer, G. W. Sol-gel-glass: I. Gelation and gel structure. Journal of Non-crystalline Solids (1985), 70, 301-322.

47. Mukherjee, S. P. Sol-Gel processes in glass science and technology. Journal of Non-crystalline Solids (1980), 42, 477-488.

48. Zelinski, B. J. J., Uhlmann, D. R. Gel technology in ceramics. Journal of Physics and Chemistry of Solids (1984), 45, 1069-1090.

49. Bradt, R. G., Hasselman, D. P. H., Lange, F. F. Fracture mechanics of ceramics. Volume 3. Flaws and testing, Plenum Press, New York; 1978.

50. Lower, S. K. Electrochemistry-Chemical reactions at an electrode, galvanic and electrolyte cells. A Chem-1 Reference Text, Simon Fraser University; 2004.

51. Bagotsky. V. S. Fundamentals of electrochemistry. John Wiley & Sons, Inc., New York; 2006.

52. Greef, R., Peat, R., Peter, L. M., Pletcher, D., Robinson, J. Instrumental methods in electrochemistry. John Wiley & Sons, Inc., New York; 1985.

53. Bard, A. J., Abruna, H. D., Chidsey, C. E., Faulkner, L. R., Feldberg, S. W., Itaya, K., Majda, M., Melroy, O., Murray, R. W. The electrode/electrolyte interface - a status report. Journal of Physical Chemistry (1993), 97, 7147-73.

54. Bott, A. W. Practical problems in voltammetry: preparation of working electrodes. A Report of Bioanalytical Systems, Inc.; 2002.

55. Brett, C. M. A., Brett, A. M. O. Electrochemistry: Principles, methods and applications. Oxford University Press, Inc., New York; 1993.

56. Schenk, J. O., Patterson, T. A., McElvain, J. A. Rotating disk voltammetric measurements in neurobiology and neuropharmacology. Trends in Analytical Chemistry (1990), 9, 325-330.

57. Wiegenstein, C. G., Schulz, K. H. A four-point surface conductivity probe suitable for in – situ ultrahigh vacuum conductivity measurements. Review of Scientific Instruments (1997), 68, 1812-1813.

58. National Nanotechnology Initiative. http://www.nano.gov/html/facts/whatIsNano.html; 2006.

59. Athene, D. M. The use of environmental scanning electron microscopy for imaging wet and insulating materials. Nature Materials (2003), 2, 511-516.

60. Crewe, A. V. The physics of the high-resolution scanning microscope. Reports on Progress in Physics (1980), 43, 621-639.

61. Rau, E. I., Gostev, A. V., Zhu, S., Phang, D., Chan, D., Thong, D., Wong, W. Comparative analysis of scanning electron microscopy techniques for semiconductors: Electron-beam induced potential method, single-contact electron -beam-induced current method, and thermoacoustic detection. Russian Microelectronics (2001), 30(4), 207-218.

62. Joy, D. C. Scanning electron microscopy for materials characterization. Current Opinion in Solid State & Materials Science (1997), 2, 465-468.

63. Breger, D. SEM basic theory questionnaire. Materials Department, Drexel University, Pennsylvania; 2004.

64. Gregg, S. J., Sing, K. S. W. Adsorption, Surface Area and Porosity. Academic Press, London; 1982.

65. Wei, Y., Xu, J., Dong, H., Dong, J. H., Qiu, K., Jansen-Varnum, S. Preparation and physisorption characterization of glucose-templated mesoporous silica sol-gel materials. Chemistry of Materials (1999), 11(8), 2023-2029.

66. Lee, C. K., Chiang, A. S. T., Tsay, C. S. The characterization of porous solids from gas-adsorption measurements. Key Engineering Materials (1996), 115, 21-43.

67. Barrett, E. P., Joyner, L. G., Halenda, P. P. The determination of pore volume and area distributions in porous substances. I. Computations from nitrogen isotherms. Journal of the American Chemical Society (1951), 73, 373-380.

68. http://www-cmls.llnl.gov/?url=about_cmels-print&content=data/pages/science_and_ technology/chemistry/solgel_chemistry.xml. Chemistry, Materials, Earth, and Life Sciences Directorate; 2007.

69. http://irc.nrc-cnrc.gc.ca/index_e.html. National Research Council of Canada; 2007

70. http://www.cartage.org.lb/en/themes/sciences/Chemistry/Electrochemis/Electrochemical/ElectricalDouble/ElectricalDouble.htm; 2003.

71. http://www-biol.paisley.ac.uk/marco/Enzyme_Electrode/Chapter1/Ferrocene_animated _CV1. htm. University of Paisley; 2002.

72. Alden, J. http://compton.chem.ox.ac.uk/john/Thesis/1/1.html. PhD Thesis, Oxford University; 1998.

73. http://www.purdue.edu/REM/rs/sem.htm. Radiological and Enviromental management, Purdue University; 2006.

74. http://www.concrete.cv.ic.ac.uk/durability/research%20techniques%20sem.htm. Concrete Durability Group; 2006.

75. http://serc.carleton.edu/research_education/geochemsheets/BraggsLaw.html. Intergrating research and education; 2008.

76. Sing, K. S. W., Everett, D. H., Haul, R. A. W., Moscou, L., Pierotti, R. A., Rouquerol, J., Siemieniewska, T. Reporting physisorption data for gas/solid systems with special reference to the determination of surface area and porosity (Recommendations 1984). Pure and Applied Chemistry (1985), 57(4), 603-619.

Chapter 3. A Biomimetic, Biodegradable, Biocompatible and Non-Toxic Adhesive

3.1 Introduction and Motivation

Interest in treating wounds and stopping hemorrhage can be dated back to our ancestors. Modern people have continued to refine sutures to its current status, but the search for alternative methods and devices for wound closure continues to evolve. Over the past four decades there has been a tremendous amount of effort in the biomedical industry for the exploration of biodegradable, biocompatible and non-toxic adhesives and glues that could be used as substitutes for sutures, staples and clips. The categories that these adhesives can be divided into are cyanoacrylate adhesives,[1-3] fibrin-based adhesives,[4] proteins,[5] synthetic polymers,[6,7] and cements.[8,9] Non-acrylate adhesives, including fibrin-based adhesives and other synthetic and protein polymers, have become very popular lately. Different products vary in the mechanism and how well they stick, adhere or bond. Unique mechanisms exist for each type of adhesive, but it is not in the purpose of this thesis to get in depth into them. At the present time, no adhesive fulfills all of the criteria of biodegradability, non-toxicity, biocompatibility and adequate adhesiveness in the presence of biological fluids. The formulation of such an ideal adhesive remains a big challenge within the medical and dental community.

This chapter focuses on an effort to synthesize a biomimetic system that contains the same chemical groups as the proteins that are extracted by marine organisms, which are responsible for the characteristic ability of these creatures to stick on various surfaces underwater. The formulation includes the covalent incorporation of diphenolic compounds onto the chitosan polysaccharide backbone to yield a biodegradable, biocompatible and non-toxic adhesive material. The results that are presented in this chapter indicate that these materials are

extremely promising and could potentially replace the use of staples, clips and suture placements that are currently employed in the dental and medical field. Some other formulations along with their synthesis procedures, which have been explored as potential biodegradable adhesives, are presented in Appendix B**.**

3.1.1 Chitosan

Chitosan is a natural polysaccharide that is commercially produced from chitin by deacetylation (**Figure 3-1**). Chitin is a natural biopolymer originating from crustacean shells. It is a long-chain polymer of N-acetyl-glucosamine, a derivative of glucose, and it is found in many places throughout the natural world. It is the main component of cell walls of fungi, of exoskeletons of crustaceans including crabs, lobsters and shrimps, and of insects including ants, beetles and butterflies. It is also found in mollusks and the beaks of the cephalopods, including squids and octopi. Partial deacetylation of chitin gives rise to chitosan, a linear polysaccharide composed of repeating units of D-glucosamine and acetyl-D-glucosamine. The ratio and distribution of acetyl-D-glucosamine residues, as compared to D-glucosamine residues, leads to differing physicochemical properties and biological responses.

Due to its natural abundance and specific biological properties, the applications of chitosan in the biomedical, nutritional and cosmetic care industries are innumerable. Chitosan is biocompatible and shows antimicrobial and antifungic activities, which makes it highly favorable for biomedical applications.[10] It has been proven useful in promoting tissue growth and tissue repair and in accelerating wound-healing and bone regeneration.[11-13] Additionally, chitosan has been incorporated into hydrogels and microspheres with a large potential of creating novel delivery systems.[14-16] Chitosan has a strong positive charge and studies have indicated that

chitosan's charge helps it bind to fats and cholesterol and initiates clotting of red blood cells.[17-19] In addition, chitosan's strong positive charge allows it to bind to negatively charged surfaces such as hair and skin, which makes it a useful ingredient in hair and skin products.[20] Finally, chitosan finds applications in the waste management, water treatment and agricultural industries.[21-24]

As mentioned earlier, chitosan is a linear β-1,4-linked polysaccharide that is obtained by the deacetylation of chitin. Because of the fact that chitin's deacetylation is partial, chitosan is actually a "copolymer" made from glucosamine and *N*-acetyl-glucosamine units. Payne et al. note that the term "chitosan" does not describe a single well-defined structure, but chitosans can have different molecular weights, degree of deacetylation and distribution of the acetylated moieties in the backbone.[25] The unique properties of chitosan are mainly attributed to the free amine groups that are obtained upon deacetylation of chitin and are the ones that affect the solubility, reactivity and functional properties of chitosan (**Scheme 3-1**).

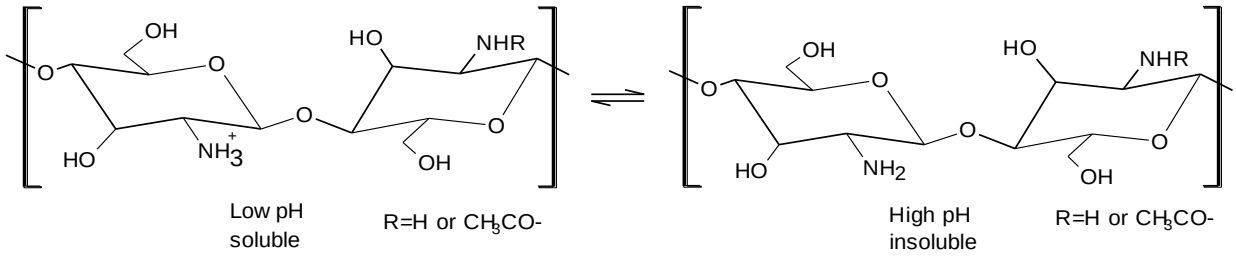

Scheme 3-1. Schematic illustration of repeating units of glucosamine and *N*-acetyl-glucosamine in chitosan.

The degree of deacetylation (DD) is defined as the content of free amino groups in polysaccharides, and can be employed to differentiate between chitin and chitosan.[26] For

example, chitin with a degree of deacetylation of 75 % or above is generally known as chitosan.[27] Deacetylation involves the removal of acetyl groups from the polymeric backbone of chitin, thereby creating a free amino group ($-NH_2$). There exist various methods for the deacetylation of chitin, including hydrolysis either with strong sodium hydroxide solution or with the utilization of enzymes (e.g., chitin deacetylase[28]). Chitosan's versatility depends mainly on this degree of chemically reactive amino groups. Several methods are available to increase or decrease the degree of deacetylation. Increase either of the temperature or the concentration of sodium hydroxide solution, utilized in the process of deacetylation, would increase the amount of acetyl groups removed from chitin. This could result in a range of different chitosan macromolecules with different properties and hence different applications.[29] All of the above suggest that it is of crucial importance to characterize chitosan by determining its degree of deacetylation prior to its utilization for basic or applied research.[30] The degree of deacetylation (DD) of the chitosans used during this research have been calculated from the integration of the appropriate peaks of the respective ^{1}H-NMR spectra as will be explained in later sections.

3.1.2 Adhesive Proteins

It is well known that marine organisms, such as barnacles and mollusks, adhere themselves onto wet surfaces, such as rocks, stones and other. The past twenty five years extensive scientific research has been devoted to understand and explain the mechanism and the molecular interactions that rely behind this adhesiveness.[31-32] This led to the very interesting discovery that some proteins with specific chemical groups that are extracted by these organisms are responsible for this characteristic ability of these creatures to stick on various surfaces underwater.[33-39] Accordingly, a biomimetic system that would contain the structural moieties

present in the aminoacids that confer adhesiveness to the mollusk proteins could be a key aspect towards the goal of the formulation of a biocompatible, biodegradable, non-toxic and versatile glue that could provide adhesiveness on a diversity of wet surfaces. One such approach would be to attach the key molecular features present in the proteins to the backbone of a biodegradable, biocompatible and nontoxic polymeric backbone

The research in this field has revealed that the curing of the marine adhesive proteins occurs possibly through the quinone equivalent of the polyphenolic groups that they contain.[38] Most studies have indicated that one of the characteristics of these marine adhesive proteins is the presence of the amino acid L-3,4-dihydroxyphenylalanine (DOPA), which is believed to play an important role in the bonding of these creatures onto wet surfaces.[39] The exact mechanism behind this adhesiveness remains still a point of study.[40-42] Following the polyphenolic hypothesis, several research groups have incorporated DOPA, or other compounds that contain the same functional groups, onto the backbone of polymeric materials, and have found that the adhesive properties of the obtained materials have improved.[43-48] Moreover, other researchers have studied the rheological properties of chitosan solutions upon addition of diphenolic compounds and enzymes, which promote the oxidation to quinone structures, and which could lead to water-resistant adhesives.[49,50]

In this chapter, the modification of chitosan via amide formation with 3,4-dihydroxybenzoic acid (DHBA) to yield a biodegradable, biocompatible and non-toxic adhesive material is presented. The aim was to make a biodegradable adhesive product that would find applications in the dental and biomedical industry. The tensile and shear adhesive strengths of these materials have been tested on various surfaces including porcine skin and beef bone. This

was done in order to create a controlled environment that would simulate the surfaces on which these materials are intended to be used. Adhesiveness was achieved without added enzymes or oxidants. Infrared spectroscopy (IR), nuclear magnetic resonance spectroscopy (NMR) and ultraviolet-visible spectroscopy (UV) have been used in order to qualitatively and quantitatively establish the amount of the diphenolic moiety present on the backbone of the biodegradable polymer. Degradation studies indicate that the degradation rate is dependent on the molar ratio of the dihydroxybenzoic groups to chitosan.

3.2 Experimental Section

3.2.1 Materials

Chitosan of high, medium and low molecular weight (Brookfield viscosity = 800,000 cps, 200,000 cps and 20,000 cps, respectively), N-(3-dimethylaminopropyl)-N'-ethylcarbodiimide hydrochloride (EDC, commercial grade) and N-hydroxysuccinimide (NHS, 98%) were purchased from Sigma Aldrich. 3,4-Dihydroxy benzoic acid (DHBA, 98%), 2,5-dihydroxybenzoic acid (98%) and 3,4,5-trihydroxybenzoic acid (THBA, 99%) were purchased from TCI America. Acetic acid (reagent grade) was purchased from Corco Corporation. All chemicals were used as received. The degree of deacetylation (DD) of the chitosans used, as calculated from their ^{1}H-NMR spectra, was 72, 78 and 65 for high, medium and low molecular weight chitosans, respectively.[51] For the mechanical testing, beef jaw bone and pork were bought from a local slaughter house.

3.2.2 Synthetic Procedures

A schematic illustration of the synthesis procedure is given in **Scheme 3-2.** First, a desired amount of chitosan was dissolved in 1 wt% acetic acid in H_2O (*sol* A) in a single-neck

round bottom flask. Specific amounts of EDC, NHS and DHBA were then charged in a small vial, that contained 1 wt% acetic acid in water, and stirred for 5 minutes until full dissolution (*sol* B). *Sol B* was then added drop-wise into *sol A* and the obtained solution was stirred for 24 hr at room temperature. Several different mole ratios of chitosan, DHBA, EDC and NHS have been tried in order to find the optimum reactant ratio that gives the highest yield of DHBA grafting onto the chitosan polymeric backbone. As an example of a typical procedure (sample DHBA-Ch-1 from **Table 3-1**), 0.2 g of chitosan was dissolved in 20 ml of 1 wt% acetic acid in H_2O (*sol* A) in a 50-ml single-neck round bottom flask. 0.096 g of DHBA, 0.12 g of EDC and 0.02 g of NHS were then charged in another vial, which contained 10 ml of 1 wt% acetic acid in distilled water, and stirred for 5 minutes until full dissolution (*sol* B). *Sol B* was then added drop-wise into *sol A*, and the obtained mixture was stirred for 24 hr at room temperature. For this example, the mole feeding ratio of Chitosan/DHBA is equal to 2, based on the repeating unit of chitosan (molecular weight of the repeating unit ~157 amu). EDC and NHS have been used as the activating agents for the amide bond formation.[52] The modified chitosan was recovered with the addition of a large amount of acetone. After filtration, washing with copious amounts of acetone and drying under continuous flow of nitrogen, the materials were stored under a nitrogen atmosphere. Soxhlet extraction with acetone for 24 hours was used to further wash the material from potential impurities and/or any unreacted compounds.

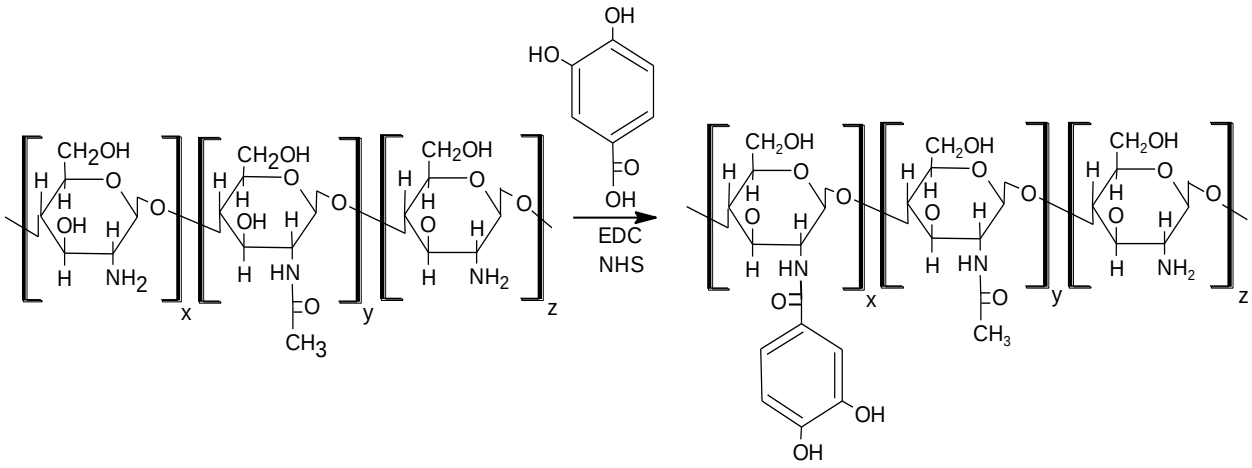

Scheme 3-2. Synthesis procedure of chitosan modified with 3,4-dihydroxybenzoic acid. Parameters x, y, and z depend on the degree of deacetylation of chitosan and the yield of the reaction.

In order to make a comparative study and verify the adhesive capabilities that the diphenolic moieties impart to the modified chitosan, some additional synthesis procedures of modified chitosans, with other diphenolic compounds, also have been conducted. These include the modification of chitosan with 2,5-dihydroxybenzoic acid and 3,4,5-trihydroxybenzoic acid (THBA). The synthesis procedure followed was the same as the one used to modify chitosan with 3,4-dihydroxybenzoic, as described above. As a typical procedure for the synthesis of a THBA-modified chitosan (sample THBA-Ch from **Table 3-1**), 0.2 g of chitosan was dissolved in 10 ml of 1 wt% acetic acid in H_2O (*sol* A) in a 50-ml single-neck round bottom flask. 0.108 g of THBA, 0.12 g of EDC and 0.02 g of NHS were then charged in another vial that contained 10 ml of 1 wt% acetic acid in distilled water and stirred for 5 minutes until full dissolution (*sol* B). *Sol B* was then added drop-wise into *sol A*, and the obtained solution was stirred for 24 hr at room temperature. The mole feeding ratio of repeating unit of chitosan to THBA for the above

example is equal to 2. The modified chitosan was precipitated as solid with the addition of a large amount of acetone. After filtration, washing with copious amounts of acetone and drying under continuous flow of nitrogen, the materials were stored under a nitrogen atmosphere. Soxhlet extraction with acetone for 24 hours was used to further wash the material from potential impurities and/or any unreacted compounds. For the modification of chitosan by 2,5-dihydroxybenzoic acid a similar synthesis procedure has been followed.

3.2.3 Instrumentation and Methods

3.2.3.1 Spectroscopic Methods

An ATR Perkin Elmer (Spectrum 1) spectrometer was employed for the IR measurements of all samples. Each IR spectrum was acquired with the accumulation of 30 scans at a scan resolution of 4 cm^{-1} between 800 and 4000 cm^{-1}. The polymeric material was pressurized with a glass slide on top of the quartz window of the ATR instrument. ^{1}H-NMR spectra of the modified chitosans were obtained with an Oxford NMR instrument at 500 MHz at room temperature using 1% deuterated acetic acid in D_2O as solvent. Feed compositions of DHBA in chitosan were calculated from the integration of the appropriate peaks.[18] UV-vis spectra measurements were done on a Perkin Elmer Lambda 35 UV-VIS spectrometer. The slit width of the detector was 1 nm and the scan speed used was 480 nm/min. Absorption was recorded between 300 nm and 900 nm.

3.2.3.2 Mechanical Testing

For the evaluation of the adhesive properties of the as-synthesized materials, an Instron instrument (model: 8872) was used for all tests. Tensile strength testing was performed on beef bone surfaces. Shear testing was employed for the evaluation of the ability of the biodegradable

materials to adhere two porcine skin surfaces together or a filter paper on a beef bone surface. For the tensile strength tests, the bone specimens were cut according to the ASTM standards for measuring the tensile strength of adhesives by means of bars or rod specimens (ASTM designation: D 2095-92). The specific dimensions of the substrates used can be seen in **Figure 3-2**. Prior to testing, 200 mg of the dry polymeric materials were added in 1 ml of de-ionized water and mixed with a spatula until a viscous homogeneous paste was obtained. The adhesive material was then applied on both of the two surfaces to be examined. In order to set the adhesive, a maximum compression force of 0.1 MPa, between the two joints, was applied. The strain rate used for tensile strength experiments was 2 mm/min. The tensile strength was calculated as the maximum load divided by the bond area (i.e. 12 mm x 12 mm) in mega-Pascals (MPa). Three tests were performed for each sample, and the average of these values is reported with the appropriate standard deviations on the graphs. Unless otherwise indicated, the curing time of the adhesive materials for the tensile strength experiments was 5 min. The surface of the bone specimens was washed with copious amounts of distilled water before each test.

Shear strength experiments were performed to evaluate the efficiency of the as-synthesized modified chitosans to adhere two porcine skin surfaces together. Porcine skin was used because of the similarity of its physical properties to human tissue. For the shear strength tests the substrates used followed the ASTM standards for measuring the strength properties of tissue adhesives in lap-shear by tension loading (designation: F 2255-05). The specific dimensions of them can be seen in **Figure 3-3**. Pork was bought from a local slaughterhouse and thin strips of skin (approximately 15 x 4 cm) were cut from the hide and scrubbed thoroughly with warm water. A razor was used to remove the hair that resided on one side of the skin, and

Super Glue® (Pacific World Corp., Lake Forest, Ca) was used to attach that side on the surface of aluminum metal substrates that were used for these shear tests (**Figure 3-3**). The extra skin that was extending beyond the surface of the substrate was cut with a razor to the final dimensions of 2.5 cm x 2.5 cm. The average thickness of the porcine skin sample was about 2.5 mm. While not in use, the pork skin was immersed in a PBS buffer solution (pH = 7.4 at 24 ^{o}C).

Prior to testing, 200 mg of the as-synthesized modified polysaccharides were added in 1 ml of de-ionized water and mixed with a spatula until a viscous homogeneous paste was obtained. The viscous mixture containing the adhesive material was casted on both of the two porcine skin surfaces which were then brought in contact. In order to set the adhesive, a weight of 500 g was placed on top of the aluminum surfaces directly over the surface of interest (e.g. where the two porcine skin surfaces overlap). The strain rate, used for the shear tests experiments, was 1 mm/min. The shear strength was calculated as the maximum load divided by the bond area (i.e., 25 mm x 10 mm) in mega-Pascals (MPa). Three tests were performed for each sample and the average mean values along with their standard deviations are presented. Unless otherwise indicated, curing time for shear tests was 30 minutes.

In addition to the above mechanical tests, the evaluation of the efficiency of the as-synthesized bioadhesives to adhere filter paper (P8, coarse porosity, Fisher scientific) on pork bone has also been conducted by shear testing. The reason for this study is that the modified chitosan might find applications in dentistry, when bone loss in the jaws, as a result of periodontal disease, trauma, tooth loss, endodentic failures or tooth fractures, occurs. Generally, bone grafting, using natural or synthetic bone, is used to augment this lost bone. A membrane, either resorbable or non-resorbable, is used to cover the graft and to prevent cells other than bone

cells from entering the site. This modified chitosan might be a means of stabilizing this membrane during mucosal suturing, thus ensuring proper healing of the tissue. This may involve the application of this biodegradable, biocompatible and non-toxic adhesive material between the membrane and the bone to ensure that the membrane stays in the desired position while covering the bone graft. Due to the limited access to such membranes, it was impossible to perform the shear tests on these membranes. The similarity in porosity and texture of the filter paper and these dental membranes, though, suggests that the evaluation of adhesion that this material confers between the filter paper and the beef bone is a means of predicting the efficiency of this adhesive to bond the dental membranes with bone. The specific dimensions of the substrates used for this shear testing, followed the ASTM standards for strength properties of tissue adhesives in lap-shear by tension loading (designation: F 2255-05), and can be seen in **Figure 3-4.** The average thickness of the filter paper sample was about 0.5 mm. Super Glue® (Pacific World Corp., Lake Forest, Ca) was used to attach one side of the filter paper on the surface of the aluminum metal substrates that were used for shear testing (**Figure 3-4**). 200 mg of the as-synthesized modified polysaccharides were again mixed with 1 ml of de-ionized water. The viscous mixture, containing the adhesive material, was casted on both of the two surfaces of interest. In order to set the adhesive, a weight of 500 g was placed on top of the aluminum surfaces directly over the surface of interest (e.g. the filter paper-bone interface). The shear strength was again calculated as the maximum load divided by the bond area (i.e., 2.5 cm x 1 cm) in mega-Pascals (MPa). Three tests were performed for each sample, and the average of these values is reported with the appropriate standard deviations. Curing time of the adhesive materials for these shear tests was again 30 minutes.

3.2.3.3 Degradation Studies

Experiments for the hydrolytic degradation of the biodegradable materials were carried out in phosphate buffer solutions (PBS, pH=7.4 at 24 ^{o}C).[39] A weighted amount of the material (e.g., 0.01 g) was immersed in 10 ml of the buffer solution, and the vial was kept in an air oven at 37 ^{o}C. At predetermined times, acetone was added, resulting in the precipitation of the modified polysaccharides. After filtering and drying the material under a stream of nitrogen, weight loss was examined gravimetrically by measuring the remaining weight. Each experiment was repeated twice and the values are expressed as average values.

3.3 Results and Discussion

3.3.1 Synthesis and Characterization of Modified Chitosans

Chitosans of high, medium and low molecular weight, as defined by Aldrich by their Brookfield viscosity of 800,000 cps, 200,000 cps and 20,000 cps, respectively, were used for this study. A series of modified chitosans with different molecular weights and different compositions, have been synthesized. Different feeding ratios of DHBA, as compared to chitosan's repeating unit, have been investigated, and the obtained materials showed dependence of their adhesiveness and physical properties on the amount of diphenolic groups grafted onto chitosan. Generally, modified chitosans of low molecular weight present poor adhesive properties, whereas modified chitosans of high and medium molecular weight showed almost the same results.

3.3.2 ^{1}H-NMR Spectroscopy

A representative ^{1}H-NMR spectrum of pure chitosan of medium molecular weight, along with the peak assignments, can be seen in **Figure 3-5.** The proton assignment of chitosan is as

follows: δ 2.0-2.1 (br m, 3 H, acetyl group of chitosan), δ 3.1 (s, 1 H, H-2 of GlcN residue), δ 3.4-3.8 (m, 6 H, H-2', 3, 4, 5, 6, 6' of chitosan), δ 3.9-4.1 (s, 1H, H-1 of chitosan). The degree of deacetylation (DD) of chitosans can be calculated from their ^{1}H-NMR spectra according to the following equation:[53]

$$D_{deac} = \{1 - \left(\frac{\frac{1}{3}\ signal\ intensity\ due\ to\ acetyl\ group}{\frac{1}{6}\ signal\ intensity\ due\ to\ H-2,3,4,5,6,6'} \right) x\ 100$$

The DD of the chitosans used during this research, as calculated from the integration of the appropriate peaks of their ^{1}H-NMR spectra, was 72, 78 and 65 for high, medium and low molecular weight chitosans respectively.

The molar ratio compositions of the feeding materials and of the final products, as calculated from ^{1}H-NMR, for medium molecular weight chitosans are summarized in **Table 3-1**. A representative ^{1}H-NMR spectrum of a modified chitosan (sample DHBA-Ch-1) of theoretical molar feeding ratio of Chitosan/DHBA= 2 with regards to the repeating unit of chitosan, with the assigned NMR peaks is shown in **Figure 3-6**. The proton assignment is as follows: δ 2.0-2.1 (br m, 3 H, acetyl group of chitosan), δ 3.1 (s, 1 H, H-2 of GlcN residue), δ 3.4-3.8 (m, 6 H, H-2', 3, 4, 5, 6, 6' of chitosan), δ 3.9-4.1 (s, 1H, H-1 of chitosan), δ 7.5-8.0 (m, 3H, H-arom. from DHBA). The quantitative determination of the experimental degree of substitution of DHBA on the modified chitosan was calculated by the following equation: [18,54]

$$DHBA\%(mole) = \frac{[1_{(c-2)}x(signal\ intensity\ due\ to\ aromatic\ H)]}{[3_{(arom)}x(signal\ intensity\ due\ to\ H-2)]}x100\%$$

3.3.3 FT-IR Spectroscopy

FT-IR spectra of pure chitosan, DHBA and modified chitosan (DHBA-Ch-1) in 1 wt% of acetic acid solution can be seen in **Figure 3-7**. Chitosan was found to exhibit characteristic absorptions at 1649 cm^{-1} and 1588 cm^{-1}, which are attributed to the N-H bending vibration of primary amines and to the presence of acetylated groups, respectively.[55] The other characteristic peaks of the saccharide structure of chitosan appear at 1154 cm^{-1}, 1082 cm^{-1} and 1032 cm^{-1}.[56] The spectrum of DHBA shows the characteristic carboxyl peak at 1664 cm^{-1}, whereas in the spectrum of the modified chitosan there is no peak corresponding to the carboxyl group of the DHBA due to the amide bond formation between DHBA and the amine group of chitosan. The prominent peaks at 1642 and 1552 cm^{-1}, which are observed in the IR of the modified chitosan are assigned to the carbonyl stretching vibration of amides (amide I) and the carbonyl bending vibration of amides (amide II).[57] These findings illustrate the conformational changes that chitosan experienced after the reaction with DHBA.

3.3.4 Ultraviolet-Visible Spectroscopy (UV-vis)

The UV-vis spectra of DHBA and of pure and modified chitosan (sample DHBA-Ch-1) in 1 wt% acetic acid solution, with and without the addition of H_2O_2, can be seen in **Figure 3-8.** H_2O_2 was added in order to investigate the effect that oxidation, with a strong oxidizer, has on the visible spectrum and color of the modified chitosan. 100 mg of the compound to be tested were dissolved in 3 ml of 1% acetic acid in distilled water. The obtained absorbance spectra, for

all of the compounds tested, correspond well to previously published data.[58] Pure chitosan shows no absorption peaks in this wavelength range from 200 nm to 800 nm. On the other hand, in the spectrum of DHBA the characteristic absorbance peaks of diphenolic compounds can be seen. 2 peaks, at around 270 nm and 300 nm, which correspond to the diphenolic structure and to quinone structures respectively, are observed. The same absorption peaks can be seen in the UV spectrum of modified chitosan, without the addition of H_2O_2. This is justified by the fact that the structural moieties of DHBA for absorption in the UV-visible range are also present in modified chitosan. In addition, when modified chitosan was treated with H_2O_2 (6 wt%), a weak broad absorption peak at around 400 nm, which has been attributed by many researchers to oxidation products of the quinone structures, is starting to evolve.[42,59] It is noteworthy that the solutions of modified chitosan would change from colorless to yellowish red with time, which is attributed to the so called "quinone-tanning" that is observed upon oxidation of this type of diphenolic compounds.[60] This darkening of the modified chitosans was reasonably much faster when H_2O_2 was added.

3.3.5 Mechanical Testing

3.3.5.1 Tensile Strength Tests

Prior to testing, the dry polymeric materials were blended with deionized water, at a concentration of 200 mg in 1 ml, and mixed with a spatula until a viscous homogeneous paste was obtained. Within about 1-2 minutes, the adhesive material was applied on both of the two surfaces to be examined. In order to set the adhesive, a maximum compression force of 0.1 MPa between the two joints was applied for the tensile tests. If not specified, the time period between application of the adhesives and mechanical testing was 5 min at room temperature. The

mechanical testing results for the tensile loading are summarized in **Figure 3-9**. As can be seen from that figure, different molecular weight chitosans do not have much difference in the values obtained, when one is to compare the high with the medium molecular weight modified chitosans. Modified chitosan of low molecular weight though gave adhesive values substantially lower. This may be attributed to the decreased intermolecular cohesion of the low molecular weight materials. The obtained results indicate that the amount of DHBA present in the polysaccharic backbone has a profound effect on the adhesiveness of the bulk material. The mean values ranged from 0.55 MPa when substitution of DHBA was 27 mol % (**Figure 3-9, 1:2** or sample DHBA-Ch-1 from **Table 3-1**) to 0.19 MPa when substitution of DHBA was 4 mol % (**Figure 3-9, 1:10** or sample DHBA-Ch-2 from **Table 3-1**). As shown in the same figure, pure chitosans give poor tensile strength values on bone surfaces. This indicates that DHBA, and more specifically the phenolic groups of this compound, impart adhesive properties to the polysaccharide of chitosan and are responsible for the chemisorption to the surfaces and the crosslinking of the material. The tensile load, with respect to the curing time, of a modified chitosan sample (DHBA-Ch-1) is presented in **Figure 3-10**. As one would assume, higher curing times of the modified chitosan lead to higher intramolecular and intermolecular crosslinking density, which subsequently results in higher values of adhesive strength. In the same figure, the dependence of tensile strength on the curing time for pure chitosan is also given. The tensile load of pure chitosan increases as well by time, though not significantly enough. This increase of tensile strength of pure chitosan may be attributed to the formation of a dried thin film.

To further support the above findings, the adhesive capabilities of the as-synthesized modified chitosans were tested on bone surfaces, upon addition of a small amount of hydrogen

peroxide (H_2O_2) solution. This was done in order to further verify that the adhesive ability of the modified chitosans should be attributed to the diphenolic groups, which are readily oxidized by air to highly reactive quinone structures. H_2O_2 is a strong oxidizer and thus will result in the faster oxidation of the diphenolic groups of DHBA to highly reactive quinones. For these experiments, 1 part of H_2O_2 (30 w/w aqueous solution) was mixed with 4 parts of 1 wt% acetic acid aqueous solution. 200 mg of modified chitosan were mixed with 1 ml of the above mixture, with a spatula until a viscous homogeneous paste was obtained. The viscous suspension was then applied on both of the two beef bone surfaces at room temperature. In order to set the adhesive, a maximum compression force of 0.1 MPa between the two joints was applied. Interestingly, the adhesion of modified chitosan increases upon addition of H_2O_2. Thus, samples DHBA-Ch-1 and DHBA-Ch-2 from **Table 3-1** show maximum tensile loads of 0.64 MPa and 0.60 MPa, respectively, when the solvent that was used for "wetting" contained H_2O_2. On the other hand, when the materials were dissolved in 1 wt% acetic acid aqueous solutions the observed maximum tensile loads were 0.51 MPa and 0.54 MPa for samples DHBA-Ch-1 and DHBA-Ch-2, respectively (**Table 3-2**). These findings further support that the adhesive ability of the as-synthesized modified chitosans probably originates from the diphenolic groups of DHBA, which are readily oxidized by air to highly reactive quinone structures, as many other researchers have indicated.[43, 44, 47]

Tensile strength measurements of modified chitosan with 2,5-dihydroxybenzoic acid and 3,4,5-trihydroxybenzoic acid (THBA) have also been conducted to further investigate this phenomenon. THBA-modified chitosan (sample THBA-Ch from **Table 3-2**) shows maximum tensile load strength equal to 0.47 MPa, which is comparable to the loads obtained for DHBA-

modified chitosans. This adhesive capability of THBA-modified chitosan may be attributed to the three hydroxyl groups of THBA and may also be oxidized to quinone structures similar to the ones obtained upon oxidation of DHBA. In addition, chitosan modified with 2,5-dihydroxybenzoic acid (sample 2,5-DHBA-Ch from **Table 3-2**) show maximum tensile load of 0.38 MPa. The tensile strength results for chitosan modified with 2,5-dihydroxybenzoic acid further suggest that the diphenolic structure is the one that imparts adhesive capabilities in the modified chitosan. All of the tensile strength experimental results are summarized in **Table 3-2**.

3.3.5.2 Shear Strength Tests

Shear test results of the modified chitosans between two porcine skin surfaces are summarized in **Table 3-2**. 200 mg of the respective modified polysaccharic adhesive were mixed with 1 ml of deionized water with a spatula until a viscous homogeneous paste was obtained. Within about 1-2 min, the adhesive material was applied on both of the surfaces of interest, which were brought in contact. In order to set the adhesive, a weight of 500 g was placed on top of the aluminum surfaces directly over the surface of interest (e.g., where the two porcine skin surfaces overlap). Adhesives were let to cure for 30 minutes at room temperature before the shear testing experiments. Samples tested include medium molecular weight chitosan, modified with 3,4-dihydroxybenzoic acid, at a theoretical feeding molar ratio of repeating unit of chitosan to DHBA equal to 2, 4 and 10, respectively. The products from the reaction of chitosan with 3,4,5-trihydroxybenzoic acid and with 2,5-dihydroxybenzoic acid, at a feeding molar ratio of repeating unit of chitosan to phenolic compound of 2:1, have been also evaluated for their adhesiveness on porcine skin. As shown in **Table 3-2**, all of these values were substantially lower than the tensile strength results on bone surfaces. This may be attributed to the moisture

that is present between the overlapping porcine skin surfaces, which is difficult to remove. This consequently makes the complete curing of the applied bioadhesive practically impossible. Nevertheless, the amount of DHBA grafted on the polysaccharic backbone has again a profound effect on the adhesiveness of the modified chitosans. The mean values ranged from 0.10 MPa when substitution with DHBA was 27 mol % (DHBA-Ch-1 from **Table 3-2**) to 0.02 MPa when substitution with DHBA was 4 mol % (DHBA-Ch-2 from **Table 3-2**). This is another justification that DHBA, and more specifically the phenolic groups of this compound, impart adhesive properties to the polysaccharide of chitosan. The shear test results obtained for modified chitosans with 2,5-dihydroxybenzoic acid and THBA are also given in the same table.

As mentioned earlier, evaluation of the efficiency of the as-synthesized bioadhesives to adhere filter paper on beef bone has been also conducted by shear testing. For these tests, 200 mg of the as-synthesized modified polysaccharides were again mixed with 1 ml of de-ionized water. The viscous mixture containing the adhesive material was cast on both of the two surfaces of interest, namely the beef bone and the filter paper surface, which were then brought in contact. In order to set the adhesive, a weight of 500 g was placed on top of the aluminum surfaces directly over the overlapping surface between the filter paper and the bone. Adhesives were let to cure for 30 min at room temperature before shear test experiments. Samples tested include medium molecular weight chitosan modified with 3,4-dihydroxybenzoic acid in a theoretical feeding molar ratio of repeating unit of chitosan to DHBA equal to 2:1, 4:1 and 10:1. The products from the reaction of chitosan with 3,4,5-trihydroxybenzoic acid and 2,5-dihydroxybenzoic acid, at a feeding molar ratio of repeating unit of chitosan to phenolic compound of 2:1, have also been evaluated for their effectiveness of adhering filter paper on bone. The results from these shear

strength tests are summarized in **Table 3-2**. DHBA-Ch-1, which has a molar ratio substitution of DHBA to chitosan equal to 27 mol %, shows a maximum shear load of 0.21 MPa, while DHBA-Ch-2, which has a molar ratio substitution of DHBA to chitosan equal to 19 mol %, shows a maximum shear load of 0.17 MPa. These results suggest again that the amount of DHBA grafted on the polysaccharic backbone has a profound effect on the adhesiveness of the final product. Low values obtained from pure chitosan's shear testing further prove that DHBA, and more specifically, the phenolic groups of this compound impart adhesive properties to the polysaccharide of chitosan. The shear test results obtained for modified chitosans with 2,5-dihydroxybenzoic acid and THBA are also shown in the same table. Again, the quinone structures that are formed upon oxidation of the diphenolic groups that all of these modified chitosans contain seem to play a key role in their adhesive capabilities.

3.3.6 Degradation Studies

Experiments for the hydrolytic degradation of the materials were carried out in phosphate buffer solutions (PBS, pH = 7.4 at 24 ^{o}C). A weighted amount of the material (0.01 g) was immersed in 10 ml of the buffer solution and the vial was kept in an air oven at 37 ^{o}C. Acetone was added in predetermined periods of time, resulting in the precipitation of the product. After filtering and drying of the material under a stream of nitrogen, weight loss was examined gravimetrically, by measuring the remaining weight. Each experiment was repeated twice and the values are expressed as average values. The percentage of degradation as a function of time can be seen in **Figure 3-11**. From this figure, degradation seems to be faster initially. All of the samples tested experienced dramatic weight loss during the first 3-4 days. Additionally, it seems that the degradation rate depends on the amount of the dihydroxybenzoic acid group grafted onto

the chitosan backbone. Thus, a 27 mol % substitution of DHBA with regards to the chitosan repeating unit (DHBA-Ch-1) leads to a weight loss of 9 % of the original weight (w/w) after three days in a PBS buffer solution at 37 ^{o}C. On the other hand, a 4 mol % substitution of DHBA with regards to the chitosan repeating unit (DHBA-Ch-3) shows a weight loss of 17 % of the original weight (w/w) after three days. This suggests that the higher the content of DHBA in the polysaccharic backbone of chitosan, the slower the hydrolytic degradation becomes. This may be attributed to the hydrophobic nature of the dihydroxybenzoic acid moiety and/or the crosslinking between different polymeric chains that the diphenolic moieties promote.

3.4 Several Considerations

The majority of the previous work, presented by other research groups, that focused on synthesizing biomimetic polymeric materials for applications as bone and/or tissue adhesives, typically employed oxidizing agents or enzymes in order to promote the quinone structure.[41,49] Other studies, though, have shown that although these oxidizing agents improve the cross-linking ability, they might also reduce the adhesive property of these polymers, especially if used in high concentrations.[61,62] The ability of the modified chitosans to adhere on a variety of other surfaces, including metal, glass and plastic, has been also tested in our study. These tests were informal and the obtained results are only empirical. Nevertheless, it was found that metal surfaces including Al, Pt and Fe, formed the strongest bonding, then glass surfaces and lastly plastic surfaces. Several mechanisms have been proposed for these phenomena but unfortunately very few have been verified.[18] Nevertheless, the highly reactive o-quinones that result from the oxidation of the phenolic groups present in DHBA by oxygen of air seem to play an important role in the crosslinking and the surface adhesion of the obtained materials (**Scheme 3-3**).

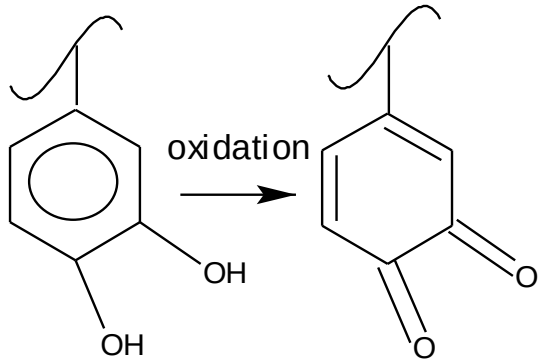

Scheme 3-3. The oxidation of the diphenolic groups to highly reactive o-quinones seems to play a crucial role in the intramolecular and intermolecular crosslinking, and the adhesion to various surfaces.

3.5 Conclusions

In this work, a series of modified chitosans have been synthesized by a simple method in an effort to create a biodegradable, biocompatible and non-toxic adhesive that mimics marine adhesive proteins. The adhesive strength of these materials varies with the molecular weight of the polysaccharide, the amount of diphenolics present and the curing time. Adhesiveness was achieved without added enzymes or oxidants. Infrared spectroscopy (IR), nuclear magnetic resonance spectroscopy (NMR) and ultraviolet-visible spectroscopy (UV) were used in order to qualitatively and quantitatively establish the amount of the diphenolic moiety present on the backbone of the biodegradable polymer. Degradation studies indicate that the degradation rate depends on the diphenolic moiety present on the biodegradable backbone. Bearing in mind that chitosan itself has been used in a number of applications as a wound dressing material, the as-synthesized polymers combine both the adhesive capability of the diphenolic function and the

healing effect of chitosan. The biocompatibility and biodegradability of these modified chitosans, offer the promise of utility of these materials in the form of novel dental and medical devices.

3.6 Acknowledgements

I would like to express my gratitude to Dr. Jack Baldwin, Dr. David Soll, Dr. Cyrial Evian, Dr. Shuxi Li and Dr. Zhongtao Zhang for their assistance and valuable suggestions in this work. I especially want to express my thankfulness to Dr. Palmese from the Chemical Engineering Department of Drexel University for the use of the Instron instrument and to Dr. Geng for his non-stop assistance and effort to facilitate the usage of that instrument. This work was supported by the National Institutes of Health (NIH No. DE09848).

Table 3-1. Comparison of the theoretical and the experimental degree of chitosan substitution with DHBA. Medium molecular weight chitosan was used for these experiments.

Sample code	Substitution targeted[a]	Substitution obtained[b]
DHBA-Ch-1	50%	27%
DHBA-Ch-2	25%	19%
DHBA-Ch-3	10%	4%

[a] With respect to the theoretical mole feeding compositions of reactants.

[b] As calculated by the integration of the appropriate ^{1}H-NMR peaks.

Table 3-2. Tensile and shear strength results of modified chitosans on a variety of surfaces. Three tests were performed for each sample and the average of these values is reported with the appropriate standard deviations.

Sample	Wetting solvent	Tensile strength[a]	Shear strength[b]	
		Maximum load between two beef bone surfaces (MPa)	Maximum load between two porcine skin surfaces (MPa)	Maximum load between filter paper and beef bone (MPa)
DHBA-Ch-1	**De-ionized water**	0.51 ± 0.07	0.10 ± 0.04	0.21 ± 0.05
DHBA-Ch-2	**De-ionized water**	0.54 ± 0.04	0.08 ± 0.02	0.17 ± 0.03
DHBA-Ch-3	**De-ionized water**	0.23 ± 0.02	0.02 ± 0.01	0.09 ± 0.02
DHBA-Ch-1	**6 wt% H_2O_2 in de-ionized water**	0.64 ± 0.06	-	-
DHBA-Ch-2	**6 wt% H_2O_2 in de-ionized water**	0.60 ± 0.09	-	-
THBA-Ch	**De-ionized water**	0.47 ± 0.03	0.07 ± 0.02	0.14 ± 0.04
2,5-DHBA-Ch	**De-ionized water**	0.38 ± 0.01	0.05 ± 0.01	0.09 ± 0.01
Chitosan (Medium MW)	**De-ionized water**	0.11 ± 0.02	-	0.02 ± 0.01
Chitosan (Medium MW)	**6 wt% H_2O_2 in de-ionized water**	0.10 ± 0.02	-	0.02 ± 0.01

[a] Tensile strength (MPa) was calculated as the maximum load divided by the bond area (i.e., 12 mm x 12 mm). Curing time of the adhesive materials was 5 minutes. The surface of the bone specimens was washed with copious amounts of distilled water before each test.

[b] Shear strength (MPa) was calculated as the maximum load divided by the bond area (i.e., 25 mm x 10 mm). Curing time of the adhesive materials was 30 min.

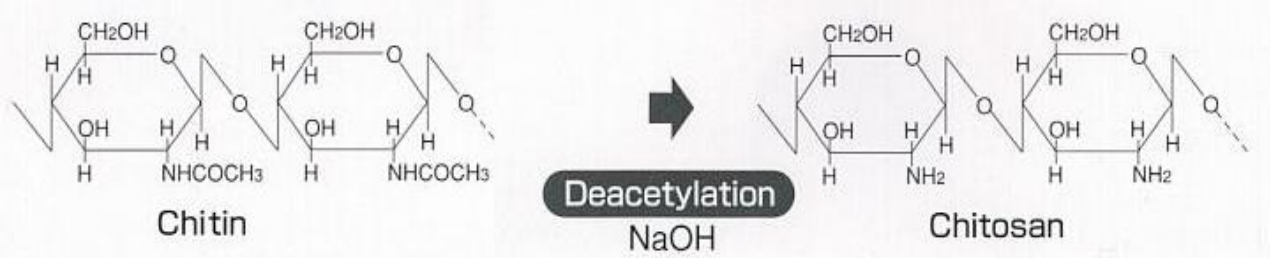

Figure 3-1. Deacetylation of chitin produces chitosan.[63] In this example, deacetylation of chitin is assumed to be 100 %.

(a)

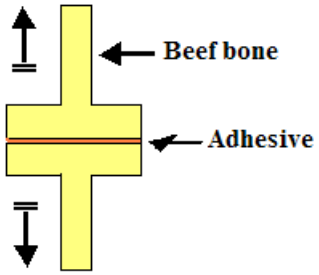

(b)

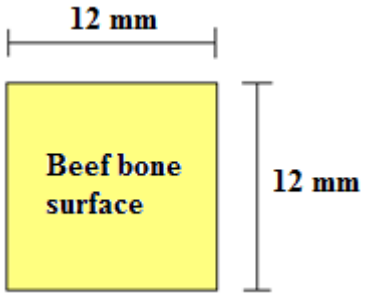

Figure 3-2. Schematics (a: perpendicular view, b: top view) illustrate the beef bone substrate that was used for the tensile tests. Bone specimens were cut according to the ASTM standards for measuring the tensile strength of adhesives by means of bars or rod specimens (D 2095-92). The surface of the beef bone specimens was washed with copious amounts of distilled water before each use.

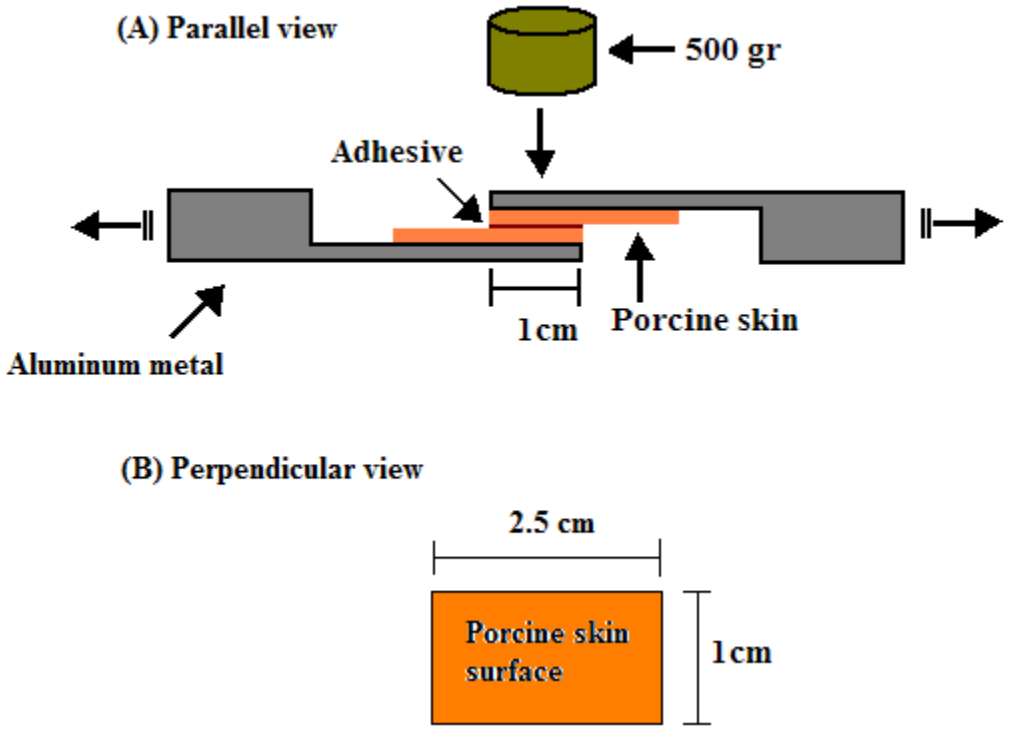

Figure 3-3. Schematics (A: parallel view, B: perpendicular view) illustrate the porcine skin substrates that were used for the shear tests. Prior to testing, the dry polymeric material was mixed with de-ionized water in a ratio of 200 mg to 1 ml and mixed with a spatula until a viscous homogeneous paste was obtained. The adhesive material was then applied on both of the two surfaces to be examined. The average thickness of the porcine skin sample was about 2.5 mm. While not in use, the pork skin was immersed in a PBS buffer solution (ph=7.4 at 24 ^{o}C).

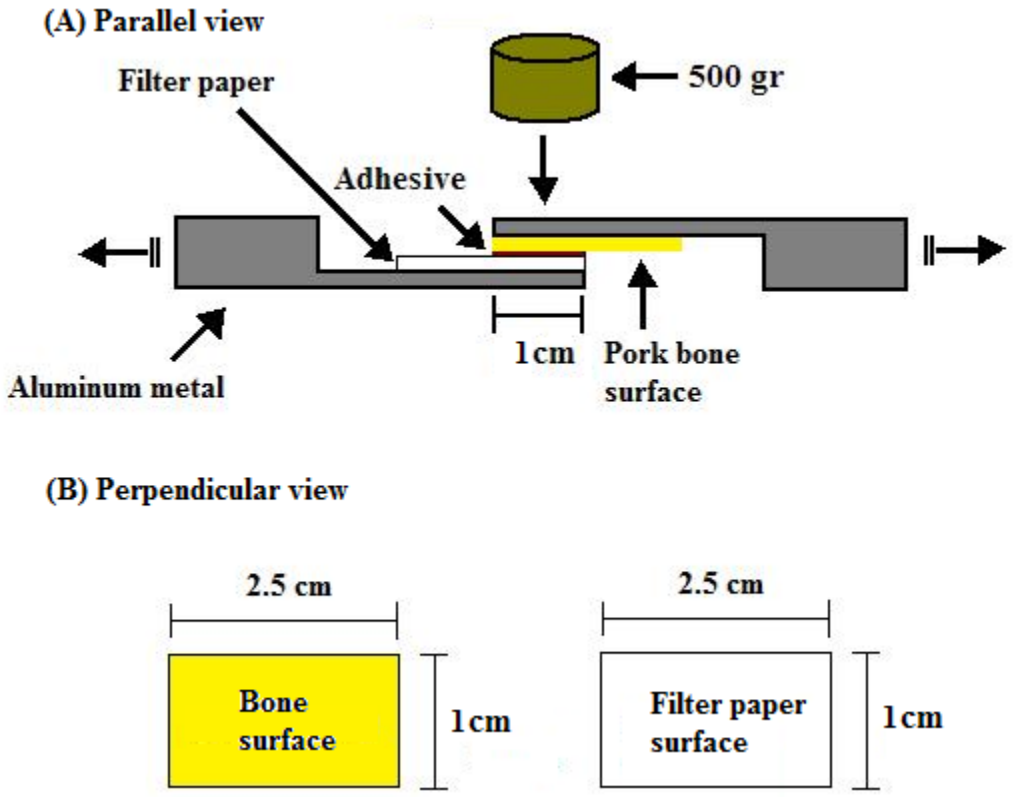

Figure 3-4. Schematics (a: parallel view, b: perpendicular view) illustrate the beef bone and filter paper substrates that were used for the shear tests. Prior to testing, the dry polymeric material was mixed with de-ionized water in a ratio of 200 mg to 1 ml and mixed with a spatula until a viscous homogeneous paste was obtained. The adhesive material was then applied on both of the two surfaces to be examined. The average thickness of the filter paper sample was about 0.5 mm.

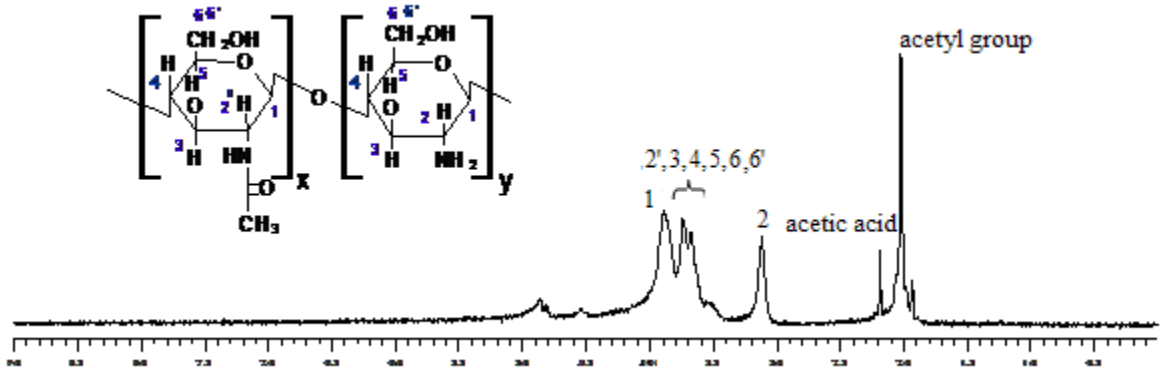

Figure 3-5. ^{1}H-NMR spectrum of pure chitosan of medium molecular weight. 1 wt% deuterated acetic acid in D_2O was used as the solvent. The proton assignment is as follows: δ 2.0-2.1 (br m, 3 H, acetyl group of chitosan), δ 3.1 (s, 1 H, H-2 of GlcN residue), δ 3.4-3.8 (m, 6 H, H-2', 3, 4, 5, 6, 6' of chitosan), δ 3.9-4.1 (s, 1H, H-1 of chitosan).

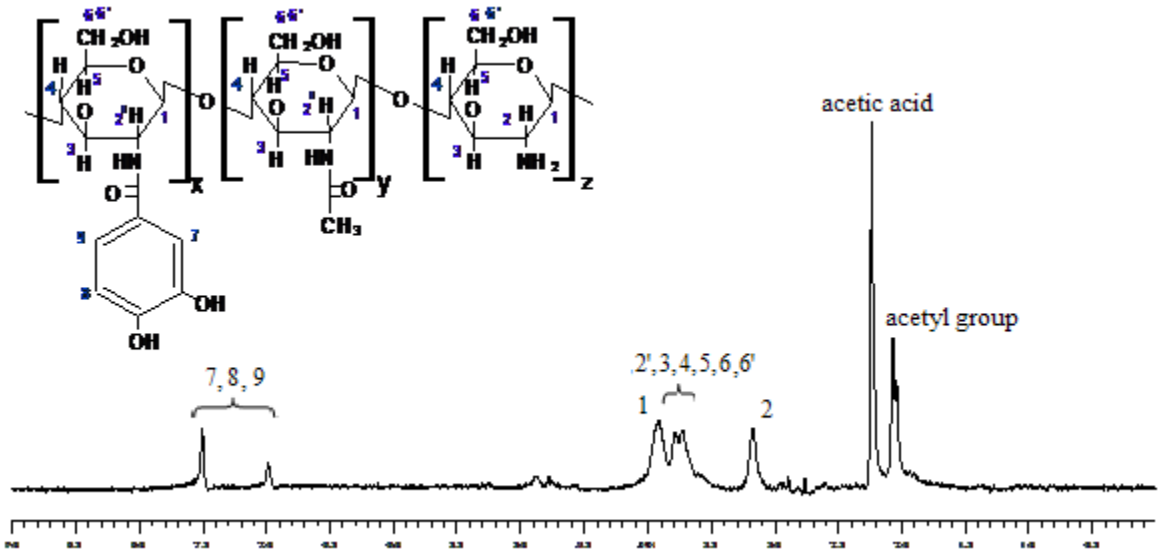

Figure 3-6. ^{1}H-NMR spectrum of modified chitosan with DHBA (27% mole). 1 wt% deuterated acetic acid in D_2O was used as the solvent. The proton assignment of modified chitosan is as follows: δ 2.0-2.1 (br m, 3 H, Acetyl group of chitosan), δ 3.1 (s, 1 H, H-2 of GlcN residue), δ 3.4-3.8 (m, 6 H, H-2', 3, 4, 5, 6, 6' of chitosan), δ 3.9-4.1 (s, 1H, H-1 of chitosan), δ 7.5-8.0 (m, 3H, H-arom. from DHBA).

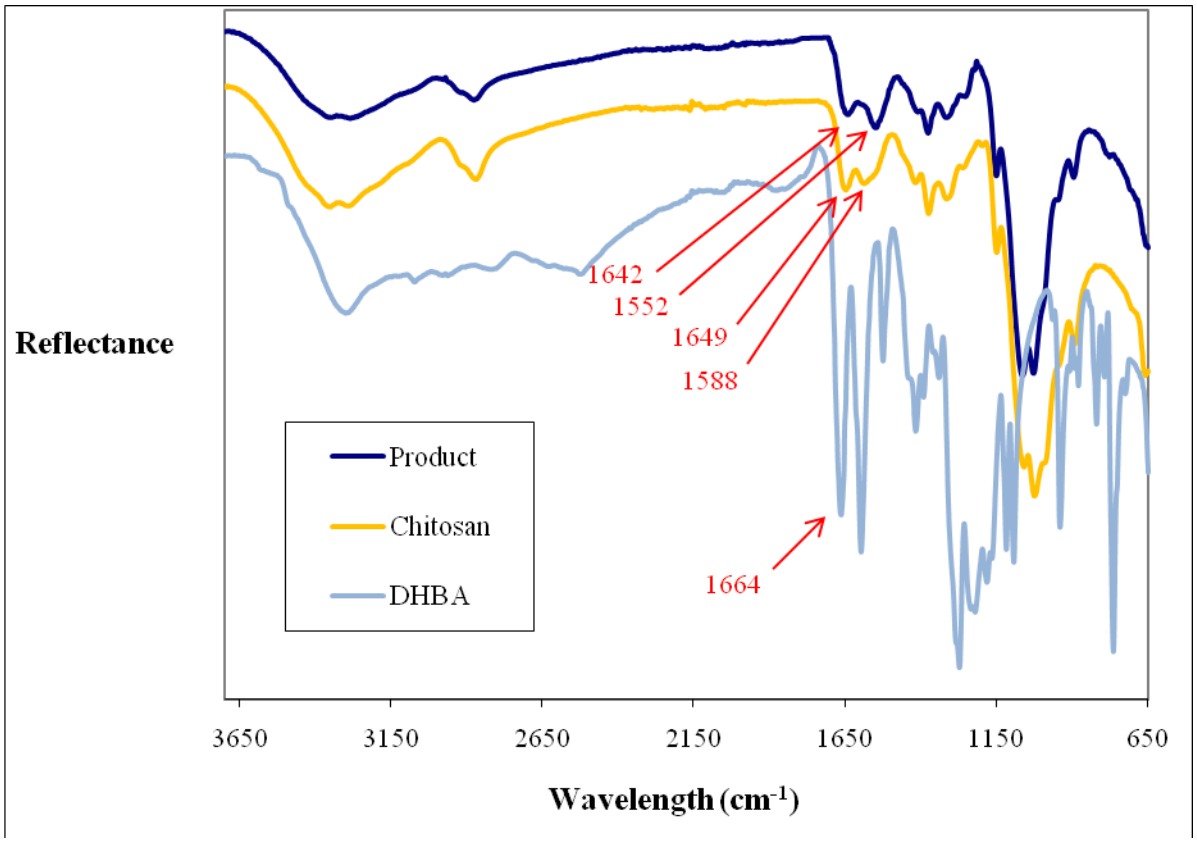

Figure 3-7. FT-IR spectra of chitosan, DHBA and modified chitosan (DHBA-Ch-1). The polymeric material was pressurized with a glass slide on top of the quartz window of the ATR instrument. Each IR spectrum was acquired with the accumulation of 30 scans at a scan resolution of 4 cm^{-1} between 800 and 4000 cm^{-1}.

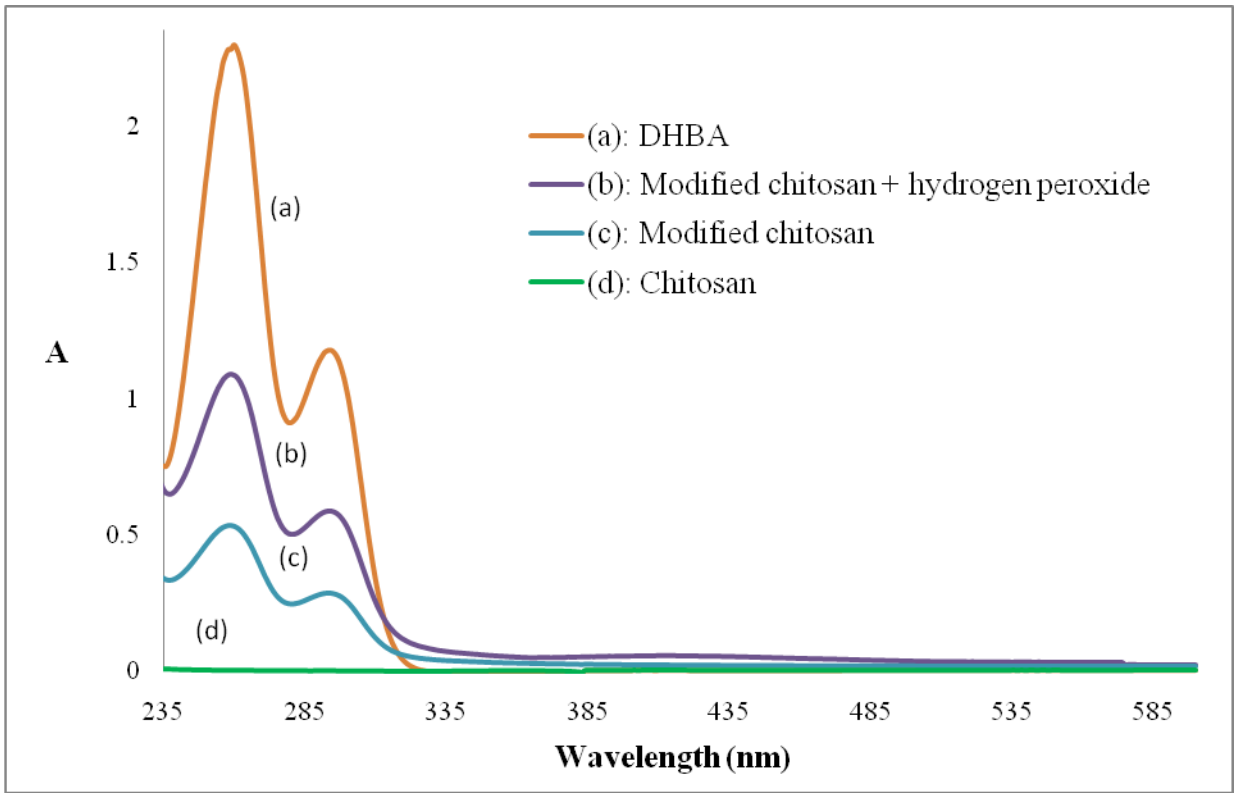

Figure 3-8. UV-vis spectra of: (a) DHBA in 1 wt% acetic acid, (b) modified chitosan (DHBA-Ch-1) upon addition of 6 wt % of H_2O_2 in 1 wt% acetic acid, (c) modified chitosan (DHBA-Ch-1) in 1 wt% acetic acid and (d) pure chitosan in 1 wt% acetic acid. The slit width of the detector was 1 nm, and the scan speed used was 480 nm/min.

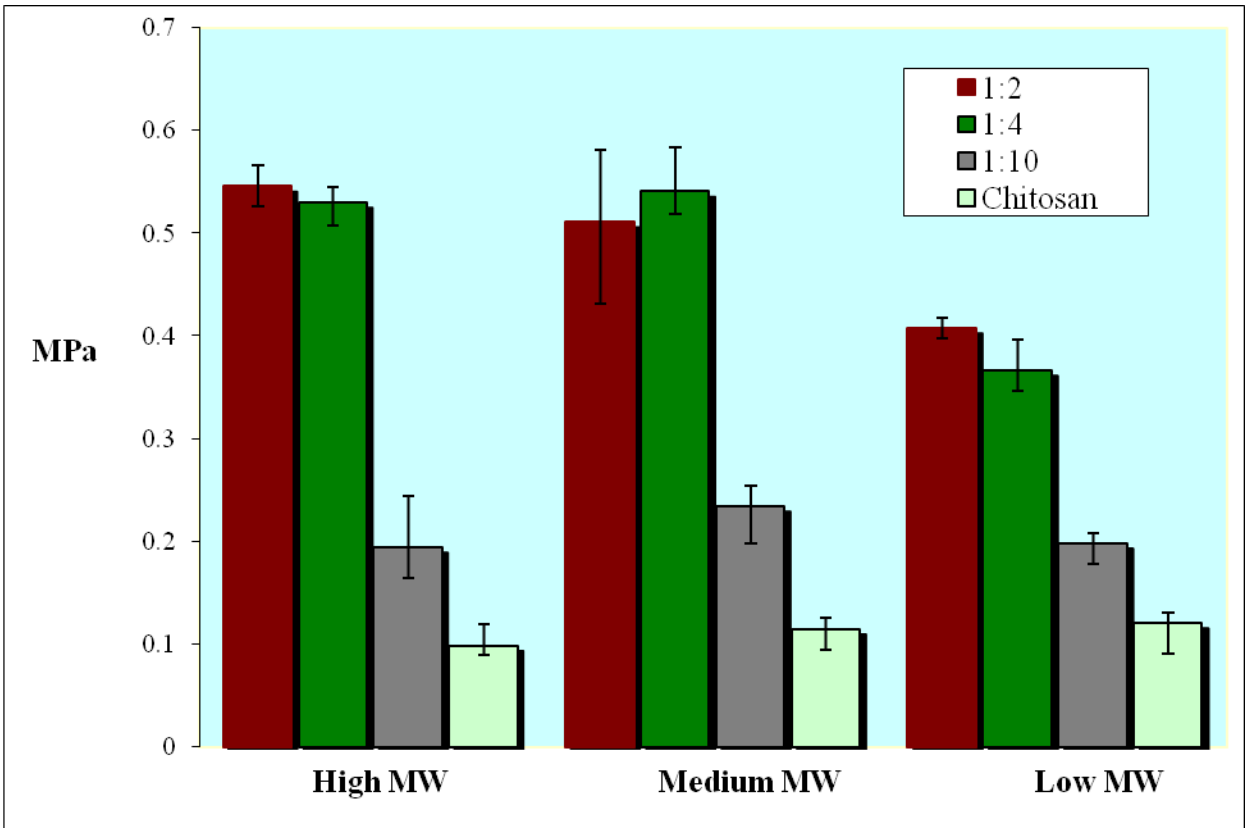

Figure 3-9. Tensile strength on beef bone as a function of the molecular weight and the composition of the materials. (DHBA-Ch-1: DHBA/Chitosan = 1/2-theoretical feeding = 27 %-experimental, DHBA-Ch-2: DHBA/Chitosan = 1/4-theoretical feeding = 19 %-experimental, DHBA-Ch-3: DHBA/Chitosan = 1/10-theoretical feeding = 4 %-experimental). Prior to testing, the dry polymeric materials were blended with deionized water in a ratio of 200 mg in 1ml and mixed with a spatula until a viscous homogeneous paste was obtained. The adhesive material was then applied on both of the two surfaces to be examined. In order to set the adhesive, a maximum compression force of 0.1 Mpa between the two joints was applied for the tensile tests.

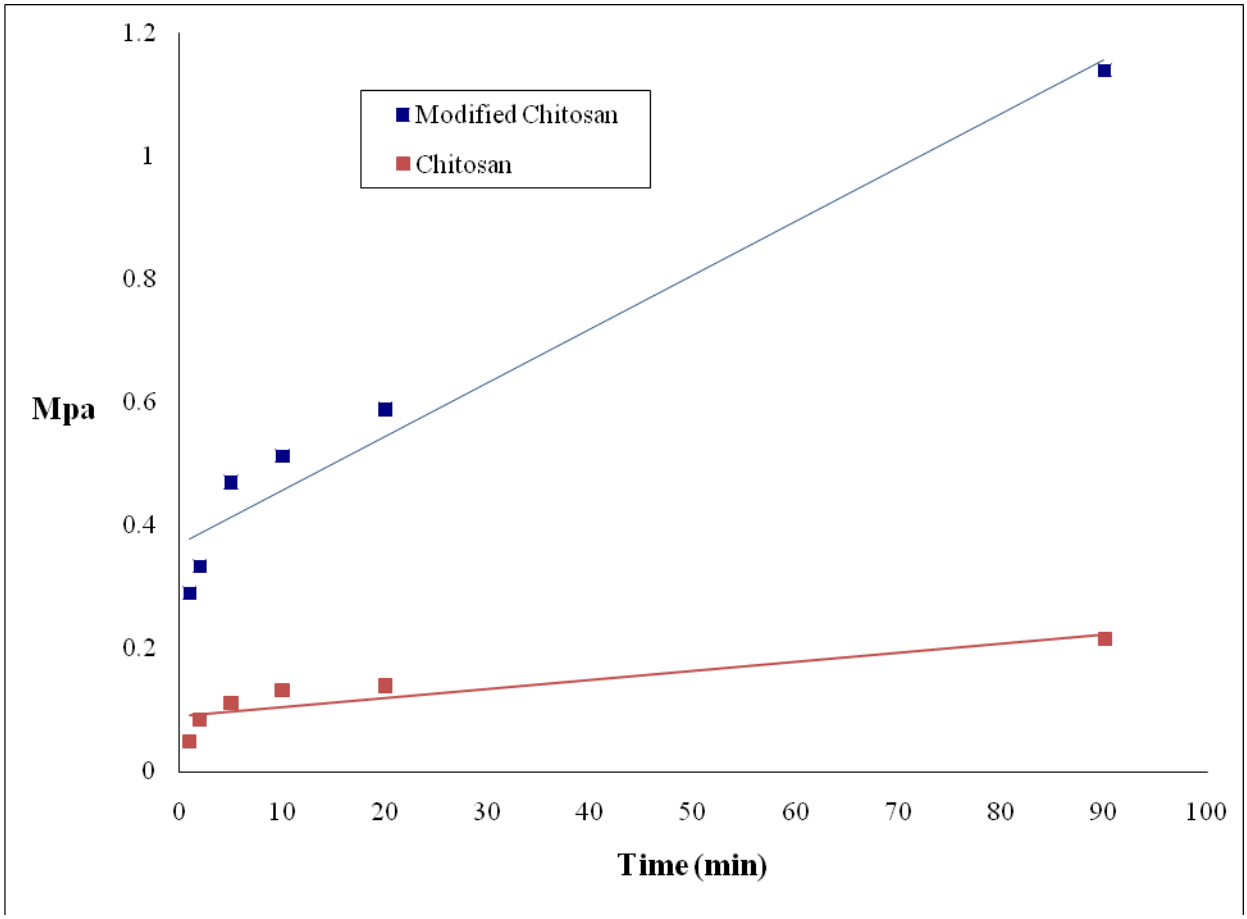

Figure 3-10. Tensile load on beef bone as a function of curing time of (a) medium molecular weight modified chitosan with theoretical mole feeding ratio of chitosan/DHBA = 2/1 (DHBA-Ch-1) and (b) medium molecular weight pure chitosan. Prior to testing, the dry polymeric materials were blended with deionized water in a ratio of 200 mg in 1 ml and mixed with a spatula until a viscous homogeneous paste was obtained. The adhesive material was then applied on both of the bone surfaces to be examined. In order to set the adhesive, a maximum compression force of 0.1 Mpa between the two joints was applied.

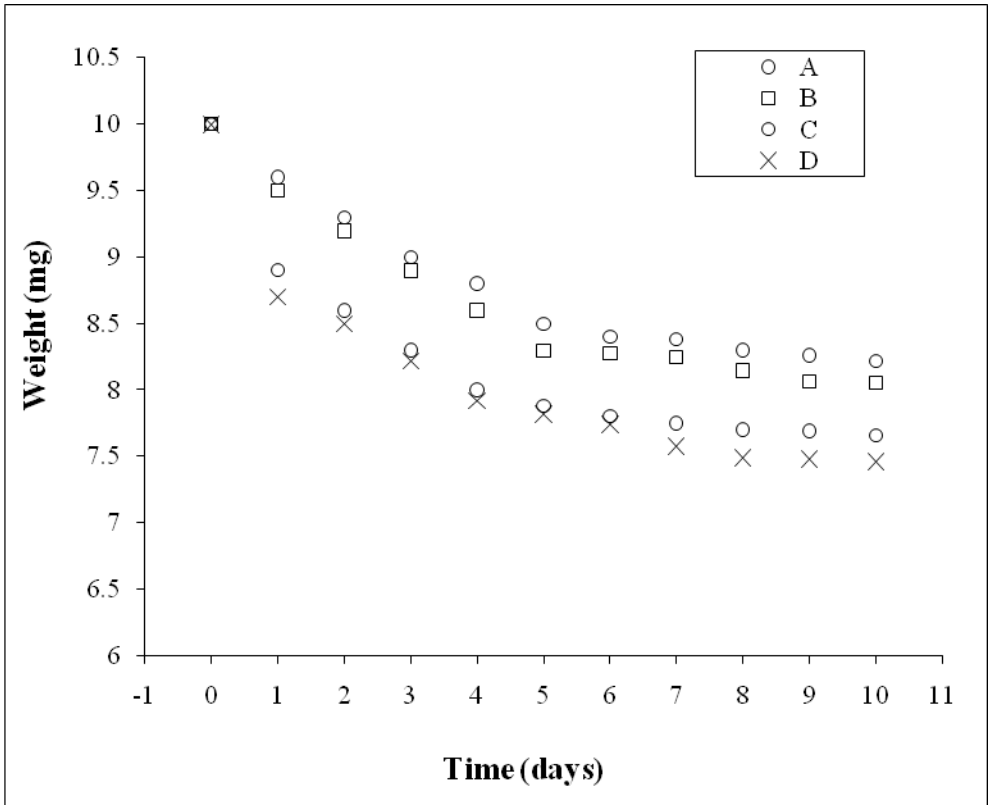

Figure 3-11. Hydrolytic degradation of the polymeric materials as a function of time of (A) DHBA-Ch-1 with a mole ratio of DHBA/ repeating unit of chitosan = 27%, (B) DHBA-Ch-2 with a mole ratio of DHBA/ repeating unit of chitosan = 19%, (C) DHBA-Ch-3 with a mole ratio of DHBA/ repeating unit of chitosan = 4% and (D) pure chitosan (medium molecular weight). Experiments for the degradation of the materials were carried out in phosphate buffer solutions (pH = 7.4 at 24 ^{o}C). A weighted amount of the material (0.01 g) was immersed in 10 ml of the buffer solution and the vial was kept in an air oven at 37 ^{o}C. Weight loss was examined gravimetrically, by measuring the remaining weight at predetermined times, for a period of 10 days.

3.7 Reference List

1. Sniezek, P. J., Walling, H. W., DeBloom, J. R., Messingham, M. J., VanBeek, M. J., Kreiter, C. D., Whitaker, D. C., Arpey, C. J. A randomized controlled trial of high-viscosity 2-octyl cyanoacrylate tissue adhesive versus sutures in repairing facial wounds following Mohs micrographic surgery. Dermatologic Surgery (2007), 33(8), 966-971.

2. Eaglstein, W. H., Sullivan, T. Cyanoacrylates for skin closure. Dermatologic Clinics (2005), 23(2), 193-198.

3. Sierra, D. H., Eberhardt, A. W., Lemons, J. E. Failure characteristics of multiple-component fibrin-based adhesives. Journal of Biomedical Materials Research (2002), 59, 1-11.

4. Lorthois, S., Schmitz, P., Angles-Cano, E. Experimental study of fibrin / fibrin-specific molecular interactions using a sphere/plane adhesion model. Journal of Colloid and Interface Science (2001), 241, 52-62.

5. Baar, S., Schorner, C., Rollinghoff, M., Radespiel-Troger, M., Hummer, H. P., Carbon, R. T. Collagen patches impregnated with antimicrobial agents have high local antimicrobial efficacy and achieve effective tissue gluing. Infection (2001), 29, 27-31.

6. Bhatia, S. K., Arthur, S. D., Chenault, H. K., Kodokian, G. K. Interactions of polysaccharide-based tissue adhesives with clinically relevant fibroblast and macrophage cell lines. Biotechnology Letters (2007), 29, 1645-1649.

7. Mo, X., Iwata, H., Matsuda, S., Ikada, Y. Soft tissue adhesive composed of modified gelatin and polysaccharides. Journal of biomaterials science. Polymer Edition (2000), 11, 341-351.

8. Donkerwolcke, M., Burny, F., Muster, D. Tissues and bone adhesives-historical aspects. Biomaterials (1998), 19, 1461-1466.

9. Akinmade, A. O., Nicholson, J. W. Glass-ionomer cements as adhesives. Part I. Fundamental aspects and their clinical relevance. Journal of Materials Science: Materials in Medicine (1993), 4, 95-101.

10. Shigemasa, Y., Minami, S. Applications of chitin and chitosan for biomaterials. Biotechnology and Genetic Engineering Reviews (1995), 13, 383-420.

11. Muzzarelli, R. A. A., Biagini, G. Role and fate of exogeneous chitosans in human wound tissues. Ed: Chitin Enzymology, European Chitin Society, Ancona; 1993.

12. Nishimura, K., Nishimura, S., Nishi, N., Saiki, I., Tokura, S., Azuma, I. Immunological activity of chitin and its derivatives. Vaccine (1984), 2, 93-99.

13. Choi, B. K., Kim, K. Y., Yoo, Y. J., Oh, S. J., Choi, J. H., Kim, C. Y. In vitro antimicrobial activity of a chito-oligosaccharide mixture against Actinobacillus actinomycetemcomitans and Streptococcus mutans. International Journal of Antimicrobial Agents (2001), 18, 553-557.

14. Ruel-Gariepy, E., Chenite, A., Chaput, C., Guirguis, S., Leroux, J. C. Characterization of thermosensitive chitosan gels for the sustained delivery of drugs. International Journal of Pharmaceutics (2000), 203, 89-98.

15. Vila, A., Sanchez, A., Tobio, M., Calvo, P., Alonso, M.J. Design of biodegradable particles for protein delivery for protein delivery. Journal of Controlled Release (2002), 78, 15-24.

16. Janes, K.A., Fresneau, M.P., Marazuela, A., Fabra, A., Alonso, M.J. Chitosan nanoparticles as delivery systems for doxorubicin. Journal of Controlled Release (2001), 73, 255-267.

17. Borchard, G. Chitosans for gene delivery. Advanced Drug Delivery Reviews (2001), 52, 145-150.

18. Wydro, P., Krajewska, B., Wydro, K. H. Chitosan as a lipid binder: A Langmuir monolayer study of chitosan-lipid interactions. Biomacromolecules (2007), 8, 2611-2617.

19. Aiba, S.I. Studies on chitosan : 6. Relationship between N-acetyl group distribution pattern and chitinase digestability of partially N-acetylated chitosans. International Journal of Biological Macromolecules (1993), 15, 241-245.

20. Wang, J., Chang, D. P-Acetaminobenzoyl chitosan for sunscreen and hair shampoo and its preparation method. Faming Zhuanli Shenging Gongkai Shuomingshu, 8pp; 2007.

21. http://www.fhwa.dot.gov/engineering/geotech/policymemo/tanks.cfm. U.S. Department of Transportation. Federal Highway Administration.

22. Casal,E., Montilla, E., Moreno,F. J., Olano, A., Corzo, N. Use of Chitosan for Selective Removal of ß-Lactoglobulin from Whey. Journal of Dairy Science (2006), 89, 1384-1389.

23. Bittelli, M., Flury, M., Campbell, G. S., Nichols, E. J. Reduction of transpiration through foliar application of chitosan. Agricultural and Forest Meteorology (2001), 107 (3), 167-175.

24. No, H.K., Meyers, S.P., Prinyawiwatkul, W., Xu, Z. Applications of chitosan for improvement of quality and shelf life of foods: A review. Journal of Food Science (2007), 72 (5), 87-100.

25. Yi, H., Wu, L. Q., Bentley, W. E., Ghodssi, R., Rubloff, G. W., Culver, J. N., Payne, G. F. Biofabrication with chitosan. Biomacromolecules (2005), 6, 2881-2894.

26. Khan, T. A., Peh, K. K., Ch'ng, H. S. Reporting degree of deacetylation values of chitosan: the influence of analytical methods. Journal of Pharmacy and Pharmaceutical Sciences (2002), 5, 205-212.

27. Baxter, A., Dillon, M., Taylor, K. D. A., Roberts, G. A. F., Improved method for i.r. determination of the degree of N-acetylation of chitosan. International Journal of Biological Macromolecules (1992), 14, 166-169.

28. Tsigos, I., Bouriotis, B. Purification and characterization of chitin deacetylase from Colletotrichum lindemuthianum. The Journal of Biological Chemistry (1995), 270, 26286-26291.

29. Li, J., Revol, J.F., Marchessault, R. H., Effect of degree of deacetylation of chitin on the properties of chitin crystallites. Journal of Applied Polymer Science (1997), 65, 373-380.

30. Mima, S., Miya, M., Iwamoto, R., Yoshikawa, S., Highly deacetylated chitosan and its properties. Journal of Applied Polymer Science (1983), 28, 1909-1917.

31. Ayako, A., Kousaku, O., Ikuo, U., Hiroyuki, Y. Green mussel Perna Viridis L.: Attachment behavior and preparation of antifouling surfaces. Biomolecular Engineering (2003), 20, 381-7.

32. Camilla, F., Hans, E., Fredrik, H. The influence of cross-linking on protein-protein interactions in a marine adhesive : the case of two byssus plaque proteins from the blue mussel. Biomacromolecules (2002), 3, 732-41.

33. Baty, A. M., Leavitt, P. K., Siedlecki, C. A., Tyler, B. J., Suci, P. A., Marchant, R. E., Geesey, G. G. Adsorption of adhesive proteins from the marine mussel, Mytilus Edulis, on polymer films in the hydrated state using angle dependent X-ray photoelectron spectroscopy and atomic force microscopy. Langmuir (1997), 13, 5702-5710.

34. Ohkawa, K., Ichimiya, K., Nishida, A., Yamamoto, H. Synthesis and surface chemical properties of adhesive protein of the asian freshwater mussel, Limnoperna Fortunei. Macromolecular Bioscience (2001), 1, 376-386.

35. Yamamoto, H., Nagai, A. Polypeptide models of the arthropodin protein of the barnacle Balanus balanoides. Marine Chemistry (1992), 37, 131-43.

36. Waite, J. H. Marine adhesive proteins: natural composite thermosets. International Journal of Biological Macromolecules (1990), 12, 139-44.

37. Yamamoto, H., Nagai, A., Okada, T., Nishida, A. Synthesis and adhesive studies of barnacle model proteins. Marine Chemistry (1989), 26, 331-338.

38. Li, K., Geng, X., Simonsen, J., Karchesy, J. Novel wood adhesives from condensed tannins and polyethilenimine. International Journal of Adhesion and Adhesives (2004), 24, 327-333.

39. Wang, J., Liu, C., Lu, X., Yin, M. Co-polypeptides of 3,4-dihydroxyphenylalanine and L-lysine to mimic marine adhesive protein. Biomaterials (2007), 28, 3456-3468.

40. Yu, M., Hwang, J., Deming, T. J. Role of L-3,4-dihydroxyphenylalanine in mussel adhesive proteins. Journal of the American Chemical Society (1999), 121, 5825-5826.

41. Monahan, J., Wilker, J. J. Cross-linking the protein precursor of marine mussel adhesives: bulk measurements and reagents for curing. Langmuir (2004), 20, 3724-3729.

42. Monahan, J., Wilker, J. J. Specificity of metal ion cross-linking in marine mussel adhesives. Chemical Communications (2003), 14, 1672-1673.

43. Lee, B., Chao, C.Y., Nelson, N. F. Motan, E., Shull, K. R. Messersmith, P. Rapid gel formation and adhesion in photocurable and biodegradable block copolymers with high DOPA content. Macromolecules (2006), 39, 1740-1748.

44. Burke, S.A., Ritter-Jones, M., Lee, B.P., Messersmith, P.B. Thermal gelation and tissue adhesion of biomimetic hydrogels. Biomedical Materials (2007), 2(4), 203-10.

45. Lee, B.P., Huang, K., Nunalee, F.N., Shull, K.R., Messersmith, P.B. Synthesis of 3,4-dihydroxyphenylalanine (DOPA) containing monomers and their co-polymerization with PEG-diacrylate to form hydrogels. Journal of Biomaterials Science. Polymer Edition (2004),15,449-464.

46. Lee, H., Bruce P. Lee, B. P., Messersmith, P.B. A reversible wet/dry adhesive inspired by mussels and geckos. Nature (2007), 448, 338-341.

47. Lee, B. P., Dalsin, J. L., Messersmith, P. B. Synthetic polymer mimics of mussel adhesive proteins for medical applications. Bioadhesives (2006), 257-278.

48. Hu, B. H., Messersmith, P. B. Enzymatically cross-linked hydrogels and their adhesive strength to biosurfaces. Orthodontics and Craniofacial Research (2005), 8, 145–149.

49. Payne, G.F., Chaubal, M.V. Enzyme-catalyzed polymer modification:reaction of phenolic compounds with chitosan films. Polymer (1996), 37, 4643-4648.

50. Yamada, K., Chen, T., Kumar, G., Vesnovsky, O., Topoleski, L.D.T., Payne, G.F. Chitosan based water-resistant adhesive. Analogy to Mussel Glue. Biomacromolecules (2000), 1, 252-258.

51. Hirai, A., Odani, H., Nakajima, A. Determination of degree of deacetylation of chitosan by ^{1}H-NMR spectroscopy. Polymer Bulletin (1991), 26, 87-94.

52. Sehgal, D., Vijay, I. K. A method for the high efficiency of water-soluble carboiimide-mediated amidation. Analytical Biochemistry (1994), 218, 87-91.

53. Hirai, A., Odani, H., Nakajima, A. Determination of degree of deacetylation of chitosan by H-NMR spectroscopy, Polymer Bulletin (1991), 26, 87-94.

54. Thatte, M. R. Synthesis and antibacterial assessment of water-soluble hydrophobic chitosan derivatives bearing quaternary ammonium functionality. Doctor's Thesis, Louisiana State University and A&M College, Los Angeles; 2004.

55. Peniche, C., Arguelles-Monal, W., Davidenko, N., Sastre, R., Gallardo, A., Roman, J. S. Self-curing membranes of chitosan/PAA IPNs obtained by radical polymerization: preparation, characterization and interpolymer complexation. Biomaterials (1999), 20, 1869-1878.

56. Tajmir-Riahi, H. A. Sugar complexes with calcium ion: infrared spectra of crystalline D-glucuronic acid and its calcium complexes. Carbohydrate Research (1983), 122, 241-248.

57. Chung, T. W., Yang, J., Akaike, T., Cho, K. Y., Nah, J. W., Kim, S. L., Cho, C. S. Preparation of alginate/galactosylated chitosan scaffold for hepatocyte attachment. Biomaterials (2002), 23, 2827-2834.

58. Hatzipanayioti, D., Karaliota, A., Kamariotaki, M., Veneris, A. Electrochemical and spectroscopic studies of 2,3-dihydroxy-benzoic acid, its oxidation products and their interaction with manganese(II), in dimethyl sulfoxide solutions. Transition Metal Chemistry (1998), 23, 407-416.

59. Jimenez, M., Garcia-Carmona, F., Garcia-Canovas, F., Iborra, J.L., Lozano, J.A., Martinez, F. Chemical Intermediates in Dopamine Oxidation by Tyrosinase, and Kinetic Studies of the Process, Archives of Biochemistry and Biophysics (1984), 235, 438-448.

60. Smyth, J. D., McManus, D. P. The physiology and biochemistry of cestodes, Cambridge University Press (1989), 172.

61. Huang, K., Lee, B. P., Ingram, D. R., Messersmith, P. B. Synthesis and characterization of self-assembling block copolymers containing bioadhesive end groups. Biomacromolecules (2002), 3, 397-406.

62. Schnurrer, J., Lehr, C. M. Mucoadhesive properties of the mussel adhesive protein. International Journal of Pharmaceutics (1996), 141, 251-256.

63. http://www.ybsweb.co.jp/chitosan.jpg. YBS Corporation website. Japan; 1998.

Chapter 4. Synthesis and Characterization of Novel Organic-Inorganic Poly(HEMA-GMA-Silica) Hybrid Materials

4.1 Introduction and Motivation

The sol-gel process, which is mainly dealing with inorganic polymerization reactions, is a chemical synthesis procedure used generally for the preparation of inorganic materials, such as glasses and ceramics.[1] It basically involves an inorganic polymerization, which leads to a highly cross-linked solid through a hydrolytic polycondensation. Compared to other inorganic network forming reactions, the sol-gel method uses mild reaction conditions and a broad solvent compatibility.[2] These two characteristics offer the possibility to carry out the inorganic network forming process in the presence of a preformed organic polymer or to carry the organic polymerization before, during or after the sol-gel process. The preparation, characterization and applications of such organic/inorganic hybrid materials have become a fast expanding area of research in the materials science due to the new and unique properties that these hybrids/nanocomposites can offer, as compared to the traditional macroscale composites and conventional materials.[3-6]

As Sharp notes in a review paper published in *Advanced Materials* though, serious material compromises usually have to be taken.[7] Substantial brittleness and loss of optical clarity and surface finish are commonly encountered during synthesis of hybrid materials when precautions are not taken. The properties of these materials depend not only on the properties of the individual components, but also on the composite's phase morphology and the interfacial properties.[8,9] These incompatibility problems mainly arise because of the domain size of the inorganic phase, which exceeds the 100-200 nanometers, and the generation of small interfacial

areas, which do not enable numerous covalent bonding that would formulate a compatibility between the two different, namely the inorganic and the organic, moieties.[10] Many researchers have addressed this problem and have sought for solutions following several different approaches.[11-15] Our group the past 2 decades has extensively investigated the incorporation of various organic groups and vinyl polymers into the sol-gel materials.[16-20] Schmidt et. al. have incorporated organoalkoxysilanes as one of the precursors in a sol-gel reaction as a method to incorporate organic groups within the inorganic network.[21] Mark et al. on the other hand have carried out sol-gel reactions inside swollen elastomers.[22] In the past several years, a richer palette of inorganic (including oxides of Sn, V and Al) and organic (including fluoropolymers, cellulosics and conductive polymers) compounds has emerged making the possibilities of incorporation of organic groups into the inorganic network innumerable.[23-25] These composites or organic-inorganic hybrid materials can be considered as nano-composites, if the size of particles in at least one direction is below 100 nm, and they remain transparent if the heterogeneity remains below 400 nm.[26,27] Sol-gel derived hybrids, have the wonderful advantage of the simplicity and versatility that is associated with the sol-gel process, which allows the easy incorporation of an organic component into a ceramic network under mild conditions.[28-32]

Optically transparent polymers, such as polyacrylates and polycarbonate, have been used in a number of applications, including shatterproof windows, coatings, reinforcement fillers, etc. In spite of their widespread use, it is desirable to improve upon their mechanical properties while maintaining their optical transparency. The motivation for this research project was the development of an organic-inorganic hybrid material that would have excellent mechanical properties, while keeping its optical transparency. Optical transparency is mainly maintained due

to the fact that the size of silica colloids or particles formed in the final hybrid is as low as 50 nm.[33] It is widely known that one of the problems associated with the preparation of sol-gel hybrids is the reproducibility of synthesis. Variability arises mainly due to the small residual byproduct molecules (e.g., water and ethanol) that are produced during sol-gel reactions. If these molecules are allowed to remain in the sol-gel system, they cause volume shrinkage as well as drastically reduce the mechanical properties of the cured polymer hybrid.[8, 9] Another problem associated with the sol-gel process is the escape of small byproduct molecules over a period of time. This subsequently creates stresses within the sample, which results in the formation of cracks and internal voids in the bulk polymeric hybrid during storage. As a consequence, the mechanical properties of the obtained sol-gel hybrids would be greatly reduced. Hence, it is beneficial to remove as much as possible the residual byproducts formed during the sol-gel reactions.

In this chapter, the synthesis of a new class of optically transparent poly(2-hydroethyl methacrylate-glycidyl methacrylate-silica) (HEMA-GMA-silica) (PHGS) hybrid materials is presented. This system was specifically designed to improve upon the mechanical properties of polymethyl methacrylate (PMMA, Plexiglass^{TM}) while maintaining its optical transparency. This new synthesis procedure enabled the almost complete removal of byproduct molecules and yielded products with no internal voids and surface cracks. Moreover, the as-synthesized poly(HEMA-GMA-silica) hybrid materials present low volume shrinkage and good reproducible mechanical properties.[34] The same synthetic concept of the covalent incorporation of organic monomers into the sol-gel intermediates can be applied to develop alternative organic-inorganic hybrid materials with tunable properties.

4.2 General Methodology

Sol-gel chemistry has been employed in this synthesis procedure in order to obtain silica-based, organic-inorganic hybrid materials with optical transparency and excellent mechanical properties. The sol-gel process, as the name implies, involves the transition of a system from a liquid "sol" (mostly colloidal) to a solid "gel" phase. The process begins with the hydrolysis (**Scheme 4-1**) and polycondensation of the precursors (e.g., tetraethylorthosilicate for our example) to form high molecular weight, yet soluble, polyintermediates defined as "sol" (**Schemes 4-2** and **4-3**). These intermediates then link together to become a three dimensional network defined as "gel".

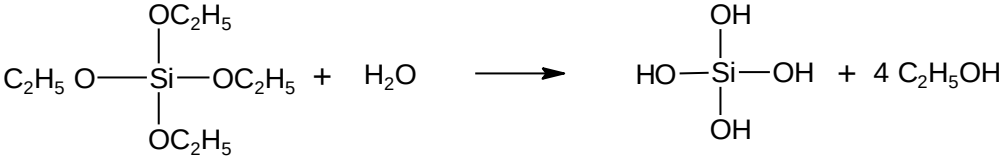

Scheme 4-1. Hydrolysis reaction of tetraethylorthosilicate with water in acidic environment.

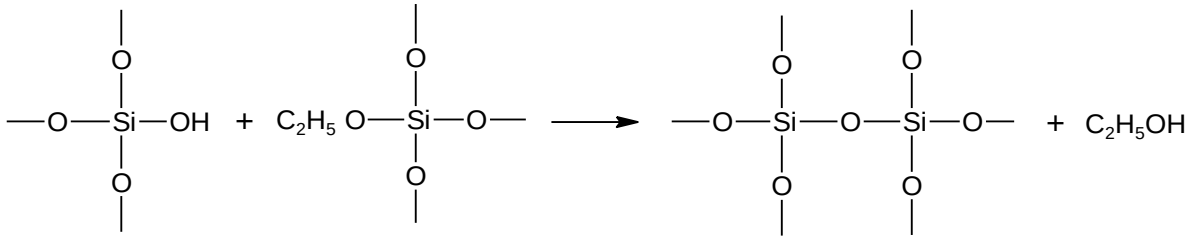

Scheme 4-2. Condensation reaction of tetraalkylorthosilicate with hydrolyzed tetraalkylorthosilicate.

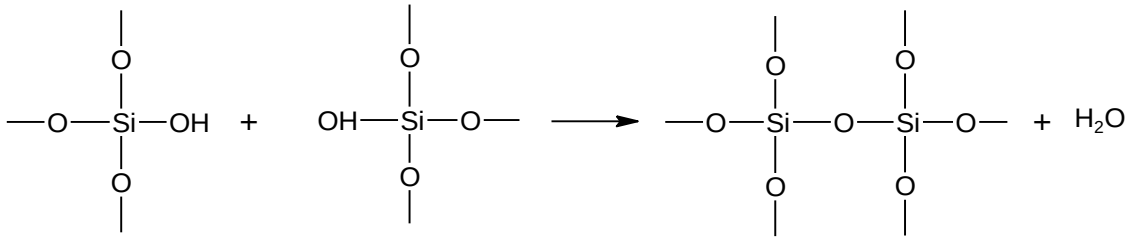

Scheme 4-3. Self condensation reaction of hydrolyzed tetraethylorthosilicate.

In the gelation step, the alkoxide gel precursors in aqueous solution after hydrolysis polymerize through alcohol- or water-producing condensations. These steps proceed simultaneously, and the extent to which each step goes depends on many factors that may be controlled by the reaction conditions. We employed acrylic monomers containing functional groups that can react with the intermediates from the sol-gel reactions. These monomers included 2-hydroxyethyl methacrylate (HEMA) and glycidyl methacrylate (GMA), which contain a hydroxyl and an epoxide group, respectively. Both of these groups can be covalently bonded with the silanol (SiOH) groups. The basic concept behind this synthesis procedure is that the sol-gel reactions of TEOS are allowed to proceed in the presence of a vinyl monomer, to a certain extent, till the organic-inorganic phase separation disappears and the system becomes homogeneous. The silanol groups in these growing silicate colloids (after hydrolysis of TEOS) react with the hydroxyl groups of HEMA and/or the epoxy groups of GMA to form covalent linkages between the acrylic monomers and the inorganic silicate component according to **Schemes 4-4** and **Scheme 4-5,** respectively. Upon radical polymerization of these acrylic monomers, a highly crosslinked, interconnected three-dimensional organic-inorganic hybrid material is obtained. All of these concepts will be explained in more detail in the following sections of this chapter.

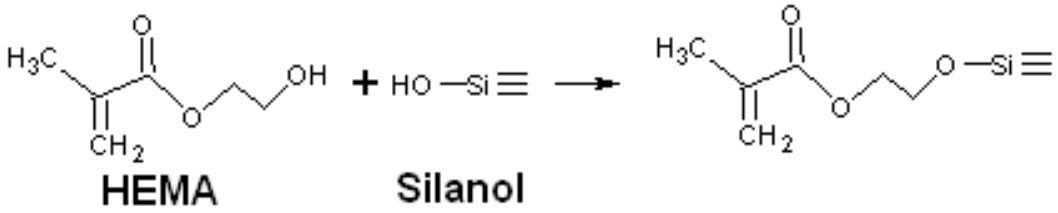

Scheme 4-4. Condensation reaction of hydrolyzed tetraalkylorthosilicate with 2-hydroxyethyl methacrylate.

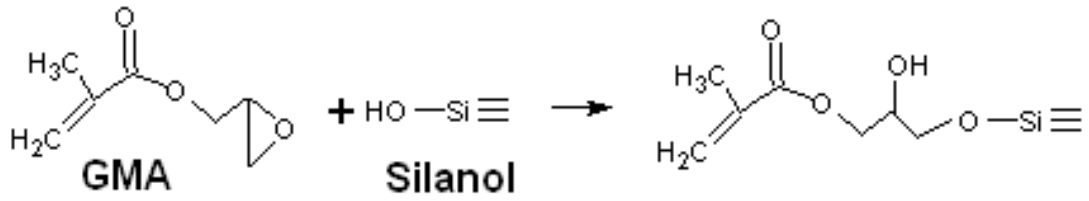

Scheme 4-5. Reaction of hydrolyzed tetraalkylorthosilicate with glycidyl methacrylate.

This new synthesis procedure enabled the almost complete removal of byproduct molecules. Thus, poly (HEMA-GMA-silica) hybrid materials with low volume shrinkage, excellent and reproducible mechanical properties, optical transparency and no surface cracking properties can be synthesized. The compression mechanical test results of these hybrid materials show the dependence of modulus, yield stress and compressive strength on silica content. Moreover, scanning electron microscopy images prove that the in-homogeneity of the two different moieties, namely organic and inorganic, remains well below the wavelength of visible light, which is also justified by the transparency of the final bulk material. Thermal analysis tests show that materials keep their structural integrity to elevated temperatures.

4.3 Experimental Section

4.3.1 Materials

Tetraethyl orthosilicate (TEOS, Aldrich), tetrahydrofuran (THF, Aldrich), tin chloride ($SnCl_4$, Aldrich) and hydrochloric acid (HCl, Fisher) were used as received. Benzoyl peroxide (BPO, Aldrich) was recrystallized from ethanol before use. 2-Hydroxethyl methacrylate (HEMA, Aldrich) and glycidyl methacrylate (GMA, Aldrich) were purified by vacuum distillation before use.

4.3.2 Methods

Hybrid monoliths, with silica content up to 30 weight percentage, have been prepared. The synthesis was carried out several times to ensure reproducibility. The compositions of the synthesized PHGS hybrids are summarized in **Table 4-1**. Pure poly(HEMA-GMA) (2:1 molar ratio) and commercially available Plexiglas™ G [poly(methyl methacrylate], PMMA) were used as controls, and their mechanical properties were compared with the mechanical properties of the as-synthesized inorganic-organic PHGS hybrids.

4.3.3 Thermal Properties

Thermogravimetric analysis was performed on a TA Q-50 thermal analysis system (TA instruments), equipped with TA Q Series Advantage Universal Analysis software, in air. The TGA was measured at a programmed heating rate of 20 °C/min in the temperature range of ~30–800 ^{o}C. Before TGA measurements, samples were ground into a fine powder and kept in a vacuum oven at 80 ^{o}C for 24 hr. A typical sample for TGA tests weighed ~5-10 mg.

Differential scanning calorimetry experiments were performed on a DSC (Q100) from TA instruments. All samples were analyzed from 20 ^{o}C to 200 ^{o}C at a heating rate of 20 ^{o}C/min.

Samples were ground into a fine powder and kept in a vacuum oven at 80 ^{o}C for 24 hr before DSC measurements. A typical sample for DSC analysis weighed ~5-10 mg.

4.3.4 Morphology

The nanoscale morphology of the composite was observed with a FEI XL30 environmental scanning electron microscope (ESEM) at a low acceleration voltage (e.g. 6-7 kV) and a beam spot size equal to 3. Before employing the microscope, the samples were coated with a Pt-Pd alloy using a sputter coater (Model G3P-8).

4.3.5 Evaluation of Mechanical Properties

Poly(HEMA-GMA-silica) hybrids were tested for compressive strength, yield stress, and modulus. The test specimens were cut (length to diameter ratio = 2:1) according to the ASTM standard (designation: D 695) using a diamond saw. The compression testing was performed using a servohydraulic machine (MTS Mini-Bionix 2, Eden Prairie, MN) at a crosshead speed of 10 mm/min. More than 6 specimens were used for each sample and the average values, with the standard deviations, are presented. The values of compressive strength (σ) were calculated using the following equation:

$$\sigma = \frac{F}{A}$$

where, F is the maximum failure load and A is the initial cross-sectional area of the specimen. The compressive modulus of the specimens was determined from the slope of a straight line fit to the initial linear portion of the stress-strain curve.

4.3.6 Synthesis Procedure of PHGS [poly (HEMA-GMA-silica)]

Poly(HEMA-GMA-silica) (PHGS) hybrid materials were prepared by the acid-catalyzed hydrolysis and polycondensation (i.e., sol-gel) reactions followed by the BPO initiated free radical polymerization of the acrylic monomers.

4.3.6.1 Hydrolysis of TEOS with HEMA

First, a desired amount of THF, HEMA, HCl (2M), distilled water and TEOS were mixed at room temperature under nitrogen atmosphere to give a two-phase mixture. After stirring for about 15 min the heterogeneous and cloudy reaction mixture became completely homogeneous and transparent. Due to the exothermic reactions, the temperature of the mixture increased from room temperature to 40 ± 5 °C. This reaction mixture was then refluxed at 60 °C for 3 hr.

4.3.6.2 Removal of Sol-Gel Byproducts

After hydrolysis, the solvent and other small molecular byproducts of the sol-gel reactions (e.g., ethanol and water) were removed using a vacuum pump (Precision vacuum pump D 25, New York, vacuum = 11 mm Hg) without heating. During this step, the temperature of the mixture dropped quickly to below 10 °C. When the weight of the mixture reached about 50-55% of the original weight (usually in 2 hr), the vacuum was discontinued. The reaction mixture stayed transparent throughout the whole period of this step.

4.3.6.3 Addition of GMA

A desired amount of GMA containing benzoyl peroxide (BPO) was then added to the reaction mixture and stirred for 3-5 min. The remaining byproducts were again removed under vacuum, until a stable weight was reached. Depending on the amounts of reagents used, this step

could take from 4 to 10 hours. At this point, the temperature of the reaction mixture gradually returned to room temperature. Tin chloride ($SnCl_4$), which was used as a catalyst for the reaction of the epoxy groups of GMA with the free hydroxyl groups of silanols, was then added, and the mixture was stirred under vacuum for about 30 more minutes.[34]

4.3.6.4 Polymerization Step and Heating Treatment

The viscous mixture was filled into polypropylene cylindrical or square window molds with typical dimensions as the ones shown in **Figure 4-1**. The further sol-gel reactions and the BPO-initiated free radical polymerization were conducted in three consecutive heating steps. The reaction mixture in the molds was first heated in an oven at 65 °C for 15-18 hr and then the temperature was increased to 85 °C for 2 hr. Finally, the transparent polymer monoliths were annealed at 125 °C for 2 hr. After curing, PHGS materials were obtained as monolithic and transparent plates, cylinders, discs and/or objects of other shapes. It is noteworthy, that the volume shrinkage from the casting solutions to the final hybrid materials was significantly lower in comparison to the conventional sol-gel process. The volume shrinkage based on the measurements of the product dimensions as compared to the dimensions of the molds was less than 5%.

As a typical procedure for the preparation of poly(HEMA-GMA-silica) hybrid materials containing 15 wt % of silica in the final product (i.e., PHGS-2-15), 52 g (0.25 mol) of TEOS and 54.97 g (0.42 mol) of HEMA were dissolved in 36 g (0.5 mol) of THF at room temperature in a 250-ml three-neck round bottom flask, which was equipped with a thermometer, a condenser and a gas inlet-outlet. To this solution, 13.35 g (0.74 mol) of distilled H_2O and 0.25 g (HCl content: 0.5 mmol) of aqueous 2 M hydrochloric acid solution were added to yield a two-phase liquid

mixture. The mixture was stirred magnetically at room temperature under nitrogen protection for about 15 min, till it became transparent and homogeneous. This mixture was further refluxed at 60 ^{o}C for 3 hr to allow for the hydrolysis of the TEOS in the presence of HEMA. After hydrolysis, the solvent and other small molecular byproducts of the sol-gel reactions (e.g., ethanol and water) were removed without heating using a vacuum pump. During this step, the temperature of the mixture dropped quickly to below 10 °C. When the weight of the mixture reached about 50-55% of the original weight the vacuum was discontinued. 30.02 g of GMA (0.21 mol) and 76.8 mg of BPO (0.3 mmol) were then added to the reaction mixture and stirred for 3-5 min. The remaining byproducts were again removed under vacuum until a stable weight was reached. Depending on the amounts used, this step may take from 4 to 10 hours. At this point, the temperature of the reaction mixture gradually returned to room temperature. 7.6 μl of $SnCl_4$ was then added, and the mixture was stirred under vacuum for about 30 more min. The viscosity of this mixture depends on the amount of TEOS in feed compositions. The higher the amount of TEOS in the feed compositions, the more viscous this final mixture becomes. Finally, the mixture was filled into polypropylene cylindrical or square window molds to complete the free radical polymerization and curing in three consecutive heating steps. The reaction mixture was first heated in an oven at 65 °C for 15-18 hr to allow for the free-radical polymerization of the acrylate groups, and then the temperature was increased to 85 °C for 2 hr. Finally, the transparent polymer monoliths were annealed at 125 °C for 2 hr. After curing, PHGS materials were completely solidified and could be obtained as monolithic and transparent windows, cylinders, discs and/or objects of other shapes (**Figure 4-2**).

4.4 Results and Discussion

4.4.1 Thermal Gravimetric Analysis (TGA)

The organic-inorganic composition of the PHGS hybrid materials was controlled by varying the amount of TEOS to the organic precursors, and a series of PHGS hybrids containing different silica wt % in the final products (represented as SiO_2 wt %) has been prepared as summarized in **Table 4-1**. In the annotation "PHGS-X-Y", X and Y represent the mole ratio of HEMA to GMA and the theoretical silica wt % in the final products (as SiO_2), respectively. Thus, the sample annotated as PHGS-2-10 represents a hybrid material with a molar ratio of HEMA to GMA equal to 2, and a theoretical silica feed composition equal to 10 wt% (calculated as SiO_2 wt% in the final product, assuming that sol-gel reactions are complete). The silica content in the final hybrid materials has been experimentally determined by thermal gravimetric analysis. A series of representative TGA curves of the as-synthesized hybrid materials can be seen on **Figure 4-3**. In general, the materials show a major weight loss at elevated temperatures (around 250 ^{o}C – 350 ^{o}C), which is attributed to the degradation of the organic polyacrylate moiety. Beyond this decomposition temperature, the TGA curves are almost flat up to 800 ^{o}C, and the final residue represents the amount of SiO_2 that is left. This residual weight % corresponds to the experimental wt % of SiO_2 (**Table 4-2**). As can be seen from that table, the obtained experimental values are quite comparable to those calculated from the stoichiometry of the reactants, which suggests that all of the reactions incorporated in this synthetic procedure have reached almost completion.

4.4.2 Differential Scanning Calorimetry (DSC)

Differential scanning calorimetry experiments have been performed on pure poly(HEMA) and poly(GMA) as controls, as well as on a series of representative poly(HEMA-GMA-silica) hybrids. Samples were first ground into fine powder form, and kept in a vacuum oven for 24 hours at 80 ^{o}C. The DSC curves shown in **Figure 4-5** reveal that pure poly(HEMA) and poly(GMA) exhibit a clear glass transition temperature at ~ 100 ^{o}C and ~ 60 ^{o}C, respectively. On the other hand, the hybrids, containing 15 wt% and 25 wt % of silica in the final products, show no clear glass transition temperatures at this range of temperatures. Such an absence of a clear calorimetric T_g suggests that the polymer chains have been confined in domains smaller than 15-20 nm from which the characteristic large scale cooperative chain segmental motions for the glass transition phenomenon are restricted.[6] This is another clear justification that the as-synthesized hybrid materials encompass a fine interpenetrating organic-inorganic morphology.

4.4.3 Synthesis Considerations

The first step in this new synthesis procedure, involves the growth of the silica phase, via hydrolysis of TEOS, up to a certain extent (**Figure 4-6**). HEMA molecules through their pendant hydroxyl groups then react, by condensation, with the silanol groups of the hydrolyzed TEOS to introduce the acrylate groups into the oligomeric silicates. The next step includes the vacuum evacuation of the solvent (THF) and some of the byproducts (namely water and ethanol) that result from the hydrolysis of TEOS, the silanol-silanol condensation and the silanol-HEMA condensation. At this stage, glycidyl methacrylate (GMA) is added to the reaction mixture and the byproducts are removed further by evaporation under high vacuum. GMA is a dual

functionality monomer that contains an epoxy and an acrylic group and has a high boiling point of 189 °C (at 760 mm Hg). In addition to GMA forming a co-polymer with HEMA and/or HEMA-silica phase during the last step of the free-radical polymerization, GMA served two other important purposes, which enabled us to overcome the problems associated with the small byproduct molecules in a typical sol-gel organic/inorganic hybrid synthesis. First, GMA has a high boiling point that enables the complete removal of lower boiling point residual byproducts (such as H_2O and ethyl alcohol) under vacuum evaporation. Second, the epoxy group of GMA can effectively react with the remaining free silanol (Si-OH) groups of the silica phase under the action of the catalyst (e.g., $SnCl_4$), thereby capping the growing silicate oligomers. This is of crucial importance because any free Si-OH groups remaining in the final grown sol-gel chains could otherwise condense over time and produce water as a byproduct. Material shrinkage, from the condensation and stresses from the escaping water, would then cause stress cracks that subsequently would decrease the mechanical properties and destroy the optical transparency of these hybrids. The final step, before the free-radical polymerization at elevated temperatures, included the addition of $SnCl_4$, which catalyzes the capping reaction of the epoxy group of GMA with the hydroxyl groups from the HEMA-silanol or silanol colloids. At this point, it must be noted that elevated temperatures (during the polymerization step) also facilitate this capping reaction and thus it is reasonable to assume that the capping reaction should be almost complete after this step. This specific capping reaction of GMA with sol-gel intermediates was further investigated and is described in chapter 5.

The final monolithic hybrid materials were formed, via free radical polymerization of the vinyl bonds of HEMA and GMA, using benzoyl peroxide (BPO) as the radical initiator. The

organic-inorganic cross-links come from the silica network that is bonded to the HEMA and GMA groups. It is expected that the improvement in mechanical properties is mainly due to the effective stress transfer between the silica phase and polymer chains through these cross-linking sites. Approximately 6 % of average volume shrinkage of these polymer hybrids has been obtained. Since the major portion, if not all, of solvent and small molecular byproducts has been removed before the gelation, the volume shrinkage from the casting step to the final products is significantly reduced in comparison to the conventional sol-gel procedures. The contribution to volume shrinkage from this stage to the final solidified products comes from two sources. One is the volume shrinkage that is caused by the radical polymerization of the acrylic groups present in the hybrids. The second source is the further condensation of the sol-gel moiety that releases small molecular byproducts. As has already been mention though, the effect of the latter factor to volume shrinkage is almost diminished by capping the free hydroxyl groups of the growing silanols by GMA. Because of this low volume shrinkage, the shrinkage-induced stress is lessened, and the probability of crack formation in the hybrid materials is, therefore, greatly reduced, if not completely eliminated.

4.4.4 Morphology and Transparency

A key issue in these novel organic-inorganic hybrid materials is the degree of mixing of the organic-inorganic components or, in other words, the homogeneity of the two different moieties. All of the as-synthesized PHGS hybrid materials are highly transparent, and this optical transparency suggests that the organic-inorganic phase separation, if any, remains below 300 nm. **Figure 4-7a** and **Figure 4-7b** show the SEM images of PHGS-2-15 and poly(methyl methacrylate) (PMMA), respectively. As can be verified from these figures, the size of the silica

particles in the PHGS sample is in the range of 50-80 nm, much smaller than the wavelength range of visible light. For comparison reasons, PMMA was also observed under the SEM microscope. In this case the material has a worm-like morphology with no particle formation. **Figure 4-8** shows the digital picture of a thick window panel (dimensions: 4" x 3.5" x 3/8") of the obtained monolithic PHGS-2-10. It appears to be completely transparent with no surface cracks or internal voids.

4.4.5 Mechanical Properties of PHGS hybrids

As shown above, all of the poly(HEMA-GMA-silica) hybrids prepared using this new sol-gel synthesis procedure were completely transparent without any surface cracks. In addition, these hybrids did not chip during cutting with a diamond saw. Compression testing was used as a means to evaluate the mechanical properties of the obtained materials (**Figure 4-9**). The values of compressive modulus, yield stress and compressive strength of the final hybrids and the controls are summarized in **Table 4-3**. Pure poly(HEMA-GMA) (2:1 molar ratio) and commercially available Plexiglas™ [poly(methyl methacrylate), PMMA] were used as controls, and their mechanical properties were compared with the mechanical properties of the inorganic-organic PHGS hybrids. Results show that the compressive modulus of poly(HEMA-GMA-silica) hybrids improves with increasing silica content up to 25 wt% (**Figure 4-10**). From the same figure it can be seen that all of PHGS hybrids exhibited higher modulus than both poly(HEMA-GMA) and PMMA (Plexiglas™). This may be attributed to the fact that silica imparts strength in the obtained PHGS hybrids creating an interlocking network through covalent bonding between the acrylic moieties and the silicates. An increase of about 50 % in modulus is seen in the 25 wt% silica hybrids when compared with pure PMMA. On the other hand, the 30 wt% silica

sample (PHGS-2-30) appeared to be more brittle and showed a decrease in the compressive modulus as compared to 25 wt%, which suggests that beyond this percentage, the silica growing moieties dominate over the silica-acrylate moieties, which tend to transmit more brittleness to the final product.

The poly(HEMA-GMA) control shows lower yield stress than Plexiglas™ (PMMA). This can be presumably attributed to the side-chain branching of HEMA and GMA such that poly(HEMA-GMA) has higher entanglement molecular weight and lower entanglement density than Plexiglas™ (PMMA). Incorporation of silica resulted in a dramatic increase in yield stress of the obtained hybrids (**Figure 4-11**). The yield stress increased from about 125 MPa for poly(HEMA-GMA) to a maximum of approximately 182 MPa for the 15 wt% silica hybrid (i.e. PHGS-2-15). This is also a 30 % higher yield stress than the Plexiglas™ (PMMA) (140 MPa). The compressive strength of these hybrid materials (**Figure 4-12**) also displayed a similar trend of composition dependence, as can seen in the yield stress behavior, despite being lower than both poly(HEMA-GMA) and Plexiglas™ (PMMA) controls. A maximum average compressive strength was obtained for the 7-10 wt % silica samples. The compressive strength decreased with increase in silica content, and this may be attributed to the fact that higher silica content, which subsequently leads to lower acrylic content, tends to make the final material more fragile.

These results clearly demonstrate the synergy of combining silica with the acrylate monomers (e.g., HEMA and GMA) to form an interpenetrating network at the molecular level (hybrids or nanocomposites). Incorporation of silica appeared to increase the crosslink density of polymer chains such that increasing silica content resulted in a simultaneous increase in modulus and yield stress when silica loading is below a threshold of 25 wt%. There appears to be

maximum silica content, about 25 wt%, associated with these poly(HEMA-GMA-silica) hybrids, above which, the formed PHGS hybrid becomes brittle, something that is exhibited by the decrease in the compressive modulus. The formation of a percolated network structure and the increased covalent bonding between the acrylic monomers and silica with further increase in silica content will ultimately hinder the extent of molecular relaxation of polymer chains within the network. Thus, these poly(HEMA-GMA-silica) hybrids can be synthesized with a compromise in the optimal silica contents to achieve the desired overall mechanical properties of the final products.

4.5 Summary and Conclusion

Poly(HEMA-GMA-silica) hybrids with various silica contents, prepared by this new sol-gel synthesis approach, were completely transparent. These hybrid materials exhibited low volume shrinkage during polymerization and were crack-free during storage (for about twelve months under ambient conditions). This proves the effectiveness of this new synthesis procedure to remove low-molecular-weight byproduct molecules and to prevent the further condensation of silanol groups during storage. The mechanical properties of these hybrid materials appear to be composition dependent. Incorporation of silica effectively increased the compressive yield stress and modulus of the obtained poly(HEMA-GMA-silica) hybrid materials. These materials seemed to reach an optimal compressive strength when the silica content is in the range of 10-20 wt%. The reproducibility of the synthesis procedure and the improvement in mechanical properties of these polymer hybrids, while not sacrificing optical transparency, demonstrate the feasibility of utilizing these materials in applications that currently utilize acrylic polymers, such as

Plexiglas^{TM}. Applications of these hybrid materials have been explored as transparent armor and as dental restoratives, among others.

4.6 Acknowledgements

This research project was in collaboration with Dr. Shuxi Li and Dr. Solomon Praveen. I would like to thank Mr. Apoorva Shah and Mr. Indraneil Mukherjee for their crucial input and valuable suggestions in this project. Financial support from the U.S. Army Research Laboratory (Contract No. W911QX-04-C-0041) and the National Institutes of Health (Grant No. DE09848) are gratefully appreciated. I would also like to thank the Materials Characterization Facility (MCF) of the A.J. Drexel Nanotechnology Institute (DNI) for the usage of the SEM instrument.

Table 4-1. Amounts of reactants used for the synthesis of PHGS hybrids containing various amounts of silica in the final product (represented as SiO2 wt-%).

	Sample code					
Reactant	**PHGS-2-7**	**PHGS-2-10**	**PHGS-2-15**	**PHGS-2-20**	**PHGS-2-25**	**PHGS-2-30**
THF (g)	28.8	36	36	28.8	36	57.6
H_2O (g)	10.8	13.9	13.3	10.8	13.3	22.3
HCl (g)	0.21	0.25	0.25	0.2	0.4	0.4
TEOS (g)	41.6	52	52	41.6	52	83.3
HEMA (g)	103.4	86	54.9	31.1	29.1	36
GMA (g)	56.5	47.7	30.1	17.1	15.9	19.8
$SnCl_4$ (µl)	14.6	12	7.6	4.5	4	5
BPO (mg)	146	122	77	43	40	50

In the annotation "PHGS-X-Y", X and Y represent the mole ratio of HEMA to GMA and the theoretical silica wt % in the final products (as SiO_2), respectively. Thus, the sample annotated as PHGS-2-10 represents a hybrid material with a mole ratio of HEMA to GMA equal to 2, and a theoretical silica feed composition equal to 10 wt% (calculated as SiO_2 wt% in the final product, assuming that sol-gel reactions are complete). It is assumed that all siloxy groups were hydrolyzed and condensed to siloxanes in the final products.

Table 4-2. Experimental and theoretical silica content (as wt % SiO_2 in the final product) in the PHGS hybrid materials.

Sample Code	SiO_2 (wt-%) Theoretical[a]	SiO_2 (wt-%) Experimental[b]
PHGS-2-7	7	6.7
PHGS-2-10	10	9.4
PHGS-2-15	15	15.6
PHGS-2-20	20	19.8
PHGS-2-25	25	24.9
PHGS-2-30	30	28.9

[a] As calculated from the theoretical silica feed compositions. It is assumed that all of the siloxyl groups have been hydrolyzed and condensed to siloxanes in the final products.

[b] As calculated from the residual weight at 800 ^{o}C in the respective TGA curves.

Table 4-3. Compressive modulus, yield stress and compressive strength of poly(HEMA-GMA-silica) at different silica weight percentages.

Sample code	Volume shrinkage (%)	Modulus average ± SD (MPa)	Yield stress average ± SD (MPa)	Compressive strength average ± SD (MPa)
PHGS-2-7	7.1	3661 ± 78	162.2 ± 3.5	204 ± 20
PHGS-2-10	6.7	3716 ± 51	172.4 ± 3.9	210 ± 26
PHGS-2-15	6.4	3843 ± 95	181.7 ± 4.7	195 ± 19
PHGS-2-20	6.3	4007 ± 102	177.8 ± 7.28	183 ± 10
PHGS-2-25	6.4	4532 ± 171	172 ± 5.35	178 ± 17
PHGS-2-30	5.9	3895 ± 166	141.2 ± 18.45	153 ± 19
Plexiglas™ (PMMA)*	N/A	3083 ± 40	139.9 ± 3.6	284 ± 2
Poly(HEMA-GMA)*	12.5	2991 ± 121	124.7 ± 2.18	230 ± 61

The test specimens were cut (length to diameter ratio=2:1) according to the ASTM standard (designation: D 695) using a diamond saw. The compression testing was performed using a servohydraulic machine (MTS Mini-Bionix 2, Eden Prairie, MN) at a crosshead speed of 10 mm/min. More than 6 specimens were used for each sample and the average values with the standard deviations are presented.

* Samples poly(HEMA-GMA) at a 2:1 mol ratio of HEMA:GMA and Plexiglas™ (PMMA) were used as controls.

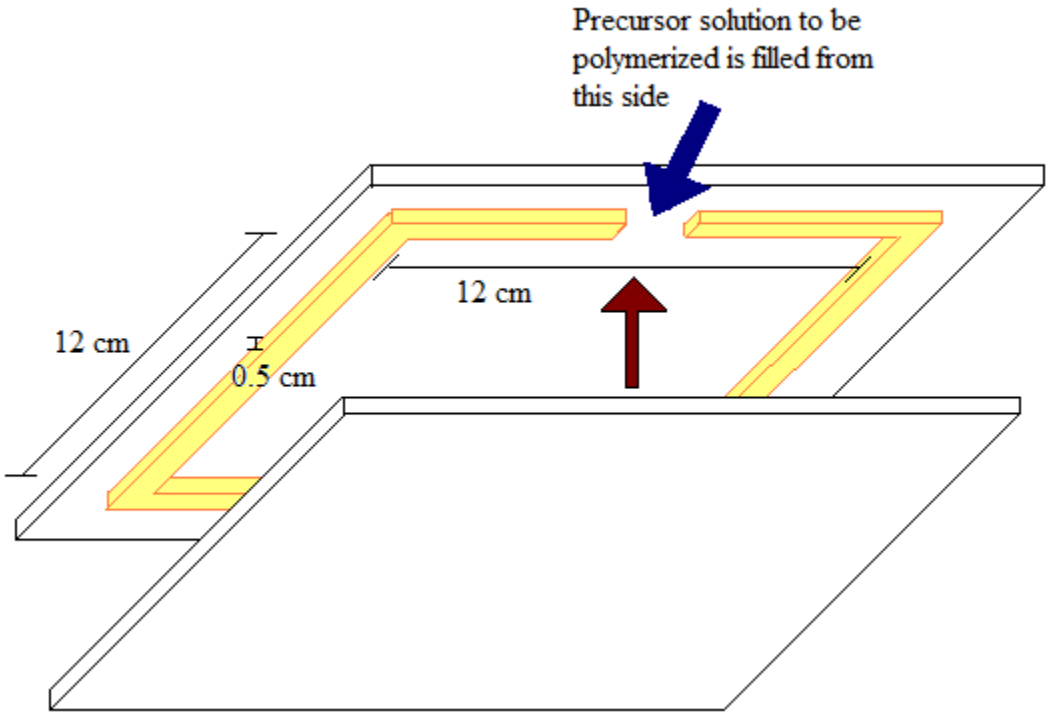

Figure 4-1. Typical dimensions of a polypropylene square mold substrate used.

Figure 4-2. These novel PHGS hybrid materials can be made various different sizes and shapes as transparent windows, cylinders, discs and cones.

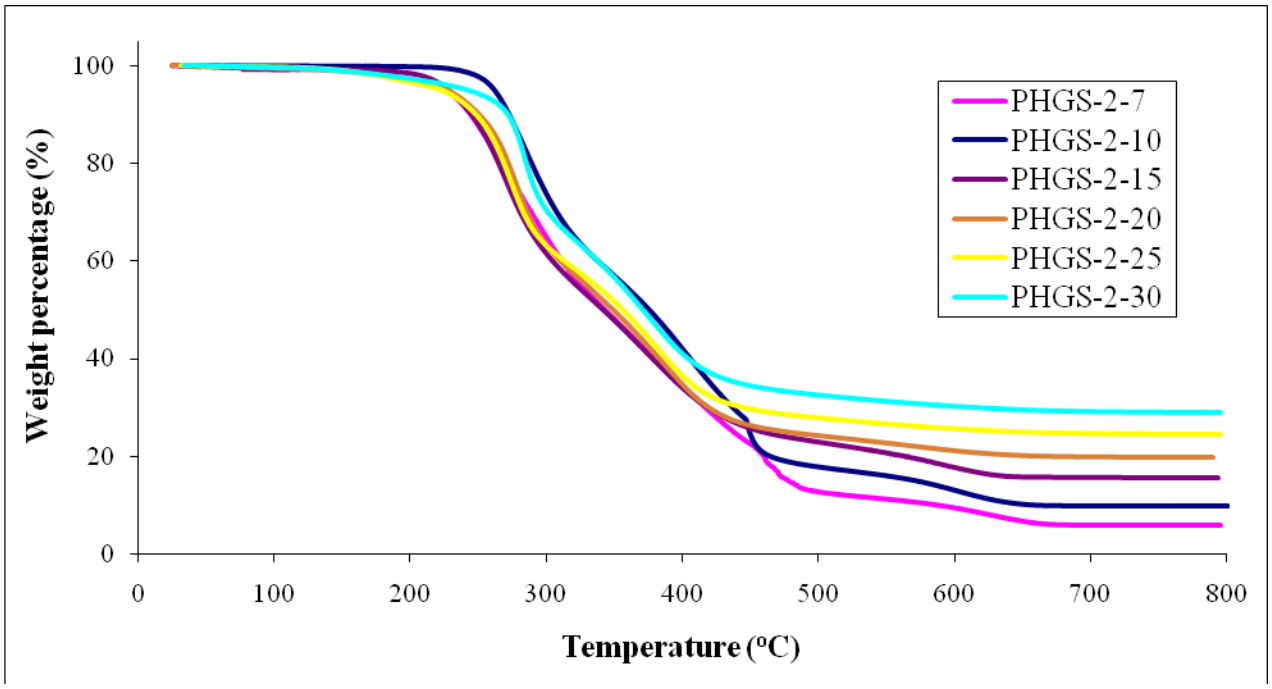

Figure 4-3. TGA curves of the as-synthesized hybrid materials from **Table 3-1**. The TGA was measured at a programmed heating rate of 20 °C/min in the temperature range of ~30–800 °C. Before TGA measurements, samples were ground into a fine powder and kept in a vacuum oven at 80 °C for 24 hr. A typical sample for TGA tests weighed ~5-10 mg.

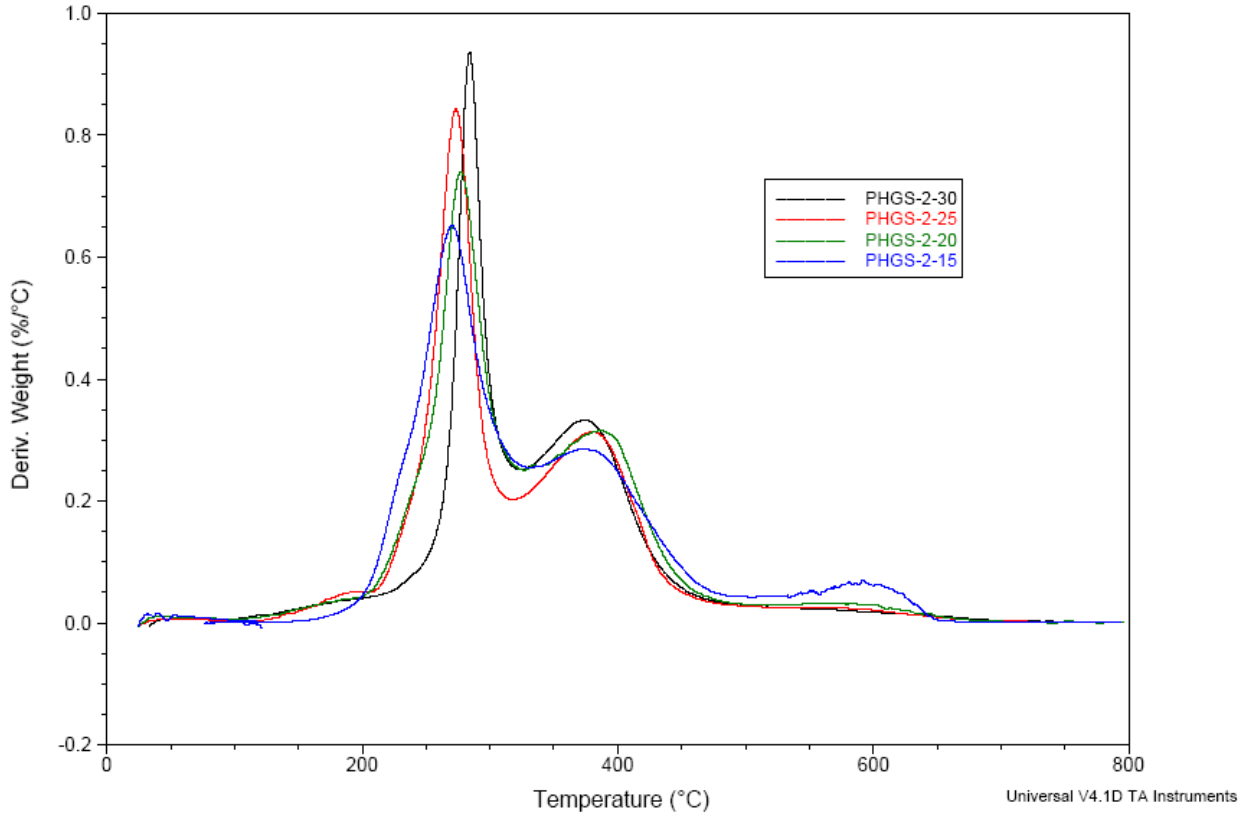

Figure 4-4. TGA differential curves of the derivative of weight percentage against temperature of the as-synthexsized hybrid materials from **Table 4-2**. TGA was measured at a programmed heating rate of 20 °C/min in the temperature range of ~30–800 ^{o}C. Before TGA measurements, samples were ground into a fine powder and kept in a vacuum oven at 80 ^{o}C for 24 hrs. A typical sample for TGA tests weighed ~5-10 mg.

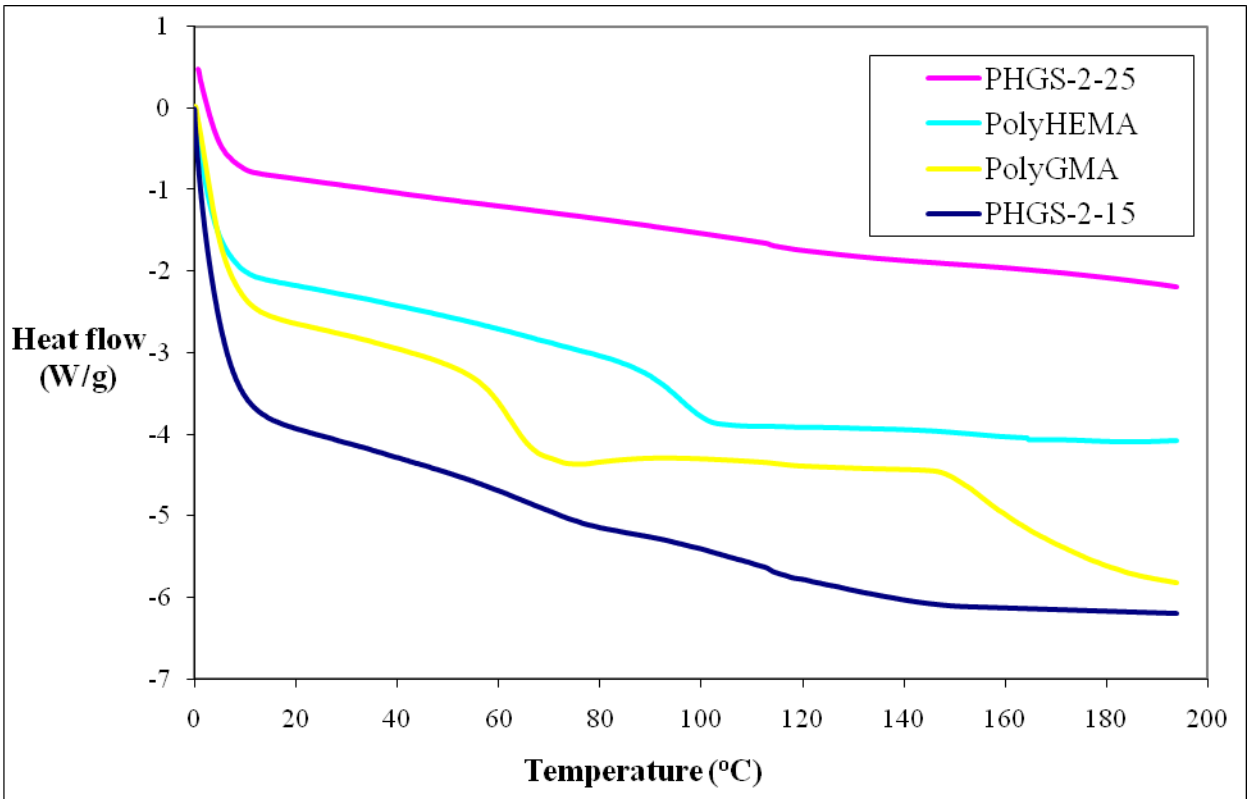

Figure 4-5. DSC curves of poly(HEMA), poly(GMA), PHGS-2-15 and PHGS-2-25 from **Table 4-2**. All samples were analyzed from 20 ^{o}C to 200 ^{o}C at a heating rate of 20 ^{o}C/min. Samples were ground into a fine powder and kept in a vacuum oven at 80 ^{o}C for 24 hr before DSC measurements. A typical sample for DSC analysis weighed ~5-10 mg.

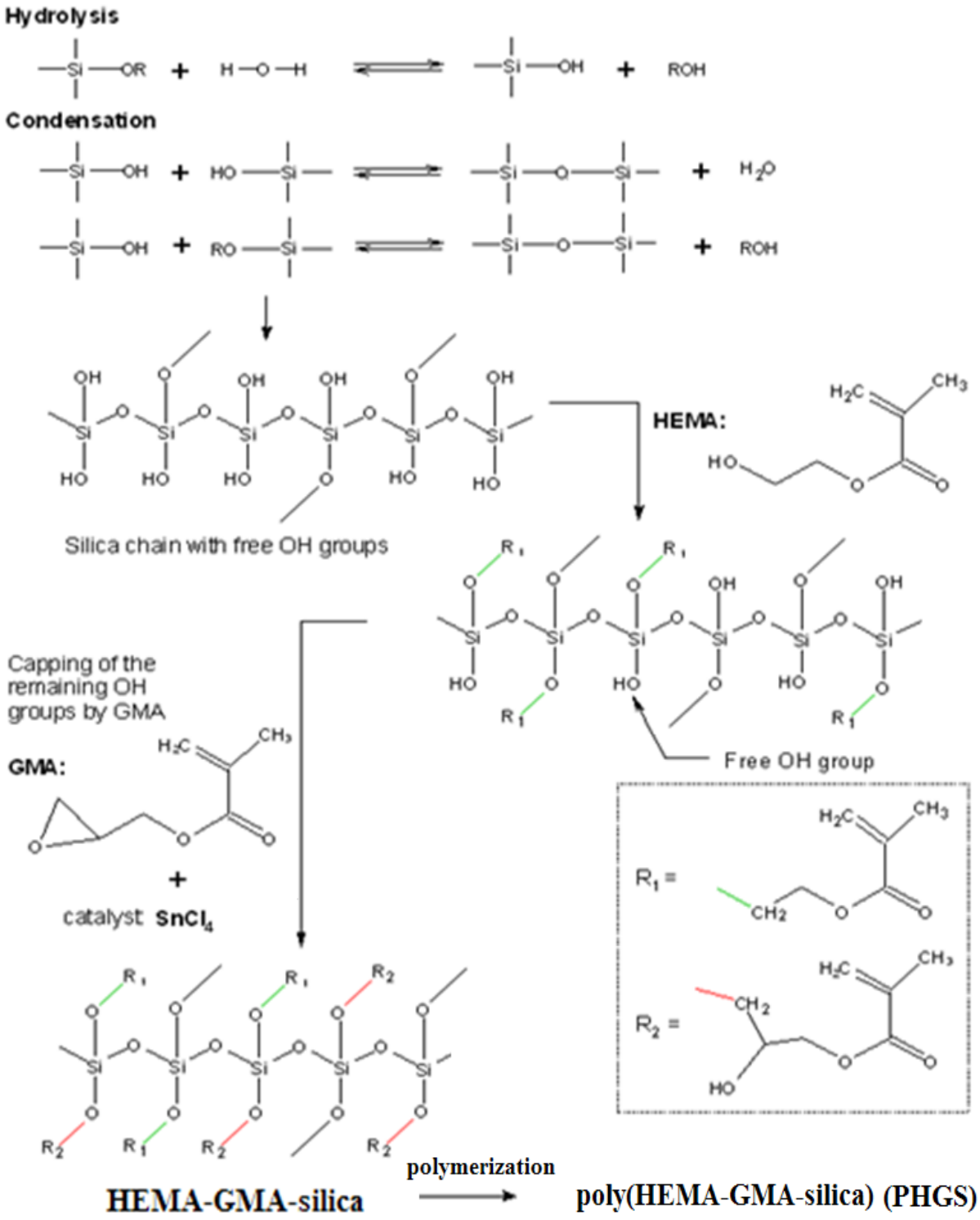

Figure 4-6. Detailed schematic of the PHGS synthesis procedure.

(a)

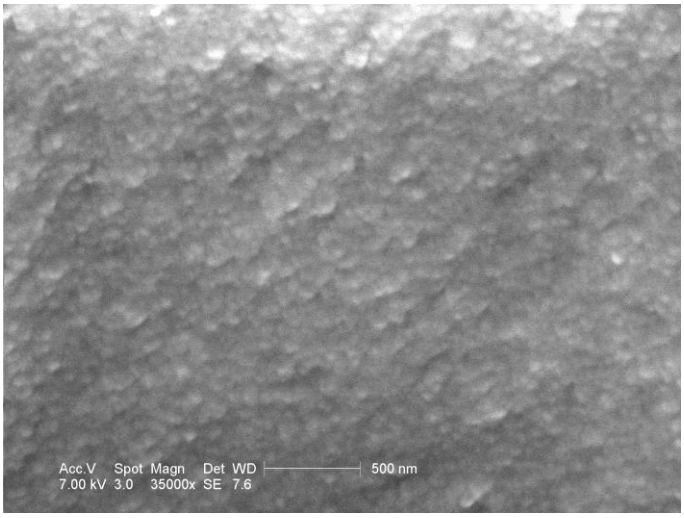

(b)

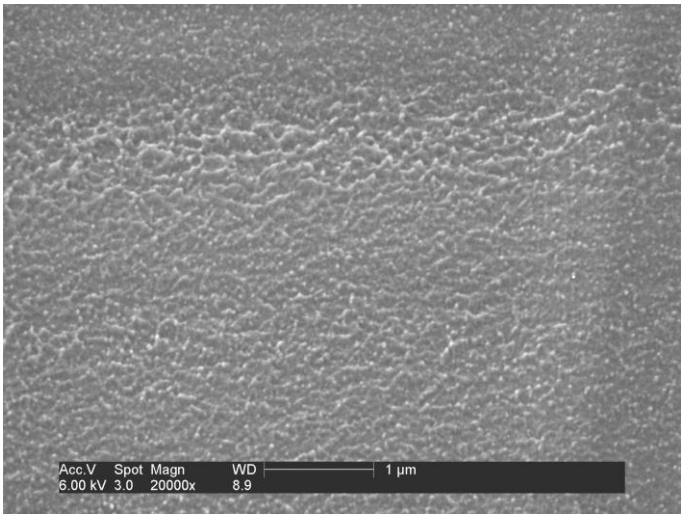

Figure 4-7. Scanning electron microscope image of: (**a**) PHGS-2-15 at 35000x magnification, acceleration voltage = 7 kV and spot size = 3. The particle formation remains smaller than 100 nm, (**b**) poly(methyl methacrylate) (PMMA) at 20000x magnification, acceleration voltage = 6 kV and spot size = 3. A worm-like structure with no particle formation is observed.

Figure 4-8. Digital picture of a monolithic transparent window product (PHGS-2-10) prepared in this study. Dimensions : 4” x 3” x 3/8”.

Figure 4-9. Hybrids were tested in compression to measure the compressive strength, yield stress, and modulus. The test specimens were cut (length to diameter ratio = 2:1) according to the ASTM standard (designation: D 695) using a diamond saw. The compression testing was performed using a servo-hydraulic machine (MTS Mini-Bionix 2, Eden Prairie, MN) at a crosshead speed of 10 mm/min.

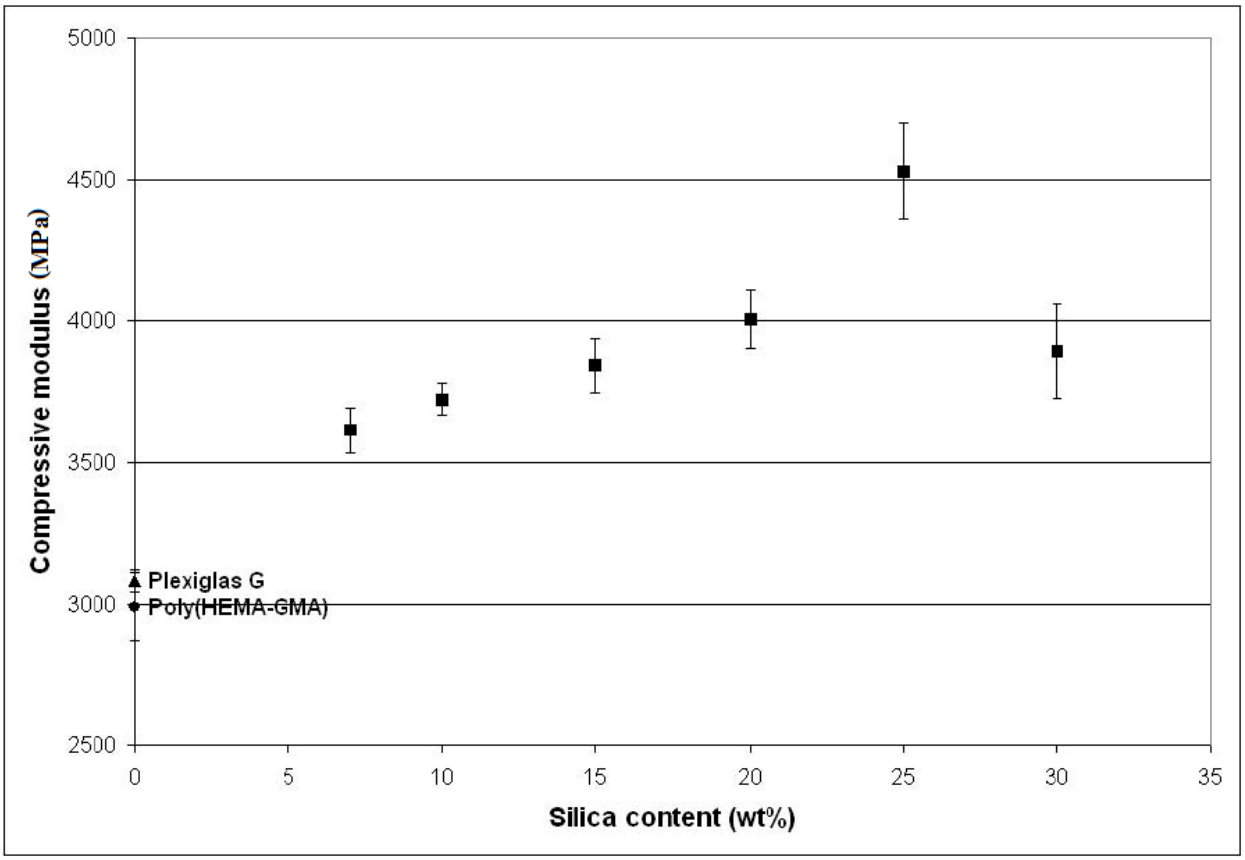

Figure 4-10. Average compressive modulus of poly(HEMA-GMA-silica) hybrids at different silica weight percentage, Plexiglas™ (PMMA) and poly(HEMA-GMA). A percolation threshold appears to be around 25 wt% of silica.

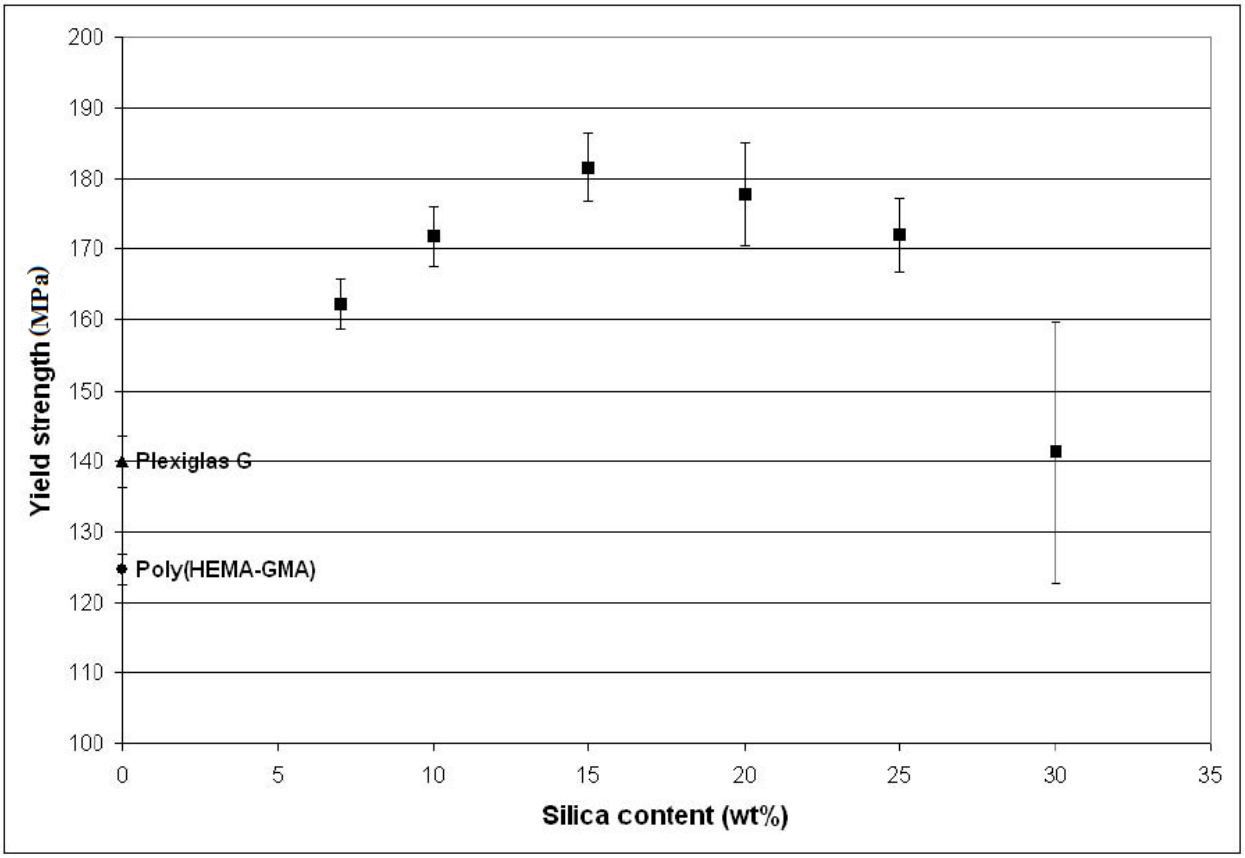

Figure 4-11. Yield stress versus silica content of poly(HEMA-GMA-silica) hybrids at different silica weight percentages, Plexiglas™ (PMMA) and poly(HEMA-GMA).

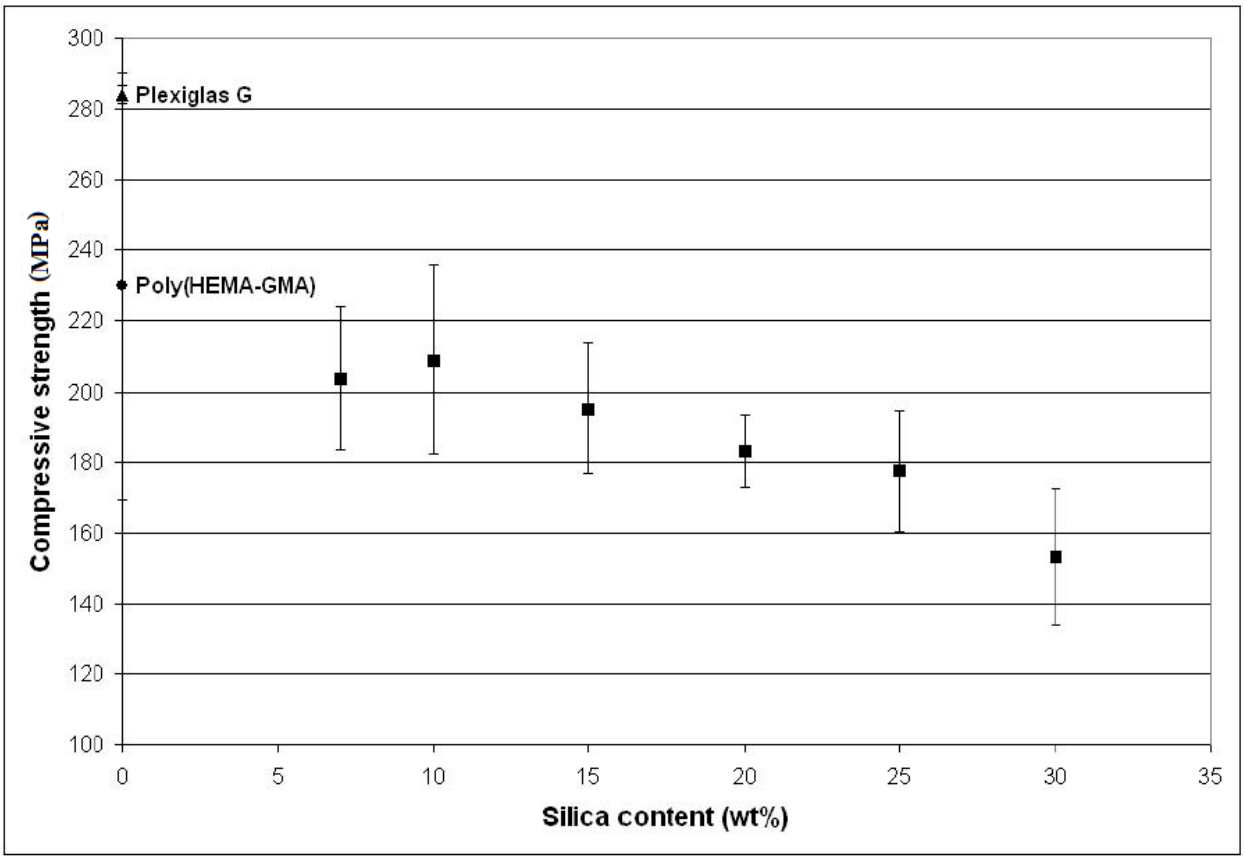

Figure 4-12. Average compressive strength of poly(HEMA-GMA-silica) hybrids at different silica weight percentages, Plexiglas™ (PMMA) and poly(HEMA-GMA).

4.7 Reference List

1. Lin, D. L., Chen, C. C., Chang, C. L., Su, Y. C., Cheng, L. P. Observation of nano-particles in silica/poly(HEMA) hybrid by electron microscopy. Journal of Polymer Research (2002), 9, 115-118.

2. Brinker C. J., Scherrer, G. W. Sol–gel science. Academic Press, San Diego; 1990.

3. Devreux, F., Boilot, J. P., Chaput, F., Lecomte, A. Sol-gel condensation of rapidly hydrolyzed silicon alkoxides: A joint ^{29}Si NMR and small-angle x-ray scattering study. Physical Review A (1990), 41, 6901-6909.

4. Bosch, P., DelMonte, F., Mateo, J. L., Levy, D. Photopolymerization of hydroxyethylmethacrylate in the formation of organic-inorganic hybrid sol-gel matrices. Journal of Polymer Science, Part A: Polymer Chemistry (1996), 34, 3289-3296.

5. Yeh, J. M., Weng, C. J., Huang, K. Y., Lin, C. C. Effect of baking treatment and materials composition on the properties of bulky PMMA-silica hybrid sol-gel materials with low volume shrinkage. Journal of Applied Polymer Science (2006), 101, 1151-1159.

6. Tanaka, K., Kozuka, H. Sol–gel preparation and mechanical properties of machinable cellulose/silica and polyvinylpyrrolidone/silica composites. Journal of Sol-Gel Science and Technology (2004), 32, 73-77.

7. Sharp, K. G. Inorganic/organic hybrid materials. Advanced materials (1998), 10, 1243-1248.

8. Messori, M., Toselli, M., Pilati, F., Fabbri, E., Fabbri, P., Busoli, S., Pasquali, L., Nannarone, S. Flame retarding poly(methyl methacrylate) with nanostructured organic-inorganic hybrids coatings. Polymer (2003), 44, 4463-4470.

9. Zhou, W., Dong, J. H., Qiu, K. Y., Wei, Y. Preparation and properties of poly(styrene-co-maleic anhydride) silica hybrid materials by the in situ sol-gel process .Journal of Polymer Science Part A: Polymer Chemistry (1998), 36, 1607-1613.

10. Novak, M. Hybrid nanocomposite materials-Between inorganic glasses and organic polymers. Advanced Materials (1993), 5, 422-433.

11. Hajji, P., David, L., Gerard, J.F., Pascault, J.P., Vigier, G. Journal of Polymer Science. Part B-Polymer Physics (1999), 37, 3172-3187.

12. Wen, J., Wilkes, G. L. Organic/inorganic hybrid network materials by the sol-gel approach. Chemistry of Materials (1996), 8, 1667-1681.

13. Wei, Y., Jin, D., Yang, C., Kels, M., Qiu, K. Organic-inorganic hybrid materials: relations of thermal and mechanical properties with structures. Materials Science and Engineering C. (1998), 6, 91-98.

14. Schubert, U., Husing, N., Lorenz, A. Hybrid inorganic-organic materials by sol-gel Processing of organofunctional metal alkoxides. Chemistry of Materials (1995), 7, 2010-2027.

15. Mammeri, F., Le Bourhis, E., Rozes, L., Sanchez, C. Elaboration and mechanical characterization of nanocomposites thin films: Part I: Determination of the mechanical properties of thin films prepared by in situ polymerisation of tetraethoxysilane in poly(methyl methacrylate). Journal of European Ceramics Society (2006), 26, 259-266.

16. Wei, Y., Jin, D., Yang, C., Wei, G. Synthesis of organic-inorganic hybrid sol – gel materials with low volume-shrinkages. Polymeric Materials Science and Engineering (1996), 74, 244-245.

17. Wei, Y., Jin, D., Wei, G., Yang, D., Xu, J. Novel organic-inorganic chemical hybrid fillers for dental composite materials. Journal of Applied Polymer Science (1998), 70, 1689-1699.

18. Guo, Y., Mylonakis, A., Zhang, Z., Lelkes, P. I., Levon, K., Li, S., Feng, Q., Wei, Y. Oligoaniline-contained electroactive silsesquioxane precursor for synthesizing novel siliceous materials. Macromolecules (2007), 40, 2721-2729.

19. Wei, Y., Wei, W., Jin, D., Yang, D., Tartakovskaya, L. Synthesis of sulfonated polystyrene-silica hybrids and their application as ion exchange materials. Journal of Applied Polymer Science (1998), 64, 1893-1902.

20. Wei, Y., Yeh, J. M., Jin, D., Jia, X., Wang, J.Composites of electronically conductive polyaniline with polyacrylate-silica hybrid sol-gel materials. Chemistry of Materials (1995), 7, 969-974.

21. Schmidt, H., Scholze, H., Kaiser, H. Principles of hydrolysis and condensation reaction of alkoxysilanes. Journal of Non-Crystallized Solids (1984), 63, 1-11.

22. Mark, J. E., Ning, Y. P. Effects of ethylamine catalyst concentration in the precipitation of reinforcing silica filler in an elastomeric network. Polymer Bulletin (1984), 12, 413-417.

23. Xu, J. W., Shi, W. F., Gong, M., Yu, F., Yan, L. F. Preparation of poly (methyl methacrylate-co-maleic anhydride) / SiO_2-TiO_2 hybrid materials and their thermo-and photodegradation behaviors. Journal of Applied Polymer Science (2005), 97, 1714-1724.

24. Kickelbick, G. Concepts for the incorporation of inorganic building blocks into organic polymers on a nanoscale. Progress in Polymer Science (2003), 28, 83-114.

25. Aparicio, M., Castro, Y., Duran, A. Synthesis and characterization of proton conducting styrene-co-methacrylate–silica sol–gel membranes containing tungstophosphoric acid. Solid State Ionics (2005), 176, 333-340.

26. Kelly, A. Concise Encyclopedia of Composite Materials. Elsevier, New York; 1994.

27. Novak, B. M., Davies, C. Inverse organic-inorganic composite materials. 2. Free-radical routes into nonshrinking sol-gel composites. Macromolecules (1991), 24, 5481-5483.

28. Klein, L. C. Sol-gel processing of silicates. Annual Review of Materials Science (1993), 23, 437-452.

29. Brinker, C. J., Scherer, G. W. Sol-gel science: The physics and chemistry of sol-gel processing. Academic Press, San Diego; 1990.

30. Wei, Y., Jin, D., Yang C., Wei, G. A fast and convenient method for the preparation of monolithic hybrid sol-gel materials without significant volume shrinkage. Journal of Sol-Gel Science and Technology (1996), 7, 191-201.

31. Xu, J. W., Shi, W. F., Gong, M., Yu, F., Yan, L. F. Preparation of poly(methyl methacrylate-co-maleic anhydride)/SiO_2-TiO_2 hybrid materials and their thermo- and photodegradation behaviors. Journal of Applied Polymer Science (2005), 97, 1714-1724.

32. Innocenzi, P., Kidchob, T., Yoko, T. Hybrid organic-inorganic sol-gel materials based on epoxy-amine systems. Journal of Sol-Gel Science and Technology (2005), 35, 225-235.

33. Chen, Y. C., Tsai, C. C., Lee, Y. D. Preparation and properties of silylated PTFE/SiO_2 organic-inorganic hybrids via sol-gel process. Journal of Polymer Science Part A: Polymer Chemistry (2004), 42, 1789-1807.

34. Li, S., Praveen, S. S., Mylonakis, A., Shah, A., Hsieh, A., Patel, A., Baran, G., Wei, Y. Synthesis of new organic–inorganic hybrids poly[2-hydroxethyl methacrylate (HEMA)-glycidyl methacrylate (GMA)-silica] and their mechanical properties. Journal of Materials Research (2008), 23, 66-71.

Chapter 5. Capping of Hydroxyl Groups in Sol-Gel Materials

5.1 Introduction and Motivation

The sol-gel method, compared to other inorganic network forming techniques, uses mild reaction conditions, such as relatively low temperatures (e.g., 30-100 ^{o}C), and is compatible with a broad range of solvents (e.g., water, alcohol, THF, etc.). These two characteristics offer the advantage to carry out the inorganic network forming reactions in the presence of a preformed organic polymer or to carry out the organic polymerization before, during or after the sol-gel process. The preparation, characterization and applications of these organic-inorganic hybrid materials have become a fast-expanding area in the search for new materials. Despite the many advantages that the sol-gel process offers, there are several severe, sometimes detrimental, problems associated with it. Amongst them, the most important are the large volume shrinkage, the crack formation and the brittleness of gels, and many attempts from various research groups have focused on how to overcome them.[1,2]

One way to solve these problems is the incorporation of organic compounds in the sol-gel matrices at the molecular or nanoscale level through a number of different synthetic routes.[3-10] Organic-inorganic hybrid materials have attracted much attention by many industrial and academic groups in the field of materials science over the past two decades because they have the potential of providing unique combinations of properties that cannot be achieved by conventional methods.[11-15] The properties of these materials depend not only on the properties of the individual components, but also on the composite's phase morphology and the interfacial properties.[16,17] These composites or organic-inorganic hybrid materials can be considered as nano-composites if the size of particles or phases, in at least one direction, is below 100 nm, and they remain transparent if the heterogeneity remains below 400 nm.[18] Sol-gel derived hybrids

have the wonderful advantage of the simplicity and versatility that is associated with the sol-gel process, which allows the easy incorporation of an organic component into a ceramic network under mild conditions.[19,20]

A big drawback of organic-inorganic hybrid materials made by the sol-gel process, though, is the inner and/or surface cracking that is observed in the obtained solidified materials after some period of time. This phenomenon is more common in the case of hybrid materials with very high inorganic content. The reason for this is the further condensation of the sol-gel materials that leads to the release of small molecular weight byproducts, which gradually create voids and cracks and subsequently greatly reduce the mechanical properties of the final materials. This is even more important when the pre-solidified materials have to be stored before use for a long period of time on the shelf or in the refrigerator. This means that the further condensation of sol-gel materials has to be hindered or completely avoided.

The synthesis and characterization of novel organic-inorganic hybrid materials, poly(HEMA-GMA-silica) (PHGS), with low volume shrinkage and excellent mechanical properties was reported in Chapter 4.[21] In this chapter, the basic concept behind the experimental approach that leads to those highly transparent monolithic hybrid materials is further investigated and described. This strategy possesses advantages over other methodologies employed to synthesize silica-containing hybrid materials, since cracking of the surface and reduction of the mechanical properties of the polymerized final materials, even after a long period of time, is lessened or avoided. This is accomplished by the capping of the remaining silanol groups in pure sol-gel materials or sol-gel hybrid materials by glycidyl methacrylate, which prevents the further condensation of the silanol groups. The progress of the capping reaction has been monitored by

thermal gravimetric analysis (TGA), near infrared spectroscopy (NIR) and gel permeation chromatography (GPC) to demonstrate the completeness of capping.

5.2 Experimental Part

5.2.1 Materials and Reagents

All reactants were purchased from Sigma Aldrich. Tetraethyl orthosilicate (TEOS), tetrahydrofuran (THF) and stannous chloride were used as received. 2-Hydroxethyl methacrylate (HEMA) and glycidyl methacrylate (GMA) were distilled under vacuum prior to use. Benzoyl peroxide (BPO) was recrystallized from methanol before use.

5.2.2 Instrumentation

5.2.2.1 Near Infrared Spectroscopy (NIR)

The near-infrared (NIR) spectroscopy apparatus consists of a NIR spectrometer from Control Development Incorporated (South Bend, IN), a custom sample chamber and a holder. The spectrometer possesses a spectral range of 1160 nm to 2250 nm with a resolution of 4 nm. The inside diameter of the testing sample tube was 1.96 mm. The reacting solutions were filled in the testing sample tube at predetermined time periods, and the epoxy concentration was monitored with NIR spectroscopy at room temperature.

5.2.2.2 Gel Permeation Chromatography (GPC)

Gel-permeation chromatography (GPC) was performed on a Waters GPC Model IIA equipped with a Model 590 solvent delivery module, a Model 410 differential refractometer as detector, and a Phenogel 10-μ column. Polystyrene standards were used for the calibration plot. THF was used as the eluent at a flow rate of 1.0 ml/min at room temperature. The samples to be

tested were diluted in THF (0.1-0.2 wt %), and 40 μl of the diluted solution were injected into the chromatography column.

5.2.2.3 Thermogravimetric Analysis (TGA)

Thermogravimetric analysis (TGA) was performed on a TA Q-50 thermal analysis system (TA instruments), equipped with TA Q Series Advantage Universal Analysis software, in air. TGA was measured at a programmed heating rate of 20 °C/min in a temperature range of ~30–700 ^{o}C. Before TGA measurements, the solidified samples were ground into a fine powder and kept in a vacuum oven at 80 ^{o}C for 24 hr. A typical sample for TGA tests weighed ~5-10 mg.

5.2.3 Synthesis Procedure

5.2.3.1 GMA-Silica Hybrids

As a general strategy to study the capping effect of GMA onto pre-hydrolyzed and partially condensed silicates, TEOS was hydrolyzed under acidic catalysis for a predetermined time, followed by condensation up to a certain point before crosslinking (i.e., gelation), under high vacuum. A predetermined portion of the above solution was mixed with GMA. In another portion of that solution, GMA was added along with the addition of $SnCl_4$ in order to study the catalytic effect that $SnCl_4$ has on the reaction of GMA with the hydroxyl groups of silanols. Finally another portion of that pre-hydrolyzed TEOS solution was mixed with GMA and $SnCl_4$, and the temperature of the obtained mixture was raised to 60 ^{o}C to study the effect that temperature has on the reaction of interest. Gel permeation chromatography and near-infrared spectroscopy studies were performed on theses non-polymerized mixtures of GMA-silica hybrids. On the other hand, thermogravimetric analysis studies were done on the polymerized

poly(GMA-silica) hybrids that were obtained upon radical polymerization of the GMA-silica hybrids thermally initiated with BPO.

As a typical procedure, 52.08 g TEOS (0.25 mol), 2.31 g of a 2M hydrochloric acid solution (0.0046 mol) and 6.69 g of water (0.371 mol) were charged in a 250-ml three-neck round-bottom flask, which was equipped with a thermometer, a condenser and a gas inlet/outlet. The mixture was stirred magnetically at room temperature under N_2 protection. The solution became homogeneous in 5 min, and in 7-8 min the temperature of the solution increased to over 60 ºC automatically. The transparent solution was stirred for 1 hr continuously without external heating. At this point the solution temperature returned to room temperature. The small molecular byproducts from the sol-gel reaction (i.e., ethanol and water) were then removed under vacuum at room temperature until the residue weight was about 60 % of the original weight solution. 5.00 g from this sol-gel mixture was mixed with 5.80 g of GMA, which is labeled as sample 1 in **Table 5-1**. An aliquot of 5.00 g from the sol-gel solution was mixed with 5.80 g GMA and 1.3 μl $SnCl_4$ and is labeled as sample 2 when stirring was done at room temperature, and sample 3 when stirring was done at higher temperature (60 ^oC) on **Table 5-1**. For thermal gravimetric analysis measurements, a predetermined amount of BPO (0.5 wt% with regards to the GMA content) was added into mixtures having the same compositions as samples 1, 2 and 3 from **Table 5-1,** followed by radical polymerization. For the polymerization step, the mixtures were kept in an air oven for 12 hr at 65 ^oC, then for 2 hr at 85 ^oC, and finally for two more hours at 125 ^oC.

5.2.3.2 GMA-HEMA-Silica Hybrids

In a similar manner to GMA-silica hybrids, GMA-HEMA-silica hybrids have been also investigated in order to study the capping efficiency of GMA onto pre-hydrolyzed and

condensed HEMA-silica hybrids. TEOS was hydrolyzed under acidic catalysis for a predetermined time in the presence of HEMA, followed by condensation up to a certain point under high vacuum. This first step in this procedure involves the growth of the silica phase via hydrolysis of TEOS up to a certain extent. HEMA molecules, through their pendant hydroxyl groups, react by condensation with the silanol groups of the hydrolyzed TEOS to introduce the acrylate groups into the oligomeric silicates. The next step includes the vacuum evaporation of the solvent (e.g., THF) and some of the byproducts (e.g., water and ethanol) that result from the hydrolysis of TEOS, the silanol-silanol condensation and the silanol-HEMA condensation respectively. A predetermined portion of the above solution was mixed with GMA. In another portion of that solution, GMA was added along with $SnCl_4$ in order to study the catalytic effect that $SnCl_4$ has on the reaction of GMA with the remaining hydroxyl groups of silanols. Finally another portion of the HEMA-silica hybrid solution was mixed with GMA and $SnCl_4$, and the temperature of the obtained mixture was raised to 60 ^oC to study the temperature effect on the reaction of interest. As in the case of GMA-silica hybrids, gel permeation chromatography and near-infrared spectroscopy studies were made on these non-polymerized mixtures of HEMA-GMA-silica (HGS) hybrids. On the other hand, thermogravimetric analysis studies were done on the polymerized poly(HEMA-GMA-silica) hybrids that were obtained upon radical polymerization of HEMA-GMA-silica hybrids by BPO.

As a typical procedure for the preparation of HEMA-GMA-silica hybrids, 52.08 g of TEOS (0.25 mol), 45.07 g of HEMA (0.346 mol), 36.05 g of THF (0.5 mol), 1.25 g of a 2M hydrochloric acid solution (0.0025 mol) and 10.52 g of H_2O (0.58 mol) were charged in a 250-ml three-neck round-bottom flask, which was equipped with a thermometer, a condenser and a nitrogen gas inlet/outlet. The opaque solution was stirred magnetically at room temperature

under N_2 protection. After about 15 minutes the mixture became transparent and the solution was refluxed for 2.5 hr at 65 ºC. After cooling down to room temperature, the solvent (e.g., THF) and byproducts from the sol-gel reaction (e.g., ethanol and water) were removed under vacuum until the residue weight was about 60 % of the original weight solution. When the solution returned to room temperature, several different sample mixtures of this hybrid with various predetermined compositions were made. The compositions of these mixtures are summarized in **Table 5-2.** The mixtures were magnetically stirred for 1 hr at room temperature before analysis tests. For thermal gravimetric analysis measurements, a predetermined amount of BPO (0.5 wt % with regards to the GMA content) was added into mixtures having the same compositions as samples 1, 2 and 3 from **Table 5-2,** followed by the radical polymerization of the acrylic groups that have been grafted on the growing silica. For the polymerization step, the mixtures were kept in an air oven for 12 hr at 65 ^{o}C, then for 2 hr at 85 ^{o}C and finally for two more hours at 125 ^{o}C.

5.3 Results and Discussion

5.3.1 Shelf Life

GMA is covalently bonded to the hydroxyl groups in pure sol-gel silica or HEMA-silica hybrids through the ring opening of the epoxy groups (**Figure 5-1**). When GMA reacts with pure sol-gel silica, organic-inorganic hybrid materials are obtained. In this case, GMA caps the hydroxyl groups of sol-gel silica directly, and the advantage is that the silica content of the final transparent products can be maximized. Shelf times observed for different hybrid compositions can be seen on **Table 5-1**. As shelf time we define the time it takes for a sol-gel material, contained in a sealed vial, to reach the gelation point when left on the bench at room temperature (i.e. 24 ^{o}C). From this table, it can be seen that pure sol-gel silica gelled in 1.5 hours, while when GMA was added into the system, without $SnCl_4$, gelation did not occur before 24 hr. On the

other hand, when $SnCl_4$, which is a catalyst for the reaction of GMA with the hydroxyl groups, was added to the above system (with or without temperature increase) the sol-gel system did not reach the gelation time before 48 days. This indicates the capping effect that GMA has onto the growing silica groups, such that the further condensation and the subsequent gelation of the obtained hybrid sol-gel materials are restricted.

Compositions and shelf times of hybrid materials obtained when GMA is added in HEMA-silica hybrids are given on **Table 5-2**. As can be seen from this table, sample 4 gelled dramatically faster (30 min) than all other samples. This is composed from HEMA-silica hybrid only, with no addition of GMA. Adding GMA to the above solution increases the shelf time by a little (i.e., sample 1 gelled in 1 day), but not sufficiently enough. On the other hand, if $SnCl_4$ is added together with GMA into the hybrid system, the shelf time increases to 21 days. Moreover, when the reaction temperature of the hybrid mixture is increased to 60 ^oC, then the shelf life of the obtained hybrid increases to 49 days.

This proves that the capping of the hydroxyl groups by GMA can be catalyzed by the addition of $SnCl_4$ and the increase of the reaction temperature. It is thus justifiable to say, that GMA is an organic group that can hinder the further condensation and the subsequent gelation of the obtained hybrid materials. This is accomplished by the complete capping of the remaining hydroxyl groups of silanols after the sol-gel reactions. An alternative route for GMA could be the reaction with water and/or ethanol groups, which result from the condensation of TEOS and have not been removed from the system upon vacuum evaporation. As IR spectroscopy experiments showed though (results not shown), these trace amounts of water and/or ethanol may be disregarded, since the extent of the reaction of the epoxy groups of GMA with the hydroxyl groups of these compounds is insignificant.

The shelf life results indicate that a catalyst (e.g., $SnCl_4$) is essential for the reaction of the epoxy groups of GMA with the hydroxyl groups of pure sol-gel silica or HEMA-silica to proceed fast. In the absence of $SnCl_4$ this reaction is slow and condensation of the sol-gel proceeds faster, which would subsequently lead to shorter gelation times. This would result in a decrease of the shelf time and in final products that tend to be more brittle and with high surface cracking upon polymerization. On the other hand, when $SnCl_4$ is added to the above-mentioned solutions, the further condensation of the sol-gel product is hindered since most, if not all, of the hydroxyl groups have been capped by GMA. This leads to hybrid solutions that have dramatically longer shelf times and to solidified products (upon radical polymerization) with low volume shrinkage and no surface cracking. It should be mentioned at this point that a basic catalyst isn't recommended in this case, because condensation under basic conditions proceeds faster as compared to acidic conditions, something that is not favorable in this case.[22]

5.3.2 Thermal Gravimetric Analysis (TGA)

Further support of the above arguments comes from the evaluation of the thermal behavior of the solidified, upon radical polymerization, hybrid materials (i.e. poly(GMA-silica) and poly(HEMA-GMA-silica)). **Figure 5-2** shows the TGA curves of the polymerized products, poly(GMA-silica), obtained upon radical polymerization by BPO (0.5 wt % with regards to the organic group) of the mixtures of GMA with pure sol-gel silica with or without the addition of $SnCl_4$ (samples 1, 2 and 3 from **Table 5-1**). The solidified product obtained upon radical polymerization of sample 1, which contained prehydrolyzed sol-gel silica and GMA but no $SnCl_4$, shows a loss of about 60% of its original weight at about 100 ^oC. This weight loss can be attributed to the byproducts that result from the further condensation of the sol-gel materials (e.g., ethanol and water). From the same figure, curves 2 and 3 correspond to the products

obtained upon radical polymerization of samples 2 and 3 from **Table 5-1,** respectively. Both of these polymerized hybrids show almost no loss at 100 ^{o}C and about 15 % loss of the original weight at 200 ^{o}C, which is attributed to the decomposition of the acrylic GMA groups. This suggests that GMA has reacted efficiently with the hydroxyl groups that remain free after the sol-gel reactions. Consequently, the further condensation of the sol-gel materials, which would lead to small molecular byproducts, has been restricted.

The thermal stability of the solidified products after the radical polymerization of the mixtures that result from the reaction of GMA with HEMA-silica hybrids with or without the addition of $SnCl_4$ has been also investigated (**Figure 5-3**). Sample 1 from **Table 5-2,** which contained no $SnCl_4$ in the reaction mixture, upon radical polymerization yielded a solidified product that shows a loss of about 35% of its original weight at 150 ^{o}C (curve 1). On the other hand, curves 2 and 3, which represent the polymerized products of samples 2 and 3 from **Table 5-2**, show a loss of 16 % and 2 % of their original weight respectively at about 150 ^{o}C. This indicates that GMA, in the presence of $SnCl_4$ and the increase of temperature, reacts efficiently with the free silanol hydroxyl groups, which remained unreacted after the sol-gel reactions of TEOS and the condensation reactions of TEOS with HEMA. This leads to products that show smaller weight loss below ~200 ^{o}C, since the further condensation of the sol-gel hybrid materials has been restricted. It has to be noted at this point, that the material that is represented by curve 1 in **Figure 5-2** shows higher weight loss at low temperatures compared to the sample that is represented by curve 1 in **Figure 5-3**. This is attributed to the fact that the latter contains HEMA organic groups, which have reacted partially with the silanol groups during the condensation step under vacuum. As a result, the amount of free hydroxyl groups remaining in this HEMA-silica sol-gel product and that could be condensed over time has been lowered.

5.3.3 Near Infrared Spectroscopy (NIR)

The capping of the silanol hydroxyl groups of the sol-gel intermediates from GMA has been monitored by means of near infrared spectroscopy (NIR).[23] The characteristic absorption peaks of the epoxy groups in this region are observed at 1644 nm and at 2209 nm, which are attributed to stretching and combination of stretching and bending vibrations, respectively.[24-26] In this study, we are particularly monitoring the peak at 2209 nm, although the peak at 1644 nm would lead us to the same conclusions.[27] The NIR spectra at different reaction times of GMA with pure sol-gel silica without addition of $SnCl_4$ at room temperature, of GMA with pure sol-gel silica in the presence of $SnCl_4$ at room temperature, and of GMA with pure sol-gel silica in the presence of $SnCl_4$ at 60 ºC can be seen on **Figures 5-4, 5-5** and **5-6,** respectively. By observing the absorption peak of the epoxy group at 2209 nm in these figures, it is apparent that even after a short period of time (e.g., 1 hr) GMA reacted faster with the hydroxyl groups in the presence of $SnCl_4$, as compared to the case where $SnCl_4$ was not present. After 7 hours of reaction, the epoxy concentration has been dramatically decreased when $SnCl_4$ has been added to the reaction system (**Figure 5-5**). As one would expect, in addition to $SnCl_4$ serving as a catalyst for this reaction, increase of the reaction temperature results in a faster reaction as well. **Figure 5-6** shows that upon increase of the reaction temperature, the peak that corresponds to the epoxy groups has almost diminished. For an even better elucidation of this phenomenon, **Figure 5-7** contains the NIR spectra of the mixtures obtained after 7 hr of reaction of GMA with sol-gel silica at room temperature, after 7 hr of reaction of GMA with sol-gel silica in the presence of $SnCl_4$ at room temperature and after 5 hr of reaction of GMA with silica at 60 ^{o}C in the presence of $SnCl_4$. It is clear that addition of $SnCl_4$ and increase of the reaction temperature to 60 ^{o}C drive the reaction of GMA with the silanol hydroxyl groups of the sol-gel intermediates to almost completion.

5.3.4 Gel Permeation Chromatography (GPC)

Gel permeation chromatography has been utilized to further prove the above findings. **Figure 5-8** presents the monitoring by GPC of the reaction of GMA with pre-hydrolyzed sol-gel silica with no addition of $SnCl_4$ or increase of the reaction temperature. The composition of this reaction system is the same as sample 1 from **Table 5-1**. Ar predetermined times, a small portion (i.e., 10 mg) of the above mixture was diluted in THF (0.1-0.2 wt%), and 40 μl of the diluted solution were injected into the GPC column. The molecular weights of the mixtures during monitoring of the reaction of GMA with pre-hydrolyzed sol-gel silica by GPC are summarized in **Table 5-3**. Initially, when no GMA has been added, only one peak, which corresponds to hydrolyzed and condensed, to a certain extent, TEOS can be seen (S curve). One hour after the addition of GMA, the graph now contains two peaks with the second peak corresponding to GMA (curve GS-1h). After 5 hr of reaction, the molecular weight of the products increases dramatically (sample GS-5h). This huge increase of the molecular weight is attributed to the condensation reactions of the sol-gel materials, which result in a highly crosslinked sol-gel product of high molecular weight.

The monitoring by GPC of the reaction of GMA with pre-hydrolyzed sol-gel silica in the presence of $SnCl_4$ and increase of temperature is presented in **Figure 5-9**. The monitoring of two different reaction systems is represented in the same figure. Both systems contained pre-hydrolyzed sol-gel silica, GMA and $SnCl_4$. The only difference between these two systems is that in one of them the reaction was done at room temperature, whereas in the other one, the reaction was done at 60 ^{o}C. The composition of these two reaction systems was the same as sample 2 and sample 3 from **Table 5-2**. In predetermined times, a small portion (i.e., 10 mg) of the above mixtures was diluted in THF (0.1-0.2 wt %), and 40 μl of the diluted solution were

injected into the GPC column. From this figure it can be seen that when $SnCl_4$ is used, the molecular weight of the mixture remains small after 1 hr of reaction. Even after 5 hr of reaction (sample GSSn-RT-5h), the molecular weight of the mixture is maintained in the small molecular weight range, which shows that the system cannot reach the gelation point. This is attributed to the fact that the further condensation of the sol-gel silica is hindered by the capping of the hydroxyl groups of the sol-gel intermediates by GMA. Moreover, adding $SnCl_4$ and increasing the reaction temperature of the solution to 60 ^oC causes the peak, that corresponds to GMA to disappear and the first peak that corresponds to the sol-gel products to be located in the low molecular weight range (GSSn-60^{o}C-2h). This is another proof of the efficiency of GMA to cap the free hydroxyl groups of the sol-gel intermediates. The further condensation of the sol-gel reactions, which would yield high molecular weight products, has thus been restricted.

5.3.5 Morphology

The synthetic approach of capping hydroxyl groups in sol-gel materials has been followed to create novel organic-inorganic hybrid materials, poly(HEMA-GMA-silica). The synthesis and characterization of these PHGS hybrids was presented in Chapter 4 of this thesis. The obtained materials were completely transparent and had excellent mechanical properties. **Figure 5-10** shows the dramatic difference between a polymerized product, when the capping procedure with GMA has been employed, and a polymerized material obtained when no capping has been utilized. Both samples were left on the lab bench at room temperature for 12 months. Sample a appears to be perfectly transparent with no surface cracks, whereas sample b shows bad surface condition with surface voids and cracks after 12 months. This resulted from the further condensation of the sol-gel that led to the release of small molecular weight byproducts, which

gradually created voids and cracks and subsequently greatly ruined the surface finish of the final materials.

5.4 Conclusions

The results of the experiments (e.g., TGA, NIR and GPC) and the physical properties of the solidified materials indicate that the hydroxyl groups in pure sol-gel silica or HEMA-silica hybrids can be efficiently capped by the epoxy groups of GMA. The two different types of reactions, that is, the capping reaction and the sol-gel condensation, are in competition. Thus, if the capping reaction proceeds fast, it can hinder the condensation reaction efficiently. Without $SnCl_4$ catalyst, though, the capping reaction proceeds slowly and the condensation of sol-gel proceeds mainly in the system, which leads to gelation. Upon increase of the temperature, the reaction of the GMA epoxy groups with the TEOS hydroxyl groups in the presence of $SnCl_4$ can be completed in about 3 to 5 hours. It is important to control the reaction conditions for optimization of the mechanical properties of the obtained materials. Except epoxy groups, the capping agents could also be anhydrides, isocyanates, silanes and others, which could lead to innumerable products with many potential applications in the chemical, materials and even biomedical industries.

5.5 Acknowledgments

This project has been conducted in cooperation with Dr. Shuxi Li and Mr. Robert Wei. This work was supported by the U.S. Army Research Laboratory and the National Institutes of Health. I would like to thank Professor Giuseppe R. Palmese and Dr. Jihean Lee from the Department of Materials Science and Engineering at Drexel University for their assistance in the NIR experiments.

Table 5-1. Compositions, reaction conditions and shelf life of products from the reaction of GMA with pure sol-gel silica.

Sample Code	Sol-gel silica (g)	GMA (g)	$SnCl_4$ (µl)	Reaction time (hr)	Shelf life (days)	SiO_2 Theore-tical (wt %)	SiO_2 Experi-mental (wt %)
1	5.00	5.80	—	6.5 at RT*	1	21.2	21.5
2	5.00	5.80	1.3	22 at RT*	Viscous after 48 days	21.2	21.7
3	5.00	5.80	1.3	6 at 60 ºC	Gelled after 48 days	21.2	21.9
4	5.00	—	—	0 at RT*	1.5 hr	48.9	52.1

*RT : Room temperature

Table 5-2. Composition, reaction conditions and shelf life of products from the reaction of GMA with HEMA-silica hybrids.

Sample Code	HEMA-silica (g)	GMA (g)	$SnCl_4$ (µl)	Reaction time (hr)	Shelf life (days)	SiO_2 Theore-tical (wt %)	SiO_2 Experime-ntal (wt %)
1	8.00	4.00	—	6 at RT*	1	18.6	18.6
2	8.00	4.00	6.7	6 at RT*	21	16.9	17.1
3	8.00	4.00	6.7	6 at 60 ºC	49	15.5	15.7
4	8.00	—	—	0 at RT*	0.5 hr	25.0	24.3

*RT : Room temperature

Table 5-3. Molecular weights of mixtures during monitoring of the reaction of GMA with pre-hydrolyzed sol-gel silica by GPC.

	First peak			Second peak		
Sample	**M_n**	**M_w**	**PD**	**M_n**	**M_w**	**PD**
S	6000	31200	5.2			
GS-1h	10200	45200	4.4	103	107	1.04
GS-5h	28500	74200	2.6	114	119	1.04
GSSn-RT-1h	6900	30300	4.4	111	123	1.11
GSSn-RT-5h	8400	39100	4.7	123	134	1.09
GSSn-60^{o}C-2h	6250	56240	9.0			

M_n: Number average molecular weight, M_w: Weight average molecular weight, PD: Polydispersity = M_w/M_n.

S: pure hydrolyzed and condensed TEOS.

GS-1h: GMA has been added in the sol-gel solution (1 hr of reaction).

GS-5h: GMA has been added in the sol-gel solution (5 hr of reaction).

GSSn-RT-1h: GMA and $SnCl_4$ have been added in the sol-gel solution (1 hr of reaction at room temperature).

GSSn-RT-5h: GMA and $SnCl_4$ have been added in the sol-gel solution (5 hr of reaction at room temperature).

GSSn-60^{o}C-2h: GMA and $SnCl_4$ have been added in the sol-gel solution (2 hr of reaction at 60 ^{o}C).

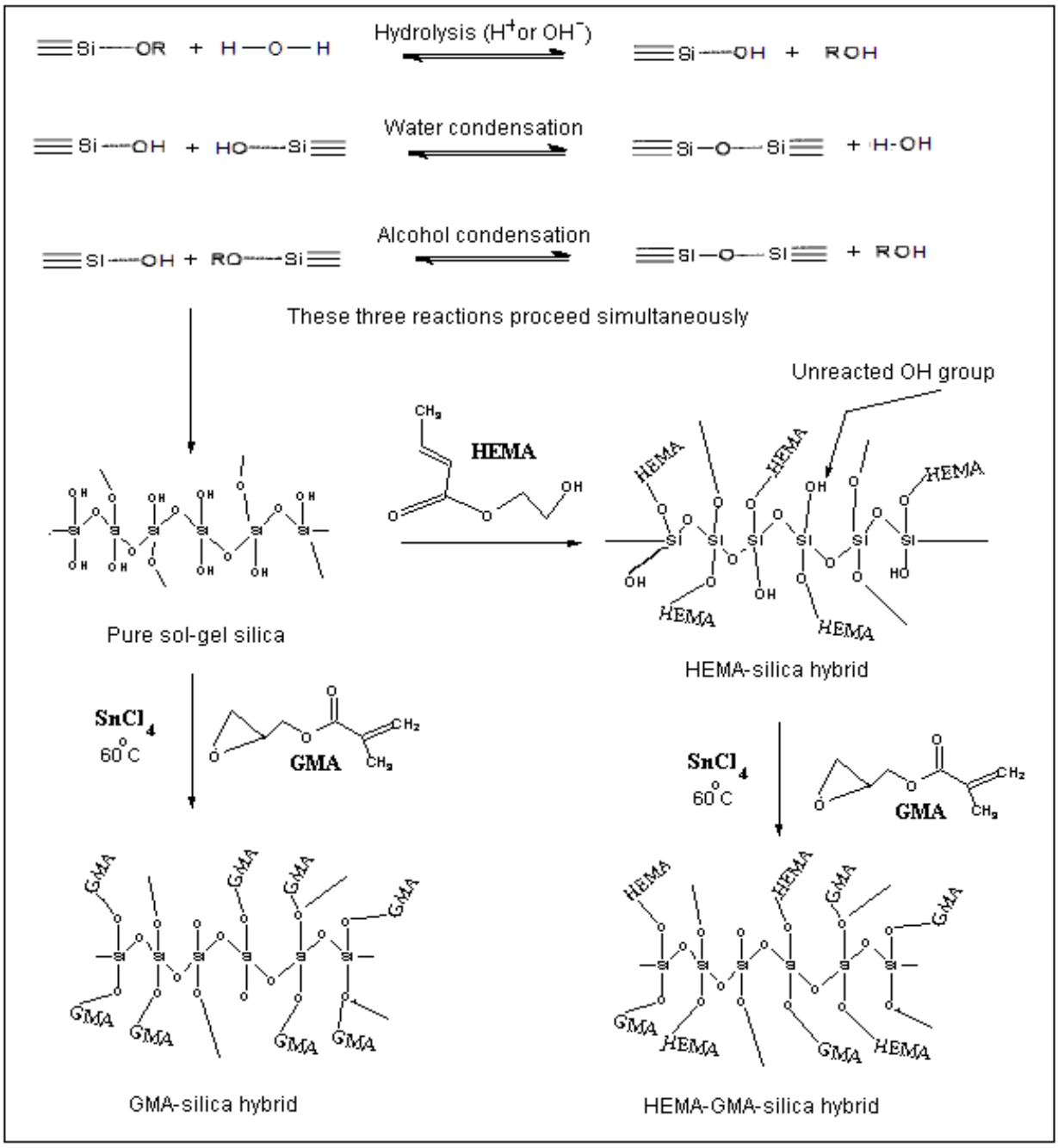

Figure 5-1. Detailed schematic showing the reactions under study.

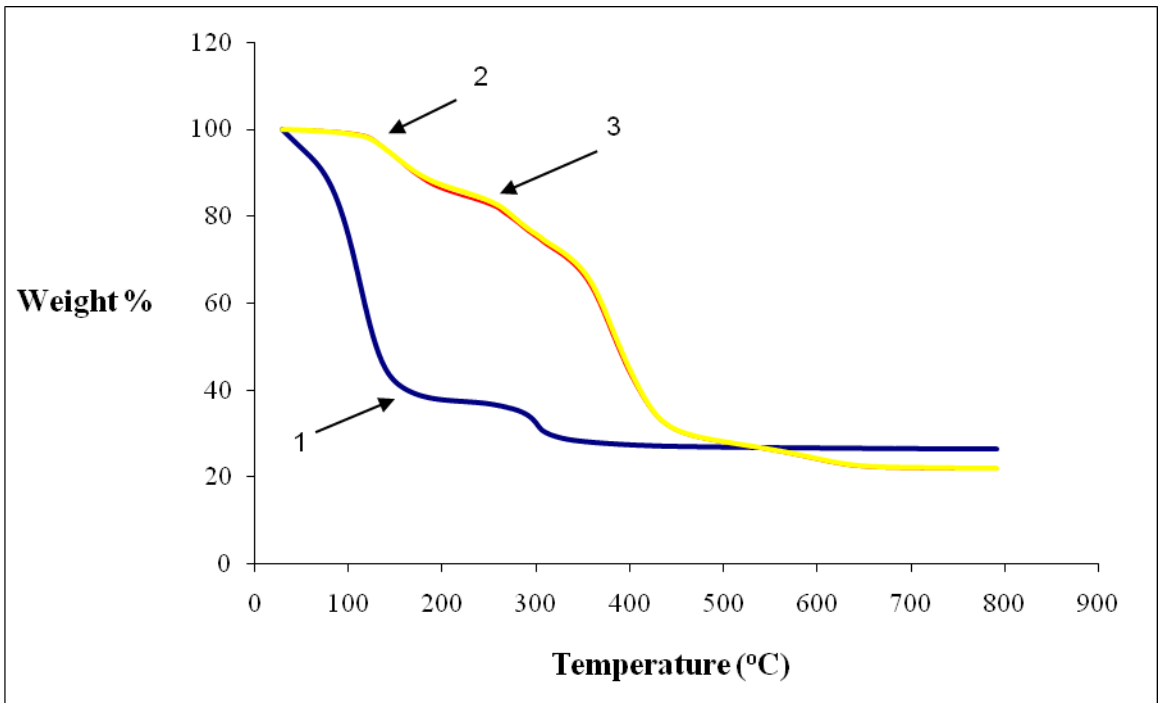

Figure 5-2. TGA curves of the solidified hybrids poly(GMA-silica) obtained upon radical polymerization by BPO (0.5 wt % with regards to the acrylic content) of GMA-silica samples: (1) no addition of $SnCl_4$, (2) in the presence of $SnCl_4$, (3) in the presence of $SnCl_4$ and increase of the reaction temperature to 60 ^oC. Curves 1, 2 and 3 correspond to the solidified hybrids obtained upon radical polymerization of samples 1, 2 and 3 from **Table 5-1,** respectively. TGA tests were perfomed at a heating rate of 20 °C/min in a temperature range of ~30–700 ^oC. Before TGA tests, the solidified samples were ground into a fine powder and kept in a vacuum oven at 80 ^oC for 24 hr.

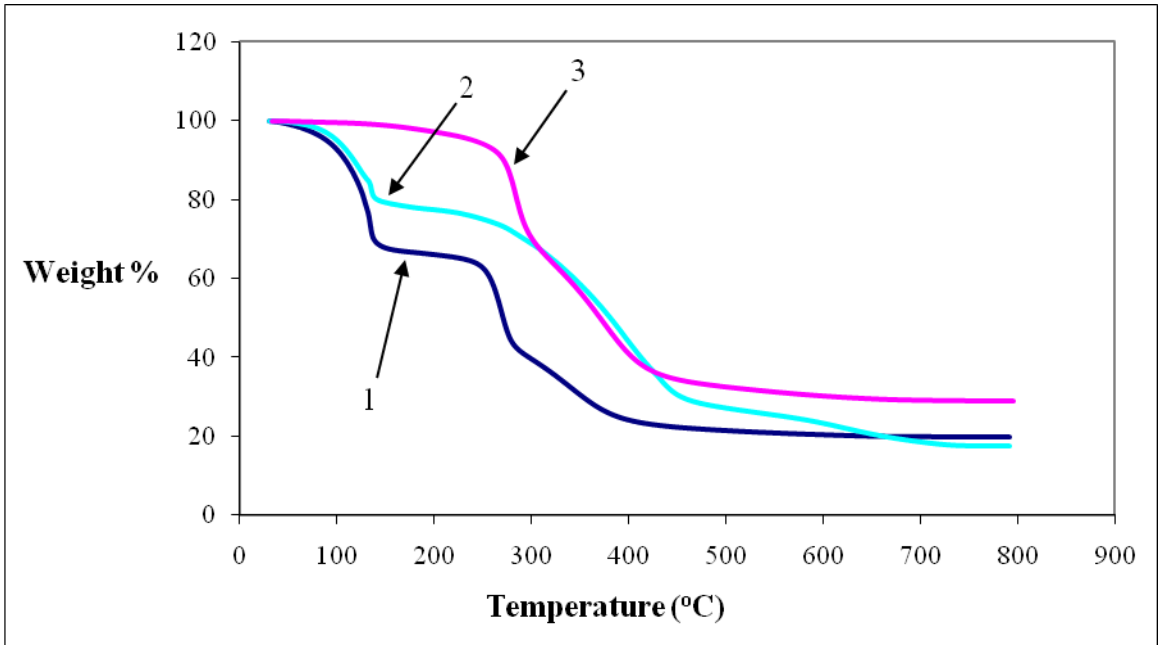

Figure 5-3. TGA curves for the solidified hybrids poly(HEMA-GMA-silica) obtained upon radical polymerization by BPO (0.5 wt % with regards to the acrylic content) of HEMA-GMA-silica: (1) no addition of $SnCl_4$, (2) in the presence of $SnCl_4$, (3) in the presence of $SnCl_4$ and increase of the reaction temperature to 60 ^oC. Curves 1, 2 and 3 correspond to the solidified hybrids obtained upon radical polymerization of samples 1, 2 and 3 from **Table 5-2,** respectively. TGA tests were perfomed at a heating rate of 20 °C/min in a temperature range of ~30–700 ^oC. Before TGA tests, the solidified samples were ground into a fine powder and kept in a vacuum oven at 80 ^oC for 24 hr.

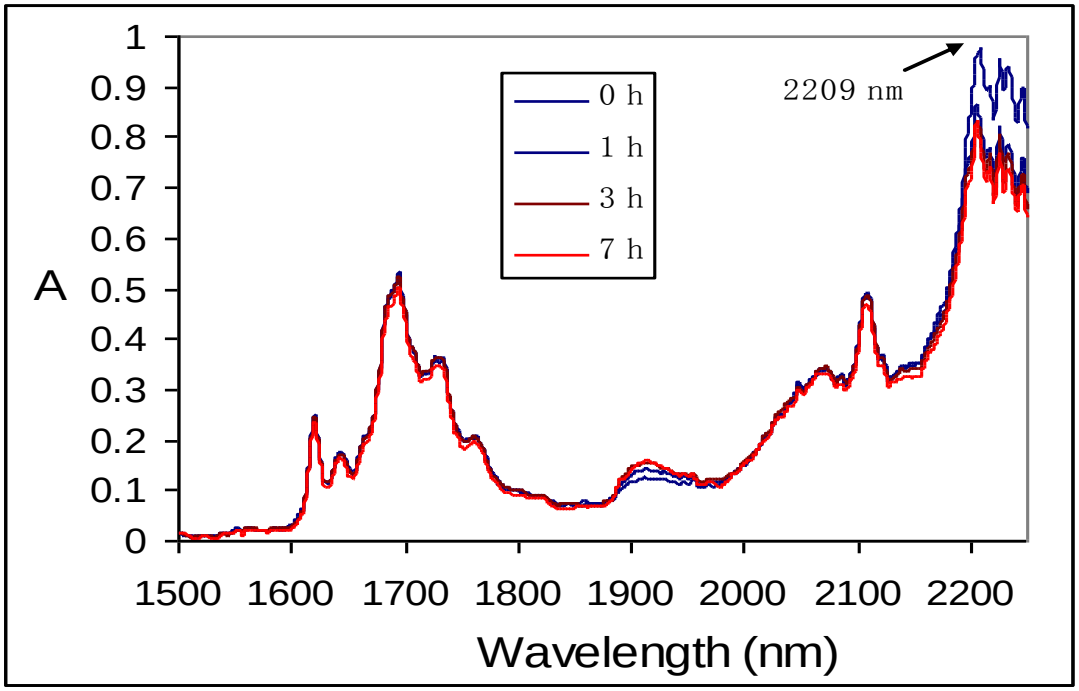

Figure 5-4. NIR monitoring of the reaction of GMA with sol-gel silica at room temperature for a period of 7 hr.

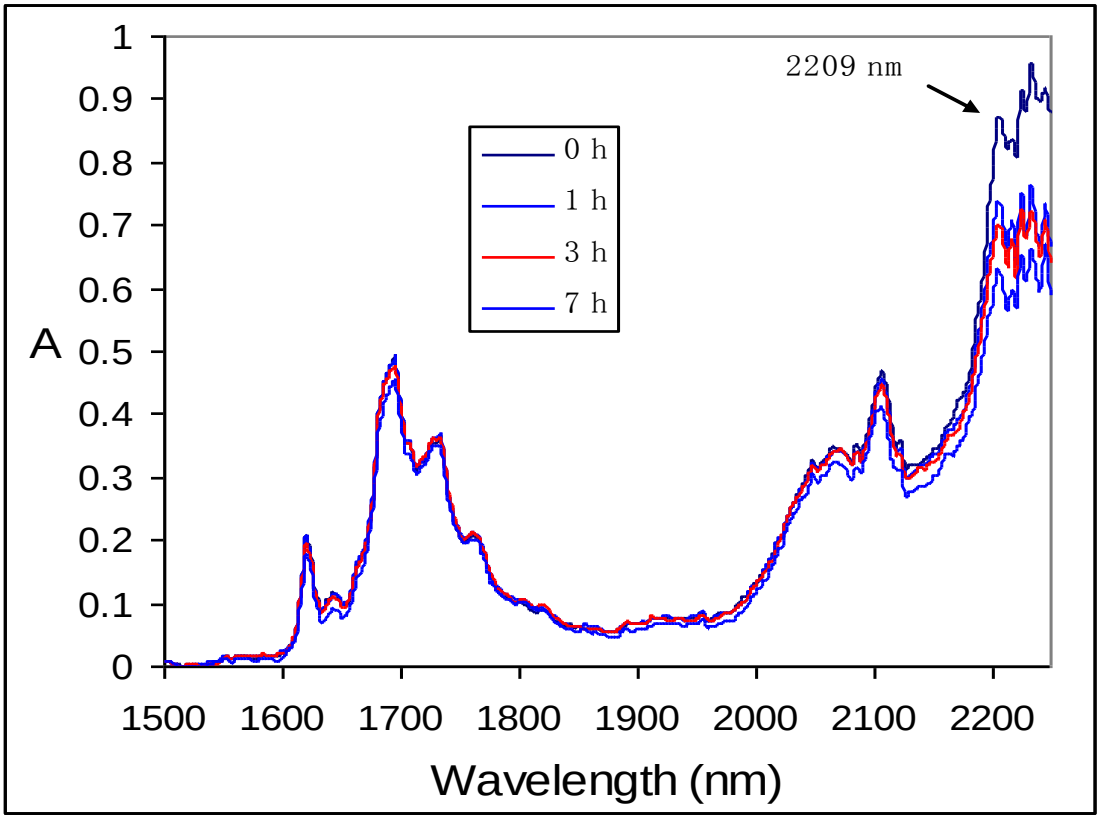

Figure 5-5. NIR monitoring of the reaction of GMA with sol-gel silica in the presence of $SnCl_4$ at room temperature for a period of 7 hr.

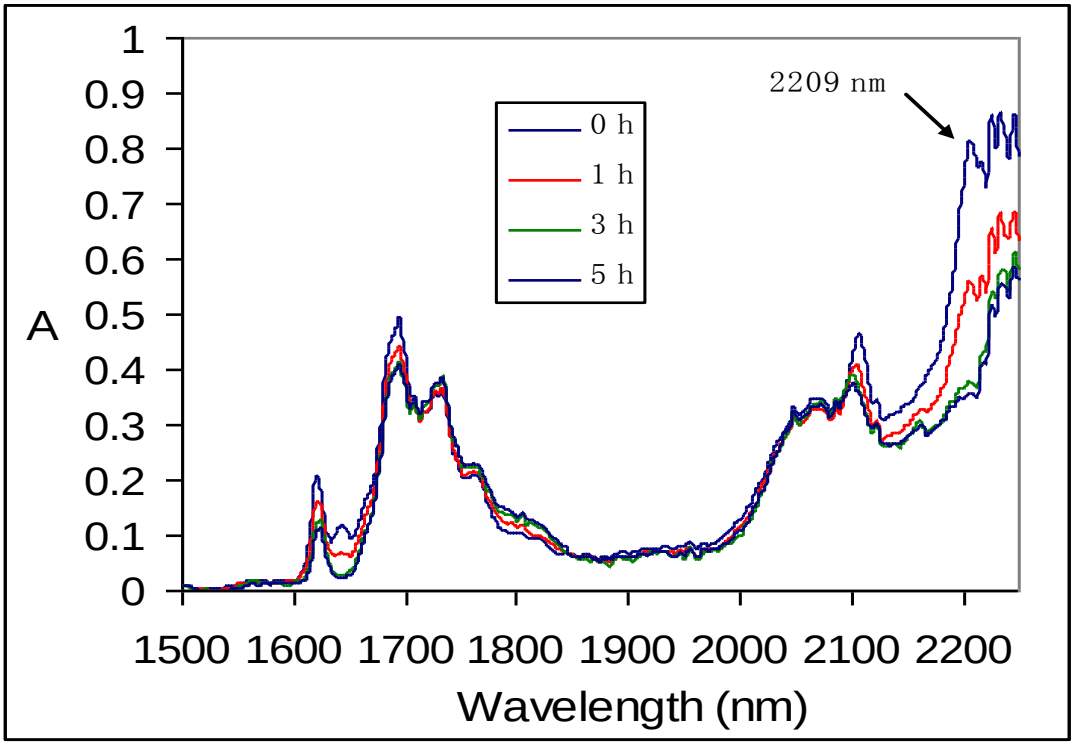

Figure 5-6. NIR monitoring of the reaction of GMA with sol-gel silica in the presence of $SnCl_4$ at 60 ºC for a period of 5 hr.

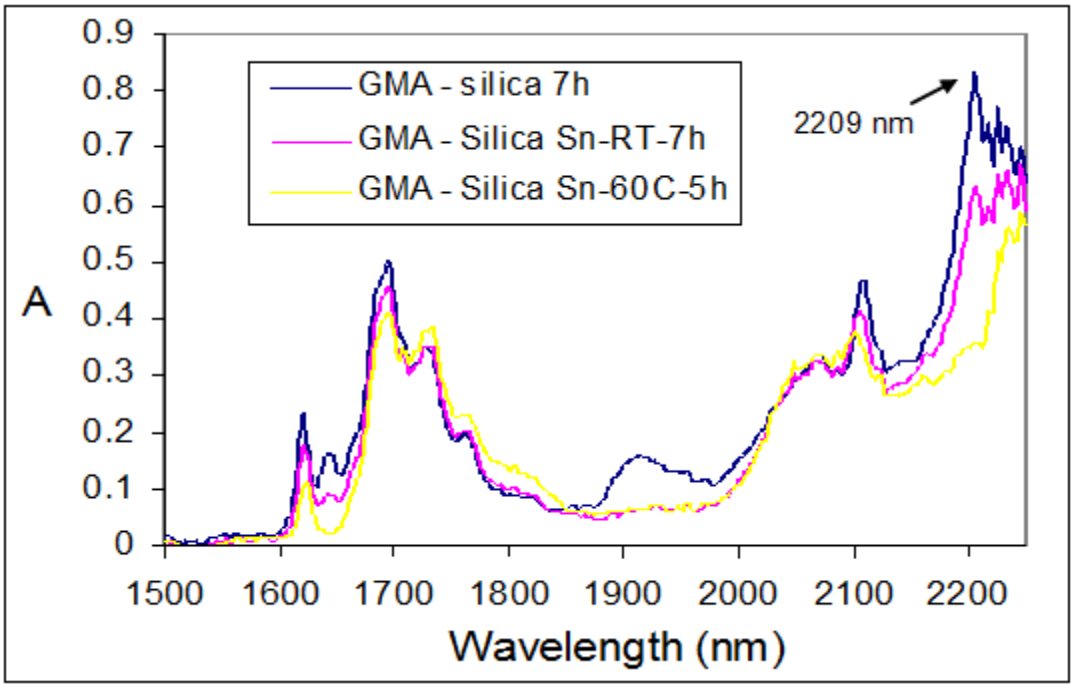

Figure 5-7. NIR curves of the reaction of GMA with sol-gel silica. GMA-silica 7h: after 7 hr of reaction of GMA with sol-gel-silica at room temperature. GMA-silica Sn-RT-7h: after 7 hr of reaction of GMA with sol-gel-silica in the presence of $SnCl_4$ at room temperature. GMA-silica Sn-60C-5h: after 5 hr of reaction of GMA with sol-gel-silica in the presence of $SnCl_4$ at 60 ºC.

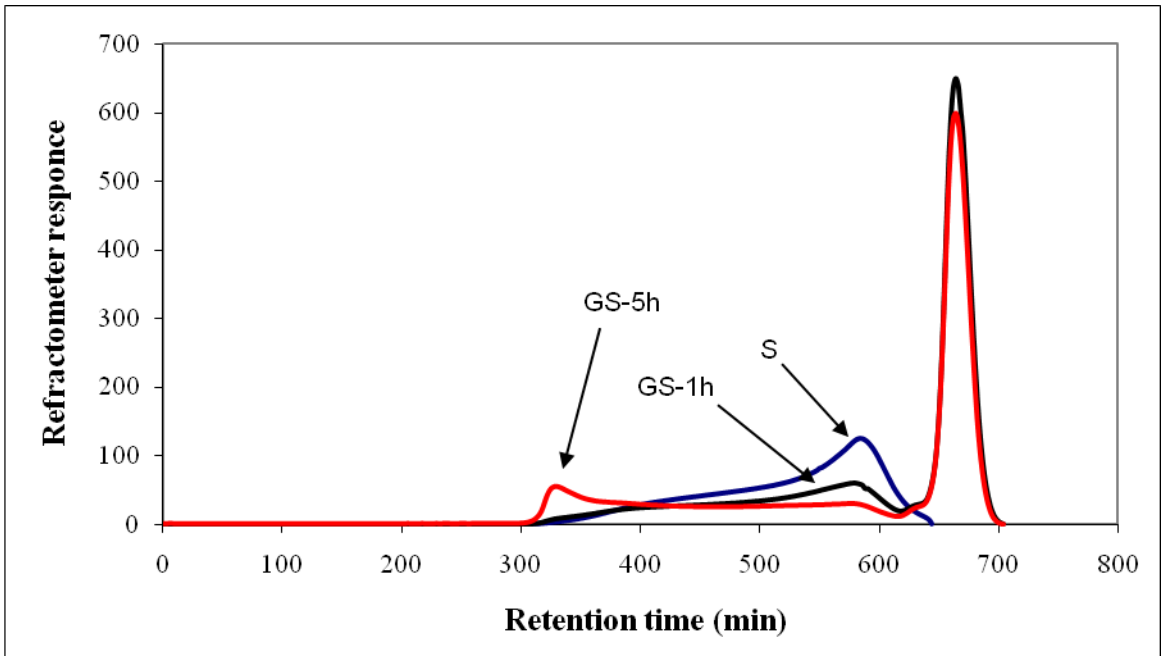

Figure 5-8. Gel permeation chromatography monitoring of the reaction of GMA with HEMA-silica hybrids at different reaction times. Polystyrene standards were used for the GPC calibration plot. THF was used as the eluent at a flow rate of 1.0 ml/min at room temperature. The samples were first diluted in THF (0.1-0.2 wt %), and 40 µl of the diluted solution were injected into the column.

S: Pure hydrolyzed and condensed TEOS.

GS-1h: GMA has been added in the sol-gel solution (1 hr of reaction).

GS-5h: GMA has been added in the sol-gel solution (5 hr of reaction).

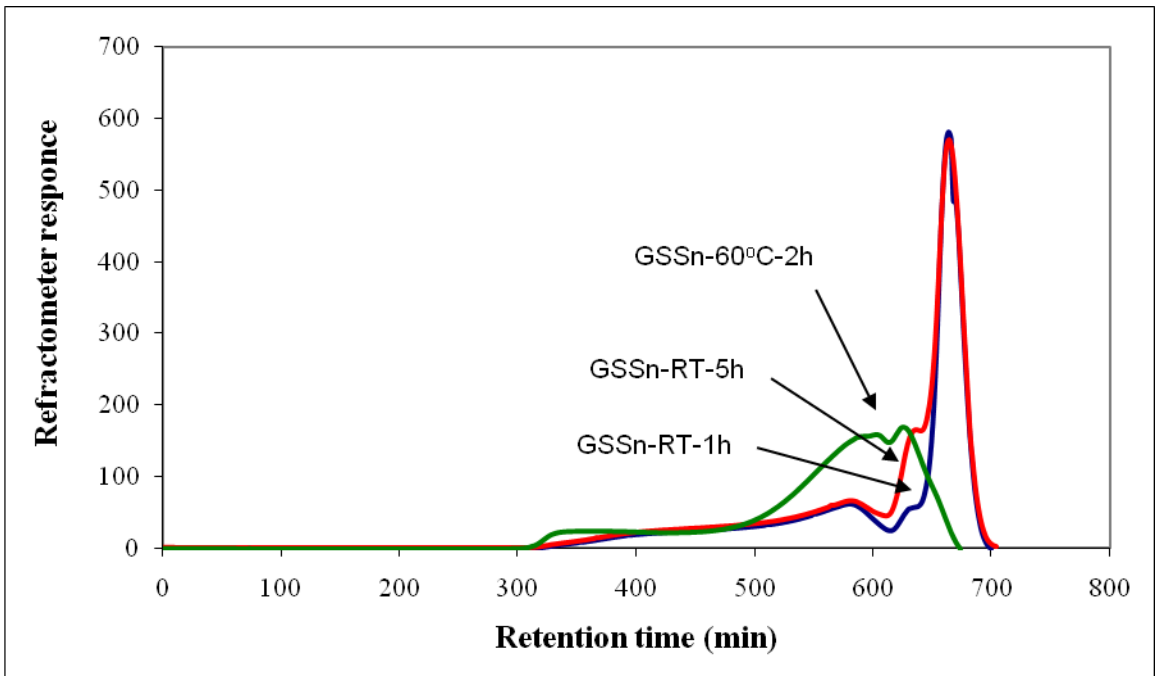

Figure 5-9. Gel permeation chromatography of the reaction of GMA with HEMA-silica at different reaction times in the presence of $SnCl_4$. Polystyrene standards were used for the GPC calibration plot. THF was used as the eluent at a flow rate of 1.0 ml/min at room temperature. The samples were first diluted in THF (0.1-0.2 wt %), and 40 µl of the diluted solution were injected into the column.

GSSn-RT-1h: GMA and $SnCl_4$ have been added in the sol-gel solution (1 hr of reaction at room temperature).

GSSn-RT-5h: GMA and $SnCl_4$ have been added in the sol-gel solution (5 hr of reaction at room temperature).

GSSn-60^{o}C-2h: GMA and $SnCl_4$ have been added in the sol-gel solution (2 hr of reaction at 60 ºC).

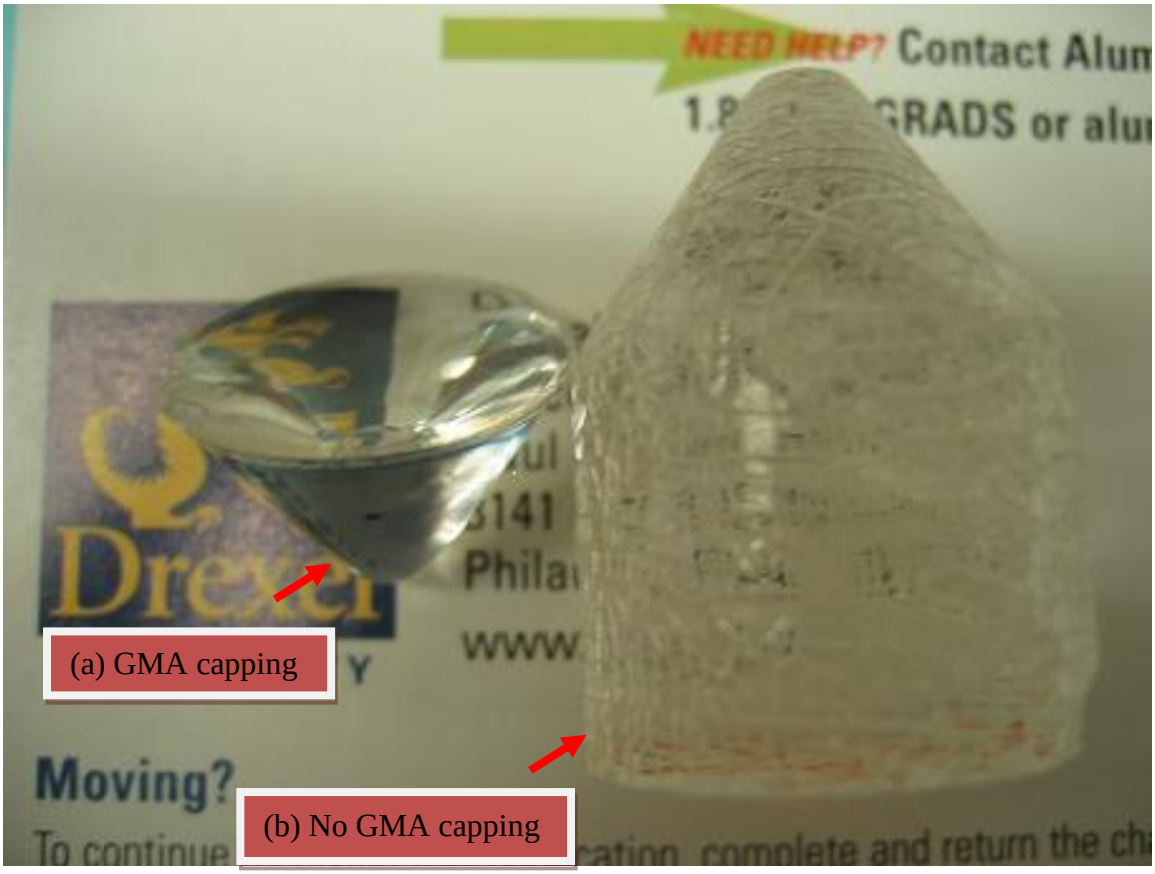

Figure 5-10. Optical picture of solidified products when (a) the capping procedure with GMA has been employed, (b) the capping procedure with GMA has not been employed. Both samples were left on the lab bench at room temperature for 12 months.

5.6 Reference List

1. Brinker, C. J., Scherer, G. W. Sol-gel science: the physics and chemistry of sol-gel processing. Academic Press, Boston; 1990.

2. Zhu, B., Katsoulis, D. E., Keryk, J. R., McGarry, F. L. Toughening of a polysilsesquioxane network by homogeneous incorporation of polydimethylsiloxane segments. Polymer (2000), 41, 7559-7573.

3. Hajji, P., David, L., Gerard, J. F., Pascault, J. P., Vigier, G. Synthesis, structure, and morphology of polymer-silica hybrid nanocomposites based on hydroxyethyl methacrylate. Journal of Polymer Science, Part B: Polymer Physics (1999), 37, 3172-3187.

4. Wei, Y., Bakthavatchalam, R., Whitecar, K. C. Synthesis of new organic-inorganic hybrid glasses. Chemistry of Materials (1990), 2, 337-339.

5. Surivet, F., Lam, T. M., Pascault, J. P., Pham, Q. T. Organic-inorganic hybrid materials. Hydrolysis and condensation mechanisms involved in alkoxysilane-terminated macromonomers. Macromolecules (1992), 25, 4309-4320.

6. Khimich, N. N. Synthesis of silica gels and organic-inorganic hybrids on their base. Glass Physics and Chemistry (2004), 30, 430-442.

7. Innocenzi, P., Kidchob, T., Yoko, T. Hybrid organic-inorganic sol-gel materials based on epoxy-amine systems. Journal of Sol-Gel Science and Technology (2005), 35, 225-235.

8. Landry, C. J. T., Coltrain, B. K., Wesson, J. A., Zumbulyadis, N., Lippert, J. L. In situ polymerization of tetraethoxysilane in polymers: chemical nature of the interactions. Polymer (1992), 33, 1496-1506.

9. Ellsworth, M. W., Novak, B. M. Mutually interpenetrating inorganic-organic networks. New routes into nonshrinking sol-gel composite materials. Journal of the American Chemical Society (1991), 113, 2756-2758.

10. Wang, S., Ahmad, Z., Mark, J. E. A polyamide-silica composite prepared by the sol-gel process. Polymer Bulletin (1993), 31, 323-330.

11. Schmidt, H., Jonschker, G., Goedicke, S., Mennig, M. The sol-gel process as a basic technology for nanoparticle-dispersed inorganic-organic composites. Journal of Sol-Gel Science and Technology (2000), 19, 39-51.

12. Landry, C. J. T., Coltrain, B. K., Landry, M. R., Fitzgerald, J. J., Long, V. K. Poly(vinyl acetate)/silica filled materials: Material properties of in situ vs fumed silica particles. Macromolecules (1993), 26, 3702-3712.

13. Huang, H. H., Orler, B., Wilkes, G. L. Structure-property behavior of new hybrid materials incorporating oligomeric species into sol-gel glasses. 3. Effect of acid content, tetraethoxysilane content, and molecular weight of poly(dimelsiloxane). Macromolecules (1987), 20, 1322-1330.

14. Garrido, L., Mark, J. E., Sun, C. C., Ackerman, J. L., Chang, C. NMR characterization of elastomers reinforced with in-situ precipitated silica. Macromolecules (1991), 24, 4067-4072.

15. Tsubokawa, N., Saitoh, K., Shirai, Y. Surface grafting of polymers onto ultrafine silica: Cationic polymerization initiated by benzylium perchlorate groups introduced onto ultrafine silica surface. Polymer Bulletin (1995), 35, 399-406.

16. Novak, M. Hybrid nanocomposite materials-between inorganic glasses and organic polymers, Advanced Materials (1993), 5, 422-433.

17. Wei, Y., Jin, D., Yang, C., Kels, M., Qiu, K. Organic-inorganic hybrid materials: relations of thermal and mechanical properties with structures. Materials Science and Engineering C. (1998), 6, 91-98.

18. Kelly, A. Concise Encyclopedia of Composite Materials. Elsevier, New York; 1994.

19. Brinker, C. J., Scherer, G. W. Sol-gel science: The physics and chemistry of sol-gel processing. Academic Press, San Diego; 1990.

20. Wei, Y., Jin, D., Yang, C., Wei, G. Synthesis of organic-inorganic hybrid sol-gel materials with low volume shrinkages. Polymeric Materials Science and Engineering (1996), 74, 244-245.

21. Li, S., Praveen, S. S., Mylonakis, A., Shah, A., Hsieh, A., Patel, A., Wei, E., Baran, G., Wei, Y. Synthesis of new organic–inorganic hybrids poly[2-hydroxethyl methacrylate (HEMA)-glycidyl methacrylate (GMA)-silica] and their mechanical properties. Journal of Materials Research (2008), 23, 66-71.

22. Moberg, C., Rakos, L., Tottie, L. Stereospecific lewis acid catalyzed methanolysis of styrene oxide. Tetrahedron Letters (1992), 33, 2191-2194.

23. Wen, J., Wilkes, G.L. Organic/inorganic hybrid network materials by the sol-gel approach. Chemistry of Materials (1996), 8, 1667-1681.

24. Poisson, N., Lachenal, G., Sautereau, H. Near- and mid-infrared spectroscopy studies of an epoxy reactive system. Vibrational Spectroscopy (1996), 12, 237-247.

25. Dean, K., Cook, W. D., Zipper, M. D., Burchill, P. Curing behavior of IPNs formed from model VERs and epoxy systems I amine cured epoxy. Polymer (2001), 42, 1345-1359.

26. Su, C. C., Woo, E. M., Chen, C.Y. NMR and FT-IR studies on trans-reactions and hydroxyl exchanges of bisphenol-A polycarbonate with an epoxy upon heating. Polymer (1997), 38, 2047-2056.

27. Mijovic, J., Andjelic, S. A study of reaction kinetics by near-infrared spectroscopy. Comprehensive analysis of a model epoxy/amine system, Macromolecules (1995), 28, 2787-2796.

Chapter 6. Covalent Incorporation of Polyaniline in Sol-Gel Materials

6.1 Introduction and Motivation

In the past 20 years, an increasing number of investigations have appeared in the field of hybrid materials owing to the growing interest of chemists, physicists and materials researchers to fully exploit the technical opportunities for creating new compounds and devices that combine the benefits of both worlds, namely inorganic and organic materials. To date, the hybrid materials have found applications in optics,[1,2] electronics,[3] mechanics,[4] membranes,[5] protective coatings,[6,7] catalysts,[8] sensors,[9] etc. Organic-inorganic hybrid materials prepared via soft synthetic methods, sol-gel processing in particular, seem to present nowadays a route to almost endless new hybrid materials with innumerable applications.[10-12] Sol-gel chemistry is a simple method that can be utilized to synthesize materials from several precursors in the presence of an acidic or a basic catalyst at relatively low temperatures. This method allows the combination of the inorganic with the organic components at the molecular or nanometer level, and provides access to materials with tunable optical, mechanical, electronic, biological and other properties.

On the other hand, conductive polymers are increasingly desired for a variety of sophisticated end-uses.[13,14] Very significant progress has been made in this field as a result of the numerous potential applications of these materials in electronic, electrochromic and photoelectrochemical devices.[15,16] Among these macromolecular compounds, polyaniline has been extensively studied due to its rather easy preparation, good environmental stability, as well as interesting redox properties.[17,18] Numerous research groups have intensively studied various possible routes of incorporating the

electrochromic, electroactive and conducting capabilities of polyaniline into conventional polymers, which can have tunable mechanical properties. These include the incorporation of polyaniline inside porous Vycor glass,[19] polyaniline grown in porous sol-gel films,[20] hybrid films employing polyaniline and polyurethane-silica,[21] hybrid materials based on electrostatic interactions,[22] polyaniline-silica composites,[23-25] etc. To the best of our knowledge, there has been no systematic study so far in incorporation of polyaniline into polyacrylate-silica hybrid materials with covalent bonding amongst all the molecular components.

Our group has been interested in both sol-gel hybrid materials and electronically conducting polymers for many decades.[26-33] Recently we have integrated electroactive polymers or oligomers into biocompatible polymers or inorganic molecular sieves for tissue engineering and other biomedical applications.[34,35] In Chapter 4, the synthesis and characterization of a novel organic-inorganic hybrid material (poly(HEMA-GMA-silica)), with low volume shrinkage and better mechanical properties compared to poly(methyl methacrylate) (PMMA), was reported. In this chapter, a series of new electroactive hybrid materials that have been synthesized by covalent incorporation of polyaniline into polyacrylate-silica hybrids is going to be presented. The formulation involves the radical co-polymerization of glycidyl methacrylate-polyaniline (GMA-PANi) and glycidyl methacrylate-2-hydroxyethyl methacrylate-silica (GMA-HEMA-silica) to yield poly(HEMA-GMA-silica)-polyaniline (PHGS-PANi) hybrids. This strategy possesses advantages over polyaniline-inorganic macro-composites because polyaniline is homogeneously dispersed at the molecular level across the polyacrylate-silica hybrid and thus, the properties that polyaniline imparts to the final material are

evenly distributed throughout the bulk of the final product. The chromoelectrochemical study suggests that these materials can have tunable colors upon change of potential and/or pH, and thus may find applications as chemical or biological sensors and electro-optical devices. Moreover, conductivity measurements and mechanical testing of these materials show that these materials can be prepared to have both a reasonably high conductivity and excellent mechanical properties. The mechanical testing reveals greater modulus upon increasing the silica content, and greater compressive strength upon increasing, to a certain extent, the amount of the organic moiety. The materials have also been characterized by infrared spectroscopy and thermal gravimetric analysis to demonstrate the covalent incorporation of polyaniline into sol-gel materials. In addition, as a proof of concept for the reaction of polyaniline with GMA the experiments of the reaction of GMA with aniline, of GMA with phenylene diamine, and GMA with aniline trimmer have been conducted. The ^{1}H-NMR spectra of the obtained products have been investigated in order to further support the covalent incorporation of polyaniline with GMA.

6.2 Experimental Section

6.2.1 Materials and Reagents

Polyaniline (PANi, Aldrich, emeraldine base, MW=10000), tetraethyl orthosilicate (TEOS, Aldrich), tetrahydrofuran (THF, Aldrich), tin chloride, ($SnCl_4$-Aldrich), hydrochloric acid (HCl, Fisher Scientific) and sulfuric acid (H_2SO_4, Fisher Scientific) were used as received. Benzoyl peroxide (BPO, Aldrich) was recrystallized from methyl alcohol before use. 2-Hydroxethyl methacrylate (HEMA, Aldrich) and glycidyl methacrylate (GMA, Aldrich) were purified by vacuum distillation before use.

6.2.2 Methods and Instrumentation

6.2.2.1 Conductivity Measurements

Electrical conductivity measurements were done by using the standard four probe method on an EG &G potentiostat/galvanostat (Model 173) with a universal programmer (Model 175). The conductivity experiments were performed with the four probe method on rectangular PHGS-PANi hybrid windows with dimensions of 1" x 0.5" x 1/8". In order to dope the polyaniline and make it conductive, the hybrids were sealed for 48 hr in a saturated acidic atmosphere (HCl, pH=1) before the conductivity tests.

6.2.2.2 Electrochemical Study

Electrochemical measurements were performed on an Epsilon Potensiostat (BASi, West Lafayette, IN) interfaced and monitored with a PC computer.

6.2.2.2.1 Cyclic Voltammetry

A three-electrode system with a Pt-wire as the auxiliary electrode and Ag/AgCl, as the reference electrode was employed for all the cyclic voltammetry measurements. A platinum disk electrode with a surface area of 0.02 cm^2 was used as the working electrode. The polymerized hybrid material was pressurized on top of the working electrode, and the testing was conducted in a solution of hydrochloric acid (pH=1). The scan rate used for these experiments was 50 mV/sec.

6.2.2.2.2 Electrochromic Analysis

A three-electrode system with a Pt-wire as the auxiliary electrode and Ag/AgCl as the reference electrode was employed. For spectroelectrochemical experiments, a glass slide with a conductive indium tin oxide (ITO) coating on one side was used as the

working electrode. This ITO glass electrode was washed with copious amounts of acetone and distilled water before use. The mixtures obtained upon mixing glycidyl methacrylate-polyaniline (GMA-PANi) and glycidyl methacrylate-2-hydroxyethyl methacrylate-silica (GMA-HEMA-silica) were cast on top of indium tin oxide (ITO) glass slides followed by radical polymerization in an air oven to yield the polymerized hybrid PHGS-PANi films. The electrolyte solution for the spectroelectrochemical tests was H_2SO_4 (0.5M) following previous studies. The scan rate used for these experiments was 50 mV/sec.

6.2.2.3 UV-vis Spectroscopy

UV-vis spectroscopy measurements were performed on a Perkin Elmer Lambda 35 UV-VIS spectrometer. The slit width of the detector was 1 nm and the scan speed used was 480 nm/min. The absorption of the hybrid materials was recorded between 300 and 900 nm.

6.2.2.4 Fourier Transform Infrared Spectrophotometer (FT-IR)

An ATR Perkin Elmer (Spectrum 1) spectrometer was employed for the IR measurements of all samples. Each IR spectrum was acquired with the accumulation of 30 scans at a scan resolution of 4 cm^{-1} between 800 and 4000 cm^{-1}.

6.2.2.5 Thermogravimetric Analysis (TGA)

Studies of thermal properties, i.e., thermogravimetric analysis, were done on a TA Q-50 thermal analysis system (TA instruments), equipped with TA Q Series Advantage Universal Analysis software, in air. All the samples were heated in air from room

temperature to 750 ^{o}C at a rate of 10 ^{o}C/min. During the heat treatment, degradation of the PHGS-PANi hybrids takes place.

6.2.2.6 Mechanical Testing

Poly(HEMA-GMA-silica)-PANi hybrids were tested in compression to measure their compressive strength, yield stress, and modulus. The test specimens were cut (length to diameter ratio=2:1) according to the ASTM standard (designation: D 695) using a diamond saw. The compression testing was performed using a servohydraulic machine (MTS Mini-Bionix 2, Eden Prairie, MN) at a crosshead speed of 10 mm/min. 6 or more tests were performed for each sample. The values of compressive strength were calculated using the following equation:

$$\sigma = \frac{F}{A}$$

where σ is the compressive strength, F is the maximum failure load and A is the initial cross-sectional area of the specimen. The compressive modulus of the specimens was determined from the slope of a straight line fit to the initial linear portion of the stress-strain curve.

6.2.3 Synthesis Procedure

6.2.3.1 *Sol A*: (HEMA-GMA-silica) (HGS)

The detailed synthesis procedure of the HEMA-GMA-silica precursors has been described earlier in **Chapter 4**. Generally, for a sample that would contain 10 wt% SiO_2 in the final product, 26 g of tetraethyl orthosilicate (0.125 mol, TEOS) were hydrolyzed with 43.65 g of 2-hydroxylethyl methacrylate (0.336 mol, HEMA) and 6.98 g of H_2O

(0.375 mol) under acidic catalysis of hydrochloric acid (0.25 mol, HCl) in 18 g of tetrahydrofuran (0.249 mol, THF). This reaction mixture was refluxed, under constant stirring at 60 °C for 3 hr, under nitrogen protection. The solvent (THF) and small molecular byproducts (e.g., water and ethanol) from the sol-gel reaction were then removed without heating using a vacuum pump. During this step, the temperature of the mixture dropped quickly to below 10 °C. When the weight of the mixture reached about 50-55% of the original weight, vacuum was discontinued. Then, 23.84 g of glycidyl methacrylate (GMA, 0.17 mol) and 0.06 g benzoyl peroxide (BPO, 0.25 mmol) were added and the reaction mixture was stirred for 3-5 min. The remaining byproducts were again removed under vacuum until a stable weight was reached. At this point, the temperature of the reaction mixture gradually returned to room temperature. 6 µL of tin chloride ($SnCl_4$), which is used as a catalyst for the reaction of GMA with the silanol hydroxyl groups, was then added in the mixture, followed by stirring under vacuum for about 30 min. This mixture is called *sol A* and while not in use was kept in a moisture free freezer at -20 ^{o}C.

6.2.3.2 *Sol B*: Polyaniline-GMA

To prepare polyaniline-GMA, 0.1 g of polyaniline (PANi, Mn=10,000) and 0.8 g of GMA were dissolved in 50 ml of dimethylsulfoxide (DMSO) in a three-neck round bottom flask, equipped with a thermometer and a gas inlet/outlet. The molar ratio of the reactants used was polyaniline (repeating unit): GMA = 2:1. The mixture was refluxed for 3 hr at about 90 °C under constant stirring in a nitrogen atmosphere. After cooling down to room temperature, the solvent was removed under vacuum up until the point when the solution became very viscous and no bubble formation was observed. This

viscous mixture is called *sol B* and while not in use was kept in a moisture free freezer (at -20 ^{o}C).

6.2.3.3 Mixing of *Sol A* with *Sol B* and Polymerization Step

The two solutions (*sol A* and *sol B*) were mixed together in predetermined weight ratios to give the HEMA-GMA-silica-PANi (HGS-PANi) hybrid precursors. The obtained mixtures depending on the specific method of analysis that would follow were either filled into polypropylene cylindrical or square window molds for mechanical testing, or cast on top of indium tin oxide (ITO) glass slides for spectroelectrochemical tests. To complete the free radical polymerization and curing steps, the appropriate mold, containing the solution mixture, was put in an air oven, where three consecutive heating steps took place. The reaction mixture was first heated in an oven at 65 °C under air for 15-18 hr, and then the temperature was increased to 85 °C for 2 more hr. Finally, the polymeric monoliths were annealed at 125 °C for 2 hr.

6.3 Results and Discussion

6.3.1 Synthesis Considerations

As has already been described in previous chapters of this thesis (i.e., chapters 4 and 5), GMA, in addition to forming a co-polymer with HEMA and/or HEMA-silica phase during free-radical polymerization, served two other important purposes that enabled us to overcome the problems associated with the small byproduct molecules in the typical sol-gel organic-inorganic hybrid synthesis. Firstly, because of its high boiling point, it allowed the complete removal of the lower boiling point residual byproducts (e.g., water and ethanol) under vacuum evaporation. Moreover, the epoxy group of GMA effectively reacts with the free silanol (Si-OH) groups of the silica phase under the action

of the catalyst (e.g., $SnCl_4$), thereby capping the growing silica oligomers (**Figure 6-1**). Thus, any free Si-OH groups that could possibly remain in the final polymer chains and could possibly condense over time and produce water as a byproduct, which would decrease the mechanical properties and the optical transparency of the obtained hybrids, may be considered insignificant. Besides, GMA is now also a means of incorporating, by covalent bonding, conductive polyaniline into the organic-inorganic framework. The detailed synthesis procedure of PHGS-PANi can be seen in **Figure 6-2.**

6.3.2 Thermogravimetric Analysis (TGA)

The obtained polymerized PHGS-PANi materials were light to dark purplish-blue in color depending on the weight percentage of polyaniline. The hybrids had various compositions of polyaniline with respect to the poly(HEMA-GMA-silica) content as summarized on **Table 6-1**. Silica content of *sol A* before mixing with *sol B* was 10 wt % as calculated by TGA. Typical TGA curves of the PHGS-PANi hybrids can be seen in **Figure 6-3**. All samples were heated in air, from room temperature to 750 ^{o}C, at a rate of 10 ^{o}C/min. In general, there appear to be several stages of weight loss upon heating starting at around 200 ^{o}C and ending at around 600 ^{o}C. The residual weight at the final temperature of 750 ^{o}C consists of SiO_2 and corresponds to the experimental percentage of silica wt (%), which can be reasonably compared to the theoretical feeding compositions of silica in these hybrid materials. Decomposition of pure polyacrylates like poly(GMA) and poly(HEMA) would start at about 200 ^{o}C. In this case, though, the acrylate polymer decomposition for the low polyaniline content hybrids starts at slightly higher temperatures presumably due to the silica incorporation in the polyacrylate matrix that imparts stiffness and rigidity to the final materials. There appears to be a threshold in

polyaniline content (curve c in **Figure 6-3**), beyond which the material seems to be decomposed at lower temperatures. This may be attributed to the fact that silica content is not high enough to form a completely cross-linked interpenetrating network that would impart rigidity and structural integrity to the bulk of the material, and would make the decomposition of the hybrids more difficult.

6.3.3 Fourier Transform Infrared Spectra (FT-IR)

The representative FT-IR spectra of the product from the reaction of polyaniline with GMA in DMSO at 90 ^{o}C for 3 hr (*sol B*), of the blend obtained upon mixing polyaniline with GMA, of pure polyaniline and of pure GMA can be seen in **Figure 6-4**. Upon reaction of the epoxy group of GMA with the polyaniline amine groups, the epoxy ring of GMA opens and carbon-nitrogen covalent bonds are formed, followed by the formation of a hydroxyl group. The broad peak at around 3400 cm^{-1} is attributed to these hydroxyl groups, which are formed upon the ring opening of the epoxy groups of GMA. In contrast, the IR spectra for pure GMA and GMA/aniline composite show no peak above 3200 cm^{-1}, which indicates that no hydroxyl groups exist in these compounds. The stretching bands for the carbonyl groups of the acrylates appear at ~1730 cm^{-1}, whereas the characteristic bands of polyaniline appear around 1500 cm^{-1}. These results indicate that polyaniline is covalently bonded with GMA and that all of the components in the final hybrids keep their structural integrity.

6.3.4 ^{1}H-NMR Spectroscopy

As a proof of concept for the reaction of polyaniline with GMA, the experiments of the reaction of GMA with aniline, of GMA with phenylene diamine, and GMA with aniline trimer have been conducted, and the ^{1}H-NMR spectra of the obtained products

have been investigated. In a small vial, 0.2 g (2.1×10^{-3} mol) of aniline and 0.3 g of GMA (2.1×10^{-3} mol) were dissolved in 5 ml of deuterated DMSO, and the mixture was stirred at 90 ^{o}C for 3 hr. The ^{1}H-NMR spectra of pure GMA, of pure aniline and of the product after the reaction of GMA with aniline can be seen in **Figures 6-5**, **6-6** and **6-7,** respectively. Support for the reaction of the epoxy group of GMA with the amine groups of aniline comes from the evaluation of these spectra, which show that the GMA epoxy group reacts, by covalent bonding, with the amine group of aniline. The same concept is presumed to be true for the reaction of polyaniline with GMA, as many researchers have verified.[36-39]

The assignment of the ^{1}H-NMR peaks is as follows:

- ^{1}H-NMR of GMA in deuterated DMSO: δ 1.9 (t, 3H, -CH_3), δ 2.62-2.8 (m, 2H, -CH_2- of epoxy ring), δ 3.2 (m, 1H, -CH- of epoxy ring), δ 3.9-4.42 (m, 2H, C(O)-O-CH_2-), δ 5.7-6.05 (dd, 2H, CH_2=).

- ^{1}H-NMR of aniline in deuterated DMSO: δ 3.62 (s, 2H, -NH_2), δ 6.85 (m, 2H, arom. ortho-H), δ 6.9 (m, 1H, arom. para-H), δ 7.2 (m, 2H, arom. meta-H).

- ^{1}H-NMR of product from reaction of aniline with GMA at 80 ^{o}C under constant stirring in deuterated DMSO (3hrs, 1 to 1 mole ratio): δ 1.9 (m, 3H, -CH_3 from GMA), δ 2.92 (s, 2H, -NH-), δ 3.2-3.3 (m, 2H, -CH_2-NH- after epoxy ring opening), δ 4.1 (m, 2H, -CH_2 (OH)- after epoxy ring opening), δ 4.2 (m, 2H, -CH_2-), δ 5.7-6.05 (m, 2H, CH_2=), δ 5.7-6.05 (m, 2H, CH_2=), δ 5.7-6.05 (dd, 2H, CH_2=), δ 6.75-7.2 (m, 5H, arom.-H).

The ^{1}H-NMR spectra of the products from the reactions of GMA with phenylene diamine and aniline trimer with the respective peak assignments are given in Appendix E.

6.3.5 Mechanical Properties

All of the as-synthesized PHGS-PANi hybrids, prepared using this new sol-gel synthesis procedure, were completely transparent without any surface cracks and did not chip during cutting with a diamond saw. The values of compressive modulus, yield stress and compressive strength of the as-synthesized hybrids and the control (e.g., poly(HEMA-GMA-silica), 10 wt % silica) are summarized on **Table 6-1**. The compressive modulus of PHGS-PANi hybrids improves with increasing silica content. On the other hand, the modulus decreases slightly when the wt % of *sol B* increases as one would expect. For example when *sol B* is 1 wt % in the final product the compressive modulus is 3.9 MPa, whereas when the wt % of *sol B* in the final material is 10 wt %, then the compressive modulus drops to 3.63 MPa. A similar trend exists for the yield stress so that PHGS-PANi hybrid with 3 wt % *sol B* (e.g., sample 4 from **Table 6-1**) shows a yield stress value equal to 179 MPa whereas when the *sol B* content increases to 10 wt % (e.g., sample 6 from **Table 6-1**) the yield stress drops to 168 MPa. This may be attributed to the fact that silica increases the cross-linking density of the polymer chains in the hybrids, such that increasing silica content resulted in a simultaneous increase in compressive modulus and yield stress. The compressive strength of these hybrid materials displays a similar trend of composition dependence. The compressive strength decreased with increasing silica content, and this is due to the fact that higher silica content tends to make the composite more brittle, whereas higher organic content (e.g., GMA, HEMA and PANi) tends to make the material more elastic. A comparison of sample 1 with sample 4 from **Table 6-1**, shows that 0.5 wt % of *sol B* in the final material yields a hybrid product with a compressive strength of 236 MPa whereas when the wt %

of *sol B* increases to 3 wt %, the compressive strength increases to 293 MPa. It is apparent from this table that, up to a threshold, the higher the PANi content the higher the compressive strength, or in other words, the higher the silica content the lower the compressive strength. These results clearly show that these materials have excellent tunable mechanical properties and reveal the synergy of combining silica with HEMA-GMA and GMA-PANi to form an interpenetrating network.

6.3.6 Conductivity Measurements

The conductivity experiments were performed with the four-probe method on rectangular PHGS-PANi hybrid windows with dimensions of 1" x 0.5" x 1/8". The materials were sealed for 48 hr in an acidic (HCl, pH=1) saturated atmosphere in order to dope the polyaniline and make it conductive. Conductivity results of these hybrid materials (**Figure 6-8**) show that the higher the weight percentage of *sol B* in the hybrid, the higher the conductivity of the obtained material, or in other words the higher the PANi content, the higher the conductivity, as one would expect. In contrast, the higher the percentage of poly(GMA-HEMA-silica) the lower the electric conductivity, which can be justified by the fact that HEMA, GMA and silica that are main components of the hybrids are insulators and don't contribute to the overall conductivity.

6.4.7 Cyclic Voltammetry

Cyclic voltammetry experiments were performed to study the electroactivity of the obtained hybrids. A three-electrode system with a platinum wire as the auxiliary electrode and Ag/AgCl as the reference electrode was employed. The polymerized PHGS-PANi hybrid material (sample 4 from **Table 6-1**) was pressurized on top of the platinum disk working electrode, and the electrochemical testing was conducted in a

solution of hydrochloric acid (pH=1). The hydrochloric acid serves both as the electrolyte and as the conductivity dopant for polyaniline. At higher potentials the polyaniline is oxidized to the pernigraniline form, while at lower potentials the polyaniline converts to the fully reduced form of leukoemeraldine (**Scheme 6-1**). **Figure 6-9a** shows the cyclic voltammogram for the PHGS-PANi hybrid material. In this cyclic voltammogram the two known redox peak pairs of polyaniline can be observed.

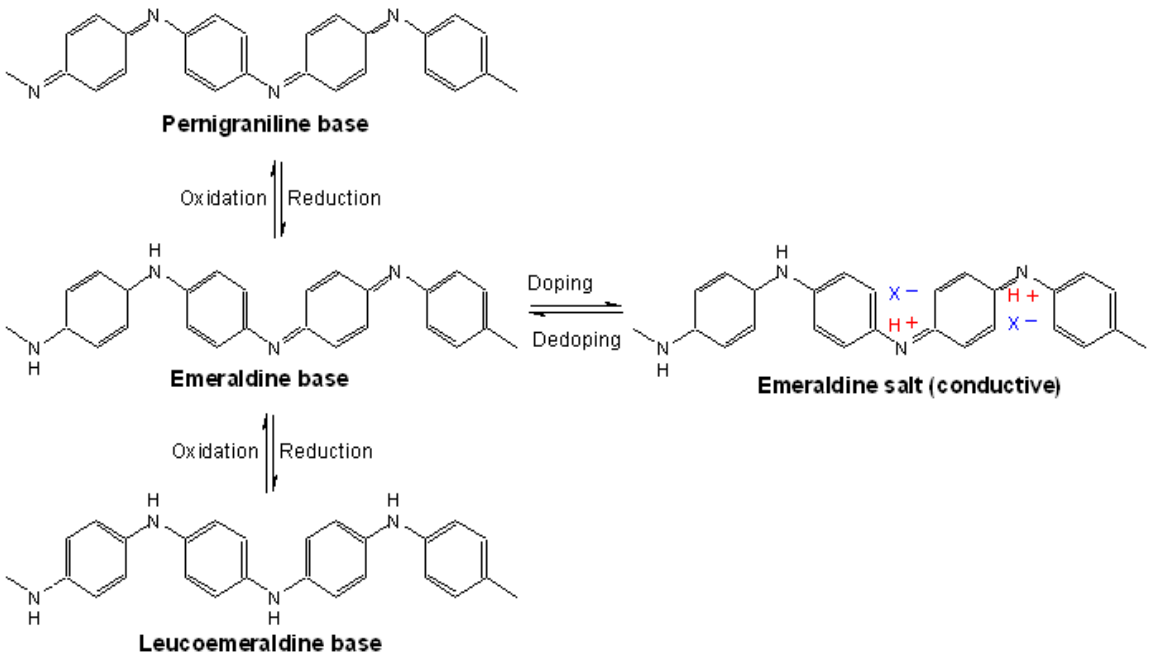

Scheme 6-3. Chemical structures and redox states of polyaniline.

Compared to pure polyaniline (**Figure 6-9b**), there is a reduction in the intensity of the obtained redox peaks that can be explained by the fact that the material is composed mostly of silica inorganic and acrylic organic groups that are electrochemically inert. The rigid inorganic silica framework makes the removal of electrons from polyaniline more difficult and causes an anodic shift of the redox peaks compared to pure polyaniline. The electrochemical activity of the polyaniline redox sites is established by

direct electron transfer from the working electrode surface to the electroactive sites of polyaniline and/or via long range electron transfer through electron exchange between the adjacent electroactive moieties (electron hopping). It should be noted that extensive scanning of the potential led to the reduction of these two redox pairs and eventually to the appearance of a small middle peak, which may be attributed to degradation products of polyaniline.[40]

6.4.8 Spectroelectrochemical Study

The spectroelectrochemical study that was conducted reveals the conversion of these PHGS-PANi hybrids from light yellowish-green to dark bluish-green as the applied potential is scanned from low to higher values, respectively. In order to conduct the spectroelectrochemical studies, *sol A* was mixed with *sol B* and the obtained mixture (same composition as sample 4 from **Table 6-1)** was cast on top of an indium-tin oxide electrode, followed by the polymerization of these precursors in an air oven. The electrolyte solution used for these experiments was H_2SO_4 (0.5M), following previous studies. Upon immersion of the hybrid in the electrolyte, the color would change from purplish-blue to dark green, which corresponds to the conducting emeraldine salt of polyaniline. **Figure 6-10** shows the UV-vis spectra of PHGS-PANi obtained upon application for 20 min of two different potentials, namely 50 mV and 900 mV.[41] Polyaniline shows various distinctive peaks in its UV-visible spectrum depending on its oxidation state as several researchers have pointed out.[42,43] A band at around λ = 300 nm corresponds to the $\pi \rightarrow \pi^*$ transition of benzenoid rings, which is characteristic of the leucoemeraldine form of polyaniline.[44,45] As can be seen from **Figure 6-10**, this band decreases when the applied voltage increases from 50 mV to 900 mV. The broad band

peak that can be seen at the red region of the UV-Vis spectra is attributed to the conducting emeraldine state of PANi. As the applied potential is increased, this band is showing a hypsochromic shift accompanied by an increase in intensity. This corresponds to the oxidation of aniline from its fully reduced form of leucoemeraldine, which contains benzenoid rings, to its fully oxidized form of pernigraniline, which contains conjugated quinoid rings.[46,47] Additionally, a shoulder peak that appears around 430 nm is slightly decreasing in intensity as the applied potential is increased.[48,49] This peak has been assigned by other researchers to charged para-coupled phenyl structures, which correspond presumably to localized phenyl ring polarons. **Figure 6-11** presents the optical pictures of the polymerized hybrid material cast on the ITO electrode at different applied potentials. Initially, the as-synthesized PHGS-PANi hybrid film, cast on top of the ITO electrode, has a purplish-blue color. When the ITO electrode, along with the hybrid, is immersed inside the acidic electrolyte the color changes to green, which corresponds to the doped polyaniline conductive form. Upon applied voltage of 50 mV for 20 minutes, the material acquires a pale yellow-green color, which is attributed to the fully reduced form of polyaniline (i.e. leucoemeraldine). On the other hand, when the applied potential is 900 mV the hybrid material acquires a dark blue color, which is attributed to the fully oxidized form of polyaniline, i.e., pernigraniline. It has to be mentioned here that these hybrid materials were much more adhesive on the indium tin oxide slide compared to PANi itself, where it would peel off after some potential cycles. That is presumably because of the silicates that these hybrid materials contain, which imparts better thermodynamic compatibility and bonding with the inorganic substrate.

6.4 Conclusions

This new synthesis procedure provides materials that can combine the excellent mechanical and optical properties of silica with the flexibility of incorporating conducting, electroactive and electrochromic polyaniline at the molecular level. The results indicate the electrochromic nature of these hybrid materials and the various colors that they attain depending on the applied potential. The final electroactive, electrochromic, conducting and mechanical properties of these hybrid materials can be easily varied by changing the ratios of the initial precursors. Reasonably higher amounts of the electroactive and electrochromic polyaniline result in more profound electrochemical and electrochromic features of the final materials. Certainly, an increase in the content of the conducting polyaniline yields the increase of the conductivity of the hybrid bulk materials. As far as the mechanical properties, the higher the silica content in the hybrids, the greater the mechanical modulus of the obtained materials. On the other hand, the higher, within a threshold, the organic content the greater the elasticity of the obtained materials. In summary, the obtained hybrid materials show good mechanical properties, tunable colors, electroactivity and conductivity that depend on the amount of polyaniline present in the hybrid. The same synthetic concept can be applied in order to incorporate various other conducting or non-conducting polymers that can introduce alternative properties to the sol-gel materials. This new type of hybrid material can be fabricated easily into products with the desirable size and shape, and potential applications may include fabrication of electronic, optical and sensor devices.

6.5 Acknowledgments

This project has been conducted in collaboration with Dr. Yi Guo. I would like to thank Dr. Solomon S. Praveen for the mechanical testing measurements and Mr. Indraneil Mukherjee for his valuable input on the drawing of the schematics. This work was supported in part by the US Army Research Office (ARO) and the National Institutes of Health (No. DE09848).

Table 6-1. Mechanical and conductivity testing results of PHGS-PANi hybrids.

Sample	Weight ratio (*Sol B*)/(*Sol A*) (mg/mg)	Modulus Average ± SD (MPa)	Yield stress Average ± SD (MPa)	Compressive strength Average ±SD (MPa)	Conductivity (S/cm)
1	5:2995	3.97 ± 0.06	179 ± 10	235 ± 21	N/A
2	10:2990	3.90 ± 0.07	176 ± 2	236± 67	$2.4x10^{-3}$
3	30:2970	3.90 ± 0.18	172 ± 4	254 ± 53	$7.2x10^{-3}$
4	50:2950	3.85 ± 0.11	173 ± 1	293 ± 28	$2.1x10^{-2}$
5	100:2900	3.88 ± 0.1	168 ± 3	184 ± 18	$7.5x10^{-2}$
6	300:2700	3.63 ± 0.6	168 ± 3	168 ± 27	$2.5x10^{-1}$
7	500:2500	3.21 ± 0.3	160 ± 2	159 ± 20	$4.3x10^{-1}$
PHGS[a]	0	3.95 ± 0.06	180 ± 8	235 ± 19	N/A

For the mechanical testing, specimens were cut (length to diameter ratio = 2:1) according to the ASTM standard (designation: D 695). Compression testing was performed at a crosshead speed of 10 mm/min. 6 or more tests were performed for each sample. Conductivity experiments were performed with the four-probe method on rectangular PHGS-PANi hybrid windows with dimensions of 1” x 0.5” x 1/8”. Hybrids were sealed for 48 hr in a saturated acidic atmosphere (HCl, pH=1) before the conductivity tests.

[a] Poly(HEMA-GMA-silica) hybrid (10 wt% of silica) was used as control.

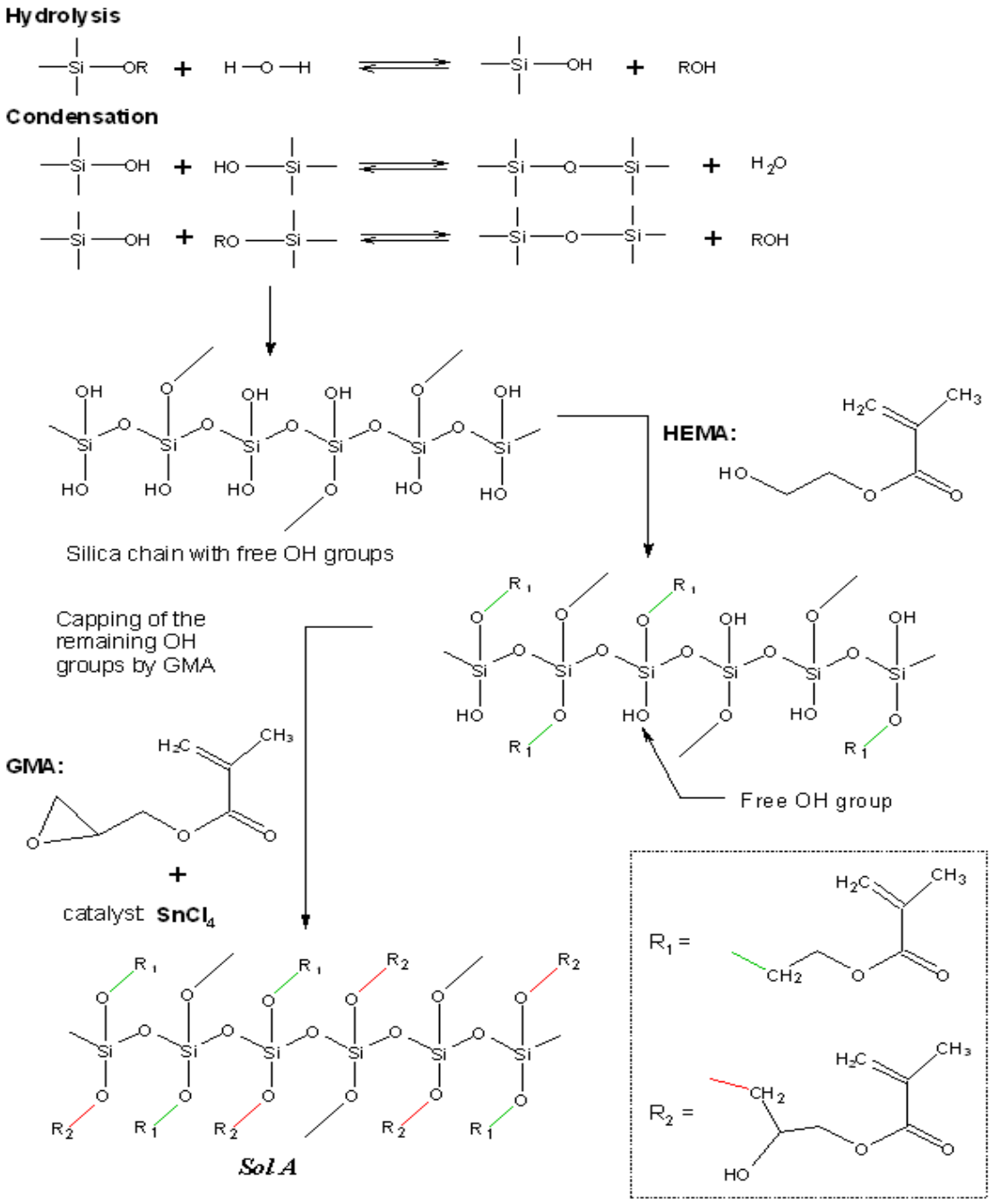

Figure 6-1. Detailed synthesis procedure of HEMA-GMA-silica (HGS) precursor (*sol A*).

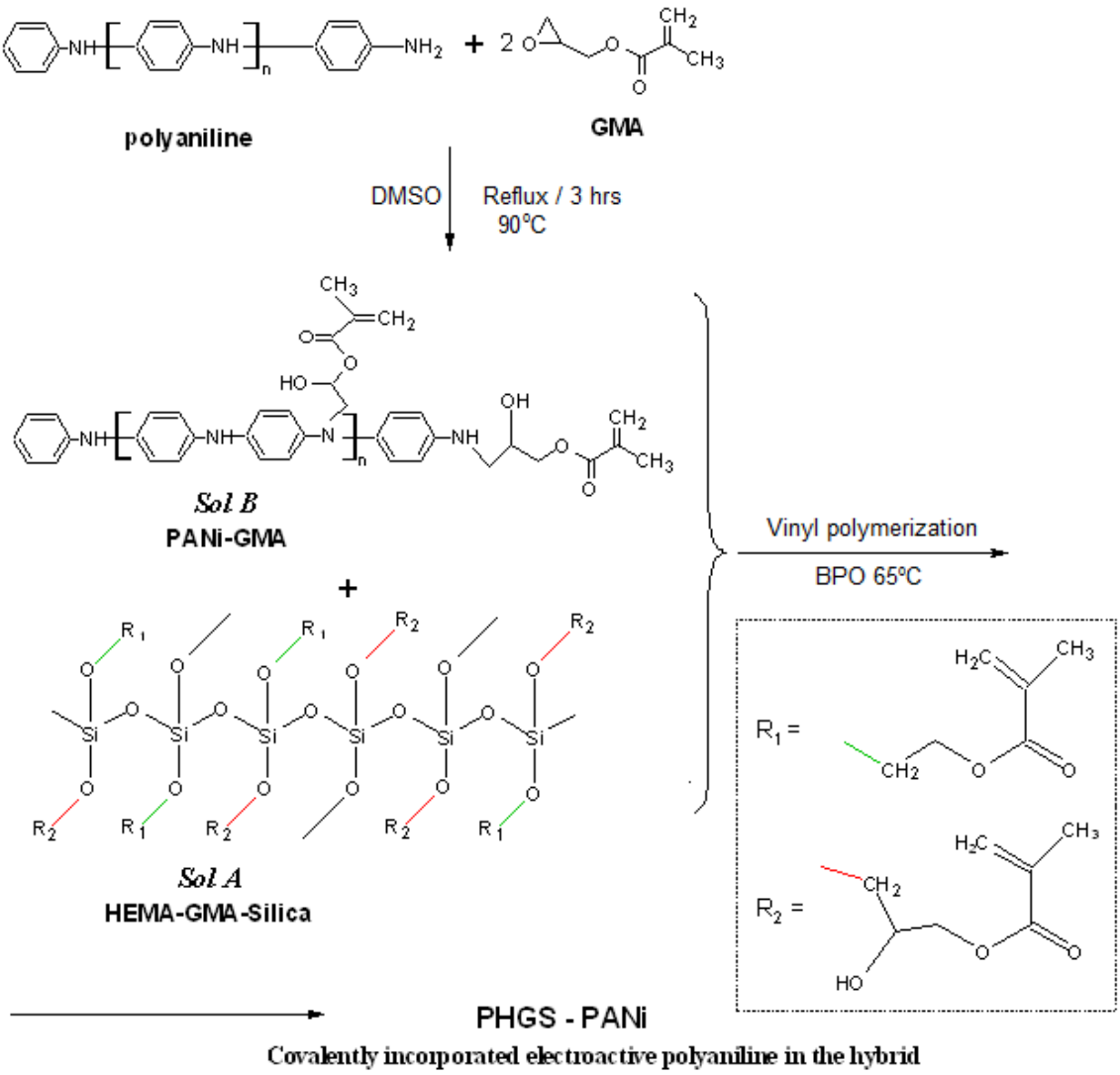

Figure 6-2. Schematic of the detailed synthesis procedure of the PHGS-PANi hybrid materials, which includes the synthesis of GMA-polyaniline (*sol B)* (100 % yield of reaction is assumed for depiction simplicity), the mixing of *sol A* (HEMA-GMA-silica) with *sol B* (GMA-PANi) and the radical copolymerization of HEMA-GMA-silica-PANi to yield poly(HEMA-GMA-silica)-polyaniline (PHGS-PANi).

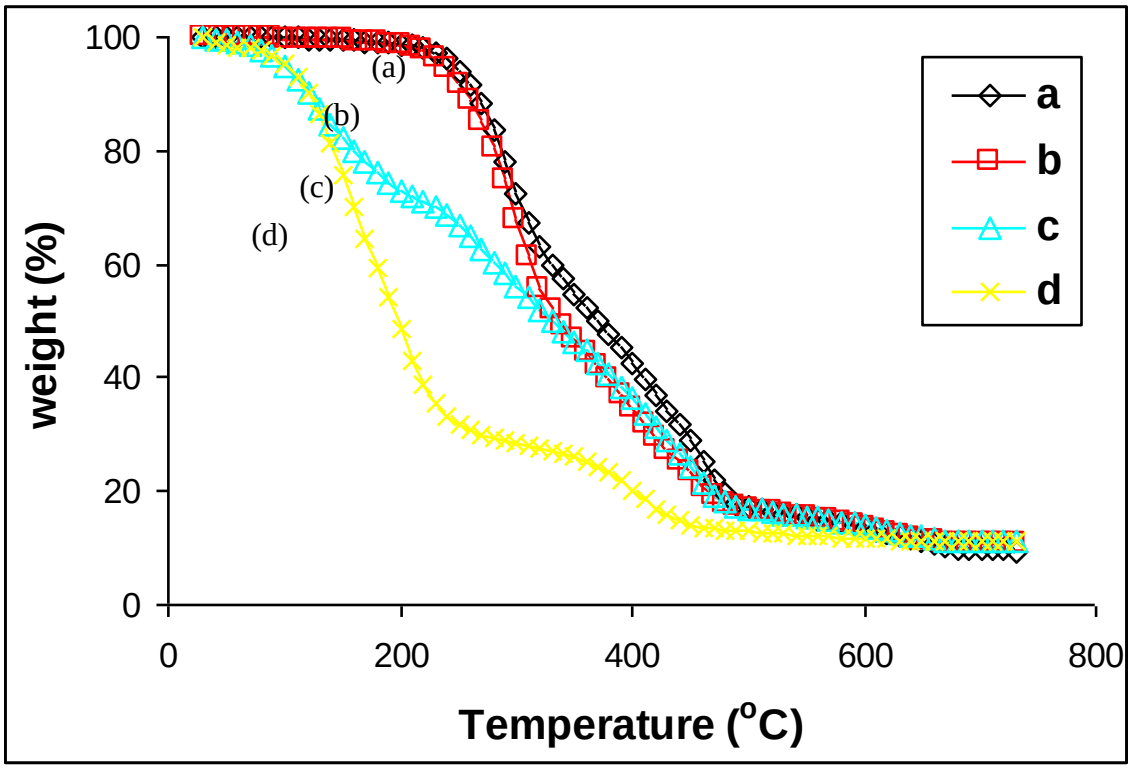

Figure 6-3. Thermogravimetric curves of PHGS-PANi samples containing: (a) 0.5 wt% *sol B,* (b) 2 wt% *sol B,* (c) 4 wt% *sol B* and (d) 16 wt% *sol B.* Thermal analysis measurements were done at a programmed heating rate of 20 °C/min in air. Samples a, b, c and d correspond to samples 1, 3, 4 and 6 from **Table 6-1,** respectively.

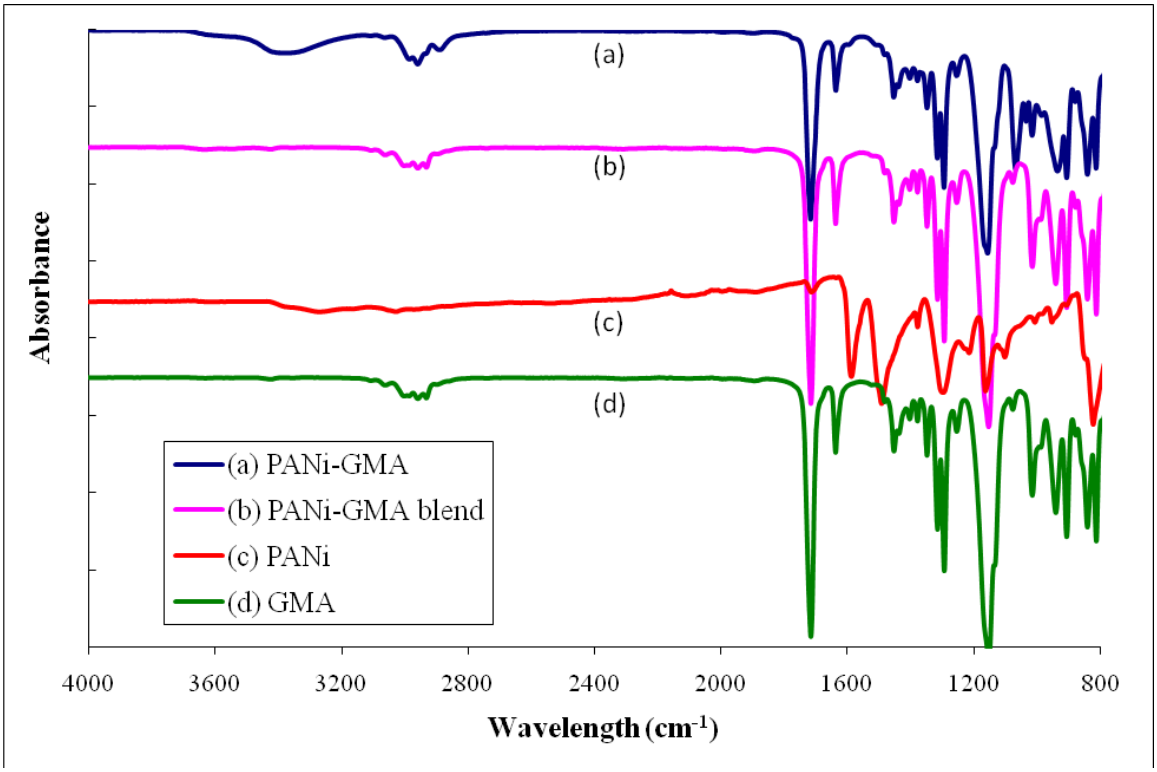

Figure 6-4. FTIR spectra of *sol B*, of polyaniline-GMA blend, of pure polyaniline and pure GMA. The spectra were collected after 30 scans at a scan resolution of 4 cm^{-1}.

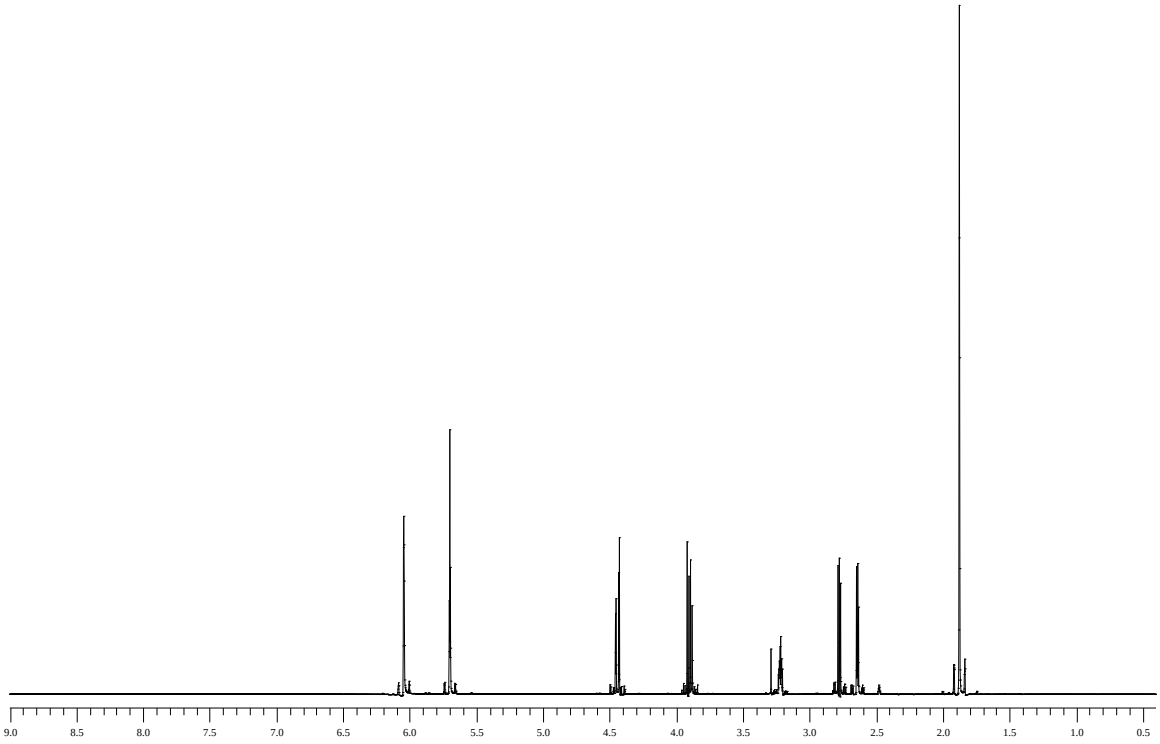

Figure 6-5. ^{1}H-NMR of GMA in deuterated DMSO: δ 1.9 (t, 3H, -CH_3), δ 2.62-2.8 (m, 2H, -CH_2- of epoxy ring), δ 3.2 (m, 1H, -CH- of epoxy ring), δ 3.9-4.42 (m, 2H, C(O)-O-CH_2-), δ 5.7-6.05 (dd, 2H, CH_2=).

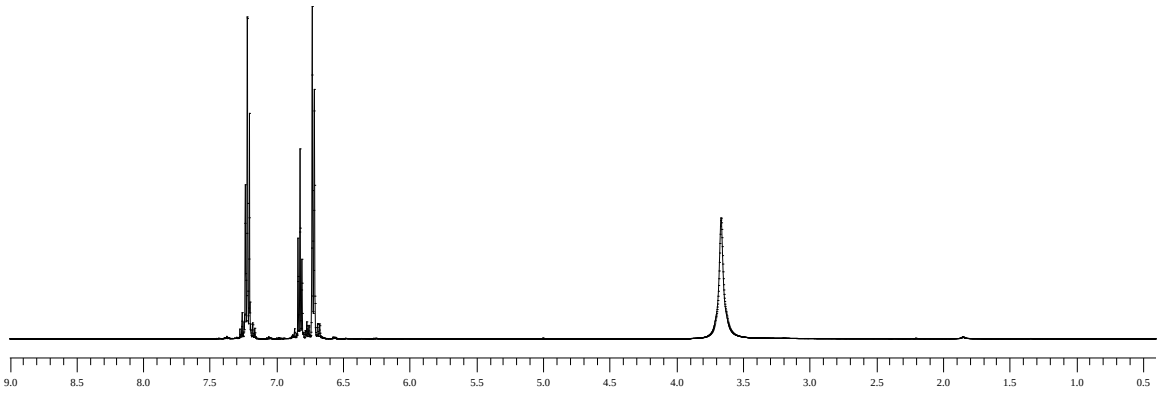

Figure 6-6. ^{1}H-NMR of aniline in deuterated DMSO: δ 3.62 (s, 2H, -NH_2), δ 6.85 (m, 2H, arom. ortho-H), δ 6.9 (m, 1H, arom. para-H), δ 7.2 (m, 2H, arom. meta-H).

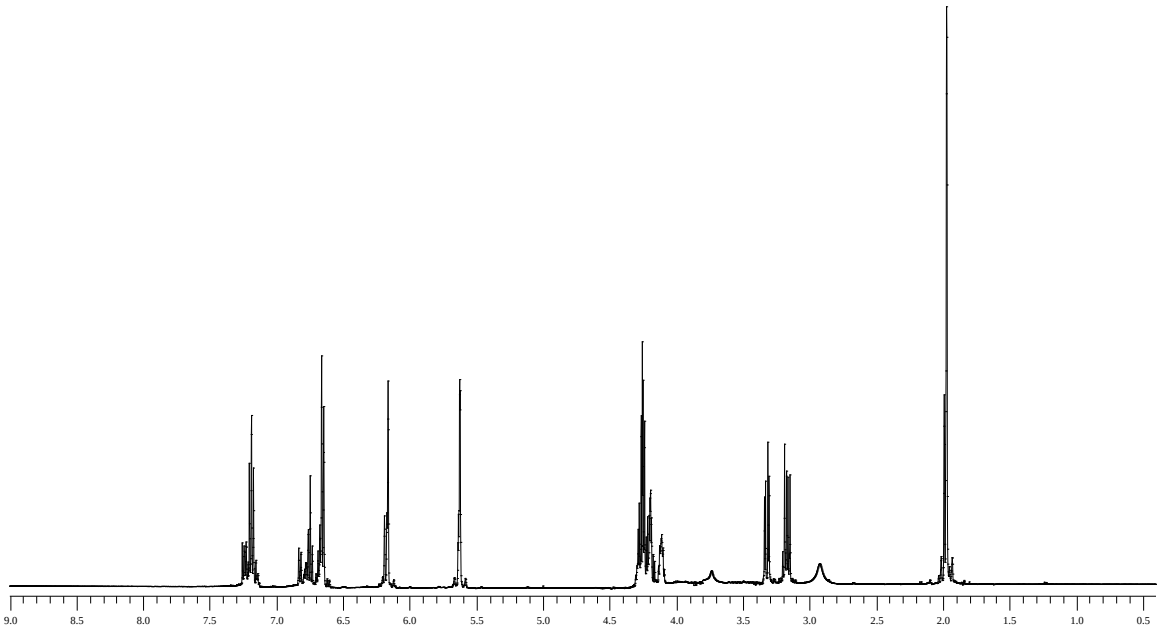

Figure 6-7. ^{1}H-NMR spectrum of the product from the reaction of aniline with GMA (3hrs, 1 to 1 mole ratio) at 90 ^{o}C under constant stirring in deuterated DMSO: δ 1.9 (m, 3H, -CH_3 from GMA), δ 2.92 (s, 2H, -NH-), δ 3.2-3.3 (m, 2H, -CH_2-NH- after epoxy ring opening), δ 4.1 (m, 2H, -CH_2 (OH)- after epoxy ring opening), δ 4.2 (m, 2H, -CH_2-), δ 5.7-6.05 (m, 2H, CH_2=), δ 5.7-6.05 (m, 2H, CH_2=), δ 5.7-6.05 (dd, 2H, CH_2=), δ 6.75-7.2 (m, 5H, arom.-H).

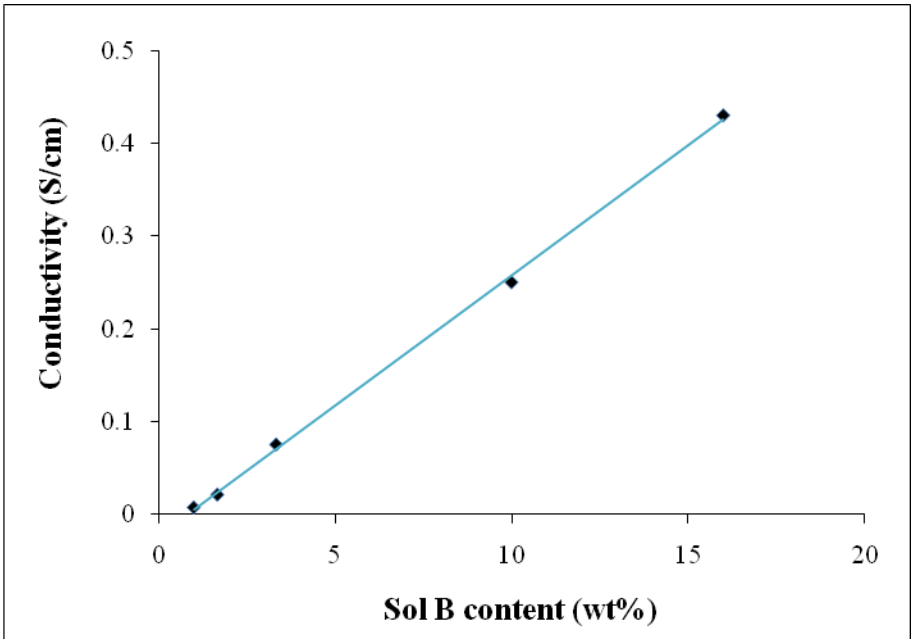

Figure 6-8. Dependence of conductivity of PHGS-PANi hybrids on *sol B* content. Experiments were performed with the four-probe method on rectangular PHGS-PANi hybrid windows with dimensions of 1" x 0.5" x 1/8". Prior to conductivity measurements, the materials were sealed for 48 hr in a saturated atmosphere of acid (HCl, pH=1).

(a)

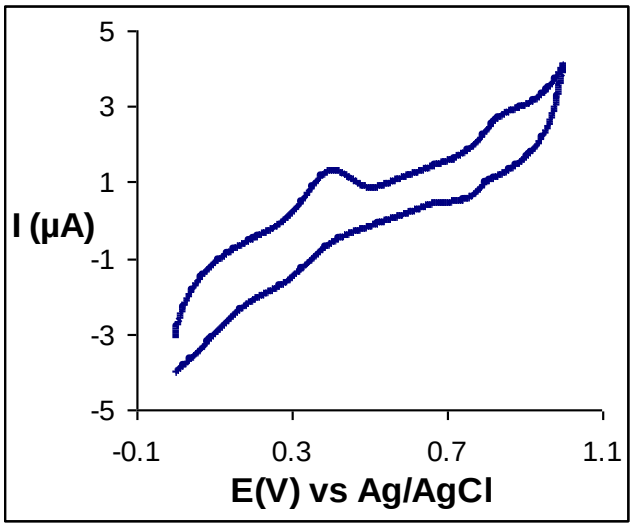

(b)

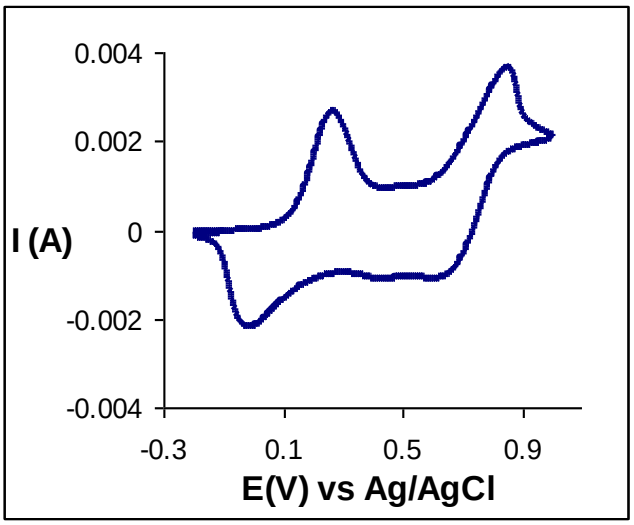

Figure 6-9. Cyclic voltammograms of: (a) PHGS-PANi hybrid (sample 4 from **Table 6-1**). The polymerized hybrid material was pressurized on top of the platinum working electrode. (b) Polyaniline. Both electrochemical tests were conducted in a solution of hydrochloric acid (pH=1). Voltage was scanned between 0 and 1000 mV at a scan rate of 50 mV/sec.

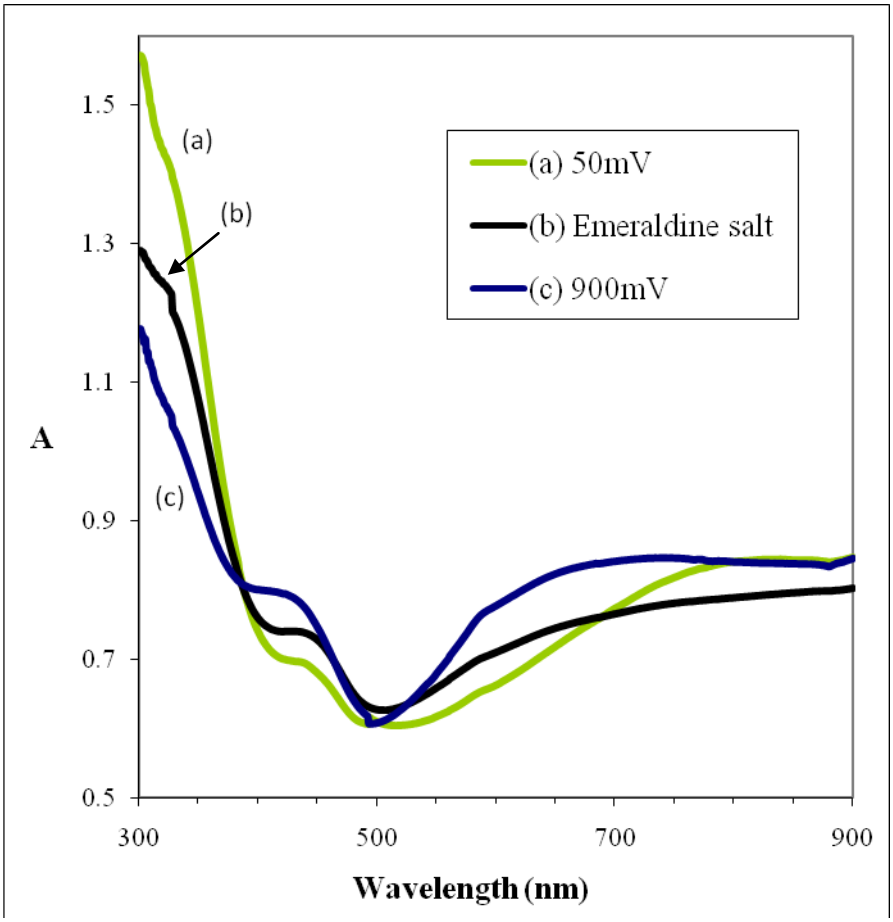

Figure 6-10. UV-visible spectra of PHGS-PANi hybrid (a) at an applied potential of 50 mV vs Ag/AgCl, (b) at the emeraldine state of polyaniline, (c) at an applied potential of 900 mV vs Ag/AgCl. For the electrochromic study, the prepolymerized hybrid HGS-PANi material was cast on top of an ITO working electrode followed by radical polymerization in air oven at 65 ^{o}C. Two different potentials (50 mV and 900 mV) were applied to the PHGS-PANi hybrid material for 20 min by controlled potential electrolysis before the UV measurements.

(a) (b)

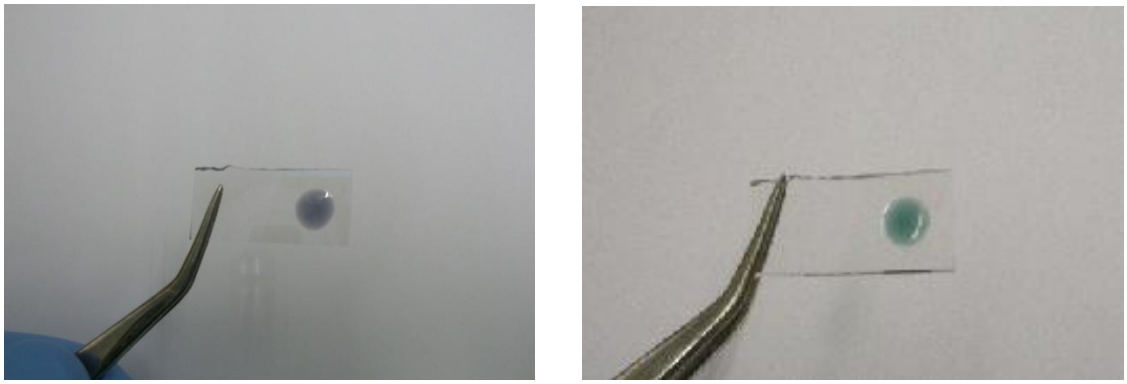

(c) (d)

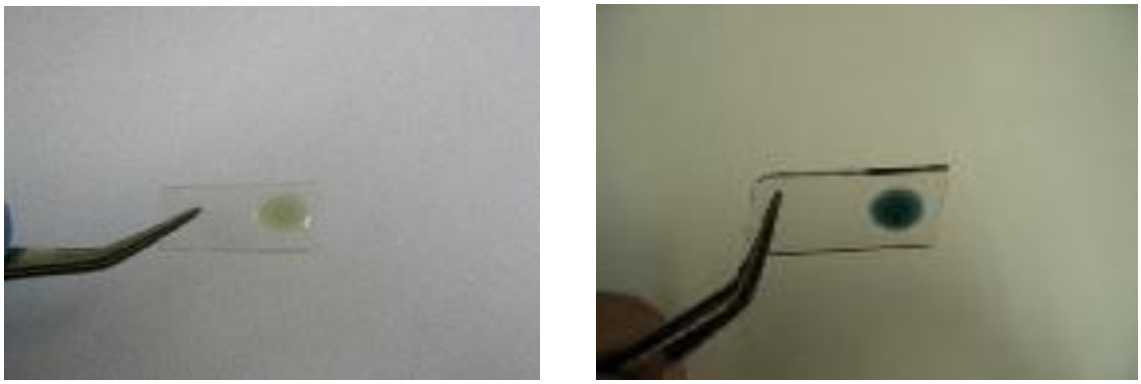

Figure 6-11. Optical pictures of PHGS-PANi hybrid (same composition as sample 4 from **Table 6-1**): (a) at the emeraldine state of polyaniline, (b) at the emeraldine salt state of polyaniline after the immersion in H_2SO_4 (0.5M) (c) after 20 minutes of an applied potential of 50 mV vs Ag/AgCl, (d) after 20 minutes of an applied potential of 900 mV vs Ag/AgCl.

6.6 Reference List

1. Que, W., Hu, X. Optical switch and luminescence properties of sol–gel hybrid organic–inorganic materials containing azobenzene groups and doped with neodymium ions. Applied Physics B, Laser and Optics (2007), 88, 557-561.

2. Li, S., Shah, A., Hsieh, A. J., Haghighat, R., Praveen, S. S., Mukherjee, I., Wei, E., Zhang, Z., Wei, Y. Characterization of poly(2-hydroxyethyl methacrylate-silica) hybrid materials with different silica contents. Polymer (2007), 48, 3982-3989.

3. Tour, J. M. Transition to organic materials science. Passive, active, and hybrid nanotechnologies. Journal of Organic Chemistry (2007), 72, 7477-7496.

4. Mohan, K., Yip, T. H., Sridhar, I., Seow, H. P. Design of hybrid sandwich panel with aluminum foam core and carbon fiber reinforced plastic face sheets under three-point bending. Solid State Phenomena (2006), 11, 63-66.

5. Wu, C., Wu, Y., Xu, T., Fu, X. Novel anion-exchange organic-inorganic hybrid membranes prepared through sol-gel reaction and UV/thermal curing. Journal of Applied Polymer Science (2007), 107, 1865-1871.

6. Zielecka, M., Bujnowska, E., Bajdor, K. Siloxane-containing polymer matrices as coating materials. Journal of Coatings Technology and Research (2007), 4, 275-281.

7. Roux, S., Audebert, P., Pagetti, J., Roche, M. Electrochemical growth of conducting polymer into zirconium oxopolymers sol-gel coatings. Journal of Sol-Gel Science and Technology (2003), 26, 435-439.

8. Maillet, C., Janvier, P., Pipelier, M., Praveen, T., Andres, Y., Bujoli, B. Hybrid materials for catalysis? Design of new phosphonate-based supported catalysts for the hydrogenation of ketones under hydrogen pressure. Chemistry of Materials (2001), 13, 2879-2884.

9. Conklin, S. D., Heineman, W. R., Seliskar, C. J. Spectroelectrochemical sensing based on multimode selectivity simultaneously achievable in a single device. 19. Preparation and characterization of films of quaternized poly(4-vinylpyridine)-silica. Electroanalysis (2007), 19, 523-529.

10. Schneider, B., Doskocilova, D., Stokr, J., Tlustakova, M., Kalal, J. Structure of the product of polymerization of 2,3-epoxypropyl methacrylate in the presence of porous glass. Acta Polymerica (1979), 30, 283-289.

11. Li, S., Praveen, S. S., Mylonakis, A., Shah, A., Hsieh, A., Patel, A., Baran, G., Wei, Y. Synthesis of new organic–inorganic hybrids poly[2-hydroxethyl methacrylate (HEMA)-glycidyl methacrylate (GMA)-silica] and their mechanical properties. Journal of Materials Research (2008), 23, 66-71.

12. Luo, C. J., Wang, X., Li, J., Zhao, X., Wang, F. Conductive hybrid film from polyaniline and polyurethane–silica. Polymer (2007), 48, 4368-4374.

13. Rohlfing, D. F., Rathousky, J., Rohlfing, Y., Bartels, O., Wark, M. Functionalized mesoporous silica films as a matrix for anchoring electrochemically active guests. Langmuir (2005), 21, 11320-11329.

14. Genies, E. M., Lapkowiski, M., Santier, C., Vieil, E. Polyaniline, spectroelectrochemistry, display and battery. Synthetic Metals (1987), 18, 631-636.

15. Bauerle, P. Intrinsically conducting polymers. Advanced Materials (1993), 5, 879-886.

16. Xing, S., Zhao, C., Jing, S., Wang, Z. Preparation of polyaniline dispersions with different assembly structure. Journal of Materials Science (2006), 41, 2761-2766.

17. Duek, E. A. R., De Paoli, M. A., Masragostino. An electrochromic device based on polyaniline and prussian blue. Advanced Materials (1992), 4, 287-291.

18. Kuzmany, H., Sariciftci, N. S. In situ spectro-electrochemical studies of polyaniline. Synthetic Metals (1987), 18, 353-358.

19. Verghese, M. M., Ramanathan, K., Ashraf, S. M., Kamalasanan, M. N., Malhotra, B. D. Electrochemical growth of polyaniline in porous sol-gel films. Chemistry of Materials (1996), 8, 822-824.

20. Zarbin, A. J. G., De Paoli, M. A., Alves, O. L. Nanocomposites glass/conductive polymers. Synthetic Metals (1999), 99, 227-235.

21. Doherty, W. J., Armstrong, N. R., Saavedra, S. S. Conducting polymer growth in porous sol-gel thin films: Formation of nanoelectrode arrays and mediated electron transfer to sequestered macromolecules. Chemistry of Materials (2005), 17, 3652-3660.

22. Wang, Q. G., Wang, X. H., Li, J., Zhao, X. J., Wang, F. S. Water-borne conductive polyaniline doped by acidic phosphate ester containing polysilsesquioxane precursor. Synthetic Metals (2005), 148, 127-132

23. Ita, M., Uchida, Y., Matsui, K. Polyaniline/silica hybrid composite gels prepared by the sol-gel process. Journal of Sol-Gel Science and Technology (2003),26, 479-482.

24. Wang, Y., Wang, X., Li, J., Mo, Z., Zhao, X., Jing, X., Wang, F. Conductive polyaniline/silica hybrids from sol-gel process. Advanced Materials (2001),13, 1582-1585.

25. Jang, S. H., Han, M. G., Im, S. S. Preparation and characterization of conductive polyaniline/silica hybrid composites prepared by sol–gel process. Synthetic Metals (2000), 110, 17-23.

26. Wei, Y., Jin, D., Yang, C., Wei, G. Synthesis of organic-inorganic hybrid sol-gel materials with low volume-shrinkages. Polymeric Materials Science and Engineering (1996), 74, 244-245.

27. Wei, Y., Jin, D., Yang, C., Wei, G. A fast convenient method to prepare hybrid sol-gel materials with low volume-shrinkages. Journal of Sol-Gel Science and Technology (1996), 7, 191-201.

28. Wei, Y., Jia, X., Jin, D., Mathai, M., Yeh, J. M., Narkis, M., Siegmann, A. Synthesis of aniline oligomers with controlled molecular weight and narrow molecular weight distribution. Polymer Preprints (1998), 39, 115-116.

29. Wei, Y., Yu, Y. H., Zhang, W. J., Wang, C., Jia, X. R., Jansen, S. A. A new approach to electroactive polymers via well-defined oligomers with further polymerizable end-groups. Chinese Journal of Polymer Science (2002), 20, 105-118.

30. Wei, Y., Yeh, J. M., Jin, D., Jia, X., Wang, J. Composites of electronically conductive polyaniline with polyacrylate-silica hybrid sol-gel materials. Chemistry of Materials (1995), 7, 969-974.

31. Wei, Y., Jin, D., Wei, G., Yang, D., Xu, J. Novel organic-inorganic chemical hybrid fillers for dental composite materials. Journal of Applied Polymer Science (1998), 70, 1689-1699.

32. Wei, Y., Wei, W., Jin, D., Yang, D., Tartakovskaya, L. Synthesis of sulfonated polystyrene-silica hybrids and their application as ion exchange materials, Journal of Applied Polymer Science (1998), 64,1893 – 1902.

33. Guo, Y., Li, M., Mylonakis, A., Han, J., MacDiarmid, A. G., Chen, X., Lelkes, P. I., Wei, Y. Electroactive oligoaniline-containing self-assembled monolayers for tissue engineering applications. Biomacromolecules (2007), 8, 3025-3034.

34. Guo, Y., Mylonakis, A., Zhang, Z., Lelkes, P. I., Levon, K., Li, S., Feng, Q., Wei, Y. Oligoaniline-contained electroactive silsesquioxane precursor for synthesizing novel siliceous materials. Macromolecules (2007), 40, 2721-2729.

35. Li, M., Bidez, P., Guterman-Tretter, E., Guo,Y., MacDiarmid, A. G., Lelkes, P. I., Yuan, X., Sheng, J., Li, H., Song, C., Wei, Y. Electroactive and nanostructured polymers as scaffold materials for neuronal and cardiac tissue engineering. Chinese Journal of Polymer Science (2007), 25, 331-339.

36. Hunter, T. C., Price, G. J. Glycidyl methacrylate and N-vinylpyrrolidinone copolymers: synthesis and nuclear magnetic resonance characterization. Polymer (1994), 35, 3530-3534.

37. Yasuda, T., Yamaguchi, I., Yamamoto, T. Preparation of N-grafted polyanilines with oligoether side chains by using ring-opening graft copolymerization of epoxide, and their optical, electrochemical and thermal properties and ionic conductivity. Journal of Materials Chemistry (2003), 13, 2138-2144.

38. Gawdzik, B., Kovtun, O. Synthesis of glycidyl amine adducts and their copolymerization with glycidyl methacrylate. Journal of Applied Polymer Science (2005), 98, 2461-2466.

39. Titier, C., Pascault, J. P., Taha, M., Rozenberg, B. Epoxy-amine multimethacrylic prepolymers, kinetic and structural studies. Journal of Polymer Science: Part A: Polymer Chemistry (1995), 33, 175-184.

40. Genies, E. M., Lapkowski, M., Penneau, J. F. Cyclic voltammetry of polyaniline: interpretation of the middle peak. Journal of Electroanalytical Chemistry (1988), 249, 97-107.

41. Dominis, A. J., Spinks, G. M., Kane-Maguire, L. A. P., Wallace, G. G. A de-doping/re-doping study of organic soluble polyaniline. Synthetic Metals (2002), 129, 165-172.

42. Genies, E. M., Penneau, J. F., Lapkowski, M., Boyle, A. Electropolymerisation reaction mechanism of para-aminodiphenylamine. Journal of Electroanalytical Chemistry (1989), 269, 63-75.

43. Malinauskas, A., Holze, R. An in situ spectroelectrochemical study of redox reactions at polyaniline-modified ITO electrodes. Electrochimica Acta (1998), 43, 2563-2575.

44. Malinauskas, A., Holze, R. Cyclic UV-Vis spectrovoltammetry of polyaniline. Synthetic Metals (1998), 97, 31-36.

45. Shreepathi, S., Holze, R. Spectroelectrochemistry and preresonance raman spectroscopy of polyaniline-dodecylbenzenesulfonic acid colloidal dispersions. Langmuir (2006),22, 5196-5204.

46. Stilwell, D. E., Park, S. M. Electrochemistry of conductive polymers. Journal of the Electrochemical Society (1989),136, 427-433.

47. Delongchamp, D. M., Hammond, P. T. Multiple-color electrochromism from layer-by-layer-assembled polyaniline/prussian blue nanocomposite thin films. Chemistry of Materials (2004),16, 4799-4805.

48. Nekrasov, A. A., Ivanov, V. F., Vannikov, A. V. Effect of pH on the structure of absorption spectra of highly protonated polyaniline analyzed by the Alentsev–Fock method. Electrochimica Acta (2001), 46, 4051-4056.

49. Koziel, K., Lapkowski, M., Lefrant, S. Spectroelectrochemistry of polyaniline at low concentrations of doping anions. Synthetic Metals (1995), 69, 137-138.

Chapter 7. Electrochemical Study of Aniline Trimers and other Aniline Oligomers with End Group Substitution

7.1 Introduction and Motivation

Explosive growth of research in the field of conductive polymers was triggered by the discovery, by MacDiarmid, Heeger and Shirakawa in 1977, that the electronic conductance of polyacetylene could be further increased by many orders of magnitude, by "doping it" with electron acceptors (p-type dopants), such as iodine.[1,2] During the last three decades, very significant progress has been made in this field as a result of the numerous potential applications of conductive polymers. Among these macromolecular compounds, polyaniline was much studied due to its rather easy preparation, good stability under the medium conditions, as well as to its interesting redox properties. One big drawback of polyaniline though is its poor processability.

On the other hand, due to molecular structure regularity, good electroactivity, and easy processing, polyaniline oligomers have become ideal candidates for investigating the properties of polyaniline,[3] or even substitute polyaniline in several applications.[4] Aniline oligomers have been extensively studied by our group as model compounds, and explored as new electroactive materials. According to the differences in the end groups, aniline oligomers can be mainly divided into three groups: parent aniline oligomers (capped with a phenyl group at one end and an amino group at the other), amino-capped aniline oligomers (capped with an amino group at both ends) and phenyl-capped aniline oligomers (capped with a phenyl group at both ends).[5] Conceivably, the terminal-functionalized aniline oligomers are valuable building blocks for making polyaniline-like, new electroactive polymers.[6] These polyaniline-like polymers may also contain inorganic

moieties, and subsequently, great interest has been shown in inorganic-organic hybrid materials that can combine the properties of both inorganic and organic materials and which can have various applications in catalysis,[7] chemical separation technology[8] and biosensors.[9]

In this chapter, a comparative study of several well-defined aniline trimers with end group substitution is presented, in order to establish possible electrochemical mechanisms and to investigate the effects of molecular structure on the electronic structure and the electronic properties of these electroactive aniline oligomers. Both aqueous and non-aqueous experiments have been performed, and the dependence of the redox peaks on the scan rate, the pH, the solvent and the supporting electrolyte has been investigated. Additionally, for a deeper comparative study, the detailed cyclic voltammetry data of some other aniline oligomers (e.g., amine and phenyl capped aniline dimers) are also presented. These include N-phenyl-1,4-phenylene diamine, N,N-diphenyl-1,4-phenylene diamine, 2,5-dimethyl-1,4-phenylenediamine and 2,3,5,6-tetramethyl-1,4-phenylene diamine, whose electrochemical behavior is also examined under virtually identical conditions. Moreover, during this electrochemical study, a novel aniline trimer-silane compound, N,N'-bis(4'-(triethoxysilylpropyl-ureido)phenyl)-1,4-quinone-dimine (TSUPQD), which is a precursor for periodic mesoporous organosilica that was synthesized and characterized from our group has been also extensively investigated.[10] N-4-aminophenyl-N'-4'-(3-triethoxysilylpropyl-ureido)phenyl-1,4-quinonenediimine (ATQD), which contains the same chemical core as TSUPQD but has only one end group substitution, has been also electrochemically studied. In addition, the

electrochemistry of the polymerized material derived from this aniline trimer-silane compound has been explored and is going to be presented.

7.2 Experimental Section

7.2.1 Materials

N-Phenyl-1,4-phenylene diamine (97%), N,N-diphenyl-1,4-phenylene diamine (98%), 2,5-dimethyl-1,4-phenylenediamine (99%) and 2,3,5,6-tetramethyl-1,4-phenylenediamine (99%), acetonitrile (anhydrous, 98%), propylene carbonate (anhydrous, 97%), methane sulfonic acid (99.5%), trifluoroacetic acid (99+%, spectrophotometric grade), perchloric acid (volumetric standard, 0.105N in glacial acetic acid), tetrabutylammonium tetrafluoroborate (99%), tetraethylammonium tetrafluoroborate (99%), tetrabutylammonium bromide (99%) and tetrabutylammonium iodide (99%) were purchased from Sigma Aldrich. Dimethyl sulfoxide (99.7%) and N,N-dimethylformamide (99.5%) were purchased from Spectrum. Tetramethylammonium perchlorate, tetrabutylammonium perchlorate and tetrabutylammonium hexafluorophosphate were of electrochemical grade and were purchased from Alfa products. Tetrapentylammonium iodide (99%) was purchased from City Chemical Corporation. All chemicals were used as received with no further purification.

7.2.2 Electrochemical Measurements

Electrochemical measurements were performed on an Epsilon Potensiostat interfaced and monitored with a PC computer. A three-electrode system was employed for all the electrochemical experiments. The working electrodes used for the cyclic voltammetry experiments were a platinum disk electrode with a surface area of 0.02 cm^2 and a platinum foil electrode with a surface area of 0.25 cm^2. For the rotating disk

electrode experiments, the working electrode was a glassy carbon rotating disk electrode with a surface area of 0.27 cm^2. A platinum wire was used as an auxiliary electrode for all electrochemical studies. The reference electrodes used were Ag/AgCl for aqueous solutions and Ag/Ag^+ (silver ions as $AgNO_3$ (0.01M) in a solution of MeCN containing 0.1M Et_4NBF_4) for non-aqueous solutions. Unless otherwise indicated, the scan rate used for all the experiments was 60 mV/sec. Nitrogen gas was purged for 10 minutes in the solution under study before measurements. A nitrogen gas blanket on top of the solutions was maintained during measurements.

7.2.3 Synthesis Procedures

7.2.3.1 Synthesis of Aniline Trimer: N,N'-bis(4'-aminophenyl)-1,4-quinonedi-imine (APQD)

The preparation of aniline trimer was achieved by following the one-step approach from N,N'-diaminodiphenylamine, developed in our group.[11] Briefly speaking, aniline monomer was added and reacted in a mixture of N,N'-diaminodiphenylamine, ammonium persulfate solution, sodium chloride and hydrochloric acid under vigorous stirring at –11 ^oC for 2 hr. After quenching of the reaction by saturated oxalic acid solution, the dark blue residue was obtained by filtering through a Buchner funnel, then washed with 1M HCl, followed by neutralization with NH_4OH and finally dried in a vacuum oven for 48 hr. Soxhlet extraction for 24 hr with acetone was used to further wash the final product. As a typical procedure, 35 g of NaCl were dissolved in 400 ml of HCl (1M) in a 1000-ml three-neck round bottom flask equipped with a thermometer and a mechanical stirrer. 12.7 g of N,N-diaminodiphenylamine sulfate (0.036 mol) and 3.4 ml (0.036 mol) of aniline were then added into the above mixture while stirring. At that

point the flask was transferred to a refrigerated bath, and the reaction system was cooled down to -11 ^{o}C under constant mechanical stirring. A solution of 9.93 g (0.051 mol) of ammonium persulfate in 60 ml of HCl (1M) was then transferred into the flask, through a dropping funnel, under vigorous mechanical stirring at a speed of ~60 drops per minute. After the addition of ammonium persulfate the mixture was stirred for 2 hr at -11^{o}C. A fresh solution of saturated oxalic acid was then added to the solution to quench the reaction, and the flask was held into the refrigerated bath for 15 more min under vigorous stirring. The dark blue reaction mixture was then filtered, and the wet dark residue was transferred to a 1000-ml beaker, where it was neutralized with 200 ml of 15% (w/w) ammonium hydroxide under strong magnetic stirring. This mixture was stirred over night. The dark blue solid was then filtered and washed thoroughly with copious amounts of distilled water. The residue was dried in a vacuum oven at 45 ^{o}C for 3 days (yield: 58 %).

7.2.3.2 Synthesis of N,N'-bis(4'-(3-triethoxysilylpropyl-ureido)phenyl)-1,4-quinonedi-imine (TSUPQD)

The synthesis procedure has been described elsewhere.[10]

7.2.3.3 Synthesis of N-(4-aminophenyl)-N'-(4'-(3-triethoxysilylpropyl-ureido)phenyl-1,4-quinonenedi-imine) (ATQD)

The synthesis procedure has been described elsewhere.[12]

7.2.3.4 Synthesis of N,N'-bis(4'-(dodecyl-amide)phenyl)-1,4-quinonedi-imine (DAPQD)

332.5 mg (1.2 mmole) of finely divided amine capped aniline trimer were

dissolved in 10 mL of dry dichloromethane. The solution was stirred and purged with nitrogen gas before adding 470 mg (2.5 mmoles) of 1-n-dodecalyl acid chloride drop-wise over a 5-min period. The mixture was stirred at room temperature for 18 hr, filtered and dried under high vacuum to yield the solid dark product (82 % yield).

7.2.3.5 Synthesis of N,N'-bis(4'-(N,N-dibutyl-amino)phenyl)-1,4-quinonedi-imine (BAPQD)

542 mg (5 mmol) of 1,4-phenylenediamine were added in a 250-mL round-bottom flask that contained 2.05 g (10 mmol) of N,N-dibutylaniline, 40 mL of 1M HCl, and 50 mL of ethanol. The contents were stirred as the solution was cooled to 5 °C with an ice bath. Once at 5 °C, 2.29 g (10 mmoles) of ammonium persulfate were added in one portion. The solution was stirred for 1.5 hr at 5 °C and for an additional hour at room temperature, diluted with 100 mL of 1M HCl and then vacuum filtered. The collected residue was then washed with 50 mL of distilled water and dried in vacuum. The obtained solid material was dissolved in 15 mL of acetone and then precipitated again with 200 ml of 1M HCl. The precipitate was collected by vacuum filtration and dried under air (18 % yield).

7.2.3.6 Synthesis of N,N'-bis(4'-(N-hexyl-amino)phenyl)-1,4-quinonedi-imine (HAPQD)

The same synthesis procedure used to synthesize BAPQD was followed to synthesize HAPQD, except that 542 mg (5 mmol) of 1,4-phenylenediamine and 1.77 g (10 mmol) of N-hexylaniline were used (49 % yield).

7.2.3.7 Synthesis of N,N'-bis(4'-(N,N'-dihexyl-amino)phenyl)-1,4-quinonedi-imine (DHAPQD)

N,N'-dichlorodi-imine (160 mg, 1 mmol) in 5 mL of acetonitrile was added to a stirring solution of N,N-dihexylaniline (523 mg, 2 mmol) in 15 mL of acetonitrile. The solution was allowed to stir for 15 min before 200 mg (1.5 mmol) of sodium oxalate were added in 40 mL of acetonitrile. The obtained mixture was refluxed for 3 hr under constant stirring. After reflux, the mixture was additionally stirred for 3 days at room temperature. The solvent was removed under high vacuum, and the solid collected was washed with copious amounts of diethylether (42 % yield).

7.3 Results and Discussion

7.3.1 Non-Aqueous Solutions

The electrochemical behavior of amine-capped aniline trimer, aniline trimers with end-group substitution, as well as other phenyl- and amine-capped aniline dimers, has been examined in non-aqueous solutions. Several combinations of solvent-electrolyte systems have been tried. Solvents like propylene carbonate, dimethyl sulfoxide (DMSO), dimethyl formamide (DMF) and acetonitrile (MeCN) have been used to find the one that gives the optimum redox peaks for the compounds analyzed. Various tetraalkylammonium salts have been explored as supporting electrolytes, including Me_4NClO_4, n-Bu_4NBF_4, Et_4NBF_4, n-Bu_4NPF_6, Et_4NClO_4, Bu_4NBr_4 and $(C_3H_7)_4NI$. Overall, the best results were obtained for the acetonitrile-Et_4NBF_4 system. Several doping acids were tried including methane sulfonic acid, trifluoroacetic acid and perchloric acid.

7.3.1.1 Amine Capped Aniline Trimer (APQD)

The electrochemical behavior of amine-capped aniline trimer and polyaniline have been investigated in acetonitrile containing 0.1M Et_4NBF_4 and 0.77M $MeHSO_4$, as the electrolyte and the doping acid, respectively. In the cyclic voltammogram of amine-capped aniline trimer, a pair of well defined redox peaks at around 350 mV that represents a removal/addition of 2 electrons was obtained (**Figure 7-1**). This pair is attributed to the oxidation/reduction of the ‘‘leukoemeraldine’’ form to the ‘‘emeraldine’’ form and back, respectively (**Scheme 7-1**). At higher potentials, i.e., 850 mV, the second pair of redox peaks represents the oxidation/reduction of the ‘‘emeraldine’’ form to the ‘‘pernigraniline’’ form and back, respectively. The identical chemical structure of aniline trimer and polyaniline suggests that the electrochemical behavior of both should be almost the same. As expected, aniline trimer gave two pairs of redox peaks almost identical with polyaniline. Thus, the two formal redox potentials for aniline trimer are displayed at 350 mV and 850 mV, as compared to 300 mV and 900 mV for polyaniline. The two redox peaks represent a removal/addition of two electrons each, as in the case of polyaniline according to the following scheme:

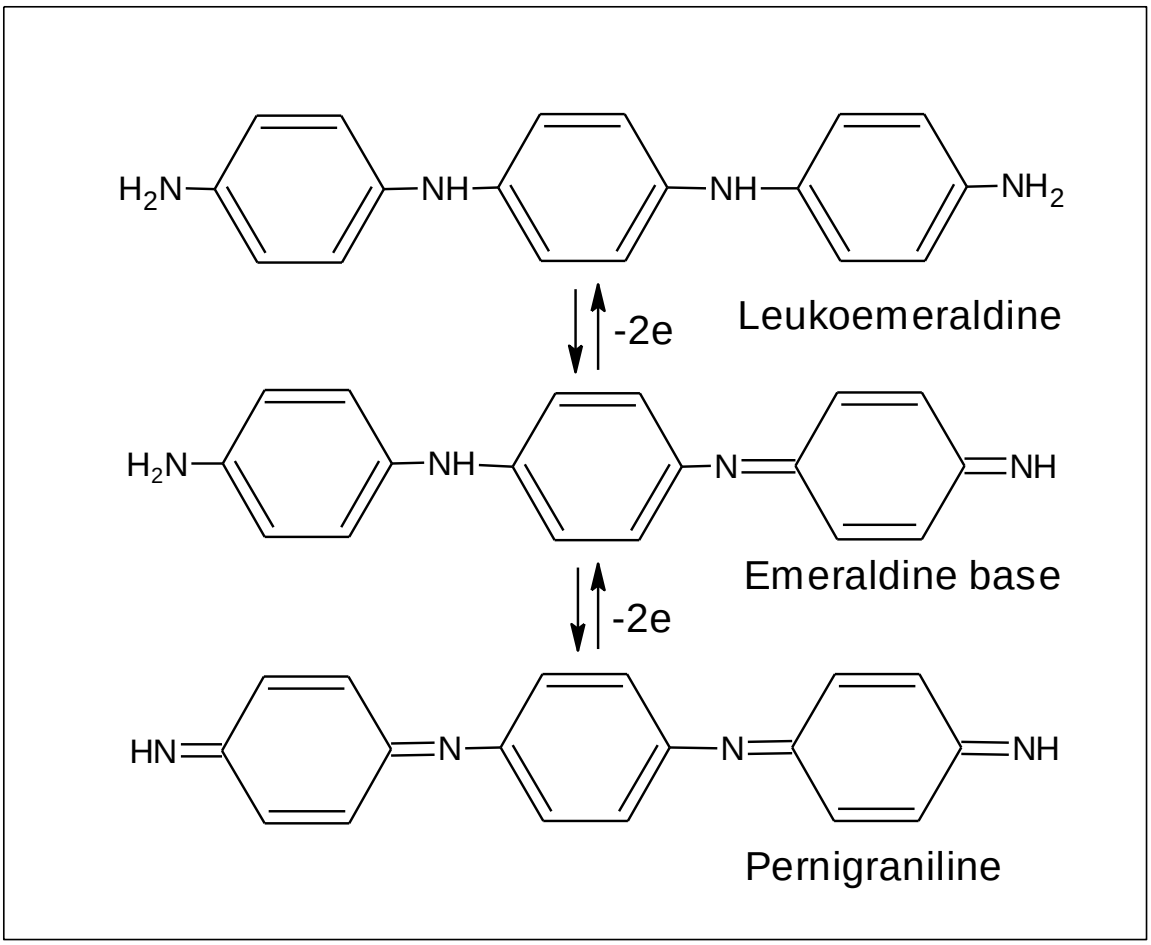

Scheme 7-1. Oxidation states of aniline trimer

7.3.1.2 Substituted Amine-Capped Aniline Trimers

Several well-defined aniline trimers, with amine end group substitution, have been examined in non-aqueous solutions of acetonitrile. The goal was a comparative study and an investigation of the effect that amine end-group substitution has on the electroactivity of the aniline trimers. The compounds that were tested can be seen on **Table 7-1**. Interestingly, replacement of the amine end-group hydrogen, by electron-withdrawing or electron-donating groups, has a profound effect on the redox peaks obtained. Depending on the substitution, the electronic cloud around the amine end groups might be more or less stabilized, which makes the removal of electrons from these

amines more or less difficult respectively. At this point, it must be emphasized that the effect of the different substitutes is manifested more profoundly for the second pair of redox peaks, since this pair of peaks involves the removal/addition of electrons that are bound on the substituted amines.

As can be seen from **Figure 7-2a,** trimer DHAPQD gave redox peaks with the lowest formal potentials, that is 164 mV and 424 mV. This is consistent with the fact that the two hexyl groups that are bound on each amine end group push the electron cloud more than any other trimer tested, which makes the electrochemical oxidation of this trimer easier. HAPQD on the other hand, which has only one hexyl group attached on each amine end group, shows formal potentials that are shifted slightly anodically, that is 322 mV and 516 mV (**Table 7-2**). Trimer BAPQD shows redox peaks at higher potentials than trimer DHAPQD, since the substitution now involves butyl groups instead of hexyl groups. This trimer gives formal redox potentials at 308 mV and 504 mV (**Figure 7-2b**). On the other hand, trimer DAPQD, which contains a substitute that has a carbonyl group next to the amine end group, shows formal redox potentials at 520 mV and 1020 mV respectively, due to the electron pulling effect of the substitutes (**Figure 7-3**). This compound gives redox peaks at almost the same potentials as TSUPQD, as will be shown in later sections of this chapter.

7.3.1.3 Other Aniline Oligomers

Several other aniline oligomers (**Table 7-3**) have been also examined to better elucidate and investigate the effects of molecular structure on the electronic properties of electroactive aniline oligomers. The electrochemical response varies also for these compounds depending on the substitution of the amine end groups and/or the phenyl end

groups. It must be pointed out here that each redox peak of these aniline oligomers represents a one-electron transfer, and thus if somebody was to compare these results to the ones obtained for the end-group substituted aniline trimers, then only the first redox pair of peaks of the latter's should be considered. A direct comparison though would not be very reliable, since different concentrations of doping acids have been used for these studies in each case. In the case of these oligomers, trifluoro acetic acid (1.3×10^{-2}M) has been used as the doping acid in order to get the optimum redox peaks. Nevertheless, this comparison can manifest the effect that end-group substitution has on the electroactivity of aniline oligomers.

As can be seen on **Table 7-3**, amongst the aniline oligomers tested, 2,3,5,6-tetramethyl-1,4-phenylenediamine is the most readily oxidized oligomer, with formal potentials at -175 mV and 340 mV. A slightly more difficult to oxidize oligomer is 2,5-dimethyl-1,4-phenylenediamine, with a first formal potential at -100 mV and a second formal potential at 445 mV. These results indicate that substitution of the phenyl rings of 1,4-phenylenediamines with alkyl groups shifts the redox peaks of the amine groups to lower potentials, due to the electron donating effect of the alkyl groups. On the other hand, substitution of hydrogen of the amine end group of N-phenyl-1,4-phenylenediamine with a phenyl group causes delocalization of the electron cloud of this oligomer, or in other words stabilization of it, and thus makes the removal of electrons harder. This is the reason that N,N'-diphenyl-1,4-phenylenediamine has higher redox formal potentials than N-phenyl-1,4-phenylenediamine. The cyclic voltammograms of these compounds in acetonitrile can be seen in **Figure 7-4**.

7.3.2 Electrochemical Study of a Precursor of Periodic Mesoporous Organosilica

As has already been mentioned, the electrochemistry of a novel aniline trimer-silane compound, that is N,N'-bis(4'-(3-triethoxysilylpropyl-ureido)phenyl)-1,4-quinonedi-imine (TSUPQD), which is a precursor for periodic mesoporous organosilica, has been extensively investigated due to the importance of this class of compounds. Both aqueous and non-aqueous experiments have been performed. N-(4-aminophenyl)-N'-(4'-(3-triethoxysilylpropyl-ureido)phenyl-1,4-quinonenedi-imine) (ATQD), which contains the same chemical core as TSUPQD but only one end-group substitution, has been also electrochemically studied. Moreover, the electrochemical investigation of the polymerized material poly(TSUPQD), which resulted from hydrolysis and co-condensation of TSUPQD with tetraethyl orthosilicate, is also presented.

7.3.2.1 Aqueous Solutions

7.3.2.1.1 TSUPQD

The cyclic voltammogram of TSUPQD was recorded in an aqueous solution of HCl (1M). Due to the insolubility of the analyte in aqueous solutions, a film was deposited on the electrode by casting a solution of TSUPQD in ethanol (5 mg/ml) on top of the working electrode and drying it in air. In the potential range of 0-1000 mV, a pair of well-defined redox peaks at around 500 mV that represents a removal/addition of two electrons was obtained (**Figure 7-5**). This pair is attributed to the oxidation/reduction of the ''leukoemeraldine'' form to the ''emeraldine'' form and back, respectively (**Scheme 7-2**).

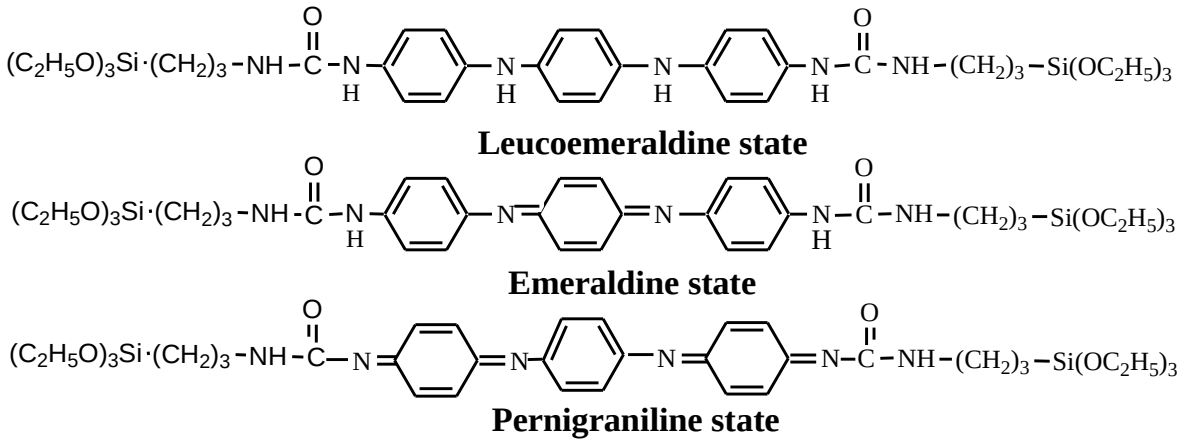

Scheme 7-2. Redox forms of the electroactive TSUPQD.

At potentials higher than 1000 mV, the strong background current from the oxidation of water makes it impossible to observe the second pair of voltammetric peaks of TSUPQD in aqueous media. This redox pair would be the one that corresponds to the oxidation/reduction of the ‘‘emeraldine’’ form to the ‘‘pernigraniline’’ form and back, respectively. Below a scan rate of 130 mV/sec the current peaks were linearly proportional to the scan rate, as can be seen from **Figure 7-6,** which is justified by the fact that the electron transfer is associated with a surface attached species.

The peak potentials of TSUPQD depend a lot on the acidity of the solution, as could be expected, due the resemblance with the polyaniline system, where proton-controlled pH dependence in the low pH region exists.[13-17] $E_{1/2}$ decreases linearly as the pH of the solution is increased up to 1. At a pH higher than 1 and up to a pH of 2, $E_{1/2}$ remained almost constant. At a pH higher than 2 no deconvolution of peaks was possible whereas at pHs higher than 4, TSUPQD completely lost its electroactivity. In a highly acidic environment (pH=1) it was even possible to observe the radical cation (polaron[18]) formation at around 250 mV, which represents a removal/addition of one electron (**Figure 7-7**). At even lower pHs, though, the first redox pair of peaks shifts anodically,

and converges with the second redox pair of peaks, to form one redox pair of peaks that represents a removal/addition of two electrons. In the graph of the peak potential against the pH, a slope of 57 mV/pH should be obtained for a redox reaction that involves equal number of electrons and protons.[19] In the TSUPQD case, the slope, at a pH lower than 1, turns out to be equal to 56 mV/pH, which reveals that equal number of protons and electrons are involved at this first redox process. The pH dependence of the half-wave potential is consistent with the following half-reaction:

$$\text{Leukoemeraldine} \rightarrow \text{Emeraldine} + 2e^- + 2H^+ \qquad E_o = 0.54 \text{ V vs Ag/AgCl}$$

7.3.2.1.2 Aniline Trimer (APQD)

The cyclic voltammogram of amine capped aniline trimer was recorded under the same conditions as TSUPQD, for comparison reasons. A film of aniline trimer was cast on top of the Pt working electrode, and the cyclic voltammograms were recorded in an aqueous solution of HCl (1M). A pair of well-defined redox peaks that correspond to the oxidation/reduction from the ‘‘leukoemeraldine’’ form to the ‘‘emeraldine’’ form and back was similarly observed. The linear dependence of the current peaks to the scan rate justifies again a species attached on the surface of the working electrode, whereas the pH dependence of the redox peaks was almost similar to the one obtained for TSUPQD. Compared to TSUPQD, the difference here is that in the very low pH region (pH~-1), it was even possible to see the second pair of redox peaks that correspond to the oxidation/reduction from the ‘‘emeraldine’’ form to the ‘‘pernigraniline’’ form and back, respectively (**Figure 7-8**). The electron-withdrawing ureido group doesn’t allow for this second peak to be shown in the cyclic voltammogram of TSUPQD in aqueous solutions, because it makes the removal of electrons from the side amine end groups more difficult

compared to aniline trimer.

7.3.2.2 Non Aqueous Solutions

7.3.2.2.1 TSUPQD

7.3.2.2.1.1 Cyclic Voltammetry

Similarly to what occurred in aqueous solutions, in the lower potential range of the cyclic voltammogram of TSUPQD, a pair of well defined redox peaks, which represent the oxidation/reduction of the ‘‘leukoemeraldine’’ form to the ‘‘emeraldine’’ form and back respectively, was observed in acetonitrile. Without the high background of water though, it is even possible to observe the second pair of peaks, which correspond to the oxidation/reduction of the “emeraldine” form to the “pernigraniline” form with a formal potential at 925 mV (**Figure 7-9**). As in the case of the aqueous solutions, dependence of the redox peaks on the pH of the solution in non-aqueous solutions is observed as well. When the concentration of methane sulfonic acid is small, only the first pair of peaks can be observed (**Figure 7-10a**). By adding more acid, or alternatively by doping TSUPQD, the second pair of peaks at around 850 mV starts to evolve (**Figure 7-10b**). Finally, after a certain amount of acid added, it is possible to observe the second pair of peaks. The first pair of peaks seems to be split into two individual redox peaks, and this phenomenon is more profound in the cathodic part of the cyclic voltammogram. This is caused by the fact that this peak represents a removal/addition of two electrons, which in a specific concentration of acid can give two distinct electrochemical waves, with the former representing the polaron formation. This is even more obvious when trifluoroacetic acid is used as the doping acid, where two redox pairs of peaks at 60 mV and 325 mV that each represents a removal/addition of one electron can be identified

(**Figure 7-11**). From the same figure, two small bumps at 700 mV and 1000 mV vs Ag/Ag^{+}, which correspond to the oxidation/reduction of the "emeraldine" form to the "pernigraniline" form, are also evident. Higher concentration of trifluoroacetic acid would cause these peaks to grow bigger, would shift them anodically and would make them combine into one peak.

7.3.2.2.1.2 Rotating Disk Polarography of TSUPQD

Rotating disk polarography experiments were performed in order to further support that equal number of electrons is involved in the two pairs of redox peaks of TSUPQD. Increase of the obtained current with the increase of the rotational speed verifies a mass transport limited process. In **Figure 7-12**, the distance of the plateaus of the current response for the two formal potentials is equal, which suggests that the same number of electrons is involved for these two redox pairs of peaks. A diffusion coefficient of 1.17×10^{-6} cm^2/sec in acetonitrile was obtained for TSUPQD at 24 ^{o}C according to the equation of mass transport limited current that was presented in section 2.3.4.2.2 of Chapter 2.

7.3.2.2.1.3 Effect of the Supporting Electrolyte

The supporting electrolyte composition affects the electrochemistry of polyaniline as has been proposed by several authors.[18-21] In the same manner, the electrochemistry of TSUPQD is also altered by changing the composition of the supporting electrolyte. By comparing the results of experiments that used different supporting electrolytes, it was noted that by changing the cation of the electrolyte, the differences of the voltammograms obtained were almost not observable. On the other hand, the effect of

different anions used in the redox peaks obtained for TSUPQD was profound. Thus, by changing the anion of the electrolyte, peaks were shifted and appeared to be smaller or bigger depending on the electrolyte used. It may be stated that this greater effect of anions suggests a stronger tendency of insertion during the redox process compared to cations.

7.3.2.2.2 Electrochemical study of N-(4-aminophenyl)-N'-(4'-(3-triethoxysilylpropyl-ureido)phenyl-1,4-quinonenediimine) (ATQD)

To better support the above findings, the electrochemical investigation of N-(4-aminophenyl)-N'-(4'-(3-triethoxysilylpropyl-ureido)phenyl-1,4-quinonenedi-imine) (ATQD), which contains the same chemical core as TSUPQD but has only one end-group substitution, has been also electrochemically studied. The cyclic voltammogram of ATQD, recorded in a non-aqueous solution of MeCN containing 0.1 M Et_4NBF_4 and 0.77M $MeHSO_4$, can be seen in **Figure 7-13.** The first two pairs of the well-defined redox peaks at 320 mV and 440 mV represent the removal/addition of 1 electron each, and can be attributed to the reversible redox process from the "leucoemeraldine'' to the ''emeraldine'' form. Moving progressively to higher potentials two reversible redox peaks with formal potentials of 650 mV and 740 mV can be observed, each of which represents the removal/addition of 1 electron. These are assigned to the oxidation/reduction of the "emeraldine" form to the "pernigraniline" form and correspond to the non-substituted amine end group of the ATQD. At even higher potentials (~ 950 mv), another pair of redox peaks that also represents the oxidation/reduction of the "emeraldine" to the "pernigraniline" form, but corresponds to the substituted end of the aniline trimer moiety, is observed. These well-defined redox peaks represent the

removal/addition of 2 electrons. The electron-withdrawing ureido group causes the redox peaks of the substituted end group to be shifted anodically, and makes them discernible from the redox peaks of the non-substituted end group. This phenomenon is a perfect example of how substitution on the amine end groups affects the electrochemical behavior of these electroactive aniline oligomers.

7.3.2.2.3 Polymerized TSUPQD

As has already been mentioned, *N,N'*-bis(4'-(3-triethoxysilylpropyl-ureido)phenyl)-1,4-quinonene-di-imine (TSUPQD), synthesized from the emeraldine base form of aniline trimer,[23] was used as the precursor, which underwent hydrolysis and co-condensation with TEOS in a cetyltrimethylammonium bromide (CTAB) templating hydrothermal sol-gel method, using acetone as the co-solvent. Removal of CTAB surfactants, from the hexagonally ordered oligoaniline-containing silica, afforded the novel electroactive periodic mesoporous organosilica (TSU-PMOs), which has high surface area and contains uniformly distributed electroactive units inside the pores. As has been reported earlier in this chapter,[23] the precursor TSUPQD showed essentially similar electrochemical behavior as polyaniline but with slightly higher redox peak potentials, which are attributed to the electron withdrawing ureido groups, attached to the main chain of the amino-capped aniline trimer. Based on this, the electrochemical behavior of the TSU-PMOs, in both aqueous and non-aqueous solutions, has been also explored.

Cyclic voltammograms obtained in strongly acidic aqueous solutions of HCl (1M) for TSU-PMOs with two different TSU contents are shown in **Figure 7-14**. Because the analytes were insoluble in aqueous solutions, the samples had to be wrapped into a

platinum foil that was used as the working electrode. In the scanned potential range shown (i.e. 0 - 1.0 V), one well defined redox pair of peaks was found at around 0.55 V against the reference electrode (Ag/AgCl), which corresponds to the transition from the "leucoemeraldine" to the "emeraldine" form of the aniline oligomer and represents the removal/addition of two electrons.[34] As seen in this figure, 66 wt% TSU-PMO shows at least one order of magnitude higher currents compared to the low content (33 wt%) TSU-PMOs, which is consistent with the fact that 66 wt% TSU-PMO has more redox sites than the lower content TSU-PMOs. The second redox pair of peaks, which correspond to the oxidation of the "emeraldine" form to the "pernigraniline" form, cannot be detected in aqueous solutions due to the background current limit from water. In order to observe this second redox pair of peaks, experiments had to be conducted in non-aqueous solutions. **Figure 7-15** shows the CV, obtained in acetonitrile, of the electroactive hybrid made from 100 wt% of TSUPQD, which clearly shows two pairs of redox peaks. The cyclic voltammograms indicate that the electroactivity coming from the electroactive aniline trimer moiety is still maintained in TSU-PMOs. The substantially lower intensities of the redox peaks obtained for TSU-PMOs, as compared to the ones of the electroactive precursor (TSUPQD) under the same conditions, are attributed to the co-condensation with the electrochemically inert TEOS and the formation of a rigid inorganic silica framework. It is not surprising to see that the introduced electroactive function can be well controlled by adjusting the content of oligoaniline bridges in the organosilica.

The electrochemical activity of these redox sites is established by direct electron transfer from the working electrode surface to the electroactive sites[35] and/or via long-range electron transfer, through electron exchange between the adjacent electroactive

moieties (electron hopping).[19,36] It is worth mentioning that the electrochemical behavior of the mesoporous TSU-PMOs is significantly different from that of the non-porous TSU-PMO (**Figure 7-16**). This may be attributed not only to the fact that the uniform mesopores provide more rapid electrolyte diffusions, but also to enhanced ordering of adjacent electroactive groups, which facilitates the electron exchange between the active redox centers and the working electrode. From this electrochemical study, it can be stated that the MCM-41 mesoporous structure makes this series of hybrid materials not only retain the anticipated electroactivity, but even enhance the electrochemical performance compared to conventional bulk materials.

7.4 Conclusion

The redox processes of amine end-group substituted aniline trimers were correlated with the variation in side-group substitution. These results demonstrate that substitution with electron-donating or electron-withdrawing groups has a profound effect on the electrochemistry of these compounds and of other aniline oligomers. By introducing alkoxylsilyl groups in the aniline trimer, it was possible to prepare an electroactive organic-inorganic hybrid material. The aniline trimer containing silsesquioxane compound behaved electrochemically like polyaniline with regard to protonation and ion insertion during the redox process. The electrochemical study of the polymerized material, obtained upon hydrolysis and co-condensation with TEOS, shows that the introduced electroactive function can be well controlled by adjusting the content of oligoaniline bridges in the organosilica.

The electroactive conjugated oligomers of well-defined structures have many significant advantages, including the much easier processability over their corresponding

polymers. End group substitution of these oligomers offers the ability to control the ionization potentials of oligomers, and thus provide materials with several potential applications. Taking advantage of their well-defined structures and designable end groups, properly functionalized oligomers could form a variety of molecular or supramolecular assemblies for potential electronic and optical applications[1]. Like polyaniline, these oligomers and their derivatives can be used in the fabrication of electrochromic, electroluminescent and biosensor devices, as well as for the preparation of anticorrosion and antistatic coatings.

7.5 Acknowledgements

A portion of this work has been in collaboration with Dr. Yi Guo and Mr. Mathew Zagorski. I would like to thank the Commonwealth of Pennsylvania through a grant to the Nanotechnology Institute of Southeastern Pennsylvania for their support in this project. I would also like to thank Dr. Shuxi Li for his valuable input in this project.

Table 7-1. Aniline trimers with end-group substitution that have been electrochemically investigated in non-aqueous solutions.

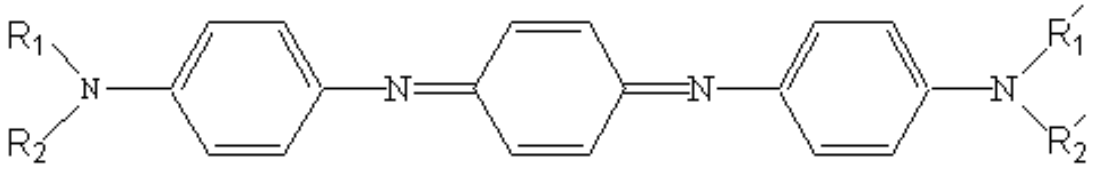

Trimer	R_1 / R_2	R_1' / R_2'
APQD	H / H	H / H
TSUPQD	C(O)-N-C-Si-O(C_2H_5)$_3$ / H	C(O)-N-C-Si-O(C_2H_5)$_3$ / H
ATQD	C(O)-N-C-Si-O(C_2H_5)$_3$ / H	H / H
BAPQD	nC_4H_9 / nC_4H_9	nC_4H_9 / nC_4H_9
HAPQD	nC_6H_{13} / H	nC_6H_{13} / H
DHAPQD	nC_6H_{13} / nC_6H_{13}	nC_6H_{13} / nC_6H_{13}
DAPQD	C(O)-$C_{11}H_{23}$ / H	C(O)-$C_{11}H_{23}$ / H

Table 7-2. Formal redox potentials of substituted amine-capped aniline trimers.

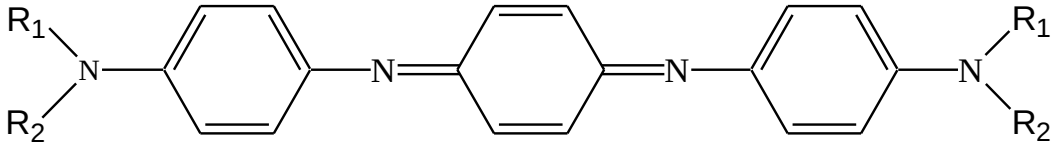

Trimer	R_1	R_2	1^{st} $E_{1/2}$ *(mV)*	2^{nd} $E_{1/2}$ *(mV)*
BAPQD	nC_4H_9	nC_4H_9	308	504
HAPQD	nC_6H_{13}	H	322	516
DHAPQD	nC_6H_{13}	nC_6H_{13}	164	424
DAPQD	$C(O)\text{-}C_{11}H_{23}$	H	520	1020

Table 7-3: Other aniline oligomers tested in non-aqueous solutions.

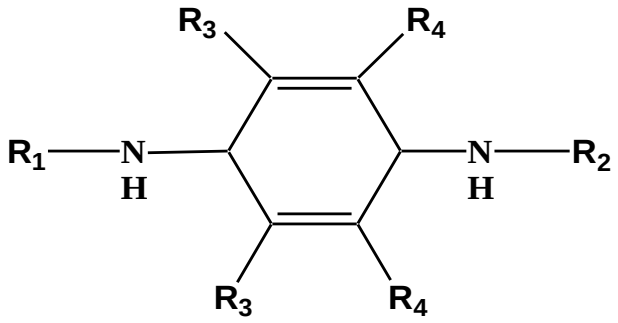

Oligomer	R1	R2	R3	R4	1st $E_{1/2}$ (mV)	2nd $E_{1/2}$ (mV)
N-phenyl-1,4-phenylenediamine	C_6H_5	H	H	H	35	525
N.N-diphenyl-1,4-phenylenediamine	C_6H_5	C_6H_5	H	H	145	550
2,5-dimethyl-1,4-phenylenediamine	H	H	CH_3	H	-100	445
2,3,5,6-tetramethyl-1,4-phenylenediamine	H	H	CH_3	CH_3	-175	340

(a)

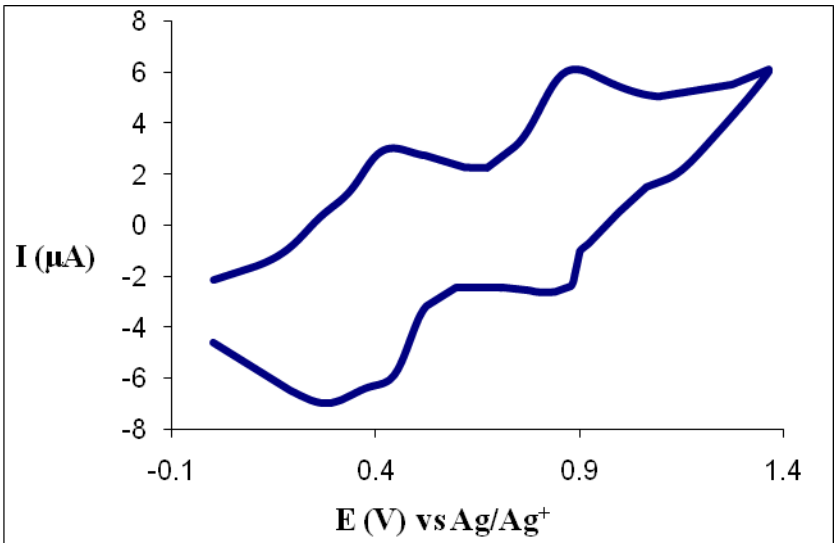

(b)

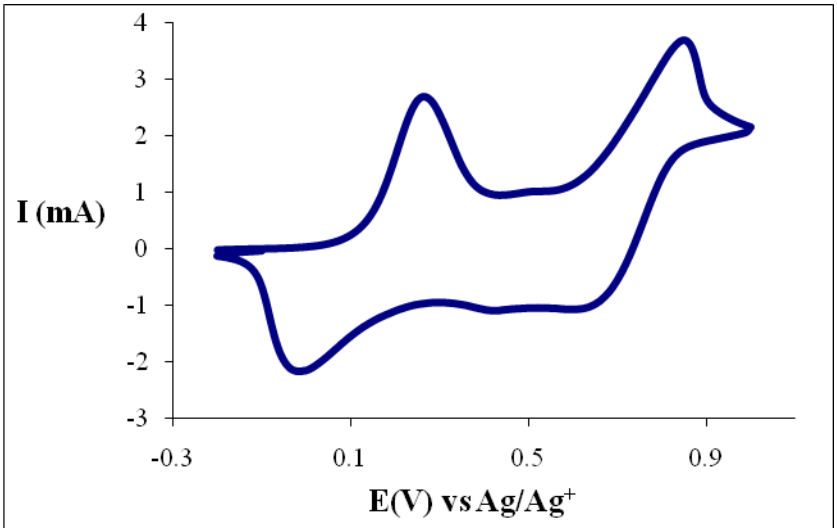

Figure 7-1. Cyclic voltammogram of: (a) amine-capped aniline trimer, (b) polyaniline, in acetonitrile containing 0.1M Et_4NBF_4 and 0.77M $MeHSO_4$. Scan rate used was 60 mV/sec.

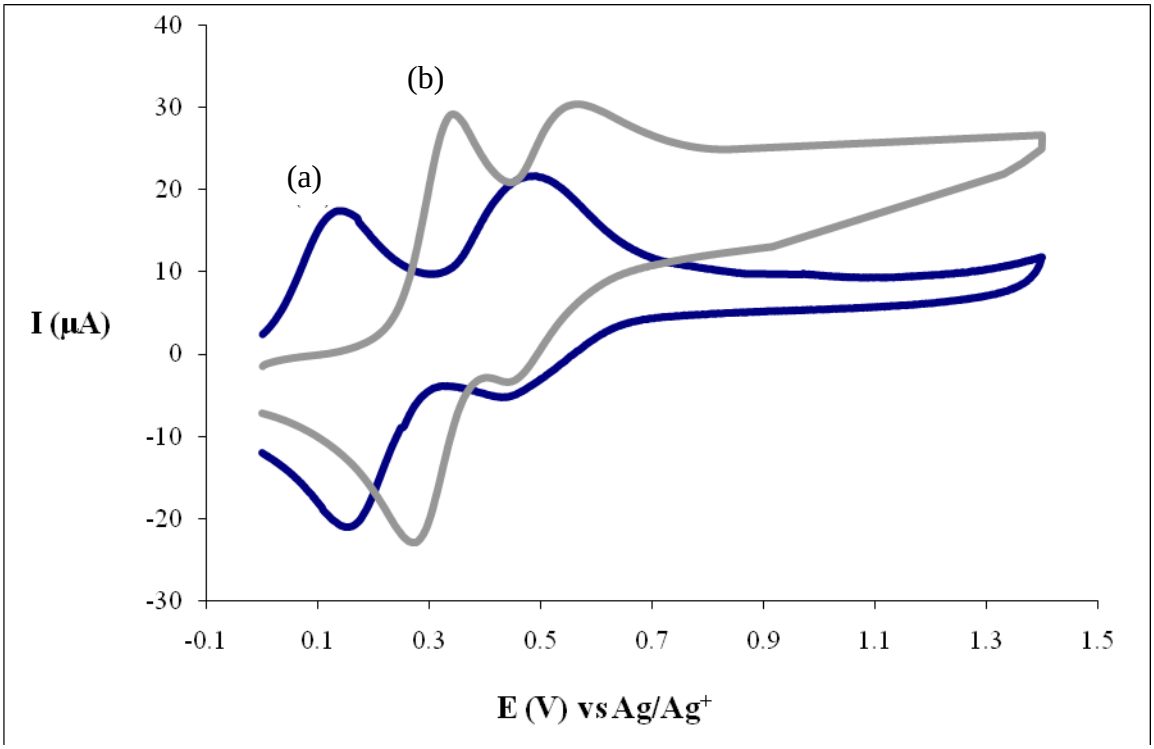

Figure 7-2. Cyclic voltammograms of aniline trimers with end-group substitution by: (a) hexyl groups (DHAPQD), (b) butyl groups (BAPQD), in acetonitrile containing 0.1M Et_4NBF_4 and 0.77M $MeHSO_4$. Scan rate used was 60 mV/sec.

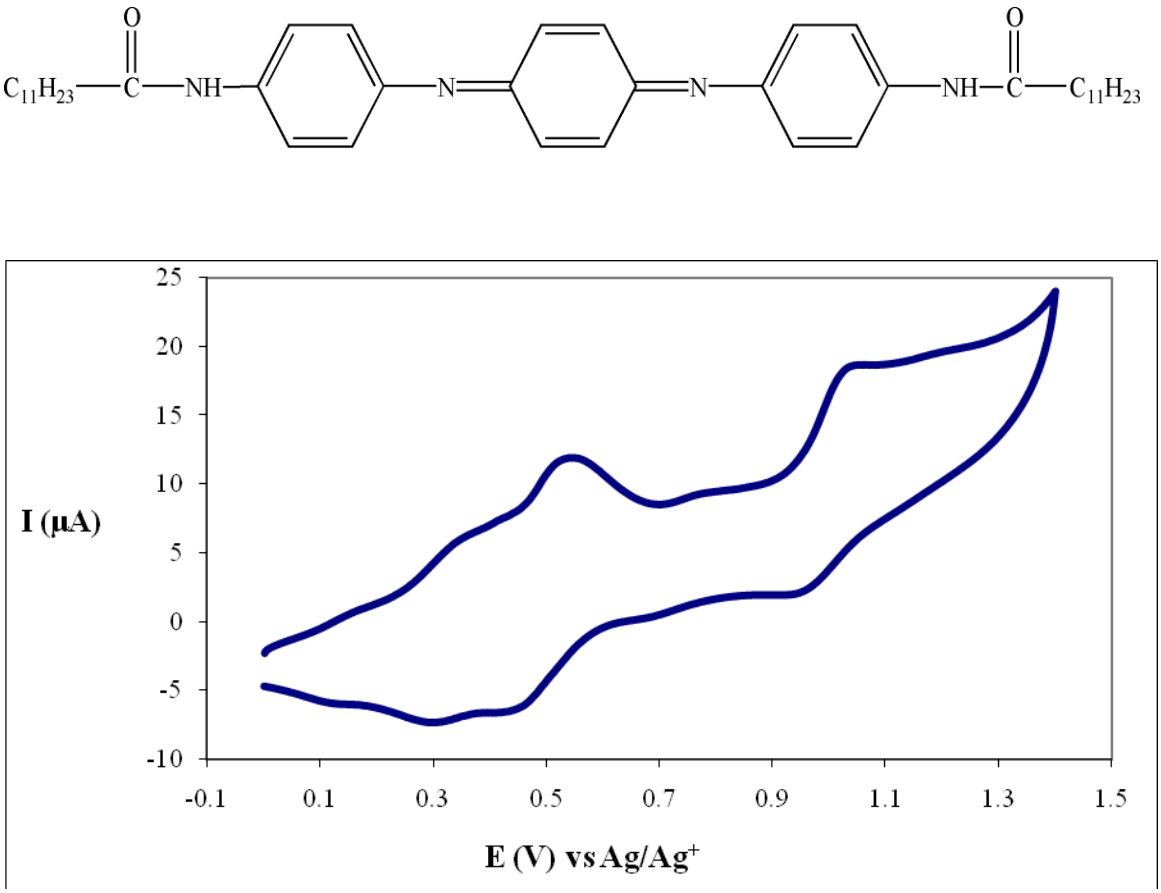

Figure 7-3. Chemical structure and cyclic voltammogram of end group substituted aniline trimer with dodecarboxyl group in acetonitrile containing 0.1M Et_4NBF_4 and $15x10^{-3}$M $MeHSO_4$. Scan rate used was 60 mV/sec.

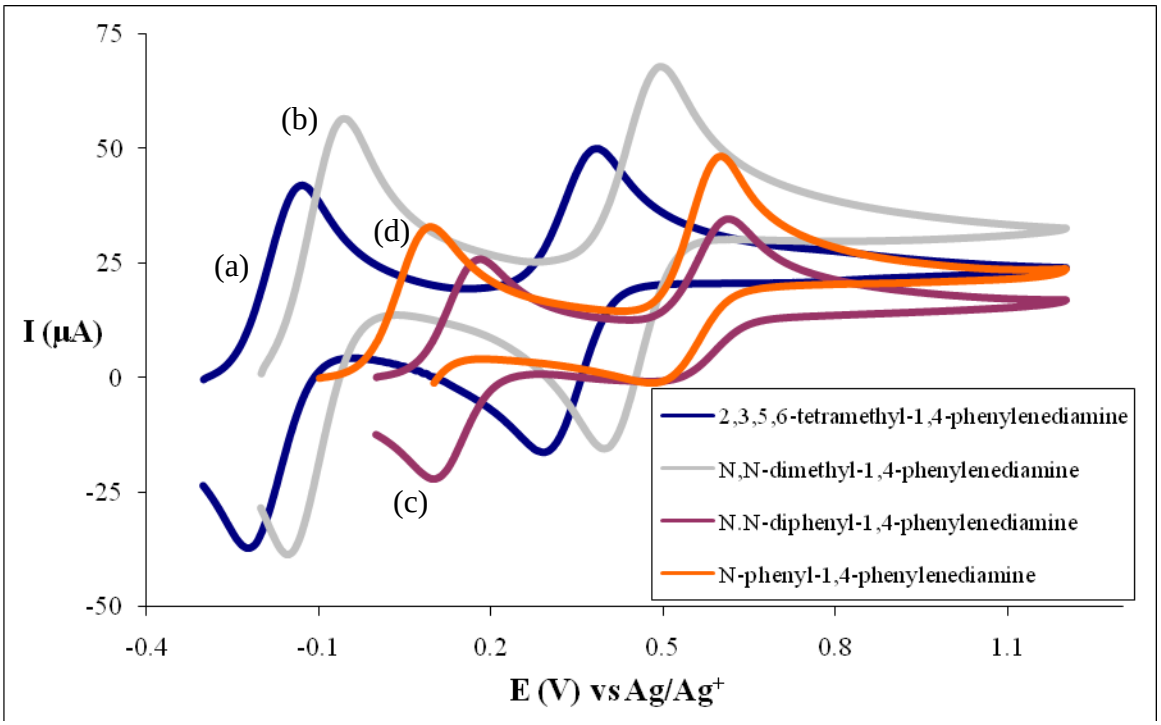

Figure 7-4. Cyclic voltammogram of: (a) 2,3,5,6-tetramethyl-1,4-phenylene diamine, (b) 2,5-dimethyl-1,4-phenylene diamine, (c) N,N-diphenyl-1,4-phenylene diamine, (d) N-phenyl-1,4-phenylene diamine, in acetonitrile containing 0.1M Et_4NBF_4 and1.3 x 10^{-2}M of CF_3COOH. Scan rate used was 60 mV/sec.

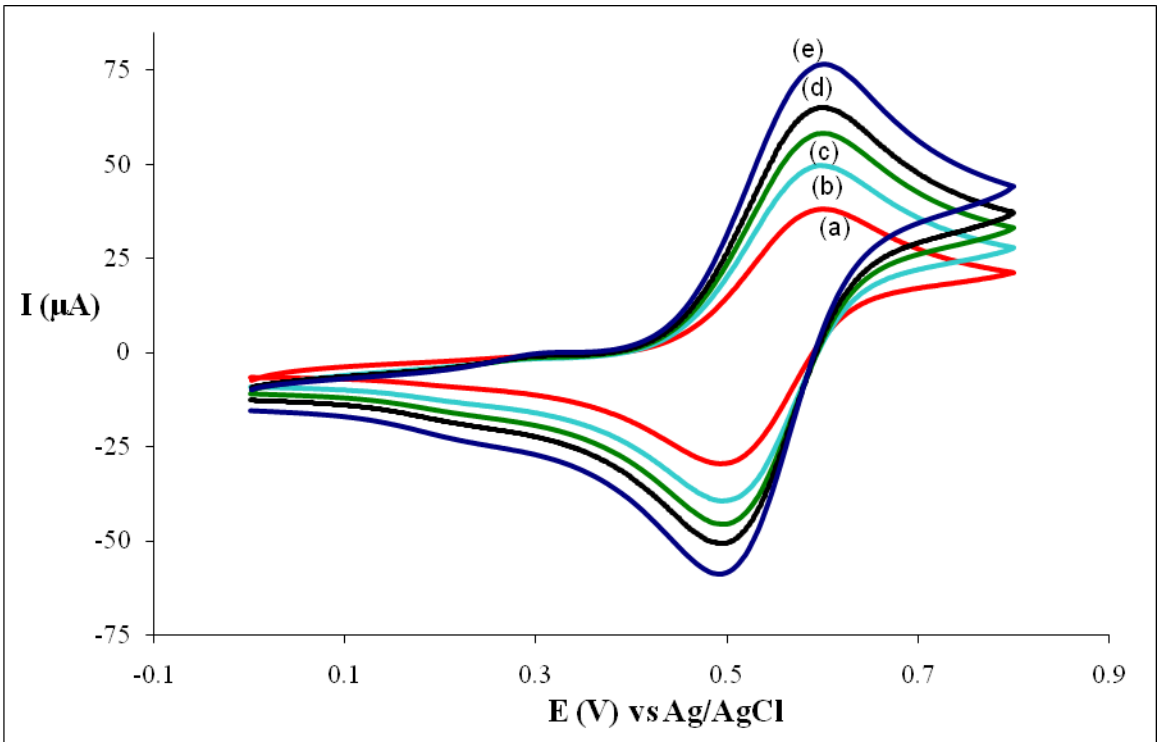

Figure 7-5. Cyclic voltammogram of TSUPQD in HCl (1M) at different scan rates: (a) 20 mV/sec, (b) 40 mV/sec, (c) 60 mV/sec, (d) 80 mV/sec, (e) 120 mV/sec.

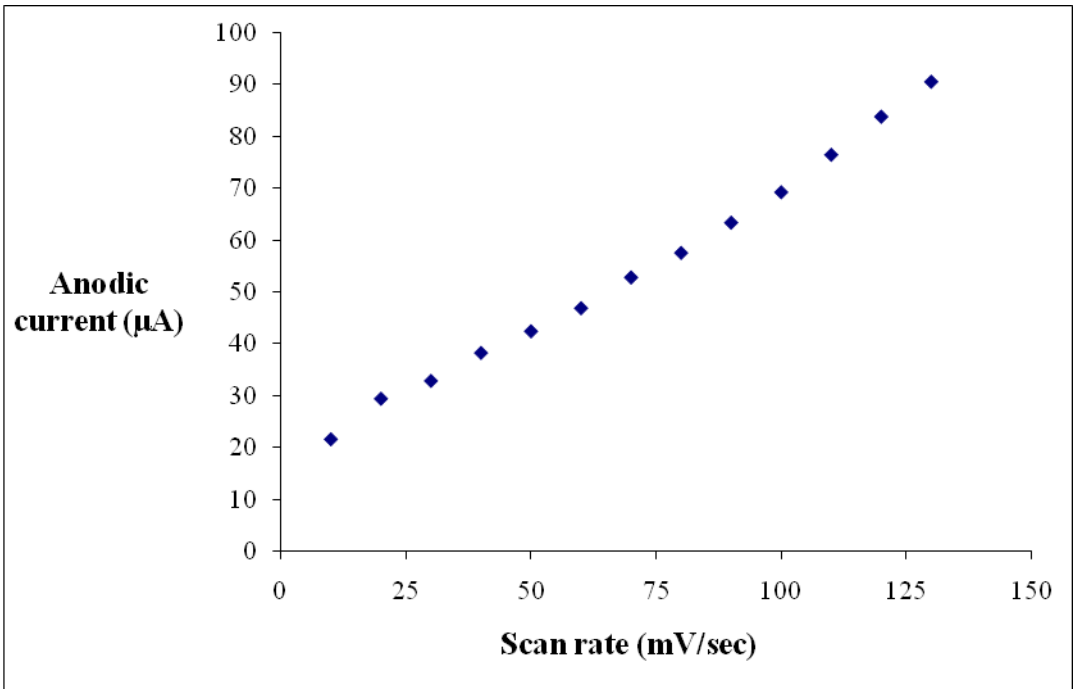

Figure 7-6. Dependence of anodic current on scan rate for TSUPQD in HCl at pH=1.

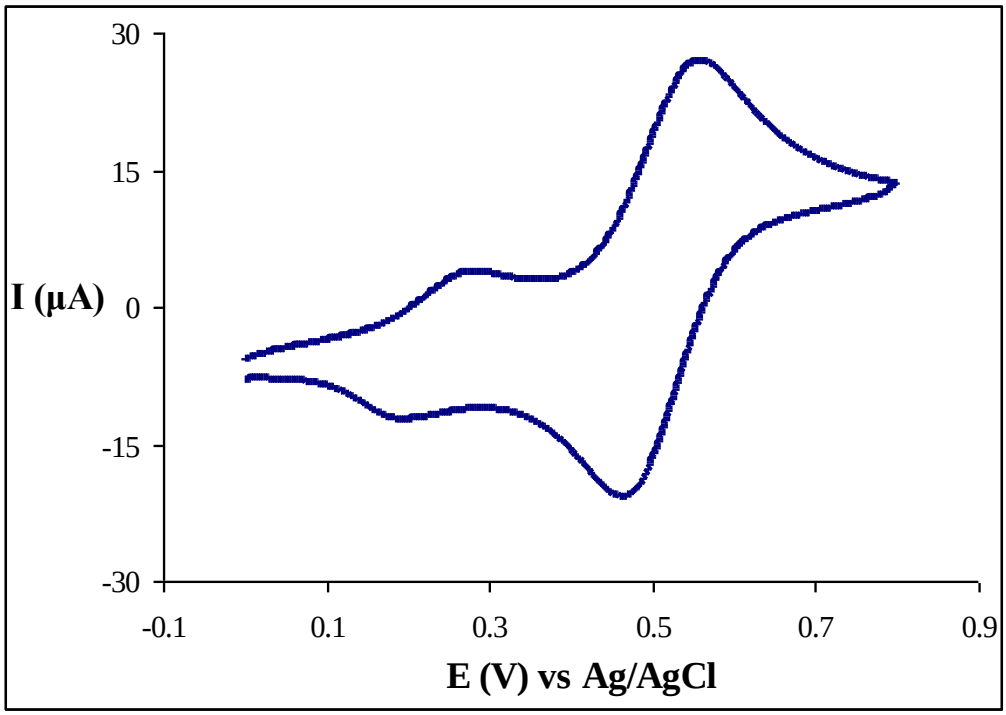

Figure 7-7. Cyclic voltammogram of TSUPQD in HCl (pH=1 at 24 ^{o}C). The polaron formation can be observed.

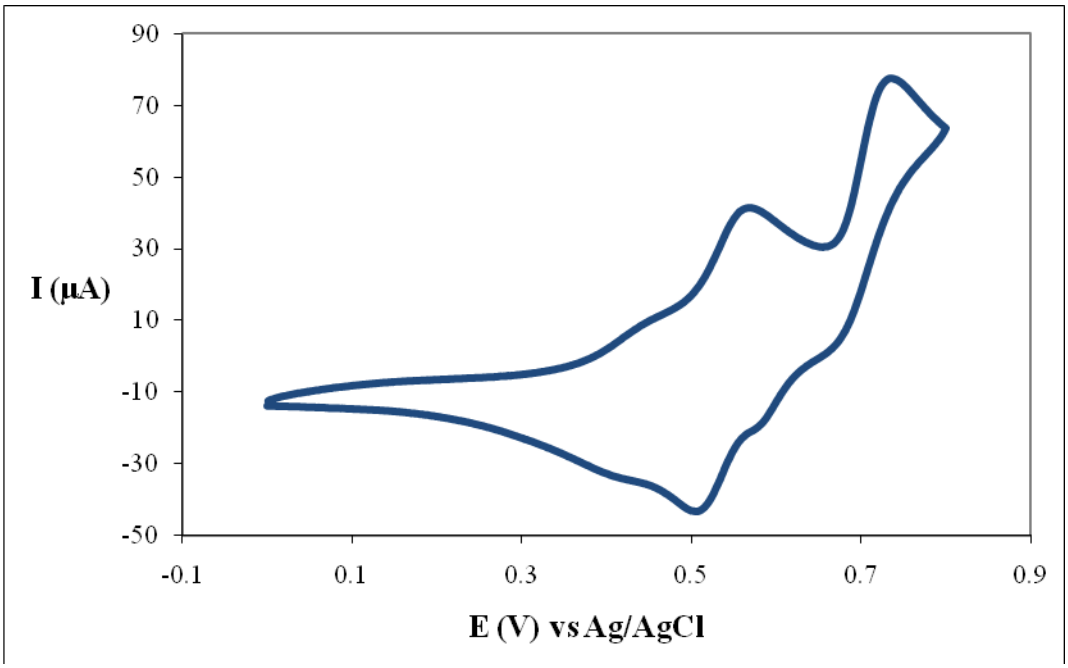

Figure 7-8. Cyclic voltammogram of amine-capped aniline trimer in HCl at very low pH (pH=-1 at 24 ^{o}C). The second redox peak, which corresponds to the oxidation/reduction of the emeraldine form to the pernigraniline form and back, respectively, can be observed.

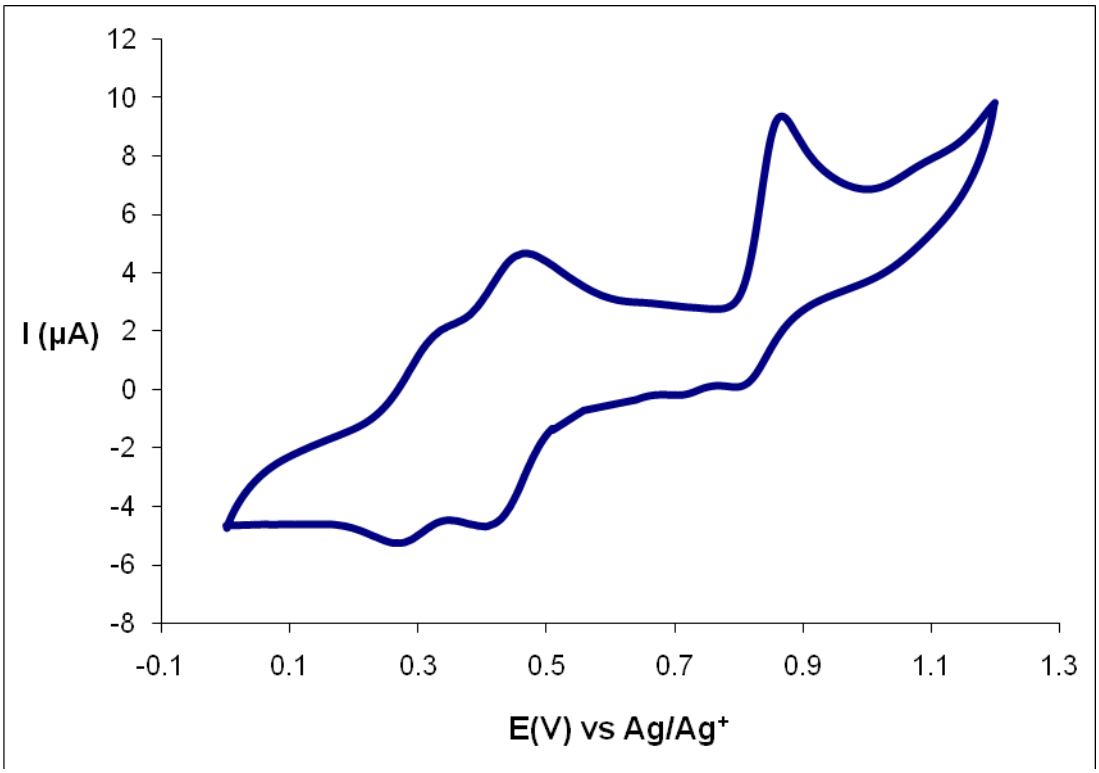

Figure 7-9. Cyclic voltammogram of TSUPQD in acetonitrile containing 0.1M Et_4NBF_4 and 0.77M $MeHSO_4$ as electrolyte and doping acid, respectively. Scan rate used was 60 mV/sec.

(a)

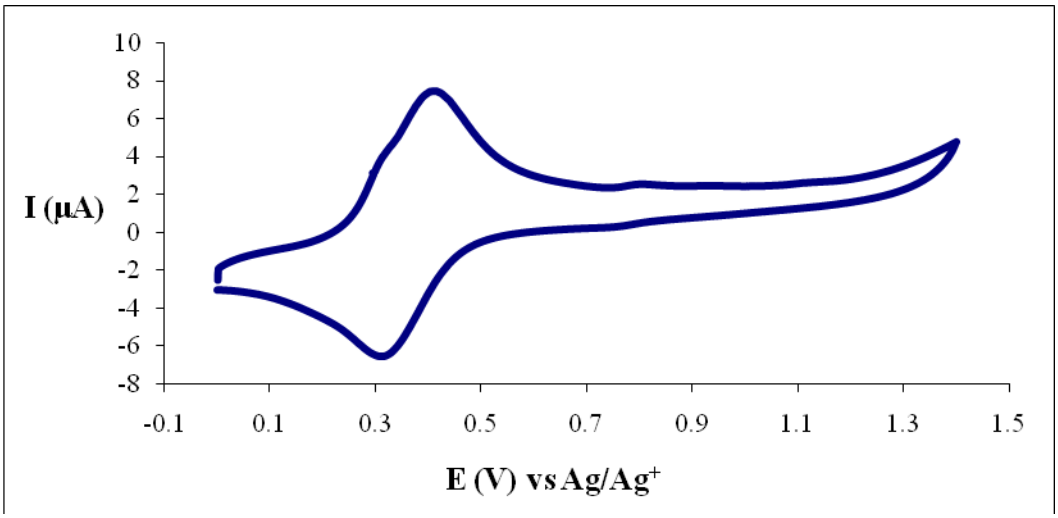

(b)

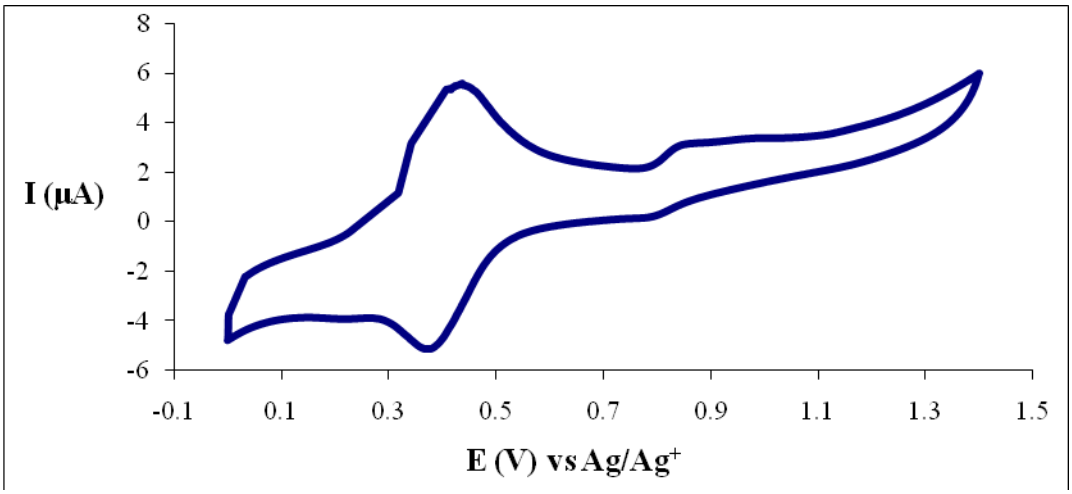

Figure 7-10. Cyclic voltammogram of TSUPQD in acetonitrile containing: (a) 0.1M Et_4NBF_4 and 0.12M $MeHSO_4$, (b) 0.1M Et_4NBF_4 and 0.32M $MeHSO_4$, as electrolyte and doping acid, respectively.

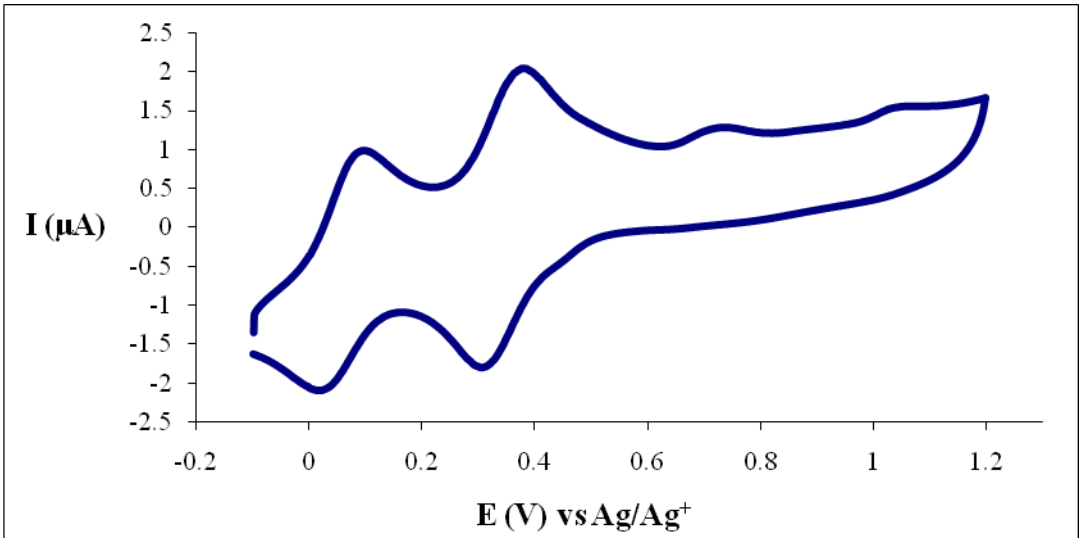

Figure 7-11. Cyclic voltammogram of TSUPQD in acetonitrile containing 0.1M Et_4NBF_4 and 0.16M CF_3COOH as electrolyte and doping acid, respectively.

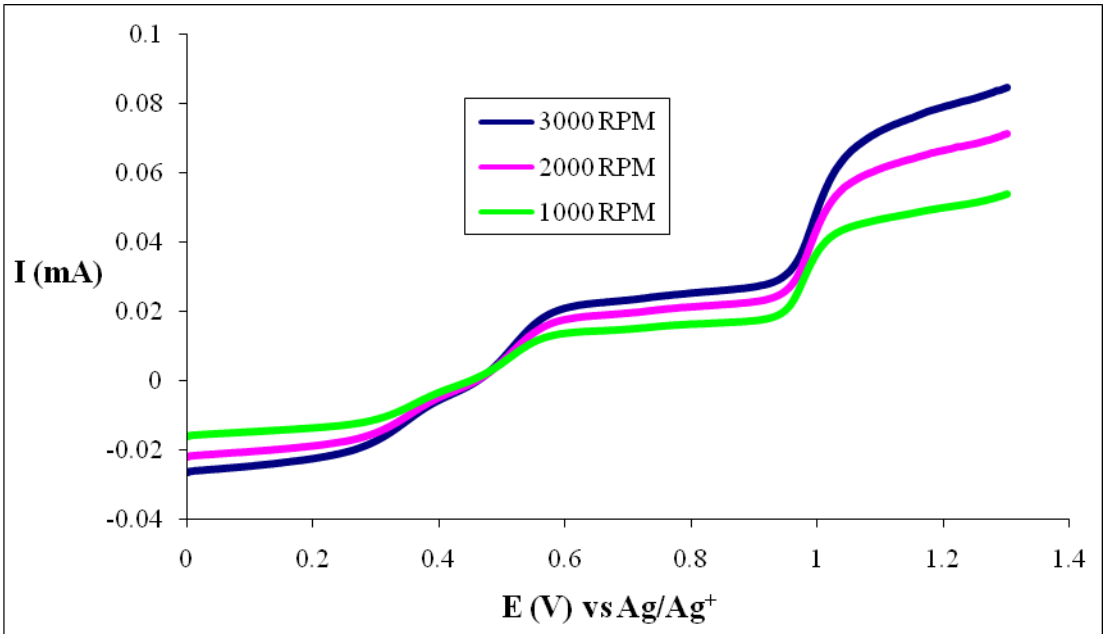

Figure 7-12: RDP experiments of TSUPQD in acetonitrile containing 0.1M Et_4NBF_4 and 0.77M $MeHSO_4$ as electrolyte and doping acid, respectively, at different rotation speeds: (a) 1000 rpm, (b) 2000 rpm, (c) 3000 rpm.

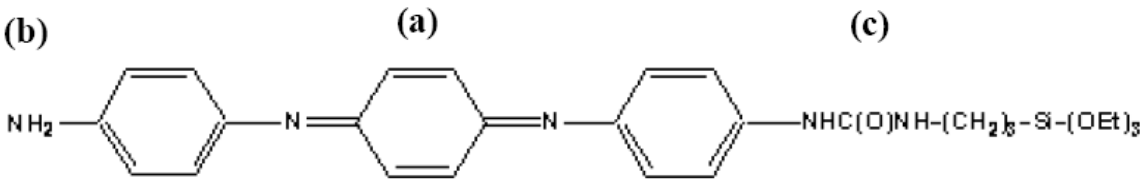

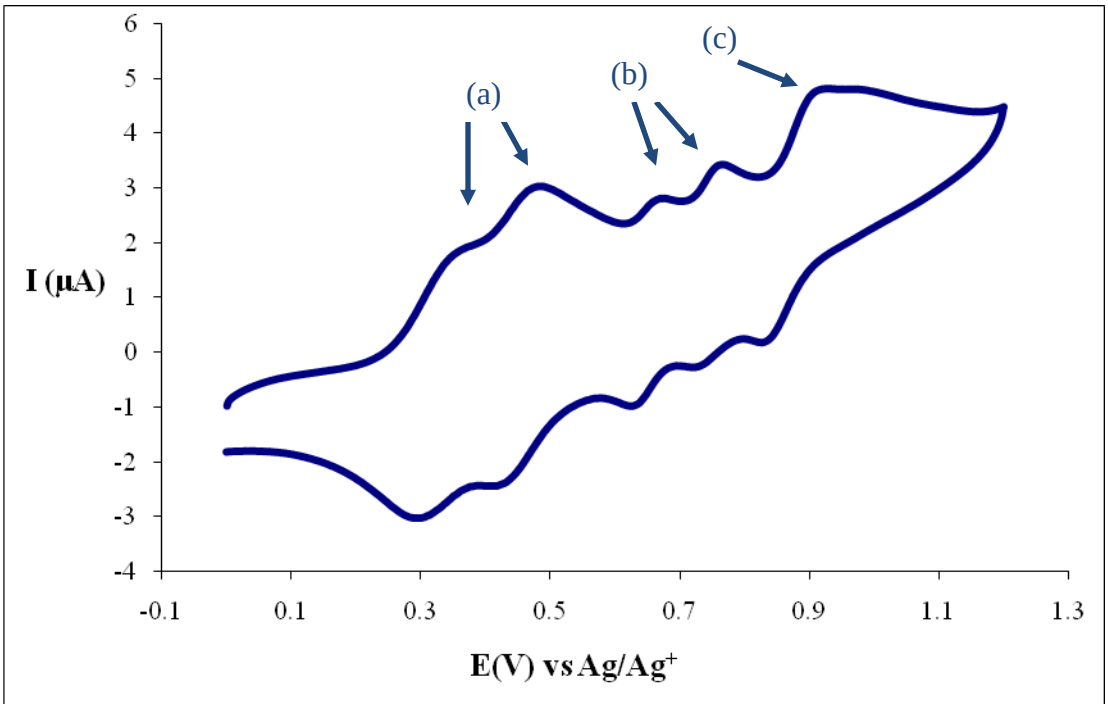

Figure 7-13. Cyclic voltammogram of ATQD in acetonitrile containing 0.1M Et_4NBF_4 and 0.77M $MeHSO_4$. Scan rate used was 60 mV/sec.

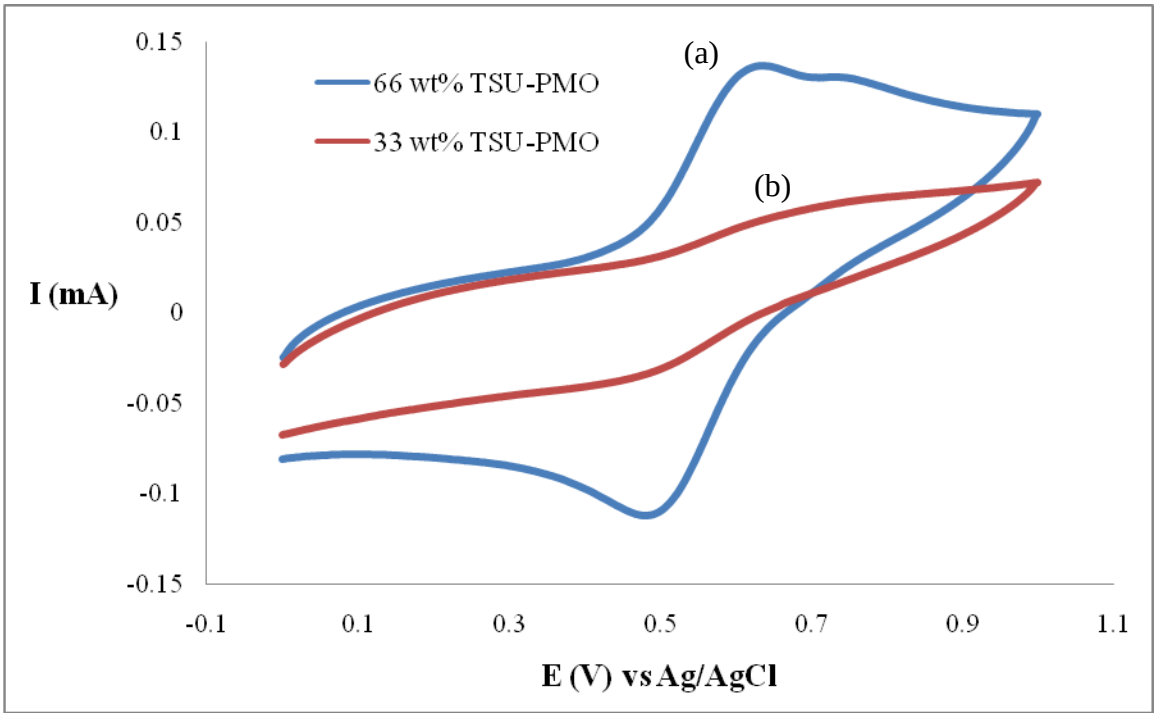

Figure 7-14. Cyclic oltammograms of (a) 66 wt% TSU-PMO and (b) 33 wt% TSU-PMO, in HCl (1M). Scan rate used was 60 mV/sec.

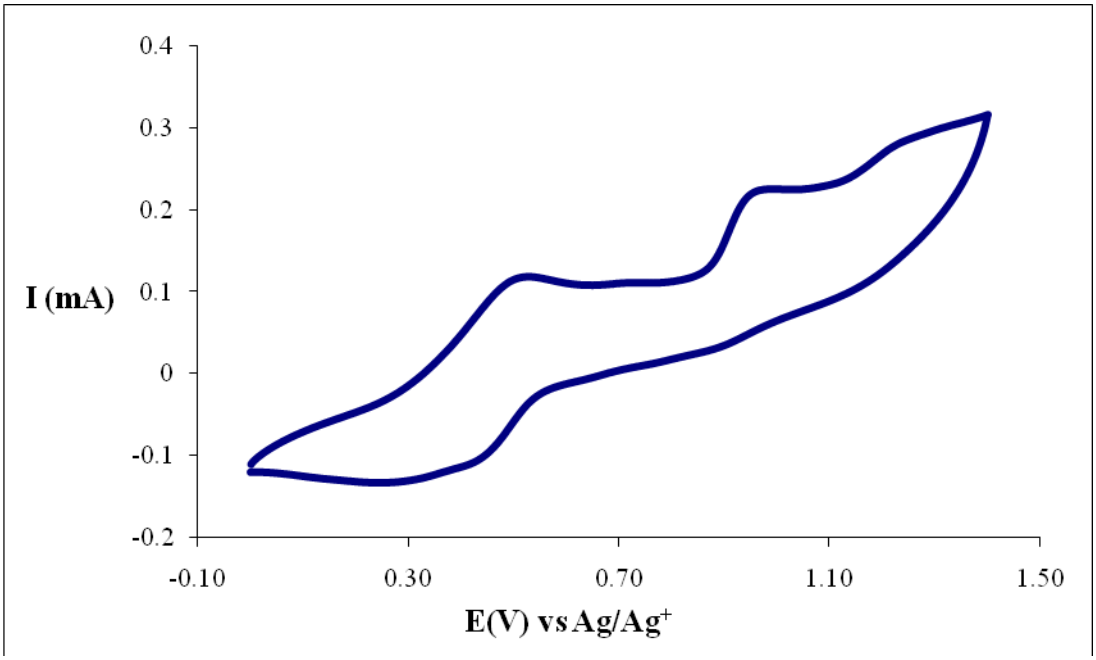

Figure 7-15. Cyclic voltammogram of polyTSUPQD in acetonitrile containing 0.1M Et_4NBF_4 and 0.77M $MeHSO_4$. Scan rate used was 60 mV/sec.

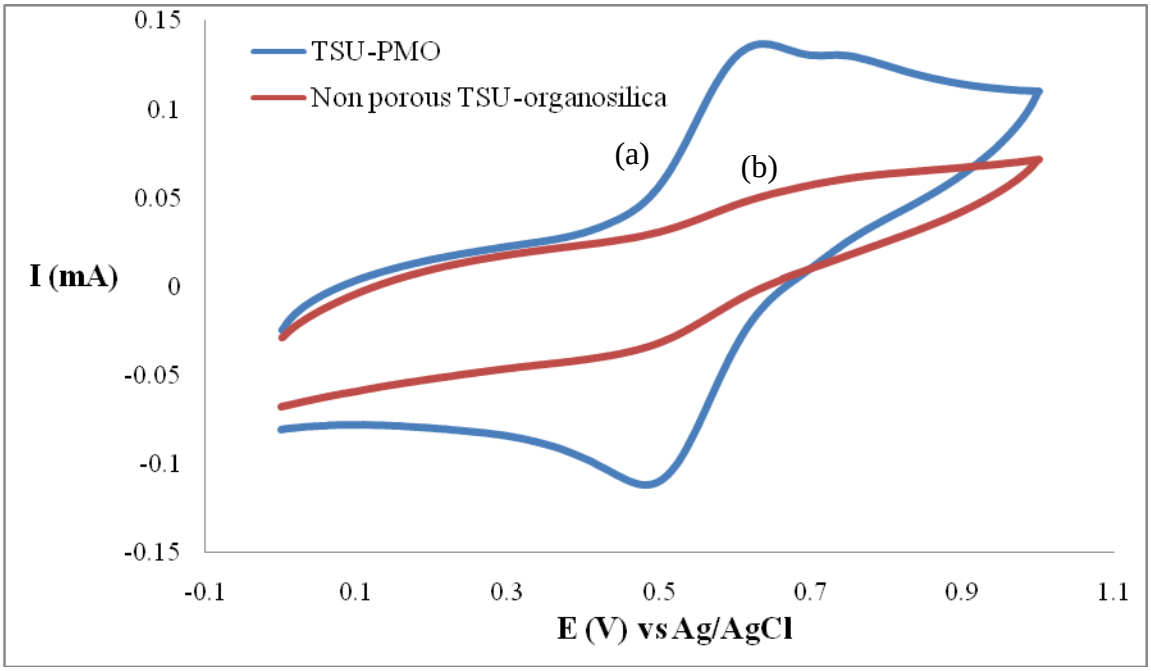

Figure 7-16. Cyclic voltammograms of (a) 66 wt% TSU-PMO and (b) 66 wt% nonporous TSU-organosilica in HCl (1M). Scan rate used was 60 mV/sec. Substantially lower currents for the nonporous material can be observed.

7.6 Reference list

1. Shirakawa, H. Ikeda, S. Simultaneous polymerization and formation of polyacetylene film on the surface of concentrated soluble Ziegler-type catalyst solution. Journal of Polymer Science (1974), 12, 11-20.

2. Shirakawa, H., Louis, E. J., MacDiarmid, A. G., Chiang, C. K., Heeger, A. J. Synthesis of electrically conducting organic polymers: halogen derivatives of polyacetylene, $(CH)_x$, Journal of Chemical Society, Chemical Communications (1977), 578-580.

3. Chen, L., Yu, Y., Mao, H., Lu. X., Zhang, W., Wei, Y., Synthesis of parent aniline tetramer and pentamer and redox properties. Materials Letters (2005), 59, 2446- 2450.

4. Li, W. G., Wang, H. L. Oligomer-assisted synthesis of chiral polyaniline nanofibers. Journal of the American Chemical Society (2004), 126, 2278-2279.

5. Chen, L., Yu, Y., Mao, H., Lu, X., Zhang, W., Wei, Y. Synthesis of parent aniline tetramer and pentamer and redox properties, Materials Letters (2005), 59, 2446-2450.

6. Wang, Z. Y., Yang, C., Gao, J. P., Lin, J., Meng, X. S., Wei, Y., Li, S. Electroactive poly-imides derived from amino-terminated aniline trimer, Macromolecules (1998), 31, 2702-2704.

7. Hench, L. L., Araujo, F. G., West, J. K., La Torre, G. P. Gel-silica optics: theory and application. Journal of Sol-Gel Science and Technology (1994), 2, 647-655.

8. Kuraoka, K., Kakitani, T., Suetsugu, T., Yazawa, T. Methanol vapor separation through the silica membrane prepared by the CVD method with the aid of evacuation. Separation and Purification Technology (2001), 25, 161-166.

9. Kuenzelmann, U., Boettcher, H., Biosensor properties of glucose oxidase immobilized within SiO_2 gels. Sensors and actuators, B: Chemical (1997), 39, 222-228.

10. Guo, Y., Mylonakis, A., Zhang, Z., Yang, G., Lelkes, P.I., Che, S., Lu, Q., Wei, Y. Templated synthesis of electroactive periodic mesoporous organosilica bridged with oligoaniline. Chemistry (2008), 14, 2909-2917.

11. Wei, Y., Yang, C., Ding, T. A one-step method to synthesize N,N′-bis(4′-aminophenyl)-1,4-quinonenediimine and its derivatives. Tetrahedron Letters (1996), 37, 731-734.

12. Guo, Y., Li, M., Mylonakis, A., Han, J., MacDiarmid, A.G., Chen, X., Lelkes, P.I., Wei, Y. Electroactive oligoaniline-containing self-assembled monolayers for tissue engineering applications. Biomacromolecules (2007), 8, 3025-3034.

13. Takashima, W., Nakashima, M., Pandey, S.S., Kaneto, K. Enhanced electrochemo-mechanical behaviors of polyaniline films by chloride concentrations. Chemistry Letters (2003), 32, 990-992.

14. Chiang, J. C., MacDiarmid, A. G. Polyaniline: Protonic acid doping of the emeraldine form to the metallic regime. Synthetic Metals (1986), 13, 193-205.

15. Wu, T., Megumi, N., Shyam, P., Keiichi, K. Enhanced electrochemomechanical activity of polyaniline films towards high pH region: contribution of Donnan effect. Electrochimica Acta (2004), 49, 4239-4244.

16. Genies, E. M. Tsintavis, C. Redox mechanism and electrochemical behaviour or polyaniline deposits. Journal of Electroanalytical Chemistry and Interfacial Electrochemistry (1985), 195, 109-128.

17. Genies, E. M., Syed, A. A., Tsintavis, C. Electrochemical study of polyaniline in aqueous and organic medium. Redox and kinetic properties. Molecular Crystals and Liquid Crystals (1985), 121, 181-186.

18. Bredas, J. L., Street, G. B. Polarons, bipolarons, and solitons in conducting polymers. Accounts of Chemical Research (1985), 18, 309-315.

19. Huang, W. S., Humphrey, B. D., MacDiarmid, A. G. Polyaniline, a novel conducting polymer. Morphology and chemistry of its oxidation and reduction in aqueous electrolytes. Journal of the Chemical Society, Faraday Transactions 1:Physical Chemistry in Condensed Phases (1986), 82, 2385-2400.

20. Borole, D. D., Kapadi, U. R., Mahulikar, P. P., Hundiwale, D. G. Electrochemical behavior of polyaniline, poly(o-anisidine) and their copolymer thin films in inorganic and organic supporting electrolytes. Polymer-Plastics Technology and Engineering (2004), 43, 1443-1458.

21. Lu, W., Meng, X.S., Wang, Z.Y. Electrochemical behavior of a new electroactive polyimide derived from aniline trimer. Journal of Polymer Science: Part A:Polymer Chemistry (1999), 37, 4295-4301.

Chapter 8. Study of the Oxygenation of Phthalocyanines

8.1 Introduction and Motivation

The word phthalocyanine is derived from the Greek for naphtha (rock oil) and cyanine (blue). Phthalocyanine is a planar 18π-electron heterocyclic aromatic system with a very close structure to porphyrin. The molecule is able to coordinate hydrogen and metal cations in its center by coordinate bonds with the four isoindole nitrogen atoms (**Figure 8-1**). The ease of preparation of phthalocyanines from inexpensive compounds, the ideality as a molecule for theoretical study, and the practical uses for a variety of applications have made phthalocyanines an object of research and of practical application.[1] To date, phthalocyanines have found applications as electrochemical catalysts, photosensitizers, gas sensors and as heterogeneous catalysts.[2-6] In particular, phthalocyanines are often used as models for investigating the chemistry and biology of porphyrins in hemoglobin for the reversible oxygenation. Phthalocyanines can acquire two different well-characterized forms, namely α-form and β-form. The β-form exists as a purple needle-like crystal, whereas the α-form usually exists as a blue very fine powder.[7] The α-form is metastable and obtained either as a polycrystalline powder or as a thin film formed by vacuum deposition onto a cold substrate. The β-form is more stable and may be obtained by sublimation as a single crystal or by heating the α-form to 350 ^{o}C for a few hours.[8,9] Essentially, the main difference between the two forms lies in the orientation of the flat molecules with respect to the crystallographic axis, where the perpendicular distance between the stacks of molecules remains approximately the same, namely 0.338 nm.[10] The inclination of the molecular stacks in the β-polymorph is much larger than that in the α-form (**Figure 8-2**). Thus, the distance between the central metal atoms in the adjoining stacks is about 0.48 nm in the β-form versus 0.38 nm in the α-form.[11] In the β-form, the nitrogen atoms in the neighboring

molecules are present axially above and below the central metal atom at a distance of about 0.338 nm.[12] The Mössbauer parameters, namely isomer shifts and quadrupole splittings of the two polymorphs of $Fe^{II}Pc$, are different because of the interaction of the central atom with the axial nitrogen atoms in β-form.[13]

There is considerable interest in the interaction of oxygen with phthalocyanines, particularly because of the use of oxygen adducts for the formation of Co and Fe nanoparticles coated with carbon. Recently, our collaborators and we reported formation of a variety of oxygen adducts with β-$Fe^{II}Pc$, which are stabilized in the solid matrix and do not exist in solution.[10-13] Oxygen is assumed to be introduced in the interlayers of metal phthalocyanines. An oxygen ambient is known to greatly increase both the dark and the photoconductivity of phthalocyanines.[14] This exposure to oxygen increases the conductivity by several orders of magnitude due to p-type doping. Herein, the dry and in-solution oxygenation of both forms (i.e., α- and β-form) of iron phthalocyanine at relatively low temperatures (i.e., 50 ^{o}C) for a prolonged period of time (i.e., 75 days) is investigated to study the effect that prolonged time of oxygenation has in the nature and structure of the obtained oxygen adducts. Mössbauer spectroscopy, IR spectroscopy and X-ray diffractometry have been used to study the crystal structures of the obtained materials. These studies indicate that when oxygenation is carried out at 50 °C in aqueous suspension or in the dry state for prolonged periods of time, then interesting oxygen adducts are formed and a much larger fraction of the compound of both α- and β- forms is oxygenated. Compared to our earlier studies, the interplanar spacing for the β-FePc seems to have substantially increased due to longer period of oxygenation. In addition, the evaluation of the obtained Mossbauer spectra of both FePc forms indicates that diffusion of oxygen between

the interlayers is further facilitated in the presence of water. Preliminary results for the oxygenation of α-FePc suggest that oxygenation of this form for prolonged periods of time results in the formation of interesting oxygen adducts. Some initial evaluations of the obtained results for the oxygenation of α-form, which are still under investigation are introduced.

8.2 Experimental

8.2.1 Materials

Iron(II) phthalocyanine (Fe(II)Pc, Sigma Alrich, 97%) was used as received for the synthesis of α-FePc and β-FePc. Oxygen and argon (Grade 5.0) were obtained from BOC GASES.

8.2.2 Instrumentation and Methods

IR measurements of the pristine forms of both α-Fe^{II}Pc and β-Fe^{II}Pc and their oxygen adducts were made on an ATR Perkin Elmer (Spectrum 1) spectrometer. Infrared spectra were recorded by an accumulation of 30 scans between 650 and 2000 cm^{-1} at a scan resolution of 4 cm^{-1}. ^{57}Fe Mössbauer spectra of pristine β-Fe(II)Pc and α-Fe(II)Pc and their oxygen adducts were recorded in the regular constant acceleration mode in the temperature range of 78 to 300 K. A ^{57}Co(Rh) source was used to supply the γ-rays. The isomer shifts are reported with respect to α-iron measured at room temperature. MOSSWIN program was used for computer fitting of the complex Mössbauer spectra. X-ray data of the pristine forms of Fe(II)Pc and its oxygen adducts were collected by fixing aliquots of the sample powder on glass slides. A Rigaku XRD Giegerflex D/max-11B instrument that had a horizontal goniometer and a Cu X-ray tube running at 45 kV and 30 mA was employed for the XRD studies.

8.2.3 Sublimation/Purification Procedure

The high vacuum needed to sublime the iron phthalocyanines was achieved by an apparatus that was custom made in our lab and which employed a diffusion pump (**Figure 8-3**). The gas pressure was kept at less than 0.1 Torr. Ultra pure argon was used to purge the whole apparatus before heating. The α-form of FePc was synthesized by vacuum sublimation of $Fe^{II}Pc$ (~100 mg) at about 400 ^{o}C and deposition on a cold substrate, utilizing a "cold finger". Cold tap water was run through the 'cold finger' to yield a deep blue powderish product on the outer surface of the wall of the finger. The β-form of $Fe^{II}Pc$ was synthesized by vacuum sublimation of $Fe^{II}Pc$ (~200 mg) at ~400 ^{o}C in a tubular furnace and deposition on a substrate that was held at about 300 ^{o}C to yield a purple needle-like product. The whole procedure for the sublimation and purification of each form takes about 6 to 8 hr. The obtained materials were tested by infrared-red spectroscopy and X-ray diffractometry to verify the purity of the obtained materials.

8.2.4 Dry and "In Solution" Oxygenation

Both alpha and beta forms of $Fe^{II}Pc$ were oxygenated under O_2 flow in a dry state or in a suspension in water. Dry oxygenation was done by passing O_2 for 75 days through a flat bottomed flask where $Fe^{II}Pc$ was evenly dispersed on the bottom of the flask at 50 ^{o}C. For the solution oxygenation 100 mg of the respective form of $Fe^{II}Pc$ were suspended in 200 ml of distilled water in a three-neck round bottom flask equipped with a thermometer and a gas inlet-outlet. In solution oxygenation was accomplished by bubbling O_2 (at a flow rate of about 10 bubbles per second) in the aqueous suspensions of $Fe^{II}Pc$ at 50 ^{o}C for 75 days. Samples oxygenated in solution were filtered and dried under the stream of ultrapure argon for five days at room temperature and in a vacuum oven for two days before further characterizations.

8.3 Results and Discussion

After sublimation and purification of the respective forms, sufficient amounts of pure β-form and α-form of iron phthalocyanine were obtained. The pristine forms were first crushed into a very fine powder with a mortar and a pestle and then characterized by powder X-ray diffractometry (XRD) and IR spectroscopy in order to verify the purity of each form. Once the purity was confirmed, then prolonged oxygenations for 75 days at 50 ^{o}C of both forms in solution and in the dry state would be carried out. Mössbauer spectroscopy, IR spectroscopy and X-ray diffractometry have been used to study the crystal structures and physical properties of the obtained materials after prolonged oxygenation and the evaluation of the results is presented. Elemental analysis of the α- and β-forms of FePc, oxygenated in the dry state and in solution, has also been performed and the obtained results are summarized in **Table 8-1.** These results show a substitution of 6 oxygen atoms per one iron atom for dry oxygenation of α-FePc, 8 oxygen atoms per one iron atom for in-solution oxygenation of α-FePc, 2 oxygen atoms per one iron atom for dry oxygenation of β-FePc and 12 oxygen atoms per one iron atom for in solution oxygenation of β-FePc with regards to the theoretical calculated weight percentage compositions of the pristine FePc. At a first glance, the numbers of oxygen atoms per iron atoms for all samples seem to be very high, substantially higher as compared to the proposed configurations of the oxygenated species formed upon prolonged oxygenation and which are going to be presented in later sections. These discrepancies may be attributed to oxygen physisorbed on the iron phthalocyanines upon prolonged dry and in-solution oxygenation, which in addition to oxygen diffused in the interplanar layers of FePcs, is also analyzed during the elemental analysis.

8.3.1 Infra-red Spectroscopy (IR)

The IR spectra of the pristine β-FePc and α-FePc can be seen in **Figures 8-4** and **8-5** respectively**.** These spectra correspond well to the literature data. The difference of the two polymorphs is exhibited in their respective IR spectrums. Pristine α-form shows a peak at 770 cm^{-1} while pristine β-form has a peak at 780 cm^{-1}. The IR spectra after prolonged oxygenation (e.g. 75 days) of both forms of Fe(II)Pc in the dry state and in an aqueous suspension at 50 ºC can be seen in **Figure 8-6** and **Figure 8-7**. IR spectroscopy indicates that both forms show noticeable changes in their IR spectrums after oxygenation for 75 days at 50 ^{o}C for both the dry state and in-solution as compared to their respective pristine forms. One can see noticeable changes in the 1600-1750 cm^{-1}, 1200 cm^{-1} and the 890 cm^{-1} region. The first region can be ascribed to diatomic oxygen physisorbed to the phthalocyanines rings, the second to superoxo attachment in a coordinate position (either end-on or side-on), and the third region is due to Fe-O bridging.[10] The more profound difference of these IR spectra can be seen for the oxygenation in solution, and the β-form in particular. These spectra reveal that prolonged oxygenation causes the formation of novel oxygen adducts and the diffusion of oxygen in the interplanar structures of both forms of iron(II) phthalocyanines.

8.3.2 X-ray Diffraction

Both pristine forms of Fe(II)Pc, namely α- and β-form, were also characterized by XRD spectroscopy before the oxygenation process. Before the XRD measurements the as-synthesized sublimates were first crushed to a fine powder by means of a mortar and a pestle. The obtained XRD spectra of the purified β-FePc and α-FePc can be seen in **Figure 8-8** and **Figure 8-9,** respectively. All the diffraction lines in the XRDs of the pristine α- and β-forms can be attributed

to lines of a monoclinic lattice and are in agreement with those that have been reported earlier. Once it was verified that the XRD spectra corresponded to the respective pure forms of Fe(II)Pc, then the oxygenation in the dry state and in-solution for both forms would start. The XRD spectra of the obtained materials after prolonged oxygenation (e.g., 75 days) at 50 ^{o}C for both forms in the dry state and in-solution can be seen in **Figure 8-10** and **Figure 8-11**. As can be seen from these figures, the monoclinic structure of both α- and β-forms is preserved after the prolonged oxygenation process. In addition though, some extra diffraction lines have appeared in the XRD spectra of the oxygenated samples as compared to the respective XRD spectra of their pristine forms. This may considerably suggest that oxygenation leads to modification to some extent of the crystal structure, which may subsequently verify the insertion of oxygen adducts in the crystal structures of the phthalocyanines. One can also observe considerably increased background due to lack of coherence resulting from a breakdown of long range order, presumably because of inhomogeneous distribution of oxygen. The broadening of the lines, which is more profound in the XRD spectra of oxygenated in-solution β-FePc, may be also attributed to the same reason. Oxygenation of both forms leads to an expansion of the lattice as can be verified from the calculated cell parameters from the respective XRD spectra. Another interesting result that is worth mentioning is an extra peak that appears in the solution oxygenated α-form sample. This dominant peak, which appears at around 2θ of 21^{o}, does not belong to the crystalline structure of pristine α-Fe^{II}Pc. It may be associated either with formation of iron oxides in solution (e.g., maghemite or iron oxyhydroxide), or due to the incorporation of oxygen atoms between the interlayers of α-Fe^{II}Pc in an ordered way. The interpretation of this specific peak is still under study although the formation of iron oxides seems not very probable since there is no typical change in color when the sample was put into concentrated HCl solution.

Electron microscopy experiments have also indicated a homogeneous morphology and not a segregation of iron oxides or iron oxyhydroxides. In addition, the Mossbauer spectrum of α-FePc oxygenated in solution, which is going to be presented later, clearly shows a considerable amount of oxygen incorporated between the interlayers of FePc, which could presumably be arranged in such an ordered form as to give extra reflections in the XRD spectrum.

8.3.3 Mössbauer Spectroscopy

As has been reported in previous studies from our collaborators and our group, the formation of oxygenated species of β-FePc has been accomplished by oxygenation of β-FePc in solution for 45 days at 50 ^{o}C.[6-9] Stereochemical constraints imposed in the solid β-FePc resulted in the formation of interesting oxygenated adducts, which cannot be synthesized by regular solution chemistry. The possible configurations of these four oxygenated species are shown in **Figure 8-12**. The oxygen-bridged compounds formed in the solid matrix bear no resemblance to the ones formed by solution chemistry. The aim of the study, presented in this thesis, is the investigation of prolonged dry and in solution oxygenation of β-FePc and α-FePc. As compared to the previous reported studies where oxygenation would take place for 45 days, the oxygenation of β-FePc and α-FePc would now be performed for 75 days. The Mössbauer spectra of dry and in solution oxygenated samples of β-Fe$^{(II)}$Pc as a function of the temperature of analysis can be seen in **Figure 8-13** and **Figure 8-14,** respectively. The computer analysis of the obtained Mossbauer spectra of β-FePc oxygenated in solution can be seen in **Table 8-2**. The obtained spectra were fit with four species, the original pristine β-Fe^{II}Pc with large quadrupole splitting (a) and three oxygen adducts (b, c, and d from **Figure 8-12**) formed with β-Fe^{II}Pc. A

very important feature that these results suggest is that prolonged oxygenation in solution yields a much larger fraction of oxygenated β-Fe^{II}Pc.

The apparent decrease of abundance that is observed for the pristine un-oxygenated Fe(II)Pc (species a), in highly oxygenated sample as a function of temperature, is very conspicuous. For instance, for β-Fe(II)Pc, oxygenated in solution, decreases from about 21% at 30 K to 7% at 293 K. This anomalous behavior reveals interesting and insightful information about the molecular dynamics. As known, the Mössbauer method registers recoil-free events only. The anomalous decrease in recoil-free events at higher temperatures is indicative of the fact that the molecules of Fe(II)Pc are no longer as tightly bound as they would be in the lattice of pristine unoxygenated iron phthalocyanine. In our samples, oxygenated for 75 days, the residual un-oxygenated component is only about 21 %. As mentioned earlier, the diffusion of H_2O and O_2 between the Pc layers and the bridging of O_2 with Fe atoms in adjoining layers results in the expansion of the lattice. In the expanded lattice the molecules are much freer to vibrate and consequently the recoil-free events diminish. Let us compare this behavior with materials that have undergone limited degree of oxygenation, like dry oxygenation at 50 ^{o}C for 75 days, or solution oxygenation at 50 ^{o}C for 45 days (**Figure 8-15)**. If we now normalize the observed percentage abundances of (c) and (d), correcting for the anomalous decrease in abundance of unoxygenated Fe(II)Pc, then we can observe clearly the spin transition of low-spin (d) species to the high-spin (c) species as the temperature increases (**Figure 8-16**). It is apparent that species (d), which is abundant at low temperatures, is converting into species (c) as the temperature increases and that at each temperature, the sum of the abundances of the two species is constant as expected. Assuming that all species are bound with equal tightness, their abundances can only

change due to spin transitions. Spin transitions, though, can occur only in oxygenated species, which further justifies the existence of such oxygen adducts as the ones shown in **Figure 8-12**. The abundances (normalized areas) of the species (a), (c) and (d) for dry oxygenated β-FePc are plotted as a function of temperature in **Figure 8-17**. Although the concentration of oxygen adducts in this case is much lower, the transformation of species (d) into species (c) undoubtfully exists while unoxygenated pristine β-Fe^{II}Pc, which is designated as (a), exhibits insignificant changes in its abundance ratio when temperature is increased. Comparing the above findings with the results obtained for oxygenation of β-Fe(Pc) for 45 days, it is apparent that prolonged oxygenation of β-FePc leads to a much larger fraction of β-Fe(Pc) oxygen adducts. Additionally, it is evident that water facilitates interlayer oxygen diffusion. The area of oxygenated species is much larger when oxygenation was performed in solution. It seems that oxygen diffuses much more rapidly in the presence of water because water molecules tend to expand the intermolecular spacing, thus allowing rapid diffusion of O_2.

The Mössbauer spectra of α-FePc after prolonged oxygenation for 75 days in the dry state and in an aqueous suspension at 50 ºC can be seen in **Figure 8-18** and **Figure 8-19** respectively. These studies have been conducted at three different temperatures: 20K, 80K and 293K. The computer analysis of the obtained Mössbauer spectra of α-FePc oxygenated in solution can be seen in **Table 8-4**. The obtained spectra were fit with three species, the original pristine α-Fe^{II}Pc with large quadrupole splitting (species (a)) and two other species, presumably oxygen adducts defined as species (2) and species (3) of α-FePc. Mössbauer parameters of doublets for species (a) can be well interpreted based on the electronic and crystal structure of the compound, which is well known from the literature data. Generally, the parameters of the

doublets (2) and (3) reflect Fe(III) microenvironments, somewhat similar to those found in the oxygenated β-FePc earlier. A very interesting magnetically split sextet component appeared in the spectrum of solution oxygenated sample at 20K, which does not exist at 80K and 293K. Although a definite interpretation of this component is still under study, this may be interpreted as a result of superparamagnetic relaxation due to small grain related microenvironments being related to oxygen incorporated between the layers. Nevertheless, the isomer shift of the sextet reveals Fe(III) microenvironments. In the Mössbauer-spectra of dry oxygenated α-Fe^{II}Pc 3 doublets that represent iron microenvironments also exist. Although the concentration of oxygen adducts, as in the case of dry oxygenated β-FePc, is much lower, the interconversion of species upon increase of the analysis temperature is still evident. However, in comparison to the solution treated α-FePc no magnetic sextet was observed in its Mössbauer spectra. Following the same concept as for β-FePc, it may be supposed that for both α-FePc (e.g., dry and in solution oxygenated), oxygen is localized mainly between the interlayers of the α-FePc stacks since the original structure of the pristine α-form was mainly preserved according to the XRD results. As in the case of beta form, it is obvious that the presence of H_2O enhances the rate of diffusion of oxygen. It seems that water molecules penetrate between the planes and increase the interplanar spacing, which facilitates a faster rate of oxygen diffusion.

From the evaluation of the Mössbauer spectra of both forms, the nature of oxygen-adducts formed in α- versus β-Fe^{II}Pc seems to be different. The abundances of species (2) and species (3) vary with temperature in an apparently erratic fashion for α-form, unlike species (c) and species (d) for β-form. The complexity in behavior most probably arises primarily from the fact that one of the α-form oxygen adducts is ferromagnetic and it exhibits superparamagnetic

behavior. This behavior is superimposed on spin transitions between the two other species (namely, species (2) and (3) for α-form). The question arises as to the origin of ferromagnetism and its superparamagnetic manifestation. Bearing in mind that the Fe-to-Fe distance between neighbors on adjoining layers is somewhat shorter in α- than in β-form, consequently the Fe-O=O-Fe bridge is not strained, but continues over several planes instead of terminating with O_2, as in the case of oxygen adducts of β-form (**Figure 8-20**). There is also a distribution in length of these ferromagnetic chains (i.e., O_2-Fe-O=O-Fe-O=O-Fe-O=O-Fe-O_2). Such ferromagnetic chains have been previously reported by other researchers.[15] At low temperature, the longer chains will exhibit a magnetically split six-line spectrum with perfect alignment of Fe atoms, while the available thermal energy is sufficient for smaller regions to fluctuate rapidly so that the nuclei experience effectively zero magnetic field and one observes a doublet instead of a sextet. At a higher temperature on the other hand, the sextet vanishes almost completely as the thermal energy is sufficient to cause rapid fluctuations in longer chains also. The exact configurations of these α-FePc oxygenated species are still under investigation.

At this point, it has to be mentioned that the differences that are observed between the Mössbauer parameters of the corresponding adducts in α-Fe^{II}Pc and β-Fe^{II}Pc may be also attributed to the different average grain of the two forms (**Figures 8-21** and **8-22**). The rate is faster in α-Fe(II)Pc than β-Fe(II)Pc, and this may be mainly due to the fact that the average size of particles of α-form is half of that for β-form resulting in four times larger surface exposed for the case of α-form compared to that of the β-form. It seems that the structural differences between the two polymorphs may also play an important role into the obtained oxygen adducts. The different angles of the flat layers, with respect to the crystallographic axis, may influence

both the electron density and the electric field gradient, which govern both the isomer shift and quadrupole splitting in Mössbauer spectroscopy.

8.4 Conclusion

The oxygenation of both forms (i.e., α- and β-forms) of phthalocyanines at 50 ^{o}C for prolonged periods of time (e.g., 75 days) in the dry state and in aqueous suspension has been investigated to study the effect that prolonged time of oxygenation has on the nature and structure of the obtained oxygen adducts. These results indicate that when oxygenation is carried out at 50 °C in aqueous suspension, or in the dry state, for prolonged periods of time, then interesting oxygen adducts are formed and a much larger fraction of the compound of both α- and β- forms is oxygenated. Compared to our earlier studies, the interplanar spacing for the β-FePc seems to have substantially increased due to longer period of oxygenation. Additionaly, the facilitation of diffusion of oxygen between the interlayers of iron phthalocyanines in the presence of water has been further justified for both forms. The formation of interesting α-Fe^{III}Pc oxygen adducts by both wet and dry prolonged oxygenation has been also accomplished. Proposed configurations of α-FePc oxygen adducts, which are still under investigation, have been proposed.

8.5 Acknowledgements

This project was performed in collaboration with Dr. Amar Nath from the Department of Chemistry in the University of North Carolina and Dr. Erno Kuzmann and Zoltan Homonnay from the Eötvös Lorand University in Budapest.

Table 8-1. Weight percentage compositions of α-FePc and β-FePc after prolonged oxygenation for 75 days at 50 ^{o}C in the dry state and in aqueous solution.

Theoretical weight percentage composition of pristine $Fe^{(II)}Pc$

C (%)	H (%)	N (%)	Fe (%)
67.38	3.18	19.64	9.79

α-FePc after 75 days of dry oxygenation

C (%)	H (%)	N (%)	Fe (%)
57.55	2.69	16.9	8.2

α-FePc after 75 days of solution oxygenation

C (%)	H (%)	N (%)	Fe (%)
52.8	2.53	15.9	7.41

β-FePc after 75 days of dry oxygenation

C (%)	H (%)	N (%)	Fe (%)
64.1	2.82	18.75	9.26

β-FePc after 75 days of solution oxygenation

C (%)	H (%)	N (%)	Fe (%)
50.2	2.36	14.6	7.01

Table 8-2. Computer evaluation results of the Mössbauer spectra of in solution oxygen-treated β-$Fe^{II}Pc$.

Species (a)			
T (K)	A [%]	δ [mm/s]	Δ [mm/s]
30	21.1	0.49	2.61
50	17.5	0.48	2.62
70	19.9	0.49	2.62
110	14.5	0.48	2.61
150	12	0.47	2.66
293	6.9	0.4	2.72

Species (c)			
T (K)	A [%]	δ [mm/s]	Δ [mm/s]
30	21.2	0.3	0.35
50	28.9	0.35	0.39
70	22.4	0.3	0.38
110	47.7	0.43	0.55
150	49.2	0.41	0.45
293	65.5	0.34	0.46

Species (d)			
T (K)	A [%]	δ [mm/s]	Δ [mm/s]
30	57.7	0.26	1.24
50	53.6	0.27	1.24
70	57.7	0.26	1.24
110	37.8	0.29	1.24
150	38.8	0.3	1.23
293	27.6	0.29	1.2

A = abundance, δ = chemical shift and Δ = quadrupole splitting.

Table 8-3. Computer evaluation results of the Mössbauer spectra of β-Fe^{II}Pc oxygenated in the dry state.

Species (a)			
T (K)	**A [%]**	**δ [mm/s]**	**Δ [mm/s]**
30	75.2	0.48	2.65
50	76.1	0.49	2.65
150	75.5	0.46	2.62
293	74.5	0.39	2.58

Species (c)			
T (K)	**A [%]**	**δ [mm/s]**	**Δ [mm/s]**
30	12.1	0.35	0.36
50	11.9	0.35	0.35
150	13	0.32	0.34
293	17.8	0.3	0.31

Species (d)			
T (K)	**A [%]**	**δ [mm/s]**	**Δ [mm/s]**
30	12.7	0.41	1.12
50	12	0.42	1.11
150	11.5	0.39	1.13
293	7.7	0.36	1.13

A = abundance, δ = chemical shift and Δ = quadrupole splitting.

Table 8-4. Computer evaluation results of the Mössbauer spectra of in solution oxygen-treated α-Fe^{II}Pc.

Species (a)			
T (K)	**A [%]**	**δ [mm/s]**	**Δ [mm/s]**
20	4.6	0.45	2.47
80	5	0.45	2.47
293	3.3	0.35	0.43

Species (2)			
T (K)	**A [%]**	**δ [mm/s]**	**Δ [mm/s]**
20	26.8	0.32	1.151
80	46.9	0.3	1.264
293	24.7	0.285	1.055

Species (3)			
T (K)	**A [%]**	**δ [mm/s]**	**Δ [mm/s]**
20	28.8	0.48	0.6
80	48.2	0.466	0.651
293	69.9	0.324	0.648

Sextet		
T (K)	**A [%]**	**δ [mm/s]**
20	41.6	0.519

A = abundance, δ = chemical shift and Δ = quadrupole splitting

Table 8-5. Computer evaluation results of the Mössbauer spectra of α-Fe^{II}Pc oxygenated in the dry state.

Species (a)			
T (K)	**A [%]**	**δ [mm/s]**	**Δ [mm/s]**
30	75.2	0.48	2.65
50	76.1	0.49	2.65
150	75.5	0.46	2.62
293	74.5	0.39	2.58

Species (2)			
T (K)	**A [%]**	**δ [mm/s]**	**Δ [mm/s]**
30	12.1	0.35	0.36
50	11.9	0.35	0.35
150	13	0.32	0.34
293	17.8	0.3	0.31

Species (3)			
T (K)	**A [%]**	**δ [mm/s]**	**Δ [mm/s]**
30	12.7	0.41	1.12
50	12	0.42	1.11
150	11.5	0.39	1.13
293	**7.7**	0.36	1.13

A = abundance, δ = chemical shift and Δ = quadrupole splitting

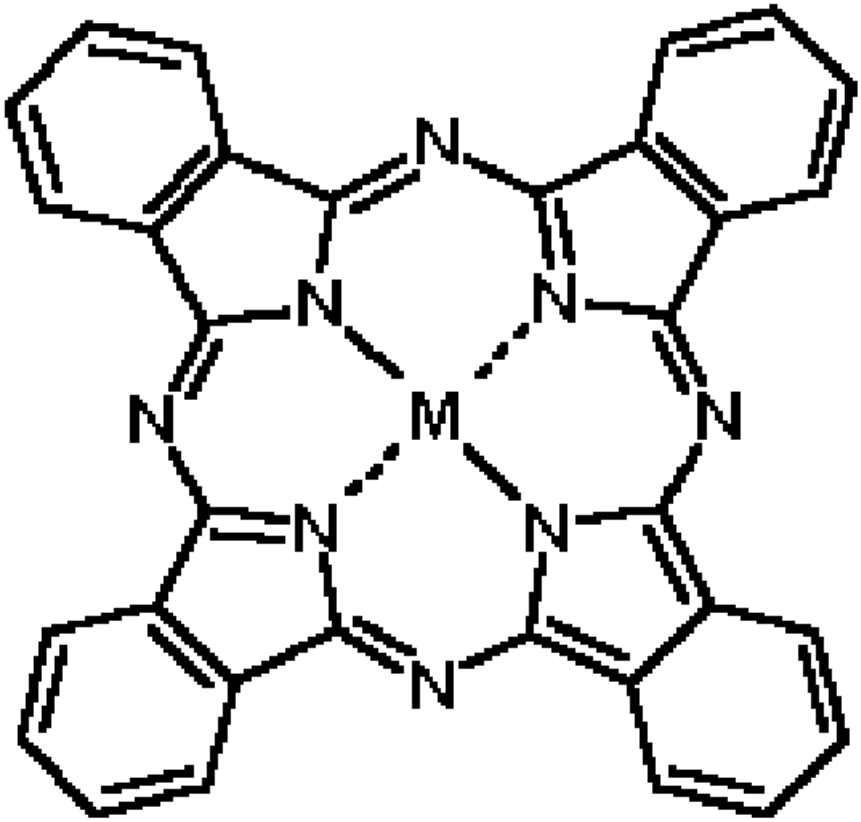

Figure 8-1. Basic structure of phthalocyanine.

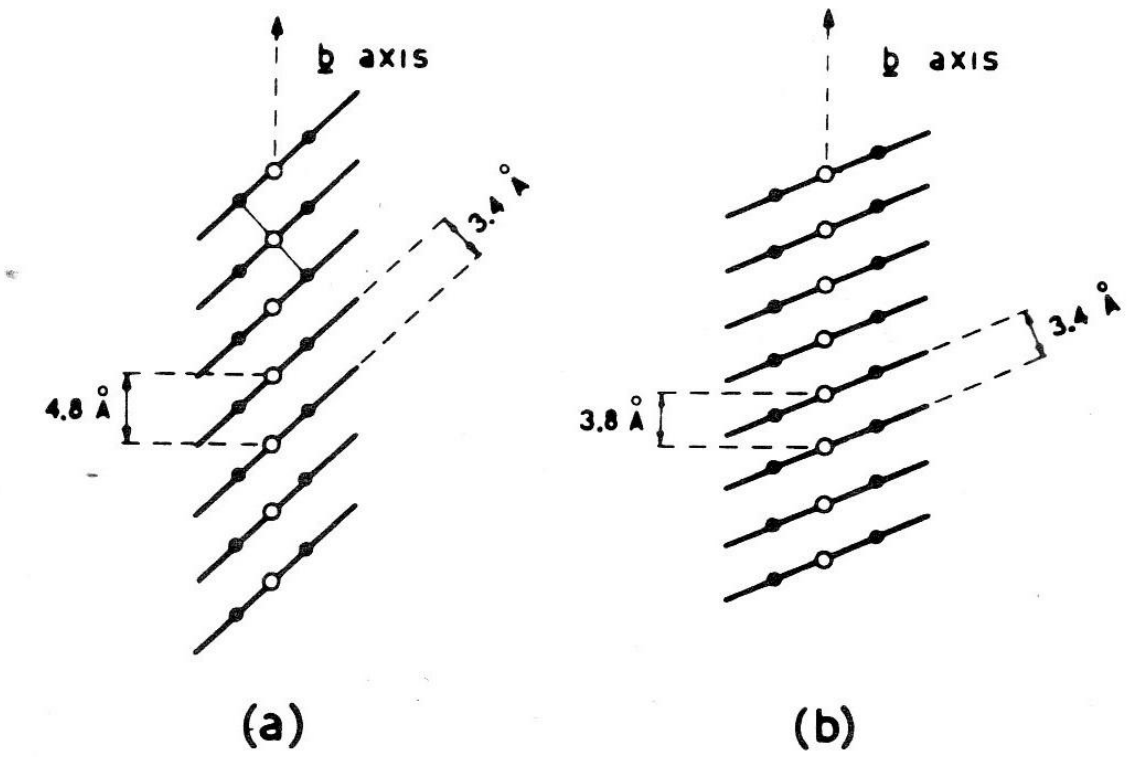

Figure 8-2. Schematic representation of the arrangement of the molecules in the beta (a) and alpha (b) polymorphs of the metal phthalocyanines.

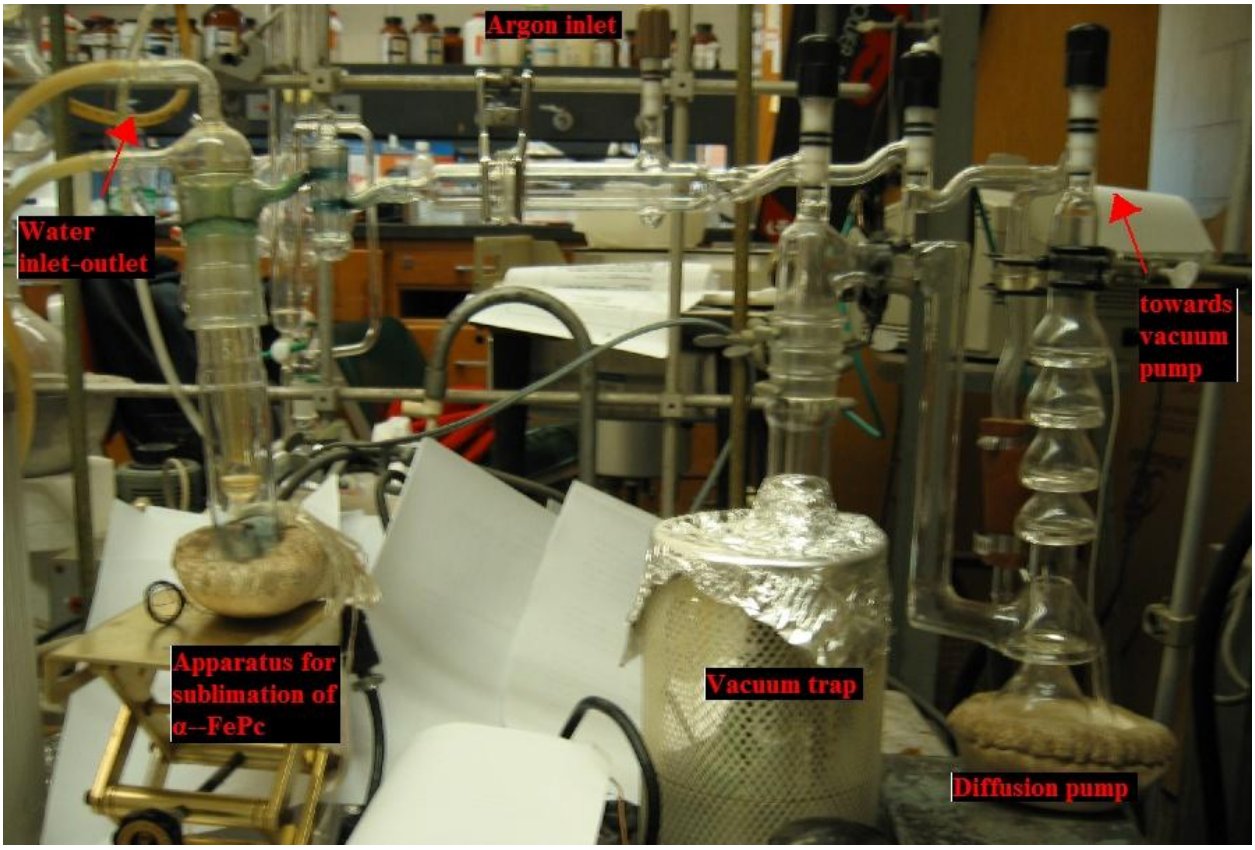

Figure 8-3. Picture of the custom-made diffusion vacuum pump apparatus utilized to synthesize pure α-Fe^{II}Pc. A similar configuration was used to synthesize β-Fe^{II}Pc except that instead of the cold finger, a tubular furnace was utilized.

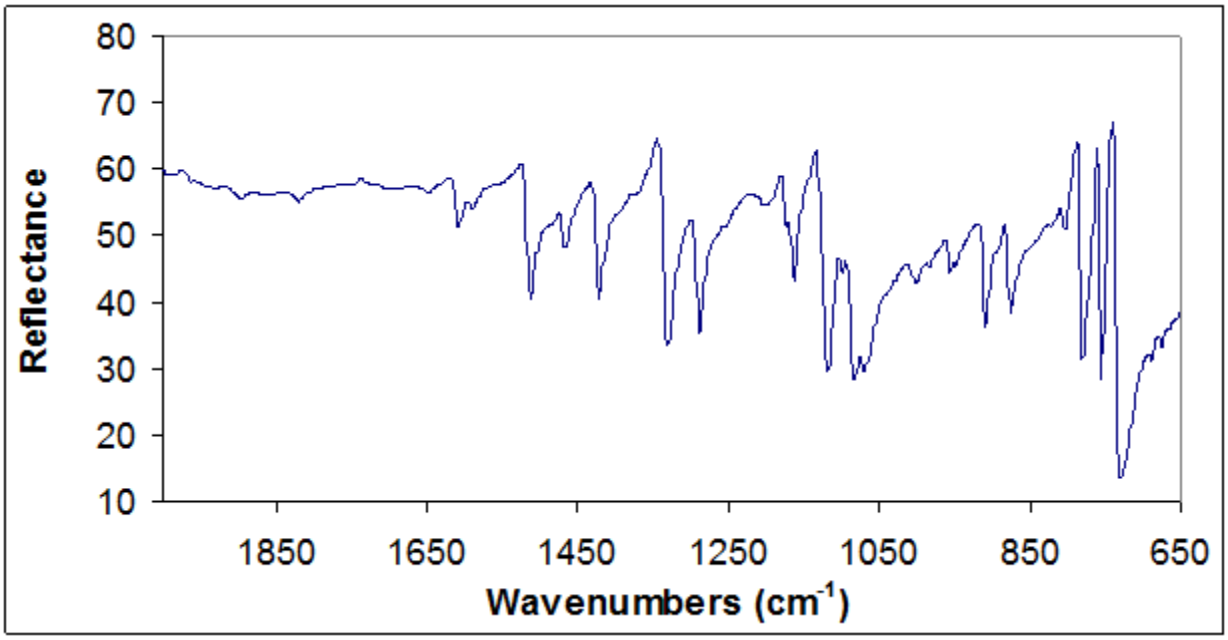

Figure 8-4. Infrared spectrum of pristine β-FePc.

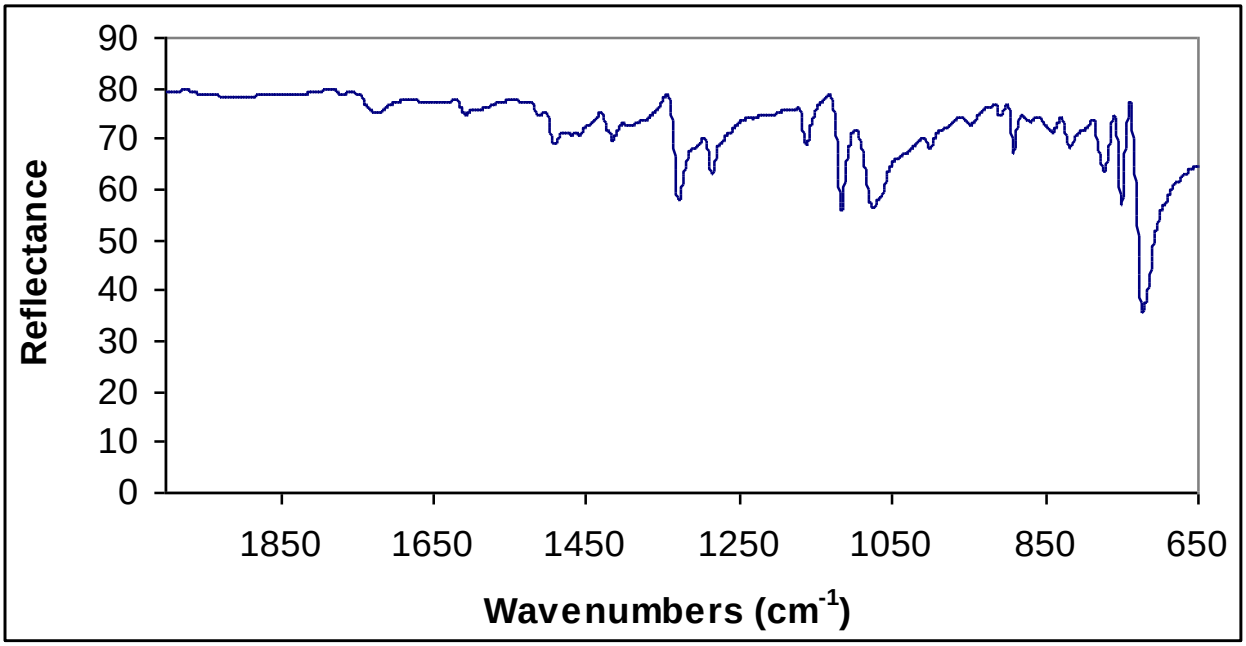

Figure 8-5. Infrared spectrum of pristine α-FePc.

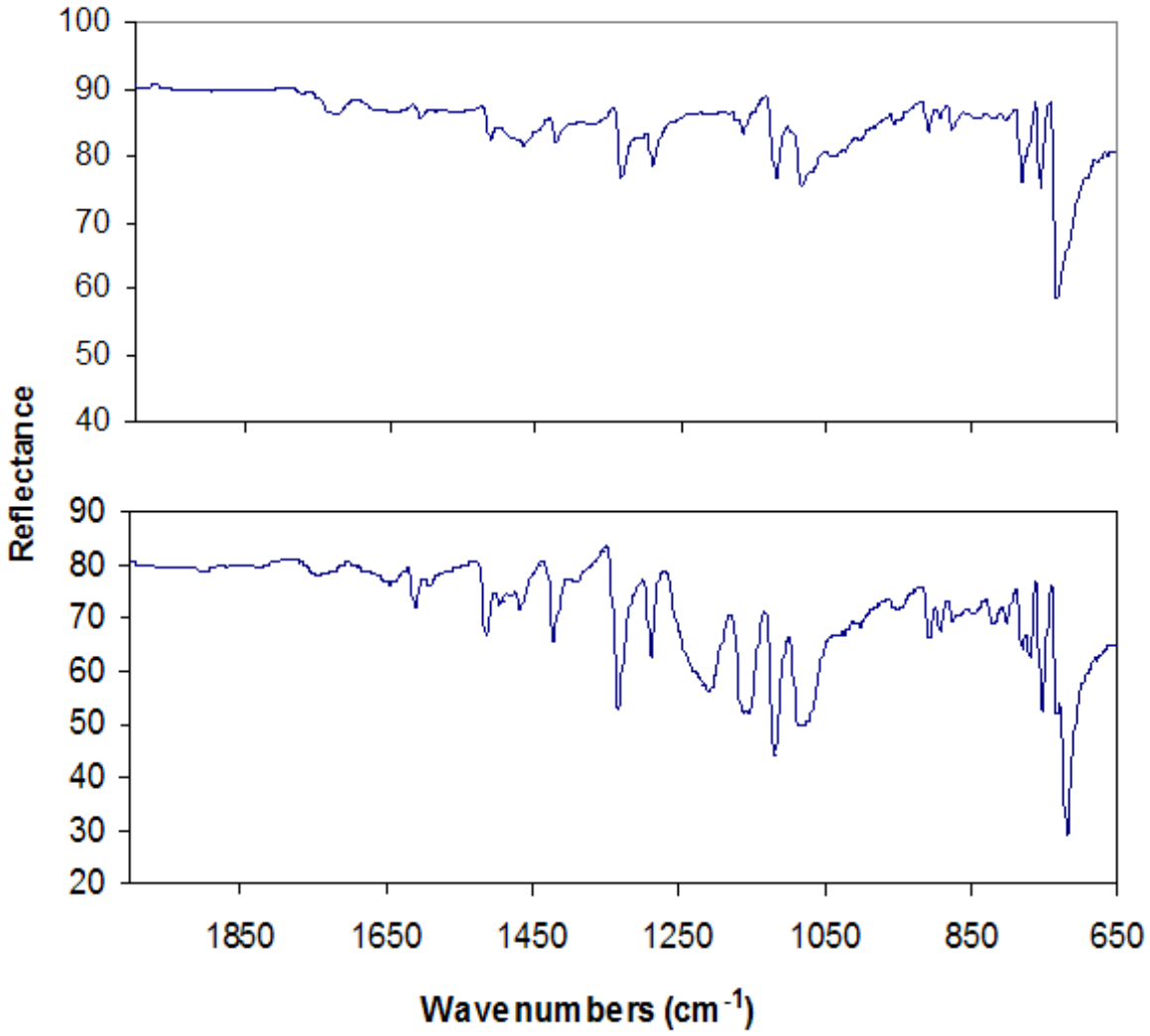

Figure 8-6. Infrared spectra of dry (top) and in solution (bottom) oxygenation of β-form FePc.

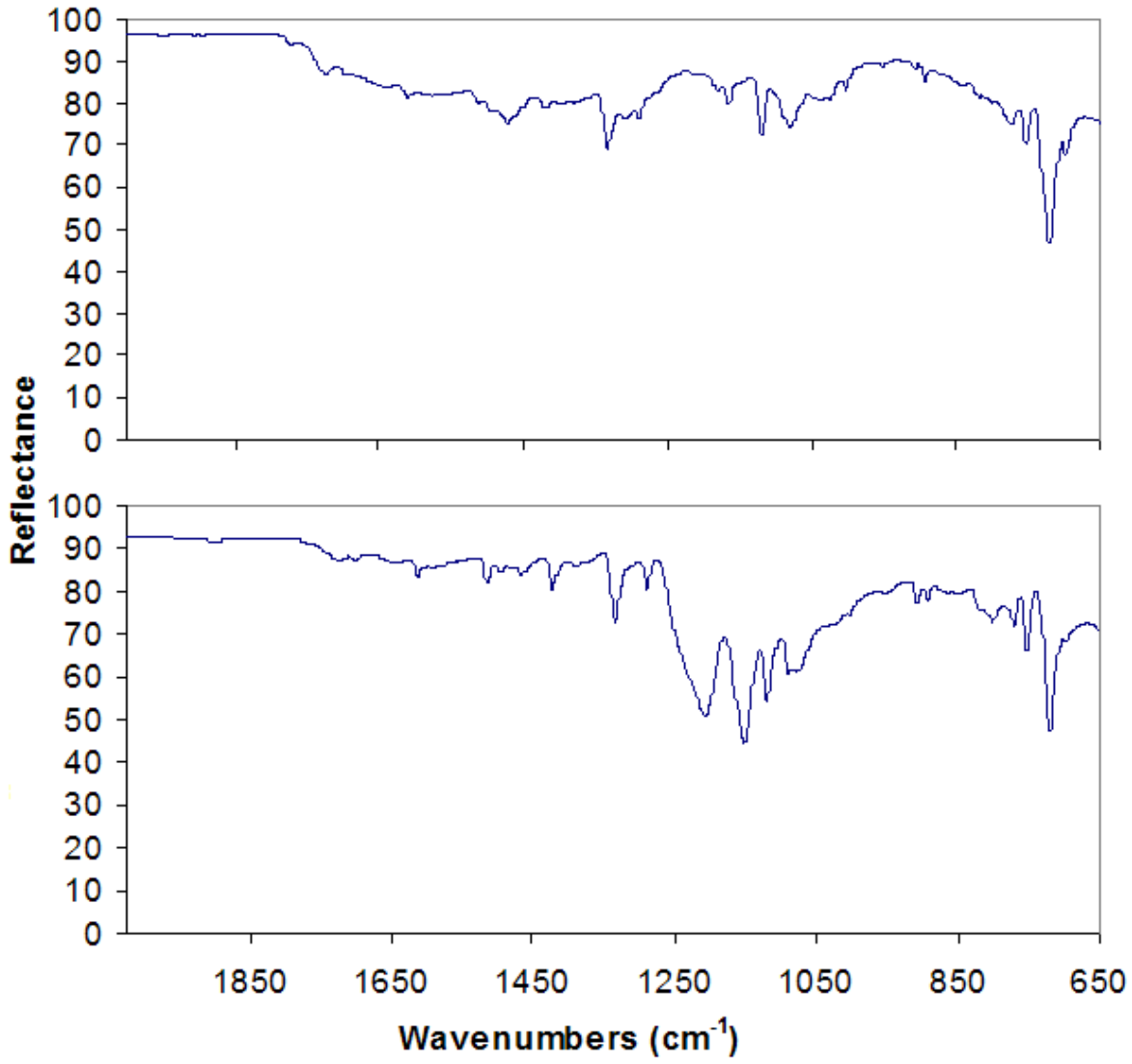

Figure 8-7. Infrared spectra of dry (top) and in solution (bottom) oxygenation of α-form FePc.

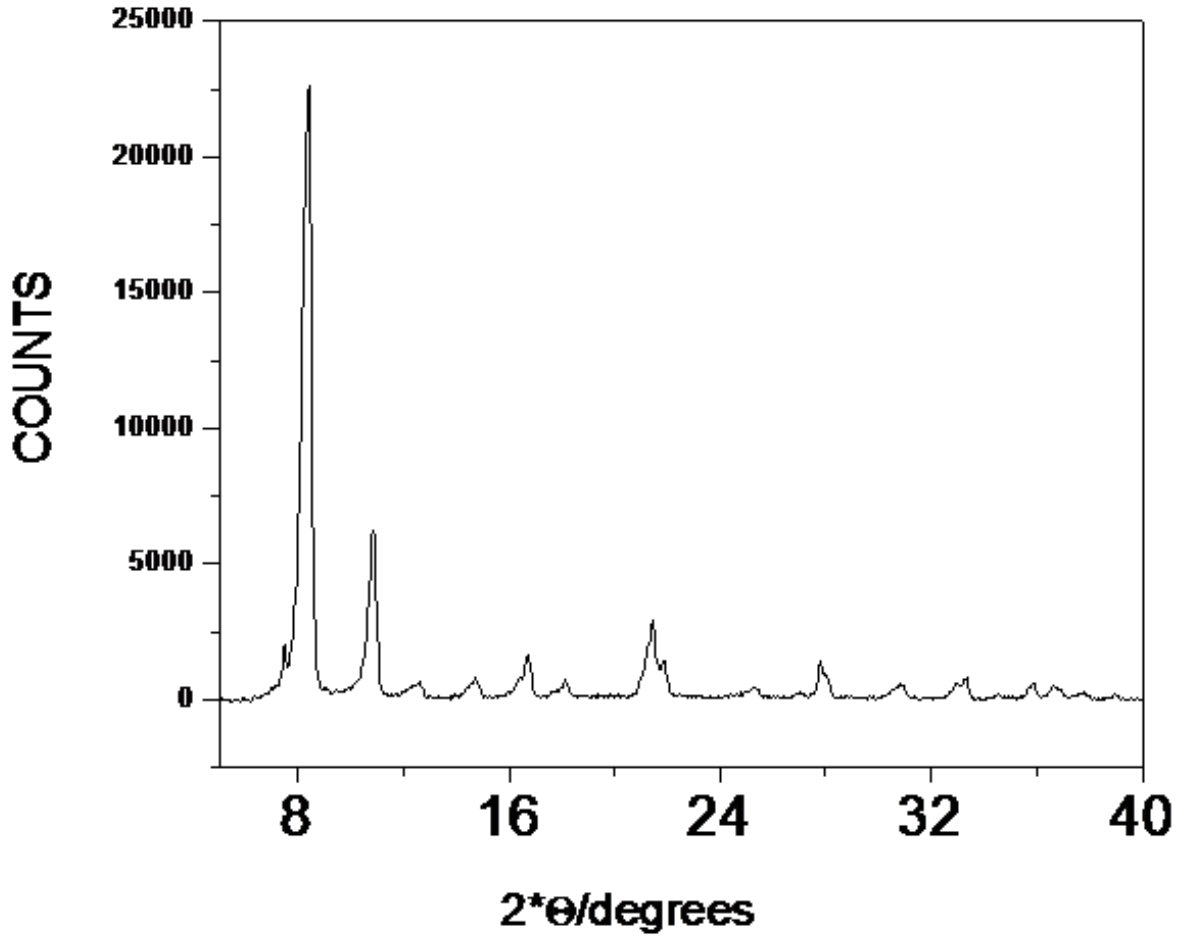

Figure 8-8. XRD spectrum of pristine β-form of FePc. Cell parameters calculated: a = 14.61 Å, b = 4.8 Å, c = 19.41 Å, β = 121.56^{o}.

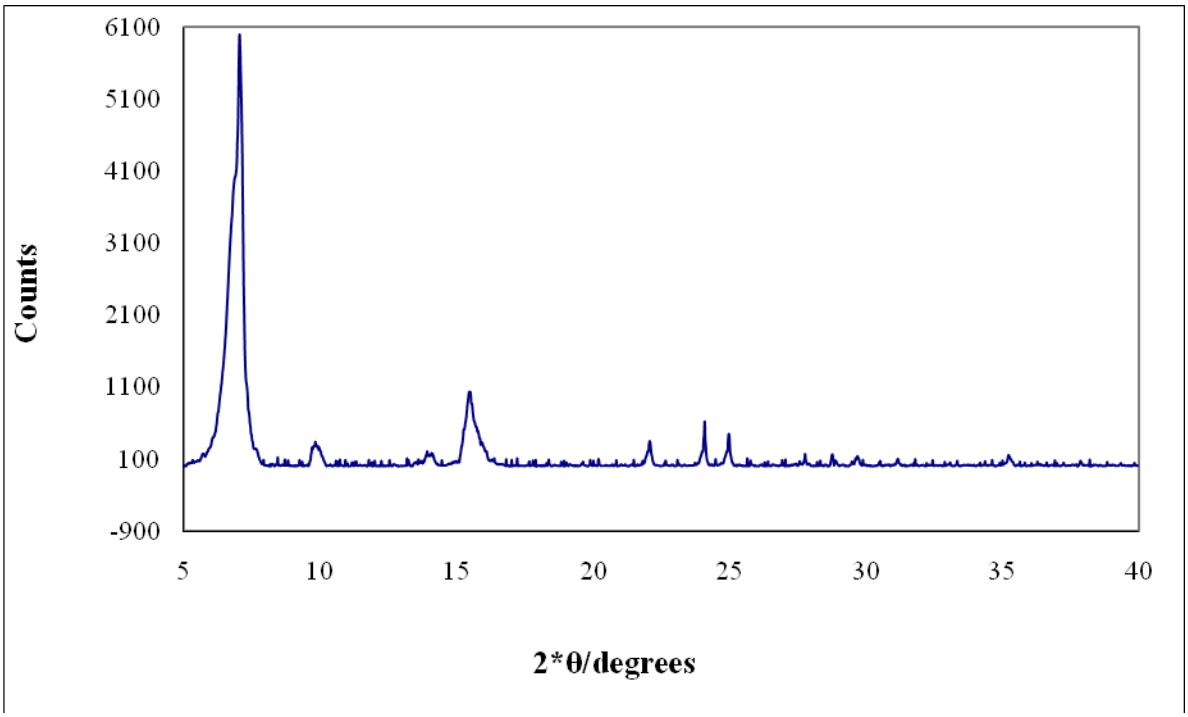

Figure 8-9. XRD spectrum of pristine α-form of FePc. Cell parameters calculated: a = 25.30 Å, b = 3.69 Å, c = 25.89 nm, β = 89.16^{o}.

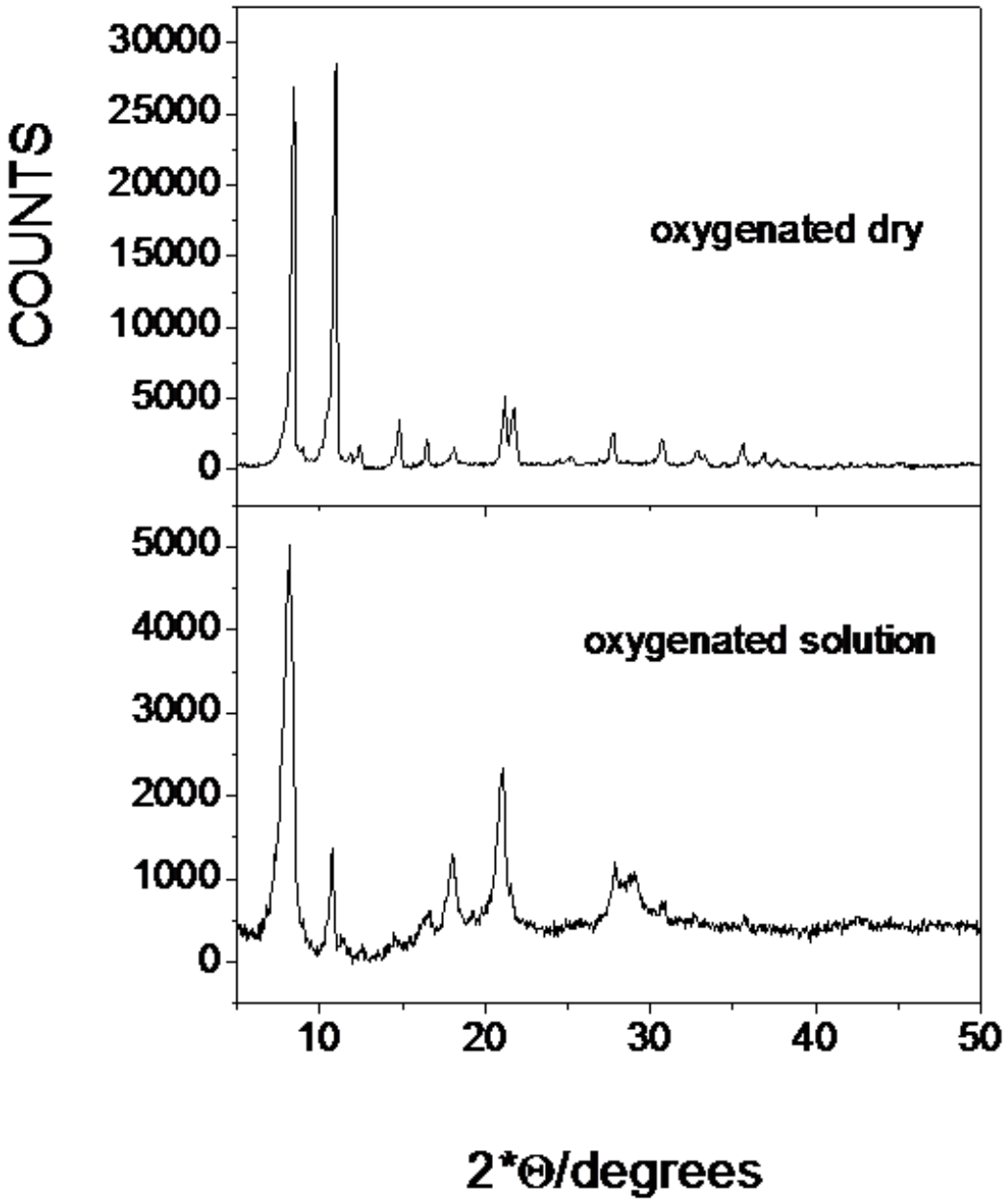

Figure 8-10. XRD spectrum of β-FePc after dry oxygenation (top) and oxygenation in solution (bottom) for 75 days at 50 ^{o}C. Cell parameters calculated for dry oxygenation: a = 14.54 Å, b = 4.83 Å, c = 19.34 Å, β = 120.51^{o}. Cell parameters calculated oxygenation in solution: a = 15.02 Å, b = 4.80 Å, c = 19.54 Å, β = 121.54^{o}.

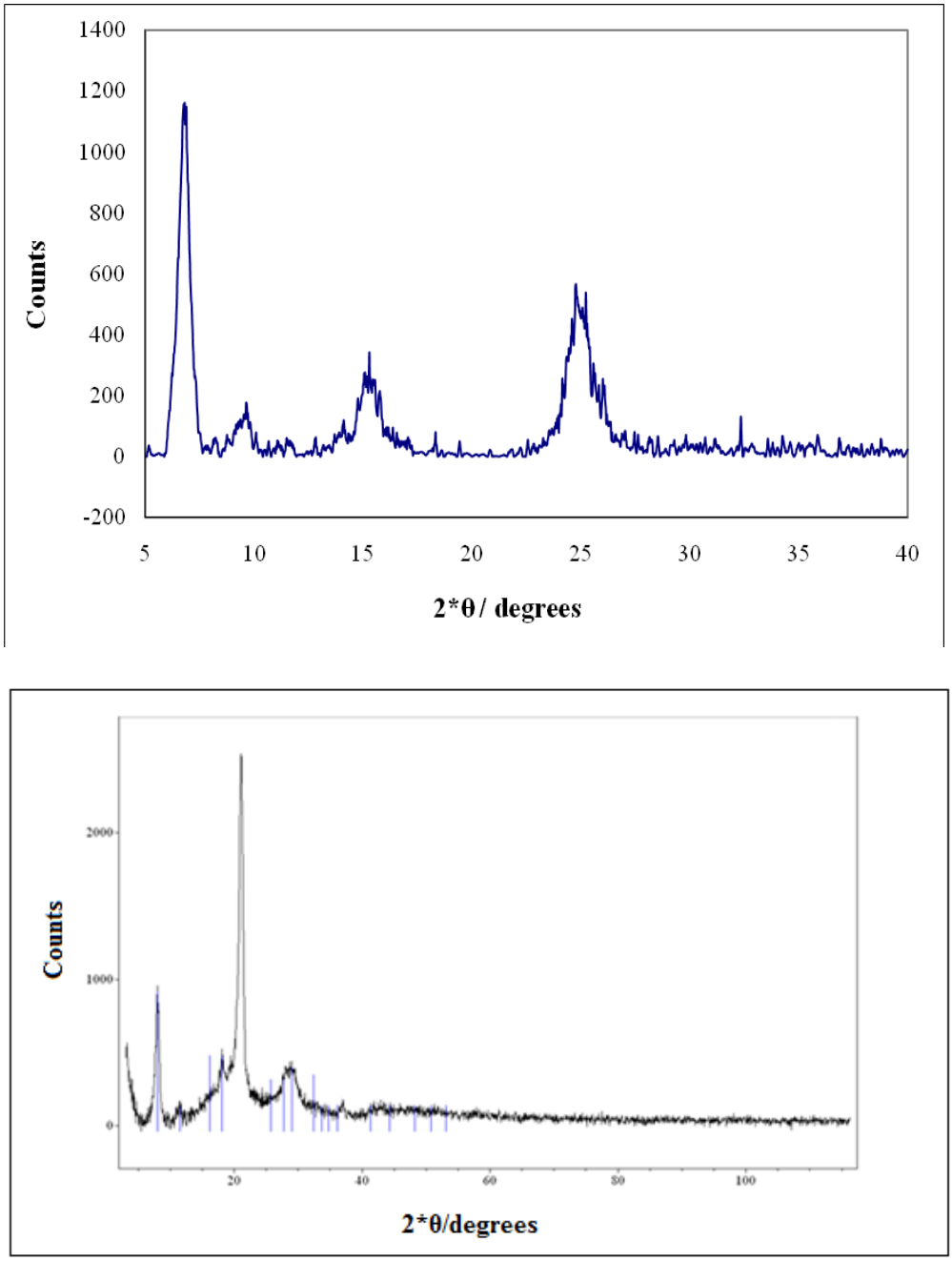

Figure 8-11. XRD spectrum of α-FePc after dry oxygenation (top) and oxygenation in solution (bottom) for 75 days at 50 ^{o}C. Cell parameters calculated for dry oxygenation: a = 25.07 Å, b = 3.67 Å, c = 25.87 Å, β = 89.2^{o}. Cell parameters could not be calculated for oxygenation in solution.

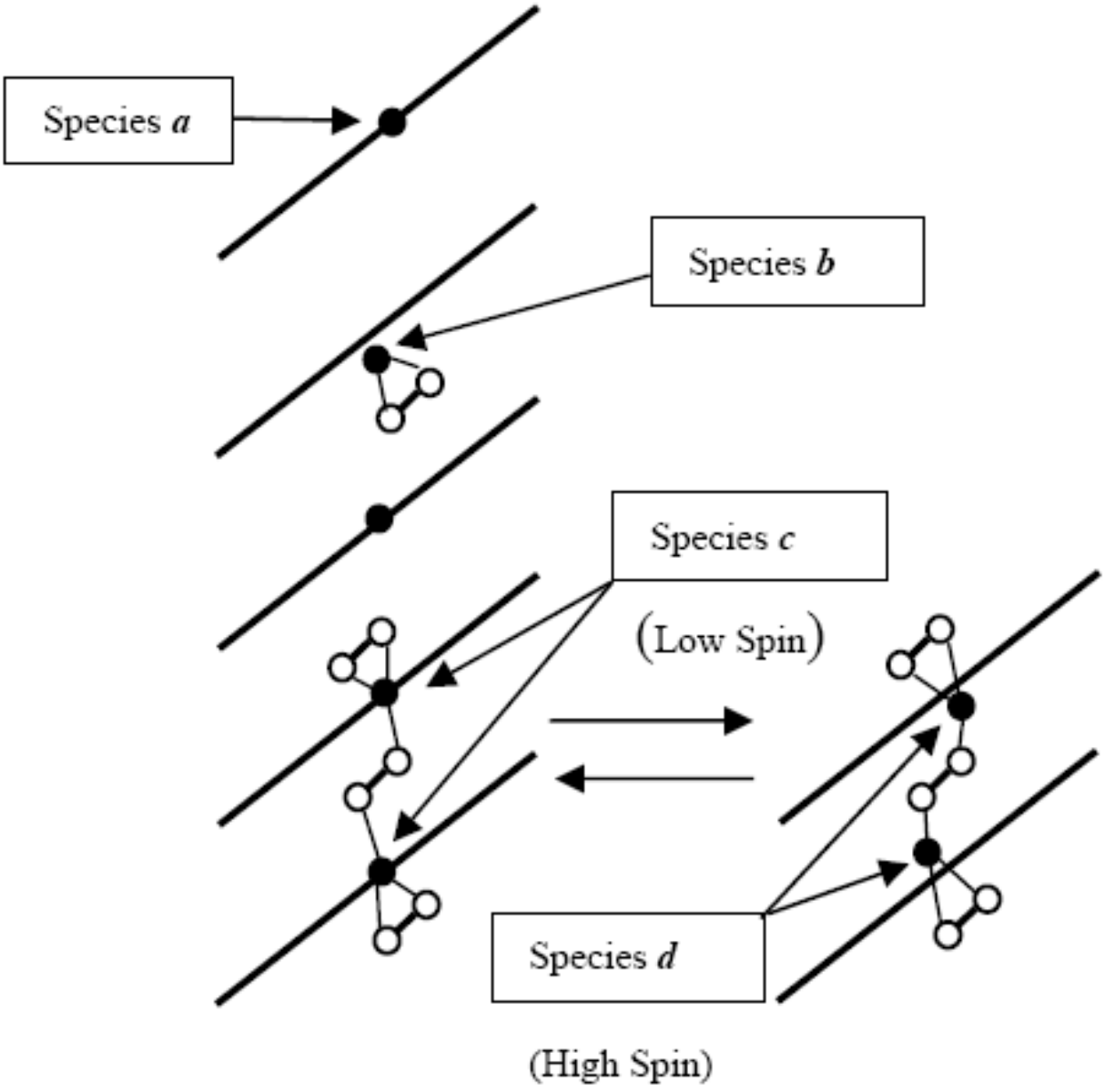

Figure 8-12. Suggested structures of four species observed in oxygenated solid β-Fe^{II}Pc. The tilted bars show the plane of the Pc rings stacked in the lattice; black and white circles represent iron and oxygen atoms, respectively.[12]

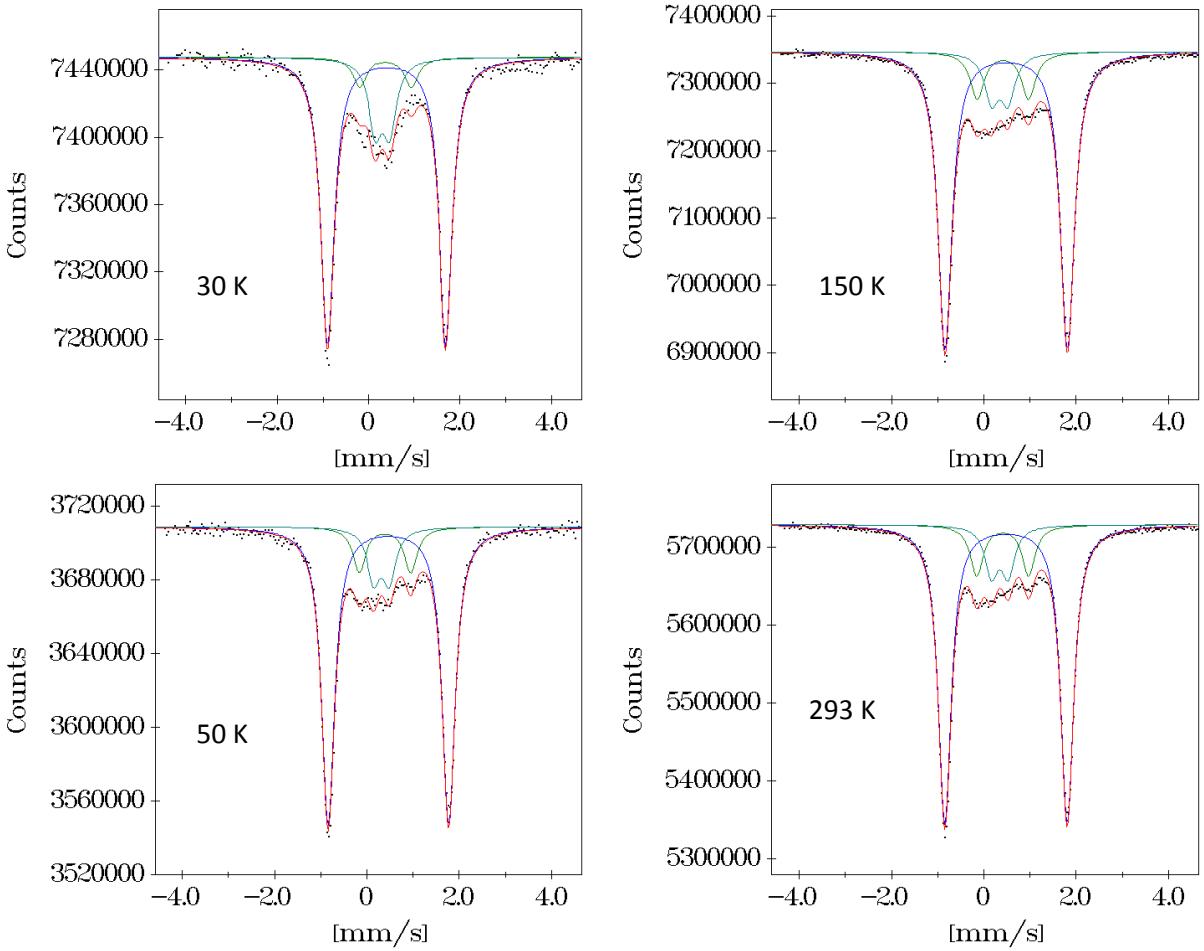

Figure 8-13. Temperature dependence of the Mössbauer spectra of β-Fe^{II}Pc dry oxygenated for 75 days at 50 ^{o}C. The interconversion of the HS species (c) to LS species (d) with increasing temperature is observed.

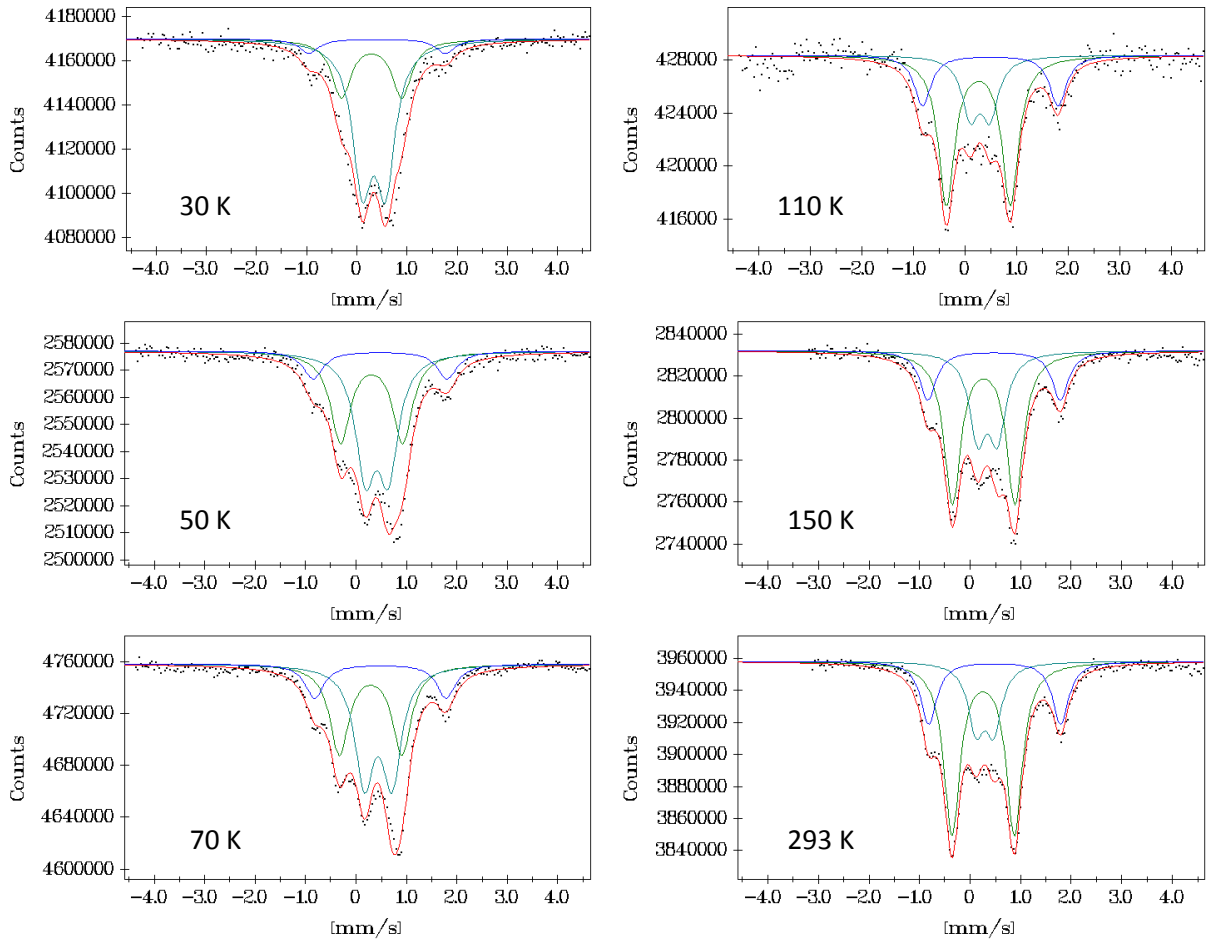

Figure 8-14. Temperature dependence of the Mössbauer spectra of β-Fe^{II}Pc oxygenated in solution for 75 days at 50 ^{o}C. The interconversion of the HS species (c) to LS species (d) with increasing temperature is observed.

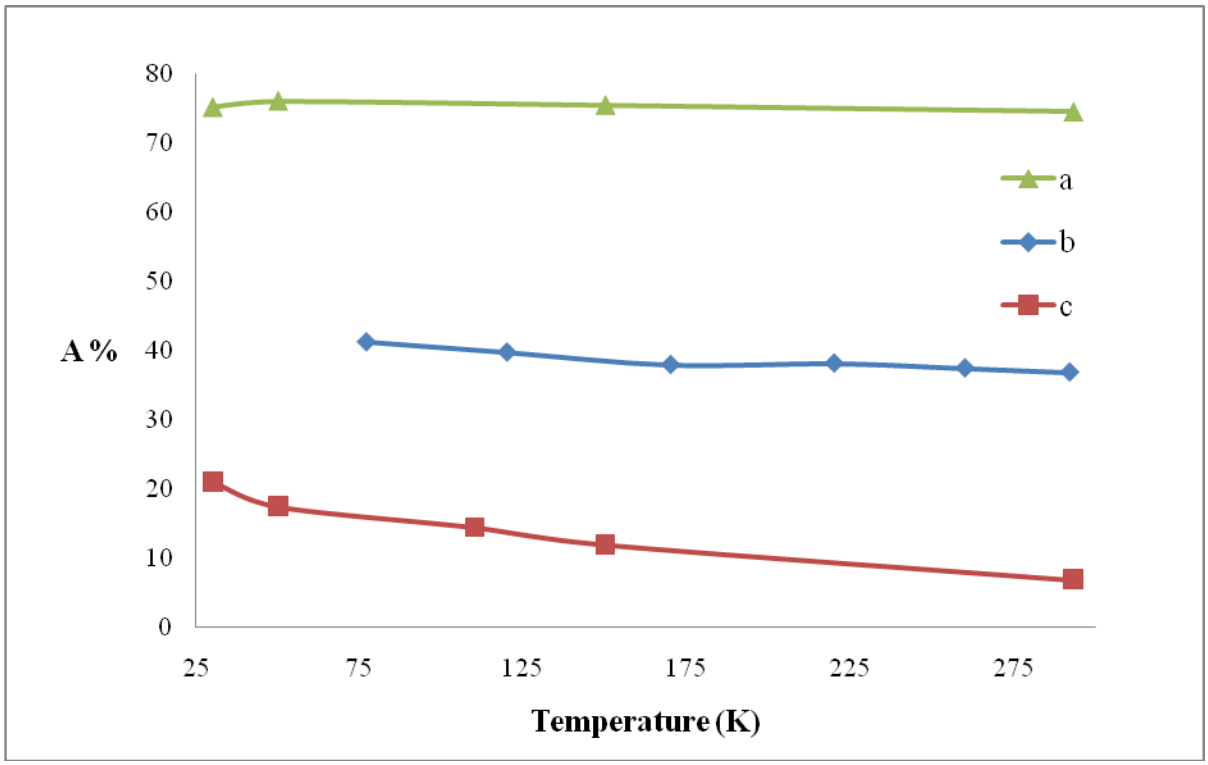

Figure 8-15. Temperature dependence of the absorption area of doublets corresponding to unoxygenated species (a) obtained from the Mössbauer spectra of β-Fe^{II}Pc after: a) dry oxygenation for 75 days at 50 ^{o}C, b) oxygenation in solution for 45 days at 50 ^{o}C and c) oxygenation in solution for 75 days at 50 ^{o}C.

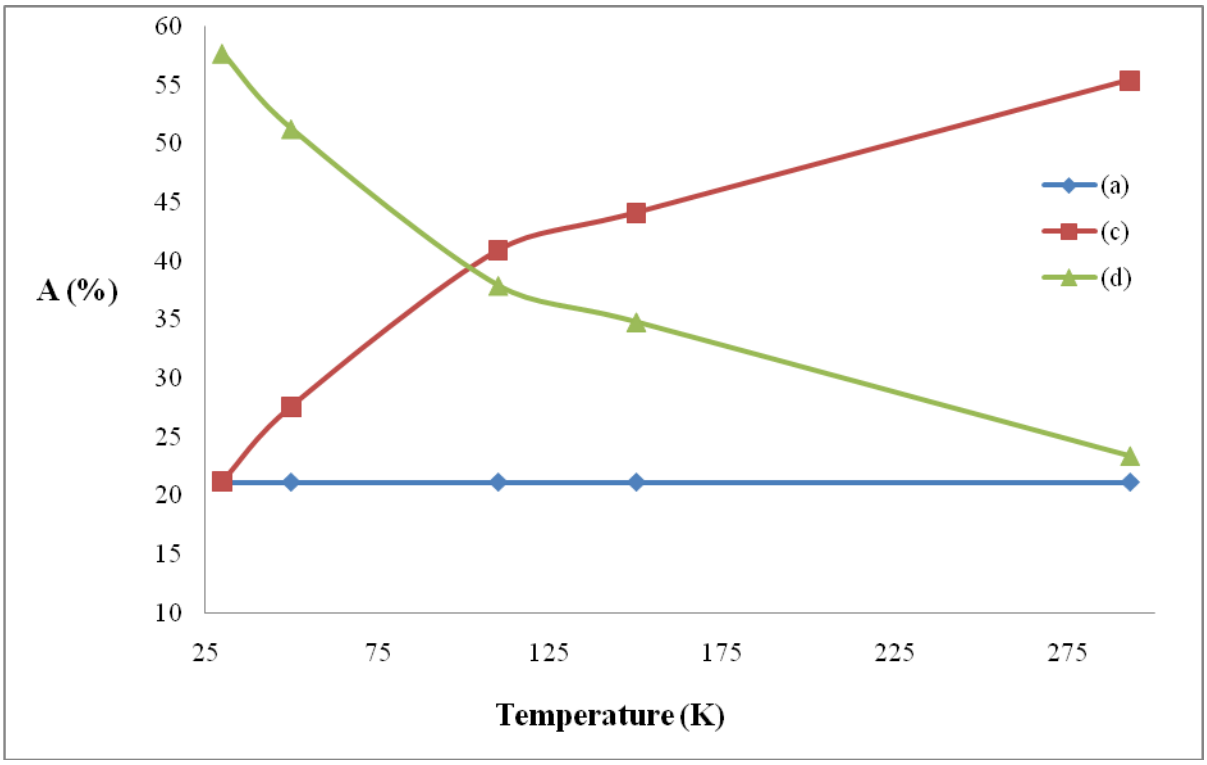

Figure 8-16. Temperature dependence of the absorption area of doublets corresponding to species (a), (c), and (d) (see figure 8-13) obtained from the Mössbauer spectra of β-Fe^{II}Pc oxygenated in solution for 75 days at 50 ^{o}C, after correcting for the anomalous decrease in abundance of unoxygenated Fe(II)Pc.

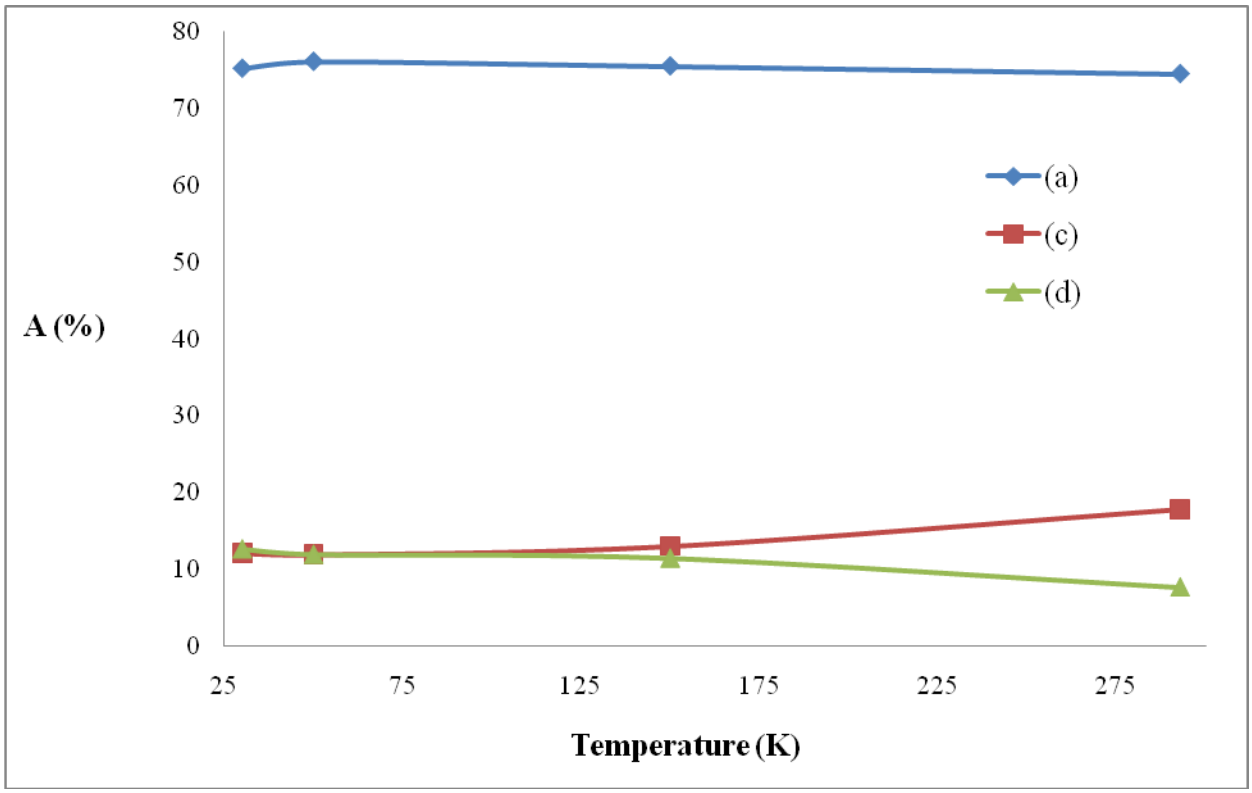

Figure 8-17. Temperature dependence of the absorption area of doublets corresponding to species (a), (c), and (d) (see figure 8-13) obtained from the Mössbauer spectra of β-Fe^{II}Pc after dry oxygenation for 75 days at 50 ^{o}C.

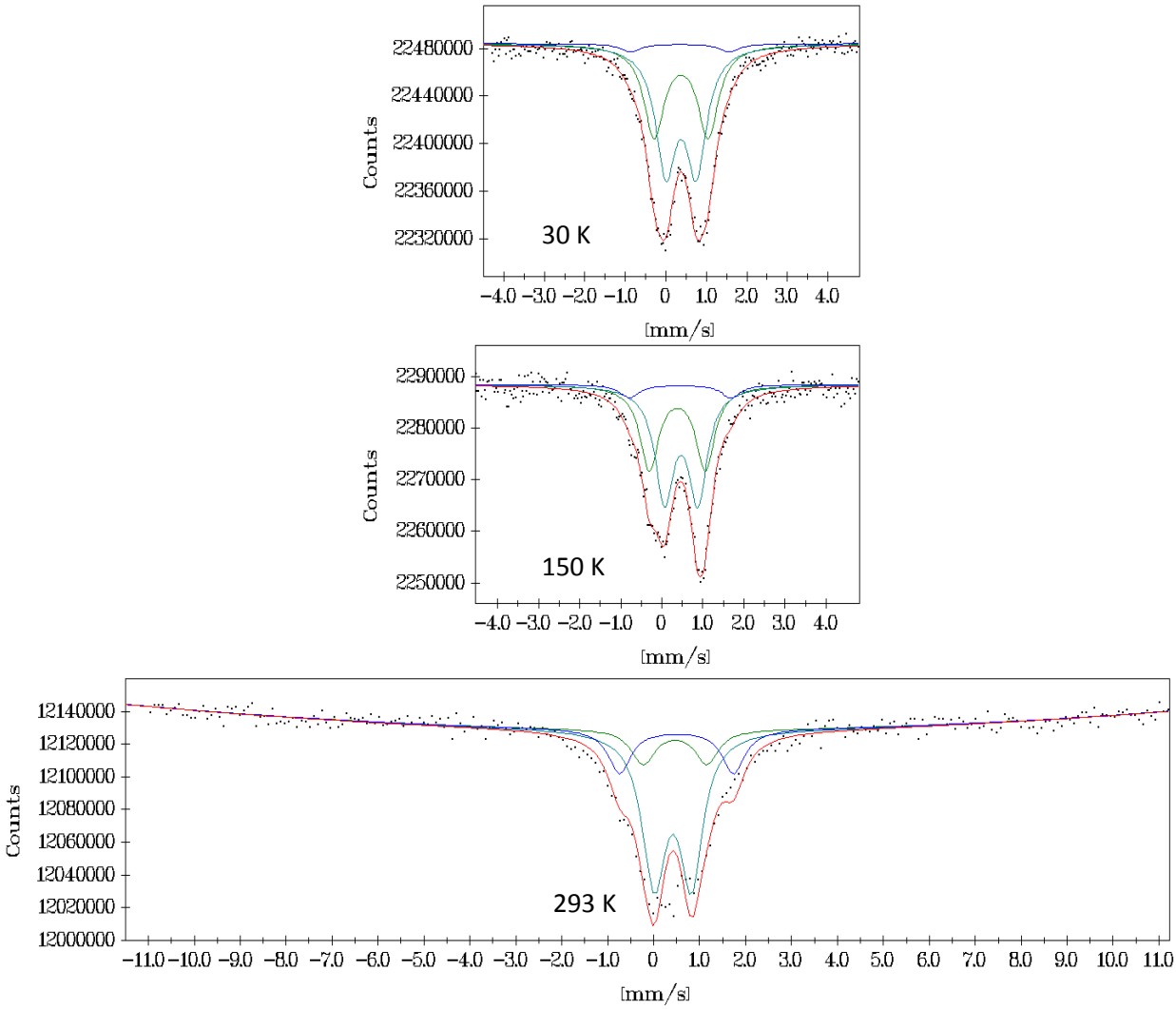

Figure 8-18. Temperature dependence of the Mössbauer spectra of α-Fe^{II}Pc dry oxygenated for 75 days at 50 ^{o}C.

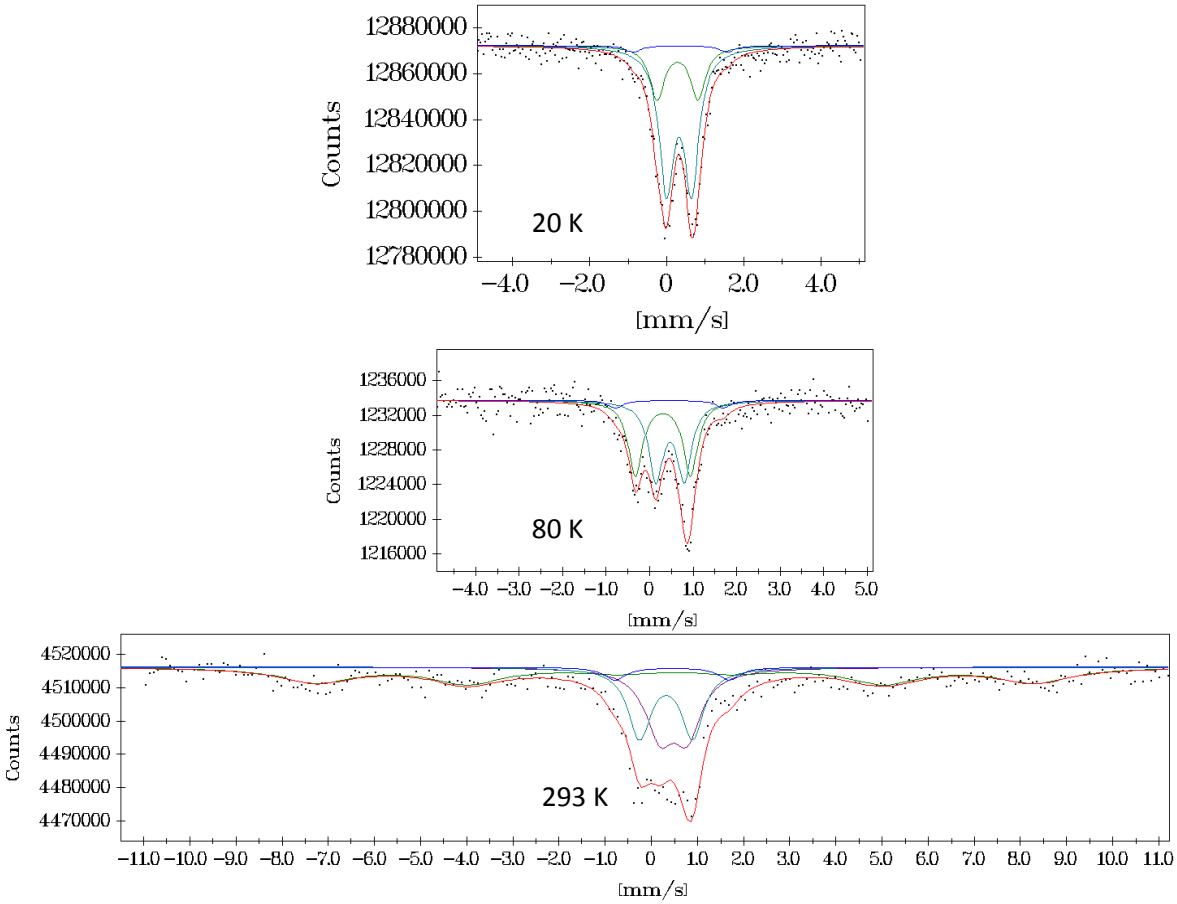

Figure 8-19. Temperature dependence of the Mössbauer spectra of α-Fe^{II}Pc oxygenated in solution for 75 days at 50 ^{o}C.

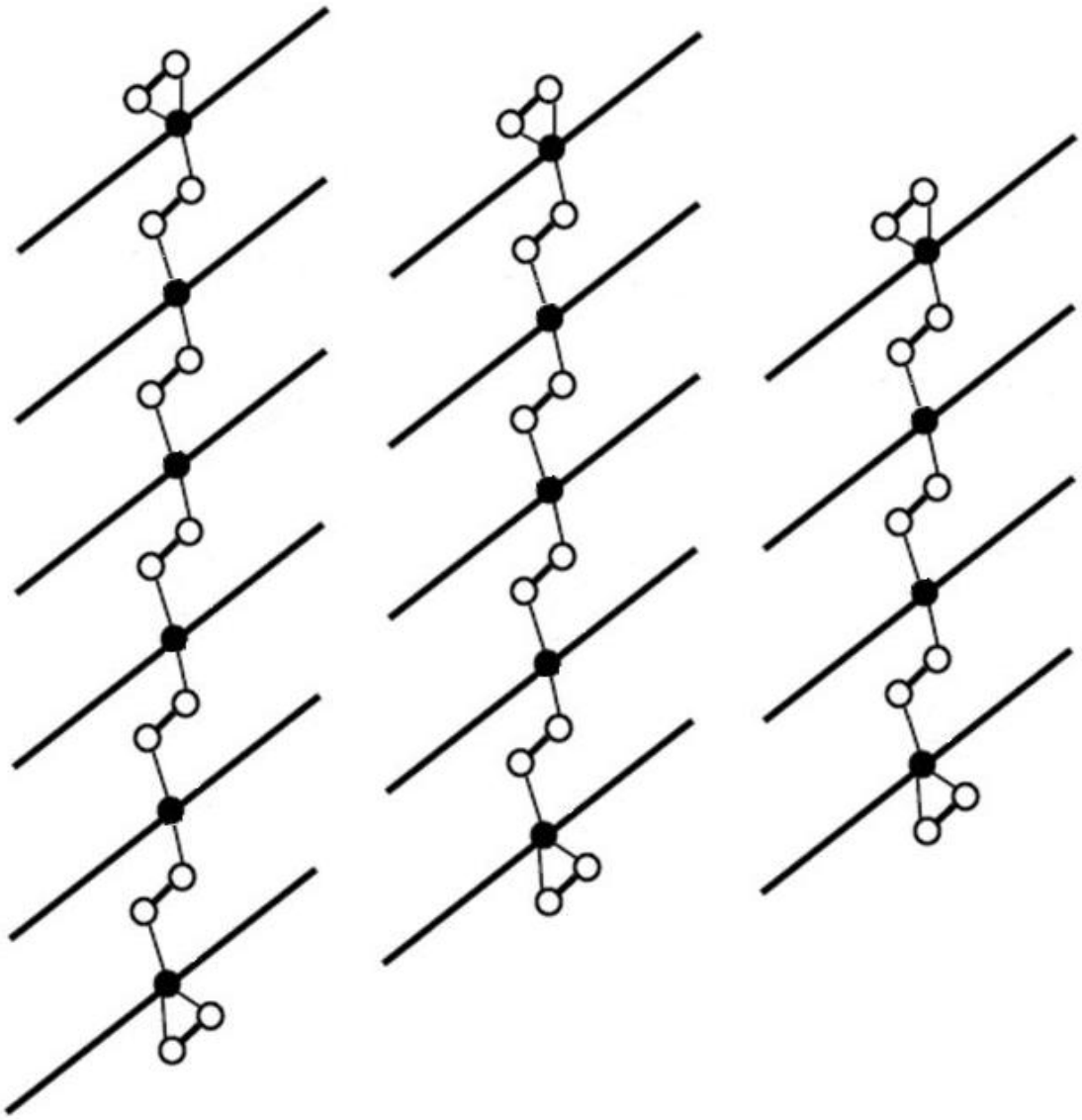

Figure 8-20. Suggested structures of species (2) observed in oxygenated solid α-Fe^{II}Pc with a distribution of chain lengths. The tilted bars show the plane of the Pc rings stacked in the lattice; black and white circles represent iron and oxygen atoms, respectively.

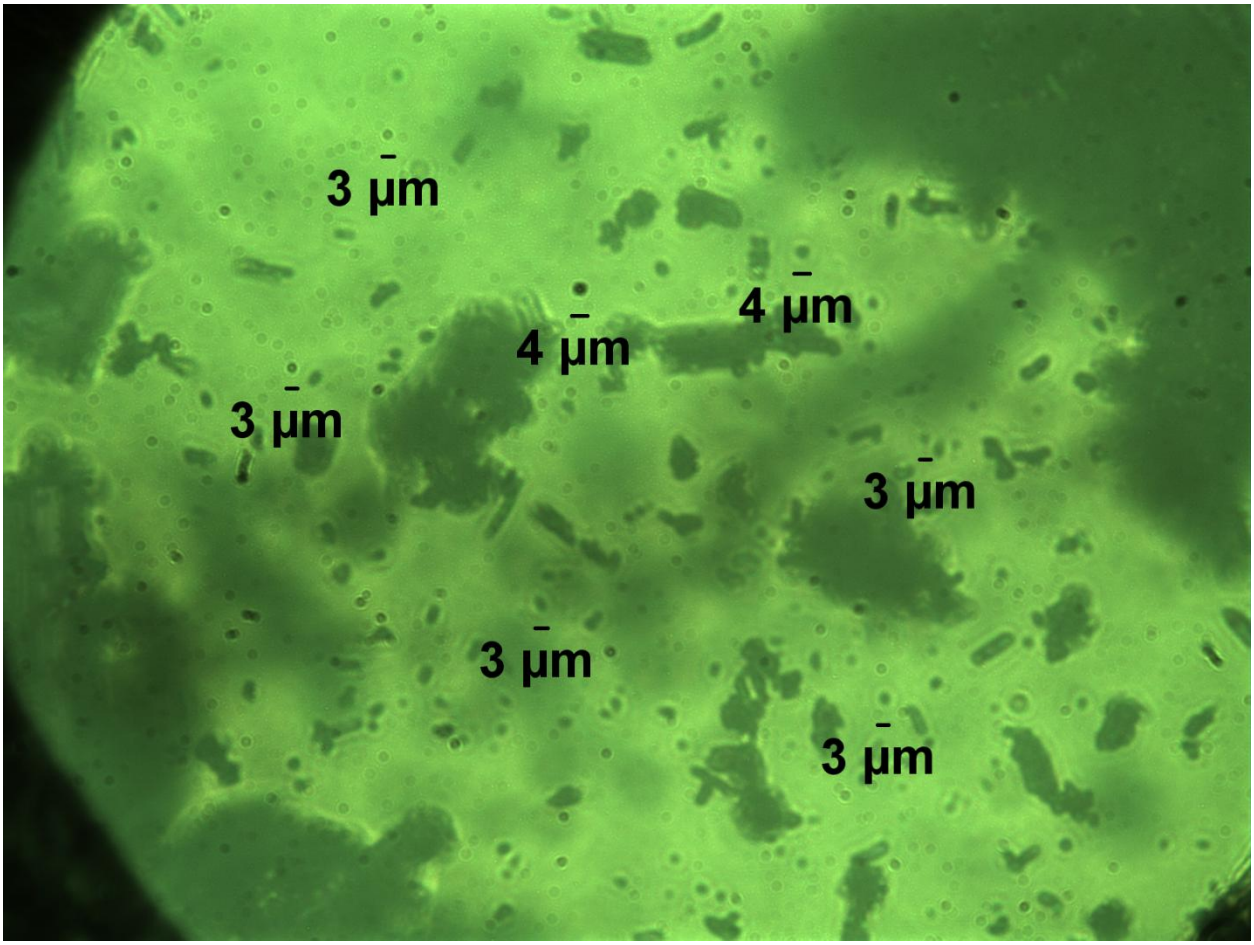

Figure 8-21. Average grain size of β-FePc under an optical microscope.

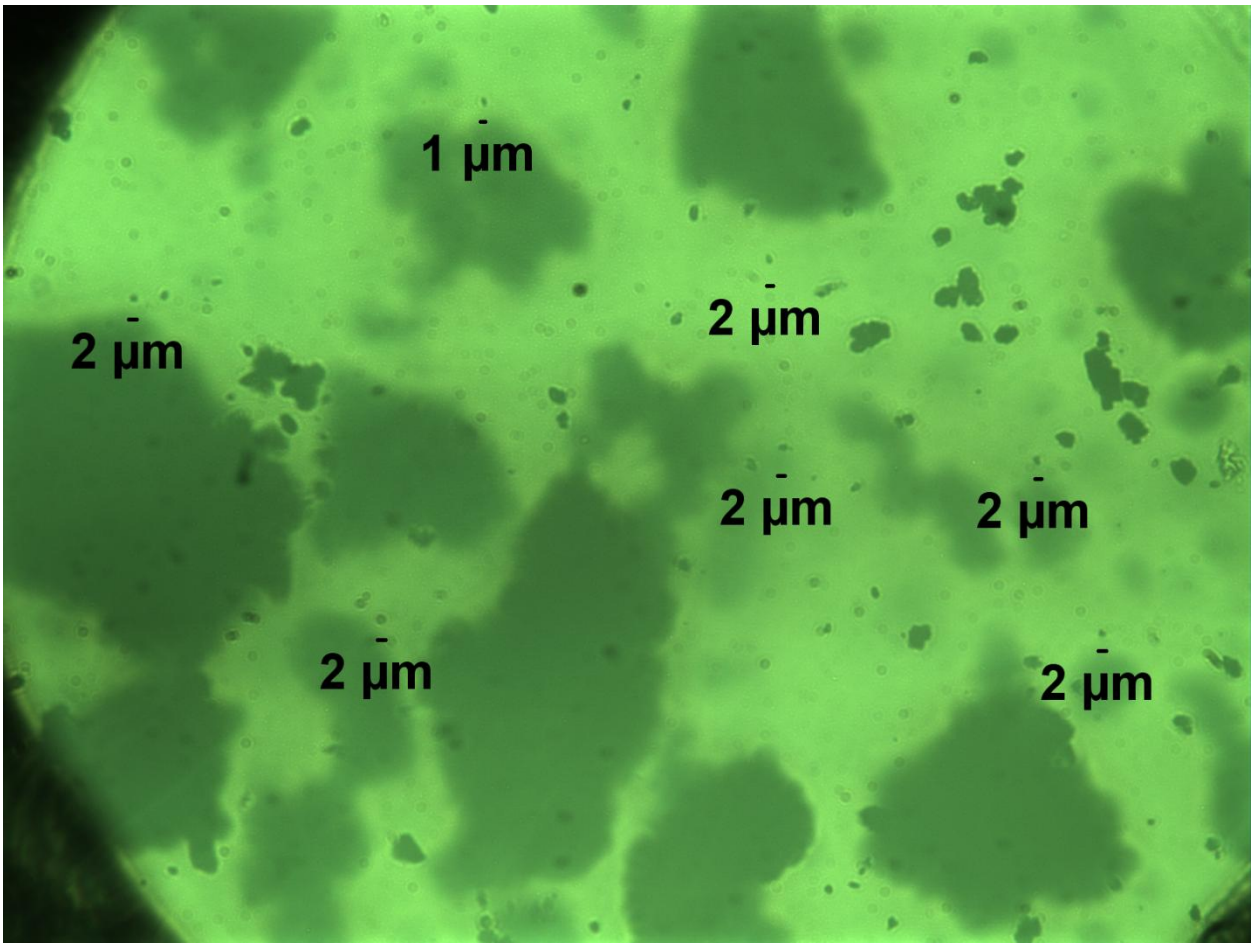

Figure 8-22. Average grain size of α-FePc under an optical microscope.

8.6 Reference List

1. Thomas, A. L. Phthalocyanine research and applications. CRC Press, Boca Raton, FL, 1990.

2. Zagel, J. H. Coord. Chem. Rev. 1998, 119, 89-136.

3. Meunier, B.; Sorokin, A., Acc. Chem. Res. 1991, 30, 470-476.

4. Chen, M. J.; Rathke, J. W. Trends in Inorg. Chem. 1998, 5, 29-41.

5. McKeon,N.B. "Phthalocyanine Materials",Cambridge Univ. Press (1998)

6. Guillaud,G.; Simon,J.; Germain, J. P., Coord. Chem. Rev. 1998, 178- 80, 1443-1484.

7. Isoda, S., Haishi, T., Yoshida, K., and Kobayashi, T. Structures of copper phthalocyanine crystals grown in inert gases. Molecular Crystals and Liquid Crystals Science and Technology, Section A: Molecular Crystals and Liquid Crystals. 2001, 370, 227-230.

8. Evangelisti, M., Bartolome, J., De Jongh, L.J., Filoti, G. Magnetic properties of α-iron (II) phthalocyanine. Physical Review B (2002), 66, 144410.1-144410.10.

9. Ballirano, P., Caminity, R., Ercolani, C., Maras, A., Orru, M. A. X-ray powder diffraction structure reinvestigation of the α and β forms of cobalt phthalocyanine and kinetics of the α→β phase transition. Journal of the American Chemical Society (1998), 120, 12798-12807.

10. Yin, H. Nanoprobes, Nanostructured Materials and Solid State Materials. PhD Thesis, Drexel University, Pennsylvania; 2005.

11. Yin, H., Kubuki, S., Homonnay, Z., Kuzmann, E., Vértes, A., Wei, Y., Nath, A. A mössbauer study of the low spin-high spin transition of an oxygen adduct formed in solid β-Fe(II) Phthalocyanine. The Open Inorganic Chemistry Journal. 2008. (In press)

12. Kuzmann, E., Homonnay, Z., Vértes, A., Li, S., Yin, H., Kubuki, S., Wei, Y., Nath, A., Chen, X., Li, J. Mössbauer studies of the interaction of oxygen with solid β-Fe(II) Phthalocyanine. Journal of Solid State Chemistry (2003), 170, 118-123.

13. Kuzmann, E., Nath, A., Chechersky, V., Li, S., Wei, Y., Chen, X., Li, L., Homonnay, Z., Gal, M., Garg, V.K., Klencsar, Z., Vertes, A. Mossbauer study of oxygenated iron-phthalocyanines, a precursor of magnetic storage material. Hyperfine Interactions (2002), 139/140, 631-639.

14. McKeon, N.B. Phthalocyanine materials. Cambridge University Press, Cambridge, London; 1998.

15. Goldberg, D. P., Telser, J., Bastos, C. M., Lippard, S. J. Ferromagnetic versus antiferromagnetic exchange in five structurally analogous carboxylate-bridged trinuclear ferrous complexes. Inorganic Chemistry (1995), 34, 3011-3024.

Chapter 9. Encapsulation of Enzymes in Mesoporous Hybrid Materials

9.1 Introduction and Motivation

The development of bioengineering and biotechnology gave a boost to increasing interest for encapsulation of enzymes and other biomacromolecules in inorganic or polymeric materials, because of the various potential applications of such materials in optical and electrochemical sensors, diagnostic devices, catalysts and even bioartificial organs.[1-3] There is currently a great interest in enzyme immobilization to maintain the enzymatic activity after prolonged periods of storage. As Mohan et al. note, "Enzymes can act on specific recalcitrant pollutants to remove them by precipitation or transformation to other (innocuous) products and also can change the characteristics of a given waste to render it more amenable for treatment".[4] In the case of waste treatment, several limitations prevent the use of free enzymes, including the decrease of stability with the complexity of effluents. Many of these limitations may be overcome by the utilization of enzymes in immobilized form, which can act as catalysts with longer lifetime. Immobilization with different inorganic or polymeric materials is nowadays studied for enzyme encapsulation along with their application in treatment with various pollutants. Additionally, many compounds of interest to the pharmaceutical industry exhibit poor solubility and may undergo deleterious side reactions (i.e., hydrolysis) in water. As a result these compounds are not amenable to enzymatic reactions in conventional media. Non-aqueous biocatalysts, including enzymes in anhydrous organic solvents, have emerged lately as an alternative approach to circumvent the above limitations of aqueous-based reaction systems.[5] However, the catalytic activity of enzymes in organic solvents is often orders of magnitude lower than those in aqueous solutions.

Many researchers have focused on efforts to overcome these problems by following various approaches. Several techniques for immobilization of enzymes have been investigated, including adsorption to solid supports, covalent attachment and entrapment in polymers. Previously, we presented the encapsulation of a variety of enzymes in mesoporous silica, utilizing a nonsurfactant-templated sol-gel method that was invented in our lab.[6-8] In a similar manner, Xiao et al. have encapsulated enzymes in macroporous cages utilizing a surfactant-templated method.[3] Following another route, our research group presented the encapsulation of horseradish peroxidase in electrospun porous silica fibers with potential biosensor applications.[9] Enzyme horseradish peroxidase also has been stabilized with cellulose by immobilization utilizing a cellulose binding domain.[10] Extensive research in this field has also revealed the salt-induced activation of enzymes, in aqueous and non-aqueous solvents, as a means of maintaining or even enhancing the enzymatic activity in these media.[11-13] Appropriate selection of the encapsulation material specific to the enzyme and optimization of the process conditions is still under investigation by many research groups.

Our group has developed a simple and environmentally friendly nonsurfactant-templated synthetic route to mesoporous sol-gel materials, where nonsurfactant organic compounds, such as D-glucose, D-fructose, D-maltoze, dibenzoyl-L-tartaric acid and numerous others, are employed as templates. Removal of the template by water or other solvent extraction leads to mesoporous metal oxide (e.g., silica) materials. In this Chapter, encapsulation of horseradish peroxidase (HRP) and alpha glucosidase is presented, as model enzymes for a range of applications. The enzymes were encapsulated in various mesoporous metal oxides and hybrid materials, via the nonsurfactant templating method. Several different precursors have been

investigated to find the optimum formulation, and the obtained materials have been characterized by thermogravimetric analysis (TGA) and nitrogen adsorption analysis (BET). Enzymatic assays for HRP and α-glucosidase revealed the percentage of residual activity of the encapsulated enzymes.

In addition, a novel technology for maintaining the enzymatic activity during storage in harsh media, such as organic solvents and high pH aqueous solutions, has also been developed. The non-surfactant templated sol-gel method again has been utilized to incorporate HRP enzyme into the pores of mesoporous organosilicates. The dry sol-gel organosilica, containing HRP, was then crushed into a fine powder, followed by covering with a second acrylic monomer coating. This coating was composed of triethyleneglycol dimethacrylate (TEGDMA), polyethylene glycol (PEG) and photoinitiators, which upon phopolymerization yielded a second acrylic protective layer. Results indicate that the encapsulates in high pH buffer solution , detergent, ethanol and toluene showed many orders of magnitude higher residual activity compared to the native enzyme. Since this “double encapsulation” technique is completely independent of the nature of the enzyme, it is expected to be useful for stabilizing other enzymes, biomacromolecules and bioactive/biomedical agents in such hostile environments as well.

9.2 Organic-Inorganic Hybrid Mesoporous Materials

A typical organic material is characterized by its flexibility, low density, toughness and formability, whereas a typical inorganic ceramic is characterized by excellent mechanical and optical properties, such as surface hardness, modulus, strength, transparency and high refractive index. Introduction of organic moieties within the silicate framework could yield materials with enhanced flexibility and decreased brittleness, as compared to the individual conventional

components. When the initial reactants are combined effectively, a new class of high performance and highly functional organic-inorganic hybrid materials may be obtained. The sol-gel method, which is the versatile solution process that involves the transition of a system from a liquid "sol" into a solid "gel" phase, has been described in earlier sections of this thesis. It is a powerful approach for the preparation of organically modified inorganic materials with a tailored microstructure. While the early developments of the sol-gel process were mainly based on simple, readily available precursors, the huge potential of new precursors, chemically tailored for special applications, is more and more realized.[14-19] A considerable amount of literature has described the use of organotrialkoxysilanes, organodisilicates, and polysiloxanes for the development of novel sol-gel derived hybrid materials.[20-24]

Among all of the organosiloxanes, trifunctional alkoxysilanes, $R'Si(OR)_3$, offer many advantages for basic or applied research in fields such as optics, catalysis, selective membranes, molecular recognition, sensors, or molecular imprinting.[25-30] Alkyltrialkoxysilanes with various alkyl chain lengths and different functionalities have been explored. For example, methylthrimethoxy silane is often used to impart some hydrophobicity to the silica matrix or to modify its mechanical properties. On the other hand, phenyltrimethoxy silanes are preferred when one wants to synthesize hybrids with increased thermal stability, glass transition temperature or refractive index. The general procedure may involve the co-condensation of several different precursors, such as tetraalkyl orthosilicates (e.g., tetraethyl orthosilicate, tetramethyl orthosilicate, etc.) with various organosiloxanes (e.g., methyltrimethoxy silane, phenyltrimethoxy silane, etc.). The main advantage of this approach is the feasibility of obtaining a wide range of organically modified hybrid silica materials under mild reaction conditions without macroscopic phase separation. This method is also an effective means of synthesizing

and designing hybrid materials with nanometer-scale architecture. These sol-gel derived hybrid materials with tunable properties can have applications in many fields that are far beyond the scope of applications of traditional composite materials. More importantly, because of the mild and biocompatible conditions (e.g., low temperature and neutral pH aqueous solvents) that would be employed, the sol-gel method can be used to encapsulate numerous biological molecules within the sol-gel derived inorganic or hybrid matrixes.

9.3 Immobilization of Enzymes by the Sol-Gel Method

In recent years, there has been a considerable demand for enzymes used as industrial catalysts. However, the practical use of enzymes often requires the utilization of them under denaturing conditions, such as high temperature and organic-inorganic environment. To further expand their utilization, effective enzyme immobilization techniques that would maintain the residual enzymatic activity and would consequently reduce the overall cost are of great interest. A broad range of immobilization methods have been investigated, including adsorption to several substrates, covalent attachment and entrapment in a range of organic-inorganic materials. Adsorption techniques usually result in weak bonding with the respective substrate and thus are lacking the degree of stabilization that may be feasible by encapsulation or covalent attachment. On the other hand, the techniques that utilize covalent attachment are often very tedious and usually require several chemical steps, which often result in a decrease of the enzymatic activity.

A variety of enzymes and other biomolecules have been encapsulated in inorganic oxides, such as silica, for several applications. Compared to other immobilization methods the sol-gel derived materials offer many advantages including:

- Easy processability and synthesis procedure ;
- Prevention of leaching of the entrapped biomolecules due to effective caging;
- Enhancement of the stability of the encapsulated enzymes;
- Better thermal stability compared to organic molecules;
- Controllable surface area, average pore size and pore size distribution;
- Do not photo-degrade and can be transparent into the UV range.

However, there are still many problems associated with the conventional sol-gel materials, which hinder their utilization for the encapsulation of enzymes. The microporous nature of the conventional sol-gel materials results in a decrease of the catalytic activities of the enzymes due to the low diffusion rates of the substrate molecules and the poor accessibility of the encapsulated enzymes. Previous work in our lab has shown that neutral non-surfactant organic compounds (e.g., D-glucose, D-fructose, D-maltose, etc.) can be used as pore-forming templates for the development of mesoporous sol-gel hybrid materials.[6-9] This novel non-surfactant sol-gel chemistry method and modifications of it have been explored for the development of host matrices for the immobilization of a variety of enzymes, including horseradish peroxidase (HRP), alkaline phosphatase, acid phosphatase and lipase. A typical laboratory procedure includes the hydrolysis and co-condensation of a variety of tetraalkyl orthosilicates (e.g., tetraethyl orthosilicate, tetramethyl orthosilicate, etc.) with various organosiloxanes (e.g., methyltrimethoxy silane, phenyltrimethoxy silane, etc). The biomaterial to be encapsulated is added to the sol after partial removal of the solvents used (e.g., water) and the small molecular byproducts from the sol-gel reactions (e.g., water, ethanol, methanol, etc). By this method it is crucial to obtain a homogeneous solution in order to uniformly coagulate the

enzyme to be encapsulated. A direct comparison of the obtained results is difficult since, in addition to different immobilization methods, a variety of enzymes and assays also have been used. In this work I have investigated a series of different precursors and ratios of them to encapsulate HRP and α-glucosidase in mesoporous hybrid sol-gel materials. The formulations include precursors, such as tetraethylortho silicate, tetramethylortho silicate, methyltrimethoxy silane and phenyl trimethoxy silane. These hybrid materials were also explored as a method to protect and to maintain the activity of the encapsulated enzymes during storage in hostile environments with, however, ambiguous results.

Consequently, a different approach, which again includes the utilization of the nonsurfactant-templated sol-gel method, has been developed. In this case, though, the mesoporous hybrid materials containing enzymes were coated with an acrylic monomer. This coating was composed of triethyleneglycol dimethacrylate (TEGDMA), polyethylene glycol (PEG) and photoinitiators, which upon photopolymerization yielded a second protective layer. The doubly encapsulated HRP samples were immersed in harsh aqueous and non-aqueous environments for a predetermined period of time to test for the efficiency of this double encapsulation method, and the obtained values of residual enzymatic activities are presented. This “double encapsulation” technique is completely independent of the nature of the enzyme, and thus, it may be expected to provide a method useful for stabilizing other enzymes in hostile environments as well.

9.4 Model Enzymes (Horseradish Peroxidase, α-Glucosidase)

In this work, horseradish peroxidase and alpha-glucosidase have been investigated as model enzymes for organophosphorous acid anhydrolases (OPAA) due to the similarities that

these enzymes present in their size and hydrophobicity. OPAA enzymes have the potential for decontamination of toxic organophosphorous compounds (OPs), including some warfare nerve agents, by catalyzing the hydrolysis of P-F or P-CN bonds. Unfortunately, and due to the limited access to OPAA enzymes, it was not possible to perform their encapsulation in mesoporous hybrid materials. Such a study has been already conducted in our group.[39] Thus, and as has already been mentioned, HRP and α-glucosidase have been encapsulated in a variety of different mesoporous organic-inorganic hybrid materials by utilizing the nonsurfactant-templated sol-gel method, in an attempt to imitate the encapsulation of OPAA enzymes and possibly give new insights to such technology.

Horseradish peroxidase, which can be found in the plant called horseradish, is an enzyme that belongs to the large family of peroxidases. Peroxidases are increasingly important in the biochemical research fields where they typically catalyze a reaction of the form:[31,32]

$$ROOR' + \text{electron donor } (2\ e^-) + 2H^+ \rightarrow ROH + R'OH$$

Horseradish peroxidase can use a variety of organic compounds as electron donors and acceptors. It is a heme-containing enzyme comprised of a single polypeptide of 308 amino acid residues. Quite recently, the three-dimensional structure and the molecular description of the intermediates in the catalytic cycle of horseradish peroxidase were revealed giving new insights to the enzyme functionality and the catalytic mechanism.[33,34] HRP is used extensively in molecular biology applications primarily for its ability to amplify a weak signal and increase detectability of a target molecule. HRP is often used in conjugates (molecules that have been joined genetically or chemically) to determine the presence of a molecular target. For example, an antibody conjugated to HRP may be used to detect a small amount of a specific protein in a

western blot. Here, the antibody provides the specificity to locate the protein of interest, and the HRP enzyme, in the presence of a substrate, produces a detectable signal. Numerous substrates for the horseradish peroxidase enzyme have been described and commercialized to exploit the desirable features of HRP.[35]

Alpha-glucosidase is the second enzyme that has been encapsulated in the mesoporous organic-inorganic hybrid materials. This enzyme is also known as maltase, and it catalyzes the hydrolysis of maltose to glucose units.[36] Alpha-glucosidase is used for assaying the activity of alpha amylase and for the determination of maltose in brewing. Alpha-glucosidase catalyzes the following reaction:

$$\text{a-D-Glucoside} + H_2O \rightarrow \text{D-Glucose} + \text{Alcohol}$$

The membrane-bound intestinal alpha-glucosidases hydrolyze oligosaccharides, trisaccharides, and disaccharides to glucose and other monosaccharides in the small intestine. Nowadays, a very important issue with respect to these intestinal α-glucosidases is the use of α-glucosidase inhibitors.[37,38] These inhibitors are a class of saccharide compounds that are used for the treatment of type II diabetes. Their function relies on the fact that they decrease the absorption of carbohydrates from the intestine, resulting in a slower and lower rise in blood glucose throughout the day, especially right after meals. Before carbohydrates are absorbed from food, they must be broken down into smaller sugar particles, like glucose, by enzymes in the small intestine. One of the enzymes involved in breaking down carbohydrates is the α-glucosidase. By inhibiting this enzyme, carbohydrates are not broken down as efficiently and glucose absorption is delayed.

9.5 Experimental

9.5.1 Materials

Tetramethyl orthosilicate (TMOS, 98%), tetraethyl orthosilicate (TEOS, 98%), methyltrimethoxysilane (MTMS, 98%), phenyltrimethoxysilane (PhTMS, 97%), triethyleneglycol dimethacrylate (TEGDMA, 95%), polyethylene glycol (PEG, MW:4,600), ethanol, toluene, carboxymethyl cellulose sodium salt, camphorquinone (CQ, 97%) and N-phenyl-glycine (NPG, 95%), hydrochloric acid, D-fructose (98%), pyrocatechol (98%), hydrogen peroxide (30 wt% in water), L-glutathione (reduced, 99%), 4-nitrophenyl-α-D-glucopyranoside (99%), horseradish peroxidase (peroxidase type II from horseradish, 181 purpogallin units/mg) and α-glucosidase (α-glucosidase type I from baker's yeast) were purchased from Aldrich and used as recieved. The PBS (pH=10 at 24 ^{o}C) buffer solution was made by mixing appropriate amounts of potassium carbonate, potasium borate and potasium hydroxide. Aniline (97%, Aldrich) was purified by vacuum distillation before use.

9.5.2 Methods

9.5.2.1 Encapsulation of Enzymes in Organic-Inorganic Hybrid Mesoporous Materials

The preparation of organic-inorganic hybrid mesoporous silica materials in the presence of D(-)fructose, as template, and hydrochloric acid, as the acidic catalyst, followed similar procedures that have been reported by our group.[39,40] In order to investigate the effect of the organosiloxanes on the structure of the hybrid silica materials and the residual activity of the encapsulated enzymes different precursors, including tetramethyl orthosilicate, methyltrimethoxy silane and phenyl trimethoxy silane, have been tried. Several different ratios of the tetralkyl orthosilicate to the alkyltrialkoxy silane have been also investigated to find the optimum

formulation for the respective enzyme. Weight percentage of the template (D-fructose) has been varied between 0 wt% and 60 wt%. A series of different hybrid mesoporous materials have been synthesized and characterized as summarized in **Table 9-1**. Four series of hybrid organosilica materials, denoted as HIF, HIIF, HIIIF and HIIIF, were prepared corresponding to molar ratios of TMOS/MTMS = 1, TMOS/MTMS = 2, TMOS/MTMS = 3 and TMOS/PhTMS = 20, respectively. The annotations are followed by a number that represents the weight percentage of fructose used. For example a hybrid with code HIIF20, corresponds to a sample with TMOS/MTMS=2 mole ratio and 20 wt% of fructose.

Generally, a tetralkyl orthosilicate and an alkyltrimethoxy silane precursor were hydrolyzed and co-condensed under acidic catalysis for about 30 min until a transparent solution was obtained. During this period, the temperature of the solution increased to about 40-50 ^{o}C due to the exothermic reactions. Upon the return of the solution temperature to room temperature, the mixture would usually become completely homogeneous. Depending on the procedure that would follow and the enzyme to be encapsulated, the mixture system containing the sol-gel intermediates would sometimes be put under high vacuum until most of the solvent (e.g., H_2O) and the sol-gel byproducts (e.g., EtOH or MeOH, which are harmful to enzymes) be removed. The next step included the addition of distilled water, containing the appropriate amount of fructose, which was used as the non-surfactant template. After stirring for about 5 min, the mixture would be transferred onto an ice bath until the temperature of the solution would drop down to about 2-4 ^{o}C. The required amount of enzyme, dissolved in the appropriate buffer solution, would then be added into the above mixture, and the samples would be sealed with a paraffin film with about 15-20 pin-holes to allow the further condensation and evaporation of the

solvents and the sol-gel byproducts. At this point, and due to the buffer addition, the gelation of the "sol" samples was fast. The samples were stored for 24 hr in a 3-5 ^{o}C refrigerator and then put under high vacuum until a constant weight would be reached (<0.5 % in weight change in a 24-hr period). The dried solids would be then crushed into a fine powder and stored, in a moisture-free freezer at -20 ^{o}C, for further characterizations.

As a typical procedure, for the synthesis of an HRP-doped sol-gel sample, denoted as HIIIF50 (**Table 9-1**), 3.197 g of TMOS (21 mmol), 0.953 g of MTMS (7 mmol), 0.945 g of H_2O (52 mmol) and 30 μl of a 40 mM HCl solution (1.5 x 10^{-2} mmol) were charged in a 50-ml single-neck flask. The mixture was magnetically stirred at room temperature in air. Within a few minutes the mixture became homogeneous accompanied by the raise in temperature. After about 20 min, the solution came back to room temperature. The next step included the removal of the solvent and the sol-gel byproducts under high vacuum until a highly viscous solution (~ one air bubble per second) was obtained. 2.57 g of fructose in 2.57 g of distilled water were then added into 5.09 g of the above viscous solution under agitation, and the solutions were transferred into an ice bath until the temperature of the mixture reached 2-4 ^{o}C. 1.0 ml of HRP solution, prepared by dissolving 1.0 mg of HRP in 1 ml of PBS buffer solution (potassium phosphate buffer solution 0.2 M, pH=7.2 at 24 ^{o}C), was then added into the above mixture and the samples were sealed with a paraffin film with about 15-20 pinholes to allow for the further condensation and evaporation of solvents and byproducts of the sol-gel reactions (e.g., water and methanol). The samples were kept in a refrigerator (at 3-5 ^{o}C) for 24 hr, before they were transferred into a container, which was held under high vacuum in an ice-water bath, held at 3-5 ^{o}C. The samples were checked occasionally for weight loss, and they remained under high vacuum until constant

weight was reached (< 0.5 % in weight change in a 24-hour period). The solid monolithic and transparent disk was then crushed into a fine powder using a mortar and a pestle and stored in a -20 ^{o}C freezer for further characterizations.

9.5.2.2 Characterization of the Sol-Gel Materials

9.5.2.2.1 Thermal Gravimetric Analysis

Thermogravimetric analysis (TGA) was performed on a TA 9900 thermal analysis system equipped with a TGA (TA Q 50 model) in air. TGA was measured at a programmed heating rate of 20 °C/min at the temperature range of 30-750 ^{o}C. Before TGA measurements, the solidified samples were ground into a fine powder by means of a mortar and a pestle, passed through a 30 square mesh wire cloth and kept in a vacuum oven at 60 ^{o}C for 24 hr. Thermal gravimetric analysis curves in air were used to calculate the experimental SiO_2 weight percentage in the as synthesized hybrid mesoporous materials. This was done by recording the residual weight at 750 ^{o}C, which is presumed to be composed of SiO_2 only.

9.5.2.2.2 Nitrogen Adsorption

The N_2 physisorption characterization of the crashed hybrid samples was conducted on a Micrometrics ASAP 2010 surface area and pore size analyzer (Micrometrics, Inc., Norcross, GA) at -196 ^{o}C. Before this N_2 desorption analysis, fructose was completely removed from the samples to be tested by extensive washing for 24 hr with water at room temperature. The water-extracted sol-gel hybrid materials were first dried in a vacuum oven at 100 ^{o}C and then degassed at 120 ^{o}C and 1 Pa overnight prior to measurements. The surface and pore structure parameters were calculated from the N_2 adsorption-desorption isotherms by using the accompanying software provided by Micrometrics, Inc.

9.5.2.2.3 Activity Assay of Free and Immobilized Horseradish Peroxidase (HRP)

An adapted colorimetric assay procedure, using aniline, catechol and hydrogen peroxide as the dye-generating compounds, has been employed to estimate the catalytic activity of free and immobilized HRP.[41] The activity of HRP was determined from the change in absorbance at 510 nm by using a UV-Vis spectrophotometer (Perkin Elmer Lambda 2, Norwalk, CT). The absorbance increase was due to the formation of the colored compound, 4-(phenylamino)benzene-1,2-diol as illustrated in **Sceme 9-1**.

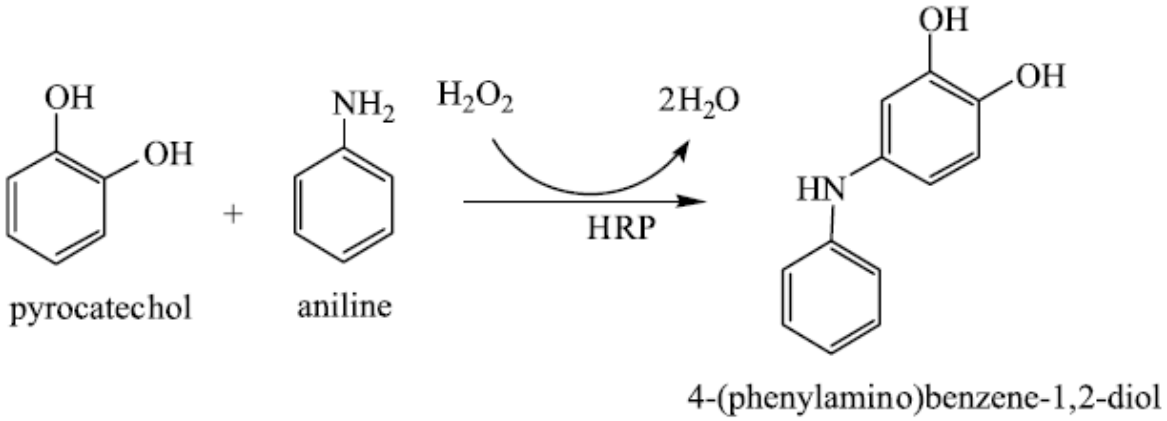

Scheme 9-1. Reaction between aniline and pyrocatechol under HRP biocatalytic activity.[40]

The difference in absorbance, at 510 nm per min, was used to calculate the activity of HRP according to the following equation:

$$Units/mg = \frac{\frac{\Delta A}{min}}{\varepsilon \times \frac{mg\ of\ enzyme}{ml\ of\ reaction\ mixture}}$$

where ε is the extinction coefficient for the colored compound of interest, which for 4-(phenylamino)benzene-1,2-diol is equal to 5 mM^{-1} cm^{-1}. For free HPR, 1 mg of HRP was dissolved in 1.0 ml of PBS buffer solution (potassium phosphate buffer solution (0.2 M, pH=7.2 at 24 ^{o}C)). A mixture of pyrocatechol (170 mM) and aniline (2.5 mM) was prepared in the phosphate buffer solution (PBS). 3-ml glass cuvettes were used for the UV measurement. To each blank and sample cuvette, 1350 μl of the above mixture solution and 1500 μl of hydrogen peroxide were pipetted. 150 μl of diluted HRP and 150 μl of PBS were then added to the sample and the blank cuvette, respectively. The spectrophotometer was adjusted to 510 nm and the increase in absorbance per minute was recorded for each sample.

For HRP encapsulated in the hybrid materials, all samples were first washed extensively with a dilute buffer solution before the activity measurements. A certain amount of solid (e.g. 10.3 mg for HIIIF50) was weighed into a 10-ml centrifuge tube. 10 ml of potassium phosphate buffer solution (0.2 M, pH 7.2 at 24 ^{o}C) was then added in the tube to soak the samples under agitation. After 2 hr of continuous agitation, the washing solution was separated from the solid by decantation after centrifugation. This procedure was repeated twice for a 2-hr interval each. The HRP-containing mesoporous hybrids were then assayed, following the same procedure as for the free enzyme, except for substituting the enzyme solution with a predetermined amount of the hybrid material and 1.0 ml of PBS buffer solution. The PBS washing solutions were also

assayed for HRP activity the same way as for the free enzyme, in order to evaluate the efficiency of the encapsulation and the amount of the unbound, loosely trapped, leached or surface absorbed enzyme in the as-synthesized mesoporous materials. It is assumed that the HRP activity is not altered by the immobilization procedure or the presence of minor amounts of other chemicals (fructose, etc.).

9.5.2.2.4 Activity Assay of Free and Immobilized Alpha-glucosidase

An adapted colorimetric procedure from Sigma Aldrich (EC 3.2.1.20) was employed to evaluate the enzymatic activity of α-glucosidase. The substrate used was p-Nitrophenyl α-D-Glucoside. Enzyme α-glucosidase catalyzes the following reaction:

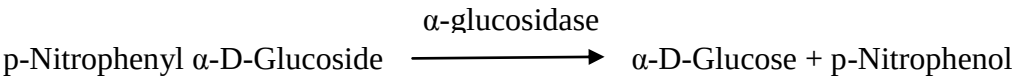

For the preparation of the assay solutions, 10 ml of p-nitrophenyl α-D-glucoside in deionized water (10mM), 50 ml of sodium carbonate in deionized water (100 mM), 10 ml of glutathione in deionized water (3 mM), 100 ml of potassium phosphate buffer in deionized water (PBS, 0.2 M, pH 6.8 at 37 ^{o}C) and an α-glucosidase enzyme solution (0.05 mg in 1 ml PBS buffer solution) were freshly prepared. For the assay procedure of free α-glucosidase, 10-ml conical plastic tubes were used. Two tubes were used for each run. One tube contained the sample under investigation and was named as “sample tube”. The other tube contained everything but the sample and was named as “blank tube”. To each blank and sample tube, 5 ml of PBS buffer solution and 0.2 ml of the glutathione solution were added. 0.2 ml of the enzyme solution were added in the sample tube, whereas 0.2 ml of deionized water were added in the blank tube. Both tubes were agitated and equilibrated at 37 ^{o}C, before 0.5 ml of the p-nitrophenyl α-D-glucoside solution were added

to both of the tubes. The solutions were then equilibrated at 37 ^{o}C for 20 min. 2 ml of each mixture (sample and blank) were pipetted in two separate suitable vials, and 8 ml of the sodium carbonate solution were added in both mixtures. The absorption of both mixtures at 400 nm was recorded using a UV-Vis spectrophotometer (Perkin Elmer Lambda 2, Norwalk, CT). The enzymatic activity was calculated using the following equation:

$$\text{Units/(ml enzyme)} = \frac{(A_{400nm}\ \text{Test} - A_{400nm}\ \text{Blank})(v)(V)\ (df)}{(\varepsilon)(t)(v)(0.2)}$$

where v is the volume (in ml) of colorimetric determination (10 ml), V is the volume (in ml) of reaction mixture (5.9 ml), df is the dilution factor, ε is the millimolar extinction coefficient of p-nitrophenol at 400 nm (18.3), t is the time (in minutes) of the assay (20 min.) and ν is the volume (in ml) of the reaction mixture used in the colorimetric determination (2 ml).

For the hybrid materials containing α-glucosidase, all samples were first washed extensively with a dilute buffer solution before the activity measurements. A specific amount of solid (e.g., 5.1 mg for HIIF50) was weighed into a 10-ml centrifuge tube. 10 ml of potassium phosphate buffer solution (PBS, 0.2 M, pH=6.8 at 37 ^{o}C) were then added in the tube to soak the samples under agitation. After 2 hr of continuous agitation, the washing solution was separated from the solid by decantation after centrifugation. This procedure was repeated twice for a 2-hr interval each. The above-mentioned assay procedure was used to test for the activity of the encapsulated α-glucosidase except for replacing the 0.2 ml of enzyme solution in the sample tube with a predetermined amount of powdered material (e.g., 5.1 mg for HIIF50) and 0.2 ml of buffer PBS solution.

The PBS washing solutions that were used to wash the powdered hybrid materials, which contained the encapsulated α-glucosidase, were also assayed for α-glucosidase activity the same way, as in the case of HRP, to evaluate the efficiency of the encapsulation. Same as HRP, it is assumed that the α-glucosidase activity is not altered by the immobilization procedure or the presence of minor amounts of other chemicals (fructose, etc.). Activity assay results of these washing solutions indicate that the amount of the unbound, loosely trapped, leached or surface absorbed α-glucosidase in the as-synthesized mesoporous materials may be considered insignificant.

9.6 Results and Discussion

9.6.1 Synthesis and Compositions

Alkyl-modified (methyl and phenyl) mesoporous hybrid silica materials have been synthesized via the acid-catalyzed hydrolysis and co-condensation of TMOS with MTMS or PhTMS in the presence of fructose as the pore-forming agent. Upon removal of the template by washing, the mesopores of the hybrid materials become accessible, and the encapsulated enzyme is now free to interact with any substrate that may enter through the pores of the organosilica. The compositions of the hybrid organosilica materials, prepared via the nonsurfactant-templated sol-gel method, and the pore parameters of these mesoporous materials upon removal of the nonsurfactant template are summarized in **Table 9-1** and **Table 9-2**, respectively**.** The theoretical fructose compositions, calculated from the initial feed stoicheiometry, are also presented in the same table and compared to those determined from the TGA experiments. The small discrepancies that are observed may be attributed to incomplete hydrolysis/condensation of the

sol-gel products and/or incomplete removal of the volatile solvents and the sol-gel by-products (e.g., water and alcohol).

9.6.2 Surface Area and Pore Structure

Among many techniques to characterize the porous structure of solid materials, the nitrogen adsorption method is the most popular. By utilizing this technique, one can obtain the total pore volume, the BET surface area and the pore size distribution. **Figure 9-1** depicts representative N_2 adsorption-desorption isotherms for water-extracted methyl-containing hybrid materials. When no template has been added, the specific surface area for sample HIIIF0 is equal to 0.007 m^2/g and the pore volume equal to 0.018 cm^3/g, which is justified from the fact that material is a nonporous solid. On the other hand, as the fructose content is increased, the isotherms change gradually from the reversible type I, typical for microporous solids (HIIIF20), to that similar to type IV with H2 hysteresis for mesoporosity (HIIIF50). For example, HIIIF50 sample, which contains 50 wt% of fructose, shows high surface area (~511 m^2/g), high pore volume (~ 0.3 m^3/g) and H2 hysteresis indicative of mesoporosity (**Figure 9-1**). From **Table 9-2,** it is evident that phenyl-modified hybrids show a similar trend as the methyl modified ones, with greater surface area and pore volume upon increase of the fructose percentage. It is noteworthy that the phenyl-modified hybrid materials show lower surface area and pore volume compared to the methyl-modified, which may be attributed to the larger phenyl group. It has also to be noted that there exists a threshold of the ratio of TMOS to PhTMS, below which there exists a phase separation of the precursors, and the solidified material appears opaque. Similar to previous studies conducted in our lab, this threshold appeared to be at a TMOS/PhTMS molar ratio equal to 20, and thus lower molar ratios of TMOS/PhTMS were not further investigated.

9.6.3 Preparation of Enzyme-Containing Hybrid Sol-Gels

A series of different hybrid materials have been investigated to evaluate their efficiency on immobilizing and protecting horseradish peroxidase and α-glucosidase. Formulations tried include precursors such as TMOS, MTMS, PhTMS, and different ratios of them. The highest activities obtained, for all of the as-synthesized hybrids, were observed for those with 50 wt% of fructose as template. Higher percentages of fructose (e.g., 60 wt%) generally led to inhomogeneous mixtures and were not further investigated.

9.6.3.1 Evaluation of Encapsulation Efficiency

This nonsurfactant-templated method, which has been invented in our lab, has been previously utilized to encapsulate and protect a variety of enzymes.[6-9] Herein, I am presenting the investigation of this approach to encapsulate and maintain the enzymatic activity of horseradish peroxidase and α-glucosidase. The encapsulation of these two enzymes was accomplished by simply adding the buffer solution, containing the respective enzyme, with a specific amount of fructose into the sol-gel intermediates before gelation occurred. Aging and drying of the resulting gel yielded an enzyme-containing hybrid material. It has to be noted that the gelation of these hybrid materials was significantly shortened upon addition of the fructose and the enzyme solution, because of the raise of the solution's pH to neutral values of pH, which facilitates gelation.

The activity values of horseradish peroxidase immobilized in a variety of different organosilica hybrids are summarized on **Table 9-3**. Different compositions have been explored by changing the type of precursors, the ratios of them and the amount of template used. Increasing the amount of template, up to a threshold, leads to increased catalytic activities of

immobilized HRP. The control sample (e.g., HIFO) prepared in the absence of fructose exhibits extremely low activity, whereas the HRP-containing hybrids synthesized in the presence of template show dramatically higher activities (e.g., HIIF50 =27.9 u/mg). HRP appears to be more efficiently encapsulated in TMOS/MTMS with a molar ratio of 3:1. HIIIF50 sample shows 54 % of residual activity with regard to the free enzyme. In order to evaluate for the efficiency of the encapsulation method, the buffer solutions, used for removing the template of the as-synthesized hybrid materials, were collected after washing. Activity assays of these washing solutions were performed following the same, previously mentioned, procedures. The zero catalytic activity values obtained for these solutions proved the almost-complete and efficient entrapment of HRP within the organo-silica matrix.

The encapsulation of α-glucosidase in hybrids of different compositions has been also investigated. Just as in the case of HRP, increasing the amount of template up to a threshold, leads to increased catalytic activities of immobilized α-glucosidase. A control sample (e.g., HIIF0) prepared in the absence of fructose shows almost no remaining activity, whereas the α-glucosidase-containing hybrids, synthesized in the presence of 50 wt% of fructose template (e.g., HIIF50), show 12% of residual activity compared to the native enzyme. Alpha-glucosidase appears to be more efficiently encapsulated in TMOS/PhTMS with a molar ratio of 20:1. HIIIIF50 sample shows 19 % of residual activity with regard to the free enzyme. As in the case of HRP, and in order to evaluate for the efficiency of the encapsulation method, the buffer solutions, used for washing during the activity assays of the as-synthesized powdered materials, were also tested for catalytic activity (presented zero catalytic activities). In a similar manner to HRP, these results prove the almost complete and efficient entrapment of α-glucosidase within

the organosilica matrix. Consequently, for both types of enzymes (i.e., HRP and α-glucosidase), the amount of unbound, loosely trapped, leaching or surface absorbed enzyme in the as-synthesized hybrid materials may be considered insignificant.

The as-synthesized HRP-containing organosilicas have been further tested for enzymatic activity after a prolonged storage in hostile environments such as organic solvents, laundry detergent and high pH aqueous solvents. The powdered hybrid materials containing the encapsulated HRP have been evaluated for their residual enzymatic activity after storage for 24 hr in non-aqueous solvents, such as toluene and ethanol, laundry detergent (purex) and aqueous buffer solutions of high pH values. These activity values can be seen on **Table 9-4**. Unfortunately these values seem not satisfactory, and thus another approach that involves a double encapsulation procedure has been explored, as will be explained below.

9.6.4 Double Encapsulation Process

9.6.4.1 Synthesis Procedure

A double encapsulation approach has been developed as a means to protect HRP and maintain its enzymatic residual activity, after storage in harsh aqueous and non-aqueous media, for a prolonged period of time. This double encapsulation method comprises a two-step procedure. First, the nonsurfactant-templated sol-gel method has been again utilized to encapsulate HRP into mesoporous hybrid organosilica. For this study, the composition that was used was the one that employed TMOS and MTMS, in a ratio of 3 to 1, since this is the one that showed the highest residual enzymatic activity of encapsulated HRP, as reported in the previous sections of this chapter. For the first encapsulation step, an aqueous solution of fructose (used as the nonsurfactant template) was added to a prehydrolyzed solution of tetramethyl orthosilicate

(TMOS) and methyl trimethoxysilane (MTMS) catalyzed by HCl. The phosphate buffer solution (0.2 M PBS, pH = 7.2 at 24 ^{o}C), containing the enzyme, was then added to the above mixture and allowed to gel, followed by the evaporation of the solvents and the small molecular byproducts of the sol-gel reaction (e.g., methanol and water). The dry sol-gel hybrid was then crushed into a fine powder by means of a pestle and a mortar. The powdered enzyme-containing silica hybrid was then coated with a mixture of triethyleneglycol dimethacrylate (TEGDMA), polyethylene glycol (PEG) and catalytic amounts of the photoinitiators, i.e., camphorquinone (CQ) and N-phenyl glycene (NPG). Photopolymerization of the obtained viscous suspension for 4.5 min resulted in a composite, which was crushed again to produce the second protective layer.

As a typical procedure for the synthesis of an HRP-doped sol-gel doubly encapsulated hybrid, 3.19 g of TMOS (21 mmol), 0.95 g of MTMS (7 mmol), 0.94 g of H_2O (52 mmol) and 650 μL of a 40 mM HCl aqueous solution (1.5 x 10^{-2} mmol) were charged in a 50-ml single-neck flask. The mixture was magnetically stirred at room temperature in air. Within a few minutes, the mixture became homogeneous, accompanied by the raise in temperature. After about 20 min of stirring, the solution came back to room temperature. 2.57 g of fructose and 2.57 g of distilled water were added in 5.09 g of the above solution under agitation, and the resulting solution was transferred into an ice bath until the temperature of the mixture reached 2-4 ^{o}C. 1.0 ml of HRP solution, prepared by dissolving 1.0 mg of HRP in 1 ml of PBS buffer solution (0.2 M, pH = 7.2 at 24 ^{o}C), was then added into the above mixture and the sample was sealed with a paraffin film with about 15-20 pinholes to allow for the further sol-gel condensation and the evaporation of solvents and byproducts of the sol-gel reactions (e.g., water and methanol). The sample was kept in a refrigerator (at 3-5 ^{o}C) for 24 hr, before it was transferred into a container that was held

under high vacuum (about 11 mm Hg) in an ice-water bath held at 3-5 ^{o}C. The product was checked occasionally for weight loss and it remained under high vacuum until constant weight was reached (< 0.5 % in weight change in a 24-hr period). The obtained solidified HRP-containing hybrid was then crushed into a fine powder by means of a mortar and a pestle, passed through a 30-square mesh wire cloth and stored in a moisture-free freezer at -20 ^{o}C for the next step to follow.

For the second encapsulation step, camphorquinone (0.5 wt %) and N-phenylglycine (0.3 wt %) were dissolved in 10 g of triethyleneglycol dimethacrylate (TEGDMA) under sonication until a clear yellow solution was obtained. To 9 g by weight of this mixture, 1 g of polyethylene glycol (PEG, MW=4,600) was added, and the final mixture was sonicated until a totally transparent solution was obtained. This solution needed to be kept relatively warm (~30 °C) to prevent the precipitation of polyethylene glycol. The powdered, HRP-containing silica hybrid was then thoroughly mixed with the TEGDMA/PEG mixture in a 1:1 weight ratio using a spatula. The obtained viscous suspension was cast as a thin layer (no more than 5 mm thick) onto a clean microscope slide. The slide was placed in a photo-curing oven (460 nm, LED Curedome, Prototech, OR) commonly used for polymerization of dental composites. Samples were cured for 90 sec followed by crushing by means of a mortar and a pestle and passed through a 40-square mesh wire cloth. This process was repeated three times to ensure that most of the mesoporous hybrid silica particles have been coated with the second acrylic coating, and that the surface area is as high as possible. It is worth mentioning that the photo-polymerization of the second acrylic coating was done in three separate steps of 90 sec each, instead of performing it in 270 sec all at once. This was done in order to avoid, as much as possible, the heat generated due to the

exorthemic curing, which may result in the denaturation of the encapsulated HRP. Finally, the doubly encapsulated HRP-containing organosilica was passed through a 30-mesh screen.

9.6.4.2 Protection in Harsh Enviroments

As reported earlier, encapsulated HRP in sol-gel hybrids showed medium to poor residual enzymatic activities after storage for 24 hr in harsh media. Unfortunately, these values were not satisfactory enough, since there is lots of room of improvement. With regards to that, a double encapsulation method has been investigated as a means to protect enzymes from hostile environments, such as toluene, ethanol, laundry detergent and high pH aqueous solutions. This double encapsulation process involves the encapsulation of HRP in mesoporous sol-gel hybrids followed by the application of a second acrylic layer. The outer acrylic layer, which is composed of crosslinked TEGDMA, is insoluble in high pH aqueous media as well as organic solvents. This prevents the harsh media from entering the pores of the interior organosilica moiety and denaturing the enzyme. On the other hand, the PEG component of the outer layer, which serves as the outer template, is water soluble and biodegradable. Thus, when the enzyme-containing powdered material is washed with an excess of water, the PEG dissolves, thereby creating pores in the outer layer. The fructose contained inside the mesopores of the inner hybrid sol-gel coating is also removed during washing, and the enzyme is now free to interact with any substrate that may enter through the pores of the mesoporous organosilica. It is worth mentioning that this ‘double encapsulation’ technique is completely independent of the nature of the enzyme, and thus, it may be utilized as a means of protection of a variety of enzymes from hostile environments.

9.6.4.2.1 Aqueous Solutions

Nowadays, enzymes are used for an increasing range of industrial applications, including pharmaceutical, laundering, detoxification and animal feeding industries. In many of these applications, the utilization of high pH aqueous solutions is unavoidable. As a result, it is of crucial importance to find a method to protect enzymes that are to be stored and used in such harsh enviroments, and maintain their enzymatic activity at reasonably good levels. The double encapsulation approach, which has been described earlier in this chapter, has been explored as a method to encapsulate and maintain the residual catalytic activity of HRP while storing the enzyme encapsulates in high pH aqueous and detergent solutions. 40 mg of the HRP-containing hybrid materials, synthesized by the double encapsulation method, were placed in three separate 3-ml glass UV-cuvettes. 3 ml of an aqueous buffer solution (potassium chloride 0.37 wt %, potassium hydroxide 0.1 wt %, thymol 0.05 wt %, LabChem Inc.), with a pH of 10 at 24 ^{o}C, was added in one of these cuvettes. In the next cuvette, 3 ml of a buffer solution (potassium carbonate, potassium borate and potassium hydroxide, Fisher Scientific), showing a pH equal to 13 at 24 ^{o}C, was added. Finaly in the last cuvette, 3 ml of a detergent solution (Purex, Pure Clean Technology, Dial Corp.) was added. The materials were kept in these high pH media for 24 hr under agitation before the supernatants were removed for the assay procedures to follow. All samples were first washed extensively with a dilute buffer solution before the activity measurements. 10 ml of potassium phosphate buffer solution (0.2 M, pH 7.2 at 24 ^{o}C) were added in the tube to soak the samples under agitation. After 2 hr of continuous agitation, the washing solutions were separated from the solids by decantation after centrifugation. This procedure was repeated twice for a two-hour interval each. The assay procedure that was used to test for the activity of the doubly encapsulated HRP was the same as the one used for HRP

encapsulated in sol-gel hybrids and which has been reported in section 9.4.2.3. As can be seen in **Figure 9-2**, doubly encapsulated HRP shows 29 % of residual activity after storage of the material in the pH-10 buffer solution for 24 hr. From the same figure, doubly encapsulated HRP shows 13% of the original enzymatic activity after storage for 24 hr in the detergent solution. On the other hand, the material shows 1% of the original enzymatic activity when the material was stored in a buffer solution with a pH equal to 13 (not shown in this figure). Noteworthy, the native enzyme was rendered completely inactive when stored in these high pH aqueous solutions for 24 hr. This double encapsulation technology shows promising results, and may be a means to protect a variety of enzymes from highly alkaline aqueous solutions. At this point, it should be mentioned that the purpose of testing the materials in the pH 13 aqueous buffer solution was to explore the limits of this protection method, and not because the enzyme encapsulates might be stored in such high pH environments in any specific potential applications. It seems that such highly alkaline solutions are highly corrosive for this double encapsulation technology to protect HRP. Undergoing optimization of this process in our lab may lead to an even better protection of the encapsulated enzyme from highly alkaline solutions.

9.6.4.2.2 Non-Aqueous Solvents

Enzymes have found numerous applications as catalysts in chemical and pharmaceutical syntheses, and as recognition elements in biosensors. Many of these technologies utilize the enzymatic activity in nonaqueous solutions. There are several beneficial reasons for utilizing enzymes in nonaqueous media, including the solubility of many substrates in such solvents, the inhibition of side reactions promoted by water, the enzymatic selectivity, and the ability to control this selectivity with the solvent.[42] As in the case of harsh aqueous media, the novel

double encapsulation technology has been investigated as a means to protect the encapsulated enzyme from hostile, for enzymes, organic media, including toluene and ethanol. 40 mg of the HRP-containing hybrid material, synthesized by the double encapsulation method, were submerged in 2.5 ml of toluene in a 3-ml square glass UV-cuvette. In another glass cuvette, the material was submerged in 2.5 ml of ethanol. Both samples were stored in the nonaqueous solutions for 24 hr under agitation before the supernatants were removed for the assay procedures to follow. Both enzyme encapsulates were first washed extensively with a dilute buffer solution before the activity measurements. 10 ml of potassium phosphate buffer solution (0.2 M, pH 7.2 at 24 ^{o}C) were added in the tube to soak the samples under agitation. After 2 hr of continuous agitation, the washing solutions were separated from the solid by decantation after centrifugation. This procedure was repeated twice for a two-hour interval each. The assay procedure that was used to test for the activity of the doubly encapsulated HRP was the same as the one used for HRP encapsulated in sol-gel hybrids, and which has been reported in earlier.

As can be seen in **Figure 9-3,** doubly encapsulated HRP shows 27 % of residual enzymatic activity after storage for 24 hr in ethanol. Storage of the HRP encapsulates in toluene results in 31 % of residual HRP activity with regards to the enzymatic activity of the original enzyme. It is noteworthy that the native enzyme was rendered completely inactive when stored in ethanol or toluene under the same conditions. **Figure 9-4** shows the time study that was conducted for both the sol-gel hybrid (e.g., HIIIF50) and the doubly encapsulated HRP in ethanol. The materials were stored in ethanol and were assayed for residual enzymatic activity at predetermined periods of time, following the above mentioned assay procedures. As can be seen from this figure, HRP encapsulated in sol-gel hybrids undergoes a dramatic loss of its enzymatic

activity even after one hour of storage of the material in ethanol (e.g., 11% of residual activity after 1 hour with respect to original HRP activity). On the other hand, even after 4 hours of storage in ethanol solution, doubly encapsulated HRP shows higher levels of residual enzymatic activity, that is 32 % with respect to the original HRP activity. These results indicate the promising nature of this novel double encapsulation technology. As stated earlier, this method is completely independent of the type and nature of the encapsulated enzyme and may thus be a means to protect a variety of enzymes from several non-aqueous solvents. In order to acquire higher residual enzymatic activity, optimization of the method by changing the ratios and/or types of templates that are used is under way in our laboratory.

9.6 Conclusions

The encapsulation of horseradish peroxidase (HRP) and alpha glucosidase, as model enzymes for a range of applications, in various mesoporous hybrid materials has been presented. Several different precursors have been investigated to find the optimum formulation, and the obtained materials were characterized by thermogravimetric analysis (TGA) and nitrogen adsorption analysis (BET). Enzymatic assays for HRP and α-glucosidase revealed the compositions of the organosilicas that led to the optimum residual activity of the encapsulated enzymes. In addition, a novel technology for maintaining the enzymatic activity, during storage in harsh media, such as organic solvents and high pH aqueous solutions, has been presented. The non-surfactant templated sol-gel method has been again utilized to incorporate HRP enzyme into the pores of mesoporous organosilicas followed by the application of a second acrylic protective layer. Results indicate that the doubly encapsulated HRP showed many orders of magnitude higher residual activity after storage for 24 hr in high pH buffer solution, detergent, ethanol and

toluene, as compared to the native enzyme under the same conditions. Since this ‘double encapsulation’ technique is completely independent of the nature of the enzyme, it is expected to be useful for stabilizing other enzymes in such hostile environments as well. Further optimization of this method is underway in our lab.

9.7 Acknowledgments

A portion of this work has been in collaboration with Mr. Indraniel Mukherjee and Mr. Sudipto Das. I would like to thank Mr. Tom Hughes and Mr. Colin Murray of Reacta Corporation and Dr. Joseph De Frank of US Army Edgewood Research Center, MD, for their valuable input in this project. The funding from Reacta Corporation and ATTI at Maryland TEDCO for this project is greatly appreciated.

Table 9-1. Compositions of hybrids synthesized

Sample code	TMOS (g)	MTMS (g)	PhTMS (mg)	H_2O (g)	HCl (µl) (40 mM solution)	Fructose (g)
HIF0	2.9	2.04	-	0.95	131	0
HIF20	2.9	2.04	-	0.95	131	0.67
HIF50	2.9	2.04	-	0.95	131	2.74
HIIF0	3.04	1.36	-	1.26	175	0
HIIF20	3.04	1.36	-	1.26	175	0.69
HIIF50	3.04	1.36	-	1.26	175	2.76
HIIIF0	3.19	0.95	-	0.94	130	0
HIIIF20	3.19	0.95	-	0.94	130	0.64
HIIIF50	3.19	0.95	-	0.94	130	2.57
HIIIIF0	3.2	-	208	0.78	107	0
HIIIIF20	3.2	-	208	0.78	107	0.52
HIIIIF50	3.2	-	208	0.78	107	2.1

HIFX: TMOS/MTMS mol ratio = 1, where X is the wt% of fructose added. HIIFX: TMOS/MTMS mol ratio = 2, where X is the wt% of fructose added. HIIIFX: TMOS/MTMS mol ratio = 3, where X is the wt% of fructose added. HIIIIFX: TMOS/PhTMS mole ratio = 20, where X is the wt% of fructose added. The wt% of fructose is calculated with regards to the final weight of the hybrid. It is assumed that the sol-gel reaction is driven to completeness.

Table 9-2. Pore structure parameters of hybrids investigated, after removal of template (fructose) by extensive washing with PBS buffer solution.

Sample ID	D-fructose (wt%)		S_{BET} (m^2g^{-1})[c]	V_{SP} (cm^3g^{-1})[d]	Micropore[e]	
	Theor.[a]	Exp.[b]			area (m^2g^{-1})	vol (cm^3g^{-1})
HI-F0	0	0	0.13	0.042	3.7	0.007
HI-F20	20	22	381	0.15	136	0.1
HI-F50	50	53	504	0.29	163	0.08
HII-F0	0	5	0.16	0.034	2.17	0.0017
HII-F20	20	23	481	0.27	304	0.17
HII-F50	50	55	603	0.36	206	0.11
HIII-F0	0	8	0.007	0.018	1.7	0.0007
HIII-F20	20	24	294	0.17	225	0.12
HIII-F50	50	53	511	0.29	266	0.15
HIII-F0	0	7	0.04	0.077	5.2	0.042
HIII-F20	20	23	264	0.14	167	0.04
HIII-F50	50	52	465	0.22	183	0.11

[a] Theoretical percentage with regards to the feeding compositions.

[b] Experimental percentage as determined by TGA.

[c] Average BET surface area.

[d] The single point pore volume determined at P/P_o~1.

[e] The BET pore diameter calculated from 4V/S.

Table 9-3. Activity values for enzymes encapsulated in sol-gel hybrids.

Sample code	HRP		A-glucosidase	
	Activity[a] (u/mg)	**Activity[b] (%)**	**Activity[c] (u/mg)**	**Activity[d] (%)**
HIF0	1.2	1	0.05	1
HIF20	5.1	4	0.17	3
HIF50	15.2	12	0.62	11
HIIF0	1.2	1	0.11	2
HIIF20	7.6	6	0.51	9
HIIF50	27.9	22	0.68	12
HIIIF0	2.5	2	0	0
HIIIF20	13.9	11	0.11	2
HIIIF50	68.6	54	0.62	11
HIIIIF0	2.7	2	0.04	1
HIIIIF20	8.9	7	0.63	12
HIIIIF50	15.3	12	1.08	19
Pure enzyme	127	100	5.7	100

[a] Absolute enzymatic activity values for encapsulated HRP were measured according to the activity assay procedure explained in section 9.4.2.3.

[b] Absolute enzymatic activity values for encapsulated α-glucosidase were measured according to the activity assay procedure explained in section 9.4.2.4.

[c] With regards to the enzymatic activity of native HRP.

[d] With regards to the enzymatic activity of native α-glucosidase.

Table 9-4. Residual enzymatic activity of encapsulated HRP in sol-gel hybrids, after storage for 24 hr in harsh aqueous and non-aqueous solvents.

Harsh media	**Residual HRP activity**	
	u/mg	**(%)[a]**
Toluene	10.1	8
Ethanol	5.1	4
Laundry detergent	6.3	5
PBS buffer solution (pH=10 at 24 ^{o}C)	6.2	5
PBS buffer solution (pH=13 at 24 ^{o}C)	0	0

Free HRP becomes completely inactive under the same conditions.

[a] With respect to the enzymatic activity of free HRP (127 u/mg).

Table 9-5. Residual enzymatic activity of doubly encapsulated HRP after storage for 24 hours in harsh aqueous and non-aqueous solvents.

Harsh media	**Residual HRP activity**	
	u/mg	**(%)[a]**
Toluene	39.4	31
Ethanol	34.2	27
Laundry detergent	16.5	13
PBS buffer solution (pH=10 at 24 ^{o}C)	34.3	27
PBS buffer solution (pH=13 at 24 ^{o}C)	12.7	1

Free HRP becomes completely inactive under the same conditions.

[a] With respect to the enzymatic activity of free HRP (127 u/mg).

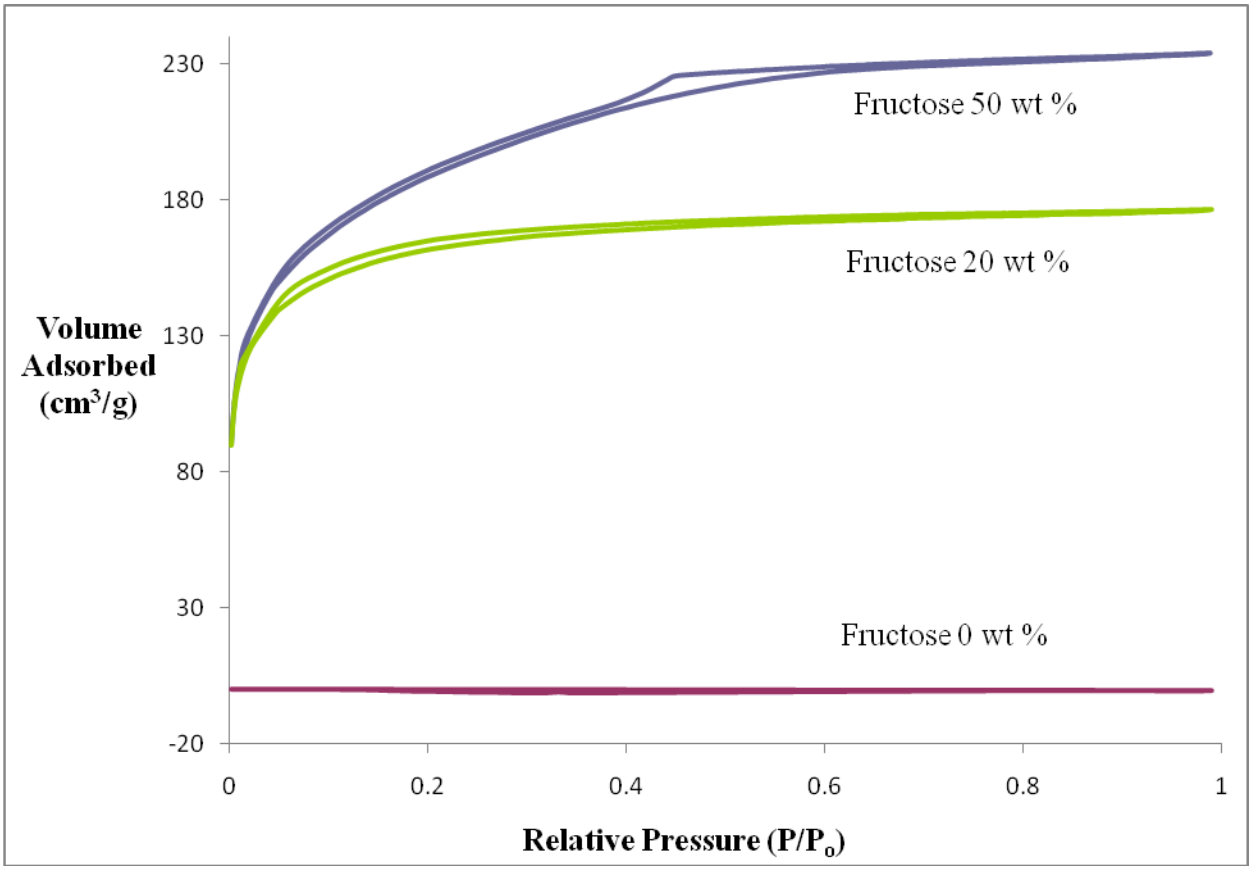

Figure 9-1. Nitrogen adsorption-desorption curves for hybrids containing 0, 20 and 50 wt % of fructose denoted as HIIIF0, HIIIF20 and HIIIF50, respectively.

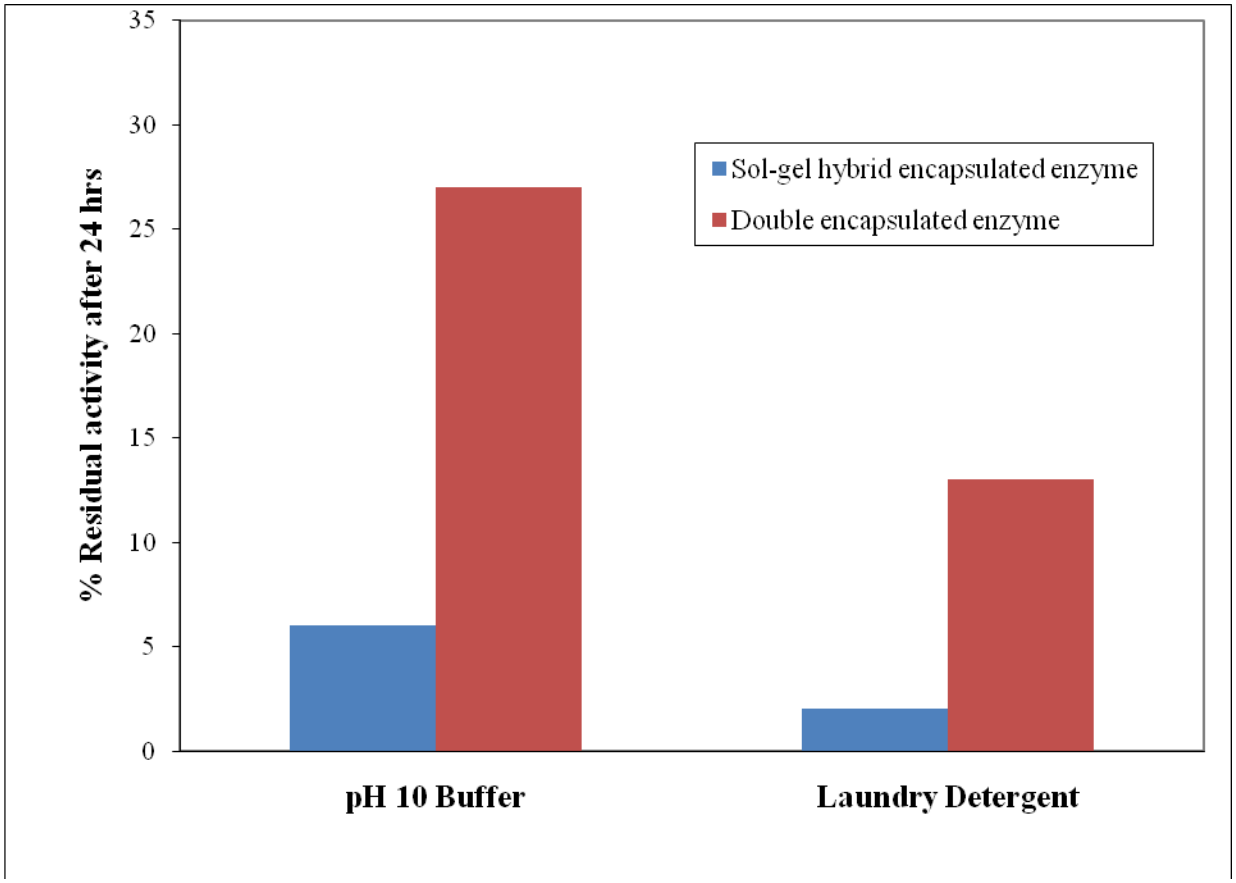

Figure 9-2. Remaining enzymatic activity of HRP encapsulated in sol-gel hybrids (e.g., HIIIF50) and in hybrids made by the double encapsulation procedure after storage under agitation for 24 hr in buffer (pH=10 at 24 ^{o}C) and detergent (purex) solutions.

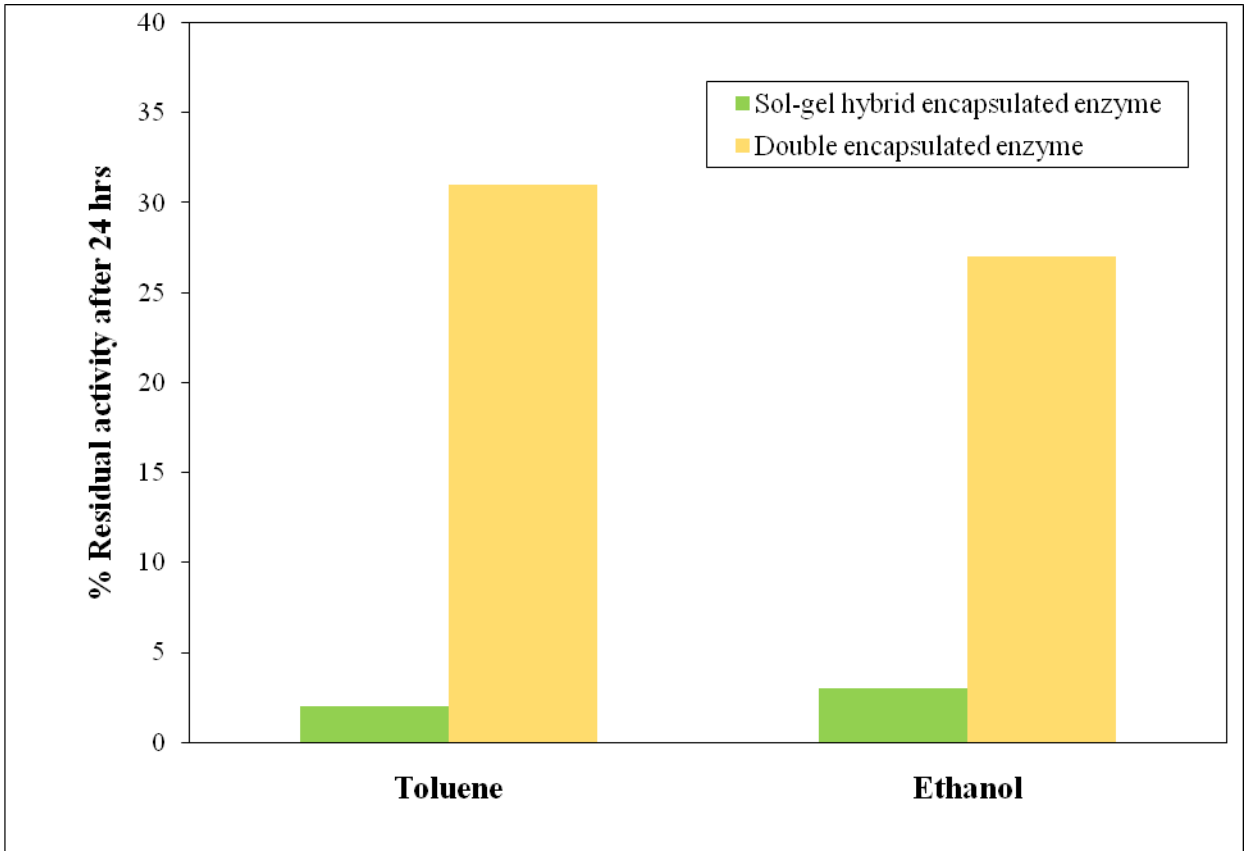

Figure 9-3. Residual enzymatic activity of HRP encapsulated in sol-gel hybrids (e.g., HIIIF50) and in hybrids synthesized by the double encapsulation procedure after storage under agitation for 24 hr in toluene and ethanol.

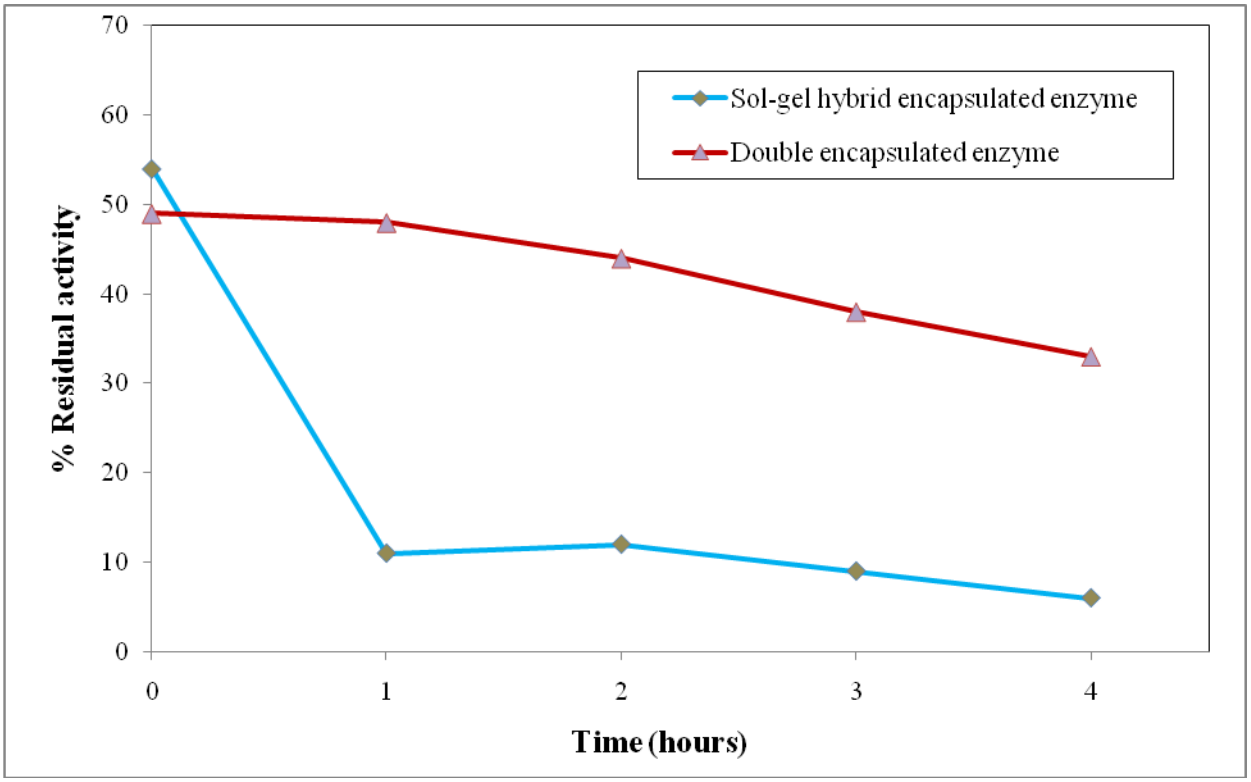

Figure 9-4. Time study of the residual enzymatic activity of HRP encapsulated in sol-gel hybrids (e.g., HIIIF50) and in hybrids synthesized by the double encapsulation procedure after storage for 4 hr in toluene.

9.8 Reference List

1. Khmelnitsky, Y., Welch, S., Clark, D., Dordick, J. Salts dramatically enhance activity of enzymes suspended in organic solvents. Journal of the American Chemical Society (1994), 116, 2647-2648.

2. Smith, K., Silvernail, N. J., Rodgers, K. R., Elgren, T. E., Castro, M., Parker, R. M. Sol-gel encapsulated horseradish peroxidase: A catalytic material for peroxidation. Journal of the American Chemical Society (2002), 124, 4247-4252.

3. Yang, X. Y., Li, Z. Q., Liu, B., Klein-Hofmann, A., Tian, G., Feng, Y. F., Ding, Y., Su, D. S., Xiao, F. S. "Fish-in-Net" encapsulation of enzymes in macroporous cages for stable, reusable, and active heterogeneous biocatalysts. Advanced Materials (2006), 18, 410-414.

4. Mohan, S. V., Prasad, K. K., Rao, N. C., Sarma, P. N. Acid azo dye degradation by free and immobilized horseradish peroxidase (HRP) catalyzed process. Chemosphere (2005), 58, 1097-1105.

5. Eppler, R. K., Komor, R. S., Huynh, J., Dordick, J. S., Reimer, J. A., Clark, D. S. Water dynamics and salt-activation of enzymes in organic media: Mechanistic implications revealed by NMR spectroscopy. Proceedings of the National Academy of Sciences of the United States of America (2006), 103, 5706-5710.

6. Wei, Y., Xu, J., Feng, Q., Dong, H., Lin, M. Encapsulation of enzymes in mesoporous host materials via the nonsurfactant-templated sol-gel process. Materials Letters (2000), 44, 6-11.

7. Wei, Y., Dong, H., Xu, J., Feng, Q. Simultaneous immobilization of horseradish peroxidase and glucose oxidase in mesoporous sol-gel host materials. ChemPhysChem (2002), 3, 802-808.

8. Wei, Y., Xu, J., Feng, Q., Lin, M., Dong, H., Zhang, W. J., Wang, C. A novel method for enzyme immobilization: Direct encapsulation of acid phosphatase in nanoporous silica host materials. Journal of Nanoscience and Nanotechnology (2001), 1, 83-93.

9. Patel, A. C., Li, S., Jian-Min, Y., Wei, Y. In situ encapsulation of horseradish peroxidase in electrospun porous silica fibers for potential biosensor applications. Nanomaterials (2006), 6, 1042-1046.

10. Fishman, A., Levy, I., Cogan, U., Shoseyov, O. Stabilization of horseradish peroxidase in aqueous-organic media by immobilization onto cellulose using a cellulose-binding-domain. Journal of Molecular Catalysis. B, Enzymatic (2002), 18, 121-131.

11. Ru, M. T., Hirokane, S. Y., Lo, A. S., Dordick, J. S., Reimer, J. A., Clark, D. S. On the salt-induced activation of lyophilized enzymes in organic solvents: Effect of salt kosmotropicity on enzyme activity. Journal of the American Chemical Society (2000), 122, 1565 -1571.

12. Ru, M. T., Dordick, J. S., Reimer, J. A., Clark, D. S. Optimizing the salt-induced activation of enzymes in organic solvents:Effects of lyophilization time and water content. Biotechnology and Bioengineering (1999), 63, 233-241.

13. Kim, J., Dordick, J. S. Unusual salt and solvent dependence of a protease from an extreme halophile. Biotechnology and Bioengineering (1997), 53, 471-479.

14. Yano, S., Iwata, K., Kurita, K. Physical properties and structure of organic-inorganic hybrid materials produced by sol-gel process. Materials Science and Engineering C (1998), 6, 75-90.

15. Husing, N., Schubert, U. Formation and structure of porous gel networks from $Si(OMe)_4$ in the presence of $A(CH_2)_nSi(OR)_3$ (A = Functional Group). Chemistry of Materials (1998), 10, 3024-3032.

16. Schwertfeger, F., Husing, N., Schubert, U., Influence of the nature of organic groups on the properties of organically modified silica aerogels. Journal of Sol-Gel Science and Technology (1994), 2, 103-108.

17. Schwerfeger, F., Glaubitt, W., Schubert, U. Hydrophobic aerogels from $Si(OMe)_4$/ $MeSi(OMe)_3$ mixtures. Journal of Non-Crystalline Solids (1992), 145, 85-89.

18. Bambrough, C. M., Slade, R. C., Williams, R. T., Burkett, S. L., Sims, S. D., Mann, S. Sorption of nitrogen, water vapor, and benzene by a phenyl-modified MCM-41 sorbent. Journal of Colloid and Interface Science (1998), 201, 220-222.

19. Mann, S., Burkett, S. L., Davis, S. A., Fowler, C. E., Menselson, N. H., Sims, S. D., Walsh, D., Whilton, N. T. Sol-gel synthesis of organized matter. Chemistry of Materials (1997), 9, 2300-2310.

20. Capozzi, C. A., Condrate, Sr., R.A., Pye, L. D., Hapanowicz, R. P. Vibrational spectral/structural changes from the hydrolysis/polycondensation of methyl-modified silicates II. Comparisons for condensates from the binary diethoxydimethylsilane/tetramethoxysilane system. Materials Letters (1992), 15, 233-241.

21. Boury, B., Chevalier, P., Corriu, R. J. O., Delord, P., Moreau, J. E., Chiman, M. W. Hybrid organic-inorganic xerogel access to meso- and microporous silica by thermal and chemical treatment. Chemistry of Materials (1999), 11, 281-291.

22. Mercier, L., Pinnavaia, T. J. Access in mesoporous materials: Advantages of a uniform pore structure in the design of a heavy metal ion adsorbent for environmental remediation. Advanced Materials (1997), 9, 500-503.

23. Shimojima, A., Sugahara, Y., Kuroda, K. Synthesis of oriented inorganic-organic nanocomposite films from alkyltrialkoxysilane-tetraalkoxysilane mixtures. Journal of the American Chemical Society (1998), 120, 4528-4529.

24. Liu, C., Komarneni, S. S., Smith, D. M., Beck J. S. Advances in porous materials. Materials Research Society, Pittsburgh (1994), 247-252.

25. Schubert, U., Hüsing, N., Lorenz, A. Hybrid inorganic-organic materials by sol-gel processing of organofunctional metal alkoxides. Chemistry of Materials (1995), 7, 2010-2027.

26. Raman, N. K., Anderson, M. T., Brinker, C. J. Template-based approaches to the preparation of amorphous, nanoporous silicas. Chemistry of Materials (1996), 8, 1682-1701.

27. Wen, J., Wilkes, G. L. Organic/inorganic hybrid network materials by the sol-gel approach. Chemistry of Materials (1996), 8, 1667-1681.

28. Interrante, L. V., Hampden-Smith, M. J. Chemistry of advanced materials, An overview. Wiley-VCH, New York; 1998.

29. Husing, N., Schwertfeger, F., Tappert, W., Schubert, U. Influence of supercritical drying fluid on structure and properties of organically modified silica aerogels. Journal of Non-Crystalline Solids (1995), 186, 37-43.

30. Lim, M. H., Branford, C. F., Stein, A. Synthesis of ordered microporous silicates with organosulfur surface groups and their applications as solid acid catalysts. Chemistry of Materials (1998), 10, 467-470.

31. Purves, D., Lichtman, J. W. Cell marking with horseradish peroxidase. Principles of Neural Development. Sinauer Associates, Inc., Sunderland; 1985.

32. Vojinovi, V., Azevedo, A. M., Martins, V. C. B., Cabral, J. M. S., Gibson, T. D., Fonseca, L. P. Assay of H_2O_2 by HRP catalyzed co-oxidation of phenol-4-sulphonic acid and 4-aminoantipyrine: characterization and optimization. Journal of Molecular Catalysis B: Enzymatic (2004), 28, 129-135.

33. Berglund, G. I., Carlsson, G. H., Smith, A. T., Szöke, H., Henriksen, A., Hajdu, J. The catalytic pathway of horseradish peroxidase at high resolution. Nature (2002), 417, 463-468.

34. Gajhede, M., Schuller, D. J., Henriksen, A., Smith, A. T., Poulos, T. L. Crystal structure of horseradish peroxidase C at 2.15 Å resolution. Nature Structural Biology (1999), 4, 1032-1038.

35. Veitch, N. C. Horseradish peroxidase: a modern view of a classic enzyme. Phytochemistry (2004), 65, 249-259.

36. Matsumoto, K., Takemata, K., Takayama, K., Kanthi, J. M., Abesundara, T. M., Katayama, H. A novel method for the assay of a-glucosidase inhibitory activity using a multi-channel oxygen sensor. Analytical Sciences (2002), 18, 1315-1319.

37. Lee, D. S., Lee, S. H. Genistein, a soy isoflavone, is a potent α-glucosidase inhibitor. FEBS Letters (2001), 501(1), 84-86.

38. Chapel, C., Garcia, C, Roingeard, P., Zitzmann, N., Dubuisson, J., Dwek, R. A., Trepo, C., Zoulim, F., Durantel, D. Antiviral effect of α-glucosidase inhibitors on viral morphogenesis and binding properties of hepatitis C virus-like particles. Journal of General Virology (2006), 87 (4), 861-871.

39. Dong, H. Organic-inorganic hybrid mesoporous silica materials and their applications as host matrix for protein molecules. PhD thesis. Drexel University, Pennsylvania; 2002.

40. Xu, J. Immobilization of enzymes in mesostructured materials via the nonsurfactant-templated sol-gel chemistry. PhD thesis. Drexel University, Pennsylvania; 2000.

41. Rad, M. A.,Ghourchian, H., Moosavi-Movahedia, A. A., Hong, J., Nazari, K. Spectrophotometric assay for horseradish peroxidase activity based on pyrocatechol-aniline coupling hydrogen donor. Analytical Biochemistry (2007), 362, 38-43.

42. Nakamura, T. Electrochemical biosensors in nonaqueous solutions and their applications. Analytical Sciences (2007), 23, 253-259.

Chapter 10. Conclusions and Future Work

This research work has been focused on polymeric materials, hybrid materials and nanomaterials. These are the three main aspects that form the foundation of this research, which includes the synthesis of biodegradable polymers with adhesive capabilities and the development of a broad range of novel organic-inorganic hybrid materials and nanomaterials for a variety of applications. Two of the main approaches in this research work were: 1) the biomimetic adhesive capabilities of certain chemical groups and 2) hybrid materials prepared via mild synthetic routes, such as the sol-gel method. Applying separately these two concepts, unique, commercially viable and versatile products have been developed. All of the obtained materials, whether these include biodegradable and biocompatible adhesive products or hybrids materials with excellent mechanical and electrochromic properties, have been tested for use in several potential applications. A short descriptive conclusion and the aims accomplished for these different projects will be briefly reviewed in this chapter. Finally some input and suggestions for future work are presented for further optimizing and improving upon the desired properties of the obtained as-synthesized products.

10.1 Modification of Chitosan to Create a Biodegradable, Biocompatible and Non-toxic Adhesive

In this work a series of modified chitosans have been synthesized by a simple method, in an effort to develop a biodegradable, biocompatible and non-toxic adhesive that mimics marine adhesive proteins. The aim was to make a biodegradable adhesive product that would find applications in the dental and biomedical industry. The tensile and shear adhesive strength of these materials has been tested on various surfaces, including porcine skin and beef bone. The

adhesive strength of these materials varies with the molecular weight of the polysaccharide, the amount of diphenolics present on the biodegradable backbone, and the curing time. Adhesiveness was achieved without added enzymes or oxidants. Infrared spectroscopy, nuclear magnetic resonance spectroscopy and ultraviolet-visible spectroscopy have been used in order to qualitatively and quantitatively establish the amount of the diphenolic moiety present on the backbone of the biodegradable polymer. Degradation studies indicate that the degradation rate depends on the diphenolic moiety present on the biodegradable backbone.

The ability of the modified chitosans to adhere to a variety of other surfaces, including metal, glass and plastic, was also tested. The highly reactive o-quinones that result from the oxidation of the phenolic groups present in DHBA by oxygen of air seem to play an important role in the crosslinking and the surface adhesion of the obtained materials. Bearing in mind that chitosan itself has been used in a number of applications as a wound dressing material, the as-synthesized polymers combine both the adhesive capabilities of the diphenol function and the healing effect of chitosan and seem to be extremely promising materials for the dental and/or medical communities. The obtained results indicate that modified chitosans have good biocompatibility and biodegradability and may serve as a substitute for the use of staples, clips and suture placements that are currently employed in the biomedical field.

10.2 Poly(HEMA-GMA-Silica) Hybrid Materials

A new class of optically transparent poly (HEMA-GMA-silica) hybrid materials has been presented. These hybrid materials exhibited low volume shrinkage during polymerization and were crack free during storage (after 12 months). This proves the effectiveness of this new synthesis procedure to remove low-molecular-weight byproduct molecules and to prevent the

further condensation of silanol groups during storage. This new procedure enabled the almost-complete removal of byproduct molecules and yielded products with no internal voids or surface cracks. This system was specifically designed to improve upon the mechanical properties of poly(methyl methacrylate) while maintaining its optical transparency. The mechanical properties of these hybrid materials appear to be composition dependent. Incorporation of silica effectively increased the compressive yield stress and modulus of poly (HEMA-GMA-silica) hybrids. The reproducibility of the synthesis procedure and the improvement in mechanical properties of these polymer hybrids, while not sacrificing optical transparency, demonstrate the feasibility of utilizing these materials in applications that currently utilize acrylic polymers, such as Plexiglas. The significance of this synthetic concept relies on the fact that it makes feasible the covalent incorporation of a variety of organic monomers on to the sol-gel intermediates to develop various organic-inorganic hybrid materials with tunable properties.

10.3 Covalent Incorporation of Polyaniline in Sol-Gel Materials

A series of novel electroactive hybrid materials that have been synthesized by covalent incorporation of polyaniline into polyacrylate-silica hybrids have been presented. The formulation involves the radical co-polymerization of glycidyl methacrylate-polyaniline (GMA-PANi) and glycidyl methacrylate-2-hydroxyethyl methacrylate-silica (GMA-HEMA-silica) to yield poly(HEMA-GMA-silica)-polyaniline (PHGS-PANi) hybrids. This strategy possesses advantages over polyaniline-inorganic macro-composites because polyaniline is homogeneously dispersed at the molecular level across the polyacrylate-silica hybrid, and thus, the properties that polyaniline imparts to the final material are evenly distributed throughout the bulk of the final product. The chromoelectrochemical study suggests that these materials can have tunable colors

upon change of applied electrical potential and/or pH value, and thus may find various applications as chemical or biological sensors and electro-optical devices. Moreover, conductivity measurements and mechanical testing of these materials show that these materials can be prepared to have both a reasonably high conductivity and excellent mechanical properties. The mechanical testing reveals good mechanical properties with greater modulus upon increasing the silica content and with greater compressive strength upon increasing, to a certain extent, the amount of the organic moiety. This new synthesis procedure provides materials that can combine the excellent mechanical and optical properties of silica with the flexibility of incorporating conducting, electroactive and electrochromic polyaniline at the molecular or nanometer level. The final electroactive, electrochromic, conducting and mechanical properties of these hybrid materials can be easily varied by changing the ratios of the initial precursors. The same synthetic concept can be applied in order to incorporate various other conducting or non-conducting polymers that can introduce desired properties to the sol-gel materials. This new type of hybrid material can be fabricated easily into products with a designable shape, and potential applications may include fabrication of electronic, optical and sensor devices.

10.4 Electrochemical Study of Aniline Trimers with End-Group Substitution

The redox processes of amine end-group substituted aniline trimers were correlated with the variation in side-group substitution. These results demonstrate that substitution with electron-donating or electron-withdrawing groups has a profound effect on the electrochemistry of these compounds and of other aniline oligomers. By introducing alkoxylsilyl groups in the aniline trimer, it was possible to prepare an electroactive organic-inorganic hybrid material. The aniline trimer containing silsesquioxane compound behaved electrochemically like polyaniline with

regard to protonation and ion insertion during the redox process. The electrochemical study of the polymerized material, obtained upon hydrolysis and co-condensation with TEOS, shows that the introduced electroactive function can be well controlled by adjusting the content of oligoaniline bridges in the organosilicates.

The electroactive conjugated oligomers of well-defined structures have many significant advantages, including the much easier processability over their corresponding polymers. End-group substitution of these oligomers offers the ability to control the ionization potentials of oligomers, and thus provide materials with several possible applications. Taking advantage of their well-defined structures and designable end-groups, properly functionalized oligomers could form a variety of molecular or supramolecular assemblies for potential electronic and optical applications. Like polyaniline, these oligoanilines and their derivatives can be used in the fabrication of electrochromic, electroluminescent and biosensor devises, as well as for the preparation of anticorrosion and antistatic coatings.

10.5 Oxygenation of Iron Phthalocyanines

The oxygenation of both forms (i.e., α- and β-forms) of phthalocyanines at 50 ^{o}C for a prolonged period of time (e.g., 75 days) in the dry state and in aqueous suspension has been investigated to study the effect that prolonged time of oxygenation has on the nature and structure of the obtained oxygen adducts. These results indicate that, when oxygenation is carried out at 50 °C in aqueous suspension, or in the dry state, for prolonged periods, then interesting oxygen adducts are formed and a much larger fraction of the compound of both α- and β- forms is oxygenated. Compared to our earlier studies, the interplanar spacing for the β-FePc seems to have substantially increased due to longer period of oxygenation. Additionaly, the facilitation of

diffusion of oxygen between the interlayers of iron phthalocyanines in the presence of water has been further justified for both forms. The formation of interesting α-Fe^{III}Pc oxygen adducts by both wet and dry prolonged oxygenation has been also accomplished. Proposed configurations of α-FePc oxygen adducts are still under investigation.

10.6 Encapsulation of Enzymes in Mesoporous Hybrid Materials

The encapsulation of horseradish peroxidase (HRP) and alpha glucosidase, as model enzymes for a range of applications, in various mesoporous hybrid materials has been presented. Several different precursors have been investigated to find the optimum formulation, and the obtained materials were characterized by thermogravimetric analysis (TGA) and nitrogen adsorption analysis (BET). Enzymatic assays for HRP and α-glucosidase revealed the compositions of the organosilicas that led to the optimum residual activity of the encapsulated enzymes. In addition, a novel technology for maintaining the enzymatic activity, during storage in harsh media, such as organic solvents and high pH aqueous solutions, has been developed. The non-surfactant templated sol-gel method has been again utilized to incorporate HRP enzyme into the pores of mesoporous organosilicates followed by the application of a second polyacrylic protective layer. Results indicate that the doubly encapsulated HRP showed many orders of magnitude higher residual activity after storage for 24 hr in high pH media, detergent, ethanol and toluene, as compared to the native enzyme under the same conditions. Since this “double encapsulation” technique is completely independent of the nature of the enzyme, it is expected to be useful for stabilizing other enzymes, biomacromolecules and bioactive agents in such hostile environments as well. Further optimization of this method is underway in our lab.

10.7 Fabrication of a Fluorescent Nanoelectrode

Nanoscale electrochemical nanoprobes have been fabricated, using electron beam deposition, on the tips of micro-sized electrodes. Electropolymerization of resorcinol, in the presence of fluorescent puronin, afforded a smooth insulating fluorescent coating that renders visibility of the nanostructures under a fluorescence optical microscope. Efforts are underway to open the insulation at the exact tip of the nanoelectrode and, thus limit the electroactive region to the extreme tip of the nanoprobe. Such a fluorescent nanoprobe is expected to have a huge impact in neuroscience area. The small size and high aspect ratio of the nanoprobes ensure that the probes can be utilized for neuron analysis in extremely small microenvironments, such as synaptic clefts. More experiments will be carried out, using these novel nanoprobes, to detect electric and electrochemical signals after the opening of the coating at the exact tip.

10.8 Future Direction

In order to further optimize upon the desired properties of the obtained materials, there are several different approaches that may lead to improved products, including:

- Incorporation of other chemical groups that have been proven to impart adhesiveness onto chitosan or other biodegradable and biocompatible materials to obtained materials with adhesive capabilities in wet and/or dry surfaces. Some of these concepts will be presented in appendix B.
- Application of the same synthetic approach as the one used to synthesize PHGS, to incorporate other acrylic monomers into sol-gel materials, which may lead to materials with alternative tunable properties.

- Incorporation of aniline oligomers into sol-gel materials may provide materials with improved mechanical and/or electrochromic properties. In addition, incorporation of other conductive polymers into sol-gel materials following the same synthetic concept may lead to innumerable products with tunable mechanical, electrochromic, electroactive and conductive properties.
- Adjustment of the ratio and/or type of the templates used in the "double encapsulation" process. In order to more efficiently protect various enzymes while storing them in harsh media, alternative acrylic monomers may also be investigated.

Appendix A. Fabrication of a Novel Fluorescent Nanoelectrode

A.1 Introduction and Motivation

Electrodes, with nanometer dimensions, provide a means for probing many electrochemical processes in various microenvironments. The small dimensions result in high current density at the electrode surface, which offers the ability to study fast heterogeneous electron transfers, molecular interactions, as well as mass transports at the nanometer scale. In addition, nanoelectrodes offer the possibility to probe cellular signals by applying and recording the neurotransmitted signals of cells. Nowadays there is huge interest in the development of practical methods to construct nanoelectrodes for a variety of applications.[1-5] Unfortunately, the currently used probes, including carbon fibers and metal microelectrodes, typically have tip diameters of a few micrometers or greater. This results in the restriction of their use in neuron analysis of extremely small dimensions. Moreover, utilizing carbon nanotubes as a method of developing nanoelectrodes presents the disadvantage of requiring many tedious steps for the construction of the probes.[6-9] Thus, it very important the development of a method that creates feasibly submicron-size or nanometer-size electrodes.

It is of crucial importance that the nanometer scale probes have a high aspect ratio to allow for the probes to pass through the cell membrane and penetrate into the neuron cell, without destructing cell viability during experiments. Several research groups, including ours, have recently demonstrated the fabrication of devices of submicron or nanometer size for the non-destructive probing of intracellular processes. These include the use of plasma-enhanced chemical vapor deposition for the fabrication of vertically aligned carbon nanofibers,[10-11] the

development of nanoelectrodes with the utilization of carbon nanotubes[12-15] and the fabrication of microelectrodes by nanomanipulated etching of metals.[16-20] Despite the many advantages, these methods are quite time and effort consuming with a low success rate. In addition, the tapering tip shapes are often poorly reproducible, and thus the utilization of these methods for the large scale production of the obtained nano-probes is often restricted. Our group recently reported the successful fabrication of nanoelectrodes by electron beam deposition as potential electrochemical neuronal probes.[21] This technology presents advantages over other existing ones in the fact that it offers the ability to reproducibly prepare sharp and single tips on a desired specific location of interest. After electrodeposition of the desired tip, phenol electropolymerization created an insulating coating according to previous published studies. After coating, the insulating polymer was removed from the exact tip of the electrode so that electrochemical activity was limited to the tip region.

Nanoelectrodes for applications in neuroscience have gotten progressively smaller and more efficient as they evolved. These nano-probes have finally gotten small enough to make it feasible to perform a test without destroying the cell under study. Up until today though, there is no means of knowing the exact position of a nanoelectrode while it is inserting into a cell membrane. The presently used procedure for probing cellular signals with the utilization of a nanoelectrode requires a nano-manipulator, an optical microscope of high magnification and a potensiostat. In this case, the nanoelectrode is brought to close proximity to the cell membrane to be examined with the help of the nano-manipulator. With the aid of the optical microscope, the nano-manipulator and the “trial-and-error” method, the aim is to insert the nano-probe inside the

membrane and record an electrical signal on the potensiostat. Once the nanoelectrode is inserted in the main body of the cell, then the recording of electrical signals is possible. If the potensiostat shows no electrical signal response, then consequently it means that the electrode is not inserted inside the cell membrane. This, in turn, demands again the utilization of the nano-manipulator to push the nanoelectrode closer to the point of interest, and the procedure goes on, up until the point that an electrical signal is recorded on the potensiostat, which verifies the insertion of the probe in the cell. Unfortunately, this procedure is very tedious and requires lots of effort and time. It is thus desirable to develop a method that enables the researcher to be able to be familiar with the exact position of the nanoelectrodes at every time, without having to invest the time and effort that the "trial-and-error" procedure requires.

Herein, the fabrication of a novel fluorescent nanoelectrode for the application in neuroscience is presented. The basic idea is quite simple. To make a nanoprobe with tip diameter of ca. 40 nm and length of a few micrometers visible under a conventional optical fluorescence microscope, as we envisioned, the surface of the nanoprobe could be coated with fluorescing compounds so that a researcher would be able to see the nanoprobe as he/she is inserting the probe into a specific part of a cell. As an analogy, a light bulb far away is not visible to naked eyes when it is off. However, when turned on, it becomes visible at the same long distance. This technology offers the advantage of knowing the exact position of the nanoprobe at every time under a conventional fluorescent microscope. This makes the cell signal probing a more feasible procedure as compared to the methods currently used. The obtained nanoprobes have tip dimensions as small as 40 nm in diameter and 1 to 2 micrometers in length. The fabrication

includes the utilization of electron beam deposition on the apex of conventional tungsten microelectrodes. To fabricate the electron beam deposited tips, the procedure followed is the same as the one that has been reported earlier by our group.[21] After electro-deposition of the desired tip, a fluorescent monomer electropolymerization creates an insulating fluorescent coating.[22-26] The obtained nanoelectrodes have been tested electrochemically before and after electropolymerization to ensure that insulation occurs throughout the whole electrode surface. After coating, the fluorescent insulating polymer has to be removed from the exact tip of the electrode so that electrochemical activity is limited to the tip region. Electrochemical studies after this step have to prove that the insulation has been stopped at the exact tip. Images taken under a fluorescent microscope verify the fluorescent nature of the applied coatings.

A.2 Materials and Instrumentation

The tip growing experiments were performed on an AMRAY 1830 scanning electron microscope (SEM). The important SEM parameters that determine the size, shape and length of the growing probes include acceleration voltage, deposition time, electron beam current, working distance, and magnification. As a typical procedure for growing a tip of about 100 nm in diameter and 1 μm in length, the following parameters were used: acceleration voltage = 30 kV, electron beam current setting = 3.5, working distance = 11 mm, deposition time = 5 min, magnification = 75,000. The observation of the tips grown on several substrates of the applied fluorescent coating, as well as of the removal of the coating at the exact tip of the nanoprobe, was performed on an environmental scanning electron microscope (ESEM-FEI XL30) featured with EDS and EBSD detectors.

Application of the fluorescent coating was conducted in both a two-electrode and three-electrode system. In the two-electrode system steel wire (0.020 inch gauge, from Malin Co., type soft SS) was used as the counter electrode. The distance between the counter electrode and the working electrode was about 2 cm. 1.0 V was applied electrolytically using a potensiostat from circuit specialists® (model: CS15003X5) for a predetermined amount of time. In the three-electrode system a Pt coil electrode was used as the auxiliary electrode while a saturated calomel electrode in MeOH was used as the reference electrode. These experiments were performed on an Epsilon Potensiostat (Model BAS 100 from Bioanalytical Systems, Inc., Indiana) interfaced and monitored with a PC computer. For the synthesis of the fluorescent coating by electropolymerization, cyclic voltammetry was employed. The potential was scanned between 0 mV and 1100 mV for 30 times at a scan rate of 100 mV/sec.

Gold wire (25 μm in diameter) was purchased from VWR. Tungsten microelectrodes (2 μm in the tip diameter) were purchased from World Precision Instruments (Florida). Steel microelectrodes (2 μm in the tip diameter) were purchased from World Precision Instruments (Florida). These tungsten wires are commonly used as microelectrodes in neural science. Phenyl-salicylate (99%, Alfa Aesar), salicylanilide (98%, Alfa Aesar), salicylamide (98%, Alfa Aesar), catechol (99%, Alfa Aesar), catechol violet (99%, Alfa Aesar), resorcinol (99%, Alfa Aesar), phenol (99%, Alfa Aesar), fluorescein (Aldrich), fluorescein isothiocyanate (Aldrich), 2,4,5,6-tetraiodofluorescein (Easman Organic Chemicals), Methanol (Aldrich), NaOH (Fluka), Na_2CO_3 (Fisher Scientific) and KCl (Fisher Scientific) were used as received. Doubly distilled, deionized water was used to make all aqueous solutions. The solutions for the preparation of insulating coatings were freshly made prior to use.

A.3 Growing of the Nanotips

The tip-growing process depends on various SEM parameters, including the acceleration voltage, the deposition time, the electron beam current, the working distance and the magnification. Several adjustments of these parameters have been performed first, in order to find the optimum conditions on the specific SEM. A series of different parameters were tested, including: an acceleration voltage between 20-30 kV, a setting for electron beam current of 2 to 5, deposition time between 3-7 min and magnification between "x 30,000" and "x 110,000". Once the optimum conditions were found for this specific SEM, tip growing was performed on mica (**Figure A-1,** parameters used: acceleration voltage of 25 kV, electron beam current setting at 3, deposition time of 5 min and magnification at "x 65,000"), gold wires (**Figure A-2,** parameters used: acceleration voltage of 30 kV, electron beam current setting at 3, deposition time of 6 min and magnification at "x 96,000") and tungsten microelectrodes (**Figure A-3,** parameters used: acceleration voltage of 25 kV, electron beam current setting at 3, deposition time of 5 min and magnification at "x 122,000"). The beam was first focused on the desired spot, and the beam setting was then switched to the spot mode for a fixed exposure time, during which a cone-shaped tip would be formed. The success of the growing tips procedure was verified by the utilization of ESEM (**FEI XL30),** which is capable of higher resolution as compared to Amray SEM.

A.4 Application of a Fluorescent Insulating Coating

Several different formulations have been tried to obtain an insulating fluorescent polymer coating of nanometer size. These include electropolymerization of phenyl-salicylate,

salicylanilide, salicylamide, catechol, catechol violet, resorcinol, phenol, in the presence or in the absence of tiny amounts of fluorescein, fluorescein isothiocyanate, 2,4,5,6-tetra-iodofluorescein and purronin. An effort to synthesize a compound containing the phenol functionality along with some groups that fluoresce (e.g., reaction of of 4-(dimethylamino) benzoyl chloride with catechol) has also been investigated. The aim was a monomer that would contain a fluoroprobe, which upon electropolymerization would lead to a fluorescent insulating thin coating. This method gave ambiguous results, with varying thickness of the obtained coating. Electropolymerization was investigated in various electrolytic solutions, including NaOH in MeOH (0.2M and 0.3M), KOH in MeOH (0.2 and 0.3M), H_2SO_4 (0.5M), HCl (0.5M), Na_2CO_3 solution and PBS buffer solution. Overall the best results so far have been obtained for resorcinol (50mM) in the presence of a tiny amount of purronin (1mM), in the H_2SO_4 (0.5M) electrolyte solution. For the coating of the grown nano-tips with fluorescent insulating polymer, two different electrochemical set ups were utilized, namely a two electrode and a three electrode set up. In the-two electrode set up the steel wire, used as an auxiliary electrode, and the microelectrode containing the grown nano-tip were immersed in a 15-ml beaker containing 10 ml of the monomer solution (e.g., 50mM of resorcinol with 1mM of purronin). The ends of both electrodes were connected to a potensiostat. The electrode to be coated with the fluorescent coating was connected to the anode of the potensiostat. A fluorescent insulating coating was obtained by the application of 1000 mV between the two ends for a predetermined period of time (1 hour for the resorcinol solution). Before the electrolysis, the coating solution was purged with nitrogen gas for 10 min. A blanket of nitrogen gas, on top of the solution, was maintained throughout the whole electrolysis period. In the three-electrode system, a Pt coil electrode and a

saturated calomel electrode were used, as the auxiliary and the reference electrode, respectively. The same solutions as the ones investigated for electrolysis have been tried for electro-polymerization by cyclic voltammetry. The potential was scanned between 0 mV and 1100 mV for 30 times at a scan rate of 100 mV/sec. The formation of a passivating film during electropolymerization of an aqueous solution of 50mM H_2SO_4 containing 50mM resorcinol and 1mM of purronin is presented in **Figure A-4**.

The last step for the construction of the novel fluorescent nanoelectrode is the opening of the insulation at the exact tip of the nanoprobe. In order to do that, the polymer coated metal substrate with the nanoprobe was placed in the SEM chamber. The electron beam was fine-focused on the tip of the nanoprobe, and the SEM mode was changed to spot mode for ten seconds at 30 kV. To ensure that the tip was exposed completely, the same procedure was repeated 2-3 times. After each step, namely the growing of the nanoprobe, the application of the fluorescent coating and the opening at the exact tip of the nanoprobe, the nanoelectrode was tested electrolytically to check for the electric resistance. At an applied potential of 1.0 V, the tungsten microelectrode with the grown tip showed current equal to 560 nA. On the other hand, when the microelectrode was coated with the fluorescent insulating coating, the current measured was 52 nA. This shows that after coating, the resistance increased by more than 10 times as compared to the uncoated electrode, which confirms the success of the coating insulation. It has to be mentioned that the current measured for the coated wire could be attributed to a very small current leakage because the coating is ultrathin. Experiments are underway in our lab for the opening of the probe at the exact tip after the application of the

fluorescent coating. This step is performed by exposing the coated nanoprobe to the electron beam in ESEM.

A.5 Conclusion and On-Going Work

Nanoscale electrochemical nanoprobes have been fabricated using electron beam deposition on the tips of micro-sized electrodes. Electropolymerization of resorcinol in the presence of puronin afforded a smooth insulating fluorescent coating. Efforts are underway to open the insulation at the exact tip of the nanoleectrode and thus, limit the electroactive region to the extreme tip of the nanoprobe. Such a fluorescent nanoprobe is expected to have a huge impact in the neuroscience area. The small size and high aspect ratio of the tips ensure that the probes can be utilized for neuron analysis in extremely small microenvironments, such as synaptic clefts. More experiments will be carried out using these novel nanoprobes to detect electric and electrochemical signals, after the opening of the coating at the exact tip, within neuron cells or other types of cells.

A.6 Fabrication of Microprobes Following Alternative Approaches

Earlier in this appendix, the effort to fabricate a novel fluorescent nanoelectrode for the application in neuroscience was presented. Herein, some other approaches that have been tried for the fabrication of nanoprobes, for applications in neuroscience, and which gave promising or ambiguous results are going to be briefly described.

One approach involved a procedure where the pipette pulling process was utilized. A glass capillary tube was put under a laser pipette pulling machine, in an attempt to obtain microprobes with a tip in the nanometer scale. The parameters of the laser pulling apparatus were

adjusted up until the point that tips, of about 200 nm in diameter, were obtained (**Figure A-10**). As shown in the obtained SEM pictures, these pulled glass pipettes are hollow inside. Two methods were tried in order to fill these pipettes with a conductive fill:

A) The glass pipettes were filled with liquid gold before pulling. At temperatures above 500 °C the liquid gold will presumably be converted into solid gold. Since the pipette pulling process is carried out at 600 °C, a thin layer of solid gold will form at that temperature. It was expected that upon laser pulling of the glass pipette, a thin continuous gold film could be obtained inside the pipette.

B) After the capillary glass pipettes were pulled to create a hollow conical tip of about 200 nm, several methods (e.g. electroplating, electroless plating, etc) have been employed in an attempt to get a continuous layer of a metal inside the capillary tube. The concept was that a thin layer of silver film would cover the inside of the pipettes, thus creating conduction between the two ends of the pipette. Both proposed methods aimed at making similar nanoprobes to those discussed in Chapter 8, that is, a nanoprobe with a conductive tip at the nanometer scale, which is coated with a nonconductive material on the outside, and where the conductive area is limited to the extreme tip. Unfortunately, both of these methods, described above, gave ambiguous results. Future work might include filling of the pipettes, to be laser pulled, with alternative solutions which upon application of the laser heating, would create a continuous layer of conductive metal.

Another approach to fabricate nanoelectrodes included the etching of several metal wires, including Pt and Au, to get a conical and sharp tip by utilizing the so called “Zone Electropolishing” method (**Figure A-11**). The etching procedure included the application of a

high voltage (20-40 V) between the wire to be etched and a graphite counter electrode. Several etching solutions of various concentrations have been tried, including NaCl, $CaCl_2$ and KCl. Overall, the sharper tips have been obtained in NaCl solution. The next step included attempts to obtain a non-conductive coating throughout the whole area of the microprobe, except the apex of the tip. To achieve that, several different approaches have been tried. One included the multiple dipping of the nanoprobes in solutions of HEMA-GMA-silica precursors containing BPO. The synthesis and characterization of such hybrid materials was explained in detail in Chapter 4. The probes were then set on a substrate perpendicularly, with the apex of the tip facing up. They were then put in a vacuum oven, where the radical polymerization of the precursors to yield non-conductive poly(HEMA-GMA-silica) (PHGS) was performed. The concept behind this approach was the formation of a smooth, thin and insulating hybrid material throughout the whole surface area of the microprobe except the apex of tip. Shrinkage upon polymerization of PHGS was expected to expose the apex of the tip, and thus create a conductive area at the exact tip of the nanoprobe. SEM pictures in **Figure A-12** and **Figure A-13** verify the smoothness and thickness respectively of the obtained insulating coating, composed of PHGS. Unfortunately, and although in general the insulating films of PGHS were completely smooth and thin, in some small areas of the microprobes, some of the coating would peel off especially after extensive probe handling. To solve for this peeling of the coating, a different approach has been also investigated. This includes the insertion of the gold microprobes in a saturated atmosphere of 3-(mercaptopropyl)trimethoxy silane. This would cause the covalent bonding of the gold metal with the sulfur atom and the subsequent grafting of the sol-gel precursor on the surface of the Au wires. The next step was the attempt to precede the sol-gel reactions of the precursors grafted on

the wire. The sol-gel reactions would be allowed to proceed upon the insertion of the microbes in a saturated atmosphere of 1% wt hydrochloric acid followed by the insertion of them in a vacuum oven. This would cause the further condensation of the 3-(mercaptopropyl)trimethoxy silane sol-gel precursors which eventually would lead to a thin and insulating sol-gel coating. In order to get a somewhat more "elastic" coating that wouldn't fail upon handling, pre-hydrolyzed HEMA-GMA-silica, has been also tried to co-condense together with 3-(mercaptopropyl)trimethoxy silane. **Figure A-14** shows the microprobe obtained after the co-condensation of 3-(mercaptopropyl)trimethoxy silane and HEMA-GMA-silica. The obtained thickness and smoothness of the final coating can be seen. Further experimentation with the amounts of precursors and the sol-gel reaction conditions is needed to get a smoother and thinner elastic and insulating coating.

Figure A-1. Tips grown on mica surface. Diagonal view.

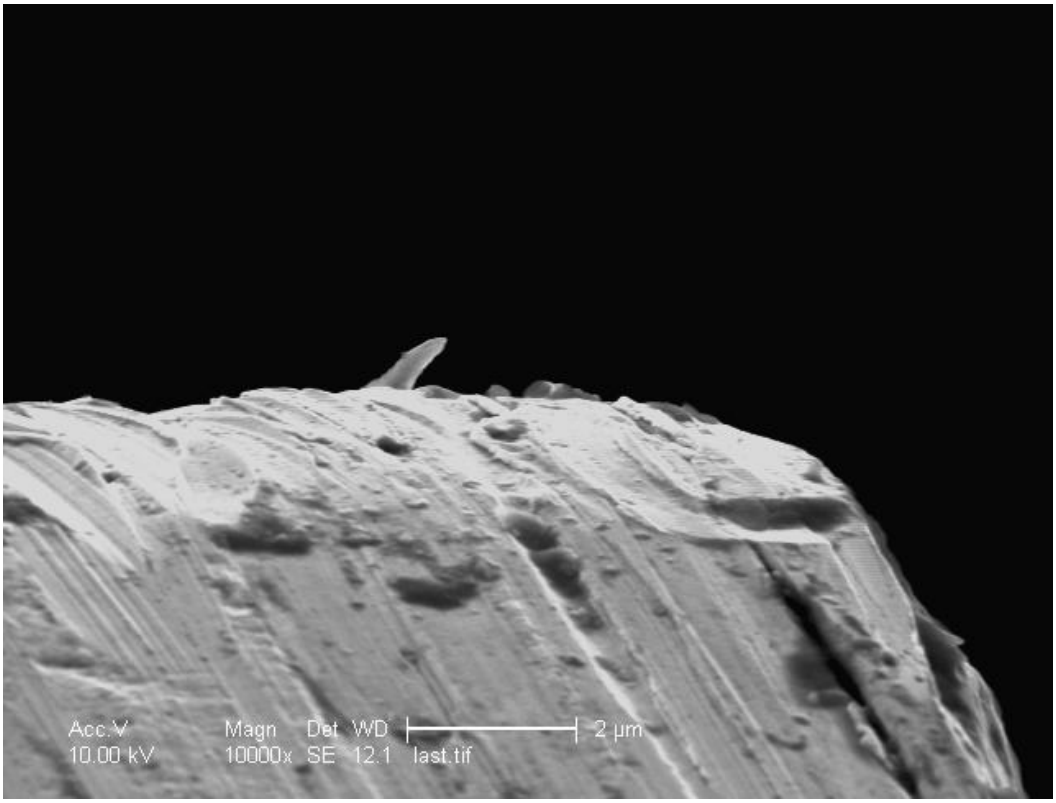

Figure A-2. SEM image of a single nanotip grown on gold wire

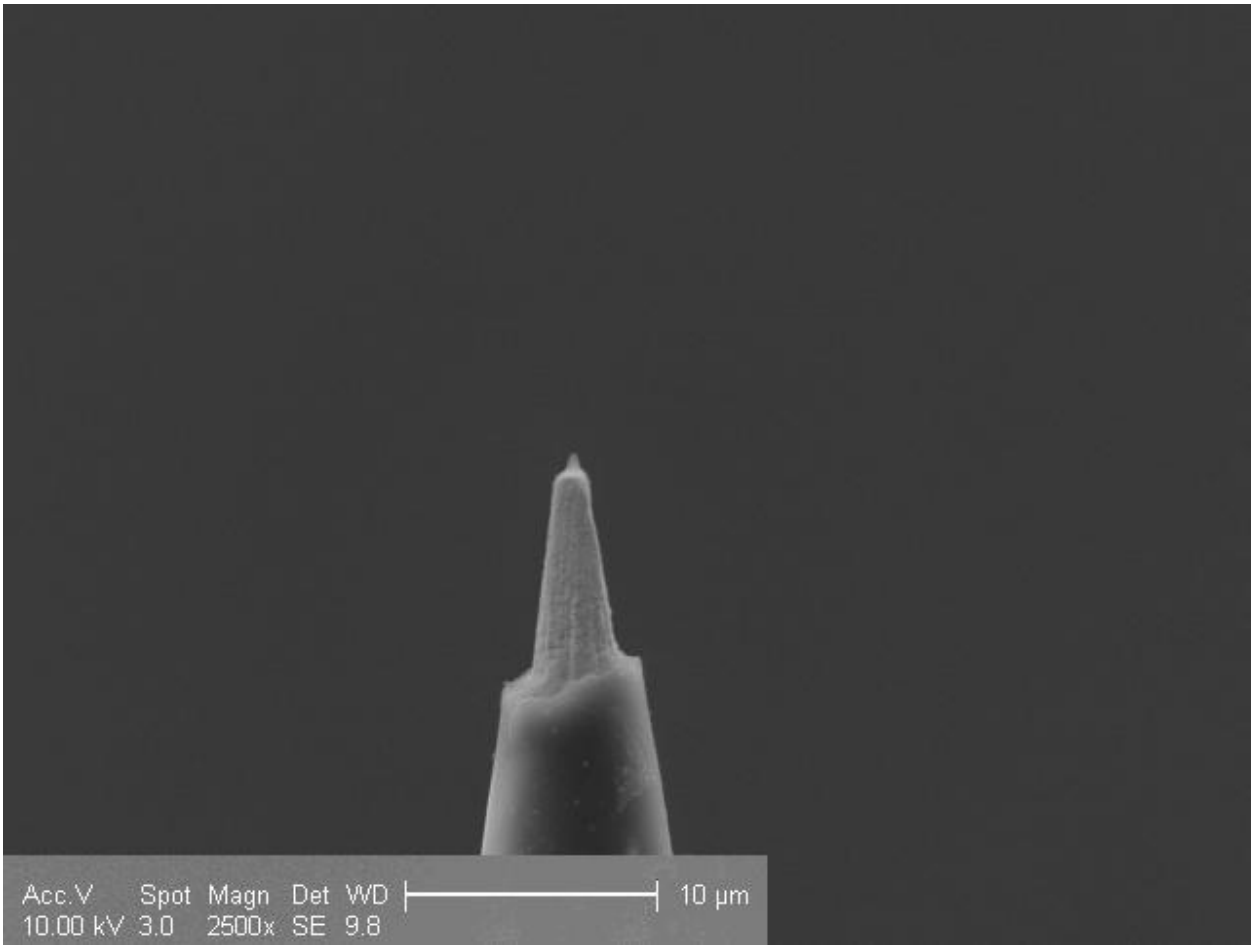

Figure A-3. SEM image of a nanotip grown on the apex of a tungsten microelectrode.

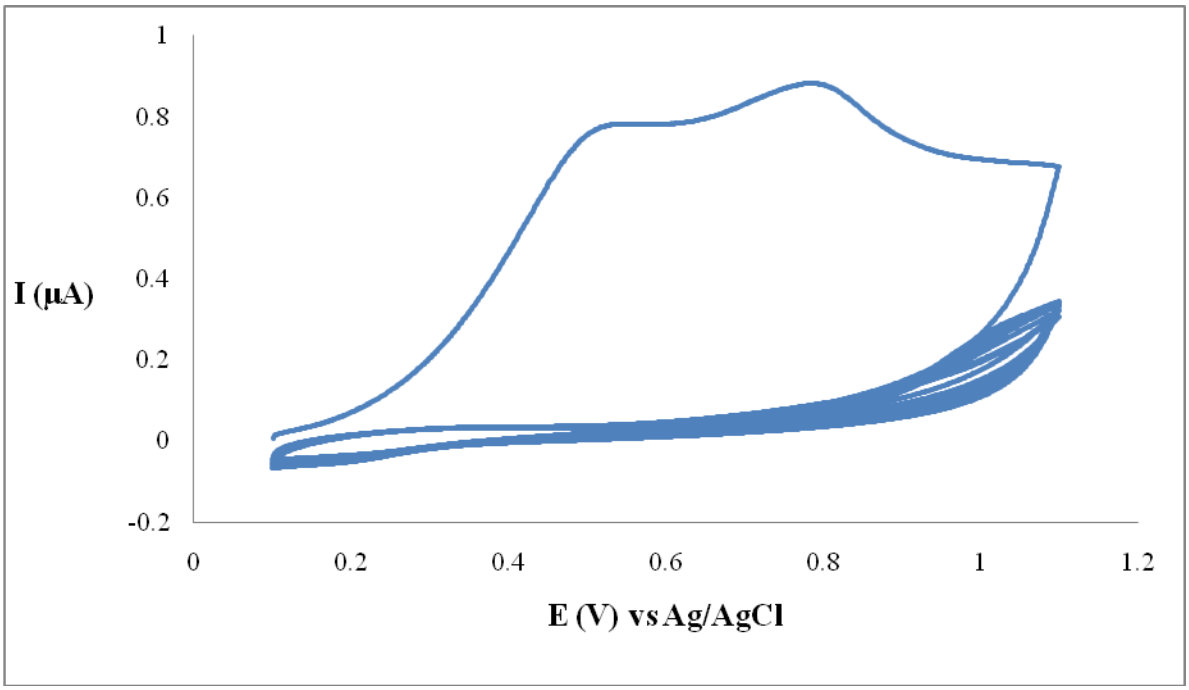

Figure A-4. Electropolymerization of an aqueous solution of 50mM H_2SO_4 containing 50mM resorcinol and 1mM of purronin during 30 cycles of cyclic voltammetry between 0 mV and 1000 mV at a scan rate of 60 mV/sec. The passivation of the electropolymerized coating after the first cycle is observed.

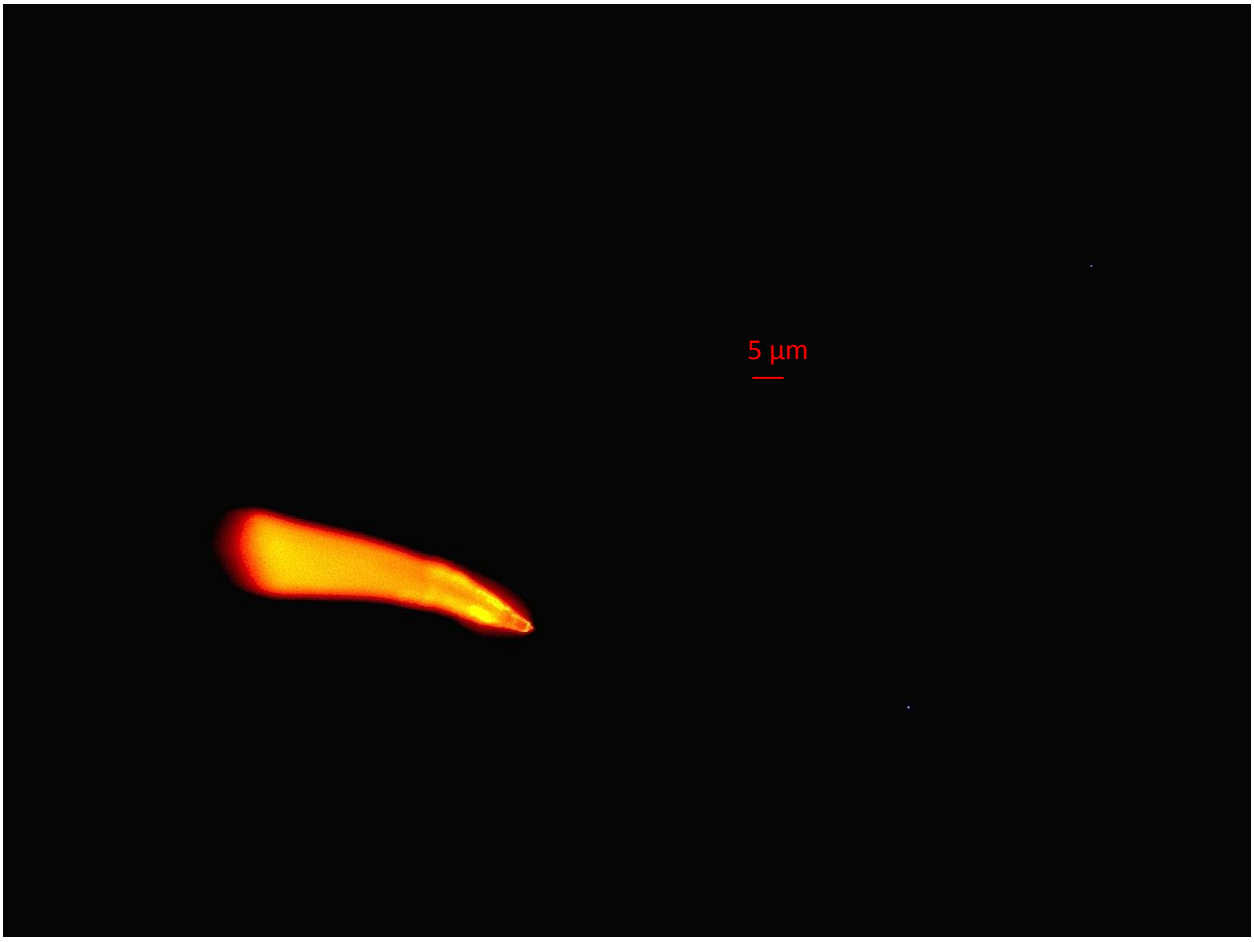

Figure A-5. Microprobe under a fluorescent microscope (x 1,000) after the application of the fluorescent coating.

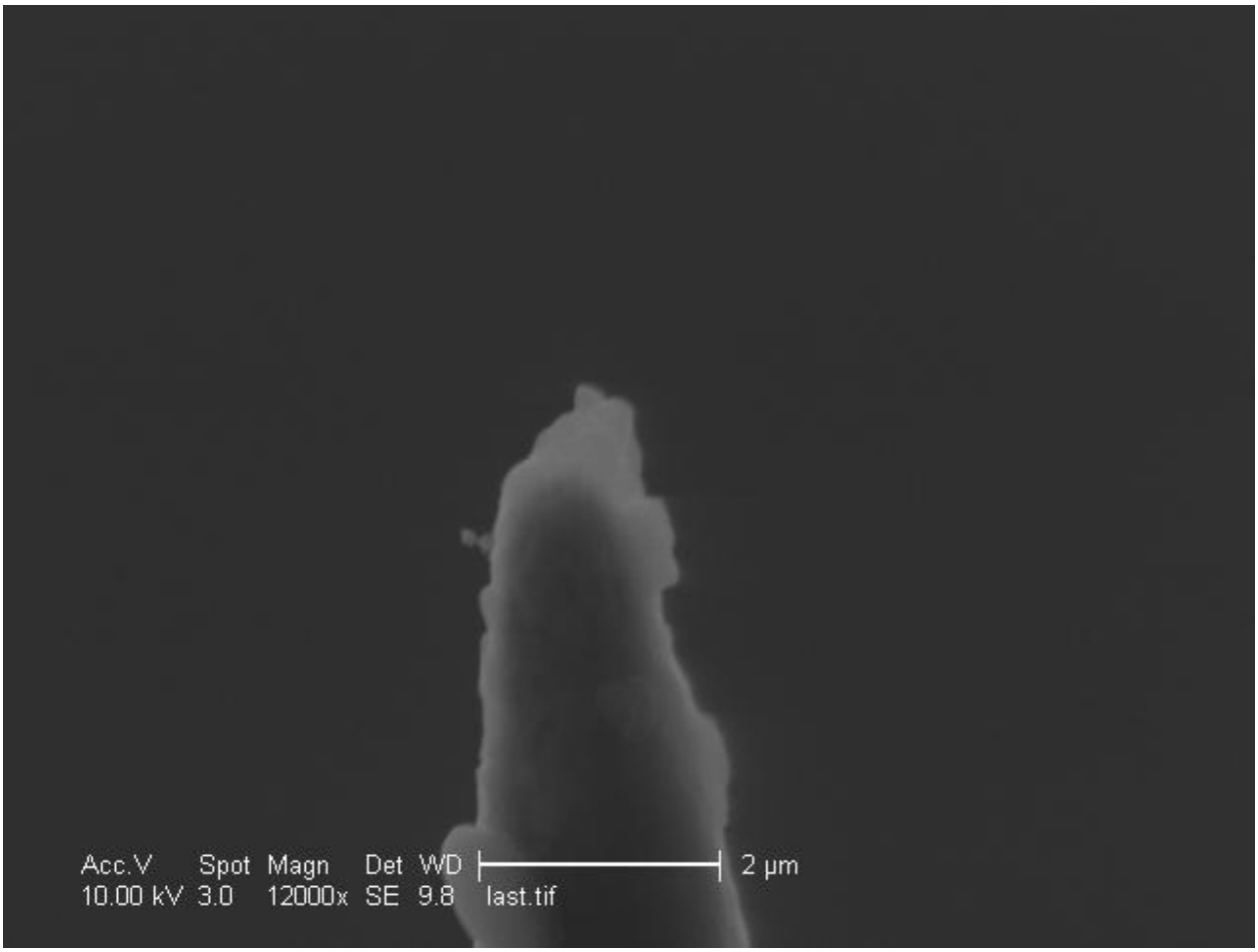

Figure A-6. Microprobe under a scanning electron microscope after the application of the fluorescent coating.

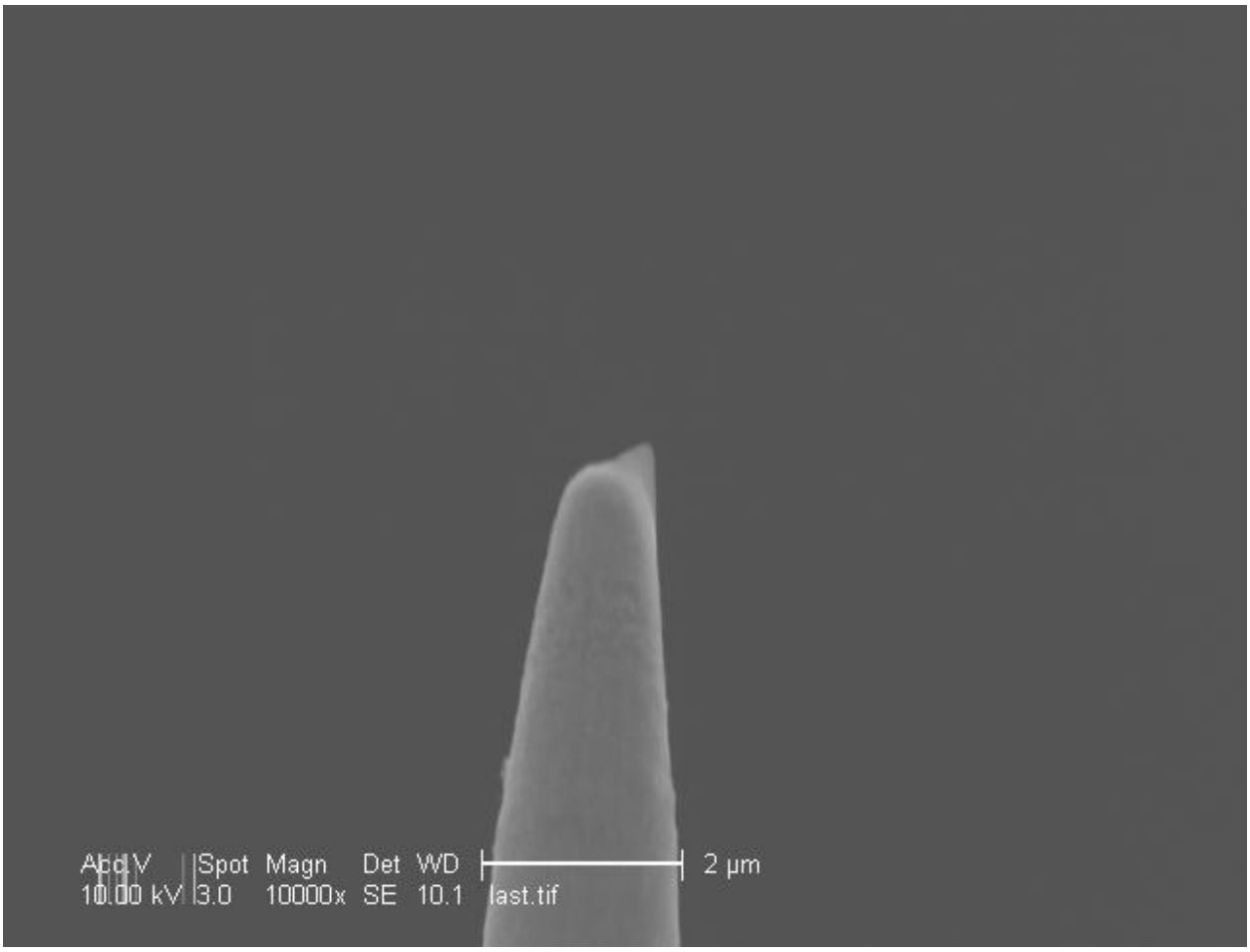

Figure A-7. Tip grown on the side of a tungsten microelectrode. It corresponds to the microprobe shown in **Figure A-6** before application of the fluorescent coating.

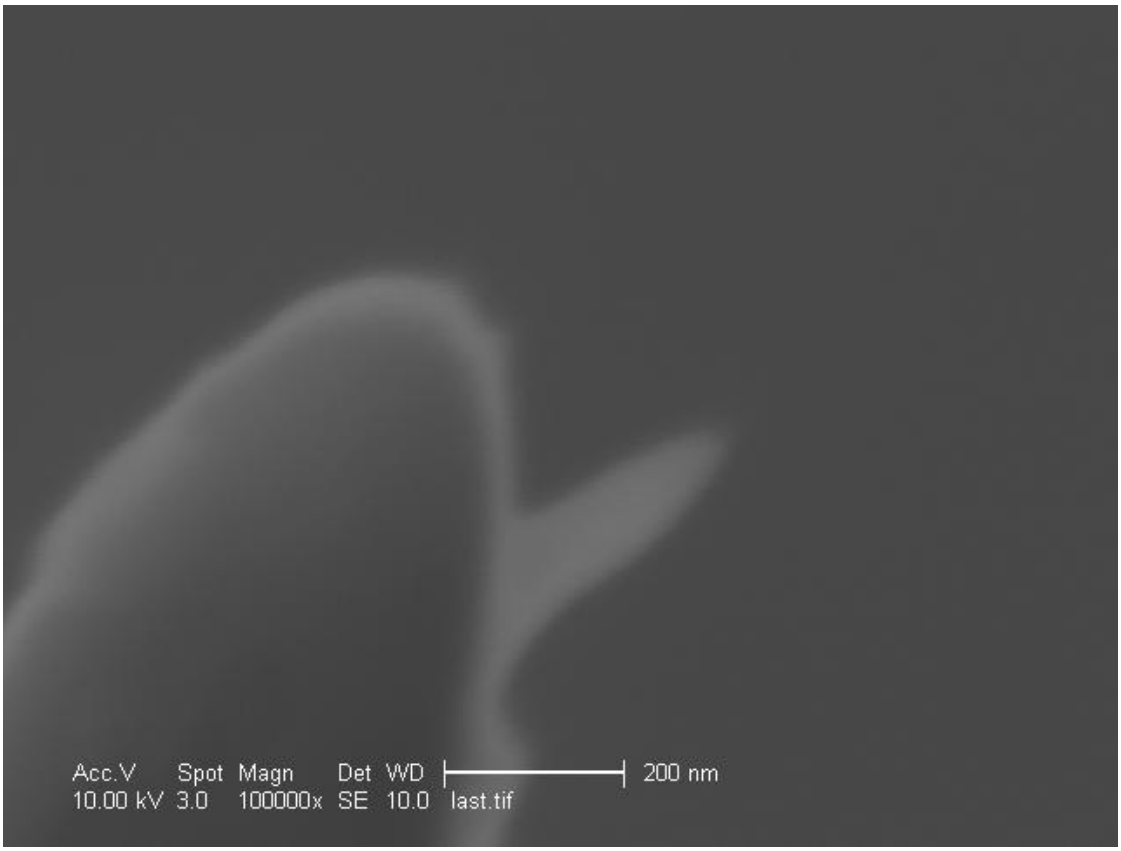

Figure A-8. SEM image of nanotip grown on the side of a tungsten microelectrode.

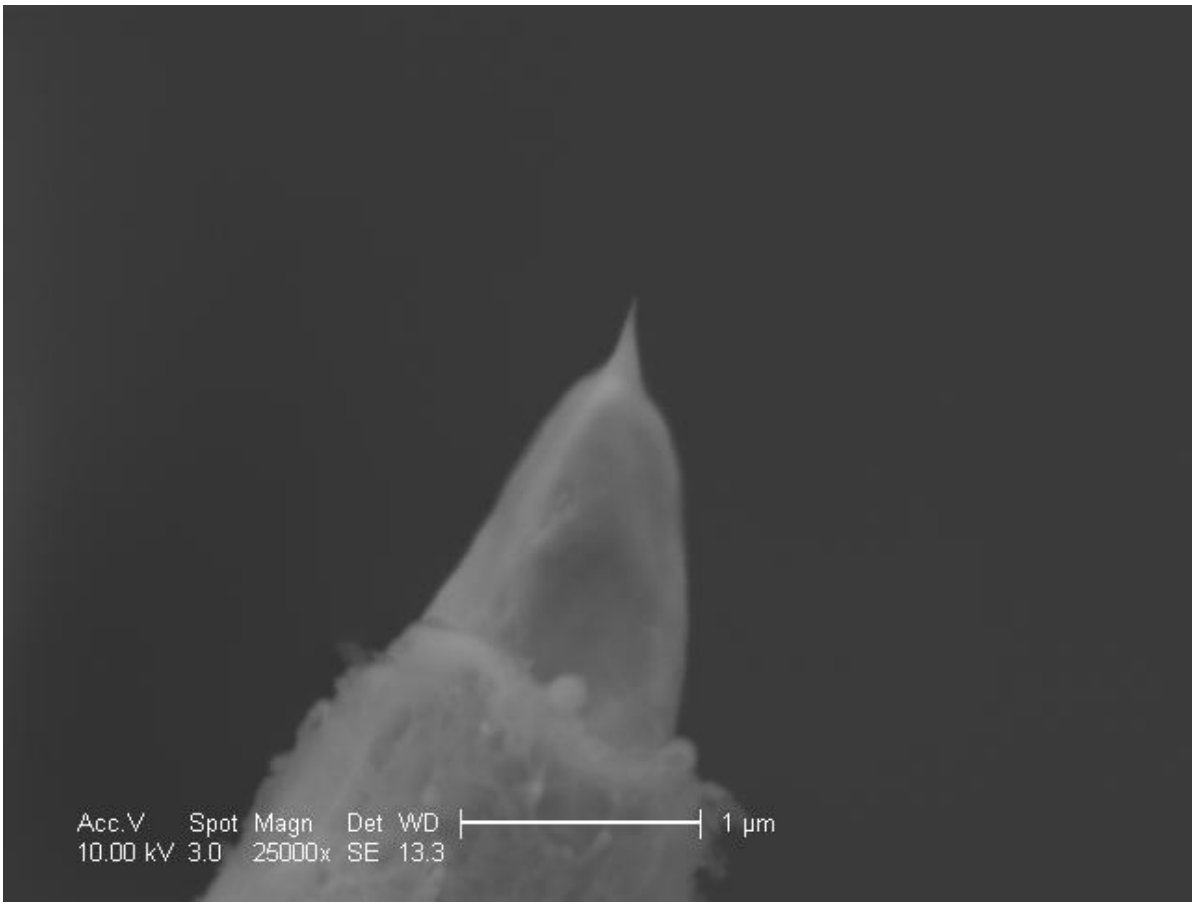

Figure A-9. SEM image of a nanotip, with a very high aspect ratio, grown on tungsten microelectrode.

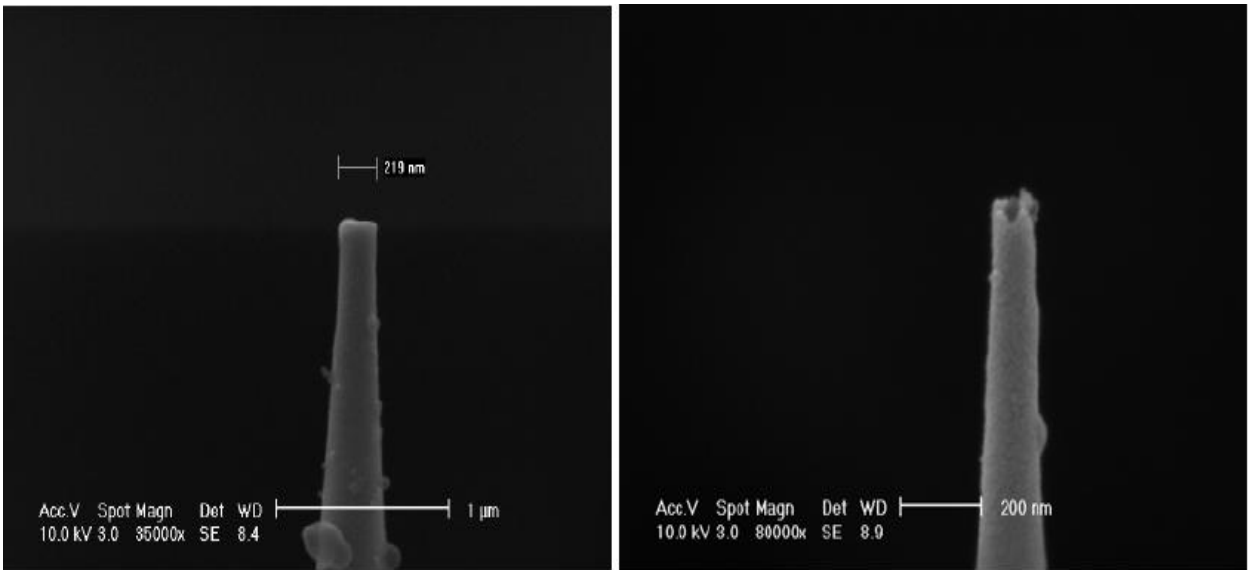

Figure A-10. SEM micrographs showing glass pipettes pulled under laser.

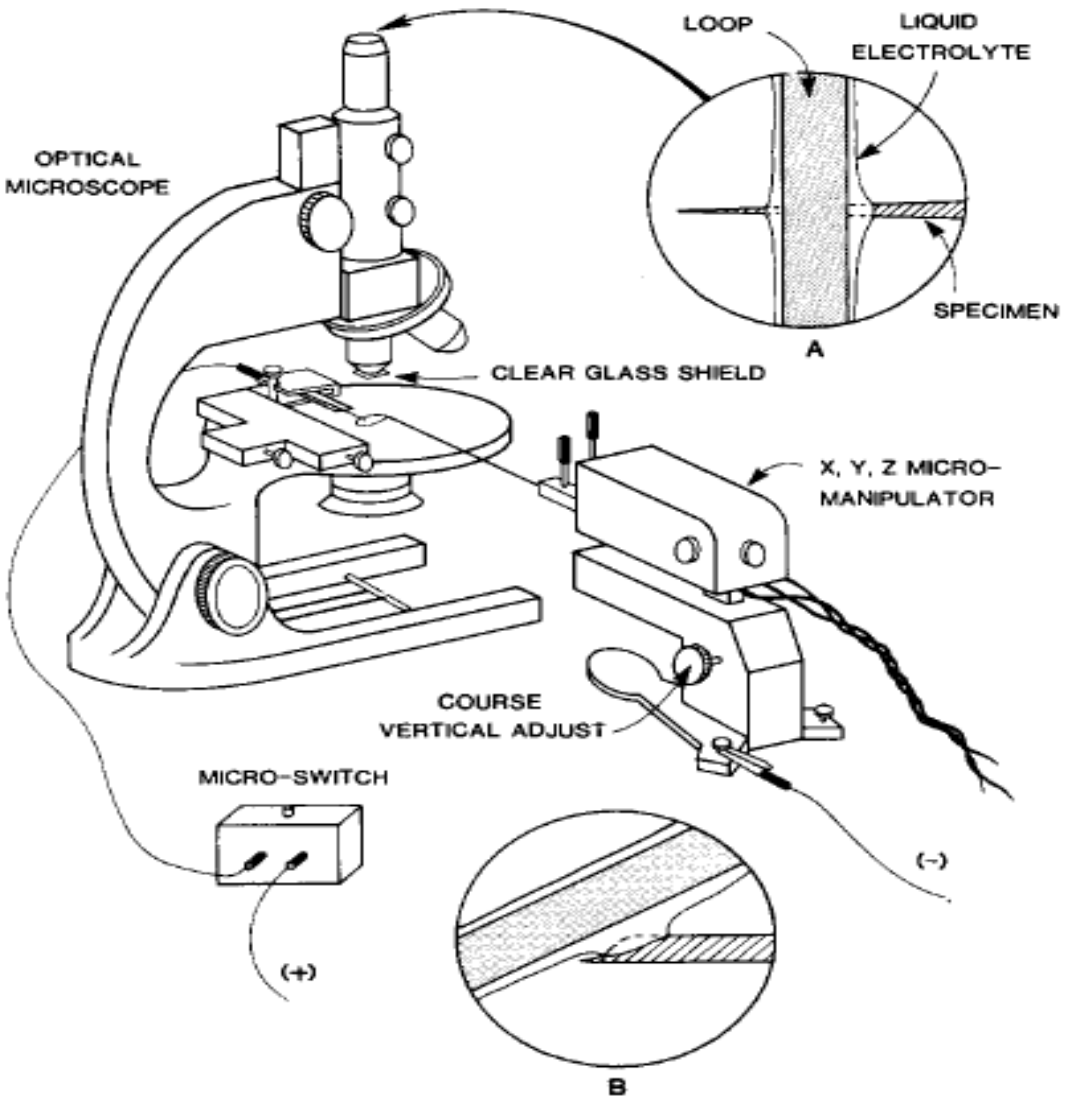

Figure A-11. Schematic of the apparatus utilizing the zone electropolishing method. A high voltage (20-40 V) between the Pt wire and a graphite counter electrode was applied. Etching solutions include NaCl, $CaCl_2$, KCl.

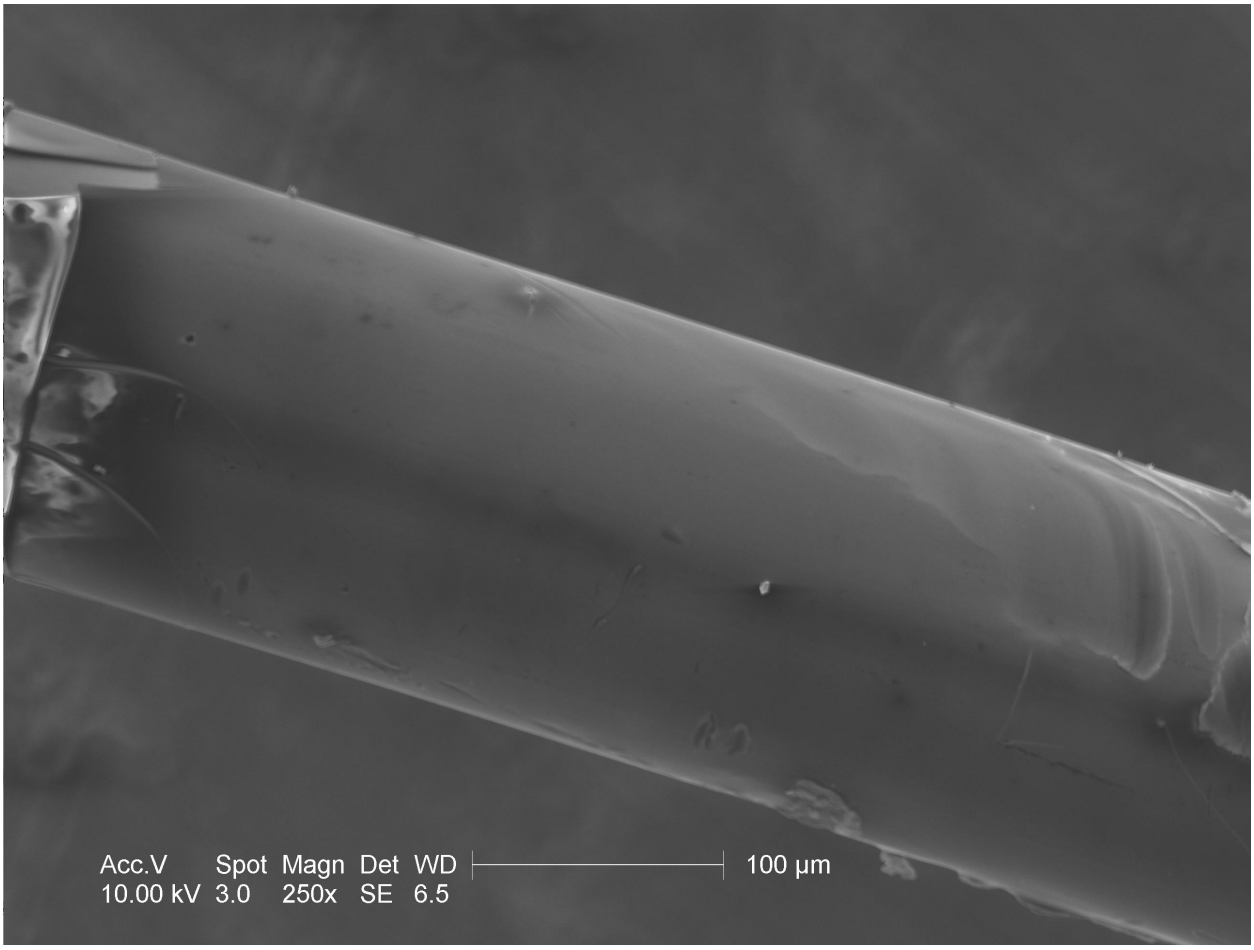

Figure A-12. SEM picture of PHGS coating applied on Pt wire. The smoothness of the insulating coating can be observed.

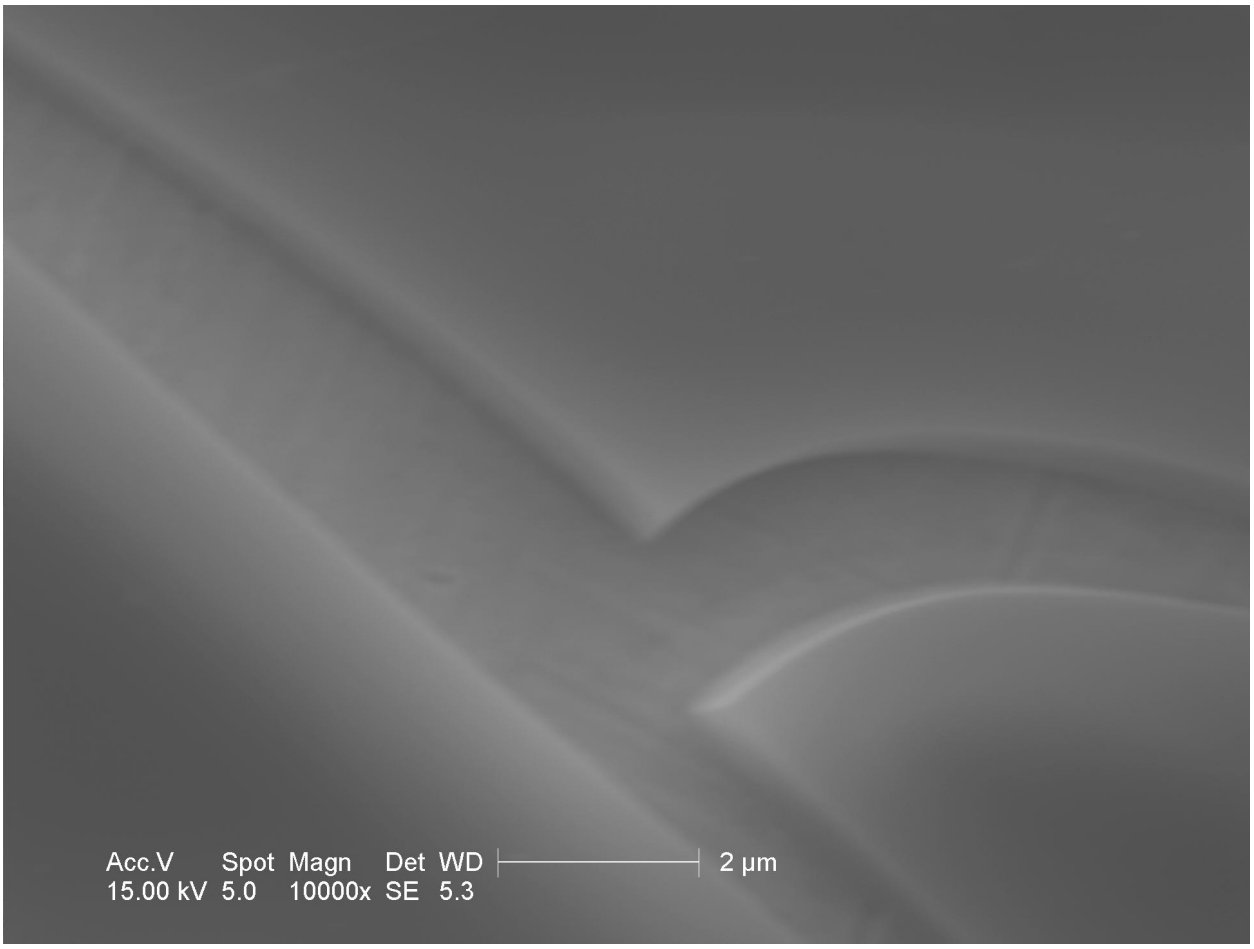

Figure A-13. SEM picture of PHGS coating applied on Pt wire. The thickness of the obtained insulating coating is about 300 nm.

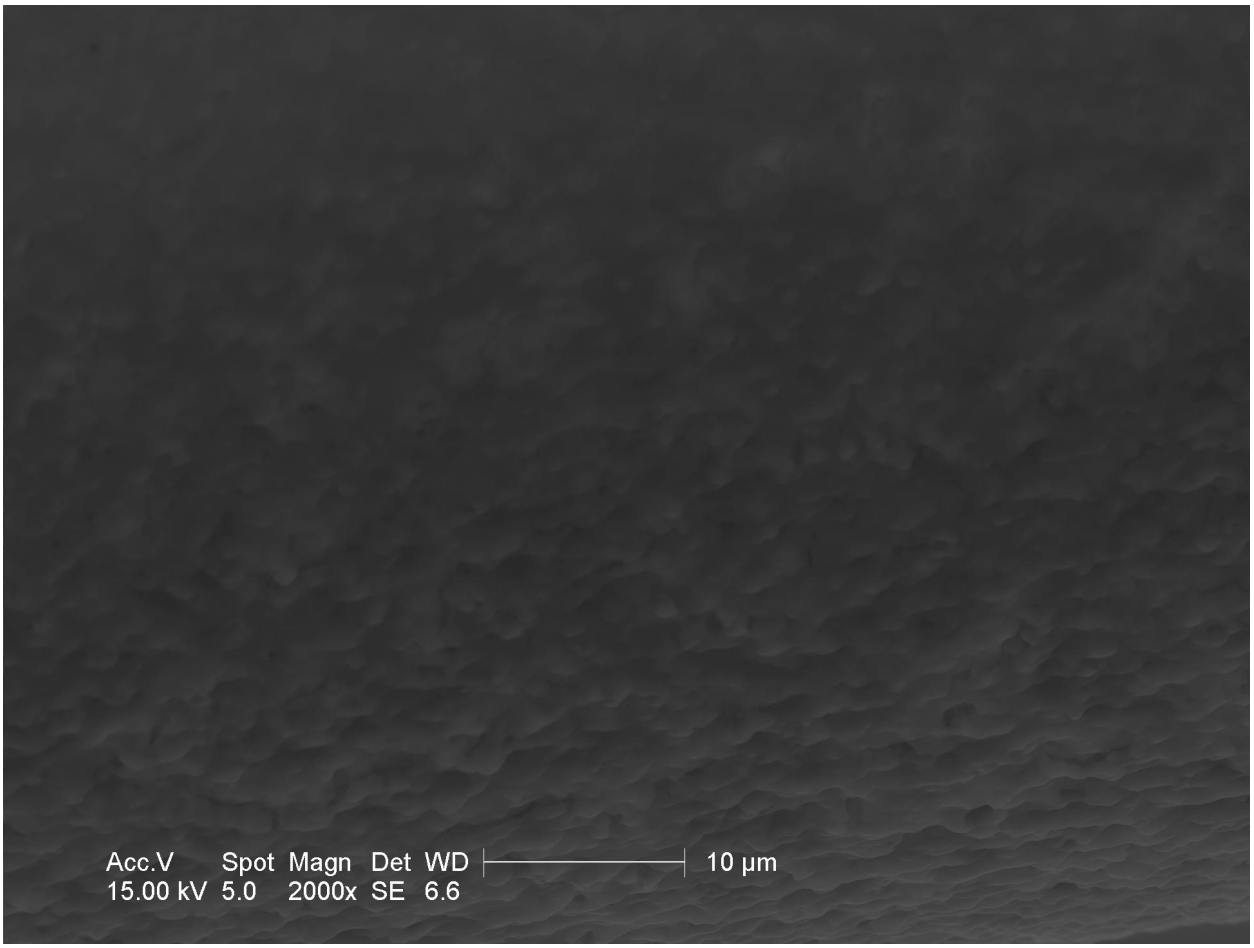

Figure A-14. SEM picture of insulating coating applied on Pt wire after the sol-gel reactions and co-condensation of 3-(mercaptopropyl)trimethoxy silane with HEMA-GMA-silica.

A.7 Reference List

1. Chen, S., Kucernak, A. Fabrication of carbon microelectrodes with an effective radius of 1 nm. Electrochemistry Communications (2002), 4, 80-85.

2. Kawagoe, K. T., Jankowski, J. A., Wightman, R. M. Etched carbon-fiber electrodes as amperometric detectors of catecholamine secretion from isolated biological cells. Analytical Chemistry (1991), 63, 1589-1594.

3. Caughman, J. B. O., Baylor, L. R., Guillorn, M. A., Merkulov, V. I., Lowndes, D. H., Allard, L. F. Growth of vertically aligned carbon nanofibers by low-pressure inductively coupled plasma-enhanced chemical vapor deposition. Applied Physics Letters (2003), 83, 1207-1209.

4. Chen, R., Huang, W., Tong, H., Wang, Z., Cheng, J. Carbon fiber nanoelectrodes modified by single-walled carbon nanotubes. Analytical Chemistry (2003), 75, 6341-6345.

5. Guillorn, M. A., McKnight, T. E., Melechko, A., Merkulov, V. I., Britt, P. F., Austin, D. W., Lowndes, D. H., Simpson, M. L. Individually addressable vertically aligned carbon nanofiber-based electrochemical probes. Journal of Applied Physics (2002), 91, 3824-3828.

6. Campbell, J. K., Sun, L., Crooks, R. M. Electrochemistry using single carbon nanotubes. Journal of the American Chemical Society (1999), 121, 3779-3780.

7. Schulte, A., Chow, R. H. Cylindrically etched carbon-fiber microelectrodes for low-noise amperometric recording of cellular secretion. Analytical Chemistry (1998), 70, 985-990.

8. Wendel, M., Lorenz, H., Kotthaus, J. P. Sharpened electron beam deposited tips for high resolution atomic force microscope lithography and imaging. Applied Physics Letters (1995), 67, 3732-3734.

9. Keller, D. J., Chou, C. Imaging steep, high structures by scanning force microscopy with electron beam deposited tips. Surface Science (1992), 268, 333-339.

10. Teo, K. B. K., Lee, S., Chhowalla, M., Semet, V., Binh, V. T., Groening, O., Castignolles, M., Loiseau, A., Pirio, G., Legagneux, P., Pribat, D., Hasko, D. G., Ahmed, H., Amaratunga, G. A. J., Milne, W. I. Plasma enhanced chemical vapour deposition carbon nanotubes/nanofibers—how uniform do they grow? Nanotechnology (2003), 14, 204-211.

11. Zhang, X., Zhang, W., Zhou, X., Ogorevc, B. Fabrication, characterization, and potential application of carbon fiber cone nanometer-size electrodes. Analytical Chemistry (1996), 68, 3338-3343.

12. Tu, Y., Lin, Y., Ren, Z. F. Nanoelectrode arrays based on low site density aligned carbon nanotubes. Nano Letters (2003), 3, 107-109.

13. Jonge, N., Lamy, Y., Kaiser, M. Controlled mounting of individual multiwalled carbon nanotubes on support tips. Nano Letters (2003), 3, 1621-1624.

14. Heller, I., Kong, J., Heering, H.A., Williams, K.A., Lemay, S.G., Dekker, C. Individual single-walled carbon nanotubes as nanoelectrodes for electrochemistry. Nano Letters (2005), 5, 137-142.

15. Koehne, J., Li, J., Cassell, A. M., Chen, H., Ye, Q., Ng, H. T., Han, J., Meyyappan, M. The fabrication and electrochemical characterization of carbon nanotube nanoelectrode arrays. Journal of Materials Chemistry (2004), 14, 676-684.

16. Qiao, Y., Chen, J., Guo, X., Cantrell, D., Ruoff, R., Troy, J. Fabrication of nanoelectrodes for neurophysiology: Cathodic electrophoretic paint insulation and focused ion beam milling. Nanotechnology (2005), 16, 1598-1602.

17. Slevin, C.J., Gray, N.J., Macpherson, J.V., Webb, M.A., Unwin, P.R. Fabrication and characterization of nanometer-sized platinum electrodes for voltammetric analysis and imaging. Electrochemistry Communication (1999), 1, 282-288.

18. Levick, W.R. Another Tungsten Microelectrode. Medical and Biological Engineering (1972), 10, 512-515.

19. Wang, C., Chen, Y., Wang, F., Hu, X. Fabrication of nanometer-sized carbon electrodes by the controllable electrochemical deposition. Electrochimica Acta (2005), 50, 5588-5593.

20. Shao, Y., Mirkin, M. Nanometer-Sized Electrochemical Sensors. Analytical Chemistry (1997), 69, 1627-1634.

21. Wei,Y., Yin, H., Cao, X., Ndungu, P., Yang, G., Bradley, J.C., Pourrezaei, K., Lelkes, P.I., Tsien, J.Z. Nanoelectrodes fabricated from electron beam deposited carbon as potential electrochemical neuronal probes. Journal of Biomedical Nanotechnology (2005), 1, 336-340.

22. MacTaylor, C. E., Ewing, A. G. Characterization of the effects of varying the pH and monomer concentrations of poly(oxyphenylene) insulating films on carbon fiber electrodes. Electroanalysis (1997), 9, 755-758.

23. Mengoli, G., Musiani, M. M. An overview of phenol electropolymerization for metal protection. Journal of Electrochemical Society (1987), 134, 643C-652C.

24. Eddy, S., Warriner, K., Christie, I., Ashworth D., Purkiss C., Vadgama P. The modification of enzyme electrode properties with non-conducting electropolymerised films. Biosensors and Bioelectrodes (1995), 10, 831-839.

25. Mengoli, G., Musiani, M. M. Phenol electropolymerization: a straight route from monomers to polymer coatings. Progress in Organic Coatings (1994), 24, 237-251.

26. Finklea, H. O., Snider, D. A., Fedyk J. Passivation of pinholes in octadecanethiol monolayers on gold electrodes by electrochemical polymerization of phenol. Langmuir (1990), 6, 371-376.

Appendix B. Biodegradable Adhesives

B.1 Introduction

In Chapter 3, the synthesis and characterization of a novel biodegradable, biocompatible and non-toxic adhesive, which was obtained by the modification of chitosan by 3,4-dihydroxybenzoic acid, was described. As mentioned in that chapter, my efforts focused on the synthesis of a biomimetic system that contains the same chemical groups, as the proteins that are extracted by marine organisms which are responsible for the characteristic ability of these creatures to stick on various surfaces underwater. Herein, some alternative approaches to obtain a biodegradable, biocompatible and non-toxic material with adhesive capabilities on wet and/or dry surfaces, and which have been experimentally investigated, are going to be briefly introduced. The same concept as the one followed for the modification of chitosan has been explored on other biodegradable polymeric backbones. Diphenolic-containing compounds have been incorporated on alternative polymeric materials that are known to be biodegradable. The synthesis procedures followed and the tests of the adhesive properties of the obtained materials are presented. Some of these materials gave interesting results and are still under investigation in our lab, while others gave ambiguous results and their investigation was stopped. Nevertheless, some of the different approaches, already tried in the lab, along with their hypothesis and concepts, are going to be described. These include the modification of polysuccinimide with 3-hydroxytyramine hydrochloride, 3,4-dihydroxy benzoic acid and 3,4-dihydroxy-L-phenylalanine. Moreover, the reaction of 3,4-dihydroxy benzoic with polyethylene glycol as a means to obtain a biodegradable adhesive is going to be briefly introduced. Finally, some novel concepts and ideas that have been planned to be investigated in our lab and which may become a key aspect towards

the goal of the development of biodegradable, biocompatible and non-toxic materials with adhesive capabilities on wet and/or dry surfaces are going to be revealed in the last section of Appendix B.

B.2 Polysuccinimide Approach

B.2.1 Materials

L-aspartic acid, hydrochloric acid, 3,4-dihydroxy-L-phenylalanine, 3-hydroxy-tyramine hydrochloride, diethylenetriamine, 1,6-diamino hexane and sodium hydrogencarbonate were purchased from Sigma Aldrich and used as received.

B.2.2 Synthesis of Polysuccinimide

The synthesis of polysuccinimide followed previously published procedures (Bennett in J. Chem. Ed.).[1,2] The thermal condensation reactions, to produce bulk polysuccinimide, were performed in a 200-ml long neck beaker. 4 g of L-aspartic acid were charged in the beaker, which was immersed in a silicon oil bath. The bath was brought quickly to 240 ^{o}C and maintained at that temperature. During the period of heating a glass stirring rode was used to agitate the contents of the beaker every minute or so, to ensure proper mixing and avoid charring of the reactants. Typical reaction times were 4-6 hours. After about 1 hour of heating, the mixture color was altered from bright white of L-aspartic acid to tan yellow of polysuccinimide. When the heating was complete, the beaker was allowed to cool down to room temperature. The obtained solid was washed with saturated aqueous $NaHCO_3$ (3 times by 5 ml), distilled water (1 time by 5 ml) and 1 % aqueous HCl (2 times x 5 ml). The washed solid was filtered and dried in a vacuum oven at 80 ^{o}C overnight. Gel permeation chromatography experiments show a molecular weight (Mn) of > 20,000 of the as-synthesized polysuccinimide.

B.2.3 Modification of Polysuccinimide

The modification of biodegradable polysuccinimide, synthesized as described above, with 3-hydroxytyramine hydrochloride, 3,4-dihydroxy benzoic acid and 3,4-dihydroxy-L-phenylalanine has been explored. A slightly different approach included the cross-linking of the as-synthesized polysuccinimide with 1,6-diamino hexane and diethylene triamine before grafting it with the phenolic-containing compounds. This approach was investigated in order to explore if increased molecular weight has any effect in the adhesive properties of the obtained final materials.

B.2.3.1 Reaction of Polysuccinimide with 3-Hydroxytyramine Hydrochloride

0.1 g of as-synthesized polysuccinimide was reacted with 0.19 g of 3-hydroxytyramine hydrochloride (DOPA) (**Figure B-1**) in a 50-ml three neck round bottom flask equipped with a thermometer and a nitrogen purge. The molar ratio of polysuccinimide/diphenol-containing compound was equal to 1/1 based on the repeating unit of polysuccinimide. 30 ml of DMF or DMSO were added in the reaction flask. The reaction was held at 60-70 ^{o}C for 2 hours. The reaction mixture was then let to reach room temperature before the solvent was removed with the aid of a rotary evaporator. The obtained dark residue was obtained as a very sticky product at the bottom of the flask.

An alternative approach that has been investigated, is the reaction of the as synthesized polysuccinimide with a cross-linker, such as 1,6-diamino hexane or diethylene triamine, before the reaction with the diphenol-containing compound. As a typical procedure, 0.1 g of polysuccinimide was reacted with 0.01 g of 1,6-diaminohexane in 20 ml of DMF at 40 ^{o}C for 1 hour. After the cross-linking reaction, the required amount of 3-hydroxytyramine hydrochloride (e.g. 0.19 g) was added in the reaction mixture and the temperature of the solution was raised to

60-70 ^{o}C for 2 more hours. The reaction mixture was then let to reach to room temperature before the solvent was again removed with the aid of a rotary evaporator. The obtained dark residue was obtained as a very sticky product at the bottom of the flask.

B.2.3.2 Reaction of Polysuccinimide with 3,4-Dihydroxy-L-phenylalanine

The same synthesis procedure as the one used above, was used for the reaction of polysuccinimide with 3,4-dihydroxy-L-phenylalanine**.** In this case, 0.2 g of 3,4-dihydroxy-L-phenylalanine was reacted with 0.1 g of polysuccinimide in 30 ml of DMSO in a three neck round bottom flask, equipped with a thermometer and a nitrogen inlet-outlet at 60-70 ^{o}C for two hours. As in the case of 3-hydroxytyramine hydrochloride, the cross-linking reaction of polysuccinimide with 1,6-diaminohexane, before the addition of 3,4-dihydroxy-L-phenylalanine in the reaction mixture, has been also investigated.

B.2.3.3 Reaction of Polysuccinimide with 3,4-Dihydroxy Benzoic Acid

Following the above mentioned synthesis procedure, the reaction of polysuccinimide with 3,4-dihydroxy benzoic acid has been also investigated.

B.2.4 Results and Discussion

The as-synthesized polysuccinimide has a molecular weight of > 20,000 according to the gel permeation chromatography experiments. All of the above mentioned obtained products were tested for adhesiveness on various wet and dry surfaces. The surfaces that these materials were tested on include plastic, glass, metal, beef bone, pork skin and pork tissue. Polysuccinimide modified with 3-hydroxytyramine hydrochloride showed the highest adhesiveness on dry surfaces. Unfortunately, all of the obtained materials show poor adhesiveness on wet surfaces. On the other hand, when one compares crosslinked with non-crosslinked polysuccinimides, the

latter ones gave stickier final products. Crosslinking of polysuccinimide seems to have a big effect on the final properties of the obtained materials as one would expect. These tend to be stickier and more viscous as compared to the products synthesized from the non-crosslinked polysuccinimide. If the surfaces are put in a series of the ones showing the highest to lowest adhesiveness that would be metals (including Pt, Fe and Ag), plastic, glass, pork bone, pork skin and pork tissue (**Table B-1**). Unfortunately all of the as-synthesized crosslinked products also showed from poor adhesiveness on wet surfaces including metals, plastic, glass, beef bone, pork skin and pork tissue (**Table B-2**). Nevertheless, these results indicate that the diphenolic moiety present in the polymeric backbone seems to play an important role in the final properties of the products. More experiments and tests are needed to support these arguments and to yield modified polyaspartates with improved adhesiveness on wet surfaces. These efforts should perhaps mostly focus on purifying the obtained products, on grafting higher amount of the diphenolic moiety on the polysuccinimide polymeric backbone, and/or on obtaining higher cross-linking density of polysuccinimide.

B.3 Polyethylene Glycol (PEO) Approach

Similarly to the case of modified polysuccinimide that was described earlier, the modification of polyethylene glycol with 3,4-dihydroxy benzoic has been investigated, in an effort to synthesize a biomimetic system that contains the same chemical groups, as the proteins that are extracted by marine organisms, which are responsible for the characteristic ability of these creatures to stick on various surfaces underwater. The 3,4-dihydroxy benzoic acid is reacted with the alcohol side groups of polyethylene glycol through esterification. The synthesis procedure and the adhesive capabilities of the obtained materials are presented.

B.3.1 Materials

Polyethylene glycol (1000 amu), 3,4-dihydroxy benzoic acid and zinc chloride were purchased from Sigma-Aldrich and used as received.

B.3.2 Synthesis Procedure

Polyethylene glycol (PEO) was reacted with 3,4-dihydroxy benzoic in toluene with the utilization of a Dean-Stark apparatus (**Figure B-3**). The Dean-Stark distillation apparatus works as follows: as the esterification reaction proceeds, water is produced. Water and toluene create an azeotrope (i.e. they will boil at a lower temperature than toluene alone). Since water has higher density than toluene, when the water-toluene mixture condenses, it flows into the Dean-Stark trap and the water now remains at the bottom. Hence, toluene overflows back into the reaction vessel, but the water that is removed from the reaction flask remains trapped. This is a simple method of removing water and pushing the equilibrium of the reaction towards the esterification reaction. Zinc chloride (1 mol %) has been used as a catalyst for the esterification. As a typical procedure, 2.5 g of PEO (5 mmol) and 1.6 g of 3,4-dihydroxy benzoic acid (10.2 mmol) were charged in a three-neck round bottom flask equipped with a thermometer and a Dean-Stark apparatus. In the above mixture, 6 mg of $ZnCl_4$ were added and the reaction mixture was refluxed at 110 ^{o}C overnight. The obtained solid was washed with copious amounts of toluene, filtered and dried under vacuum. (yield 48%)

B.3.3 Results and Discussion

The obtained products had a waxy-like form. The as-synthesized modified with 3,4-dihydroxybenzoic acid polyethylene glycols were tested for adhesion on both wet and dry surfaces including metals (e.g. Pt, Fe, Ag), glass, plastic and pork skin and pork bone. All of the as synthesized materials show promising adhesiveness on dry surfaces. If the surfaces are put in

a series of the ones showing the highest to lowest adhesiveness, that would be plastic, glass, metals (including Pt, Fe and Ag) and beef bone. The obtained products show no adhesion on pork skin and pork tissue. In addition, adhesion on wet surfaces is poor. This may be attributed to the partial dissolution of the PEG chains upon contact with water. Future experiments are needed for the optimization of this synthetic procedure. The experimental efforts should focus on the purification of the obtained products, on utilization of higher molecular weight or crosslinked polyethylene glycols, and possibly on the reaction of other diphenolic and triphenolic compounds with polyethylene glycol.

B.4 Future Directions

In Chapter 3, the synthesis and characterization of a novel biodegradable, biocompatible and non-toxic adhesive, which was obtained by the modification of chitosan by 3,4-dihydroxybenzoic acid, was described. As mentioned in that chapter, diphenolic-containing compounds have been incorporated on the backbone of the biodegradable polymer and the obtained materials showed promising results with regards to their adhesion. Following the same concept, alternative diphenolic or triphenolic compounds may be grafted on chitosan or other backbones, which are known to biodegrade. Such biodegradable polymers could be hyaluronic acid, N-acetylneuraminic acid (structures shown in **Figure B-5**), polyvinyl alcohol, polysuccinimide (some work was presented earlier), gelatin, and many others, which contain functional groups that can react further with di- or tri-phenol containing compounds. In addition, lysine, which have been proven by many research studies to impart adhesive properties, once grafted onto various polymers, may be grafted onto the backbone of a biodegradable polymer along with the diphenol containing compounds. Alternatively, another approach could be the utilization of various biodegradable polymers, like polylactic acid, polyglycolic acid,

polyfumaric anhydride, polysebasic anhydride, polyethylene oxide and copolymers of them, for the synthesis of a composite or a copolymer with cyanoacrylate moieties of various content. Many of the above mentioned approaches have been already or will be studied in our lab in the near future.

Table B-1. Compositions and adhesiveness on dry surfaces of compounds investigated

Reactants		**Surfaces tested (dry surfaces)**					
Biodegradable polymer	**Diphenolic group**	**Metal**	**Plastic**	**Glass**	**Beef bone**	**Pork skin**	**Pork tissue (liver)**
non-crosslinked polysuccinimide	3-hydroxytyramine hydrochloride	++	+	+	~	~	~
“ “	3,4-dihydroxy benzoic acid	+	~	~	-	-	-
“ “	3,4-dihydroxy-L-phenylalanine	++	+	+	-	-	-
crosslinked polysuccinimide	3-hydroxytyramine hydrochloride	+++	++	++	+	~	-
“ “	3,4-dihydroxy benzoic acid	+	~	~	~	~	-
“ “	3,4-dihydroxy-L-phenylalanine	++	++	++	+	~	-

Left rows: reactants used to synthesize the biodegradable adhesives, right rows: dry surfaces that the obtained products have been tested on. The surfaces were wiped with a kim-wipe tissue before application of the obtained material on the surface. A piece of filter paper was then pressed on top of the material and held on that place for about 5 minutes. The judgment of adhesion is empirical and no means of formal mechanical testing have been used.

+++ Very strong adhesion

++ Strong adhesion

+ Good adhesion

~ Poor adhesion

- No adhesion

Table B-2. Compositions and adhesiveness on wet surfaces of compounds investigated

Reactants		**Surfaces tested (wet surfaces)**					
Biodegradable polymer	**Diphenolic group**	**Metal**	**Plastic**	**Glass**	**Beef bone**	**Pork skin**	**Pork tissue (liver)**
non-crosslinked polysuccinimide	3-hydroxytyramine hydrochloride	~	~	-	-	-	-
" "	3,4-dihydroxy benzoic acid	-	-	-	-	-	-
" "	3,4-dihydroxy-L-phenylalanine	-	~	-	-	-	-
crosslinked polysuccinimide	3-hydroxytyramine hydrochloride	+	~	~	~	-	-
" "	3,4-dihydroxy benzoic acid	-	-	-	-	-	-
" "	3,4-dihydroxy-L-phenylalanine	-	-	~	~	-	-

Left rows: reactants used to synthesize the biodegradable adhesives, right rows: wet surfaces that the obtained products have been tested on. The surfaces were wetted with distilled water before application of the obtained material on the surface. A piece of filter paper was then pressed on top of the material and held on that place for about 5 minutes. The judgment of adhesion is empirical and no means of formal mechanical testing have been used.

+++ Very strong adhesion

++ Strong adhesion

+ Good adhesion

~ Poor adhesion

- No adhesion

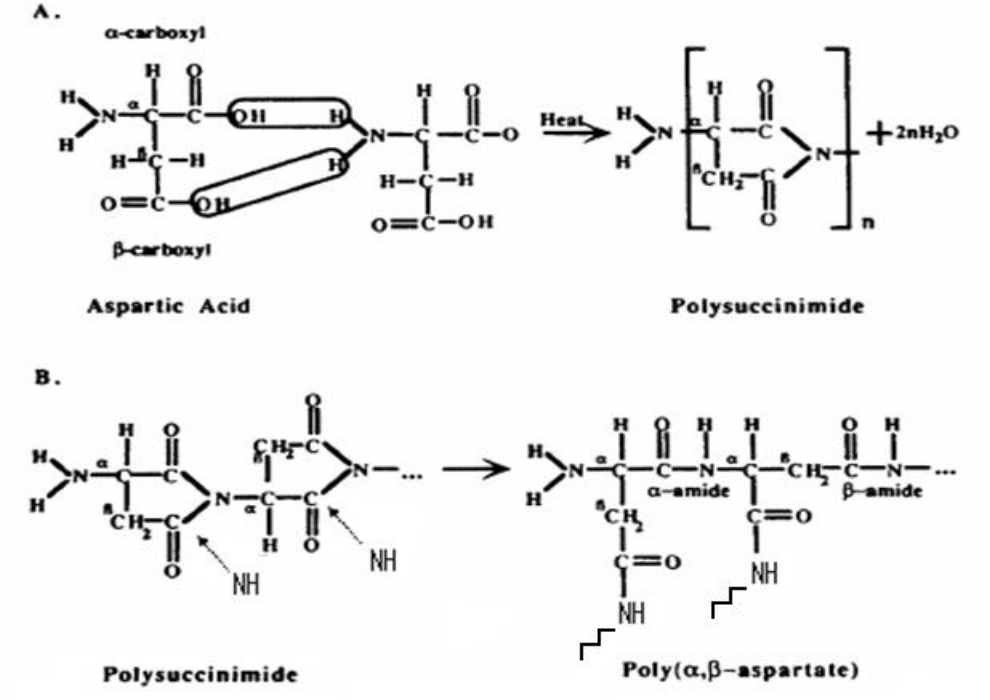

Figure B-1. (A) Thermal polycondensation of aspartic acid to form polysuccinimide, (B) reaction of polysuccinimide by opening of the ring to yield poly (α,β-aspartate).

(a)

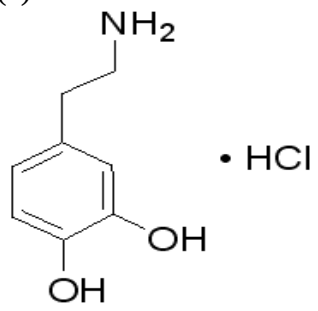

(b)

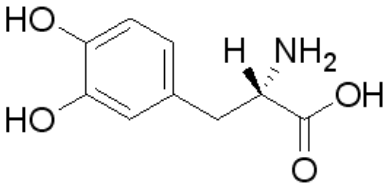

(c)

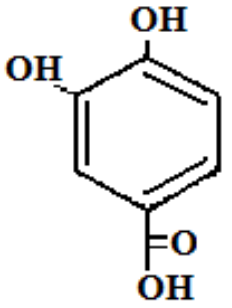

Figure B-2. Structures of diphenolic compounds investigated: (a) 3-hydroxytyramine hydrochloride, (b) 3,4-dihydroxy-L-phenylalanine, (c) 3,4-dihydroxybenzoic acid.

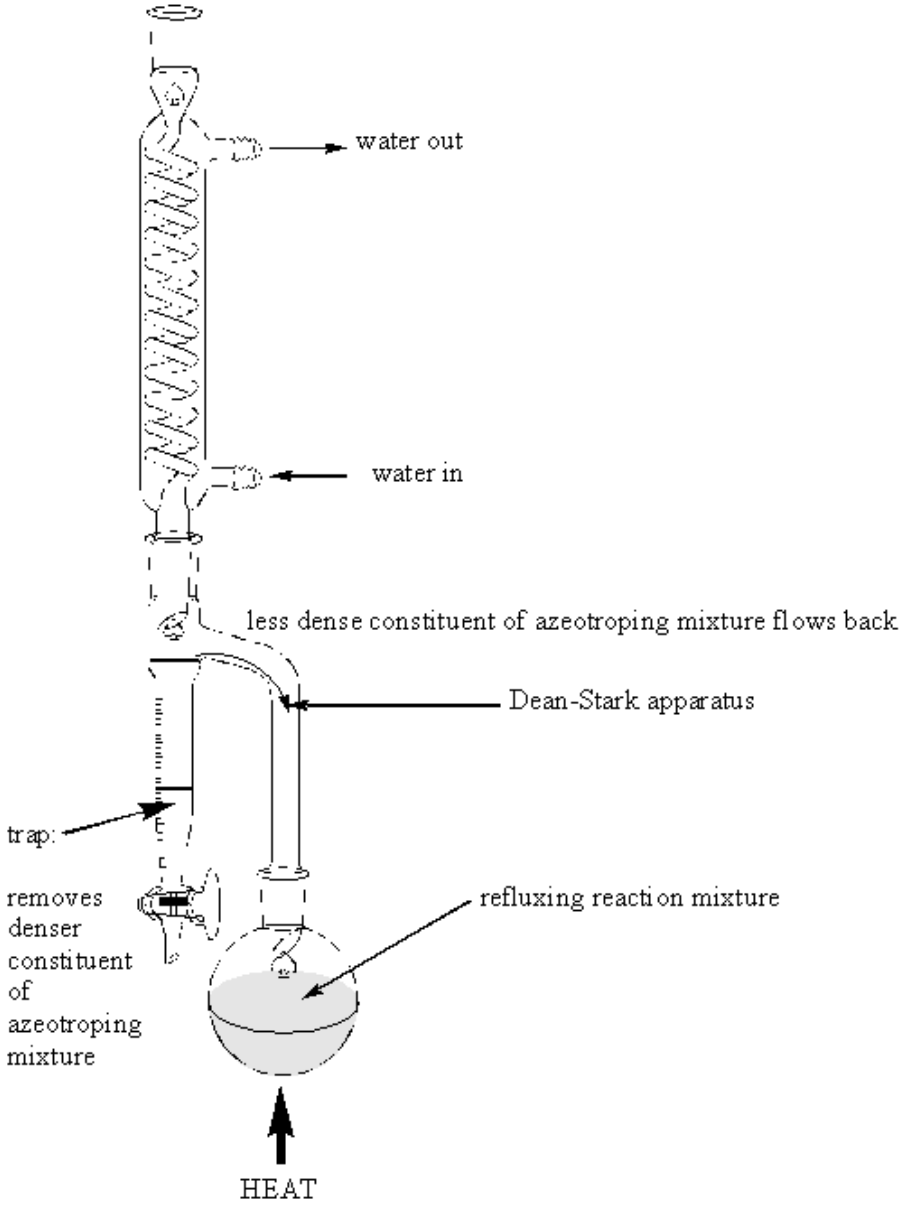

Figure B-3. General schematic of the apparatus, used for the esterification of polyethylene glycol, utilizing a Dean-Stark apparatus.

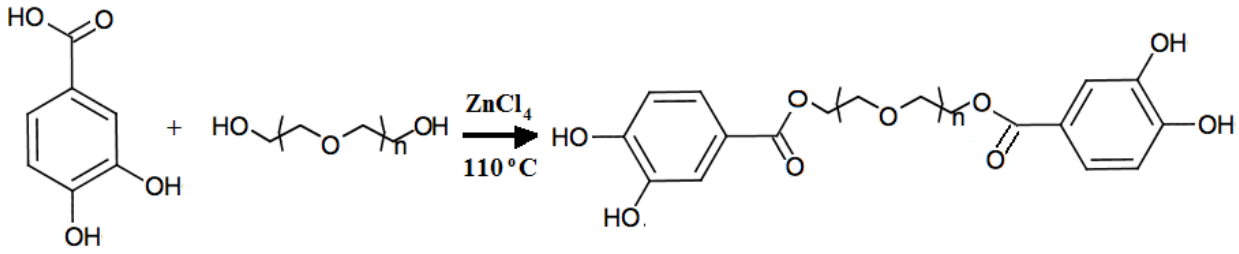

Figure B-4. Schematic of the synthesis procedure of esterification of PEG.

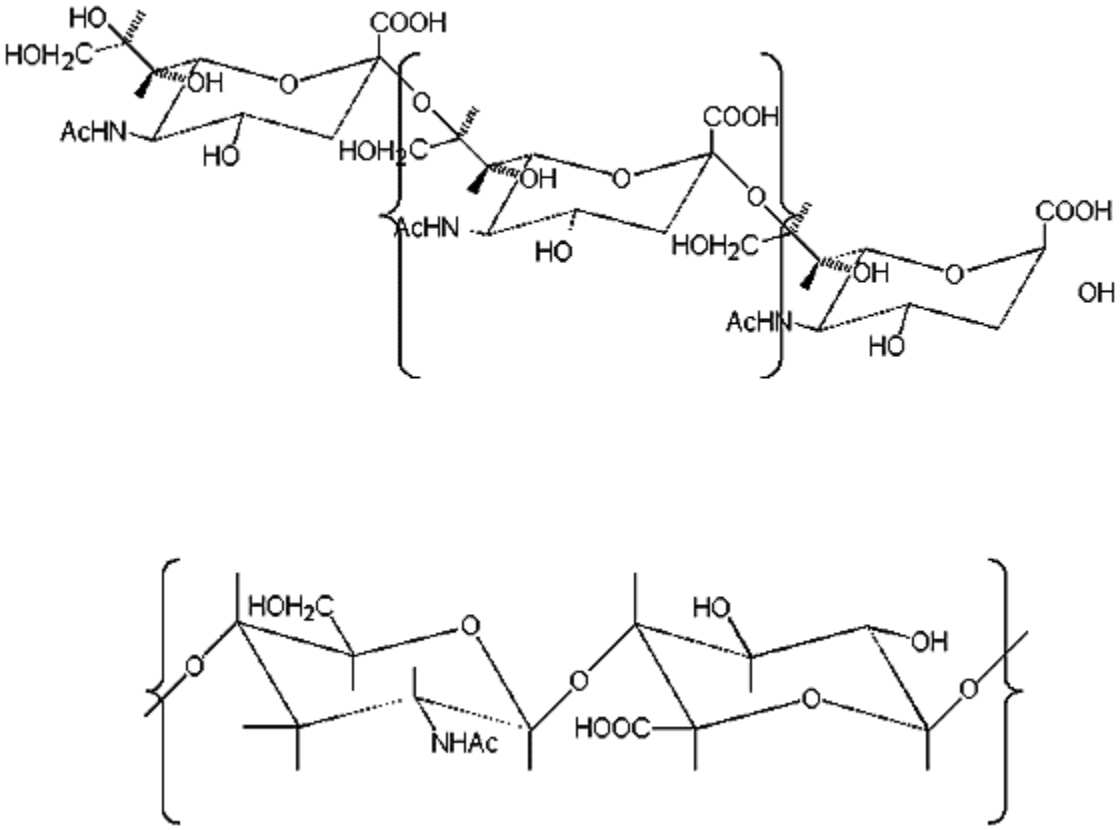

Figure B-5. Structures of hyaluronic acid and N-acetylneuraminic acid polymers.[3]

B.5 Reference List

1. Bennett, G.D. A green polymerization of aspartic acid for the undergraduate organic laboratory. Green chemistry. Journal of Chemical Education (2005), 82, 1380-1381.

2. Alford, D.D., Wheeler A.P., Pettigrew C.A. Biodegradation of thermally synthesized polyaspartate. Journal of Enviromental Polymer Degradation (1994). 2, 225-236.

3. http://www.glycoforum.gr.jp. Glycolforum; 2008.

Appendix C. Preservation of Historic Property Utilizing Bacteria and Biodegradable Polymeric Microspheres

(An Independent Research Proposal, Defended and Passed On December 15th, 2006 in Partial Fulfillment of the Requirements for the Ph.D. Candidacy)

C.1 Proposal Hypothesis

The utilization of biodegradable polymeric nanospheres and heterotrophic calcinogenic bacteria as a method to induce calcium carbonate precipitation inside the pores and on top of the stone of historic buildings or even monumental statues. The key issue of this approach is the controlled release of the nutrient, encapsulated in the polymeric nanospheres, to the bacteria that will make the regulation of the calcium carbonate precipitation feasible.

C.2 Abstract

Attempts to stop, or at least slow down, monument deterioration have been continuously made by utilization of several methods. Unfortunately, these treatments present several drawbacks and cannot fully satisfy the goal of safe conservation of historic property. Thus, the invention of a method that protects cultural heritage effectively and safely, and is environmentally friendly, is still a big challenge to be conquered. Herein, I propose the utilization of biodegradable triblock copolymers and heterotrophic calcinogenic bacteria as a method to induce calcium carbonate precipitation inside the pores and on top of the stone of historic buildings or even monumental statues. The treatment starts by applying a coating of the heterotrophic calcinogenic bacteria on the surface that is to be preserved and which consists of calcium carbonate. Biodegradable ABA triblock copolymer microspheres consisting of hydrophobic poly(D,L-lactic-co-glycolic acid) (PLGA) as A blocks and hydrophilic poly(ethylene

oxide) (PEO) as B blocks, containing calcium cations and several amino acids, will be then applied on top of the bacteria and will serve two functions. First, they are going to promote bacterial proliferation, since they contain the appropriate nitrogen and carbon sources, which will be released upon hydrolysis-biodegradation of the polymer. Secondly, the calcium cations released, shall "cooperate" with bacterial metabolism and carbonate anions towards the precipitation of calcium carbonate. Controlled release of nutrients to bacteria and the subsequent controlled calcium carbonate precipitation is thus achievable. This coating will form a smooth "blanket" several micrometers thick, which will partially fill the voids formed by the pores at the surface, and thus will become rooted in the structure of the stone. This biocalcin is going to ensure the protection of the treated surface, by restricting exchange between the interior of the stone and external atmosphere and, additionally, by limiting the penetration of degrading agents into the stone. This technique is environmentally friendly, low-cost, and presents no-risk to human health and the surfaces to be treated.

C.3 Introduction and Motivation

The use of stone, as a medium for artistic expression, has ranged from the construction of monuments and buildings to small-scale statues. While the weathering of rocks to soil formation is unquestionably essential for the evolution of life on earth, the decay of culturally significant stone artifacts represents an irretrievable loss of our heritage and history (**Figure C-1**).

The decay of rocks and freshly exposed monumental stones is a complex process, in which physical and chemical mechanisms are usually considered the main factors. It generally starts with alteration processes, due to the synergetic action of rain, wind,

sunlight and freezing/thawing cycles.[2] Thus, the initial smooth and clean stone surface becomes progressively rough and more porous, with the formation of micro cracks and fractures within crystal grains. Moreover, the pollutants, whose concentration level is continuously increasing in our atmosphere, form deposits of particles, black encrustation and leave secondary reaction products on stone surfaces. The consequence of these combined actions is a loss of cohesion with dwindling and scaling of stone material and with general weakening of the superficial structural strength.[3,4]

Attempts to stop, or at least to slow down, monument deterioration have been continuously made by application of conservative treatments with both inorganic and organic products.[5-9] The use of the latter presents some drawbacks due to their chemical composition and thermal expansion coefficient, which are quite different from that of the stone.[9] Products applied for stone conservation, such as silicones and ethyl silicates, cannot fully satisfy the goal of safe conservation. Such treatments, based on these chemical products, tend to produce a superficial skin that deteriorates with age, tends to peel off, and thus requires constant maintenance.

In fact, restorers involved in monument conservation, due to the unsatisfactory results obtained with such products, are extremely reluctant to use them as conservation products, to consolidate or protect stone surfaces. Color changes, crust formation, glossy appearance and substrate exfoliation, together with environmental pollution, due to the use of large amounts of organic solvents, are the most frequent drawbacks. These are essentially related to chemical and photochemical reactions, which cause alterations to the product's structure.[10] Furthermore the lack of standard methods for evaluating the

treatment effectiveness can lead to an over or under estimation of the amount of products to be applied.

From the above discussion, it can be easily understood that the maintenance field of historical stones needs innovative conservation strategies that can safely accomplish the objective of sustainable interventions. The invention of a method that protects cultural heritage effectively and safely and is environmentally friendly is still a big challenge to be conquered. It is essential that a method protects the surface over a large period of time without the need for numerous applications of this treatment. This proposal presents a method that utilizes biodegradable polymers and heterotrophic calcinogenic bacteria to protect effectively, and for a long period of time, historic buildings and monumental statues.

Biodegradable ABA triblock copolymer microspheres consisting of hydrophobic poly(D,L-lactic-co-glycolic acid) (PLGA) as A blocks and hydrophilic poly(ethylene oxide) (PEO) as B blocks, containing calcium cations and several amino acids, will be applied on top of the bacteria and will serve two functions. First, they contain the appropriate nitrogen and carbon sources, which will be released upon hydrolysis-biodegradation of the polymer, in order to promote bacterial proliferation. Secondly, calcium cations released, shall “cooperate” with bacterial metabolism and carbonate anions towards the precipitation of calcium carbonate. In this way, the controlled release of nutrients to bacteria and the subsequent controlled calcium carbonate precipitation is achievable. This method will make the thickness and porosity of the obtained calcium carbonate coating on the surface of the monuments experimentally controlled.

C.4 Calcinogenic Bacteria

C.4.1 Metabolic Pathways

The production of calcium carbonate particles, through bacterial mediation, can follow two different pathways. In autotrophy, three metabolic pathways are involved: non-methylotrophic methanogenesis, anoxygenic photosynthesis and oxygenic photosynthesis. All three pathways use CO_2 as carbon source to produce organic matter. In heterotrophy two bacterial processes may occur, often concurrently. These are called passive and active precipitation.

In the passive precipitation, or passive carbonatogenesis, two metabolic cycles can be involved: the nitrogen cycle and the sulphur cycle. In the nitrogen cycle, passive bacterial precipitation follows three different pathways: (a) the ammonification of amino-acids (in aerobiosis (i.e., in the presence of gaseous or dissolved oxygen), in the presence of organic matter and calcium); (b) the dissimilatory reduction of nitrate (in anaerobiosis (i.e., in the absence of oxygen) or microaerophily (i.e., in the presence of very low amounts of oxygen), in the presence of organic matter, calcium and nitrate); and (c) the degradation of urea or uric acid (in aerobiosis, in the presence of organic matter, calcium, and urea or uric acid).

These three pathways induce production of carbonate and bicarbonate ions and, as a metabolic end-product, ammonia, which induces pH increase. When proton concentration decreases, the carbonate–bicarbonate equilibria are shifted towards the production of carbonate ions. If calcium ions are present, calcium-carbonate precipitation occurs. If calcium cations (and/or divalent cations) are lacking in the medium, carbonate

and bicarbonate ions accumulate, and the pH increase and bacterial activity may favor zeolite formation.[11] This happens in soda lakes, e.g., in Kenya.[12]

Herein, the bacteria that are going to be used are metabolized through the nitrogen cycle and follow the pathway of ammonification of amino acids. Quantitatively, the production of solid calcium carbonate by these bacterial organisms depends essentially upon the strains in the bacterial population, the environmental conditions (temperature, salinity, etc), the quality and quantity of available nutrients and time.[13]

C.4.2 Mechanism of Calcium Carbonate Production

The mechanism by which the heterotrophic calcinogenic bacteria produce calcium carbonate is complex and still not well understood. Nevertheless, bacterial activity can control the crystallogenesis of carbonates, and crystals start to build up on the bacterial wall. In a few steps a kind of cocoon forms and subsequently biomineral assemblage appears progressively turning into true crystals, either well shaped or poorly organized, trapping bacteria within the mineral structure.[13,14] Differences in the type of crystal formed (vaterite, aragonite or calcite) depend both on growing features and bacterial strains. Different bacteria precipitate different types of $CaCO_3$.[15]

Carbonatogenesis appears to be the response of heterotrophic bacterial communities to an enrichment of organic matter. The phase of latency of bacterial evolution is followed by an exponential increase in bacterial growth together with the accumulation in the medium of metabolic end-products: carbonate, bicarbonate and ammonia ions (**Figure C-2**). This phase is followed by the steady state. Calcium carbonate precipitation occurs during the exponential phase and ends more or less after the beginning of the steady state.[16] In most cases, the active carbonatogenesis seems to

start first followed by the passive carbonatogenesis, which induces the growth and shape modifications of initially produced particles.

C.5 Biodegradable Polymeric Microspheres

The use of degradable polymers in environmental, medical and other applications has gained increased interest in the past 2 decades. Degradable polymers have applications as materials for bottles, packaging and other widely used consumer products that would not create environmental build-up, as well as biomedical applications, including drug delivery systems, resorbable sutures, stents and scaffolds for tissue regeneration.[17,18] In this proposal, an important class of degradable polymeric systems, that is polyesters, which undergo degradation by chemical reactions, is going to be employed. Aliphatic polyesters have utility as temporary prosthetics, surgical aids and subdermal drug delivery systems, because of their demonstrated susceptibility to biodegradation and lack of toxicity. [19]

For many, if not for all applications, whether these are medical or other, the erosion profile of polymers is of crucial importance.[20] The rate of polymer degradation depends on the molecular weight, the polydispersity, the composition and the material geometry.[21,22] In the case of a surface-eroding polymer, erosion is confined to the polymer surface, while in the case of bulk erosion, polymer matrices erode throughout their cross section (**Figure C-3**).[23,24] The biodegradable polymers, used in this proposal, were chosen specifically to erode via the bulk erosion route.

The success of this novel approach depends a lot on the degradation profile of the microspheres or nanospheres that are going to be used. The goal is that the bacteria are initially enriched with the organic matter that will be provided from the surface of the

biodegradable polymeric spheres. As soon as these microspheres start to erode at the points where they are directly touching the bacteria, the enrichment in aminoacids and Ca^{+} will begin. This, in cooperation with the bacterial metabolism that produces carbonate ions will subsequently cause calcium carbonate to be produced. In this way, the controlled release of nutrients to bacteria and the subsequent controlled calcium carbonate precipitation will be achievable. On the other hand, if surface erosion polymers were used, probably several problems would be encountered. A surface erosion polymer could yield an initial high enrichment of organic matter that would lack the presence of calcium ions and aminoacids. That in turn could yield a significant bacterium evolution that could potentially block the passages for the nutrient to reach the bacteria, which reside at the lower sections of the bacteria coating.

C.6 Proposed Research

Herein, I propose the use of heterotrophic calcinogenic bacteria (e.g. *Bacilus Cereus, Bacillus Subtillis,* etc.) as a method to induce calcium carbonate precipitation inside the pores and on top of the stone of historic buildings or even monumental statues. These bacteria are able to undertake ammonification of amino-acids, and as metabolic end-products, upon enrichment with organic nutrients, they produce carbonate, bicarbonate and ammonia ions. The treatment could start by applying a coating of these heterotrophic calcinogenic bacteria on the surface that is to be preserved and which consists of calcium carbonate.

Following this step, microspheres prepared from biodegradable ABA tri-block copolymers, consisting of hydrophobic poly(D,L-lactic-co-glycolic acid) (PLGA) as A blocks, and hydrophilic poly(ethylene oxide) (PEO) as B blocks, will be then applied on

top of the bacteria coating. These microspheres, containing calcium cations and several amino acids, will serve two functions. First, they contain the suitable organic source, namely carbon, oxygen and nitrogen resource, which is going to serve as nutrient for the bacteria. This organic nutrient is provided to the heterotrophic bacteria upon hydrolysis/biodegradation of the copolymer and results in bacterial proliferation. Secondly, the microencapsulated calcium cations and aminoacids that they contain will be gradually released when the biodegradation/hydrolysis of the biodegradable polymers reaches a specific point. These compounds upon release will "cooperate" with bacterial metabolism, which produces carbonate anions, towards the precipitation of calcium carbonate.

By employing this novel method, the controlled release of nutrients to bacteria and the subsequent controlled calcium carbonate precipitation is achievable. This method will make the thickness and porosity of the obtained calcium carbonate coating on the treated surface experimentally controlled. This coating will form a smooth "blanket" several micrometers thick, which will partially fill the voids formed by the pores at the surface and thus will become rooted in the structure of the stone. This biocalcin will ensure the protection of the treated surface by restricting exchange between the interior of the stone and external atmosphere and, additionally, by limiting the penetration of degrading agents into the stone.

C.7 Theoretical Considerations

C.7.1 Bacterial Growth and Calcite Precipitation

In the past, many different strains of bacteria have been identified as calcinogenic, and several different studies have been conducted exploring the mechanism that drives

these bacteria to produce calcium carbonate when proper nutrients are present (e.g. *Micrococcus sp., Bacillus subtilis, Bacillus pasteurii, Deleya halophila, Halomonas eurihalina, and Myxococcus xanthus*).[11-16] Various different bacteria strains can be used in this novel proposal. *Bacillus subtillis* and *bacillus cereus,* which are heterotrophic bacteria able to undertake ammonification of amino-acids, are two candidates.

Results of preliminary experiments, which have to take place in the lab before life size applications, will dictate what type of bacteria strain is going to be used in this approach for the preservation of cultural heritage. The aim of these experiments is going to be the study of the calcinogenic yield of different strains. It is important to stress out that these strains of bacteria are able to extracellularly degrade the polymeric microspheres via esterase activity and use them as a nutrient for their metabolic pathway.[25-31] In other words, the polymeric triblock copolymer degradation can be carried out either by chemical hydrolysis or by bacteria (enzymatic) biodegradation. However, most probably the mechanism of degradation of the triblock copolymer is going to be a cooperation of both of these degradation ways.

In the presence of organic matter and calcium cations, the result of their bacterial action is going to be the production of carbonate and bicarbonate ions accompanied by the increase of the pH values (**Figure C-5**). The production of solid calcium carbonate will depend essentially upon the strains in the bacterial population, the environmental conditions, the quality and quantity of available nutrients and time. The experimental conditions, which are going to be used for the study of the bacteria, should be as close as possible to the conditions at which the application of the product is going to take place. Besides, the pH plays an important role in the carbonatogenesis speed and efficiency of

these bacteria and a buffer solution might be required if the pH drops in values lower than those that result in calcium carbonate precipitation.

At this point, it has to be noted that the calcium carbonate coating that will be the end result of this process will form a smooth "blanket" several micrometers thick, which will partially fill the voids formed by the pores at the treated surface, and thus will become rooted in the structure of the stone. It may be said that the utilization of these calcinogenic bacteria is a method that will create a coating identical to the treated surface, since calcium carbonate is the main component of the surface of interest. This biocalcin will ensure the protection of this surface by restricting exchange between the interior of the stone and external atmosphere and, additionally, by limiting the penetration of degrading agents, like water and others, into the stone.

C.7.2 Microspheres Prepared from ABA Tri-Block Copolymer

The degradation rate of the polymeric spheres and the release behavior profile as a function of time are the most important design criteria. The most frequently used biodegradable polymers for drug delivery are polymers of lactic acid, glycolic acid and their copolymers, abbreviated as PLGA.[32-39] The intrinsic nature of these biomaterials renders them suitable for applications where temporally slow release of different agents is required. Degradation of PLGAs involves hydrolysis of the polymer to produce common metabolites, that is lactic and glycolic acids, which are eliminated through the Krebs cycle. The rate of degradation depends on the polymer composition, molecular weight and synthesis procedure.[40]

This copolymer represents a means of varying morphology and hydrophobicity, as well as the chemical susceptibility to ester hydrolysis. In brief, in the case of

polyglycolide (PG), amorphous regions undergo hydrolysis with random scission of ester groups followed by hydrolysis of the crystalline domains.[41] Compared to lactide, glycolide is more hydrophilic owing to the lack of pendant methyl groups. The optically active polylactide (PL) is semicrystalline and it degrades less rapidly than PG. Racemic poly(D,L-lactide) (PDLL) on the other hand, is amorphous and, therefore, will biodegrade more rapidly than its optically active counterparts, poly(L-lactide) (PLL) and poly(D-lactide) (PDL). From the above, it can be easily understood that the degradation rate of thePLGA copolymer can be adjusted by varying the lactic/glycolic ratio.

Despite the huge number of applications of PLGA copolymers, some less advantageous properties of them can be distinguished. One of these, is the relatively fixed thermomechanical properties, due to their relatively high glass transition temperature (T_g) of about 40-50 ^oC, which makes them more rigid. Secondly, a pH reduction due to the accumulation of acidic degradation products in the rigid PLGA matrix sometimes may significantly reduce the internal pH of PLGA microspheres, something that may have detrimental effects on the encapsulated agents. Another approach is to use multiblock copolymers composed of various pre-polymer building blocks of different combinations of DL-lactide (LA), glycolide (GA) and polyethylene glycol (PEG). Polyethylene glycol has been noted for being a biocompatible, nontoxic, non-immunogenic, and water-soluble material for use in pharmaceutical and biomedical applications.[42,43] By varying the molecular composition and molecular weight of the triblock copolymer, highly different functionalities can be now obtained (**Figure C-7**).

The procedure to synthesize microspheres or nanospheres with the encapsulated agents, involves a double emulsion/evaporation technique (**Figure C-8**). Polyvinylacohol

(PVA) is typically used to stabilize the emulsion. In the standard embodiment of the water-in-oil-in-water double emulsion protocol for making microspheres containing hydrophilic agents, the prepolymers are dissolved in a water-immiscible organic solvent to yield an organic phase. The hydrophilic agent is dissolved in the aqueous phase, and the two phases are then emulsified to yield a "water-in-oil" (W/O) emulsion. The W/O emulsion and a second aqueous phase are then again emulsified to yield a double "water-in-oil-in-water" (W/O/W) emulsion. The organic solvent is then removed from the W/O/W emulsion, yielding microspheres containing the hydrophilic agent, and the microspheres are recovered by ultracentrifugation.

In this novel method, the utilization of these biodegradable polymers, to preserve historic property, will have great advantages compared to other methods used. The fact that different molecular compositions and different molecular weights of the triblock copolymers result in different degradation behaviors, offers the researcher the ability to prolong or shorten the sustained release of the encapsulated agents (solution of aminoacids and calcium ions) to the calcinogenic bacteria to the favor of the sought end result. Thus, the control and adjustment of the bacterial proliferation and the subsequent biocalcin coating that will be rooted inside the pores of the treated surface will be plausible. The thickness and porosity of the obtained calcium carbonate coating on the treated surface can now be experimentally controlled.

At this point it must be noted that the size (diameter) of polymeric spheres that is going to be used will be dictated by the surface that is going to be treated. With regard to the size of the grain of the limestone used to create most of the cultural heritage monuments, two different classes can be distinguished. One class of materials is made

from coarse grain limestone and will most probably require the utilization of polymeric microspheres. On the contrary, the other class of the fine grain limestone materials will most probably require the use of polymeric nanospheres. This is because the volume of the pores on the surface is smaller, which means that in order to fill and coat the pores of the limestone surface and make the final coating of biocalcin to be rooted inside the structure of the stone, the usage of smaller particles might be necessary.

C.7.3 Agent Encapsulated in the Polymeric Spheres

The agent that contains aminoacids and calcium cations will be encapsulated in the polymeric spheres of micro or nano size and will be eventually delivered to the bacteria, upon hydrolysis/biodegradation of the polymeric spheres. The primary goal of the sustained agent release is the prolonged delivery of these aminoacids and the calcium cations to the calcinogenic bacteria, so that no repeated coatings with nutrient are necessary. The aminoacids are going to serve as a nitrogen source for the heterotrophic bacteria. The bacteria will then follow the amonification of aminoacids pathway, through the nitrogen cycle, and will produce carbonate anions. Finally, calcium cations released shall “cooperate” with bacterial metabolism towards the precipitation of calcium carbonate.

The agent encapsulated in the microspheres is going to be an aqueous solution that contains several amino-acids (e.g. L-Arginine, L-Asparagine, L-Glutamine, etc.) and $CaCl_2$ (0.5-0.75M). Which amino acids are going to be used to prepare the agent that is going to be encapsulated will be dictated by the type of the bacteria strain that is to be used. The encapsulated aminoacids should be the ones that are essential for the bacteria in order for them to proliferate and produce carbonate ions, as well as undergo other

metabolic activities. This means that a preliminary study of the aminoacids required for the bacteria-calcinogenic yield is necessary before the agent to be used is chosen.

C.8 Experimental Conditions

C.8.1 Pretreatment of the Surface

C.8.1.1 Cleaning of the Surface

In order to remove unwanted compounds and materials that reside already on the surface and in the pores of the stone, the treatment should start with a pretreatment of the surface. Identification of the factors responsible for the deterioration of the surface is a crucial step in developing a treatment strategy for an infected artwork.[44] Apart from physical reasons that lead to stone decay, common agents causing deterioration of cultural heritage are fungi and bacteria. There are several approaches that are already used to clean a surface of a stone that needs to be treated for preservation. Physical and chemical methods are used for the removal of possible dirt, foreign materials, gypsum residues and weathering crusts. These treatments might include surfactants and solubilizing agents to remove pollutants and residual substances, special mechanical tools, ultraviolet radiation, gamma rays, ultrasonic, lasers, and microorganisms.[45,46]

C.8.1.2 Consolidation of the Surface

Consolidation is the impregnation of the damaged areas of stone with a suitable product that reaches down into the underlying undamaged layers, and results in a strong cohesive structure. Consolidation usually happens after cleaning of the surface, because consolidant used at this step might cause a blockage of the pores of the stone, something that might make cleaning of the stone much harder if not impossible. Preconsolidation of

the surface may be deemed advisable before cleaning if the surface is friable or in an advanced state of decay.[47]

C.8.2 Novel Treatment Method-Preservation of the Surface

C.8.2.1 Preliminary Experiments in the Laboratory

The process has to be first simulated on miniature walls composed of both categories of limestones (e.g coarse grain limestone and fine grain limestone) before the life size applications of this method. Initially, several scientific investigations have to be undertaken. First, it is necessary to collect different carbonatogenetic bacteria strains from natural carbonate-producing environments and test them for their carbonatogenetic yield. This will then dictate what type of calcinogenic bacteria strain is going to be used in this preservation method. The experimental conditions (e.g. pH, humidity, temperature, etc.) that are going to be used for the bacteria study should be, as close as possible, to the conditions that the application of the product is going to take place. The effect of these factors, on the bacteria proliferation and the subsequent calcinogenic action, is going to be studied in order to find the optimum conditions.

C.8.2.2 Application of Heterotrophic Bacteria

The treatment of the surface after cleaning or consolidation will continue by applying a coating of the heterotrophic calcinogenic bacteria on the surface that is to be preserved. The culture of the bacteria has first to be incubated for 16-24 hours in the appropriate nutrient broth, depending on what bacteria strain is going to be used. *Bacillus* broth is an optimized medium for the growth of *Bacillus* species that can be purchased from major vendors. When the optimum density of the bacteria population has been reached, the bacteria solution can be sprayed or brushed on the surface of interest.

C.8.3 Synthesis of ABA Triblock Copolymers

ABA triblock copolymer consisting of poly(D,L-lactic-co-glycolic acid), as A blocks, and poly(ethylene oxide), as B blocks, is going to be synthesized using methods that have been described by various researchers.[48-52] Briefly, the procedure starts by mixing equimolar amounts of D,L-lactide and glycolide with poly(oxyethylene) and equivalent amounts of aluminum tri-isopropoxide in a flask under vigorous stirring and nitrogen purge. The reaction will be initiated by immersion into an oil bath preheated to 150 °C. When the reaction mixture becomes transparent, the bath temperature will be lowered to 110 °C. After 12-72 hours, the polymeric mixture will be cooled, dissolved in dichloromethane, extracted with hydrochloric acid (2N), washed with water and then precipitated with cold ethanol. The precipitated polymer will be finally dried at 50 ^{o}C under vacuum for 48 hourrs.

It must be noted that different ratios of monomers have to be tested in order to find the triblock copolymer composition that gives the optimum agent release profile for this specific application. Polymer molecular weights can be determined by gel permeation chromatography, using polystyrene as a reference material. The % molar ratios as referring to lactic acid:glycolic acid and poly(ethylene) oxide of the ABA polymer can be determined by ^{1}H-NMR spectroscopy in $CDCl_3$ solutions of the polymers containing tetramethyl silane (TMS) as reference at 25 °C.

C.8.3.1 Synthesis of Biodegradable Microspheres

Microspheres will be prepared by utilizing a double emulsion method.[48] The internal water phase (W1) will consist of aminoacids and $CaCl_2$ solution in distilled water. The organic phase (O) will contain the triblock copolymer in organic solvent

(dichloromethane). First the internal emulsion (W1/O) can be prepared using a high speed homogenizer (e.g. 20,000 rpm for 60 sec). The resulting emulsion will be then rapidly mixed with an aqueous solution of polyvinyl alcohol (W2) under stirring with another homogenizer at lower speed (e.g., 8,000 rpm), to form the (W1/O)/W2 double emulsion. For the removal of dichloromethane the double emulsion can be continuously stirred with a propeller mixer at 200 rpm for 3 hours. The solidified microspheres will be collected by centrifugation, followed by filtration and washing with distilled water. Finally the polymeric microspheres or nanospheres will be lyophilized.

C.8.3.2 Application of Biodegradable Triblock ABA Copolymers

Once the polymeric microspheres (or nanospheres depending on the porosity of the surface to be treated) with the encapsulated agent have been synthesized, the next step is to apply them, with the aid of a brush, on top of the calcinogenic bacteria coating. Special care has to be taken for difficult spots that either do not have an easy access or rely on edges. Depending on the results of the calcinogenic yield of the bacteria, it might be necessary for the microspheres to be mixed with a buffer solution, before their application on top of the bacteria coating. The detailed procedure of the application of the proposed method onto stone surfaces to be treated can be seen in **Figure C-10**, **Figure C-11** and **Figure C-12** respectively.

C.8.4 Characterization of the Treatment

The last step of this novel method for the preservation of cultural heritage will be the characterization of the obtained coating. Macroscopic observation will be definitely the first means of evaluation, because the aesthetic aspect cannot be neglected. There is no doubt though, that more scientific means of characterization have to be used in order

to evaluate the final result of this method. The identity of all crystals can be verified by X-ray crystallography and FT-IR spectroscopy, whereas the texture and morphology of the as-synthesized calcium carbonate coating on top of the treated surface can be observed through scanning electron microscopy or even optical microscopy for the case of big crystals. Measurement of the superficial water permeability (by measuring the time of water absorption using a water pipe) and probably microdrilling could be other methods to explore and evaluate the effectiveness of the biocalcin coating that this novel method will create on top of the surface of interest.

C.8.5 Possible Outcomes and Proposed Solutions

In this section some possible outcomes that may be faced during the experimental application of this novel technology, along with the proposed methods to solve for them, are briefly described. In the case that the calcine coating is too thick or too thin or peels off from the surface of interest, then a possible resolution could be to lower the population of the bacteria and/or the amount of the nanospheres. Another problem that might be faced is the lowering of the pH of the solution that contains the nanospheres. This lowering of the pH may be caused by the formation of big amounts of lactic and glycolic acid upon hydrolysis of the triblock copolymer, which in turn may cause the deactivation of the bacteria. If such a condition is faced, a good approach would be either to decrease the amount of lactide and glycolide in the as synthesized triblock copolymeric nanospheres or to use a neutral pH buffer solution. Lastly, in the unfortunate event that organic matter is left at the end of the procedure that might suggest the need to lower the amount of microspheres used or increase the population of the bacteria.

C.9 Proposed Time Frame

The proposed method can be divided into two separate phases. The first phase includes the simulation of this procedure on miniature walls, composed of both categories of limestones (e.g. coarse grain limestone and fine grain limestone), in order to find the optimum experimental conditions before the life size applications of this method. The proposed time frame for this phase is two years. The second phase contains the application of the bacteria-nanospheres formulation that showed the best results in the lab conditions onto real life applications and the evaluation of the obtained results. The proposed time frame for the second phase is one year. Thus, the time that this proposed method is going to require can be predicted into 3 years in total.

C.10 Conclusions

The proposed method is a method intended to provide a means of preservation of statues and historic property in general. This technique is environmentally friendly, low-cost and presents no-risk to human health and the surfaces to be treated. The formulation includes the utilization of biodegradable triblock copolymers and heterotrophic calcinogenic bacteria, as a method to induce calcium carbonate precipitation inside the pores and on top of the stone of historic buildings or even monumental statues. The biodegradable nanospheres used, are going to contain the appropriate nutrient, which is going to promote bacterial proliferation, since it contains the appropriate nitrogen and carbon sources, which will be released upon hydrolysis-biodegradation of the polymer. The controlled release of nutrients to the calcinogenic bacteria and the subsequent controlled calcium carbonate precipitation is, thus, going to be achievable. This coating is predicted to form a smooth “blanket” several micrometers thick, which will partially fill

the voids, formed by the pores at the surface of the stone, and thus will become rooted in the structure of the stone. This biocalcin is going ensure the protection of the treated surface by restricting exchange between the interior of the stone and external atmosphere and, additionally, by limiting the penetration of degrading agents into the stone.

Figure C-1. Influence of biodeterioration processes on an angel statue at the "Peters-Portal" on the cathedral of Cologne (Germany). Documented by (a) the original object in 1880, (b) the respective weathered statue in 1993.[1]

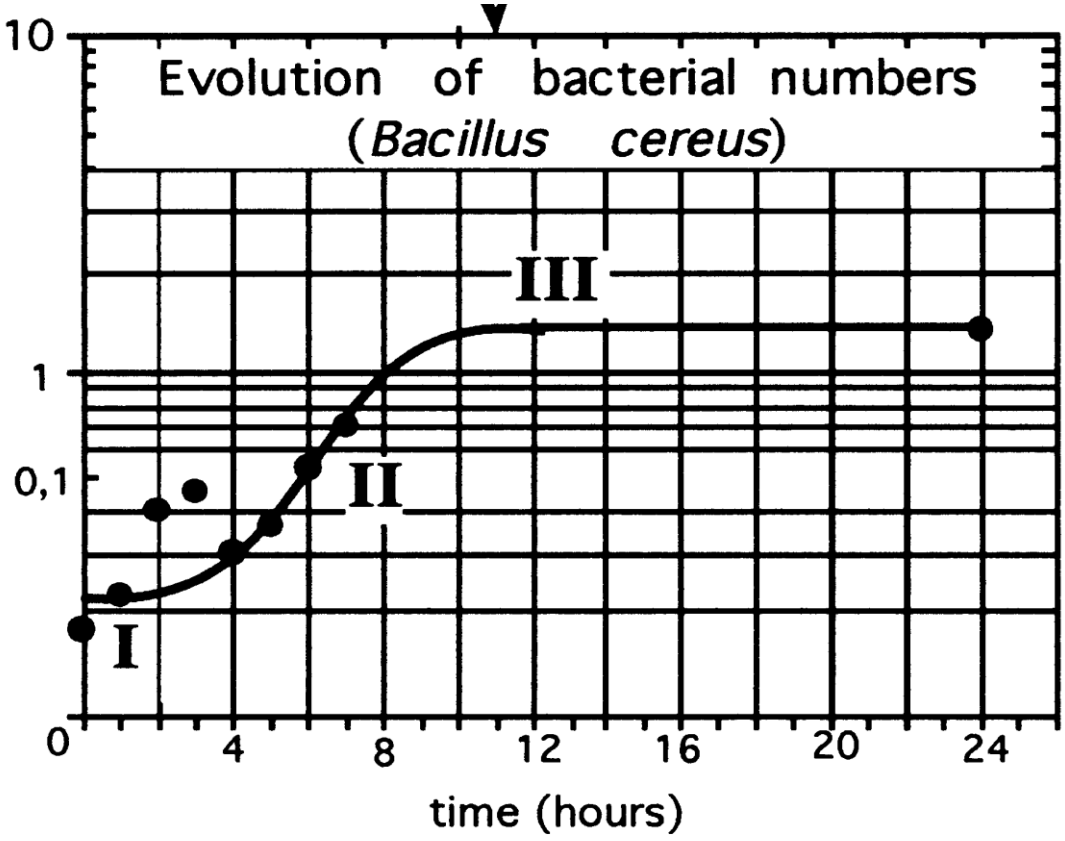

Figure C-2. I: Latency phase, II: Exponential phase and III: steady phase phase during bacterial evolution.[16]

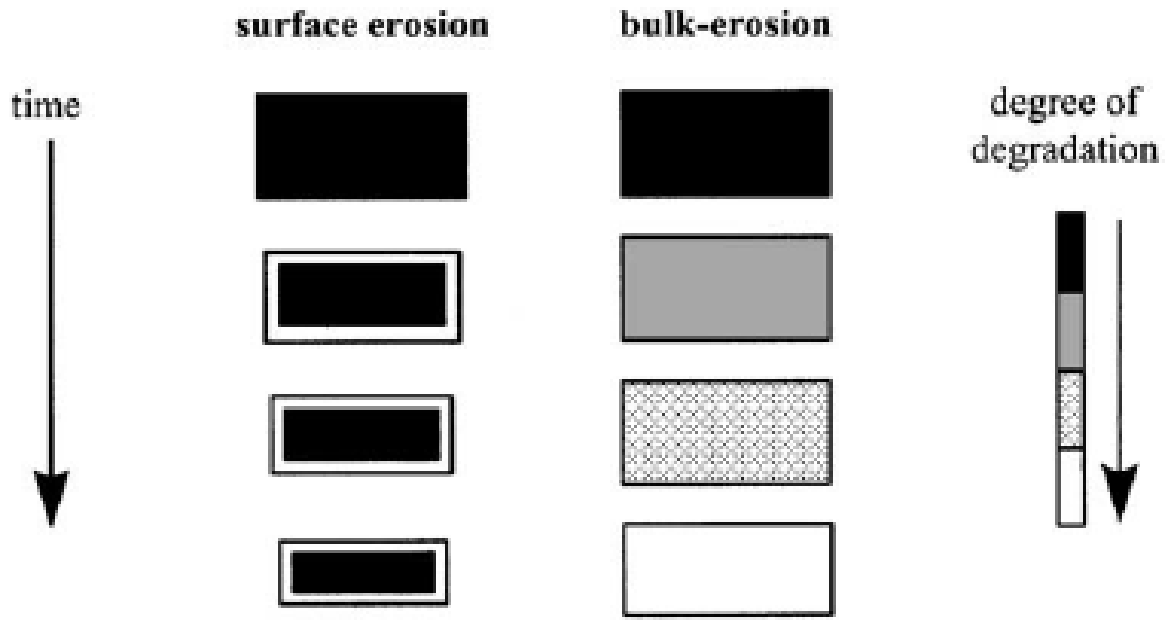

Figure C-3. Schematic illustration of the changes of a degradable polymer matrix upon degradation by: (a) surface erosion, (b) bulk-erosion.[24]

Figure C-4. Acropolis at night. Athens, Greece.

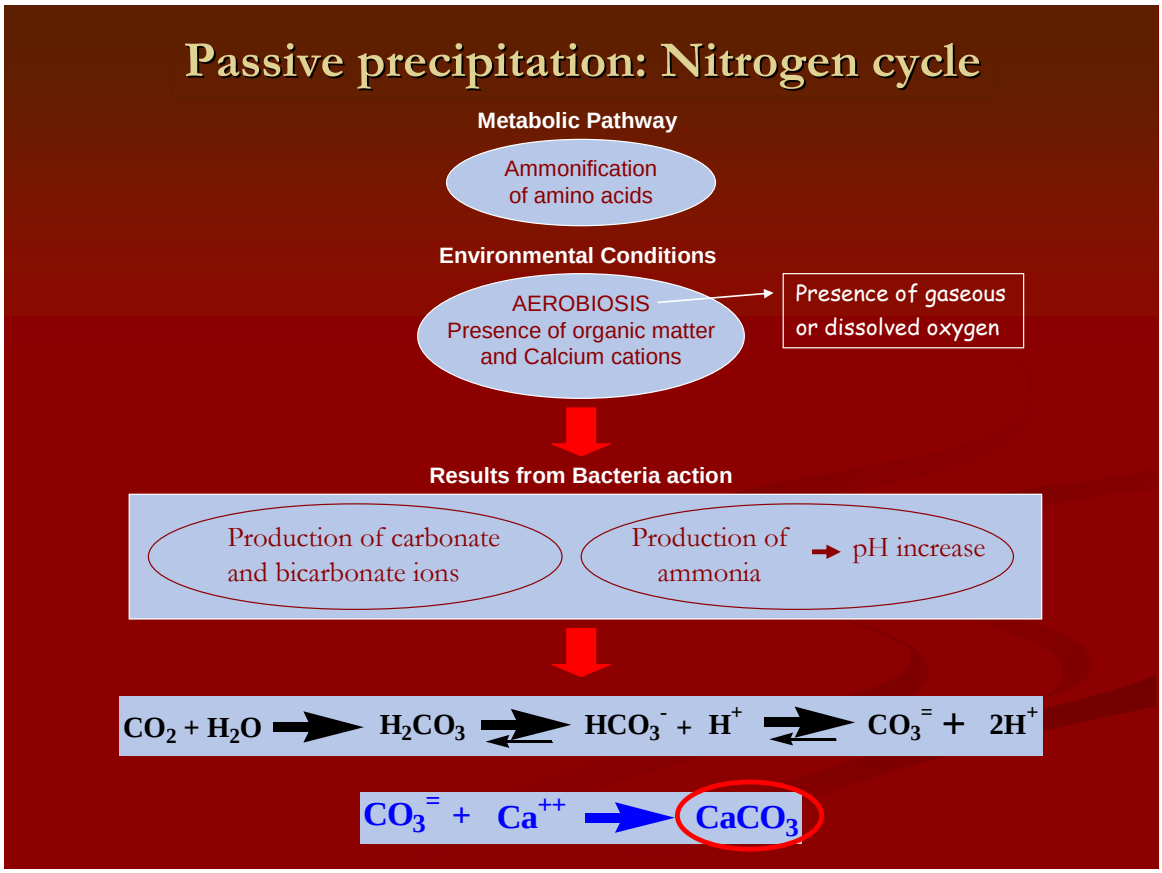

Figure C-5. Schematic of the detailed mechanism of the calcium carbonate bacterial precipitation.

(A)

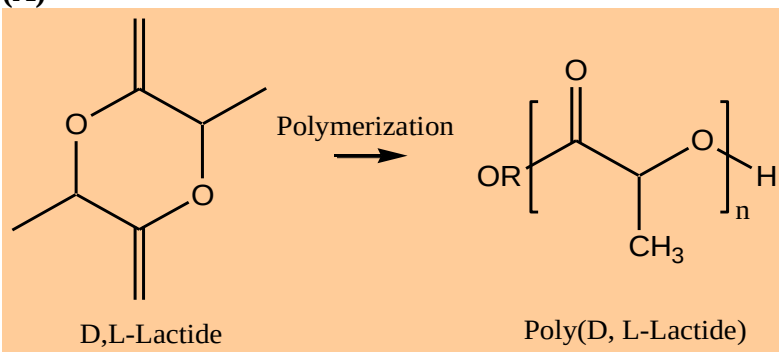

(B)

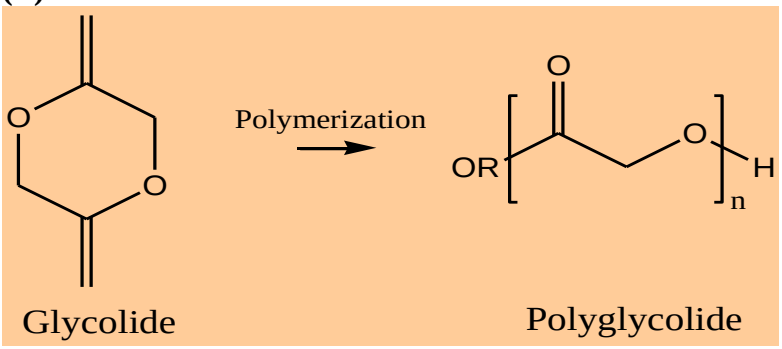

(C)

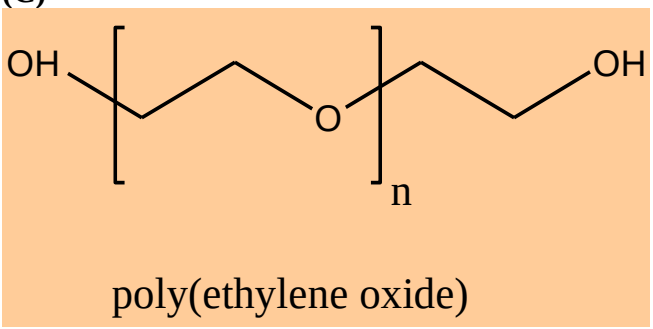

Figure C-6. Chemical structures of**:** (A) poly**(**D,L-lactide), (B) polyglycolide and (C) poly(ethylene oxide).

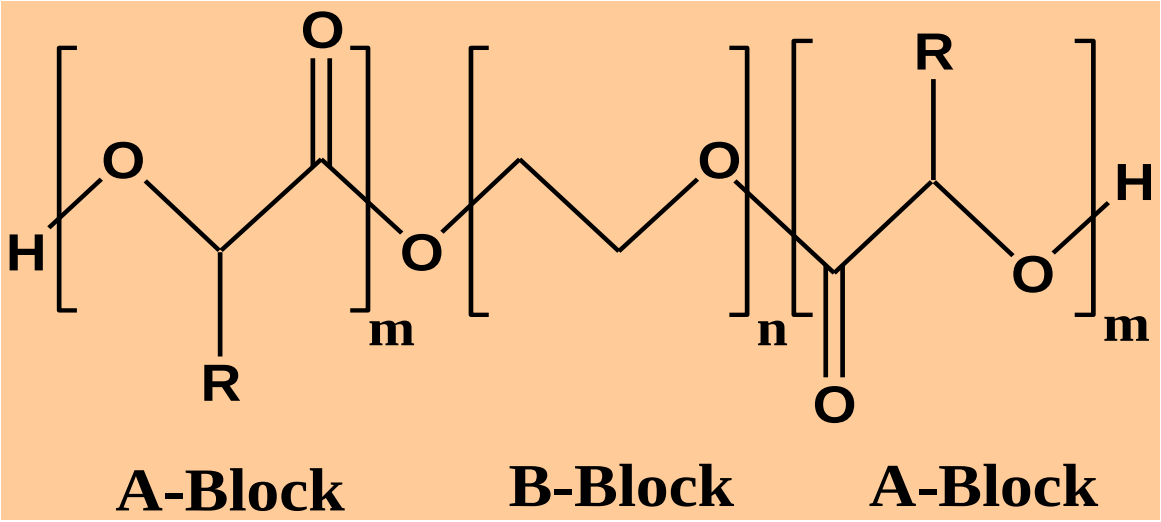

Figure C-7. ABA tri-block copolymer, consisting of poly (D,L-lactic-co-glycolic acid) (PLGA) as A blocks, and polyethylene oxide (PEO) as B blocks. (R=H or CH_3)

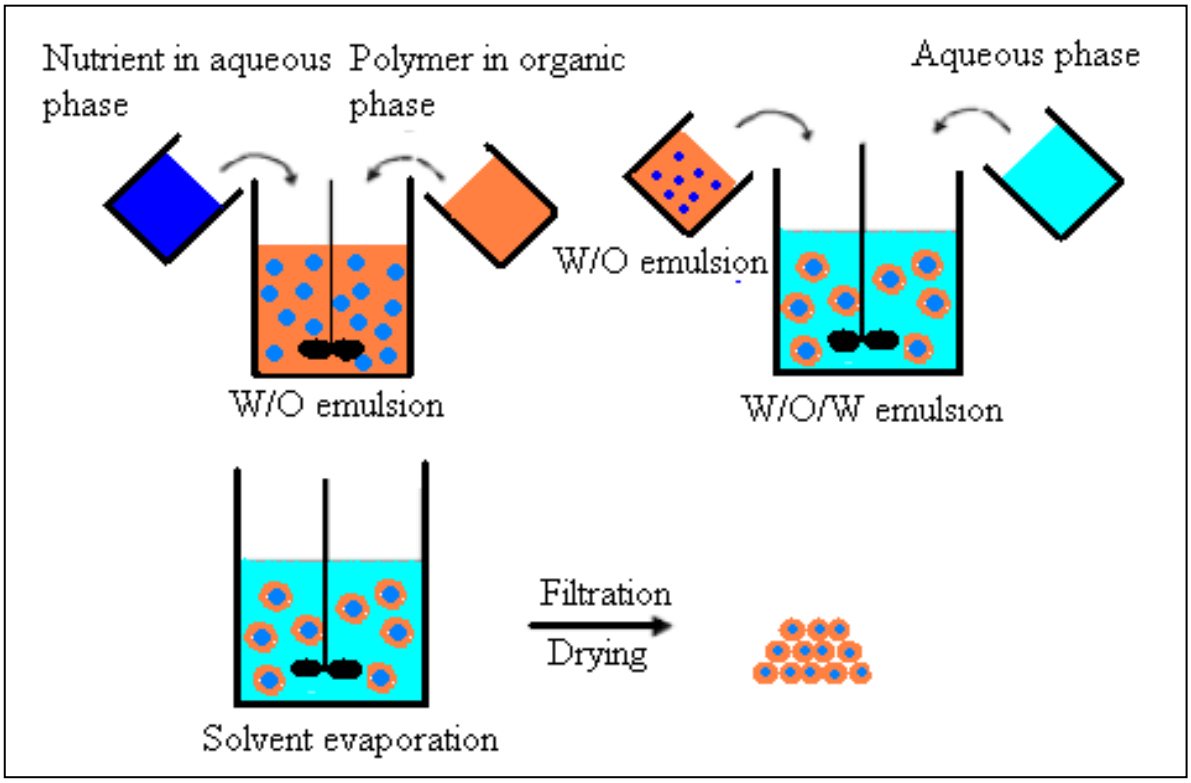

Figure C-8. Schematic of the detailed procedure of the double emulsion technique for the preparation of nanospheres.

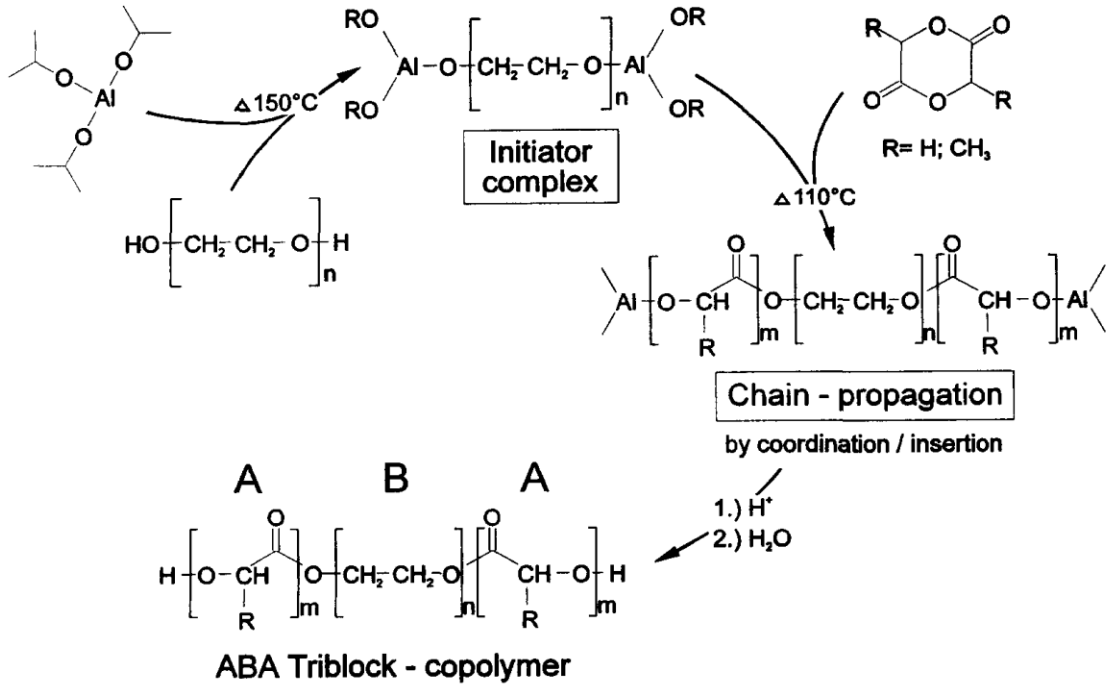

Figure C-9. Schematic diagram of the synthesis of ABA triblock copolymers using aluminum tri-isopropoxide as catalyst.[50]

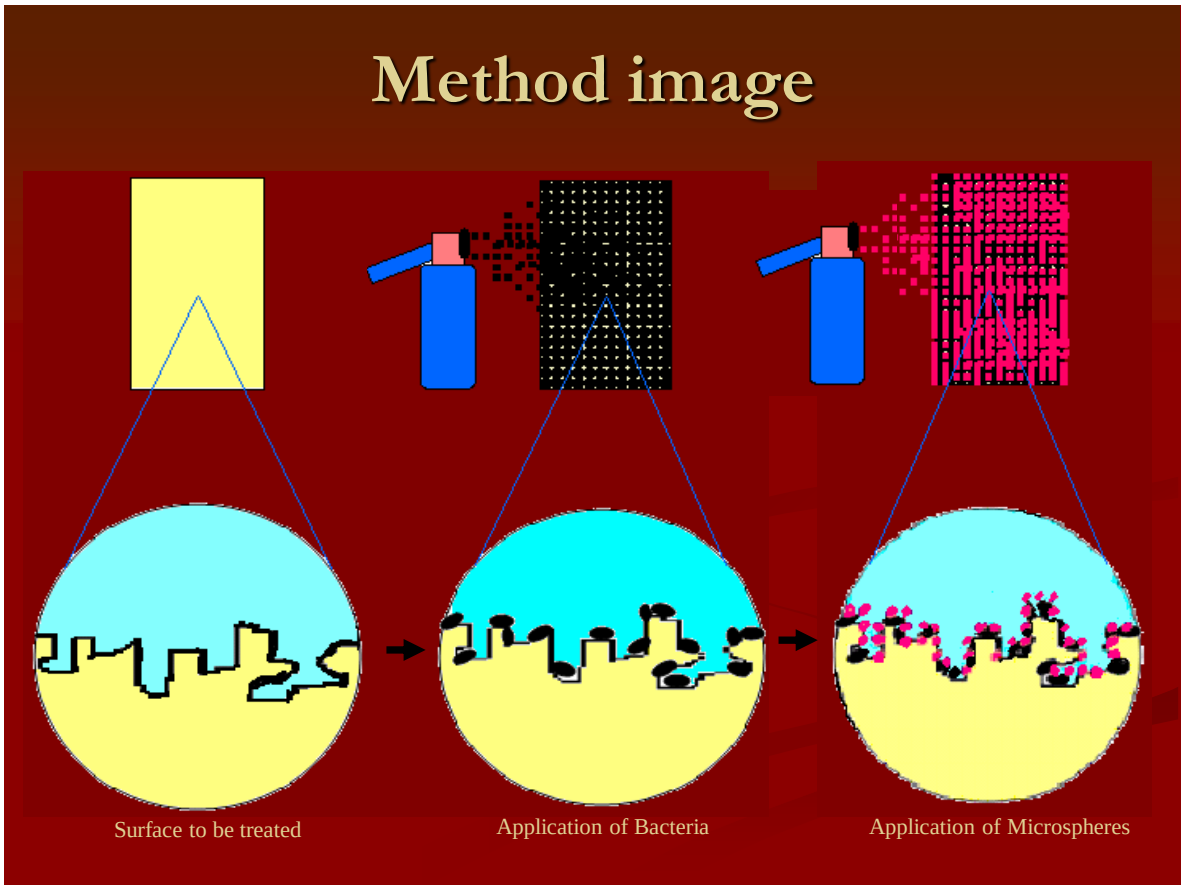

Figure C-10. Schematic diagram of the proposed procedure. It includes the application of the bacteria solution, on the surface to be treated, followed by the application of the solution containing the nanospheres. (continued in the next figure)

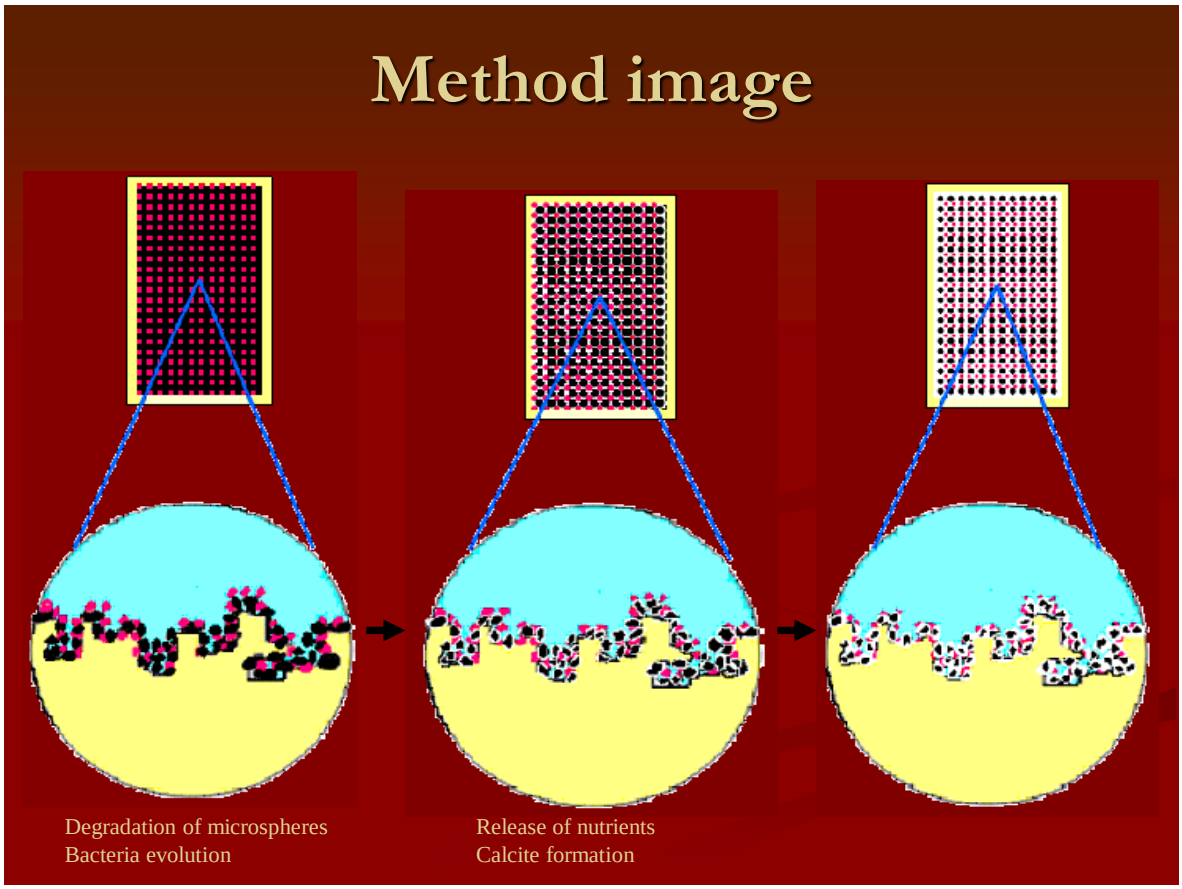

Figure C-11. Schematic diagram of the proposed procedure (continued). The degradation of the nanospheres along with the bacteria evolution can be seen. The subsequent calcite formation is also observed. (continued in the next figure)

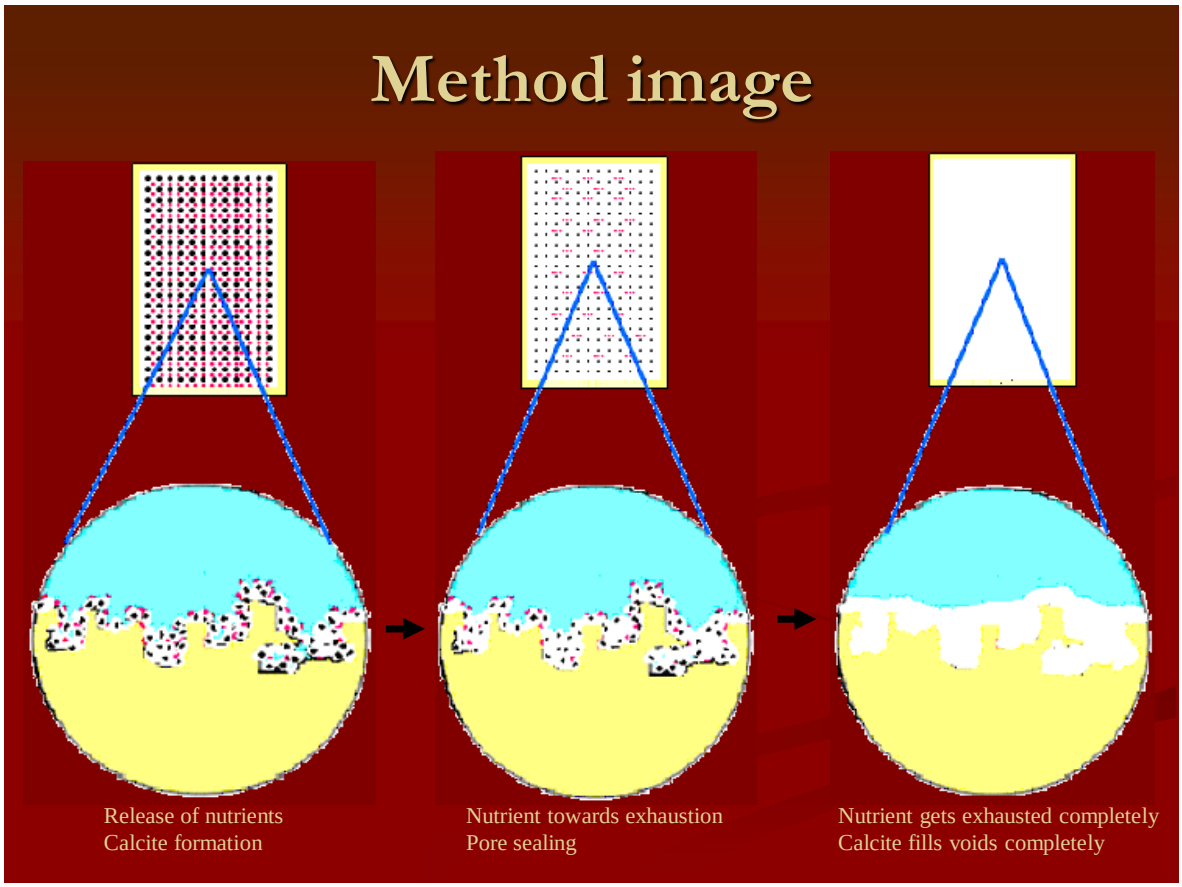

Figure C-12. Schematic diagram of the proposed procedure (continued). The calcite formation continues which results in the formation of a smooth calcite blanket and filling of the marble voids.

C.11 Reference list

1. Warscheid, T., Braams, J., Biodeterioration of stone: a review. International Biodeterioration and Biodegradation (2000), 46, 343-368.

2. Tiano, P. Biodegradation of cultural heritage: Decay mechanisms and control methods. CNR-centro di studio sulle "Cause Deperimento e Metodi Conservazione Opere d'Arte", Via G. Capponi 9, 50121 Firenze, Italy.

3. Schaffer, R. J. Causes of deterioration of building materials. I-Chemical and physical causes. Chemistry and Industry (1967), 23, 1584-1586.

4. Camuffo, D. Physical weathering of stones. The Science of the total environment. (1955), 167, 1-14.

5. Torraca, G. Treatment of stone in monuments-a review of principles and processes. Proceedings of the Conservation of Stone, Bologna (1976), 297-315.

6. Cardiano, P., Ponterio, R. C., Sergi, S., Schiavo, S. Lo, Piraino, P. Epoxy-silica polymers as stone conservation materials. Polymer (2005), 46, 1857-1864.

7. Poli, T., Toniolo, L., Sansonetti, A. Durability of protective polymers: The effect of UV and thermal ageing. Macromolecules Symposium (2006), 238, 78-83.

8. Mazzola, M., Frediani, P., Bracci, S., Salvini, A. New strategies for the synthesis of partially fluorinated acrylic polymers as possible materials for the protection of stone monuments. European Polymer Journal (2003), 39, 1995-2003.

9. Perez, J., Villegas, R., Vale, J. F., Bello, M. A., Alcade, M. Effects of consolidant and water repellent treatments on the porosity and pore size distribution of limestones. Proceedings of the International Colloquium Methods of Evaluating Products for the Conservation of Porous Building Materials in Monuments. Rome (1995), 203-211.

10. Tiano, P. Innovative treatments for stone conservation. Corrosion Reviews (2004), 22, 365-380.

11. Castanier, S., Le Me´tayer-Levrel, G., Perthuisot, J. Ca-Carbonates precipitation and limestone genesis-the microbiogeologist point of view. Sedimentary Geology (1999), 126, 9-23.

12. Castanier, S., Bernet-Rollande, M., Maurin, A., Perthuisot, J. Effects of microbial activity on the hydrochemistry and sedimentology of Lake Logipi, Kenya. Hydrobiologia (1993), 267, 99-112.

13. Cañaveras, J. C., Sanchez-Moral, S., Soler, V., Saiz-Jimenez, C. Microorganisms and microbially induced fabrics in cave walls. Geomicrobiology Journal (2001), 18, 223-240.

14. Rivadeneyra, M. A., Garcia, I. P., Salmeron, V., Cormezan, R.A. Bacterial precipitation of calcium carbonate in presense of phosphate. Soil Biology Biochemistry (1985), 17, 171-172.

15. Perito, B., Biagiotti, L., Daly, S., Galizzi, A., Tiano, P., Mastromei, G. Bacterial genes involved in calcite crystal precipitation. Of Microbes and Art. Plenum Publishers, New York (2000), 219-230.

16. Castanier, S., Le Me´tayer-Levrel, G., Orial, G., Loubiere, J., Perthuisot, J. Bacterial carbonatogenesis and applications to preservation and restoration of historic property. Of Microbes and Art. Plenum publishers, New York (2000), 203-218.

17. Angelova, N., Hunkeler, D. Rationalizing the design of polymeric biomaterials. Tibtech (1999), 17, 409-421.

18. Tamada, J. A., Langer, R. Erosion kinetics of hydrolytically degradable polymers. Proceedings of the National Academy of Sciences of the United States of America (1993), 90, 552-556.

19. Pitt, C.G., Gratzl, M.M., Kimmel, G. L., Surles, J., Schindler, A. Aliphatic polyesters II. The degradation of poly (DL-lactide), poly (E-caprolactone), and their copolymers in vivo. Biomaterials (1981), 2, 215-220.

20. Gopferich, A. Polymer bulk erosion. Macromolecules (1997), 30, 2598-2604.

21. O'Hagan, D.T., Jeffery, H., Davis, S. S. The preparation and characterization of poly (lactide-co-glycolide) microparticles: III. Microparticle/ polymer degradation rates and the in vitro release of a model protein. International Juurnal of Pharmaceutics (1994), 103, 37-45.

22. Heller, J. Polymers for controlled parenteral delivery of peptides and proteins. Advanced Drug Delivery Reviews (1993), 10, 163-204.

23. Burkersroda, F. V., Goepferich, A. M., An approach to classify degradable polymers. Materials Research Society Symposium Proceedings, Pennsylvania-USA (1999), 550-557.

24. Burkersroda, F., Schedl, L., Gopferich, A. Why degradable polymers undergo surface erosion or bulk erosion. Biomaterials (2002), 23, 4221-4231.

25. Perito, B., Mastromei, G., Conservation of monumental stones by bacterial biomineralization. Microbiology Today (2003), 30, 113-4.

26. Graae, J. Esterase activity shown by subtilisin,a proteolytic enzyme from Bacillus Subtilis. Acta Chemica Scandinavica (1954), 8, 356-7.

27. Gonzalo, S. An esterase in Bacillus Subtilis spores and its release by ballistic disintegration. Canadian Journal of Microbiology (1963), 9, 643-645.

28. Kaiser, P., Raina, C., Parshad, R., Johri, S., Verma, V., Andrabi, K., Qazi, G. A novel esterase from Bacillus subtilis (RRL 1789):Purification and characterization of the enzyme. Protein expression and purification (2006), 45, 262-268.

29. Eggert, T., Pencreach, G., Douchet, I., Verger, R., Jaeger, K. A novel extracellular esterase from Bacillus subtilis and its conversion to a monoacylglycerol hydrolase. European Journal of Biochemistry (2000), 267, 6459-69.

30. Albertsson, A. C., Karlsson, S. Chemistry and biochemistry of polymer biodegradation. Chemistry and Technology of Biodegradable Polymers. Chapman and Hall, London (1994), 7-17.

31. Riefler, J. F., Higerd, T. B. Characterization of intracellular esterase A from Bacillus Subtilis. Biochimica et Biophysica Acta (1976), 429, 191-197.

32. Jeffery, H., Davis, S., O'Hagan, D. The preparation and characterisation of poly(lactide-co-glycolide) microparticles. I:Oil-in-water emulsion solvent evaporation. International Journal of Pharmaceutics (1991), 77, 169-175.

33. Jeffery, H., Davis, S., O'Hagan, D. The preparation and characterization of Poly(lactide-co-glycolide) Microparticles. II.The entrapment of a model protein using a (water-in-oil)-in-water emulsion solvent evaporation technique. Pharmaceutical Research (1993), 10, 362-369.

34. O'Hagan, D., Jeffery, H., Davis, S. The preparation and characterization of poly(lactide-co-glycolide) microparticles: III.Microparticle/polymer degradation rates and the in vitro release of a model protein. International Journal of Pharmaceutics (1994), 103, 37-45.

35. Grodzinski, J. Biomedical application of functional polymers. Reactive & Functional Polymers (1999), 39, 99-138.

36. Angelova, N., Hunkeler, D. Rationalizing the design of polymeric biomaterials. Tibtech (1999), 17, 409-421.

37. Gunatillake, P., Adhikari, R. Biodegradable synthetic polymers for tissue engineering. Polymers for Tissue Engineering European Cells and Materials (2003), 5, 1-16.

38. Benita, M., Romeijn, S., Junginger, H., Borchard, G. PLGA–PEI nanoparticles for gene delivery to pulmonary epithelium. European Journal of Pharmaceutics and Biopharmaceutics (2004), 58, 1-6.

39. Mader, K., Bittner, B., Li, Y., Wohlauf, W., Kissel, T. Monitoring microviscosity and microacidity of the albumin microenviroment inside degrading microparticles from poly(lactide-co-glycolide) (PLG) or ABA-triblock polymers containing hydrophobic poly(lactide-co-glycolide) A blocks and hydrophilic poly(ethyleneoxide) B blocks. Pharmaceutical Research (1998), 15, 787-793.

40. Athanasiou, K. A., Niederauer, G. G., Agrawal, C. M. Sterilization, toxicity, biocompatibility and clinical applications of polylactic acid/polyglycolic acid copolymers. Biomaterials (1996), 17, 93-102.

41. Hollinger, J., Jamiolkowski, D., Shalaby, S. Bone repair and a unique class of biodegradable polymers: the poly(α-esters). Biomedical Applications of Synthetic Biodegradable Polymers. CRC Press, Florida (1995), 197-217.

42. Harris, J. M. Introduction to biotechnical and biomedical applications of poly(ethylene glycol). Poly(ethylene glycol) Chemistry: Biotechnical and Biomedical Applications, Harris J. M. Ed., Plenum Press, New York (1992), 1-14.

43. Merril, E. W. Poly(ethylene oxide) and blood contact, a chronicle of one laboratory. Poly(ethylene glycol) Chemistry: Biotechnical and Biomedical Applications, Harris J. M. Ed., Plenum Press, New York (1992), 199.

44. Ramirez, J. L., Santana, M. R., Castro, I. G., Gonzalez, A.The role of biotechnology in art. Preservation. Trends in Biotechnology (2005), 23 (12), 584-588.

45. Skoulikidis, T. N., et. al. Damage and preservation of monuments. Preservation of the surface of statues in Acropolis. Committee for the Preservation of the Statues of Acropolis, Athens (1994), 13-38.

46. Skoulikidis, T. N. Preservation of surfaces. Corrosion and preservation of compositional materials used in monuments. University of Crete editions, Heraklion (2000), 219-266.

47. Koestler, R. J. Polymers and resins as food for microbes. Of Microbes and Art. Plenum publishers, New York (2000), 153-167.

48. Youxin, L., Kissel, T. Synthesis and properties of biodegradable ABA triblock copolymers consisting of poly (L-lactic acid) or poly (L-lactic-co-glycolic acid) A-blocks

attached to central poly (oxyethylene) B-blocks. Journal of Controlled Release (1993), 27, 247-257.

49. Ronneberger, B., Kissel, T., Anderson, J. M. Biocompatibility of ABA triblock copolymer microparticles consisting of poly(L-lactic-co-glycolic-acid) A-blocks attached to central poly(oxyethylene) B-blocks in rats after intramuscular injection. European Journal of Pharmaceutics and Biopharmaceutics (1997), 43, 19-28.

50. Bittner, B., Witt, C., Mader, K., Kissel, T. Degradation and protein release properties of Microspheres prepared from biodegradable poly(lactide-co-glycolide) and ABA triblock copolymers: influence of buffer media on polymer erosion and bovine serum albumin release. Journal of Controlled Release (1999), 60, 297-309.

51. Morlock, M., Kissel, T., Li, Y. X., Koll, H., Winter, G. Erythropoietin loaded microspheres prepared from biodegradable LPLG–PEO–LPLG triblock copolymers: protein stabilization and in-vitro release properties. Journal of Controlled Release (1998), 56, 105-115.

52. Kissel, T., Li, Y. X., Volland, G, Gorich, S., Koneberg, R. Parenteral protein delivery systems using biodegradable polyesters of ABA block structure, containing hydrophobic poly(lactide-co-glycolide) A blocks and hydrophilic poly(ethylene oxide) B blocks. Journal of Controlled Release (1996), 39, 315-326.

Appendix D. Collaborative or Incomplete Work

D.1 Introduction

Research work that has been conducted in collaboration with other graduate students from our group, as well as with other research groups from other universities and companies is briefly summarized and discussed. An introduction on each project, along with an explanation of the motivation and the objectives, is given. A part of the work stated in this section, deals with the development of products for companies. Due to the confidentiality constraints, some of the work explained below is going to be kept intentionally brief. Finally, some research work, particularly in thermo-responsive hydrogels (e.g. PNiPAAm), which has not been completed, due to time constraints, is going to be briefly introduced. In addition some new ideas and concepts in some of the projects that this thesis has been focused and which may be conducted in our lab in the future are going to be revealed.

The research projects explained in the following sections of Appendix D include:

- Encapsulation of enzymes utilizing the double encapsulation method for detergent formulations.
- Incorporation of conductive aniline oligomers in PNiPAAm thermo-responsive hydrogels.

D.2 Encapsulation of Enzymes Utilizing the Double Encapsulation Method for Detergent Formulations

As has been described in Chapter 9, a novel technology for maintaining the enzymatic activity, during storage in harsh media, such as organic solvents and high pH aqueous solutions, has been explored. This technology includes the utilization of the non-surfactant templated sol-

gel method, which has been invented in our lab, to incorporate the enzyme of interest into the pores of mesoporous organosilicas, followed by the application of a second acrylic coating. The results indicated that the encapsulates after storage in high pH buffer solution , detergent, ethanol and toluene showed many orders of magnitude higher residual activity as compared to the native enzymes under the same conditions. A similar ‘double encapsulation’ technique has been extensively investigated for stabilizing and maintaining the enzymatic activity of enzymes after storage in a high pH detergent. This project deals with the development of products for companies and thus, due to the confidential constraints, some of the work explained below, is going to be kept intentionally brief. The aim of this study was to find a material that would fulfill two purposes. First the material has to be able to effectively maintain the catalytic activity of the encapsulated enzyme, while storage in detergent formulations, for as long as needed. Secondly, upon dilution of the detergent, that contains the encapsulated enzyme, in water in the laundry machine, the materials should be able to make the encapsulated enzymes accessible to the compounds of interest, which is dirt for this specific application. This double encapsulation method comprises of a two-step procedure. First, the nonsurfactant-templated sol-gel method has been utilized to encapsulate protease into mesoporous hybrid organosilica. The dry sol-gel hybrid was then crushed into a fine powder. The powdered enzyme-containing silica hybrid was then coated with a mixture of acrylic monomer and catalytic amounts of photo-initiators. Photopolymerization of the obtained viscous suspension for predetermined time resulted in a composite which was crushed again to produce the second protective layer.

The key features of this technology are the following: The outer acrylic layer is insoluble in high pH aqueous solvents. This prevents these harsh media (e.g. the detergent) from entering

the pores of the interior organosilica moiety and denaturing the enzyme. On the other hand, the outer layer contains again a template, but this time this template is slightly water soluble. Thus, when the enzyme-containing powdered material is diluted in an excess of water along with the increase of temperature and the agitation that the laundry machine procedure is associated with, the outer template dissolves, thereby creating pores in the outer layer. The inner template contained inside the mesopores of the inner hybrid sol-gel coating is also removed during washing and the protease is now free to interact with the dirt of the cloths that are washed. **Figure D-1** shows some preliminary data obtained for protease encapsulated in hybrid materials after storage for a prolonged period of time in a high pH detergent solution. As can be seen on this figure, the enzymatic catalytic activity of the protease remains in very good levels (e.g about 55 % of the original enzymatic activity) even after 30 days of storage of the materials in the detergent solution. As mentioned earlier, due to the constraints imposed, the type of the detergent and the compositions of the materials, used to encapsulate the protease, cannot be revealed. It is noteworthy though, that the native enzyme becomes completely inactive after 1 day of storage in the detergent formulations. Further experiments and evaluation of the obtained results is underway in our lab. Future work includes the adjustment of the type and the ratios of templates used (both inner and outer) in order to further optimize this novel technology and further maintain the enzymatic activity of the encapsulated enzymes.

D.3 Incorporation of Aniline Oligomers in N-Isopropylacrylamide Gels

The past 2 decades, poly(N-isopropylacrylamides) (PNIPAAm) hydrogels have been extensively studied due to their unique properties. These hydrogels are extremely thermo-sensitive and are characterized by a reversible volume decrease upon heating. These materials

exhibit a phase transition temperature (T_{tr}) or lower critical solution temperature (LCST) at ~ 32 ^{o}C. At temperatures below the LCST, PNIPAAm gel is soluble in water. As the temperature is increased above LCST, it undergoes abrupt changes in volume and precipitates suddenly from solution. This transition is attributed to the change in the balance between hydrophilic and hydrophobic interactions inside the NiPAAm moiety.

The aim of this work was the covalent incorporation of conductive and electroactive aniline oligomers into the PNiPAAm structure. Two synthetic approaches have been followed. One includes the copolymerization of N-isopropylacrylamide with a modified, with amine end group substitution by acrylic groups, aniline trimer to yield a conductive thermo-responsive hydrogel. The second approach that has been envisioned is the formation of non-covalent composites of copolymers of PNiPAAm with 2-acrylamido-2-methyl-1-propane sulfonic acid and aniline oligomers (dopped with dodecyl benzene sulfonic acid). Both of these synthetic approaches can be seen in **Figure D-3** and **Figure D-4** respectively.

D.3.1 Experimental Part

D.3.1.2 Modified Aniline Trimer

For the synthesis of a modified aniline trimer, 1.84g of N-phenyl–p-phenylene diamine, and 1.01 g of triethylamine were dissolved in 30 ml of dichloromethane in a three-neck round-bottom flask and stirred under nitrogen purge. 0.9 g of acryloyl chloride were dissolved in 30 ml of dichloromethane and added drop-wise over a period of 60 min into the above solution. The solution temperature was kept at ~ -10 – -5 ^{o}C throughout the whole period of the addition of acryloyl chloride. After this period the mixture was stirred for 3 more hours at room temperature.

The modified trimmer was precipitated in the organic phase by the addition of a big amount of distilled water. The obtained brown-grey solid was washed with copious amounts of distilled water and dried under vacuum (yield 42%).

D.3.1.3 Synthesis of Copolymer

For the synthesis of PNiPAAm as a control, 100 mg of N-isopropylacrylamide was dissolved in 1.2 ml of de-ionized water. 2.0 mg of N,N-methylene-bis-acrylamide, 20 μl of ammonium persulfate and 5 μl N,N,N',N'-tetramethylenediamine in 1 ml of de-ionized water were then added in the above acrylamide solution in one portion. After about 50 min a white hydrogel was obtained. Additional methods (already reported by other researchers) to synthesize PNiPAAm have been also explored yielding to a hydrogel formation. A similar procedure to synthesize a copolymer of the acrylic-modified aniline oligomer with N-isopropylacrylamide has been explored. A series of different compositional mole ratios have been investigated including ratios of modified trimer/acrylamide= 99/1, 95/5, 90/10, 85/15. So far, the results obtained seem ambiguous. Ratios of trimer/acrylamide= 99/1 seem to provide a crosslinked hydrogel while lower ratios show no formation of a hydrogel. More experiments are needed to support the above findings. Nevertheless, the present method seems very promising for providing novel conductive and electroactive hydrogels.

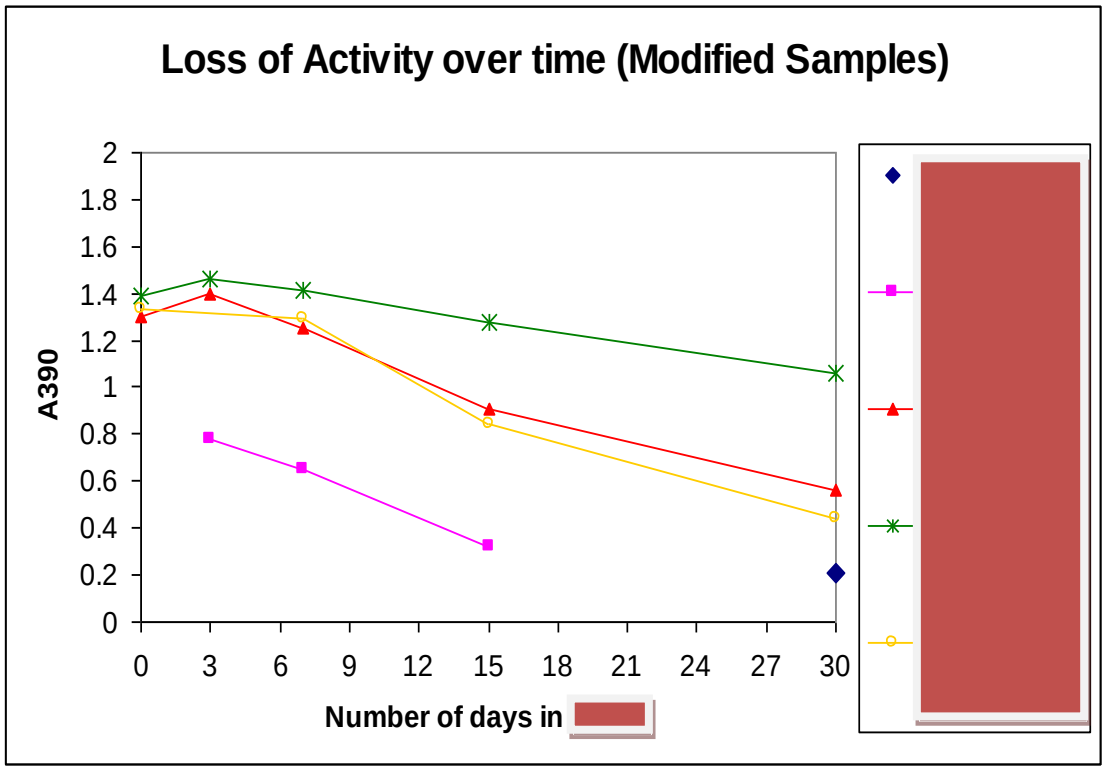

Sample	0days	3days	7days	15days	30days
					0.21 (1)
		0.78 (1)	0.65 ± 0.2 (2)	0.32 (1)	
	1.3 ± 0.16 (5)	1.4 (1)	1.25 (1)	0.91 ± 0.07 (2)	0.56 ± 0.13 (3)
	1.4 ± 0.03 (2)	1.46 (1)	1.42 ± 0.01 (3)	1.28 ± 0.08 (4)	1.06 ± 0.05 (4)
	1.33 ± 0.09 (4)		1.29 ± 0.03 (2)	0.84 ± 0.04 (3)	0.44 ± 0.01 (2)

Figure D-1. Time study of the enzymatic catalytic activity of protease encapsulated in hybrid materials by the double encapsulation method.

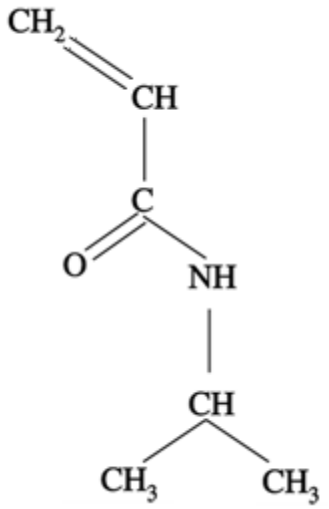

Figure D-2. Chemical formula of N-isopropylacrylamide.

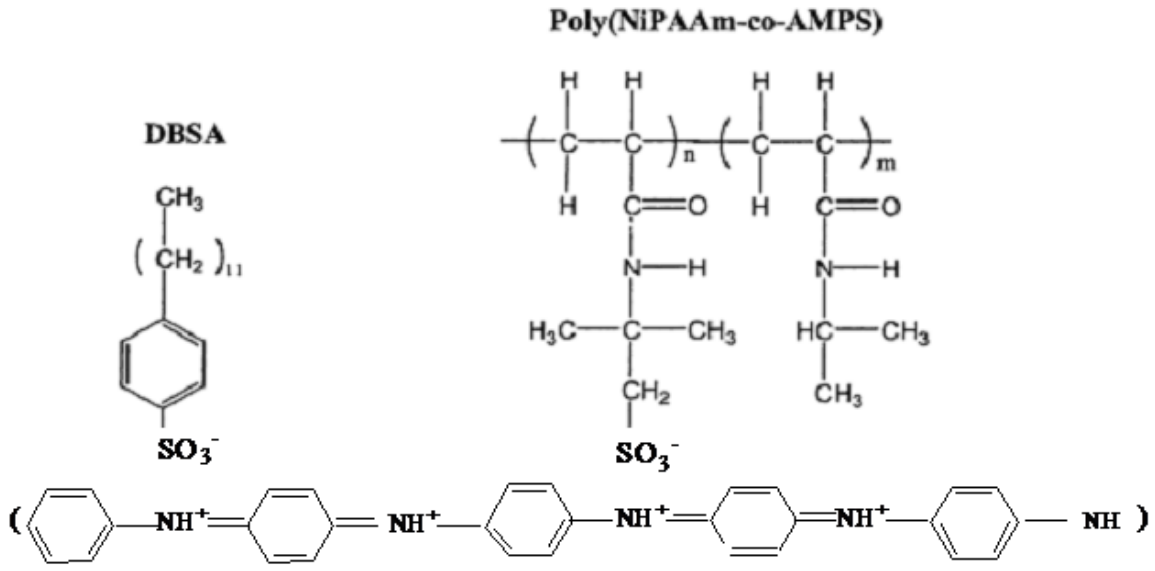

Figure D-3. Non-covalent composites of copolymers of NiPAAm and 2-acrylamido-2-methyl-1-propane sulfonic acid with aniline oligomers (aniline trimer, pentamer, heptamer,etc).

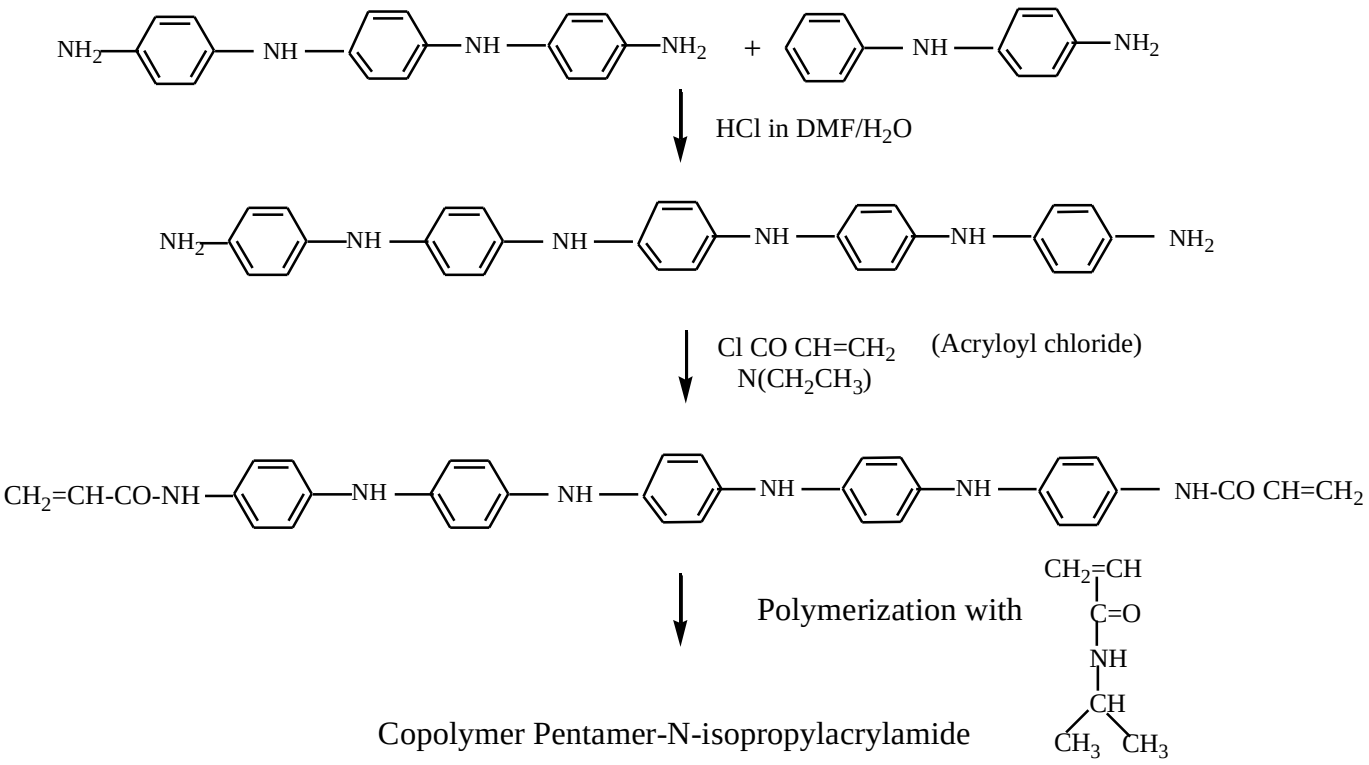

Figure D-4. Incorporation of aniline oligomers (trimer, pentamer, etc.) in PNiPAAm hydrogel.

Appendix E. Supporting Information

E.1 Additional NMR Spectra for Chapter 6

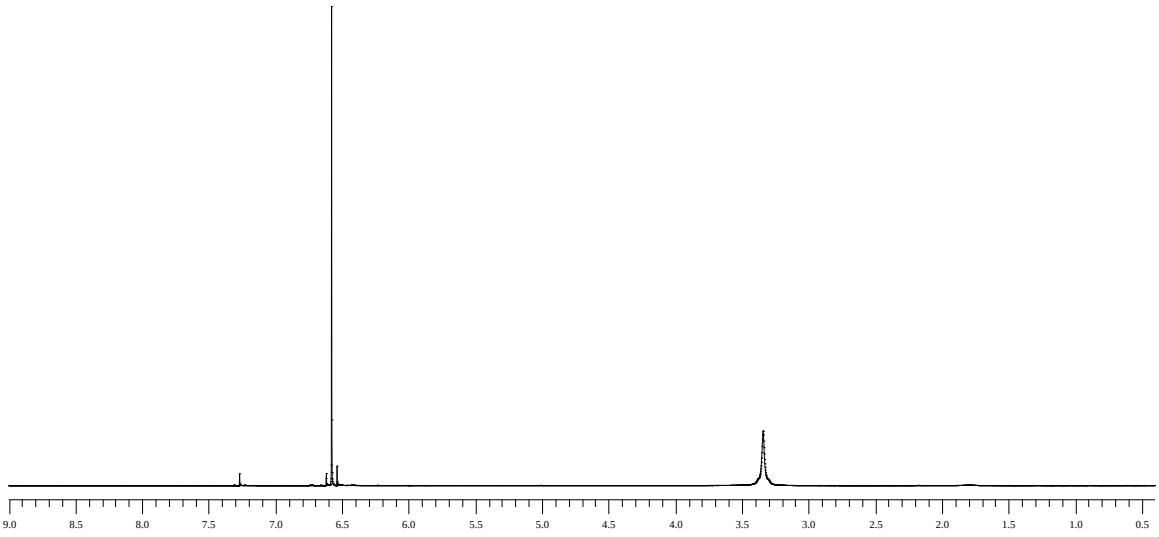

Figure E-1. ^{1}H-NMR of phenylene diamine in $CDCl_3$: δ 3.3 (s, 4H, -NH_2), δ 6.5 (t, 4H, arom.-H).

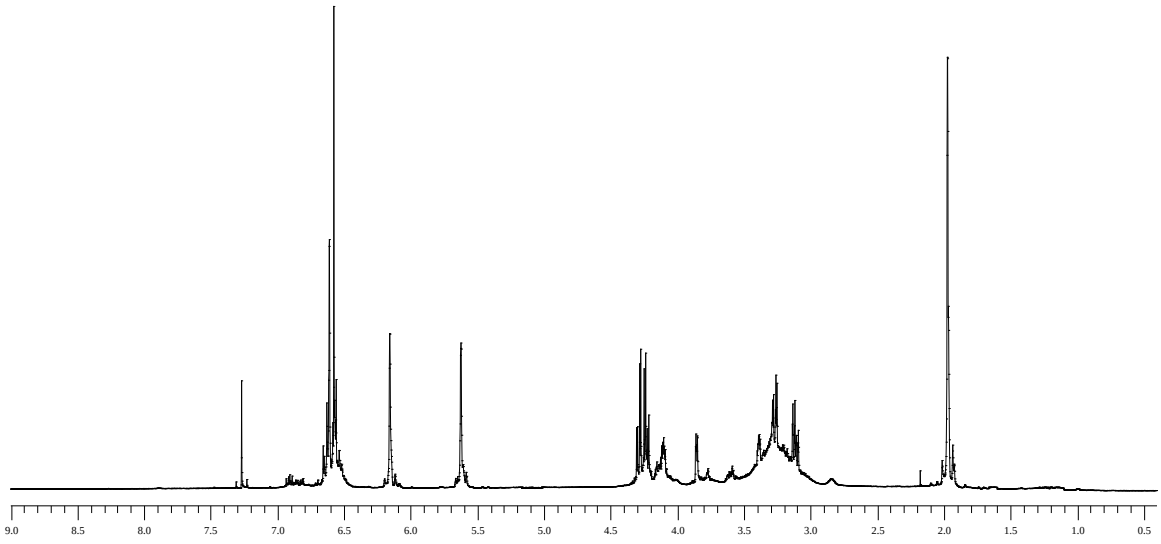

Figure E-2. ^{1}H-NMR of product from the reaction of phenylene diamine with GMA (3hrs at 90 ^{o}C, 1 to 2 mole ratio) in $CDCl_3$: δ 1.9 (m, 3H, -CH_3 from GMA), δ 2.9-3.0 (s, 2H, -NH-), δ 3.2-3.3 (m, 2H, -CH_2-NH- after epoxy ring opening), δ 3.9-4.1 (m, 2H, -CH_2 (OH)- after epoxy ring opening), δ 4.2 (m, 2H, -CH_2-), δ 5.6-6.2 (dd, 2H, CH_2=), δ 6.6 (m, 4H, arom.-H).

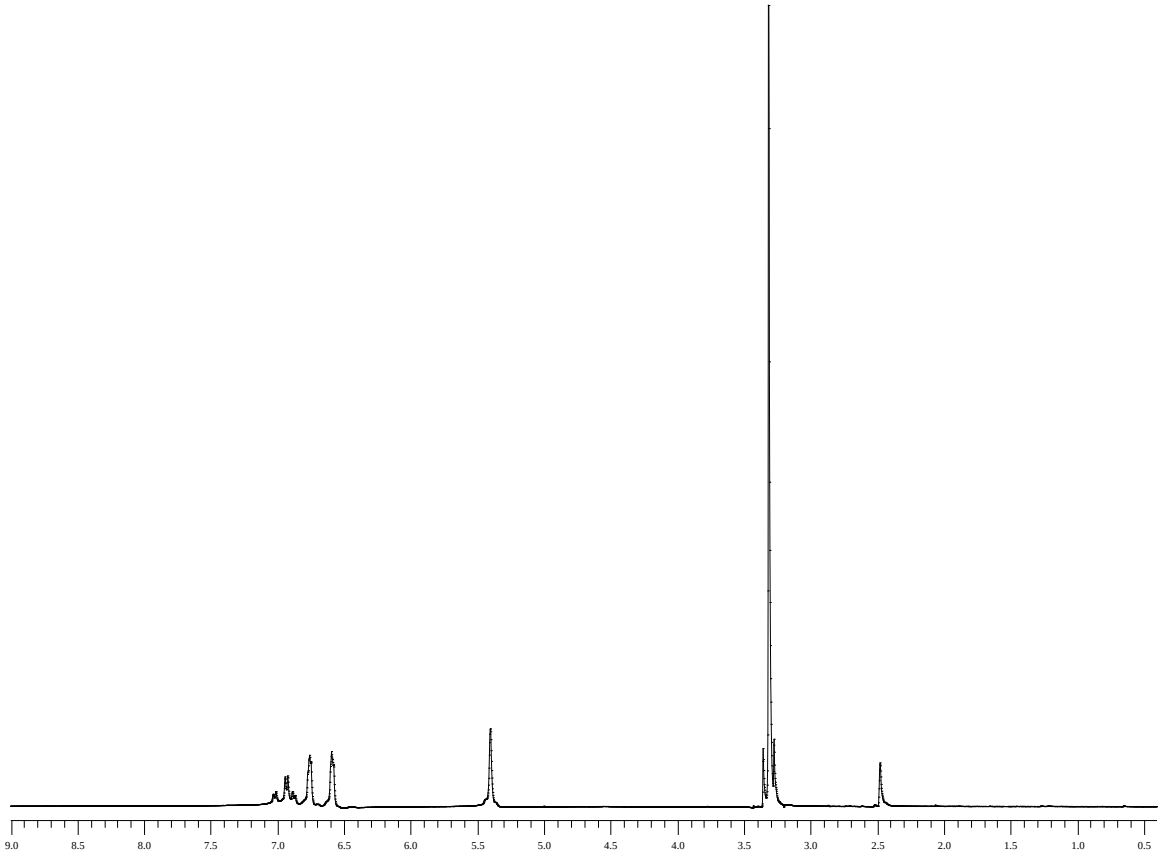

Figure E-3. ^{1}H-NMR of aniline trimer in DMSO: δ 5.4 (s, 4H, -NH_2), δ 6.6 (t, 4H, arom.-H), δ 6.8 (t, 4H, arom.-H), δ 7.0 (t, 4H, arom.-H).

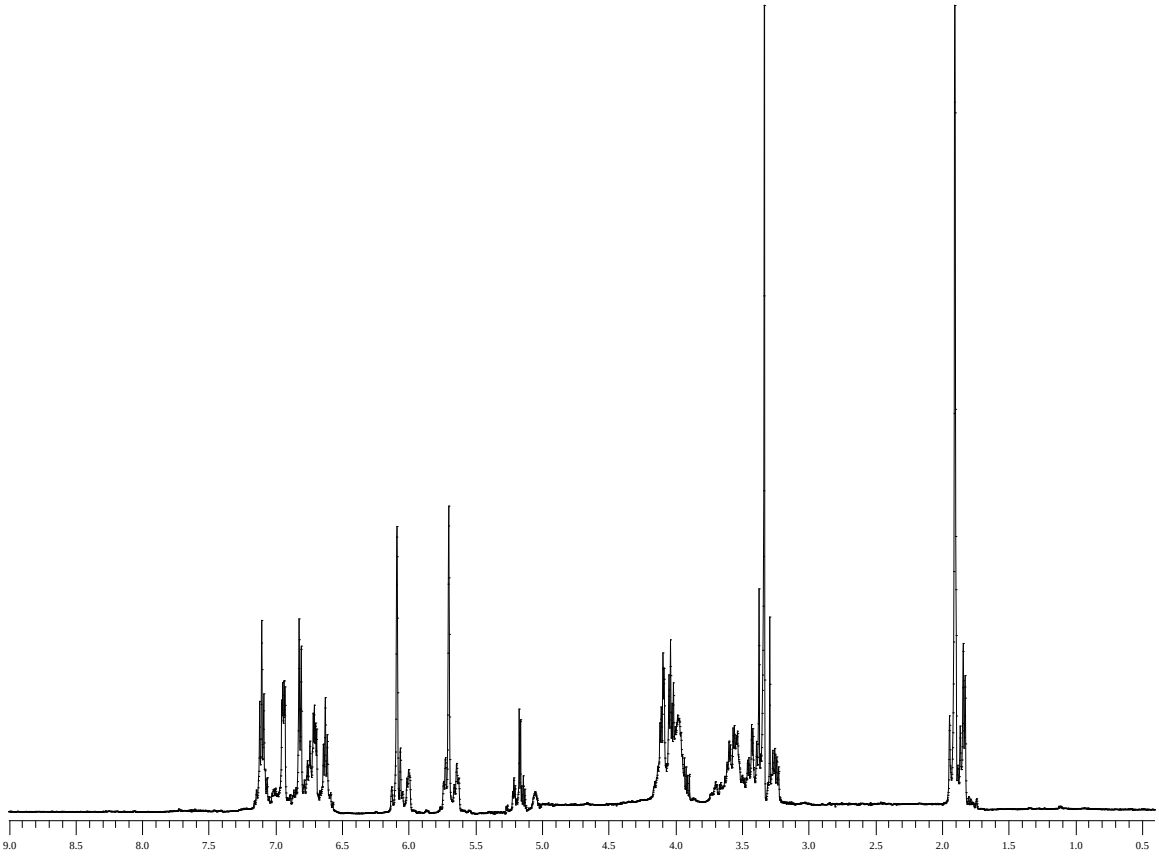

Figure E-4. ^{1}H-NMR of reaction of aniline trimer with GMA (3hrs at 90 ^{o}C, 1 to 2 mole ratio) in DMSO: δ 1.9 (m, 3H, -CH_3 from GMA), δ 3.2-3.3 (m, 2H, -CH_2-NH- after epoxy ring opening), δ 3.8 (m, 2H, -CH_2 (OH)- after epoxy ring opening), δ 4.0-4.2 (m, 2H, -CH_2-), δ 5.0-5.2 (m, 2H, -NH-), δ 5.6-6.2 (dd, 2H, CH_2=), δ 6.6-6.8 (m, 4H, arom.-H), δ 6.9 (m, 4H, arom.-H), δ 7.1 (t, 4H, arom.-H).

E.2 Additional Cyclic Voltammogram for Chapter 7

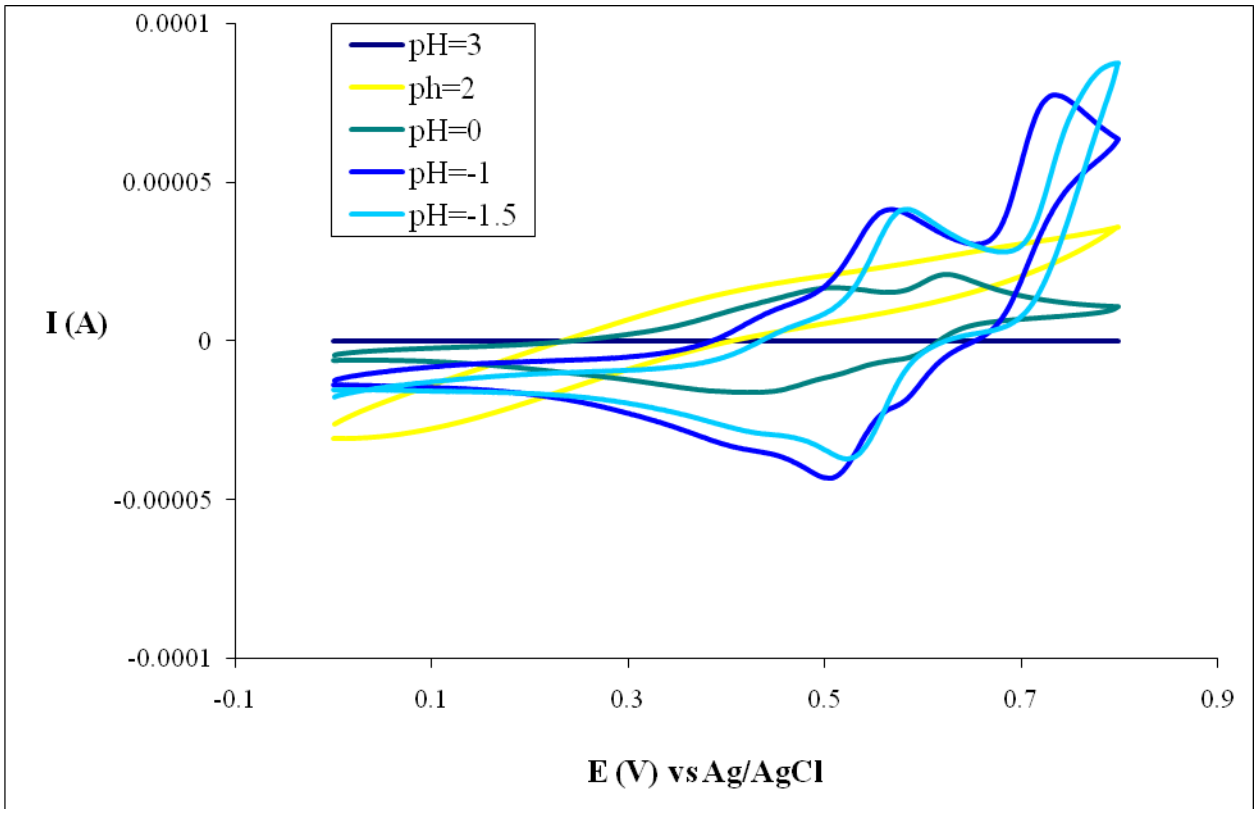

Figure E-5. Dependence of redox peaks of aniline trimer on the pH of the solution (HCl). Voltage scanned between 0 and 800 mV. Scan rate used : 60 mV/sec.

Vita

Andreas Mylonakis was born in Athens, Greece on October 28th, 1978. He received his Bachelors of Science degree in Chemistry from Aristotle University of Thessaloniki in 2002. He joined Drexel University, Philadelphia, PA in 2003 after he received a full-time scholarship from The Hellenic Foundation to pursue the PhD in Chemistry. He received his Masters of Science degree in Chemistry from Drexel University, Philadelphia, PA in 2005. From then on, he has been pursuing a Ph.D. degree under the supervision of Dr. Yen Wei from the Center of Advanced Polymers and Materials Chemistry and Department of Chemistry, Drexel University. His research interests include a wide range of fields in polymer and materials chemistry, especially novel hybrid materials, nanomaterials and biodegradable adhesives for several applications. He has developed several products for multibillion-dollar companies and has one patent in biodegradable adhesives for dental applications pending.

Selected publications:

- Mylonakis Andreas, Yi Guo, Shuxi Li, Solomon Praveen, Indraniel Mukherjee, Yen Wei. Covalent incorporation of polyaniline into sol-gel materials. Polymer (Featured article), 2008, (in revision).
- Mylonakis, A.; Economou, A.; Fielden, P. R.; Goddard, N. J.; Voulgaropoulos, A. A study of the determination of Cu(II) by anodic stripping voltammetry on a novel Nylon/Carbon fiber electrode. Electroanalysis, 2004, 16(7), 524-531.
- Shuxi Li, S. Solomon Praveen, Andreas Mylonakis, Apoorva Shah, Alex Hsieh, Alpa Patel, George Baran, Yen Wei. Synthesis of new organic–inorganic hybrids poly(HEMA-GMA-silica) and their mechanical properties. Journal of Materials Research, 2008, 23 (1), 66-71.
- Guo, Yi; Mylonakis, Andreas; Zhang, Zongtao; Lelkes, Peter I.; Levon, Kalle; Li, Shuxi; Feng, Qiuwei; Wei, Yen. Oligoaniline-contained electroactive silsesquioxane precursor for synthesizing novel siliceous materials. Macromolecules, 2007, 40(8), 2721-2729.
- Mylonakis, Andreas; Guo, Yi; Zagorski, Matthew C. R.; Li, Shuxi; Wei, Yen. Electrochemical Study of Electroactive Aniline Oligomers with Alkoxysilyl or Amine End-groups. Electroanalysis, 2008, (In revision).